



12-2013

Geologic investigations in the central Georgia Inner Piedmont and the western flank of the Carolina superterrane: Implications regarding Acadian and Alleghanian collisional orogenesis, fault reactivation, and the Mesozoic breakup of Pangea

Matthew Tiesher Huebner

University of Tennessee - Knoxville, mhuebne1@utk.edu

Follow this and additional works at: https://trace.tennessee.edu/utk_graddiss



Part of the [Tectonics and Structure Commons](#)

Recommended Citation

Huebner, Matthew Tiesher, "Geologic investigations in the central Georgia Inner Piedmont and the western flank of the Carolina superterrane: Implications regarding Acadian and Alleghanian collisional orogenesis, fault reactivation, and the Mesozoic breakup of Pangea. " PhD diss., University of Tennessee, 2013.
https://trace.tennessee.edu/utk_graddiss/2581

This Dissertation is brought to you for free and open access by the Graduate School at TRACE: Tennessee Research and Creative Exchange. It has been accepted for inclusion in Doctoral Dissertations by an authorized administrator of TRACE: Tennessee Research and Creative Exchange. For more information, please contact trace@utk.edu.

To the Graduate Council:

I am submitting herewith a dissertation written by Matthew Tiesher Huebner entitled "Geologic investigations in the central Georgia Inner Piedmont and the western flank of the Carolina superterrane: Implications regarding Acadian and Alleghanian collisional orogenesis, fault reactivation, and the Mesozoic breakup of Pangea." I have examined the final electronic copy of this dissertation for form and content and recommend that it be accepted in partial fulfillment of the requirements for the degree of Doctor of Philosophy, with a major in Geology.

Robert D. Hatcher Jr., Major Professor

We have read this dissertation and recommend its acceptance:

Theodore C. Labotka, Micah J. Jessup, Carol P. Harden

Accepted for the Council:

Carolyn R. Hodges

Vice Provost and Dean of the Graduate School

(Original signatures are on file with official student records.)

**Geologic investigations in the central Georgia Inner
Piedmont and the western flank of the Carolina
superterrane: Implications regarding Acadian and
Alleghanian collisional orogenesis, fault reactivation, and the
Mesozoic breakup of Pangea**

A Dissertation
Presented for the
Doctor of Philosophy Degree
The University of Tennessee

Matthew Tiesher Huebner
December, 2013

Copyright © 2013 by Matthew Tiesher Huebner
All rights reserved

ACKNOWLEDGMENTS

I most importantly have to thank Dr. Robert D. Hatcher, Jr. for his guidance, his perspective of our ever-changing science, the ability to adapt to new data, and of course, for his patience with a slow learner. His outlook on how to approach geologic problems, built on a foundation of strong field studies prior to incorporating other analytical techniques, is an approach that many preach yet few practice. Dr. Hatcher has given me the opportunity to approach a problem that involved a significant field component, without which our interpretations of subsequent geochronologic and geochemical data would have likely been erroneous. My committee members, Drs. Ted Labotka, Micah Jessup, and Carol Harden are thanked for their reviews and comments, discussions about geology, and an abiding willingness to help.

I must also convey a great deal of gratitude toward the “Hatcher support staff,” Nancy Meadows and Andrew Wunderlich. Nancy has always been a source of positive encouragement, grammatical edits, and of course, a sympathetic ear. Andrew Wunderlich has aided in countless projects through my years at UTK, including, but not limited to, the GIS component of our field mapping and formatting the 2011 Georgia Geological Society Fieldtrip Guidebook. Without either of these folks, much of the work that I have completed would not be nearly as clean, neat, or professional. Thank you.

Many thanks are extended to the numerous classmates (and friends) that have endured incessant questions and rants during my time at UTK. Brittany Steele (Davis) was always there for discussions during the early stages of field work in central Georgia, and certainly shaped our ideas of the geology in that region. Chris Howard was a fantastic field mate during the 2010 field season in McDonough, GA, that involved hockey, home brewing, “adventure Mexican food,” and failed experiments with breakfast burritos. Justin Rehrer has been a great office mate and source of alternative hypotheses, and is a collaborator on several manuscripts that are presented in this dissertation. Phillip Derryberry deserves thanks for teaching me a great deal about Valley and Ridge structure and stratigraphy over afternoon darts and putting practice. Last but not least, I thank Arthur Merschat, who was always willing to talk through new ideas, was always able to provide background geologic input that I wouldn’t have considered otherwise, and introduced me to the value of geologic discussion while tossing a football. Justin Rehrer, Chris Howard, and Mary Biswal deserve special thanks for helping with zircon separations during several days- to weeks-long zircon separation sessions. Additionally, the influence of countless other faculty and students in the Department of Earth and Planetary Sciences has molded my approach to scientific problems, and those folks are genuinely appreciated.

I would also like to acknowledge several individuals outside of the University of Tennessee that have provided support, geologic discussion, and encouragement. Mike Higgins, Ralph

Crawford, John Costello, and Randy Kath attended several field reviews, and their perspectives, insight, and knowledge of the regional geology were invaluable sources of guidance through the field studies. Randy Kath and Tim Chowns are especially thanked for their assistance and contributions to the 2011 Georgia Geological Society Annual Field Trip, which included all of the logistics and guidebook printing. Drew Coleman, Ryan Mills, and Jez Ingles at UNC-Chapel Hill and Calvin Miller and Abe Padilla at Vanderbilt University allowed the use of their facilities for zircon separation between 2010 and 2013. Joe Wooden, Matt Coble, and Jorge Vazquez at the SUMAC SHRIMP facility are greatly appreciated for their time and assistance with that instrument, and reduction and interpretation of those data. Most importantly, the landowners of Butts, Henry, Jasper, and Newton Counties, Georgia, many of whom shared my enthusiasm for the geology of that area, deserve thanks for their hospitality and access to their property.

Funding for this research was provided by USGS EDMAP award GO9AC00126, in addition to the University of Tennessee Science Alliance Center of Excellence and the University of Tennessee Office of Research.

Last but certainly not least, I would like to thank my family, immediate and extended, for their love and support through these years in Tennessee. My success here would not have been possible without them.

Thank you.

ABSTRACT

Detailed geologic mapping, U-Pb geochronology, igneous petrology and whole-rock geochemical analysis, and structural analysis of the Inner Piedmont and Carolina superterrane were conducted to better define the tectonic history of the southern Appalachian orogen; results yield implications for Acadian/Neocadian and Alleghanian collisional events and Mesozoic breakup of Pangea. Detailed geologic mapping was focused in the Inner Piedmont at the northeastern end of the Pine Mountain window to investigate an aeromagnetic anomaly that was hypothesized to represent the southwestern continuation of the Brindle Creek fault, which separates the Inner Piedmont terranes (Tugaloo and Cat Square). Evidence supports this hypothesis, while contrasting detrital zircon and metamorphic ages provide insight regarding the paleogeographic position of the Cat Square terrane during deposition, and to processes related to mid-crustal flow in orogenic systems.

Two tectonic models that differ in timing, kinematics, and subduction polarity have been proposed to describe accretion of the Carolina superterrane. Geochronologic and geochemical analysis of mafic plutons better define their timing and petrogenetic origin; data are consistent with derivation in a subduction-zone setting. Emplacement predates main-phase Cat Square terrane plutonism, which is a product of east-dipping B-subduction beneath the Carolina superterrane followed by shutoff of arc-magmatism during A-subduction of the eastern Laurentian margin that resulted in metamorphism and anatectic plutonism in the eastern Inner Piedmont. A hybrid tectonic model synthesizes numerous data from the orogen.

The Towaliga fault contains tectonites that formed under various P-T conditions, revealing a complex reactivation history. Towaliga fault garnet-grade mylonite formed during large-displacement Alleghanian dextral strike-slip, while isolated, km-scale rhomboidal silicified cataclasite pods likely represent ancient dilational step-overs that formed in a small-displacement sinistral strike-slip system during the Mesozoic breakup of Pangea.

The Pine Mountain terrane has a polyphase allochthonous emplacement history that can be delimited by its bounding faults, regional fabric and crosscutting relationships. Palinspastic restoration indicates the Pine Mountain terrane may have originated near the Virginia promontory. The current configuration of the Pine Mountain terrane far outboard in the orogen, combined with its near-shore Neoproterozoic-Cambrian cover strata, suggest it may represent a peri-Laurentian microcontinent that rifted from the margin sometime in the Cambrian.

Table of Contents

Introduction.....	1
References Cited.....	4

CHAPTER I

Detailed geologic map of the Inner Piedmont and Carolina superterrane at the northeast end of the Pine Mountain window, Georgia.....	5
Abstract.....	6
Introduction.....	7
Geologic Setting.....	10
Lithologic Units of the Map Area.....	14
Tectonic Synthesis.....	41
Acknowledgments.....	43
References Cited.....	44

CHAPTER II

Confirmation of the southwest continuation of the Cat Square terrane, southern Appalachian Inner Piedmont, with implications for middle Paleozoic collisional orogenesis	53
Abstract.....	54
Introduction.....	55
Geologic Setting.....	59
Attributes of the Inner Piedmont – A Summary of Results from Two Islands of Detailed Geologic Mapping.....	63
Methodology.....	82
Results.....	84
Discussion.....	113
Conclusions.....	120
Acknowledgments.....	121
References Cited.....	122

CHAPTER III

The transition from B- to A-subduction during closure of the Rheic remnant ocean: Marking the Acadian/Neoacadian accretion of the Carolina superterrane, southern Appalachians	134
Abstract.	135
Introduction.	136
Geologic Setting	140
Methods.	149
Results.	150
Discussion.	161
Conclusions.	179
Acknowledgments.	180
References Cited.	181

CHAPTER IV

Polyphase reactivation history of the Towaliga fault, central Georgia: Implications regarding the amalgamation and breakup of Pangea	196
Abstract.	197
Introduction.	198
Geologic Setting	202
Brittle and Ductile Fault Rocks of the Towaliga fault zone	204
Isolated Pods of Siliceous Cataclasite as Dilational Step-overs.	208
Discussion.	210
Conclusions.	215
Acknowledgments.	215
References Cited.	216

CHAPTER V

A new perspective on the emplacement of the Pine Mountain terrane, southern Appalachians: Evidence from the northeastern end of the Pine Mountain window, Georgia	220
Abstract.	221
Introduction.	222
Geologic Setting	223

New Observations from Detailed Mapping at the Northeast End of the Pine Mountain window.	230
A Revised Tectonic History of the Pine Mountain terrane	235
Discussion.	245
Conclusions.	247
References Cited.	248
APPENDICES.	253
Appendix I	
Structural Measurements and Outcrop Descriptions from the Covington, Jackson, Lloyd Shoals Dam, Stewart, and Worthville 7.5-minute Quadrangles.	254
Appendix II	
SHRIMP U-Th-Pb data from analysis of igneous and metasedimentary rocks from the Inner Piedmont and Carolina superterrane	315
Appendix III	
SHRIMP U-Th-Pb data from analysis of Concord Plutonic Suite mafic plutons.	327
Appendix IV	
Compiled whole-rock geochemical data of granitoids from the Inner Piedmont.	332
Appendix V	
Whole-rock geochemical data of mafic plutons from the Concord Plutonic Suite.	343
Vita	345

List of Tables

CHAPTER II

Table 2-1: Geographic locations of samples collected for SHRIMP geochronologic analysis... 83

Table 2-2: New and compiled U-Pb ages of Inner Piedmont granitoids... 98

CHAPTER III

Table 3-1: Compiled U-Pb ages of Concord-Salisbury suite plutons ... 157

Table 3-2: Compiled U-Pb ages of Paleozoic plutonic rocks from the eastern Blue Ridge, Inner Piedmont, and Carolina superterrane. ... 168

List of Figures

CHAPTER I

Figure 1-1: Simplified lithotectonic map of the southern Appalachian internides	9
Figure 1-2: Metamorphic isograd map of the southern Appalachian orogen.	13
Figure 1-3: Characteristic lithologies of the Tugaloo terrane.	15
Figure 1-4: Dominant lithologic units of the Cat Square terrane.	18
Figure 1-5: Characteristic rocks of the Pine Mountain window.	22
Figure 1-6: Selected lithologies from the Carolina superterrane in the map area.	26
Figure 1-7: Mesozoic rocks	28
Figure 1-8: High-grade fault rocks	33
Figure 1-9: Ribbon quartz mylonite.	38
Figure 1-10: Crosscutting relationships of some of the dominant lithologies in the map area . .	40

CHAPTER II

Figure 2-1: Simplified lithotectonic map of the southern Appalachian internides	57
Figure 2-2: Geologic map of the Carolina portion of the Inner Piedmont.	61
Figure 2-3: Conceptual block diagram of the infrastructural Inner Piedmont and adjacent suprastructural Carolina superterrane	64
Figure 2-4: Compiled geologic map of the central Georgia portion of the Inner Piedmont . . .	65
Figure 2-5: Characteristic exposures of igneous rocks selected for geochronologic analysis. .	70
Figure 2-6: Simplified geologic map illustrating the type locality of the Snapping Shoals Augen Gneiss.	71
Figure 2-7: Mesoscale examples of spatial relationships between major lithologies in the central Georgia Inner Piedmont.	73
Figure 2-8: Simplified geologic map illustrating the type locality of the Indian Springs Granodiorite.	75
Figure 2-9: Metamorphic isograd map of the southern Appalachian orogen	79
Figure 2-10: Zircon U-Pb concordia diagrams for plutonic rocks analyzed in this study. . . .	86
Figure 2-11: Relative probability distributions with histograms of detrital zircon data	90
Figure 2-12: Th/U data from three samples of Indian Springs Granodiorite.	93
Figure 2-13: U-Pb data and zircons from the Gladesville gabbro contact aureole	96
Figure 2-14: Relative probability distributions of compiled metamorphic ages	99
Figure 2-15: Results of major element geochemical analysis	101
Figure 2-16: Multi-element variation diagrams of granitoids geochemical data.	102
Figure 2-17: Tectonic discrimination diagrams of granitoids	105
Figure 2-18: Compiled detrital zircon analyses from the Inner Piedmont.	111
Figure 2-19: Relative probability distributions with histograms of pooled U-Pb zircon analyses from Inner Piedmont igneous rocks.	112
Figure 2-20: Tectonic model illustrating the evolution of the Cat Square terrane.	115
Figure 2-21: Estimated displacement of the Cat Square terrane	117

CHAPTER III

Figure 3-1: Simplified lithotectonic map of the southern Appalachian Inner Piedmont and adjacent Carolina superterrane with sample locations of Concord Plutonic Suite gabbros analyzed in this study.	138
Figure 3-2: Metamorphic isograd map of the southern Appalachian orogen	144
Figure 3-3: Cathodoluminescence images of representative zircons with U-Pb concordia diagrams from plutonic rocks	151
Figure 3-4: Geochemical classifications of plutonic rocks	158
Figure 3-5: Bivariate plots of major oxides versus MgO	159
Figure 3-6: Normalized trace element and REE spider diagrams	160
Figure 3-7: Ti-Zr-Y discrimination diagrams.	162
Figure 3-8: Zr-Y discrimination diagram.	163
Figure 3-9: Th-Hf-Ta and La-Y-Nb discrimination diagrams	163
Figure 3-10: Relative probability distributions of pooled U-Pb ion microprobe ages of zircon from the Inner Piedmont and Concord Plutonic suite gabbros	165
Figure 3-11: Compiled age chart of plutonic rocks, metamorphism, and cooling events in the eastern Blue Ridge, Inner Piedmont, and Carolina superterrane, with ages of ash beds in the Appalachian foreland basin	167
Figure 3-12: Spatial distribution of Devonian siliciclastics.	170
Figure 3-13: Sequential tectonic evolution of the accretion of the Carolina superterrane	174

CHAPTER IV

Figure 4-1: Idealized fault-fracture mesh	198
Figure 4-2: Simplified tectonic map showing the geographic extent of the Towaliga fault. . . .	199
Figure 4-3: Simplified geologic map of the study area	200
Figure 4-4: Crosscutting relationships between silicified faults and CAMP diabase dikes. . . .	201
Figure 4-5: Distribution of CAMP diabase dikes and silicified cataclasites of the southern Appalachian orogen	203
Figure 4-6: Brittle fault rocks from rhomboidal pods along the Towaliga fault	205
Figure 4-7: Hand specimen and photomicrographs of ribbon quartz mylonite.	206
Figure 4-8: Block diagram illustrating dilational step-over at Barnes Mountain	208
Figure 4-9: Photomicrographs and hand specimen of a hydrothermally altered Inner Piedmont granitoid adjacent to a dilational step-over	209
Figure 4-10: Temperature-time curves demonstrating the evolution of the Towaliga fault . . .	212

CHAPTER V

Figure 5-1: Simplified lithotectonic map of the southern Appalachian orogen.	224
Figure 5-2: Thickness variation of Neoproterozoic-Cambrian rifted- to passive-margin strata along the eastern Laurentian margin	225
Figure 5-3: Simplified geologic map of the Pine Mountain window and Inner Piedmont at its northeastern terminus.	227

Figure 5-4: Cross section and block diagram through the Carolina superterrane, Pine Mountain terrane, and Inner Piedmont at the northeastern end of the Pine Mountain window	229
Figure 5-5: Hand specimen, outcrop, and photomicrographs of Box Ankle and Towaliga fault mylonites	232
Figure 5-6: Inner Piedmont fabric and granitoid relationships	236
Figure 5-7: Tectonic history of the allochthonous Pine Mountain terrane	240
Figure 5-8: Schematic block diagram illustrating the relationship between the Box Ankle and Brindle Creek-Jackson Lake faults	246

List of Plates

- Plate I:** Detailed geologic map of the Stewart, Lloyd Shoals Dam, and portions of the Jackson and Worthville 7.5-minute quadrangles, Georgia MTH_Plate_I.pdf
- Plate II:** Station geologic map of the Stewart, Lloyd Shoals Dam, Jackson, and Worthville 7.5-minute quadrangles, Georgia MTH_Plate_II.pdf
- Plate III:** Detailed geologic map of the Inner Piedmont at the northeast end of the Pine Mountain window, Georgia MTH_Plate_III.pdf

Introduction

Terrane analysis has proven useful in delineating the accretionary history of cratonic margins through time, and has been applied to numerous orogens throughout the world (e.g., Coney et al., 1980; Williams and Hatcher, 1982; Ramos et al., 1986; DeCelles et al., 2000). A lithotectonic terrane is a discrete, fault-bounded, allochthonous fragment of oceanic or continental material with a distinct tectonic (magmatic, depositional, etc.) history relative to adjacent terranes, ultimately accreted to a craton at an active plate margin. Because of the internal homogeneity and regional context of lithotectonic terranes, the application of terrane analysis to orogenic belts worldwide, specifically the relationships between terranes, has yielded vital clues regarding tectonic accretionary history along cratonic margins. The primary goal of this dissertation research was to test the hypothesis that the Cat Square terrane, initially identified in western North Carolina, continues through central Georgia. Terrane analysis is an underlying theme through most of the chapters presented herein, further stressing its importance to the study of orogenic belts. Research presented in this dissertation is original, and my contributions to all included chapters are indicated at the beginning of each chapter.

This dissertation consists of five chapters, each an independent manuscript that has been or will be submitted to peer-reviewed media. Research was conducted from 2007-2013 and incorporates detailed geologic mapping, structural analysis, U-Pb SHRIMP geochronology, igneous and metamorphic petrology, geochemistry, and regional correlations between foreland deposition and tectonothermal metamorphism in the crystalline interior of the southern Appalachians. The foundation of this research, however, is unquestionably the detailed geologic mapping that was conducted over three field seasons, and is compiled as a 1:24,000 scale geologic map (Plate I). Accompanying structural and lithologic data are presented in Appendix I, with station locations illustrated in Plate II.

This dissertation can be separated into three basic sections. The first section, Chapters I – II, involves a comprehensive 1:50,000 scale compiled geologic map (Plate III) and subsequent structural, geochronologic, and geochemical work in the area. Chapter I has been submitted to the Geological Society of America Maps and Charts Series for publication, and is still in review at the time of the compilation of this dissertation. Chapter II discusses the hypothesis that the Cat Square terrane continues through central Georgia, which was the core motivation for geologic study in this region, and synthesizes numerous data from the southern Appalachian Inner Piedmont as a test of this hypothesis, in addition to better defining middle Paleozoic collisional orogenesis along the eastern Laurentian margin. This manuscript has been submitted to the *American Journal of Science*, and is currently in review.

The second section, which consists solely of Chapter III, discusses geochemical and geochronologic data that were gathered from mafic plutons along the western flank of the peri-Gondwanan Carolina superterrane. The underlying motivation for this chapter was to better understand

the nature of the accretion of the Carolina superterrane; its timing, kinematics, and subduction polarity have been the subject of debate for well over a decade (e.g., Hibbard, 2000; Merschat et al., 2005; Merschat and Hatcher, 2007; Hibbard et al., 2012). This manuscript synthesizes new data with existing structural, geochronologic, and geochemical data, and the distribution of metamorphism in the interior of the southern Appalachians, in addition to diachronous clastic deposition in the central to southern Appalachian foreland basin and spatial attributes of Ordovician through Devonian ash beds, to construct a viable tectonic model that incorporates data used to support both competing hypotheses. This paper will likely be submitted to the *Geological Society of America Bulletin* in late 2013.

The third section, Chapters IV and V, examines the polyphase history of the Towaliga fault in central Georgia (Chapter IV) and offers a new perspective on the tectonic evolution of the Pine Mountain window based on our findings from recent detailed geologic mapping, geochronologic, and structural analyses (Chapter V). Chapter IV was published in 2013 by the *Journal of Geology*, and resolved conflicting kinematic and temporal interpretations of the Towaliga fault, which involves a garnet-grade dextral Alleghanian phase that was sinistrally reactivated under brittle conditions at ~200 Ma. Chapter V presents a new hypothesis regarding the allochthonous history of the Pine Mountain terrane, which is dictated by temporal and fabric relationships between it and the Inner Piedmont, along with the timing and kinematics of its bounding faults, and restoration of major southern Appalachian fault zones. It is anticipated that this manuscript, coauthored by Justin R. Rehrer and Dr. Robert D. Hatcher, Jr., will be submitted to a peer-reviewed journal for publication in late 2013 or early 2014.

Plates included are: 1) detailed geologic map of portions of the Jackson, Lloyd Shoals Dam, Stewart, and Worthville, 7.5-minute quadrangles, Georgia; 2) accompanying station map of the Jackson, Lloyd Shoals Dam, Stewart, and Worthville quadrangles; and 3) compiled geologic map of the Inner Piedmont and Carolina superterrane at the northeast end of the Pine Mountain window, Georgia. Appendix I contains the structural data and rock descriptions that accompanies Plates I and II. Appendix II contains U-Pb SHRIMP spot analyses of zircons that accompany Chapters II and III, and Appendix III contains whole-rock geochemical data from Chapters II and III.

REFERENCES CITED

- Coney, P. J., Jones, D. L., and Monger, J. W. H., 1980, Cordilleran suspect terranes: *Nature*, v. 288, p. 329-333.
- DeCelles, P. G., Gehrels, G. E., Quade, J., LaReau, B., and Spurlin, M., 2000, Tectonic implications of U-Pb zircon ages of the Himalayan orogenic belt in Nepal: *Science*, v. 288, p. 497-499.
- Hibbard, J. P., 2000, Docking Carolina: *Geology*, v. 28, p. 127-130.
- Hibbard, J. P., Miller, B. V., Hames, W. E., Standard, I. D., Allen, J. S., Lavallee, S. B., and Bolland, I. B., 2012, Kinematics, U-Pb geochronology, and $^{40}\text{Ar}/^{39}\text{Ar}$ thermochronology of the Gold Hill shear zone, North Carolina: The Cherokee orogeny in Carolina, southern Appalachians: *Geological Society of America Bulletin*, v. 124, p. 643-656.
- Merschat, A. J., and Hatcher, R. D., Jr., 2007, The Cat Square terrane: Possible Siluro-Devonian remnant ocean basin in the Inner Piedmont, southern Appalachians, USA, in Hatcher, R. D., Jr., Carlson, M. P., McBride, J. H., and Martínez Catalán, J. R., editors, 4-D Framework of Continental Crust: Boulder, Colorado, Geological Society of America Memoir 197, p. 553-565.
- Merschat, A. J., Hatcher, R. D., Jr., and Davis, T. L., 2005, The northern Inner Piedmont, southern Appalachians, USA: Kinematics of transpression and SW-directed mid-crustal flow: *Journal of Structural Geology*, v. 27, p. 1252-1281.
- Ramos, V. A., Jordan, T. E., Allmendinger, R. W., Mpodozis, C., Kay, S. M., Cortés, J. M., and Palma, M., 1986, Paleozoic terranes of the central Argentine-Chilean Andes: *Tectonics*, v. 5, p. 855-880.
- Williams, H., and Hatcher, R. D., Jr., 1982, Suspect terranes and accretionary history of the Appalachian orogen: *Geology*, v. 10, p. 530-536.

Chapter I

Detailed geologic map of the Inner Piedmont and Carolina superterrane at the northeast end of the Pine Mountain window, Georgia

This chapter, which accompanies Plate III, has been submitted to the *Geological Society of America Maps and Charts Series* for publication. Coauthors of this manuscript include Justin R. Rehner, Robert D. Hatcher, Jr., and Andrew L. Wunderlich. My contributions to this manuscript include the majority of the writing, data collection, and compilation of the map. The use of the term “we” and “our” in the text refers to the coauthors and myself.

ABSTRACT

The accompanying geologic map is a 1:50,000-scale compilation of several 1:12,000 and 1:24,000-scale detailed mapping projects centered at the northeast end of the Pine Mountain window in central Georgia. This map includes parts of several lithotectonic terranes, including the Tugaloo and Cat Square terranes of the Inner Piedmont, the Pine Mountain window (and terrane), and the western flank of the exotic Carolina superterrane (Charlotte terrane?). Rocks through the map area have been metamorphosed under sillimanite-grade conditions during the Acadian/Neocadian orogeny, although metasedimentary cover rocks in the interior of the Pine Mountain window decrease to kyanite-grade southwest of the map area. In this region, the Tugaloo terrane (western Inner Piedmont) consists of amphibolite-rich metagraywacke and schist of the lower member of the Tallulah Falls Formation, which also includes thin, laterally extensive gondite beds. Tallulah Falls Formation rocks are intruded by the Ordovician-Silurian Lithonia Gneiss, a medium- to coarse-grained granitic gneiss that is strongly foliated and polydeformed. Both metasedimentary rocks and the Lithonia Gneiss were deformed coevally, and are truncated by the Jackson Lake fault, which separates the Tugaloo terrane from the Cat Square terrane through central Georgia. This terrane boundary is equivalent to the Brindle Creek fault recognized in the western Carolinas, although there it occurs as a gently east and southeast dipping southwest-directed thrust fault. In contrast, the Jackson Lake fault is a steeply to moderately northwest-dipping strike-slip fault. Cat Square terrane rocks consist of massive metagraywacke and sillimanite schist units intruded by the Devonian High Falls Granite, which comprises the majority of the Lloyd Shoals plutonic complex that occurs in the map area. The High Falls Granite is a medium- to coarse-grained biotite granite characterized by 1-10 cm euhedral microcline megacrysts, and is commonly strongly foliated. Foliation in the High Falls Granite is concordant with the dominant sillimanite-grade regional foliation (S_2), which coincides with peak metamorphic conditions. The High Falls Granite is the youngest granitoid crosscut by the Jackson Lake fault, which provides a maximum limit regarding the timing of deformation along the fault. Several Alleghanian granitoids also occur in the Lloyd Shoals plutonic complex, the most abundant being the Indian Springs and Dows Pulpit Granodiorites. These granitoids most commonly truncate S_2 , confirming that development of regionally penetrative peak-metamorphic fabric predated the Alleghanian orogeny. Small bodies of Indian Springs Granodiorite occur in the Tugaloo

terrane, and one body appears to crosscut the Jackson Lake fault, which indicates the Tugaloo and Cat Square terranes had been juxtaposed prior to the Alleghanian orogeny, and also provides a minimum age for the Jackson Lake fault. Alleghanian granitoids are truncated by the Towaliga fault, which separates the Inner Piedmont from the Pine Mountain window (continuing northeast through the Inner Piedmont), and contains a localized lower amphibolite-facies mylonite along the fault trace. The Pine Mountain window consists of massive Grenville basement gneisses that are overlain by Neoproterozoic-Cambrian(?) quartzite and schist of the Pine Mountain cover sequence. The Towaliga fault truncates the Jackson Lake fault, and also truncates the Box Ankle fault, an upper amphibolite-facies, north- to northwest-directed thrust fault that juxtaposes Cat Square terrane rocks above the Pine Mountain window. The Box Ankle fault is folded axial planar to S_2 , which also indicates movement along the fault predates the Alleghanian orogeny. The Inner Piedmont is separated from layered metavolcanic and mafic and felsic plutonic rocks of the Carolina superterrane by the Ocmulgee fault and Rumble shear zone. Fabric relationships also indicate these faults may be Acadian/Neoacadian features. Several small-scale lower greenschist-facies mylonite zones that are localized in quartz veins under lower greenschist-facies conditions have been identified, and may represent either late-stage Alleghanian deformation or deformation associated with the early stages of Mesozoic rifting. These shear zones appear to be spatially related to brittle silicified faults, and are everywhere overprinted by brittle deformation. Silicified faults share mutually overprinting crosscutting relationships with diabase dikes, which intruded ~200 Ma during the final stages of Pangea breakup.

INTRODUCTION

The enclosed 1:50,000-scale geologic map is a compilation of several detailed mapping projects that were completed at 1:12,000 and 1:24,000-scale at the northeast end of the Pine Mountain window (Hooper, 1986; Sneyd, 1995; Davis, 2010; Howard, 2012; M.T. Huebner, in progress; J.R. Rehrer, in progress; R.D. Hatcher, Jr., unpublished data; R. Kath, unpublished data). The map area is centered at arguably one of the most interesting locations in the southern Appalachian orogen; it includes several major tectonic boundaries that record the amalgamation of the exotic Carolina superterrane to Laurentia, deformation and juxtaposition of Laurentian terranes during middle- and late Paleozoic collisional orogenesis, and eventual brittle deformation and mafic magmatism associated with the Mesozoic breakup of Pangea. The spatial and temporal relationships between these terranes, in addition to the nature of their bounding faults, are paramount to understanding the Paleozoic evolution of the southern Appalachian orogen. The Inner Piedmont portion, however, is the focus of the recent mapping projects and this report.

The southern Appalachian Inner Piedmont extends ~700 km along orogenic strike from Winston-Salem, North Carolina, to beneath the Coastal Plain in Alabama (Fig. 1-1). It is bound to the northwest by the Brevard fault zone and to the southeast by the Central Piedmont suture. The Inner Piedmont has long been recognized for its high metamorphic grade, near wholesale migmatization, and contrasting structural style with adjacent terranes (e.g., King, 1955; Bentley and Neathery, 1970; Merschhat et al., 2005); however, rocks west of the Brevard fault (eastern Blue Ridge) cannot be separated stratigraphically from the rocks in the western Inner Piedmont, signifying that the Brevard fault zone is not a suture (e.g., Bream et al., 2001; Hatcher et al., 2007). The Inner Piedmont comprises two distinct lithotectonic terranes (Tugaloo [west] and Cat Square [east]) separated by the Brindle Creek fault, which juxtaposes the Cat Square terrane above the Tugaloo terrane.

Division of the Inner Piedmont into two discrete lithotectonic terranes was primarily the result of detrital zircon geochronology that followed numerous detailed geologic mapping projects in the North Carolina Inner Piedmont (e.g., Giorgis, 1999; Williams, 2000; Bier, 2001; Kalbas, 2002; Bream, 2003; Merschhat, 2003; Wilson, 2006; Gatewood, 2007; Byars, 2010; Gilliam, 2010). In addition to subtle lithologic distinctions, metasedimentary rocks west of the Brindle Creek fault (Tugaloo terrane) exhibit an overwhelming Grenville (Laurentian) source, while metasedimentary rocks east of the fault include detrital zircons signifying both Laurentian and peri-Gondwanan sources, along with a prominent Ordovician-Silurian suite through the Carolinas (e.g., Bream, 2003; Merschhat et al., 2010). Additional distinguishing criteria include: 1) partitioning of granitoid ages: the Tugaloo terrane was intruded by a suite of Late Ordovician-Early Silurian granitic plutons, while the Cat Square terrane includes only Devonian-Mississippian granitoids; and 2) fragments of continental Grenville basement gneisses have been identified in the Tugaloo terrane, while none have been identified (to date) in the Cat Square terrane.

While this boundary is well defined in the northern portion of the Inner Piedmont, its southwest extent has only previously been correlated with a conspicuous aeromagnetic lineament that crosses through central Georgia (Hatcher et al., 2007). The goal of recent mapping projects was to ascertain the nature of the Inner Piedmont in the vicinity of this aeromagnetic lineament, and to test the hypothesis that this lineament represents the southwest equivalent of the Brindle Creek fault. Detailed geologic mapping has revealed a high-grade ductile fault, the Jackson Lake fault, that separates distinct suites of metasedimentary and igneous rocks, and spatially corresponds with the prominent aeromagnetic lineament. Subsequent geochemical and geochronologic analyses have also been incorporated to test the hypothesis that this fault is the Brindle Creek fault equivalent; at present, results support this proposition (e.g., Huebner et al., 2010; *in review*).

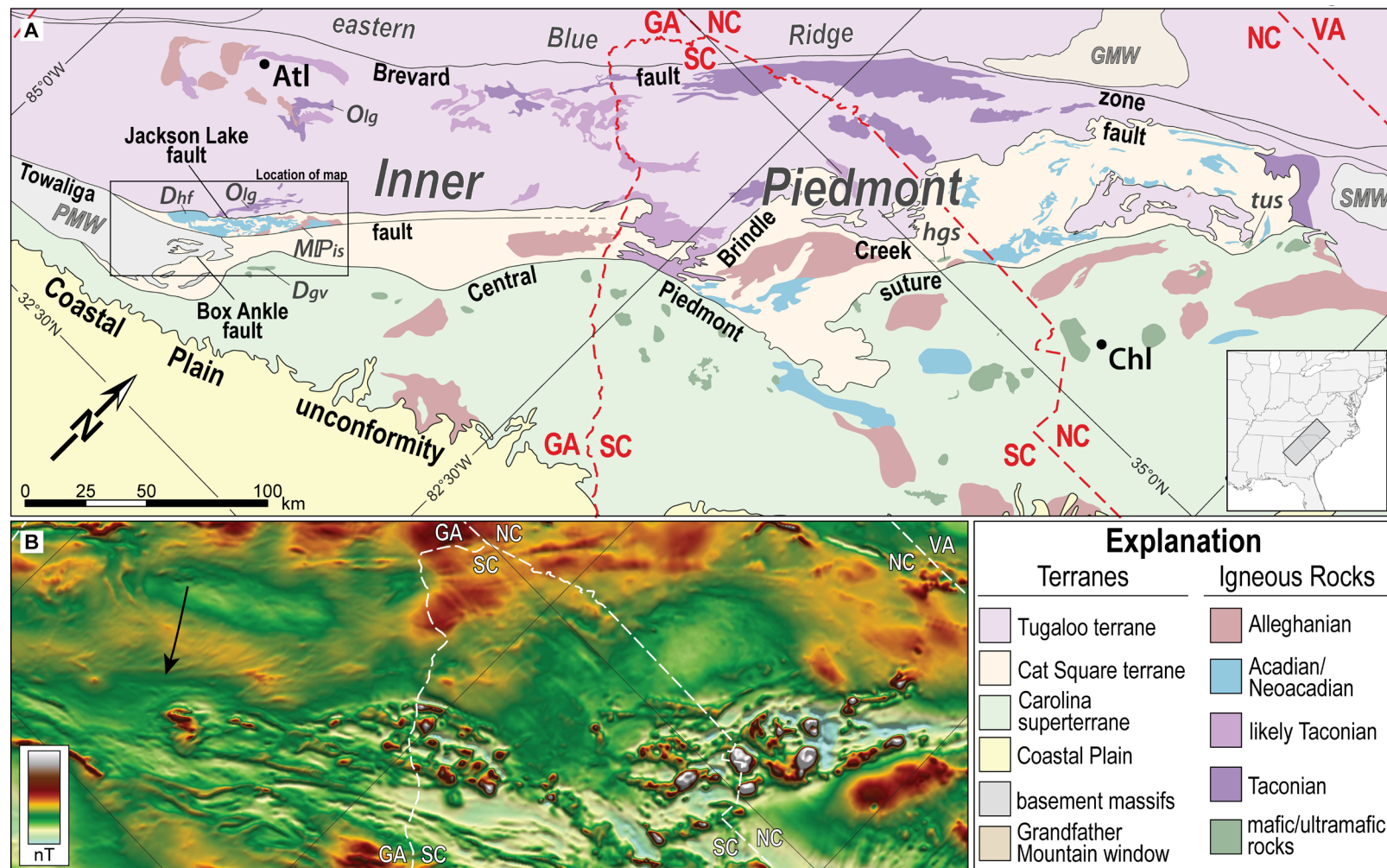


Figure 1-1: (A) Simplified lithotectonic map of the southern Appalachian internides (after Hatcher et al., 2007; Huebner et al., *in review*), with inset showing geographic location of map area. (B) Aeromagnetic map of the same extent, with black arrow pointing to the strong lineament interpreted to represent the southwest continuation of the Brindle Creek fault. Atl = Atlanta; Chl = Charlotte; Dgv = Gladesville Gabbro; Dhf = High Falls Granite; MIPis = Indian Springs Granodiorite; Olg = Lithonia Gneiss; hgs = Hammett Grove Metaigneous Suite; tus = Turnersburg Ultramafic Suite; GMW = Grandfather Mountain window; PMW = Pine Mountain window; SMW = Sauratown Mountains window.

GEOLOGIC SETTING

The dominant assemblage of metasedimentary rocks in the Tugaloo terrane (western Inner Piedmont) consists of the Tallulah Falls Formation, which contains Neoproterozoic–Cambrian(?) deep-water, siliciclastic and volcanic rocks (now biotite paragneiss, aluminous schist, and amphibolite) that have been metamorphosed under middle- and upper amphibolite facies conditions. Hatcher (1971) defined the Tallulah Falls Formation from exposures surrounding the Tallulah Falls dome in northeastern Georgia. The Tallulah Falls Formation is equivalent to the Ashe Formation (Rankin, 1970) and Lynchburg Formation (Stose and Stose, 1957) through the Blue Ridge of North Carolina and Virginia. To the south, the Tallulah Falls Formation can be correlated with Ashland supergroup (e.g., Adams, 1926; Tull, 1978), or the Zebulon Formation of Sears et al. (1981) and Higgins et al. (1988). Detrital zircon analyses indicate sediment was derived solely from Grenville source material (e.g., Bream, 2003; Merschat et al., 2010; Huebner et al., *in review*).

The Tallulah Falls Formation comprises a three-part stratigraphy, which includes a lower amphibolite-rich metagraywacke sequence and an amphibolite-poor upper metagraywacke unit, separated by a conspicuous aluminous schist member (e.g., Hatcher, 1993). In northeast Georgia and the Carolinas, these rocks are overlain by Cambrian(?) metasiltstone, quartzite, graphitic schist, and impure marble of the Chauga River Formation, which are unconformably overlain by Middle Ordovician Poor Mountain Formation metavolcanic and metasedimentary rocks (Hatcher, 1993; Bream, 1999). While Tallulah Falls Formation stratigraphy can be correlated across the Brevard fault zone, the Chauga River and Poor Mountain Formations are not known in the eastern Blue Ridge.

The Tugaloo terrane was intruded by mostly Ordovician-Silurian (470–445 Ma) peraluminous granites to granodiorites, which include several large plutons (e.g., Henderson Gneiss, Caesar’s Head). Minor Devonian granitic plutonism occurs west of the Brevard fault (Pink Beds and Looking Glass; Miller et al., 2000), and several Carboniferous plutons intruded the central Georgia Inner Piedmont (e.g., Stone Mountain, Panola; Mueller et al., 2011). Additional granitic rocks that occur in the Tugaloo terrane include several small fragments of continental Grenville basement (Heyn, 1984; McConnell, 1989; Merschat, 2003; Byars, 2010; Huebner et al., 2010); to date, no continental basement rocks have been identified in the Cat Square terrane.

Cat Square terrane metasedimentary rocks consist of massive biotite paragneiss and aluminous schist, with minor amounts of interlayered metabasalt and calc-silicate. In contrast to the Tugaloo terrane, no recognizable stratigraphy has been delineated. Detrital zircon signatures from Cat Square terrane metasedimentary rocks exhibit a relatively muted Grenvillian component, with additional peri-Gondwanan (600–500 Ma) zircons and a dominant Ordovician-Silurian

signature that is likely Laurentian-derived (Bream, 2003; Merschhat et al., 2010; Sinha et al., 2012). The most likely source of the 600–500 Ma detrital zircons is the adjacent Carolina superterrane, with detritus that was probably shed as the exotic microcontinent approached the eastern Laurentian margin (Bream, 2003; Merschhat et al., 2005). The presence of Ordovician-Silurian detrital zircons signifies the relative youth of Cat Square terrane rocks, and indicates depositional age was likely Silurian-Devonian (e.g., Bream et al., 2004). The oldest granitoid in the Cat Square terrane (Anderson's Mill, ~415 Ma; Mapes, 2002) therefore punctuates closure of the basin, revealing the short-lived nature of this transient depositional environment.

The Cat Square terrane contains Late Silurian through early Mississippian (415-355 Ma) granitoid plutons that appear to be dominantly anatectic (Mapes, 2002; Merschhat, 2009). The most abundant granitoids are the Toluca (~383 Ma; Mapes, 2002), Walker Top (407-357 Ma; Mapes, 2002; Gatewood, 2007; Byars, 2010), Cherryville (~355 Ma; Mapes, 2002), and High Falls (407-371 Ma; Huebner et al., *in review*). Several smaller Devonian granitic bodies have been identified through the Carolinas, and Pennsylvanian-Permian granitoids appear to be more abundant in the southwestern portion of the Cat Square terrane (e.g., Reedy River, Elberton, Indian Springs).

Detailed geologic mapping in central Georgia revealed a batholith-scale body of lithologically distinct granitoids in the Cat Square terrane, here termed the Lloyd Shoals Plutonic Complex. Felsic intrusives in the complex include the Devonian High Falls Granite, and Pennsylvanian-Permian Murder Creek granite, and Dows Pulpit and Indian Springs granodiorites. Although the rocks are different ages, their spatial relation is a function of their intrusive history. The Lloyd Shoals plutonic complex includes lithologies similar to the Cedar Rock Complex proposed by Atkins and Lineback (1992); however, those authors included the Odessadale gneiss (Lithonia equivalent) as part of the complex, which is spatially related to the complex by fault contact, not by intrusive history. We do not include the Lithonia Gneiss (Tugaloo terrane) as part of the proposed Lloyd Shoals Plutonic Complex.

Throughout the Carolinas, rare ultramafic and mafic rocks have been identified in the Cat Square terrane (Privett, 1984; Mittwede et al., 1987; Goldsmith et al., 1988; Giorgis, 1999; Merschhat et al., 2008). Several small bodies of altered ultramafic rocks (talc-chlorite schist) occur near the Brindle Creek fault in the South Mountains, North Carolina (Giorgis, 1999), while the largest bodies of ultramafic and mafic rocks, the Turnersburg ultramafic suite and the Hammett Grove meta-igneous suite, occur in the eastern part of the Cat Square terrane near the central Piedmont suture (Privett, 1984; Mittwede et al., 1987; Goldsmith et al., 1988). The Hammett Grove meta-igneous suite consists of serpentinized ultramafic rocks, metapyroxenite, metagabbro, amphibolite, and metachert, and may represent a dismembered ophiolite (Mittwede et al.,

1987; Mittwede, 1989). Bulk-rock geochemistry and $\delta^{18}\text{O}$ and δD isotopic data also support this interpretation (Mittwede, 1989; Chaumba, 2010a).

Based on the presence of mafic and ultramafic bodies, absence of continental basement rocks, and the mixed detrital zircon signature indicating Laurentian and peri-Gondwanan provenance, Mersch and Hatcher (2007) suggested the Cat Square terrane metasedimentary rocks were deposited on ocean crust in a remnant ocean basin that formed during diachronous accretion of the Carolina superterrane. Numerous geochronologic data indicate the entire Inner Piedmont reached peak metamorphic conditions from Devonian through Mississippian times (Mersch, 2009), which several workers attribute to subduction of the Inner Piedmont beneath the Carolina superterrane during its accretion in the Acadian/Neocadian orogeny (e.g., Mersch et al., 2005; Hatcher et al., 2007; Huebner et al., *in review*). Regional structural patterns indicate the Inner Piedmont was extruded to the southwest as a mid-crustal orogenic channel, buttressed against the Brevard fault zone, as the Carolina superterrane overrode the eastern Laurentian margin (e.g., Mersch et al., 2005; Hatcher and Mersch, 2006).

This model recalls Griffin's (1971, 1978) stockwork (suprastructure/infrastructure) model that depicts the migmatitic infrastructural Inner Piedmont overridden by the suprastructural Carolina superterrane, which was originally based on the fold-nappe structural style of the Inner Piedmont and distribution of metamorphic mineral assemblages through the Inner Piedmont and adjacent Carolina superterrane. Metamorphic isograd maps of the Inner Piedmont reveal a core of pervasively migmatitic sillimanite-grade rocks through the central Inner Piedmont, flanked by lower-grade rocks at its boundaries (Fig. 1-2). Metamorphic grade decreases to kyanite + staurolite, kyanite, and garnet grade in the western Inner Piedmont (Chauga belt), and kyanite, staurolite, and garnet grade in the eastern Inner Piedmont (Fig. 1-2). Several studies indicate the high-grade core of the Inner Piedmont reached peak conditions of 750-850°C at pressures of 500-800 MPa (Mirante and Patiño-Douce, 2000; Bier et al., 2002; Mersch, 2003), signifying metamorphism reached sillimanite I, sillimanite II, and possibly hornblende-granulite-facies conditions. Assuming moderate geothermal and geobarometric gradients, metamorphic conditions in the Inner Piedmont require burial depths of 15-20 km (Mersch and Hatcher, 2007).

Barrovian-style prograde metamorphism through the Inner Piedmont occurred during the Devonian-Mississippian Acadian/Neocadian and Pennsylvanian-Permian Alleghanian orogenies. U-Pb geochronology (monazite and zircon rims) from the Inner Piedmont across the Carolinas and northern Georgia reveals peak metamorphism occurred ~345 Ma, with apparent pulses of metamorphism at ~400, ~375, and 330-320 Ma (Dennis and Wright, 1997; Bream, 2003; Mersch, 2009). Ion-microprobe analyses of metamorphic zircon rims from central Georgia samples reveal peaks at ~380 and ~320 Ma, with a relative lull in metamorphic zircon growth at ~345 Ma (Huebner et al., *in review*). These data indicate the Inner Piedmont underwent peak metamor-

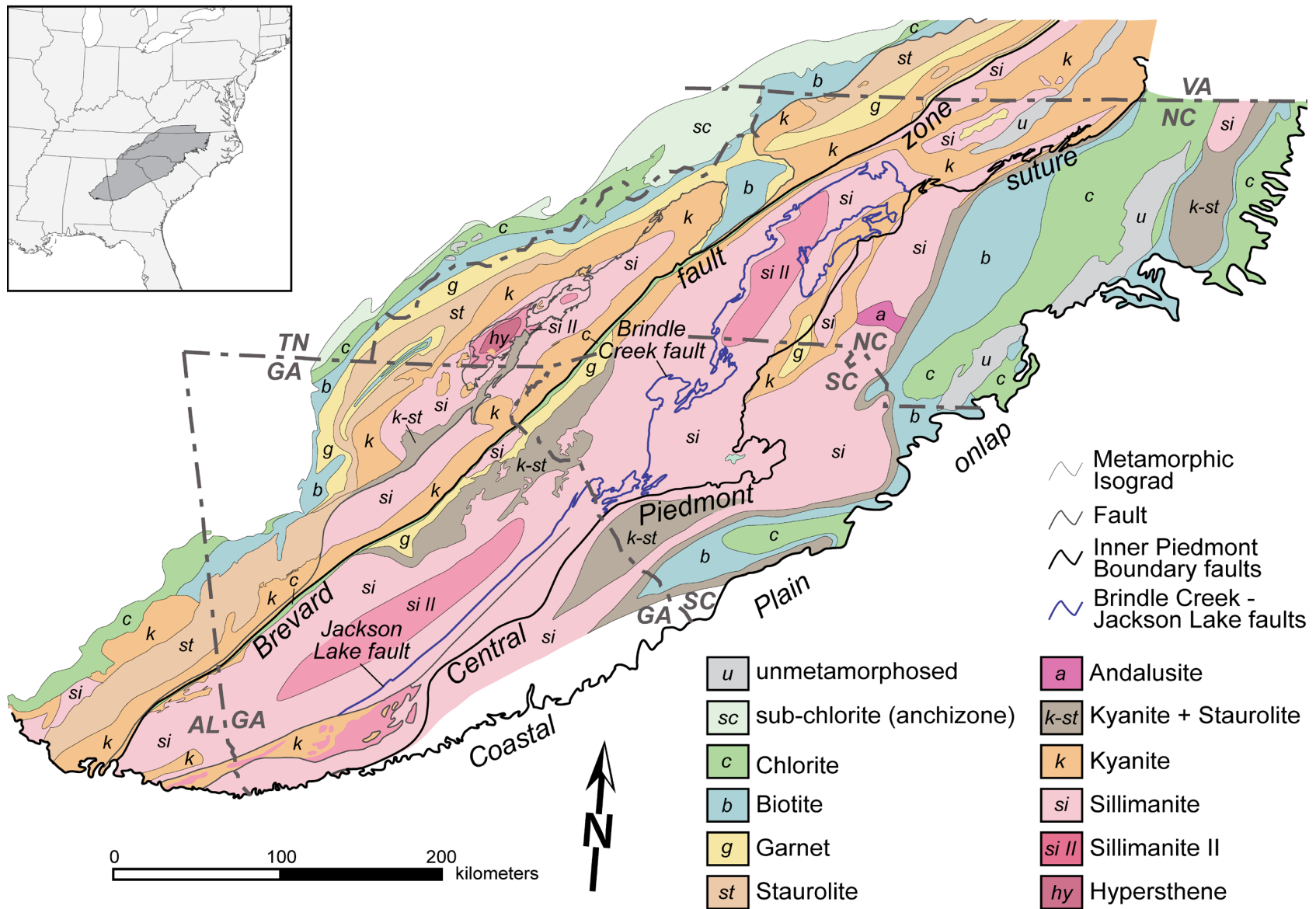


Figure 1-2: Metamorphic isograd map of the southern Appalachian orogen (modified from Mersch, 2009; Hatcher, 2004, and references therein; Huebner et al., *in review*).

phism 405-360 Ma, remained hot until ~345 Ma, cooled, and was again subjected to a thermal increase peaking 330-300 Ma (Dennis and Wright, 1997; Mersch, 2009; Huebner et al., *in review*). However, the Carolina portion of the Inner Piedmont remained at relatively high grade through the entire Devonian into the Mississippian, while the central Georgia portion peaked relatively quickly by ~380 Ma, then remained comparatively cool until the Alleghanian orogeny.

$^{40}\text{Ar}/^{39}\text{Ar}$ release spectra of biotite, muscovite, and hornblende from the Georgia Inner Piedmont and portions of the Carolina superterrane indicate cooling from a thermal event that occurred 360-350 Ma (Dallmeyer, 1978; Secor et al., 1986; Dallmeyer, 1989). Cooling ages from the Gold Hill fault zone indicate portions of the Carolina superterrane cooled from a thermal peak ~375 Ma (Hibbard et al., 2012), which coincides with prograde upper-amphibolite facies metamorphism in the Inner Piedmont. This also supports the hypothesis that the suprastructural Carolina superterrane overrode the infrastructural Inner Piedmont through the Devonian and Mississippian.

LITHOLOGIC UNITS OF THE MAP AREA

Lithologic descriptions of units from the central Georgia map area have been separated based on apparent terrane affinity. Exposed lithotectonic terranes include the Inner Piedmont terranes (Tugaloo and Cat Square), exotic Carolina superterrane, and Pine Mountain window, an allochthonous block of Grenvillian continental basement and associated Paleozoic(?) cover sequence. The Indian Springs Granodiorite occurs in both Inner Piedmont terranes, and is described separately.

Tugaloo terrane

Lower(?) Tallulah Falls Formation

The lower Tallulah Falls Formation consists of predominantly metagraywacke with locally abundant, discontinuous layers or boudins of amphibolite (Fig. 1-3). Metagraywacke is generally medium-fine to coarse-grained, thickly layered, and strongly foliated. Metagraywacke is light to dark gray in fresh exposures, while saprolite ranges from light to deep reddish-orange to dark brown. Thin, discontinuous layers of muscovite-biotite \pm sillimanite schist are common. Typical mineral assemblages of the metagraywacke include (decreasing order of abundance) quartz, biotite, alkali feldspar and plagioclase (An_{24-32}), locally with garnet, muscovite, and sillimanite. Accessory phases include sphene, epidote, apatite, zircon, and Fe oxides. Migmatization appears to increase with proximity to the Jackson Lake fault. Detrital zircon analysis of one sample yielded a Gaussian curve centered ~1.1 Ga, indicating Grenville (Laurentian) provenance (Huebner et al., 2010).

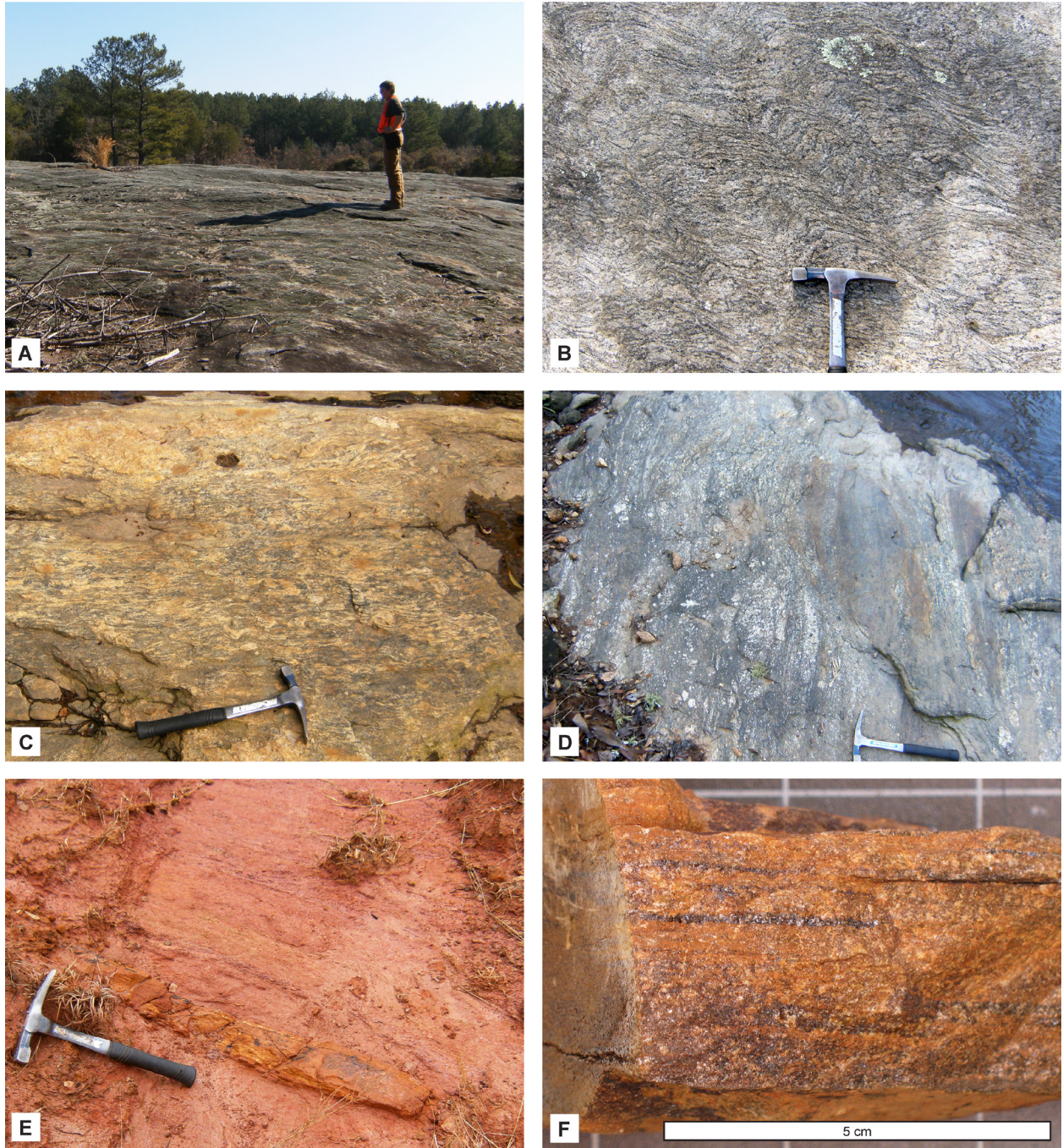


Figure 1-3: Characteristic lithologies of the Tugaloo terrane throughout the map area. (A) and (B) Lithonia Gneiss. C.W. Howard (~1.9 m tall) for scale in (A), view to the east. (B) Folia-
tion (S_2) deformed by northwest-vergent F_3 folds. (C) Snapping Shoals Augen Gneiss, view to
the northeast. (D) and (E) Lower Tallulah Falls migmatitic metagraywacke with amphibolite
boudins. (F) Hand sample of gondite.

Amphibolite boudins vary in length from 10 cm to 2 m, and are readily found as float due to resistance to chemical weathering relative to the enclosing metasedimentary rocks. Amphibolite is strongly foliated and locally preserves an early foliation although, in most occurrences, foliation parallels the surrounding biotite gneiss. Amphibolite is commonly fine- to medium-grained, composed of hornblende, plagioclase (An_{36-52}), and quartz, locally with garnet, biotite, and epidote. Amphibolite is easily identified in saprolite exposures by its characteristic orange-ochre color.

Several (one?) layers of gondite have been mapped just northwest of the Jackson Lake fault. Thickness of these layers ranges from 5 to 50 cm, although they can be traced laterally for over 30 km. Gondite is fine- to medium-grained with a granular texture, mostly made up of quartz and spessartine(?) garnet, with minor phases including muscovite, biotite, sillimanite, opaque minerals, zircon, and apatite (Fig. 1-3). Blocky weathering and dark iridescent purple to black Fe-Mn oxide staining common on weathered surfaces make gondite readily identifiable in the field. Gondite commonly occurs as float due to its relative resistance to erosion, which facilitates tracing individual layers over great distances. The protolith of this rock was likely a Mn-rich chemical precipitate that possibly formed on the deep seafloor.

Lithonia Gneiss

The Lithonia Gneiss is by far the most voluminous granitoid found northwest of the Jackson Lake fault, and has been quarried extensively for over a century north of the map area near Conyers, Georgia (e.g., Herrmann, 1954). It is light gray, medium- to medium-coarse grained granitic gneiss that is characteristically polydeformed and strongly foliated (Fig. 1-3); it weathers to a yellow-orange or orange-red sandy soil. Mineralogy consists of quartz, plagioclase (An_{9-13}), alkali feldspar, and biotite, with locally abundant garnet and/or muscovite, along with accessory sphene, zircon, apatite, and Fe oxides. Relatively large pavement exposures (10-100s km²) are common in this region, with arguably the most striking exposure located at Arabia Mountain in southeastern Dekalb County. Foliation in the Lithonia Gneiss is subparallel to regional foliation, with fold hinges trending east-southeast and west-southwest with moderate plunges and consistent southwest vergence. U-Pb ion microprobe analyses of two samples yielded Late Ordovician to Silurian ages (444 and 443 Ma; Huebner et al., *in review*).

Snapping Shoals Augen Gneiss

This rock is named Snapping Shoals Augen Gneiss for the spectacular exposure along the Yellow River at Snapping Shoals, Newton County (Huebner et al., *in review*). It is pervasively deformed, and is characterized by large (up to 10 cm), strongly sheared microcline megacrysts that exhibit dominantly dextral shear sense (Fig. 1-3). Matrix minerals consist of quartz, pla-

gioclase (An_{26-29}), microcline, and biotite, with accessory muscovite, garnet, sphene, and apatite. Only a few small exposures of the Snapping Shoals Augen Gneiss are exposed in the map area, and are found in the north-central to northwestern portion of the Worthville 7.5-minute quadrangle. This unit occurs as meter-scale xenoliths included in both lower Tallulah Falls metagraywacke and the Lithonia Gneiss. To date, this rock unit has not been found southeast of the Jackson Lake fault. Huebner et al. (2010) demonstrated these bodies represent fragments of Grenvillian continental basement.

Evidence of Mesozoic brittle deformation can readily be observed at Snapping Shoals; previous mapping indicates that a splay of the Oxford fault may trace through this locality (Gardner, 1961; Huebner et al., 2011; M.W. Higgins, unpublished data). Rocks here can exhibit almost complete retrogression from biotite to chlorite, sericitization of feldspars, and abundant secondary calcite precipitation, especially as vein fill. Sulfide mineralization is also common at this location. These textures and mineral assemblages likely resulted from an influx of hydrothermal fluids during brittle deformation (Huebner and Hatcher, 2013).

Cat Square terrane

Metasedimentary rocks

Cat Square terrane metagraywacke is medium-fine to coarse-grained, ranges from thinly to thickly layered, appears light to dark gray in fresh outcrop, and generally weathers to a deep reddish-brown (Fig. 1-4). Mineral assemblages include quartz, plagioclase, microcline feldspar, and biotite, locally with garnet, sillimanite, and muscovite. Accessory minerals include sphene, zircon, apatite, and ilmenite. Similar to the Tallulah Falls Formation, an apparent increase in migmatization occurs with proximity to the Jackson Lake fault. Although amphibolite layers and boudins are not uncommon in Cat Square terrane metagraywacke, the relative abundance of amphibolite noticeably increases northwest of the Jackson Lake fault. The occurrence of gondite has also been used as a criterion for distinguishing between Cat Square terrane metagraywacke and the lower Tallulah Falls Formation (e.g., Byars, 2010; Gilliam, 2010; Huebner, this study). Detrital zircon geochronology indicates provenance was primarily Laurentian-derived, with only a minor peri-Gondwanan component, and no Ordovician-Silurian signature has been identified (Huebner et al., *in review*; J.R. Rehrer, unpublished data). Huebner et al. (*in review*) suggested the difference in provenance may be related to proximity of different portions of the Cat Square basin to the proposed Ordovician-Silurian source material prior to translation of the Inner Piedmont along the Brevard fault zone.

Sillimanite schist is abundant in the Cat Square terrane in central Georgia. Typical mineral assemblages include biotite, muscovite, sillimanite, quartz, plagioclase, microcline, and garnet (Fig. 1-4). Both fibrous and prismatic sillimanite occur throughout the map area, along with

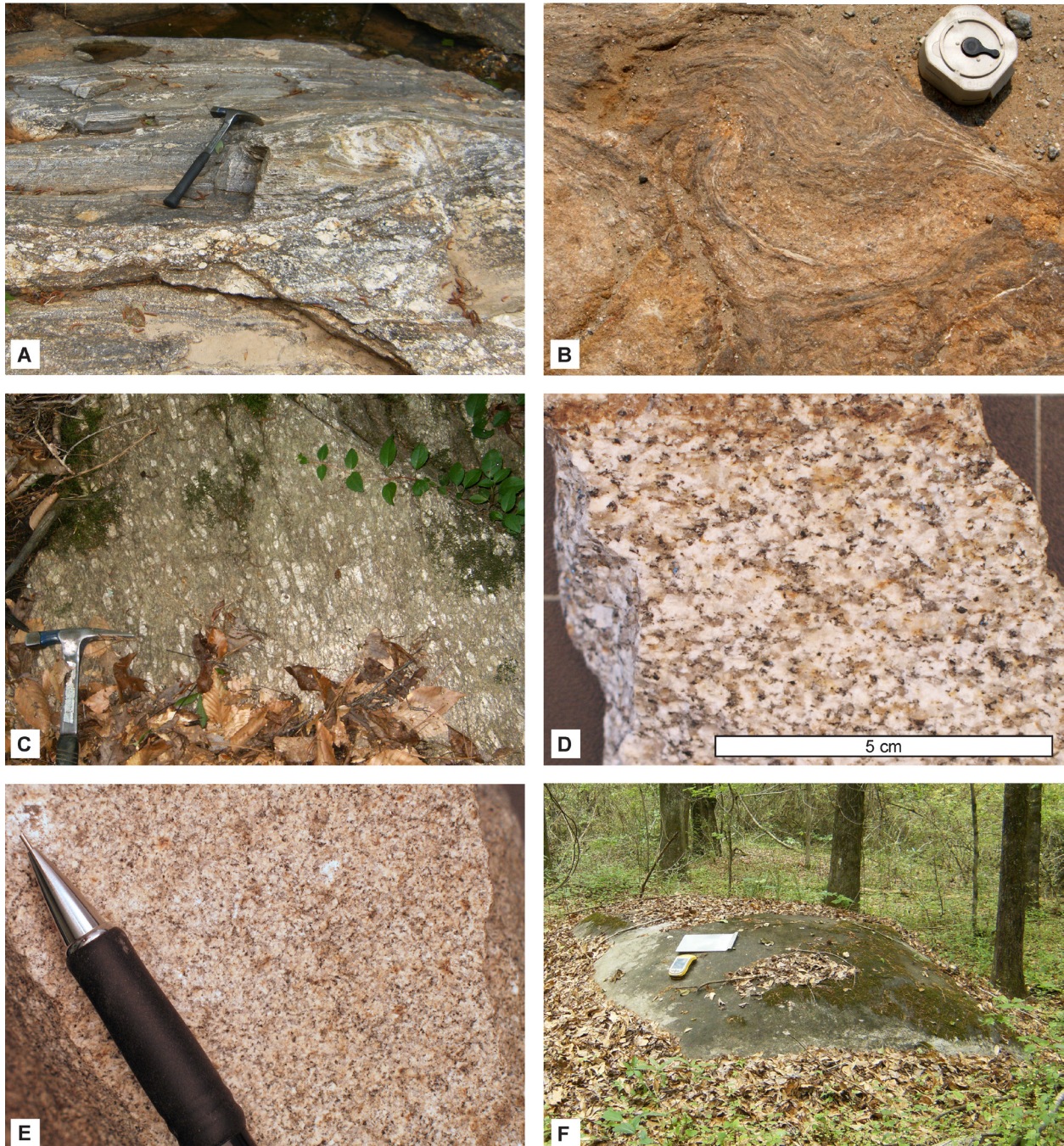


Figure 1-4: Dominant lithologic units of the Cat Square terrane. (A) Coarse-grained migmatitic metagraywacke, view to the southeast. (B) Migmatitic sillimanite schist, view to the southeast. Note the white stringers of sillimanite just below the Brunton® compass. (C) Megacrystic High Falls Granite, view to the northeast. (D) Medium-grained hand sample of Dows Pulpit Granodiorite. (E) and (F) Indian Springs Granodiorite.

blocky muscovite crystals, which may represent retrogressive pseudomorphs after sillimanite. Sillimanite schist weathers to a bright purple or light to medium brown saprolite, and soils frequently contain friable cm-scale chips of schist.

High Falls Granite

The High Falls Granite was named for excellent exposures in and around High Falls State Park (Atkins and Lineback, 1992). Pavement outcrops are common, although typical exposures occur as 0.5-10 m angular to rounded boulders. The High Falls Granite is a moderately to strongly foliated porphyritic biotite granite characterized by 1 to 17 cm-long subhedral to euhedral microcline megacrysts that commonly display Carlsbad twinning (Fig. 1-4). Matrix minerals include quartz, plagioclase (An_{27-43}), microcline, biotite, and locally garnet, with accessory opaque minerals, myrmekite, and zircon. The High Falls Granite weathers to a yellow-orange or orange-red soil, and its characteristic megacrysts can often be readily identified in saprolite exposures. Foliation is defined by parallel alignment of biotite and microcline megacrysts. Although foliation is typically concordant with foliation in the surrounding country rock, exceptions occur in isolated zones at outcrop scale, likely a result of magmatic flow during emplacement (Howard, 2012). Four samples yielded U-Pb ion microprobe ages of 407-371 Ma (Howard, 2012; Huebner et al., *in review*).

Dows Pulpit Granodiorite

The Dows Pulpit Granodiorite is a white to light gray, medium-coarse- to coarse-grained granitoid with a weakly developed foliation, and was named for exposures at Dows Pulpit, Newton County, Georgia (Davis, 2010) (Fig. 1-4). Dominant mineralogy includes smoky quartz, plagioclase (An_{10-14}), microcline, biotite, and muscovite, with accessory sphene, apatite, zircon, and opaque minerals. This rock plots both in the granite and granodiorite fields according to IUGS classification (Streckeisen, 1974), although it more commonly plots as a granodiorite (Davis, 2010). The Dows Pulpit Granodiorite is found predominantly in the northeast portion of the map area, although a few smaller bodies have been found farther southwest. One sample yielded a crystallization age of 325 ± 5 Ma (Huebner et al., *in review*).

Murder Creek granite

The Murder Creek granite is a white to light gray, medium-coarse- to coarse-grained granitoid with a moderately developed foliation, and is informally named for an exposure near Murder Creek in the Charlie Elliot Wildlife Center near Mansfield, Georgia. It is a porphyritic biotite granite characterized by 1-5 cm subhedral to euhedral microcline megacrysts, with a medium- to coarse-grained matrix consisting of quartz, plagioclase (An_{35-43}), microcline, and biotite, with mi-

nor amounts of sphene, apatite, zircon, and opaque minerals. Only one small body of this granite has been identified in the northeastern portion of the map area. The age of this granitoid is 328 ± 4 Ma (Huebner et al., *in review*)

Hornblende diorite

One small body of medium- to dark-gray, medium-grained hornblende diorite has been identified along the boundary between the Jackson and Lloyd Shoals Dam 7.5-minute quadrangles. This rock is mostly equigranular, and consists of nearly equal parts plagioclase (An_{33-45}) and hornblende, with relatively less abundant biotite, opaque minerals, epidote, apatite, and zircon. The age of this rock is unknown, but a lack of solid-state fabric within the rock suggests an Alleghanian age.

Indian Springs Granodiorite

The Indian Springs Granodiorite is a white to light gray, weakly to moderately foliated, medium- to fine-grained equigranular granodiorite, and was named for great exposure at Indian Springs State Park, Butts County, Georgia (Huebner et al., *in review*). This unit typically occurs as large (1-5 m) rounded boulders (Fig. 1-4), although relatively large pavement outcrops (up to ~ 300 m²) are also common. The Indian Springs Granodiorite weathers to a fine, sandy, yellow-orange soil. This rock unit occurs as dikes or isolated pods, as well as larger map-scale bodies. Foliation typically parallels the boundaries of Indian Springs Granodiorite bodies, suggesting a magmatic origin, and bodies of Indian Springs often truncate regional foliation. Plagioclase (An_{8-13}), quartz, microcline, and biotite are the primary phases, although muscovite can be locally abundant. Accessory minerals include sphene, chlorite, apatite, zircon, and opaque minerals. Sericitic alteration is frequently observed, along with local alteration of biotite to chlorite locally. Ion microprobe ages from three samples of Indian Springs Granodiorite reveal Alleghanian ages (317-301 Ma; Huebner et al., *in review*).

Pine Mountain Window

Pine Mountain cover sequence

Metasedimentary units in the Neoproterozoic-Paleozoic(?) cover group of the Pine Mountain window in Georgia consist of three lithologies (Hewett and Crickmay, 1937). The Sparks schist is comprised of feldspathic quartz-mica schist that lies stratigraphically between basement units of the Pine Mountain window and the Hollis Quartzite. It is not exposed in the map area; here the Hollis Quartzite is in contact with underlying basement units. The Hollis Quartzite is a fine- to medium-grained, micaceous-feldspathic, quartzite that is typically thin-bedded and interlayered

with coarse-grained muscovite that defines a foliation parallel to bedding. Locally the quartzite grades upward into a massively bedded, more pure quartzite. The Hollis Quartzite is resistant to weathering and forms steep ridges that are obvious in the topography at the southwestern portion of the map; however, where the unit has experienced extensive weathering it develops a fine-grained, sandy, light yellow to tan soil. A biotite-quartz-feldspar schist lying stratigraphically above the Hollis Quartzite has been mapped in the Barnesville (Sneyd, 1995; Kath, unpublished data) and Zebulon (Hatcher and Rehner, unpublished reconnaissance) quadrangles. Petrographic descriptions of this unit, along with stratigraphic position above the Hollis Quartzite, indicate that it is most likely part of the Manchester Schist described by Hewitt and Crickmay (1937) and Clarke (1952).

Woodland Gneiss

The Woodland Gneiss is the most widespread exposed basement gneiss within the mapped area of the Pine Mountain window, and was so named by Hewitt and Crickmay (1937) for the town of Woodland, Talbot County. This unit is composed predominantly of dark-gray coarse-grained biotite-microcline-quartz augen gneiss, consisting of large (1-2 cm long) sheared microcline feldspars distributed throughout a fine- to medium-grained biotite-quartz-feldspar matrix. Garnet locally occurs within the gneiss as a primary phase, with muscovite, apatite, sillimanite, and zircon occurring as common accessory phases. Although the Woodland Gneiss is typically observed as sheared gneiss with extensively deformed feldspars, in some locations it does occur as undeformed granitic gneiss characterized by large euhedral microcline megacrysts up to 10 cm long (Fig. 1-5). Exposures of this unit are common throughout the Pine Mountain window and generally occur as small ($< 50 \text{ m}^2$) pavement outcrops with few large ($> 1 \text{ km}^2$) outcrops occurring locally, such as the shoals in the Little Towaliga River at Higgins Mill. The weathering characteristics of this gneiss produce a deep-red colored soil and are largely responsible for the gentle rolling topography observed to the southeast of the Towaliga fault. The age of the Woodland Gneiss is $1011 \pm 12 \text{ Ma}$ (Heatherington et al., 2006).

Hornblende quartz diorite

A large body of light- to medium-gray coarse-grained quartz diorite is exposed in a klippe of Cat Square terrane rocks in the Pine Mountain window at the northwestern corner of the Johnstownville 7.5-minute quadrangle. The quartz diorite consists predominantly of plagioclase, biotite, quartz, and hornblende, with the occurrence of microcline and zircon as accessory phases. Garnet is also abundant and is typically mantled by biotite, which, along with the dark hornblende crystals, gives the rock a “speckled” appearance. A foliation defined by parallel alignment of biotite grains tends to be well developed near the contact with the enclosing Cat Square terrane rocks

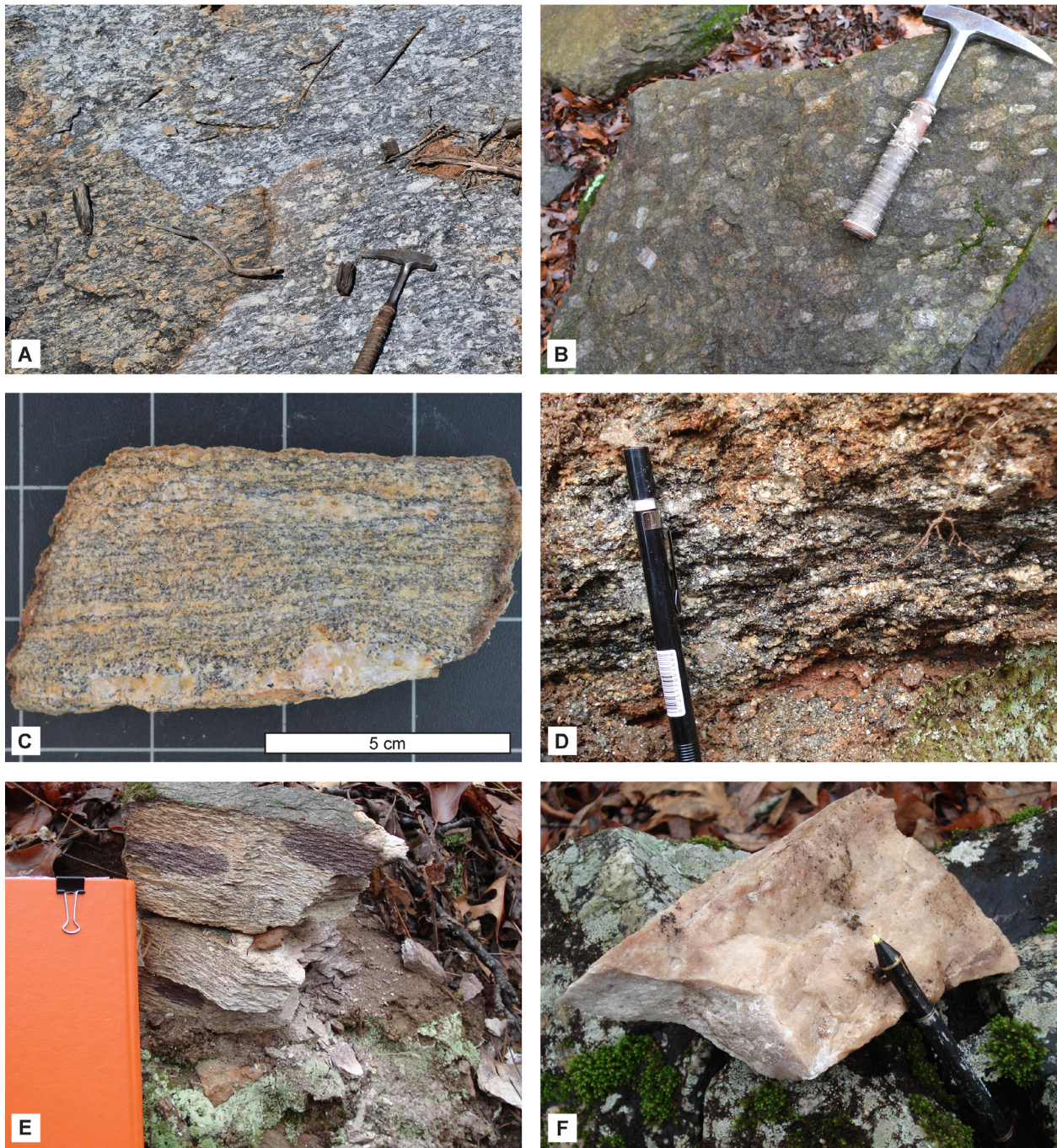


Figure 1-5: Characteristic rocks of the Pine Mountain window. (A) and (B) Woodland Gneiss, characteristically sheared in (A; view to the northwest), relatively undeformed in (B). (C) Basement gneiss Yb₂. (D) Manchester schist. (E) and (F) Hollis quartzite, which ranges from strongly foliated and micaceous (E) to massive quartzite (F).

and becomes more weakly developed and is almost not existent toward the interior of the exposure. SHRIMP analysis from one sample of quartz diorite yielded an age of 1007 ± 9 Ma (Rehrer, unpublished data). Outcrops typically occur as large (1-5 m) rounded boulders, resulting from spheroidal weathering of thick exfoliation surfaces.

Grenville basement gneiss (Yb₁)

Light pinkish gray, medium- to coarse-grained orthogneiss is exposed beneath the Hollis Quartzite in the southeastern part of the Zebulon quadrangle. This unit is polydeformed, strongly foliated, and may be the country rock into which the Woodland Gneiss and other less deformed basement granitoids were intruded. Mineralogy consists of quartz, microcline, plagioclase, and biotite, with accessory opaque minerals.

Grenville basement gneiss (Yb₂)

This basement gneiss is fine- to medium-grained, strongly foliated biotite orthogneiss that is exposed at the easternmost end of the Pine Mountain window. Dominant mineralogy includes quartz, microcline, plagioclase, and biotite, with accessory garnet, sphene, apatite, and zircon. Ion microprobe SHRIMP analysis of zircon yielded a crystallization age of 1014 ± 12 Ma (Rehrer, unpublished data).

Carolina superterrane

The Carolina superterrane in the map area consists of an assemblage of mafic and felsic metavolcanic rocks along with mostly mafic intrusive bodies. In addition, a traceable body of metaultramafic rock (soapstone) occurs here that appears to be truncated to the southwest by the central Piedmont suture immediately east of the Ocmulgee River. There also is a mappable unit of amygdaloidal metabasalt that occurs in this area near the northwest edge of the Carolina superterrane. Several large gabbro bodies intrude the volcanic complex. Hooper (1986) and Hooper and Hatcher (1989) suggested that this entire assemblage be called the Berner mafic complex. However, modern SHRIMP ages of a metagabbroic diorite body present in the complex and the contact aureole of the Gladesville Gabbro indicate that the gabbro bodies here are Paleozoic (~372 Ma), whereas the ~538 Ma age on the metavolcanic host rocks and the metagabbroic diorite clearly indicates the gabbro bodies are much younger and the volcanic assemblage that encloses these gabbros is Cambrian or older. Therefore, the term “Berner mafic complex” should be restricted to either the mid-Paleozoic gabbros or the Cambrian volcanic assemblage. Much of the following rock unit descriptions have been adapted from Hooper (1986) and Hooper et al. (1997).

Layered gneiss series

The layered gneiss series in Charlotte terrane rocks make up the bulk of the Carolina superterrane in the map area. The scale of layering in the series varies from millimeter- to meter-scale (Fig. 1-6). Layered felsic gneisses consist of quartz, plagioclase, microcline, biotite and muscovite, are locally garnetiferous, and schistose with high mica content. Subordinate volumes of mafic and intermediate gneiss occur as layers and boudins throughout the unit. Small felsic plutons of granitic to granodioritic composition locally form pavement exposures. The layered intermediate gneiss series generally consists of alternating packages of biotite-rich and/or hornblende-rich gneiss. Equal proportions of felsic gneisses are locally interlayered with the intermediate gneisses, with minor volumes of mafic gneisses occurring throughout the unit. Layered mafic gneisses include amphibolites and amphibole gneisses with localized epidote-rich zones. Minor amounts of felsic and biotite gneiss are interlayered throughout the unit. Layering is defined by varying proportions of mafic phases between layers, although it is locally enhanced by grain-size variations. These rocks are not so highly strained that original volcanic layering has been lost, but most, if not all primary pyroxenes have been converted to hornblende. Some of the felsic and mafic rocks are intimately interlayered, and also grade into each other (Hooper, 1986).

Metagabbroic diorite

Metagabbroic diorite occurs in apparent lenticular bodies in the western portion of the Carolina superterrane throughout the map area, with outcrops generally consisting of meter-scale rounded boulders. This unit is medium- to coarse-grained, medium-greenish gray, with 1-3 mm hornblende (and pyroxene?) porphyroclasts in a plagioclase, hornblende, diopside matrix with minor amounts of quartz, sphene, and zircon (Fig. 1-6). Zircon from this rock yielded a U-Pb age 538 ± 5 Ma (Huebner et al., *in review*).

Amygdaloidal amphibolite gneiss

A single layer of amygdaloidal metabasalt occurs as a narrow almost east-west-trending belt that is traceable for ~7 km along the western flank of the Carolina superterrane. Its outcrop belt is subparallel to the Ocmulgee fault (central Piedmont suture) and the unit produces abundant exposure consisting of rounded boulders that appear to not be far out of place that facilitate tracing it. It consists of metabasalt containing vesicles that were filled with quartz, epidote, and possibly a carbonate mineral. The amygdules are not highly strained, although they were deformed into ellipsoids with K values ~0.30, with the X-Y plane of the ellipsoids lying in the plane of the foliation (Fig. 1-6). The matrix of the basalt consists of hornblende (replacing clinopyroxene?), plagioclase, and minor biotite and opaque minerals (Hooper, 1986).

Metaultramafic rocks

This unit consists largely of soapstone (likely altered dunite), in addition to metapyroxenites and chlorite-actinolite schists. The rocks occur as either boudins or thin layers within the layered mafic gneisses or are associated with mafic plutonic rocks. Individual pods and layers of altered ultramafic rocks that are not traceable for long distances are also common in this part of the Carolina superterrane. All of these bodies are foliated (Hooper and Hatcher, 1989).

Paleozoic gabbro

Several mappable gabbro bodies intruded the older volcanic complex during the middle Paleozoic. These enclose the Gladesville Gabbro (studied in detail by Matthews [1967]), the Rum Creek gabbro, and several smaller gabbroic bodies. All of the gabbros appear to have well-developed contact aureoles, although in a few cases they may not have been mapped (e.g., West, 1994). Huebner et al. (*in review*) suggested the Gladesville gabbro was emplaced 372 ± 4 Ma, based on U-Pb SHRIMP ages derived from numerous metamorphic overgrowths of zircons separated from contact aureole rocks. This timing is likely the approximate age of intrusion and cooling of the other gabbro bodies in this area. While all of the gabbros here exhibit some alteration, particularly along fractures that cut the gabbros, the gabbroic bodies appear to have a similar origin (Chaumba, 2010b). The Rum Creek gabbro may be more altered than some of the others, perhaps because of its proximity to the central Piedmont suture. Alteration zones within the gabbros commonly contain chlorite, serpentine (antigorite), and occasional anthophyllite. While Matthews (1967) concluded that the Gladesville Gabbro is a layered body, Hooper (1986) was unable to resolve extensive layering in either field exposure or in drill core.

Hooper (1986) defined four distinct subsets of rock types within the main body of the Gladesville gabbro although, in general, it can be described as a medium- to coarse-grained, two-pyroxene gabbro that is locally olivine-bearing. Plagioclase is locally ophitic to sub-ophitic, and occurs as both laths and as an interstitial phase throughout the body. Minor phases include amphibole, opaque minerals, biotite, spinel, sphene, and muscovite (Hooper, 1986). Intrusion of the Gladesville Gabbro resulted in thermal alteration of surrounding country rock to conditions in the pyroxene hornfels facies.

Felsic plutonic rocks

Felsic plutonic rocks include a range of deformed tonalitic through granitic rocks that likely intruded the layered gneisses (Hooper, 1986). The rocks are dominantly quartz, plagioclase, alkali feldspar, biotite, muscovite gneisses that are locally garnetiferous and/or amphibole-bearing.

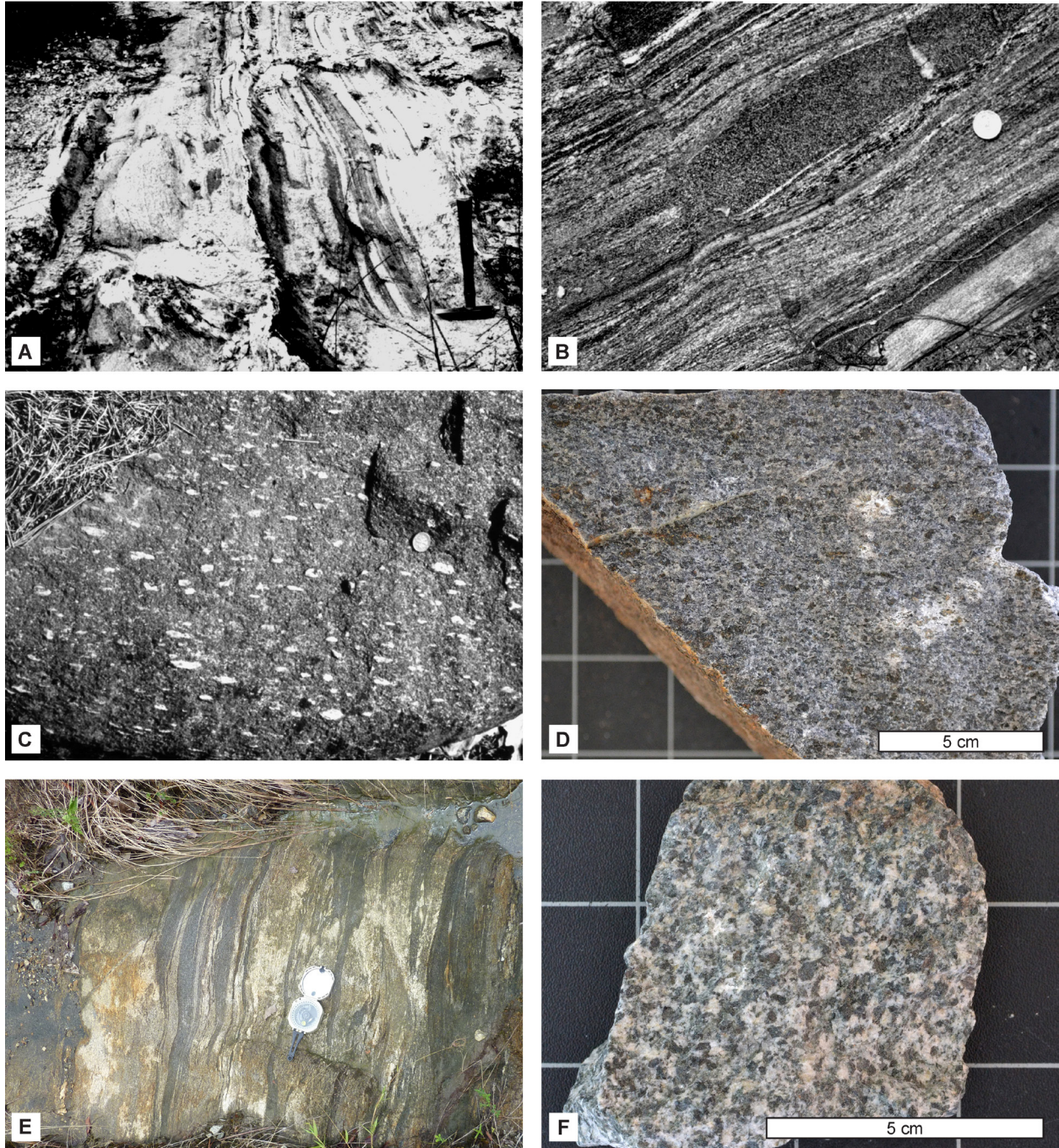


Figure 1-6: Selected lithologies from the Carolina superterrane in the map area. (A) Interlayered felsic and intermediate metavolcanic gneiss (from Hooper, 1986). (B) Intermediate gneiss with late brittle fracture, U.S. quarter for scale (from Hooper, 1986). (C) Amygdaloidal amphibolite gneiss, U.S. dime for scale. White vesicles containing quartz, epidote, and carbonate flattened parallel to foliation (from Hooper, 1986). (D) Characteristic hand specimen of Gladesville Gabbro. (E) Layered intermediate gneiss from contact aureole of the Gladesville Gabbro, view to the southwest. (F) Metagabbroic diorite.

Hooper (1986) suggested that these were Paleozoic, and suggested at least one body had an associated hornblende hornfels-grade contact aureole.

Mesozoic rocks

Diabase dikes

Several diabase dikes occur throughout the map area, and are generally < 10 m wide, although they can be traced lengthwise for tens of km. Diabase dikes are generally exposed as 0.25 to > 1 m rounded boulders that appear rusty-orange on a weathered surface (Fig. 1-7). Fresh surfaces reveal the mafic nature of these rocks, which are medium to dark gray (Fig. 1-7). Diabase is fine-grained and aphanitic, and dominant mineralogy consists of clinopyroxene (augite) and plagioclase, and olivine, with relatively minor opaque minerals and chlorite. Characteristic ophitic texture is obvious in thin section, and can be readily observed in hand samples.

Silicified cataclasite

Silicified cataclasite occurs in isolated, km-scale rhomboidal ridges of silicified breccia and cataclasite associated with small-displacement Mesozoic faults and along the Towaliga fault. Rock that comprises these ridges is almost entirely quartz, which is responsible for the striking topographic relief due to its resistance to chemical weathering relative to surrounding high-grade metamorphic and plutonic rocks. Siliceous cataclasite consists of white to light-beige or smoky quartz, with rock fabrics that range from massive vein quartz to multiply brecciated quartz vein fill with abundant wallrock clasts (Fig. 1-7). Vugs and boxwork textures are common, with individual quartz crystals up to 10 cm long. Angular breccias show little evidence of attrition, and are generally cemented with boxwork quartz. Accessory minerals include sulfides, clay minerals, and possibly relict zeolites.

Metamorphism

Metamorphic isograds through the Inner Piedmont reveal a high-grade core flanked by relatively lower grade rocks (Fig. 1-2). However, no evidence has been documented of a variation in peak metamorphic grade across the map area. Metamorphic mineral assemblages of metasedimentary rocks throughout the map area consistently indicate conditions that reached sillimanite grade during prograde metamorphism. Typical mineral assemblages of pelitic schists and schistose metagraywacke include:

muscovite + plagioclase + sillimanite + garnet + biotite + quartz ± chlorite ± epidote

muscovite + biotite + quartz + plagioclase ± chlorite

biotite + sillimanite + muscovite + quartz + garnet + apatite + rutile + sphene

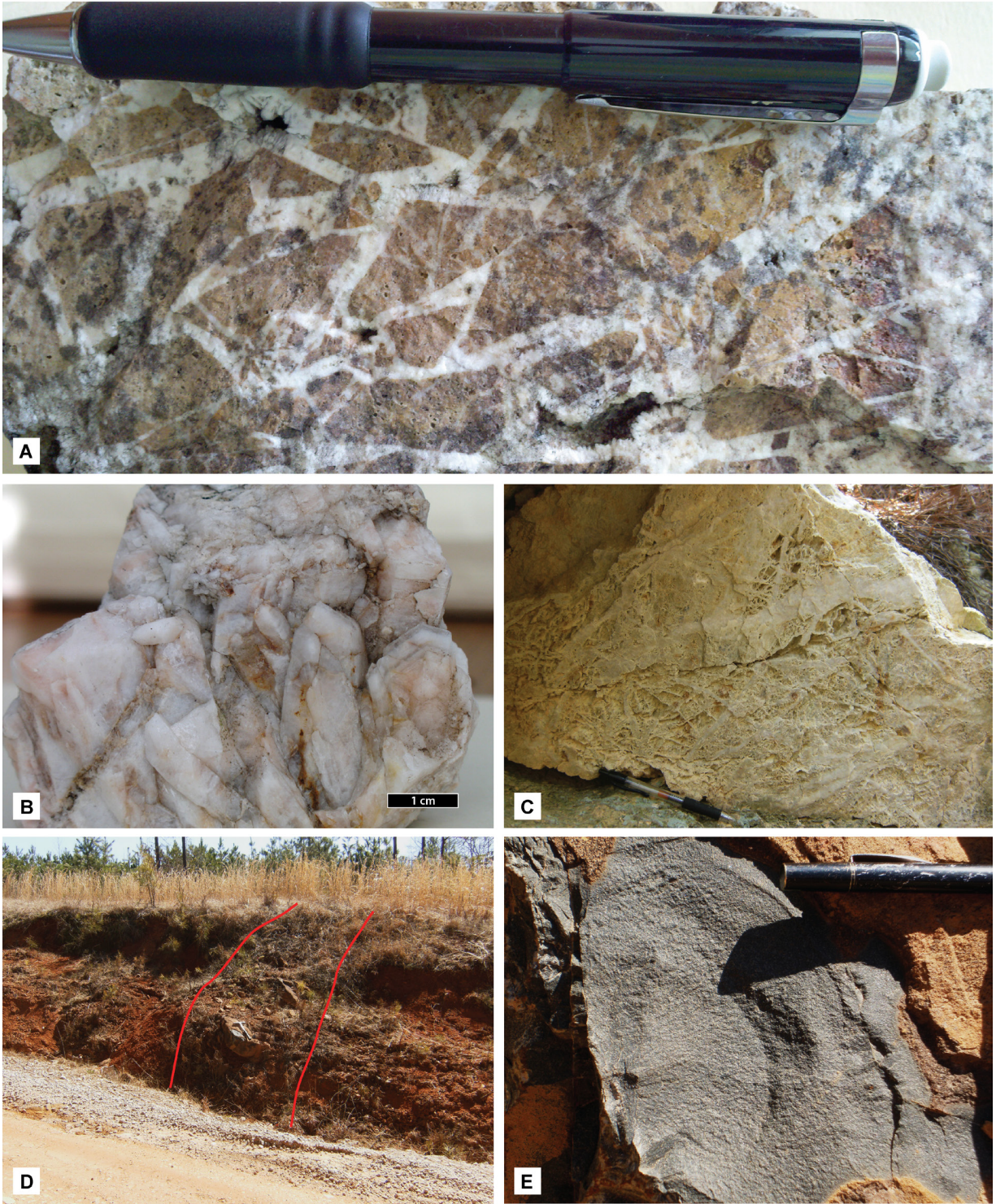


Figure 1-7: Mesozoic rocks. (A) Angular implosion breccia from the Towaliga fault, with clasts cemented by boxwork quartz. Note the vugs in the quartz cement. (B) Boxwork quartz from the Towaliga fault. Note the chemical zonation in the crystal in the right center of the image. (C) Intensely deformed quartzite from the Towaliga fault with numerous overprinting deformation events, view southwest. (D) and (E) Characteristic exposure of a diabase dike, view to the southeast.

Davis (2010) reported peak metamorphic conditions in central Georgia reached 4-5.3 kbars with temperatures ranging between 645 and 715° C. These conditions fall within the sillimanite stability field, but below sillimanite II conditions, which agrees with observed metamorphic mineral assemblages. Petrographic evidence suggests K-feldspar in metasedimentary rocks was most likely detrital, and not formed by the breakdown of muscovite.

A narrow band of lower-amphibolite facies mylonite occurs along the Towaliga fault. Hooper and Hatcher (1988a) reported mylonite records deformation of upper amphibolite-facies protolith gneisses that occurred under relatively lower (garnet grade) conditions. Current studies have revealed new exposures of mylonitic rocks along the Towaliga fault, and petrographic evidence indicates deformation occurred in the range of garnet stability. However, more precise thermobarometric estimates are limited by the lack of appropriate mineral assemblages in the rocks. Throughout the map area, breakdown of biotite, hornblende, and garnet to chlorite occurs locally, although the sporadic occurrence of these reactions indicates any retrograde overprint is generally insignificant.

Areas of low-temperature hydrothermal alteration (zeolite facies?) have been identified along brittle Mesozoic faults in the region. Country rocks exhibit complete breakdown of feldspars to clay minerals, biotite to chlorite, and secondary precipitation of calcite, oxides, sulfides, and possibly zeolites. The largest exposures of this low-temperature overprint occur in proximity to rhomboidal ridges of silicified cataclasite (dilational step-overs) that acted as loci of concentrated hydrothermal fluid flow during faulting ~200 Ma (Huebner and Hatcher, 2013).

Structure

Much of the knowledge regarding the structure of the Inner Piedmont is the result of numerous detailed geologic mapping projects in the northern portions of the Inner Piedmont (e.g., Mersch et al., 2008, and references therein). Many aspects of fabric and related deformational events appear to be similar in the southern portion of the Inner Piedmont, with subtle differences. Fabrics from the map area are discussed in terms of well-documented structural analyses throughout the northern Inner Piedmont, although differences in timing and development of various fabrics provide a new perspective into the orogenic events that shaped the southern Appalachian orogen.

Planar and Linear Fabrics

The central Georgia portion of the Inner Piedmont has been multiply deformed, and records least six deformation events. The dominant regional foliation (S_2) formed close to peak metamorphic conditions (upper amphibolite-facies), with foliation in metasedimentary rocks defined by high-temperature mineral assemblages, including prismatic and fibrous sillimanite, phyllosili-

cates, and other inequant phases. Compositional layering in migmatitic metasedimentary rocks also parallels S_2 , which indicates development of S_2 fabric occurred near peak thermal conditions. Associated mineral lineations (L_2) are abundant in the map area, locally defined by similar high-temperature minerals, and typically exhibit shallow ($< 15^\circ$) plunges. Ion microprobe analyses of metamorphic zircon rims indicate peak metamorphic conditions took place in the Middle to Late Devonian (400-380 Ma; Huebner et al., *in review*), which we interpret to represent the timing of S_2 development. Primary sedimentary structures were mostly destroyed by deformation that accompanied high-grade metamorphism, although lithologic contacts between pelitic and coarser-grained metasedimentary rocks (S_0) are consistently subparallel to the dominant S_2 foliation, likely a result of strong transposition during deformation and metamorphism.

S_2 fabric envelops amphibolite boudins that locally preserve an earlier S_1 foliation (Hopson and Hatcher, 1988; Merschat et al., 2005; Davis, 2010; this study), which Merschat et al. (2008) suggested developed during the early stages of the Acadian/Neoacadian orogeny. If the enclosing metasedimentary rocks were originally deposited in the Silurian-Devonian, development of S_1 , which had to postdate basaltic volcanism that coincided with deposition, cannot be an older fabric.

A rare secondary foliation (S_3) and mineral lineation (L_3) have been recognized in the northern Inner Piedmont, although have not been observed (to date) in central Georgia. However, the Indian Springs Granodiorite contains a weak foliation that locally appears tectonic in nature and, in places, appears to be subparallel to S_2 . On the other hand, numerous exposures through the map area indicate a magmatic origin of this fabric; contacts between the Indian Springs Granodiorite and S_2 fabric in metasedimentary rocks are more often discordant, with foliation in the Indian Springs Granodiorite parallel to discordant lithologic contacts. Petrographic evidence from several samples indicates solid-state deformation, whereas others exhibit only minor indications of solid-state fabrics, which may indicate submagmatic development (e.g., Paterson et al., 1989). Combination of these observations could be interpreted to indicate the Indian Springs Granodiorite was emplaced late syn- to post-deformation and development of S_2 and, by association, S_2 would then be an early Alleghanian fabric. However, several attributes support the hypothesis that S_2 fabric developed in the middle Paleozoic: 1) ion-microprobe ages of metamorphic zircon that indicate thermal peak occurred 400-380 Ma (Huebner et al., *in review*); 2) numerous structural data and field relationships that indicate the High Falls Granite (407-371 Ma) formed pre- to syn- S_2 ; and 3) several Alleghanian (328-301 Ma) granitoids truncate S_2 fabric. Therefore, Alleghanian orogenesis (330-300 Ma) throughout the map area was predominantly a thermal event that resulted in a pulse of granitic magmatism, metamorphic zircon growth in metasedimentary and metaigneous rocks, and sporadic development of weak (tectonic?) planar fabric (tentatively designated S_3) that has been recognized only in coeval granitic plutons.

Mylonitic foliation confined to the narrow belt of upper greenschist-facies mylonites of the Towaliga fault zone truncates S_2 fabric and several bodies of the Indian Springs Granodiorite, indicating deformation and fabric development occurred post ~300 Ma. The steeply northwest-dipping foliation and corresponding shallow-plunging mineral lineation associated with the fault zone are termed S_4 and L_4 , respectively.

Numerous small-scale shear zones occur throughout the map area that deformed quartz veins under middle- to lower-greenschist facies conditions. These shear zones are generally < 15 cm thick, and do not appear to be laterally continuous. Although no direct crosscutting relationships have been observed, the relatively low grade of deformation indicates development post-dates other fabric in the region (Huebner and Hatcher, 2013). Mylonitic foliation and lineations within these localized shear zones are designated S_5 and L_5 , respectively.

Folds

Several generations of folds have been revealed from detailed geologic mapping throughout the map area. Folding coincident with the development of S_1 , preserved locally in amphibolite boudins, occurs in the northern Inner Piedmont. The majority of mesoscale folds through the map area are passive and flexural flow, inclined to recumbent isoclinal folds that are axial planar to S_2 , and are termed F_2 . Davis (2010) suggested that F_2 should designate only intrafolial folds, whereas folds with similar characteristics that isoclinally fold S_2 , and in places, coaxially refold intrafolial F_2 folds, should be deemed F_3 . While we do not disagree with this suggestion, similar trends, characteristics, and rheologic styles of F_3 folds often make them difficult to distinguish in the field and, as we compiled different generations of detailed mapping efforts, this distinction throughout the map area is not feasible. Therefore, F_2 and F_3 folds are combined in equal-area plots of fold data (see attached map). The latest identified generation of folding, F_4 , consists of broad, upright open folds that gently warp S_2 fabric. Mesoscopic exposures of F_4 are generally rare, although structural data indicate the map area may encompass the axis of a broad macroscale F_4 antiform.

Faults

Jackson Lake fault

The Jackson Lake fault is a ~15 m thick high-grade fault zone that dips very steeply southeast at the northeast end of the map area, and changes to a moderate northwest dip toward the southwest. Granitoids and metasedimentary assemblages from both sides of the fault are truncated along this boundary. Pervasive S-C fabric, along with asymmetric σ -, δ -, and θ -porphyroclasts in the fault zone, dominantly exhibit dextral shear sense (Fig. 1-8A), while shallow-plunging mineral stretching lineations indicate predominantly strike-slip displacement. Mylonite protoliths

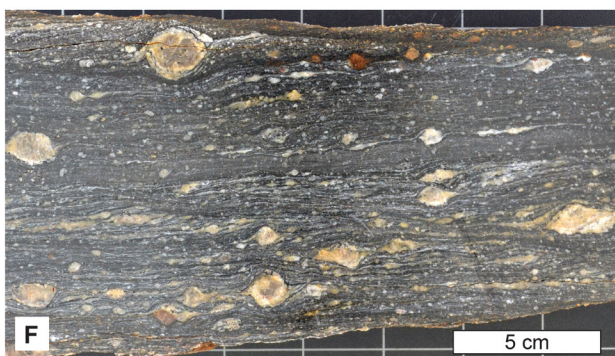
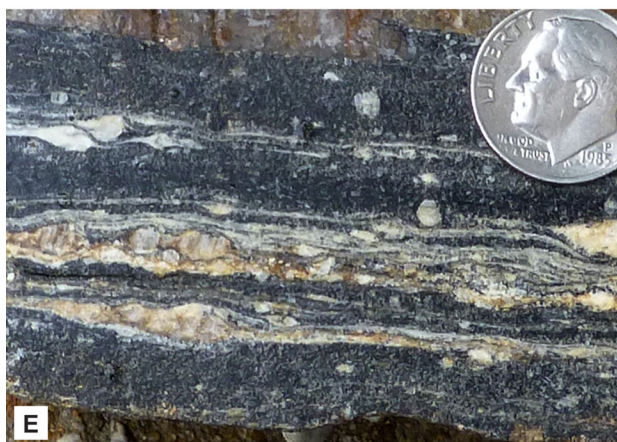
include migmatitic metagraywacke and megacrystic High Falls Granite, with porphyroclasts consisting of mostly plagioclase and microcline, with myrmekite rims visible in hand sample. Sillimanite growth within the mylonitic fabric demonstrates deformation along the Jackson Lake fault occurred under sillimanite-grade conditions, similar to S_2 fabric. In addition, mylonitic fabric is generally concordant with regional foliation, indicating the fault was active pre- to syn-peak metamorphic conditions. Granitoid ages and detrital zircon analyses strongly suggest the Jackson Lake fault is the southwest equivalent of the Brindle Creek fault, which indicates this terrane boundary extends ~500 km from just south of the Sauratown Mountains window in west-central North Carolina, likely truncated to the southwest by the Alleghanian Towaliga fault near Concord, Georgia. This boundary has not been traced in detail through central and southwestern South Carolina (Curl, 1998; Nelson et al., 1998), although detrital zircon analysis of metasedimentary rocks near Paris Mountain indicate the Cat Square terrane also occurs there (Bream, 2003; Mersch et al., 2010). The age of the Jackson Lake fault is bracketed by the youngest granitoid truncated by the fault (High Falls, ~371 Ma) and a possible stitching body of Indian Springs Granodiorite (~305 Ma). The occurrence of the Indian Springs Granodiorite on both sides of the fault also indicates deformation along the Jackson Lake fault occurred prior to the Alleghanian orogeny, likely during the Acadian/Neoacadian event.

Towaliga fault

The Towaliga fault frames the northwest side of the Pine Mountain window and continues northeast through the Cat Square terrane at a ~070 trend, changes to a ~035 trend at the northeast end of the window, and continues northeast through the Cat Square terrane (Wells, 1982; Huebner and Hatcher, 2013). The Towaliga fault contains both ductile and brittle fault rocks, recording a two-part history of deformation, with fault activity occurring during the Alleghanian orogeny and Mesozoic breakup of Pangea (Huebner and Hatcher, 2013). Both phases of faulting dip steeply northwest, and were active as strike-slip faults, although with opposite shear sense (Huebner and Hatcher, 2013). The high-temperature (Alleghanian) mylonite zone ranges from 10 m to up to 5 km thick (Steltenpohl et al., 2010), with proto- to ultramylonite exhibiting upper greenschist to lower amphibolite facies conditions during deformation. Dextral strike-slip displacement has been reported by numerous geologists (e.g., Hooper and Hatcher, 1988a; Steltenpohl, 1988; Babaie et al., 1991; Hadizadeh et al., 1991; Huebner and Hatcher, 2011, 2013).

Arguably, the most striking aspect of the Towaliga fault is the occurrence of isolated, km-scale post-Alleghanian rhomboidal ridges of silicified breccia and cataclasite that occur along its length. Huebner and Hatcher (2013) interpreted these to represent ancient dilational step-overs that formed in a small-displacement sinistral strike-slip regime. These ridges can locally exhibit > 40 m of positive relief, and northwest dip is inferred from slight asymmetry of the ridges.

Figure 1-8: High-grade fault rocks. (A) Jackson Lake fault mylonite. (B) Kinnard Creek fault mylonite with large hornblende porphyroclast, view to northwest. (C) Saprolite exposure of the Ocmulgee fault, view to northwest. (D) Box Ankle fault mylonite. (E) Hand specimen of Rumble shear zone annealed mylonite from the type area around Rumble Creek. Note the banded nature of the mylonite, the tailed porphyroclasts, and the ribbon texture in part of the rock. (F-G) Towaliga fault mylonites, illustrating different protolith material (F - likely Woodland Gneiss; G - migmatitic schist).



High-dilation breccias with angular wall-rock clasts are likely a result of hydraulic implosion (Huebner and Hatcher, 2013). Strong hydrothermal alteration of country rock adjacent to silicified cataclasite ridges also supports the hypothesis that these pods acted as dilational step-overs during faulting, since these sites would have been loci for concentrated fluid flow (Huebner and Hatcher, 2013).

The Towaliga fault abruptly truncates the Cat Square terrane plutonic complex in central Georgia, including granitoids as young as ~300 Ma. This indicates large displacement has occurred along this fault zone, which is interpreted to be a result of Alleghanian dextral strike-slip. The size of the Mesozoic step-overs, in addition to the possible ~2.5 km offset of diabase dikes along the fault, indicate Mesozoic displacement was on the order of a few km.

Box Ankle fault

The Box Ankle fault is a ~2 km-thick, gently southeast- and northwest-dipping, northwest-vergent thrust and terrane boundary that juxtaposes Cat Square terrane rocks above Pine Mountain window rocks in the footwall. Mylonite here contains an upper amphibolite facies mineral assemblage, a well-developed S-C fabric, and abundant rotated feldspar porphyroclasts (Hooper and Hatcher, 1988b) (Fig. 1-8D). Petrographic evidence indicates Box Ankle fault mylonite is relatively free of unrecovered strain (Hooper and Hatcher, 1988b), indicating thermal equilibration post-deformation. The continuity of S_2 fabric across the fault zone, in addition to evidence that the fault is folded axial planar to S_2 , indicates displacement along the fault occurred prior to the development of the dominant S_2 foliation and thermal peak (Hooper and Hatcher, 1988b, 1989). These observations call into question the ~303 Ma age of the Box Ankle fault suggested by Student and Sinha (1992), and instead indicate the Box Ankle fault is likely an Acadian/Neoacadian fault.

Kinnard Creek fault

The Kinnard Creek fault is marked by a distinctive high-temperature mylonite that characteristically contains 0.2–2 cm porphyroclasts of hornblende, garnet, and feldspar (Fig. 1-8B). This unique lithology is found only along this relatively narrow (~20 m) fault zone. The fault dips shallowly southeast, with moderately northeast-plunging mineral stretching lineations, and mylonitic foliation is generally concordant with regional foliation. Dynamic recrystallization of hornblende and alkali feldspar porphyroclasts confirms this fault was active at high temperatures (Berg, 2012). Davis (2010) interpreted this fault to be a southwest-directed, dextral-oblique thrust fault that was active during D_2 .

Ocmulgee fault

The Ocmulgee fault (central Piedmont suture) separates the peri-Laurentian Cat Square terrane from the exotic, peri-Gondwanan Carolina superterrane. In the map area, it is an amalgamation of steeply southeast-dipping, sillimanite-grade, syn- to post-metamorphic dextral strike-slip shear zones (Hooper et al., 1997). The southeast dip of the fault becomes more shallow northeast of the map area (Troyer, 1991; Hooper et al., 1997). Form surface maps indicate the S_2 fabric is not disrupted by the fault, which suggests displacement occurred prior to the development of S_2 , likely during the Acadian/Neoacadian event (e.g., Hooper and Hatcher, 1989). This calls into question the validity of the ~330 Ma upper-intercept age suggested by Student and Sinha (1992).

Rumble shear zone

The Rumble shear zone is a high-temperature zone of annealed mylonite that extends from the southeastern part of the Pine Mountain window, where it is truncated by the low temperature Dean Creek (Modoc) fault, northeastward following the Ocmulgee fault. It was named for exposures along Rumble Creek, south of Forsyth, Georgia. The Rumble shear zone splays into five or six main segments, reducing the west- to east-shear zone width from ~5 km wide to the south to individual segments < 0.5 km wide to the northeast. Splays are not confined to the boundary between the Pine Mountain window and the Carolina superterrane: some splays cross the boundary and terminate in the Carolina superterrane, while the majority propagated into Cat Square terrane rocks west of the suture. The shear zone is not traceable beyond the Towaliga River ~2.5 km upstream from its confluence with the Ocmulgee River; one of the segments merges with the Ocmulgee fault terrane boundary and terminates before reaching the Towaliga River.

The microfabric of the mylonite along the Rumble shear zone consists of thoroughly recrystallized quartz and biotite, and less common hornblende porphyroclasts, with incipient recrystallization of feldspars (mostly plagioclase) in detrital grains and tailed porphyroclasts. Sillimanite-bearing pelitic layers that occur intermittently in the shear zone confirm its high metamorphic grade. The microtexture of the annealed mylonite matrix resembles that of a recrystallized medium-grained metagraywacke with annealed quartz grains meeting at 120° angles, biotite defining a foliation, and recrystallized quartz ribbons that vary from rare to locally abundant. If the tailed porphyroclasts and quartz ribbons were not present, it would be very difficult to recognize the shear zone. There is no indication of retrogression in either the microscopic or the mesoscopic fabric. Rotated porphyroclasts consistently yield a dextral motion sense.

The longest splay of the Rumble shear zone terminates in an area of poor exposure just south of GA Highway 83 ~8 km east of Forsyth. It is possible that this splay continues northeastward to join the Kinnard Creek fault, although there are no currently available data that could test this

hypothesis. Both shear zones are sillimanite-grade faults that are dominated by dextral displacement, and both contain feldspar and hornblende porphyroclasts.

Pennsylvanian-Permian to Middle Triassic shear zones

Relatively low-temperature (chlorite-muscovite-grade) ribbon quartz mylonite has been found throughout the map area in small, isolated shear zones (Fig. 1-9). In outcrop, most ribbon quartz mylonite occurs as < 15 cm-thick quartz veins concordant with regional foliation that do not appear to be laterally continuous. The volume of quartz veins showing no evidence of shear, however, is considerably greater than the amount of ribbon quartz mylonite. These rocks are generally composed of > 95 percent quartz, with minor alkali feldspar and muscovite porphyroclasts, and rare oxides. Quartz dynamic recrystallization textures indicate temperature of deformation ~400° C, which agrees with brittle deformation of feldspar porphyroclasts enveloped by flowing quartz. Ribbon quartz mylonite occurs locally along the Towaliga fault, although it is also abundant throughout the region in the Inner Piedmont and the Carolina superterrane. *In situ* exposures of the mylonite are rare and, although we have found float along the Towaliga fault, none have been found in place. Where present in outcrop, S-C fabric and asymmetric mica fish indicate dextral shear sense.

These shear zones share an apparent spatial relationship with brittle Mesozoic faults. Previous work on brittle faults in central Newton County (e.g., Gardner, 1961; Schultz, 1961) and along the Middleton-Lowndesville fault in northeast Georgia (Davis, 1980) reported the occurrence of sheared quartz veins with similar characteristics, and those studies also indicated difficulty of finding *in situ* exposures. Where these shear zones occur together with brittle faults, ductile fabrics are exclusively overprinted by brittle deformation.

The precise timing of these shear zones remains unresolved. Based on estimated deformation temperature and thermal history of the Inner Piedmont, mylonitization likely occurred sometime between Alleghanian deformation and the motion of silicified faults that formed at the Triassic-Jurassic boundary (Huebner and Hatcher, 2013). Nearly ubiquitous brittle overprint of ribbon quartz mylonite indicates formation prior to ~200 Ma, and opposite shear sense between ribbon quartz mylonite and silicified faults suggests formation during a separate event. Babaie et al. (1991) acquired a K-Ar age of ~269 Ma from muscovite in a “quartz ribbon ultramylonite,” although those authors did not convey confidence in that analysis. Further work is needed to determine whether these shear zones were deformed during late-stage Alleghanian orogenesis or during the early stages of the Mesozoic breakup of Pangea.

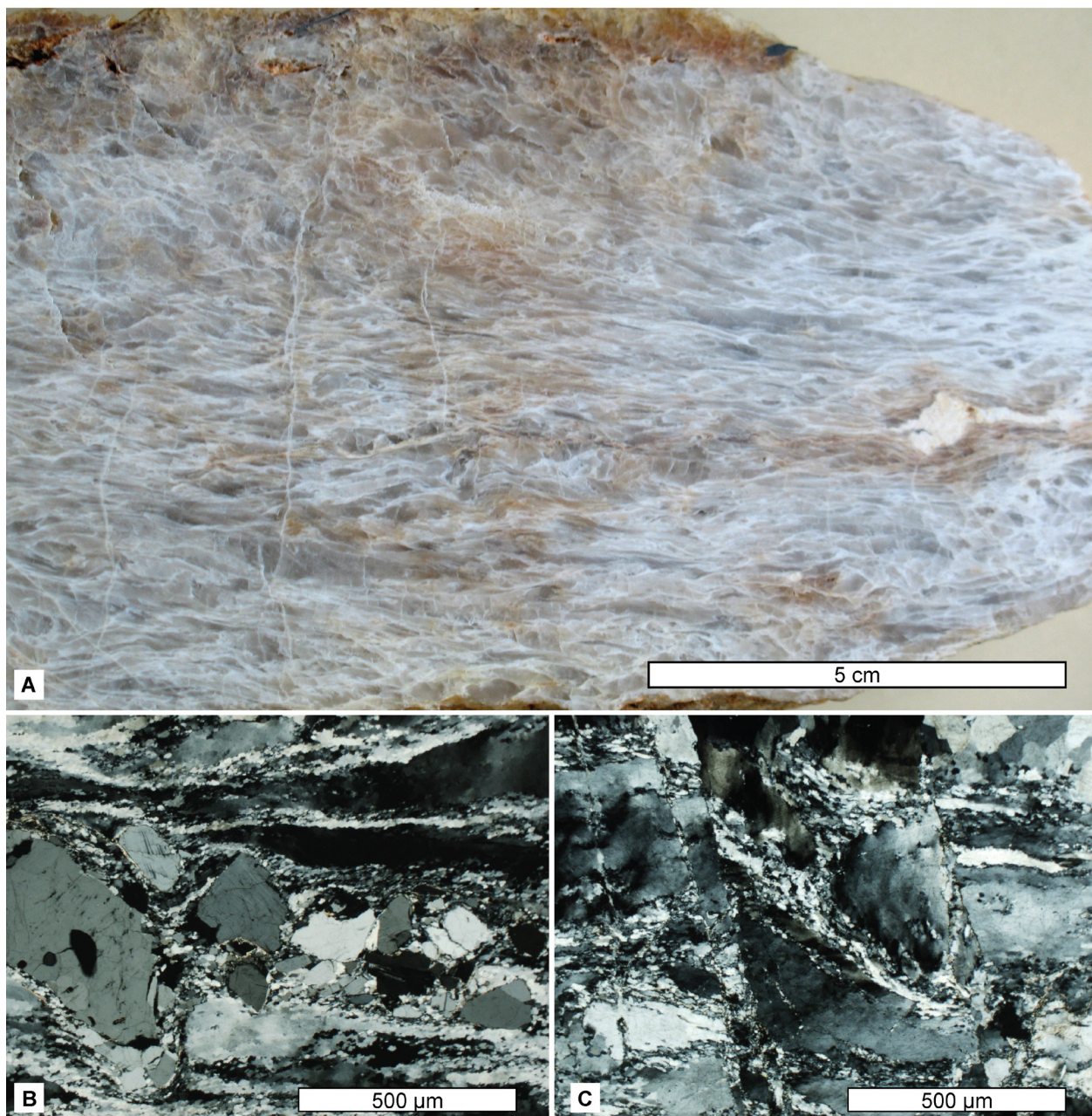


Figure 1-9: (A) Sawed hand sample of ribbon quartz mylonite. (B) and (C) Photomicrographs of ribbon quartz mylonite, cross-polarized light. Note the angular feldspar porphyroclasts enveloped in dynamically recrystallized quartz in (B). (C) Ribbon quartz mylonite overprinted by brittle deformation at ~200 Ma.

Mesozoic faults

In addition to the Mesozoic reactivation along the Towaliga fault, similar isolated pods of cataclasite have been found in other parts of the region along brittle faults that are not known to be associated with earlier ductile faults (e.g., Reade, 1960; Fountain, 1961; Jones, 1970; M.W. Higgins, unpublished data). These brittle faults share similar orientations (~070 and ~035) to the two segments of the Towaliga fault, and geometry of the ridges also suggests sinistral displacement. Silicified faults with similar characteristics are common throughout the southern Appalachians (e.g., Garihan et al., 1993), and have even been reported in New England (e.g., Robinson, 1989; Altamura, 2001).

Crosscutting relationships

Detailed geologic mapping in the study area has revealed numerous crosscutting relationships (Fig. 1-10) that provide insight regarding the relative ages of most of the rocks in the map area, in addition to the nature of the spatial relationships between the major lithologies and fault zones. The Lithonia Gneiss and surrounding Tallulah Falls Formation share contacts concordant with regional foliation that are also deformed. Lithologic contacts between the High Falls Granite and metasedimentary rocks are mostly concordant (Fig. 1-10, E-G), with rare discordant foliation likely a function of magmatic flow. Deformed contacts between the High Falls Granite and surrounding metasedimentary rocks indicate the emplacement was pre- to syn-deformational (D_2). Metasedimentary rocks, the Lithonia Gneiss, and the High Falls Granite are all truncated by the Jackson Lake fault, although a small pod of Indian Springs Granodiorite likely cuts this fault. The Dows Pulpit and Indian Springs granitoids generally cut regional foliation in metasedimentary rocks and the High Falls Granite (Fig. 1-10, A-D), although in places these contacts are concordant. Crosscutting relationships between the Dows Pulpit and Indian Springs have not been observed in the field, although radiometric ages indicate the Dows Pulpit is slightly older than Indian Springs. The Box Ankle fault, in addition to all granitic rocks located in the vicinity of the Towaliga fault, are obviously truncated, indicating the Towaliga fault is younger than ~300 Ma. Diabase dikes cut all crystalline rocks in the map area, including amphibolite- and greenschist-facies mylonite zones, although they share mutually overprinting crosscutting relationships with small-displacement brittle faults, indicating roughly coeval timing. Radiometric ages of diabase dikes surrounding the Atlantic margin indicate emplacement ~200 Ma (e.g., Hames et al., 2000; Nomade et al., 2007).

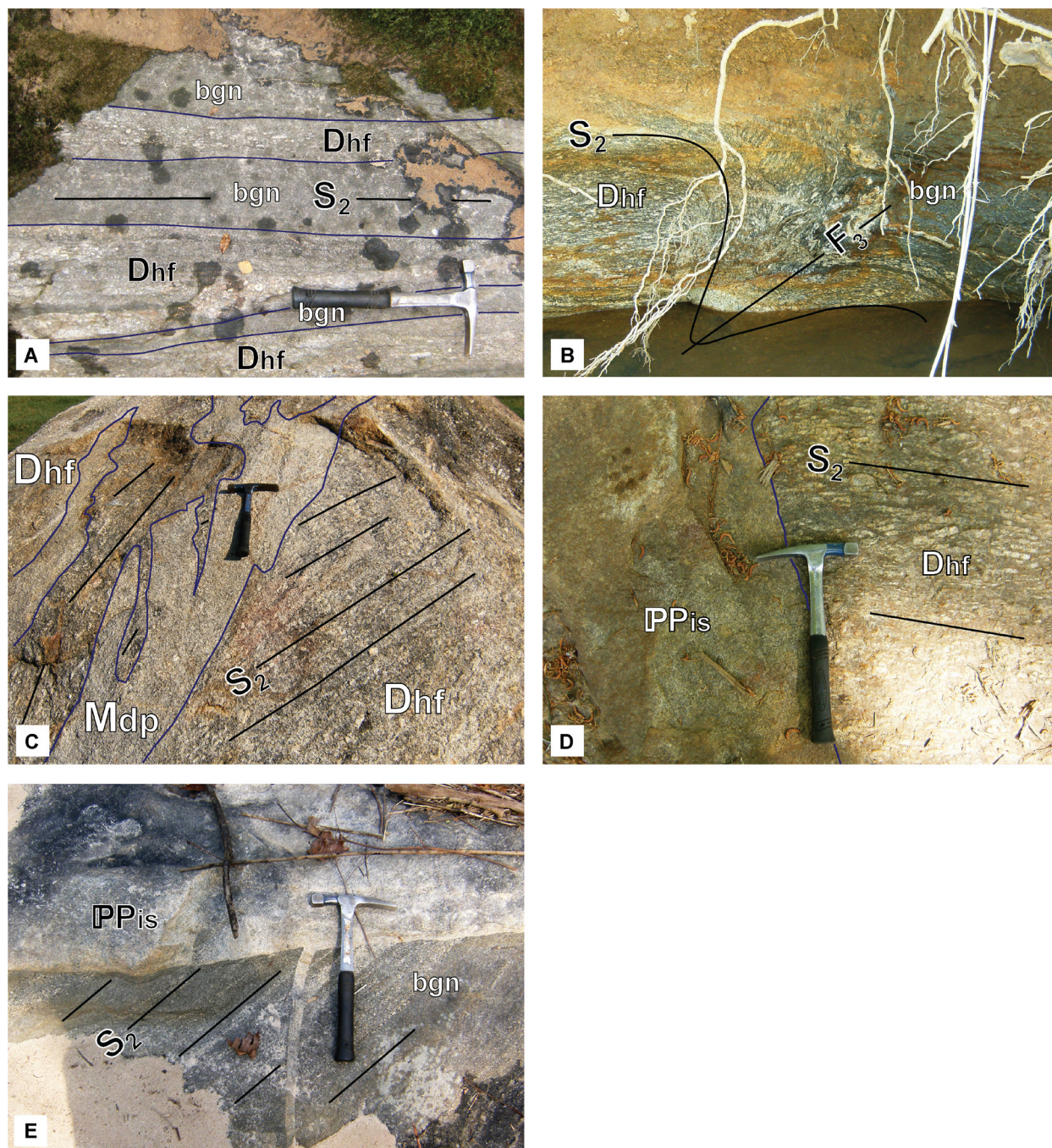


Figure 1-10: Crosscutting relationships of some of the dominant lithologies in the map area. Contacts that are difficult to see in photographs have been accented with dark blue lines. (A) Apparent interlayering of biotite paragneiss and High Falls Granite, with contacts parallel to S_2 . (B) Folded contact between biotite paragneiss and High Falls granite. Field of view ~2.5 m, view to northeast (C) Dikes of Dows Pulpit Granodiorite truncating S_2 in High Falls Granite, view to northeast. (D) Indian Springs Granodiorite truncating S_2 in High Falls Granite. (E) Indian Springs Granodiorite truncating S_2 in biotite paragneiss, view to northwest. bgn = biotite gneiss; Dhf = High Falls Granite; Mdp = Dows Pulpit Granodiorite; PPis = Indian Springs Granodiorite.

TECTONIC SYNTHESIS

The intricate tectonic history of the southern Appalachian Inner Piedmont involves two collisional orogenies that record accretion of exotic material to the eastern Laurentian margin and the formation of Pangea, followed by its eventual breakup in the Mesozoic. Details of this complex history can be elucidated from different episodes of sedimentation, deformation, metamorphism, and magmatism that comprise the defining characteristics of the Inner Piedmont. While ambiguities remain regarding the absolute timing of deformation and fabric development throughout the region, the combination of detailed geologic mapping, structural analysis, and ion-microprobe geochronology can prove useful in delimiting the timing and nature of these events, and ultimately improves our understanding of the tectonic evolution of the southern Appalachian orogen.

U-Pb geochronology of metamorphic zircon rims indicates the region underwent two distinct thermal peaks at 400-380 and 330-300 Ma, corresponding with the Acadian/Neoacadian and Alleghanian orogenies, respectively. Metasedimentary rocks throughout the map area consistently exhibit evidence of prograde metamorphism that peaked at sillimanite-grade conditions, which likely coincides with the Acadian/Neoacadian orogeny. The dominant regional foliation (S_2) developed during this event, along with the associated mineral lineation and axial planar F_2 and F_3 folds. We term this event D_2 , as the rare S_1 foliation that occurs only in amphibolite boudins was a product of D_1 . Lithologic contacts between schistose and coarser-grained metasedimentary rocks (S_0) were transposed to S_2 during this event. D_2 also involved coeval emplacement of the High Falls Granite (likely anatectic; Howard, 2012) and near ubiquitous migmatization of metasedimentary rocks. The Jackson Lake, Kinnard Creek, Box Ankle, and Ocmulgee faults likely correspond to D_2 based on fabric relationships, metamorphic grade during deformation, intensified migmatization near fault zones, and axial planar folding of fault surfaces. The development of the Rumble shear zone would also be product of D_2 based on these criteria. Timing of this event ranges from 410-370 Ma, based on ion-microprobe ages of metamorphic zircon rims, transposed contacts and concordant S_2 foliation between the High Falls Granite (407-371 Ma) and country rocks, and truncation of the High Falls Granite along the Jackson Lake fault. We attribute the high-grade Barrovian metamorphism, deformation, and magmatism associated with D_2 to the subduction of the Inner Piedmont beneath the Carolina superterrane during Acadian/Neoacadian accretion to the eastern Laurentian margin.

The Alleghanian orogeny though central Georgia is recorded by a pulse of granitic magmatism, metamorphic growth of zircon rims, and localized deformation along regional-scale shear zones. The most conspicuous manifestation of the Alleghanian orogeny in the map area is a suite of 328-301 Ma granite to granodiorite bodies (Murder Creek, Dows Pulpit, and Indian Springs) that locally contain a tectonic foliation (S_3). The development of D_3 fabric, however, is not appar-

ent in country rocks or older plutonic rocks, nor is there any evidence of an overprinting phase of Barrovian metamorphism. Nevertheless, the lack of obvious contact aureoles surrounding the granitoids, in addition to abundant metamorphic zircon growth during this time, indicate country rocks were at elevated temperatures during this event. The tectonic cause of this event is speculative, but data presented herein suggest D_3 may be related to west-directed subduction of Theic ocean crust beneath Laurentia prior to the terminal collision with Gondwana and the formation of Pangea.

Granitoids associated with D_3 are truncated by the garnet-grade Towaliga fault, which we attribute to a D_4 event. Deformation associated with D_4 appears to be localized along the Towaliga fault and similar regional-scale faults throughout the southern Appalachians (e.g., Eastern Piedmont fault system, Hatcher et al., 1977), with the development of retrograde S_4 and L_4 features restricted to the shear zones themselves. Meso- and macro-scale open, upright folds (F_4) throughout the Inner Piedmont have been correlated with this event. Displacement along regional scale fault systems during D_4 most likely marks the initial oblique collision with Gondwana, prior to the clockwise rotation of Gondwana relative to Laurentia that resulted in head-on collision in the southern Appalachians and emplacement of the Blue Ridge/Inner Piedmont megathrust sheet over the Paleozoic Laurentian platform (Hatcher, 2002).

Two late- to post-Alleghanian deformational events have been identified throughout the map area. Widespread sheared quartz veins, termed ribbon quartz mylonites, represent a late Alleghanian(?) to Middle Triassic event (D_5) (Huebner and Hatcher, 2013). D_5 fabrics include a dominantly dextral mylonitic foliation (S_5) and associated mineral lineation (L_5) that developed under middle- to lower-greenschist facies conditions, based on dynamic recrystallization textures in quartz, brittle deformation of feldspars, and ductile muscovite mica fish (Huebner and Hatcher, 2013). D_5 fabrics are overprinted by sinistral small-displacement brittle faults, including reactivation along the Towaliga fault, that coincide with Mesozoic diabase dike emplacement at ~200 Ma. This event, D_6 , marks the final breakup of Pangea, and likely coincides with the rift-to-drift transition and initial opening of the Atlantic Ocean (e.g., Withjack et al., 1998; Huebner and Hatcher, 2013).

ACKNOWLEDGMENTS

This map is a compilation of previously unpublished data (R.D. Hatcher, Jr., R. Kath), M.S. theses (B.A. Davis, C.W. Howard, T.E. West, Jr., J.R. Rehrer, in progress), Ph.D. dissertations (R.J. Hooper, M.T. Huebner, in progress), and a Georgia Geologic Survey Information Circular (D. Sneyd). Funding was provided by the grants from the National Science Foundation to RDH (EAR-7911802), USGS EDMAP Awards GO9AC00126, G11AC20114, and G12AC20116 to RDH, The University of Tennessee-Knoxville Science Alliance Center of Excellence, and The University of Tennessee Office of Research.

REFERENCES CITED

- Adams, G.I., 1926, The crystalline rocks, *in* Adams, G. I., Butts, C., Stephenson, L. W., and Cooke, W., eds., *Geology of Alabama: Geological Society of Alabama Special Report 14*, p. 25-40.
- Altamura, R.J., 2001, *Geology of the Lantern Hill silicified fault zone near North Stonington, Connecticut, with integrated geochemistry and geochronology [PhD dissertation]: State College, Pennsylvania State University*, 256 p.
- Atkins, R.L., and Lineback, J.A., 1992, Structural relations, origin and emplacement of granitic rocks in the Cedar Rock Complex, Georgia piedmont: *Georgia Geologic Survey Bulletin 115*, 40 p.
- Babaie, H.A., Hadizadeh, J., Babaei, A., and Mohammad Ghazi, A., 1991, Timing and temperature of cataclastic deformation along segments of the Towaliga fault zone, western Georgia, U.S.A.: *Journal of Structural Geology*, v. 13, p. 579-586.
- Bentley, R.D., and Neathery, T.N. 1970. *Geology of the Brevard zone and related rocks of the Inner Piedmont of Alabama: Alabama Geological Society, Eighth Annual Field Trip Guidebook*, 119 p.
- Berg, C.A., 2012, Detailed petrographic and microstructural analysis of sheared biotite gneiss within the Kinnard Creek fault, Jasper County, Georgia: *Geological Society of America Abstracts with Programs*, v. 44, no. 4, p. 29.
- Bier, S.E., 2001, *Geology of the southeastern South Mountains, North Carolina [M.S. thesis]: Knoxville, University of Tennessee*, 162 p.
- Bier, S.E., Bream, B. R., and Giorgis, S. D., 2002, Inner Piedmont stratigraphy, metamorphism, and deformation in the Marion-South Mountains area, North Carolina, *in* Hatcher, R. D., Jr., and Bream, B. R., eds., *Inner Piedmont geology in the South Mountains-Blue Ridge Foothills and the southwestern Brushy Mountains, central-western North Carolina: Carolina Geological Society Guidebook*, p. 65-100.
- Bream, B.R., 1999, *Geology of the Glenwood and Sugar Hill quadrangles, North Carolina, and the structure of the northeast end of the Henderson Gneiss [M.S. thesis]: Knoxville, University of Tennessee*, 155 p.
- Bream, B.R., 2003, *Tectonic implications of geochronology and geochemistry of para- and orthogneisses from the southern Appalachian crystalline core [Ph.D. dissertation]: Knoxville, University of Tennessee*, 262 p.
- Bream, B.R., Hatcher, R. D., Jr., Miller, C. F., and Fullagar, P. D., 2001, Geochemistry and provenance of Inner Piedmont paragneisses, NC and SC: Evidence for an internal terrane boundary?: *Geological Society of America Abstracts with Programs*, v. 33, no. 2, p. 65.

- Bream, B.R., Hatcher, R.D., Jr., Miller, C.F., and Fullagar, P.D., 2004, Detrital zircon ages and Nd isotopic data from the southern Appalachian crystalline core, Georgia, South Carolina, North Carolina, and Tennessee: New provenance constraints for part of the Laurentian margin, *in* Tollo, R.P., Corriveau, L., McLelland, J., and Bartholomew, M.J., eds., Proterozoic tectonic evolution of the Grenville orogen in North America: Boulder, Colorado, Geological Society of America Memoir 197, p. 459-475.
- Byars, H.E., 2010, Tectonic evolution of the west-central portion of the Newton window, North Carolina Inner Piedmont: Timing and implications for the emplacement of the Paleozoic Vale charnockite, Walker Top Granite, and mafic complexes [M.S. thesis]: Knoxville, University of Tennessee, 248 p.
- Chaumba, J.B., 2010a, The Hammett Grove meta-igneous suite, South Carolina: Bulk-rock, mineral composition, hydrogen, and oxygen isotope data from metagabbros: Geological Society of America Abstracts with Programs, v. 42, no. 1, p. 164.
- Chaumba, J.B., 2010b, Island arc origin for the Gladesville and associated bodies in the Carolina superterrane, central Georgia: Geological Society of America Abstracts with Programs, v. 42, no. 5, p. 307.
- Clarke, J.W., 1952, Geology and mineral resources of the Thomaston Quadrangle, Georgia: Georgia Geological Survey Bulletin 59, 99 p.
- Curl, D.C., 1998, Stratigraphy and structure of Wellford and Reidville quadrangles in part of the eastern Inner Piedmont, near Spartanburg, South Carolina [M.S. thesis]: Knoxville, University of Tennessee, 129 p.
- Dallmeyer, R.D., 1978 $^{40}\text{Ar}/^{39}\text{Ar}$ incremental-release ages of hornblende and biotite across the Georgia Inner Piedmont: Their bearing on late Paleozoic-early Mesozoic tectonothermal history: American Journal of Science, v. 278, p. 124-149.
- Dallmeyer, R.D., 1989, Late Paleozoic thermal evolution of crystalline terranes within portions of the U.S., Appalachian orogen, *in* Hatcher, R. D., Jr., Thomas, W. A., and Viele, G. W., editors, The Appalachian-Ouachita orogen in the United States: Boulder, Colorado, Geological Society of America, The Geology of North America F-2, p. 417-444.
- Davis, B.A., 2010, Tectonic evolution of the southern Appalachian Inner Piedmont: Identification and interpretation of crustal features from aeromagnetic data and detailed geologic mapping in central Georgia [M.S. thesis]: Knoxville, University of Tennessee, 222 p.
- Davis, G.J., 1980, The southwestern extension of the Middleton-Lowndesville cataclastic zone in the Greensboro, Georgia area and its regional implications [M.S. thesis]: Athens, University of Georgia, 151 p.

- Dennis, A.J., and Wright, J.E., 1997, Middle and late Paleozoic monazite U-Pb ages, Inner Piedmont, South Carolina: Geological Society of America Abstracts with Programs, v. 29, no. 3, p. 12.
- Fountain, R.C., 1961, The geology of the northwestern portion of Jasper County, Georgia [M.S. thesis]: Atlanta, Emory University, 65 p.
- Gardner, C.H., 1961, The geology of central Newton County, Georgia [M.S. thesis]: Atlanta, Emory University, 53 p.
- Garihan, J.M., Preddy, M.S., and Ranson, W.A., 1993, Summary of mid-Mesozoic brittle faulting in the Inner Piedmont and nearby Charlotte belt of the Carolinas, *in* Hatcher, R.D., Jr., and Davis, T.L., eds., Studies of Inner Piedmont geology with a focus on the Columbus promontory: Carolina Geological Society Field Trip Guidebook, p. 55-66.
- Gatewood, M.P., 2007, Structure and tectonics of the northeastern Inner Piedmont from detailed geologic mapping, geochronologic, geochemical, and petrologic studies with macro-, meso-, and microstructural analyses of ductile fault zones [M.S. thesis]: Knoxville, University of Tennessee, 279 p.
- Gilliam, W.G., 2010, Structural and metamorphic evolution of the west-central Newton window eastern Inner Piedmont, North Carolina [M.S. thesis]: Knoxville, University of Tennessee, 142 p.
- Giorgis, S.D., 1999, Inner Piedmont geology of the northwestern South Mountains near Morganton, North Carolina [M.S. thesis]: Knoxville, University of Tennessee, 191 p.
- Goldsmith, R., Milton, D. J., and Horton, J. W., Jr., 1988, Geologic map of the Charlotte 1-degree x 2-degree quadrangle, North Carolina and South Carolina: U.S. Geological Survey Map I-1251-E, scale 1:250,000.
- Griffin, V.S., Jr., 1971, The Inner Piedmont belt of the southern crystalline Appalachians: Geological Society of America Bulletin, v. 82, p. 1885-1898.
- Griffin, V.S., Jr., 1978, Detailed analysis of tectonic levels in the Appalachian Piedmont: Geologische Rundschau, v. 67, p. 179-201.
- Hadizadeh, J., Babaie, H.A., and Babaei, A., 1991, Development of interlaced mylonites, cataclastic sites and breccias: example from the Towaliga fault, south central Appalachians: Journal of Structural Geology, v. 13, p. 63-70.
- Hames, W.E., Renne, P.R., and Ruppel, C., 2000, New evidence for geologically instantaneous emplacement of earliest Jurassic Central Atlantic magmatic province basalts on the North American margin: Geology, v. 28, p. 859-862.
- Hatcher, R.D., Jr., 1971, Geology of Rabun and Habersham Counties, Georgia: A reconnaissance study: Georgia Department of Mines, Mining, and Geology Bulletin 83, 48 p.

- Hatcher, R.D., Jr., 2002, An Inner Piedmont primer, *in* Hatcher, R. D., Jr., and Bream, B. R., eds., Inner Piedmont geology in the South Mountains-Blue Ridge Foothills and the southwestern Brushy Mountains, central-western North Carolina: Carolina Geological Society Guidebook, p. 1-18.
- Hatcher, R.D. Jr., 1993, Perspective on the tectonics of the Inner Piedmont, southern Appalachians, *in* Hatcher, R.D., Jr., and Davis, T.L., eds., Studies of Inner Piedmont geology with a focus on the Columbus Promontory: North Carolina Geological Survey, Carolina Geological Society guidebook, p. 17-43.
- Hatcher, R. D., Jr., 2004, Southern Appalachian Crustal Transect: Overview, *in* Merschat, A. J., and Hatcher, R. D., Jr., editors, Trans Appalachians Internides Geotraverse: 17th International Basement Tectonics Association Field Trip Guidebook, p. 1-12.
- Hatcher, R.D., Jr., and Merschat, A.J., 2006, The Appalachian Inner Piedmont: An exhumed strike-parallel, tectonically forced orogenic channel, *in* Law, R.D., Searle, M., and Godin, L., eds., Channel flow, ductile extrusion, and exhumation of lower-mid crust in continental collision zones: Geological Society of London Special Publication 268, p. 517-540.
- Hatcher, R.D., Jr., Bream, B.R., and Merschat, A.J., 2007, Tectonic map of the southern and central Appalachians: A tale of three orogens and a complete Wilson Cycle, *in* Hatcher, R.D., Jr., Carlson, M.P., McBride, J.H., and Martínez Catalán, J.R., eds., The 4D Framework of Continental Crust: Boulder, Colorado, Geological Society of America Memoir 200, p. 595-632.
- Hatcher, R.D., Jr., Howell, D.E., and Talwani, P., 1977, Eastern Piedmont fault system: Speculations on its extent: *Geology*, v. 5, p. 636-640.
- Heatherington, A.L., Mueller, P.A., Kamenov, G., Steltenpohl, M.G., Hanley, T.B., and Wooden, J.L., 2006, Pine Mountain terrane: Geochemistry and geochronology of basement gneisses and xenoliths: *Geological Society of America Abstracts with Programs*, v. 38, no. 3, p. 63.
- Herrmann, L.A., 1954, Geology of the Stone Mountain-Lithonia mining district, Georgia: *Georgia Geological Survey Bulletin* 61, 139 p.
- Hewitt, D.F., and Crickmay, G.W., 1937, The Warm Springs of Georgia, their geologic relations and origin: a summary report: *U.S. Geological Survey Water Supply Paper* 819, 40 p.
- Heyn, T., 1984, Stratigraphic and structural relationships along the southwestern flank of the Sauratown Mountains anticlinorium [M.S. thesis]: Columbia, University of South Carolina, 192 p.
- Hibbard, J.P., Miller, B.V., Hames, W.E., Standard, I.D., Allen, J.S., Lavallee, S.B., and Boland, I.B., 2012, Kinematics, U-Pb geochronology, and ⁴⁰Ar/³⁹Ar thermochronology of the Gold Hill shear zone, North Carolina: The Cherokee orogeny in Carolina, southern Appalachians: *Geological Society of America Bulletin*, v. 124, p. 643-656.

- Higgins, M.W., Atkins, R.L., Crawford, T.J., Crawford, R.F., III, Brooks, R., and Cook, R.B., 1988, The structure, stratigraphy, tectonostratigraphy and evolution of the southernmost part of the Appalachian orogen: U.S. Geological Survey Professional Paper 1475, 173 p.
- Hooper, R.J., 1986, Geologic studies at the east end of the Pine Mountain window and adjacent Piedmont, central Georgia [Ph.D. dissertation]: Columbia, University of South Carolina, 322 p.
- Hooper, R.J., and Hatcher, R.D., Jr., 1988a, Mylonites from the Towaliga fault zone, central Georgia: products of heterogeneous non-coaxial deformation: *Tectonophysics*, v. 152, p. 1-17.
- Hooper, R.J., and Hatcher, R.D., Jr., 1988b, Pine Mountain terrane, a complex window in the Georgia and Alabama Piedmont; evidence from the eastern termination: *Geology*, v. 16, p. 307-310.
- Hooper, R.J., and Hatcher, R.D., Jr., 1989, The geology of the east end of the Pine Mountain window and adjacent Piedmont, central Georgia: Atlanta, Georgia Geological Society, Premeeting Field Trip Guide for Southeastern Section Geological Society of America, 37 p.
- Hooper, R.J., Hatcher, R.D., Jr., Troyer, P.K., Dawson, R.J., and Redmond, C.G., 1997, The character of the Avalon terrane and its boundary with the Piedmont terrane in central Georgia, *in* Glover, L., III, and Gates, A.E., eds., *Central and Southern Appalachian Sutures: Results of the EDGE Project and Related Studies*: Boulder, Colorado, Geological Society of America Special Paper 314, p. 1-14.
- Hopson, J.L., and Hatcher, R.D., Jr., 1988, Structural and stratigraphic setting of the Alto allochthon, northeast Georgia: *Geological Society of America Bulletin*, v. 100, p. 339-350.
- Howard, C.W., 2012, Investigating the evolution of two southern Appalachian terrane boundaries and a plutonic complex: Tectonic implications of structural, geochemical, and geochronologic studies in the central Georgia Inner Piedmont [M.S. thesis]: Knoxville, University of Tennessee, 222 p.
- Huebner, M.T., and Hatcher, R.D., Jr., 2011, Evidence for sinistral Mesozoic inversion of the dextral Alleghanian Towaliga fault, central Georgia, *in* Huebner, M.T., and Hatcher, R.D., Jr., eds., *The Geology of the Inner Piedmont at the Northeast End of the Pine Mountain Window*: Carrollton, Georgia Geological Society, 46th Annual Field Trip Guidebook, p. 55-72.
- Huebner, M.T., and Hatcher, R.D., Jr., 2013, Polyphase reactivation history of the Towaliga fault, central Georgia: Implications regarding the amalgamation and breakup of Pangea: *Journal of Geology*, v. 121, p. 75-90.
- Huebner, M.T., Wooden, J.L., and Hatcher, R.D., Jr., 2010, A terrane boundary in the central Georgia (USA) Inner Piedmont confirmed using new U-Pb SHRIMP ages of granitic rocks: *Geological Society of America Abstracts with Programs*, v. 42, no. 5, p. 196.

- Huebner, M.T., Hatcher, R.D., Jr., and Howard, C.W., 2011, Geologic overview of the Inner Piedmont at the northeast end of the Pine Mountain Window, *in* Huebner, M.T., and Hatcher, R.D., Jr., eds., *The Geology of the Inner Piedmont at the Northeast End of the Pine Mountain Window*: Carrollton, Georgia Geological Society, 46th Annual Field Trip Guidebook, p. 1-26.
- Huebner, M.T., Hatcher, R.D., Jr., and Mersch, A.J., Confirmation of the southwest continuation of the Cat Square terrane, southern Appalachian Inner Piedmont, with implications for middle Paleozoic collisional orogenesis: *American Journal of Science*, in review.
- Jones, D.D., Jr., 1970, Petrofabric and movement study of faults in Newton and Walton Counties, Georgia [M.S. thesis]: Atlanta, Emory University, 28 p.
- Kalbas, J.L., 2002, Geology of part of the southwestern Brushy Mountains, Inner Piedmont, North Carolina, and the geochemistry of western Inner Piedmont migmatite [M.S. thesis]: Knoxville, University of Tennessee, 206 p.
- King, P. B., 1955, A geologic section across the southern Appalachians: An outline to the geology in the segment in Tennessee, North Carolina, and South Carolina, *in* Russell, R. J., editor, *Guides to Southeastern Geology*: New York, Geological Society of America, p. 332–373.
- Mapes, R.W., 2002, Geochemistry and geochronology of mid-Paleozoic granitic plutonism in the southern Appalachian Piedmont terrane, North Carolina-South Carolina-Georgia [M.S. thesis]: Nashville, Vanderbilt University, 150 p.
- Matthews, V., 1976, Geology and petrology of the pegmatite district in southwestern Jasper County, Georgia [M.S. thesis]: Athens, University of Georgia, 68 p.
- McConnell, K.I., 1989, Geology and geochronology of the Sauratown Mountains anticlinorium, northwestern North Carolina [Ph.D. dissertation]: Columbia, University of South Carolina, 232 p.
- Mersch, A.J., 2003, Inner Piedmont tectonics in the southwestern Brushy Mountains, North Carolina: Field and laboratory data revealing 3-D crustal flow and sillimanite I and II metamorphism [M.S. thesis]: Knoxville, University of Tennessee, 198 p.
- Mersch, A.J., 2009, Assembling the Blue Ridge and Inner Piedmont: Insights into the nature and timing of terrane accretion in the southern Appalachian orogen from geologic mapping, stratigraphy, kinematic analysis, petrology, geochemistry, and modern geochronology [Ph.D. dissertation]: Knoxville, University of Tennessee, 455 p.
- Mersch, A.J., and Hatcher, R.D., Jr., 2007, The Cat Square terrane: Possible Siluro-Devonian remnant ocean basin in the Inner Piedmont, southern Appalachians, USA, *in* Hatcher, R.D., Jr., Carlson, M.P., McBride, J.H., and Martínez Catalán, J.R., eds., *4-D Framework of Continental Crust*: Boulder, Colorado, Geological Society of America Memoir 197, p. 553-565.

- Merschat, A.J., Hatcher, R.D., Jr., and Davis, T.L., 2005, The northern Inner Piedmont, southern Appalachians, USA: kinematics of transpression and southwest-directed mid-crustal flow: *Journal of Structural Geology*, 27, 1252-1281.
- Merschat, A.J., Hatcher, R.D., Jr., Byars, H.E., and Gilliam, W.G., 2008, Inner Piedmont Geotransverse from the Brushy Mountains to Lincolnton, North Carolina: Architecture of the Cat Square and Tugaloo terranes: Geological Society of America Southeastern Section, Field Trip Guidebook, 64 p.
- Merschat, A.J., Hatcher, R.D., Jr., Bream, B.R., Miller, C.F., Byars, H.E., Gatewood, M.P., and Wooden, J.L., 2010, Detrital zircon geochronology and provenance of southern Appalachian Blue Ridge and Inner Piedmont crystalline terranes, *in* Tollo, R.P., Bartholomew, M.J., Hibbard, J.P., and Karabinos, P.M., eds., *From Rodinia to Pangea: The Lithotectonic Record of the Appalachian Region*: Geological Society of America Memoir 206, p. 661-699.
- Miller, C.F., Hatcher, R.D., Jr., Ayers, J.C., Coath, C.D., and Harrison, T.M., 2000, Age and zircon inheritance of eastern Blue Ridge plutons, southwestern North Carolina and northeastern Georgia, with implications for magma history and evolution of the southern Appalachian orogen: *American Journal of Science*, v. 300, p. 142-172.
- Mirante, D.C., and Patiño-Douce, A.E., 2000, Melting and migmatization in the southern Appalachian Inner Piedmont of northeast Georgia; the Athens gneiss: *Geological Society of America Abstracts with Programs*, v. 33, no. 7, p. 297.
- Mittwede, S.K., 1989, The Hammett Grove meta-igneous suite; A possible ophiolite in the northwestern South Carolina Piedmont: *Geological Society of America Special Paper* 231, p. 45-62.
- Mittwede, S.K., Ødegård, M., and Sharp, W.E., 1987, Major chemical characteristics of the Hammett Grove meta-igneous suite, northwestern South Carolina: *Southeastern Geology*, v. 28, p. 49-63.
- Mueller, P., Heatherington, A., Foster, D., and Wooden, J., 2011, Alleghanian granites of the southern Appalachian orogen: Keys to Pangean reconstructions, *in* Huebner, M.T., and Hatcher, R.D., Jr., eds., *The Geology of the Inner Piedmont at the Northeast End of the Pine Mountain Window*: Carrollton, Georgia Geological Society, 46th Annual Field Trip Guidebook, p. 39-47.
- Nelson, A.E., Horton, J.W., Jr., and Clarke, J.W., 1998, Geologic map of the Greenville 1-degree x 2-degree quadrangle, Georgia, South Carolina and North Carolina: U.S. Geological Survey Map I-1275, scale 1:250,000.
- Nomade, S., Knight, K.B., Beutel, E., Renne, P.R., Verati, C., Féraud, G., Marzoli, A., Youbi, N., and Bertrand, H., 2007, Chronology of the Central Atlantic Magmatic Province: Implications

- for the Central Atlantic rifting processes and the Triassic-Jurassic biotic crisis: *Palaeogeography, Palaeoclimatology, Palaeoecology*, v. 244, p. 326-344.
- Paterson, S.R., Vernon, R.H., and Tobisch, O.T., 1989, A review of criteria for the identification of magmatic and tectonic foliations in granitoids: *Journal of Structural Geology*, v. 11, p. 349-363.
- Privett, D.R., 1984, The Turnersburg intrusive: Petrogenesis of a metamorphosed Alpine ultramafite in the eastern Inner Piedmont Iredell County, North Carolina: *Southeastern Geology*, v. 25, p. 55-60.
- Rankin, D.W., 1970, Stratigraphy and structure of Precambrian rocks in northwestern North Carolina, *in* Fisher, G.W., Pettijohn, F.J., Reed, J.C., Jr., and Weaver, K.N., eds., *Studies of Appalachian Geology: Central and Southern*: John Wiley and Sons, Inc., p. 227-245.
- Reade, E.H., Jr., 1960, The geology of a portion of Newton and Walton Counties, Georgia [M.S. thesis]: Atlanta, Emory University, 63 p.
- Robinson, J.C., 1989, A brittle fracture analysis of the Flint Hill fault zone, southeastern NH [M.S. thesis]: Amherst, University of Massachusetts, 90 p.
- Schultz, R.S., 1961, The geology of northwestern Newton and southeastern Walton Counties, Georgia [M.S. thesis]: Atlanta, Emory University, 46 p.
- Sears, J.W., Cook, R.B., and Brown, D.E., 1981, Tectonic evolution of the western part of the Pine Mountain window and adjacent Inner Piedmont province, *in* Sears, J.W., ed., *Contrasts in tectonic style between the Inner Piedmont terrane and the Pine Mountain window*: Alabama Geological Society, 18th Annual Field Trip Guidebook, p. 1-13.
- Secor, D.T., Jr., Snoke, A.W., and Dallmeyer, R.D., 1986, Character of the Alleghanian orogeny in the southern Appalachians: Part III. Regional Tectonics: *Geological Society of America Bulletin*, v. 97, p. 1345-1353.
- Sinha, A.K., Thomas, W.A., Hatcher, R.D., Jr., and Harrison, T.M., 2012, Geodynamic evolution of the central Appalachian orogen: Geochronology and compositional diversity of magmatism from Ordovician through Devonian: *American Journal of Science*, v. 312, p. 907-966.
- Sneyd, D., 1995, Geology of the Barnesville Hydrologic Research Site, Lamar County, Georgia: Georgia Geologic Survey Information Circular 98, 27 p.
- Steltenpohl, M.G., 1988, Kinematics of the Towaliga, Bartletts Ferry, and Goat Rock fault zones, Alabama: the late Paleozoic dextral shear system in the southernmost Appalachians: *Geology*, v. 16, p. 852-855.
- Steltenpohl, M.G., Hatcher, R.D., Jr., Mueller, P.A., Heatherington, A.L., and Wooden, J.L., 2010, Geologic history of the Pine Mountain window, Alabama and Georgia: Insights from a new geologic map and U-Pb isotopic dates, *in* Tollo, R.P., Bartholomew, M.J., Hibbard, J.P.,

- and Karabinos, P.M., eds., From Rodinia to Pangea: The Lithotectonic Record of the Appalachian Region: Geological Society of America Memoir 206, p. 837-857.
- Stose, A.J., and Stose, G.W., 1957, Geology and mineral resources of the Gossan Lead district and adjacent areas: Virginia Division of Mineral Resources Bulletin 72, 233 p.
- Streckeisen, A., 1974, Classification and nomenclature of plutonic rocks recommendations of the IUGS subcommission on the systematics of igneous rocks: International Journal of Earth Sciences, v. 63, no. 2, p. 773-786.
- Student, J.J., and Sinha, A.K., 1992, Carboniferous U-Pb ages of zircons from the Box Ankle and Ocmulgee faults, central Georgia: implications for accretionary models: Geological Society of America Abstracts with Programs, v. 24, no. 2, p. 69.
- Troyer, P.K., 1991, Geology of the Rock Eagle complex, central Georgia [M.S. thesis]: Tampa, University of South Florida, 59 p.
- Tull, J. F., 1978, Structural development of the Alabama Piedmont northwest of the Brevard zone: American Journal of Science, v. 278, p. 442-460.
- Wells, D.E., 1982, Geology and petrochemistry of the Rock Branch quadrangle, Elbert County, Georgia [M.S. thesis]: Athens, University of Georgia, 163 p.
- West, T.E., Jr., 1994, Field evidence that the Appalachian Décollement is exposed in central Georgia at the east end of the Pine Mountain terrane [M.S. thesis]: Columbia, University of South Carolina, 26 p.
- Williams, S.T., 2000, Structure, stratigraphy, and migmatization in the southwestern South Mountains, North Carolina [M.S. thesis]: Knoxville, University of Tennessee, 111 p.
- Wilson, C.G., 2006, Origin and tectonic evolution of the southern Appalachian Neoacadian crystalline core: Evidence from the geology of the Gilreath 7.5-minute quadrangle, North Carolina [M.S. thesis]: Knoxville, University of Tennessee, 200 p.
- Withjack, M.O., Schlische, R.W., and Olsen, P.E., 1998, Diachronous rifting, drifting, and inversion on the passive margin of central eastern North America: an analog for other passive margins: American Association of Petroleum Geologists Bulletin, v. 82, p. 817-835.

Chapter II

Confirmation of the southwest continuation of the Cat Square terrane, southern Appalachian Inner Piedmont, with implications for middle Paleozoic collisional orogenesis

Chapter II uses a combination of detailed geologic mapping, structural analysis, metamorphic and igneous petrology, geochemistry, and U-Pb SHRIMP geochronology to test the hypothesis that the Cat Square terrane continues through central Georgia. My coauthors are Robert D. Hatcher, Jr., and Arthur J. Merschat. This manuscript was submitted to the *American Journal of Science* in August, 2013, and at the time of this writing, is under review. My contributions include sample and data collection, compilation of geochronologic and geochemical data from the northern Inner Piedmont, synthesis and interpretation of the data, and the majority of the writing. The use of the term “we” and “our” in the text refers to the coauthors and myself.

ABSTRACT

The southern Appalachian Inner Piedmont is a vast area of exposed sillimanite-grade rock, bound to the west by the Brevard fault zone, and to the east by the Central Piedmont suture. It consists of two lithotectonic terranes, separated by the Brindle Creek fault, which juxtaposes the Cat Square terrane (eastern Inner Piedmont) above the Tugaloo terrane (western Inner Piedmont) in the northern portion of the Inner Piedmont. Peak metamorphism (upper amphibolite facies), deformation, and a pulse of magmatism occurred from Devonian into Mississippian time, likely a result of accretion of the Carolina superterrane and associated subduction of the eastern Laurentian margin. The entire Inner Piedmont may have flowed as a mid-crustal orogenic channel during this event, buttressed by the Brevard fault zone, during southwest-directed lateral extrusion related to diachronous collisional orogenesis.

Inner Piedmont terranes are distinguished by detrital zircon provenance, granitoid ages, and lithologic differences; deformation and peak metamorphic conditions occurred from the Devonian into the Mississippian in both terranes. The primary characteristic that led to the distinction of the Cat Square as a separate terrane is the distinctive detrital zircon signature, which includes a dominant suite of Ordovician-Silurian zircons, with relatively muted components representing mixed peri-Gondwanan (Carolina superterrane) and Laurentian provenance. This contrasts with provenance of Tugaloo terrane metasedimentary rocks, which indicates solely Laurentian (primarily Grenville) source. Cat Square terrane granitoids are also distinctly younger than those in the Tugaloo terrane (407-355 Ma and 450-440 Ma, respectively), providing additional criteria used in the distinction of the two terranes. Carboniferous and Permian granitoids occur in both terranes and appear to be more abundant in Georgia and South Carolina. Detailed geologic mapping, U-Pb zircon geochronology and whole-rock geochemical analyses were conducted in the central Georgia Inner Piedmont to test the hypothesis that a prominent aeromagnetic lineament represents the southwest continuation of the Brindle Creek fault (terrane boundary).

In the central Georgia Inner Piedmont, the Jackson Lake fault (Brindle Creek?) truncates lithologically distinct granitoids and metasedimentary units, and roughly corresponds with the

identified aeromagnetic lineament. SHRIMP geochronology reveals Ordovician-Silurian granitoids (~450 Ma) exclusively occur northwest of the fault, while Devonian (406-372 Ma) granitoids only occur southeast of the fault, similar to the characteristics of granitoids on either side of the Brindle Creek fault in the northern Inner Piedmont. Detrital zircon signatures from samples southeast of the Jackson Lake fault, however, reveal dominant Grenville provenance, limited peri-Gondwanan source, and no Ordovician-Silurian signature. We interpret these rocks to represent the southwest extension of the Cat Square terrane, and suggest that provenance patterns provide key insight regarding the paleogeographic position of the Inner Piedmont during Silurian-Devonian deposition in the Cat Square basin. The Ordovician-Silurian source material was likely derived from plutonic rocks in the Blue Ridge of southern Virginia, and palinspastic restoration of ~250 km along the Brevard fault zone places the northern Inner Piedmont adjacent to the possible source area, while the Georgia Inner Piedmont would be separated from the source by the Virginia promontory. The Cat Square terrane likely represents the accretionary complex that developed in front of the advancing Carolina superterrane and was subducted to mid-crustal depths during accretion.

INTRODUCTION

Terrane analysis has proven useful in delineating the accretionary history of cratonic margins through time, and has been applied to many orogens throughout the world (for example, Coney and others, 1980; Williams and Hatcher, 1982; Ramos and others, 1986; DeCelles and others, 2000). A lithotectonic terrane can be defined as a discrete, fault-bounded, allochthonous fragment of oceanic or continental material with a contrasting tectonic (magmatic, depositional, etc.) history relative to adjacent terranes, ultimately accreted to a craton at an active plate margin. The term ‘suspect terrane’ was first used by Coney and others (1980) to describe aspects of the Cordilleran margin of North America, and deemed terranes suspect based on questionable paleogeographic origin that may not have been along the cratonic margin. Williams and Hatcher (1982) were first to apply terrane analysis to the Appalachian orogen, and identified numerous terranes as suspect, some of which have since been acquitted (Hatcher, 2001a). Because of the internal homogeneity and regional context of lithotectonic terranes, the application of terrane analysis to orogens worldwide, specifically the relationships between terranes, has yielded vital clues regarding tectonic accretionary history along cratonic margins: the southern Appalachians are no exception.

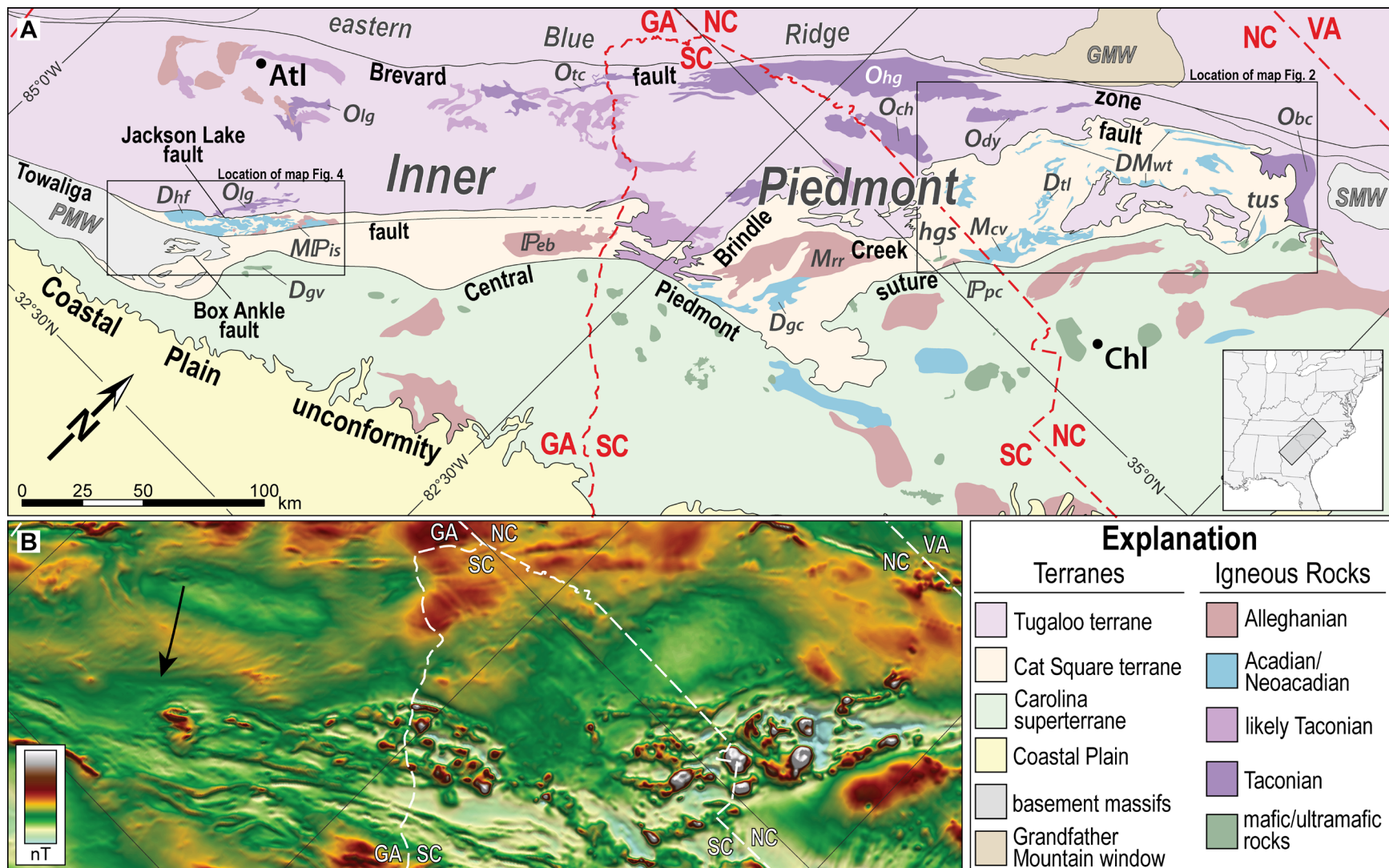
While the late Paleozoic history of southern Appalachian orogenesis is generally agreed upon by most workers, timing and kinematics of earlier orogenic activity in the outboard Laurentian and exotic terranes of the southern Appalachians remain a subject of debate (for example, Hibbard, 2000; Merschat and others, 2005). Although the primary objective of this study focuses

on the Inner Piedmont, new data reveal insight regarding the accretionary history of the exotic Carolina superterrane and high-grade regional metamorphism, which impact tectonic models of southern Appalachian orogenesis. We provide a viable, testable tectonic model based on new and compiled geochronologic and geochemical data from the Inner Piedmont.

The southern Appalachian Inner Piedmont is a vast area of exposed sillimanite-grade rock, bound to the west by the Brevard fault zone, and to the east by the Central Piedmont suture. The Inner Piedmont covers a broad area along orogenic strike from North Carolina into Alabama, and consists of two distinct lithotectonic terranes: the Tugaloo (west) and Cat Square (east) terranes, separated by the Brindle Creek fault (Bream, ms, 2003; Merschhat and Hatcher, 2007) (Fig. 2-1). The terrane distinction is primarily based on the unique detrital zircon suite revealed in Cat Square terrane metasedimentary rocks, which includes Laurentian, peri-Gondwanan, and Ordovician-Silurian (480-425 Ma) source material of Laurentian affinity (Merschhat and others, 2010; Sinha and others, 2012). Differences in recognizable stratigraphy, in addition to a distinct partitioning of granitoid ages, have also been used to discriminate between the two terranes (Merschhat and Hatcher, 2007). Furthermore, small fragments of continental basement occur throughout the Tugaloo terrane (Heyn, ms, 1984; McConnell, ms, 1990; Fullagar, 1997; Merschhat, ms, 2009); to date, none have been found in the Cat Square terrane.

Initial recognition of the Brindle Creek fault as a terrane boundary was a product of detailed geologic mapping projects and detrital zircon analyses conducted in the North Carolina Inner Piedmont (Giorgis, ms, 1999; Williams, ms, 2000; Bier, ms, 2001; Kalbas, ms, 2002; Bream, ms, 2003; Merschhat, ms, 2003; Wilson, ms, 2006; Gatewood, ms, 2007; Byars, ms, 2010; Gilliam, ms, 2010). Hatcher and others (2007) interpreted a prominent aeromagnetic lineament that truncates a suite of curved anomalies to represent the southwest continuation of the Brindle Creek fault through central Georgia, ultimately truncating against the Alleghanian Towaliga fault (Fig. 2-1B). Detailed geologic mapping in the vicinity of the aeromagnetic lineament has revealed a high-grade ductile fault, termed the Jackson Lake fault, and based on evidence presented herein, we suggest is the southwestern extension of the Brindle Creek fault and terrane boundary. Criteria used to test this hypothesis include: 1) identification of a high-grade fault that separates distinct lithologic packages; 2) a marked disparity in detrital zircon suites relative to this fault; 3) partitioning of granitoid ages on either side of the fault; and 4) the presence or absence of Grenville basement. U-Pb SHRIMP geochronologic analyses of zircon from igneous and metasedimentary rocks were employed as the primary test of this hypothesis, and whole-rock geochemical analyses of granitic rocks were also used to compare and contrast geochemical signatures of felsic magmatism between the study areas in the Carolina and central Georgia portions of the Inner Piedmont. Additional geochemical data better constrain the petrogenesis of igneous rocks throughout the Inner Piedmont, which in turn provides additional clues to the tectonic history

Figure 2-1: (A) Simplified lithotectonic map of the southern Appalachian internides (after Hatcher and others, 2007), with inset showing geographic location. (B) Aeromagnetic map of the same geographic extent, with black arrow pointing to the strong lineament interpreted to represent the southwest continuation of the Brindle Creek fault. Atl = Atlanta; Chl = Charlotte; Dgc = Gray Court granite; Dgv = Gladesville Gabbro; Dhf = High Falls Granite; Dtl = Toluca Granite; DMwt = Walker Top Granite; Mcv = Cherryville granite; Mrr = Reedy River granite; MPis = Indian Springs Granodiorite; Obc = Brooks Crossroads granite; Och = Caesar's Head Granite; Ody = Dysartsville Tonalite; Ohg = Henderson Gneiss; Olg = Lithonia Gneiss; Otc = Toccoa granite; Ppc = Pacolet granite; hgs = Hammet Grove Ultramafic Suite; tus = Turnersburg Ultramafic Suite; GMW = Grandfather Mountain window; PMW = Pine Mountain window; SMW = Sauratown Mountains window.



of the southern Appalachians through the early and middle Paleozoic. Understanding the depositional, magmatic, metamorphic, deformational, and kinematic history of the Inner Piedmont terranes is paramount to unraveling the nature of Paleozoic orogenesis in the southern Appalachians. Several mafic plutonic rocks southeast of the Ocmulgee fault (central Piedmont suture) were also dated in this study to further understand timing of magmatism in the adjacent exotic terrane.

GEOLOGIC SETTING

The Inner Piedmont has long been distinguished from surrounding masses of rock by its high metamorphic grade and contrasting structural style, which consists of shallow-dipping foliation, map-scale sheath folds, and a regional curved mineral stretching lineation pattern (for example, King, 1955; Bentley and Neathery, 1970; Griffin, 1971; Merschat and others, 2005; Hatcher and others, 2007). Overall, the Inner Piedmont consists of a gently dipping imbricate stack of large, crystalline, type F thrust sheets (for example, Griffin, 1971; Hatcher and Hooper, 1992; Hatcher, 2004a). East of the Inner Piedmont is the exotic peri-Gondwanan Carolina superterrane, a Neoproterozoic volcanic arc system that accreted to Laurentia during the middle Paleozoic. The crustal affinity of the Inner Piedmont was also suspect for a time (for example, Rankin, 1975; Williams and Hatcher, 1982; Hibbard, 2000) and, as a result, the true nature of the Brevard fault zone, the western boundary of the Inner Piedmont, remained ambiguous. Detrital zircon data, however, confirm Laurentian affinity of Inner Piedmont metasedimentary rocks, and also support the hypothesis that the Brevard fault zone is not a suture (Bream and others, 2001; Bream, ms, 2003; Hatcher and others, 2007). Additionally, identical stratigraphic sequences from both sides of the Brevard fault zone indicate the Tugaloo terrane comprises both the western Inner Piedmont and eastern Blue Ridge (Hurst, 1973; Hopson and Hatcher, 1988; Hatcher, 2001b, 2002; Hatcher and others, 2007).

The dominant lithostratigraphic unit in the Tugaloo terrane is the Tallulah Falls Formation, which consists of Neoproterozoic-Cambrian(?) deep-water siliciclastic and mafic volcanic rocks likely deposited on ocean crust and rare fragments of continental (Grenville) basement that have been metamorphosed to middle- and upper amphibolite facies assemblages (Hatcher, 1993, 2002). The Tallulah Falls Formation was first named by Hatcher (1971), and is equivalent to the Ashe Formation (Rankin, 1970) and the Lynchburg Formation (Stose and Stose, 1957). The Tallulah Falls Formation comprises a tripartite stratigraphy consisting of lower metagraywacke-amphibolite and upper metagraywacke units separated by a distinct, mappable aluminous schist unit (Hatcher, 1978, 1993). In the southern portion of the Inner Piedmont, lithologic and stratigraphic similarities permit the correlation of the Tallulah Falls Formation with the Ashland supergroup

(Adams, 1926; Tull, 1978) or the Zebulon Formation of Sears and others (1981) and Higgins and others (1988). For sake of comparison, we use the term Tallulah Falls Formation for lithologically analogous rocks with similar stratigraphic sequences and detrital zircon signatures throughout the central Georgia portion of the Inner Piedmont.

The stratigraphic relationships in the western Inner Piedmont are easiest to reconcile through the western Carolinas (for example, Hatcher, 1972, 2004; Bream, ms, 1999). In this region, the Tallulah Falls Formation is conformably overlain by Cambrian – lower Ordovician(?) siliciclastics and carbonates of the Chauga River Formation (for example, Hatcher, 2002). Partial uplift occurred that resulted in the development of a regional unconformity, after which ~460 Ma volcanic rocks of the Middle Ordovician Poor Mountain Formation were deposited (Bream, ms, 2003). These metavolcanic rocks are overlain by quartzite, felsic metavolcanics, and marbles of the Poor Mountain Formation. The Chauga River and Poor Mountain Formations occur only in the western Inner Piedmont, and are absent from the lithostratigraphy in the eastern Blue Ridge.

The Tugaloo terrane was intruded by mostly Ordovician-Silurian granitoids, with minor Devonian granitic plutonism (Pink Beds and Looking Glass, 390-380 Ma; Miller and others, 2000; Jubb, 2010) west of the Brevard fault zone in North Carolina and Carboniferous-Permian granitoids east of the Brevard fault zone in Georgia (for example, Stone Mountain ~337 Ma; Panola, 297; Mueller and others, 2011). Small bodies of continental basement (Grenville) have been identified throughout the western Inner Piedmont (for example, Heyn, ms, 1984; McConnell, ms, 1990; Fullagar, 1997; Merschat, ms, 2009; Huebner and others, 2010); to date, none have been found in the Cat Square terrane. A window of Tugaloo terrane rocks (Newton window) has been identified east of the Brindle Creek fault in North Carolina and confirmed by detrital zircon geochronology (Merschat and others, 2010) (Fig. 2-2).

The Cat Square terrane consists of massive aluminous schist and metagraywacke units, with an apparent lack of a recognizable stratigraphy similar to the Tallulah Falls Formation. The initial distinction as a separate terrane was the product of detrital zircon geochronology (Bream, ms, 2003); otherwise, the two assemblages can only be distinguished by lithologic (granitoid and metasedimentary) differences that would not warrant division as a separate lithotectonic terrane. Cat Square terrane metasedimentary rocks contain zircons that identify both Laurentian and peri-Gondwanan (likely Carolina superterrane) sources, along with a prominent Ordovician-Silurian suite that was likely Laurentian-derived (Merschat and others, 2010; Sinha and others, 2012). The presence of Ordovician-Silurian detrital zircons has been suggested to delimit the maximum age of Cat Square terrane metasedimentary rocks (Bream and others, 2004), and as a result, the terrane has been interpreted to represent a Silurian-Devonian basin (Dennis, 2007; Merschat and Hatcher, 2007). Cat Square terrane granitoid plutons are mostly Devonian to Mississippian and appear to be dominantly anatectic (Mapes, ms, 2002).

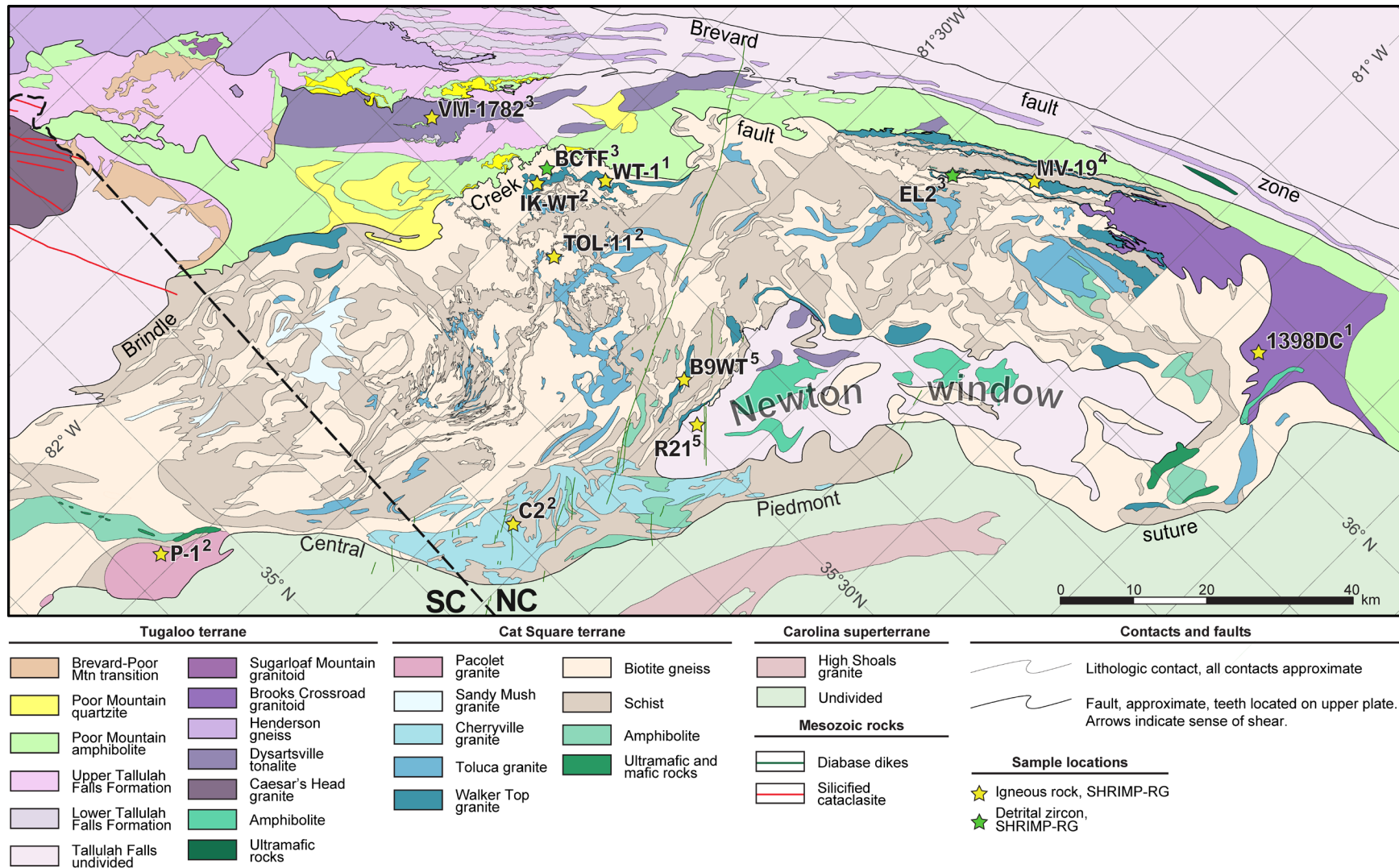


Figure 2-2: Geologic map of the Carolina portion of the Inner Piedmont (modified from Mersch, ms, 2009) with sample locations of compiled U-Pb ion microprobe granitoid ages and detrital zircon analyses. Ages summarized in table 2. Data sources: ¹Vinson (ms, 1999); ²Mapes (ms, 2002); ³Bream (ms, 2003); ⁴Gatewood (ms, 2007); ⁵Byars (ms, 2010). Location of map is indicated in Fig. 1.

Several localities of ultramafic and mafic rocks have been identified throughout the Cat Square terrane (Privett, 1984; Mittwede and others, 1987; Goldsmith and others, 1988; Giorgis, ms, 1999; Mersch and others, 2008). Small bodies of talc-chlorite schist (altered ultramafic rocks) occur near the Brindle Creek fault in the South Mountains (Giorgis, ms, 1999); however, the largest bodies of ultramafic and mafic rocks, the Turnersburg ultramafic and the Hammett Grove meta-igneous suite, occur in the eastern part of the Cat Square terrane near the central Piedmont suture (Privett, 1984; Mittwede and others, 1987; Goldsmith and others, 1988). The Hammett Grove meta-igneous suite in northwestern South Carolina consists of serpentinized ultramafic rocks, metapyroxenite, metagabbro, amphibolite, and metachert (Mittwede and others, 1987). Based on chemical analyses and a progression of metamorphosed mafic, ultramafic, and metasedimentary rocks, Mittwede (1989) interpreted the Hammett Grove suite to represent a dismembered ophiolite, which is also supported by $\delta^{18}\text{O}$ and δD isotopic data (Chaumba, 2010a). Mersch and Hatcher (2007) suggested the Cat Square terrane metasedimentary rocks were deposited on ocean crust, based on the presence of mafic and ultramafic bodies, lack of continental basement, and the mixed detrital zircon signature indicating provenance from Laurentian and peri-Gondwanan sources.

The Inner Piedmont as a mid-crustal orogenic channel

The Brevard fault zone is one of the largest faults in the southern Appalachian orogen; its deformational, kinematic, thermal, and temporal histories are vital to tectonic reconstructions regarding the accretion and translation of outboard Laurentian and peri-Gondwanan terranes. The Brevard fault zone is a complex boundary that has undergone multiple reactivation events under a variety of stress and rheologic regimes through the middle and late Paleozoic (Hatcher, 2001b). For purposes of this paper, we focus on observations from the initial high-grade deformation along the fault zone that occurred during the Devonian (for example, Vauchez and others, 1993; Hatcher, 2001b; Mersch and others, 2005).

At the western boundary of the Inner Piedmont, the Brevard fault zone is a northeast-striking, 15-20 km wide amphibolite facies dextral shear zone characterized by strongly aligned foliations and mineral stretching lineations (for example, Hatcher, 2001b). The shear zone dips southeast $10-45^\circ$, with subhorizontal mineral lineations trending northeast-southwest. Mineral lineations continue this trend into the eastern Blue Ridge for a few kilometers west of the Brevard fault zone (Hatcher, 2001b). East of the Brevard fault zone, mineral lineations become significantly less aligned, and transition to east-west and north-south trends toward the easternmost portions of the Inner Piedmont. Based on field, microfabric, and geochronologic relationships, Mersch and others (2005) concluded that the curved regional-scale lineation pattern formed during one event, and is not the product of separate overprinting deformation. The resultant curved line-

tion pattern has been interpreted to be the product of lateral extrusion of the Inner Piedmont as an orogenic channel, buttressed against the Brevard fault zone, that flowed at mid-crustal levels during oblique transpressive accretion of the overriding Carolina superterrane (Merschhat and others, 2005; Hatcher and Merschhat, 2006). This model invokes Griffin's (1971, 1978) supra-structure/infrastructure model of the migmatitic infrastructural Inner Piedmont overridden by the suprastructural Carolina superterrane, which was largely based on the regional fold-nappe structural style of the Inner Piedmont (Fig. 2-3). Griffin (1971), however, interpreted these nappes to be northwest-vergent, although more recent studies (Merschhat and others, 2005; Hatcher and Merschhat, 2006) indicate these nappes are southwest-vergent thrust sheets and macroscale sheath folds. Through the core of the Inner Piedmont, intense migmatization of footwall rocks beneath overriding thrust sheets is nearly ubiquitous, revealing the elevated thermal regime during deformation and emplacement of the Inner Piedmont thrust sheets (Griffin, 1969; Bier and others, 2002; Merschhat and others, 2005; Davis, ms, 2010).

ATTRIBUTES OF THE INNER PIEDMONT – A SUMMARY OF RESULTS FROM TWO ISLANDS OF DETAILED GEOLOGIC MAPPING

The current study is focused on the central Georgia portion of the Inner Piedmont (Fig. 2-4), although the basis of this work stems from an island of detailed geologic mapping in the northern portion of the Inner Piedmont (Fig. 2-2). We are currently testing the hypothesis that the Cat Square terrane continues through central Georgia; therefore, a basic summary of lithologic, structural, and metamorphic attributes of the composite Inner Piedmont revealed by detailed geologic mapping projects are vital for comparison between the two portions of the Inner Piedmont. Subsequent geochronologic and geochemical data provide further tests of this hypothesis, and overall provide more insight regarding the tectonic evolution of the Inner Piedmont.

Major Lithologic Units and Field Relations

The northern Inner Piedmont

Through the Carolinas, metasedimentary rocks of the western Inner Piedmont (and eastern Blue Ridge) occur in a recognizable, reproducible stratigraphy that spans the Neoproterozoic(?) through the Middle Ordovician (for example, Bier and others, 2002; Bream, ms, 2003; Hatcher, 2002). The stratigraphically lowest unit in the Tugaloo terrane, the lower member of the Tallulah Falls Formation, consists of an assemblage of dark gray, fine- to coarse-grained biotite-quartz-plagioclase paragneiss (metagraywacke) with variable amounts of biotite-muscovite schist (e.g., Hatcher, 1971). The lower member characteristically contains an abundance of thin, discontinuous layers and boudins of fine- to coarse-grained amphibolite with dominant mineralogy

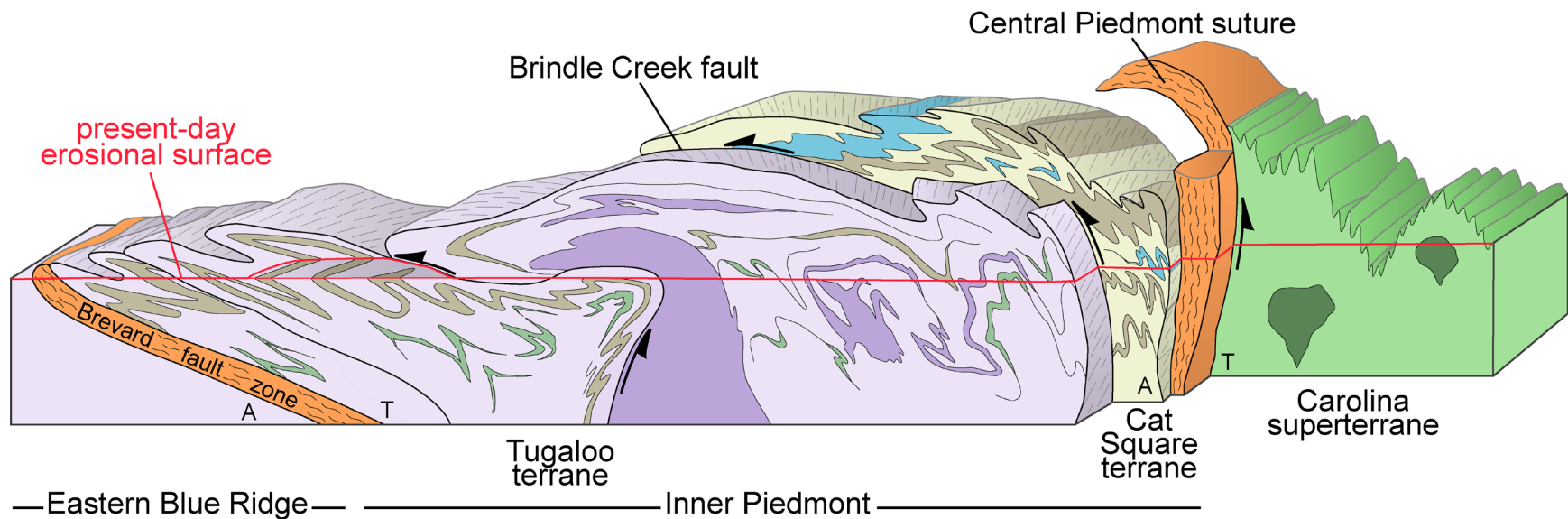


Figure 2-3: Conceptual block diagram illustrating the nappe-style deformation of the infrastructural Inner Piedmont and adjacent suprastructural Carolina superterrane (modified from Griffin, 1978). Colors of lithologic units coincide with those in Fig. 2-2, with large fault zones shown as orange. Thin lines on fault surfaces represent the megascale curved mineral lineation pattern through the Inner Piedmont.

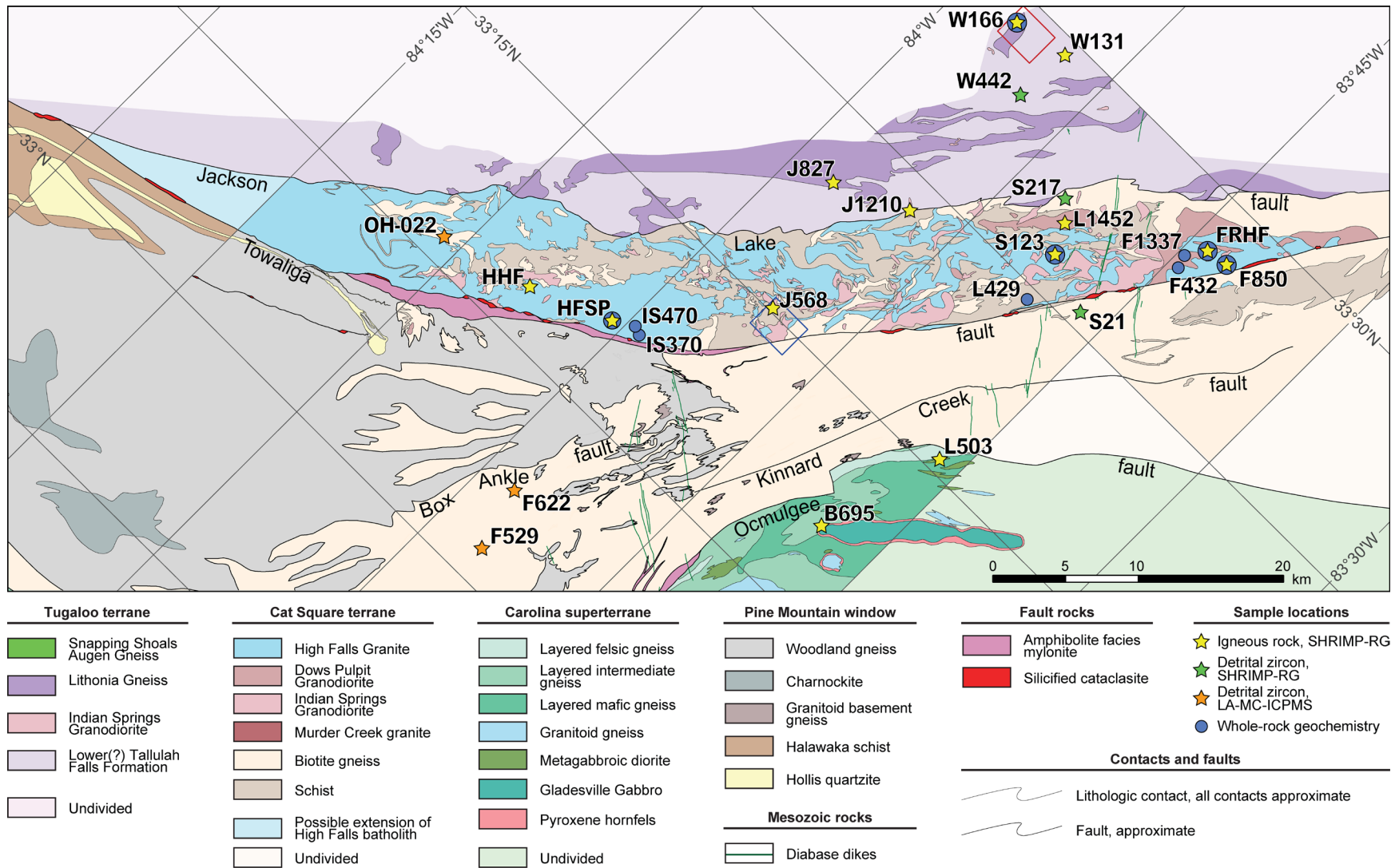


Figure 2-4: Compiled geologic map of the central Georgia portion of the Inner Piedmont with geochronologic and geochemical sample locations. Sources of geochemical data listed in appendix III. LA-MC-ICPMS detrital zircon data from J.R. Rehrer, unpublished data. The red and blue boxes indicate the locations of maps in figures 3-6 and 3-8, respectively. Location of map is shown in Fig. 2-1.

hornblende, plagioclase, and quartz, locally with garnet, biotite, sillimanite, and minor epidote and clinozoisite (Hatcher, 1971). Additionally, several 10-25 cm thick gondite layers have been mapped in the Newton window (Byars, ms, 2010; Gilliam, ms, 2010) and consist of granular, fine- to medium-grained garnetiferous (spessartine?) quartzite. Metagraywacke and schist of the upper member of the Tallulah Falls Formation are lithologically similar to units in the lower member, although the upper member, separated from the lower member by a distinct, regionally extensive aluminous schist member, is distinguished by the relative paucity of amphibolite.

The aluminous schist member has been used in numerous detailed mapping projects as a stratigraphic marker within the Tallulah Falls Formation, and has also been key in delimiting macroscale structures in the western Inner Piedmont (for example, Hatcher, 1971; Heyn, ms, 1984; Bream, ms, 1999; Hill, ms, 1999; Stahr, ms, 2008). In general, this thin (< 100 m) continuous unit is composed of garnetiferous kyanite- or sillimanite-bearing muscovite schist. It is generally silvery light-gray, with muscovite, quartz, plagioclase, and biotite present in varying amounts.

In the northwestern portion of the Inner Piedmont from central-western North Carolina to northeast of Atlanta, Georgia, the Tallulah Falls Formation is overlain by Cambrian – lower Ordovician(?) metasilstone, quartzite, graphitic schist, and impure marble of the Chauga River Formation (for example, Hatcher, 2002). This unit thins dramatically toward the eastern portion of the western Inner Piedmont through the Carolinas (for example, Bier and others, 2002). In the South Mountains, the contact with the overlying Poor Mountain Formation is sharp with limited interlayering, and when combined with the lack of evidence of faulting, has been interpreted as an unconformity (for example, Bream, ms, 1999; Hill, ms, 1999; Bier and others, 2002).

The Poor Mountain Formation consists of a basal laminated amphibolite and interlayered felsic tuff unit that grades upward into feldspathic quartzite and metatuff. Its extent may continue as far to the southwest as eastern Alabama, based on similarities with the Ropes Creek Amphibolite (for example, Bentley and Neathery, 1970; Steltenpohl, 2005). The Poor Mountain amphibolite unit consists mostly of a fine-grained, dark- to medium-gray, laminated amphibolite, with lesser amounts of interlayered feldspathic quartzite and amphibole gneiss (Hatcher, 1969; Bream, ms, 1999). The relative amount of feldspathic quartzite increases upward, eventually grading into the overlying Poor Mountain Quartzite member. Two metatuff units from the quartzite member yielded Late Ordovician ages (459 ± 4 and 445 ± 4 Ma; Bream and others, 2004).

Several large granitic bodies occur in the western Inner Piedmont in the Carolinas, including the Henderson gneiss, Dysartsville Tonalite, and the Caesar's Head Granite. Tugaloo terrane granitoids are generally peraluminous, and are classified as granites to granodiorites based on modal and normative mineral assemblages (Vinson, ms, 1999; Bream, ms, 2003). Common mineralogy consists of microcline, plagioclase, quartz, biotite, with locally abundant muscovite. The

Henderson Gneiss, arguably the largest pluton in the southern Appalachians, is a coarse-grained, porphyroclastic gneiss consisting of 1-3 cm microcline augen within a matrix of microcline, plagioclase, quartz, biotite, and muscovite (for example, Horton and McConnell, 1991; Hatcher, 1993). The Henderson Gneiss may have been emplaced as a large single thrust sheet (Liu, ms, 1991; Davis, ms, 1993; Bier and others, 2002), and the present shape of the Henderson body is thought to be the product of southwest-directed heterogeneous simple shear, with the contacts containing a greater degree of mylonitization than the internal parts of the body (Mersch et al., 2005, their Fig. 10). Detailed geologic mapping in the Newton window revealed the Reepsville orthogneiss, a migmatized porphyroclastic quartz-plagioclase-microcline-biotite gneiss, with minor garnet, muscovite, and secondary epidote (Byars, ms, 2010). U-Pb zircon geochronology indicates this unit is a small fragment of Grenvillian basement rock, but is included in what Byars (ms, 2010) interpreted as the lower Tallulah Falls Formation.

Southeast of the Brindle Creek fault, the metasedimentary assemblage consists mostly of migmatitic medium-coarse grained metagraywacke and interlayered aluminous schist (Mersch et al., 2007). Metagraywacke generally consists of K-feldspar-plagioclase-biotite-quartz gneiss with abundant quartzofeldspathic leucosome, with mesoscale variation in mineralogy likely a product of both protolith variation and degree of migmatization. Massive sillimanite schist bodies include coarse-grained poikiloblastic muscovite-sillimanite schist, migmatitic sillimanite schist, and garnet-biotite-sillimanite schist (Mersch et al., ms, 2003), although a discernable stratigraphy is not evident. In general, schist is medium grained, lepidoblastic, with garnet, fibrous sillimanite, biotite, muscovite, and quartz (Mersch et al., ms, 2003). Sillimanite schist and metagraywacke contain various amounts of pegmatite and felsic leucosome, which occur as deformed bodies concordant with regional fabrics and deformed and undeformed bodies that crosscut regional fabric (Mersch et al., ms, 2003). Relatively minor amounts of amphibolite, calc-silicate, and ultramafic rocks occur southeast of the Brindle Creek fault.

Abundant peraluminous granitoids occur southeast of the Brindle Creek fault in the Cat Square terrane; the most voluminous are the Toluca, Walker Top, and Cherryville Granites. The Toluca Granite (Griffitts and Overstreet, 1952) is a garnet-muscovite bearing, massive, equigranular to locally porphyritic, medium- to coarse-grained, weakly to strongly foliated granite with contacts that are generally concordant to oblique to regional fabrics (for example, Bier, ms, 2001; Mersch et al., ms, 2003). Dominant mineralogy consists of microcline, plagioclase, quartz, muscovite, biotite, garnet, and minor sillimanite (for example, Bier, ms, 2001; Mersch et al., ms, 2003). The Walker Top Granite (Giorgis, ms, 1999) is a distinct porphyritic granite with characteristic subhedral to euhedral K-feldspar megacrysts in a medium-grained K-feldspar, biotite, plagioclase, quartz matrix that locally contains garnet and muscovite (Giorgis, ms, 1999; Mersch et al., ms, 2003). Immediately east of the Brindle Creek fault, the Walker Top Granite occurs as a series of

linear, laterally extensive bodies that parallel regional structural trends (Mersch, ms, 2003). The Cherryville Granite is a non- to weakly foliated, medium-grained peraluminous two-mica monzogranite (Goldsmith et al., 1988; Horton and McConnell, 1991; Mapes, ms, 2002).

Several relatively less abundant granitoids occur east of the Brindle Creek fault in the Carolinas Inner Piedmont, some of which may be related to more abundant Inner Piedmont igneous intrusions. The Anderson Mill is a medium- to coarse-grained biotite augen gneiss composed of plagioclase porphyroclasts within a plagioclase, quartz, biotite, microcline, garnet, and muscovite matrix (Curl, ms, 1998). The Gray Court granitoid is a strongly foliated, equigranular to porphyritic biotite granite (Horton and McConnell, 1991; Mapes, ms, 2002). The Pelham granitoid is a strongly deformed augen gneiss with garnet and feldspar porphyroclasts (Mapes, ms, 2002). The Pacolet monzogranite, an equigranular to porphyritic granitoid composed of plagioclase, microcline, quartz, biotite, and muscovite, has been depicted as a stitching pluton across the Inner Piedmont and Carolina superterrane (Mittweide and Fullagar, 1987; Horton and McConnell, 1991; Hatcher et al., 2007) and as part of the Carolina superterrane (Dennis, 1991). An unnamed granite that crosscuts the central Piedmont suture in north-central South Carolina (Cold Point pluton) was dated by Dennis and Wright (1995) at 326 ± 3 Ma, and provides a minimum age limit to ductile deformation along the exposed suture.

The central Georgia Inner Piedmont

In the central Georgia portion of the Inner Piedmont, the dominant metasedimentary assemblage identified northwest of the Jackson Lake fault consists of predominantly metagraywacke with thin layers of aluminous schist and locally abundant discontinuous layers or boudins of amphibolite. Metagraywacke is generally medium-fine to coarse-grained, thickly layered, and strongly foliated. Typical mineral assemblages of the metagraywacke include quartz, biotite, alkali feldspar and plagioclase, locally with garnet, muscovite, and sillimanite. Amphibolite boudins vary from 10 cm to 2 m long, and are generally fine- to medium-grained, composed of hornblende, plagioclase, and quartz, locally with garnet, biotite, and epidote. Thin layers of muscovite-biotite \pm sillimanite schist are common, although they are difficult to trace along strike. Additionally, several (one?) laterally extensive layers of fine- to medium-grained gneiss have been identified within this metasedimentary assemblage. We interpret this assemblage of metasedimentary rocks to be equivalent to the lower member of the Tallulah Falls Formation based on the lithologic similarities.

Southeast of the Jackson Lake fault, metasedimentary rocks consist of massive metagraywacke and sillimanite schist units. Metagraywacke is generally medium-fine to coarse-grained, ranges from thinly to thickly layered, and is predominantly composed of quartz, plagioclase, alkali feldspar and biotite, locally with garnet, sillimanite, and muscovite. Sillimanite schist is

relatively more abundant southeast of the Jackson Lake fault, with typical mineral assemblages of biotite, muscovite, fibrous and prismatic sillimanite, quartz, plagioclase, alkali feldspar, and garnet. Although amphibolite layers and boudins are not uncommon southeast of the Jackson Lake fault, the relative abundance of amphibolite is undoubtedly much greater northwest of the fault.

Several granitic units have been identified northwest of the Jackson Lake fault in central Georgia. In this region, the Lithonia gneiss is by far the most voluminous granitoid. It is a light gray, strongly foliated and folded, medium- to medium-coarse grained granitic gneiss (Fig. 2-5B). Mineralogy consists of quartz, plagioclase, alkali feldspar, and biotite, with locally abundant garnet, along with accessory sphene, zircon, and apatite, and rare muscovite. Relatively large pavement exposures (10-100s km²) are common in this region, with the most striking exposures located in the Stone Mountain-Lithonia mining district (Herrmann, 1954). Foliation in the Lithonia gneiss is subparallel to regional foliation, and elongate bodies on the surface may occupy map-scale upright to inclined isoclinal folds.

Few small exposures of the Snapping Shoals Augen Gneiss (named here, type area around Snapping Shoals [33°29' 02.89" N, 83°57'11.60" W]; Fig. 2-6) are exposed in this area. This augen gneiss is pervasively deformed, characterized by large (up to 10 cm), strongly sheared alkali feldspar megacrysts that exhibit dominantly dextral shear sense (Fig. 2-5A). Matrix minerals consist of quartz, plagioclase, microcline, and biotite, with accessory muscovite, garnet, sphene, and apatite. Small bodies occur within both lower Tallulah Falls Formation metagraywacke and the Lithonia Gneiss, and none (to date) have been identified southeast of the Jackson Lake fault.

The most abundant granitoid southeast of the Jackson Lake fault is the High Falls Granite, named for excellent exposures in and around High Falls State Park (Atkins and Lineback, 1992), which comprises the most voluminous lithology in the Lloyd Shoals plutonic complex (Huebner and others, in submission). The High Falls Granite is a moderately to strongly foliated porphyritic biotite granite characterized by 1-20 cm long blocky, euhedral to subhedral microcline megacrysts that commonly display carlsbad twinning (Fig. 2-5C). Matrix phases include quartz, plagioclase, biotite, and quartz, with locally abundant garnet or muscovite. Foliation is defined by parallel alignment of biotite and microcline megacrysts, and is typically concordant with foliation in the surrounding country rock. In places, lithologic contacts between the granite and country rock are deformed coevally (Fig. 2-7). Exceptions occur in isolated zones at outcrop and map scale, with perturbations in the foliation likely related to magmatic flow or nappe-style folding of the pluton (Howard, ms, 2012). The High Falls Granite is texturally, mineralogically, and geochemically similar to the Walker Top Granite in the North Carolina Inner Piedmont (Davis, ms, 2010; Howard, ms, 2012).

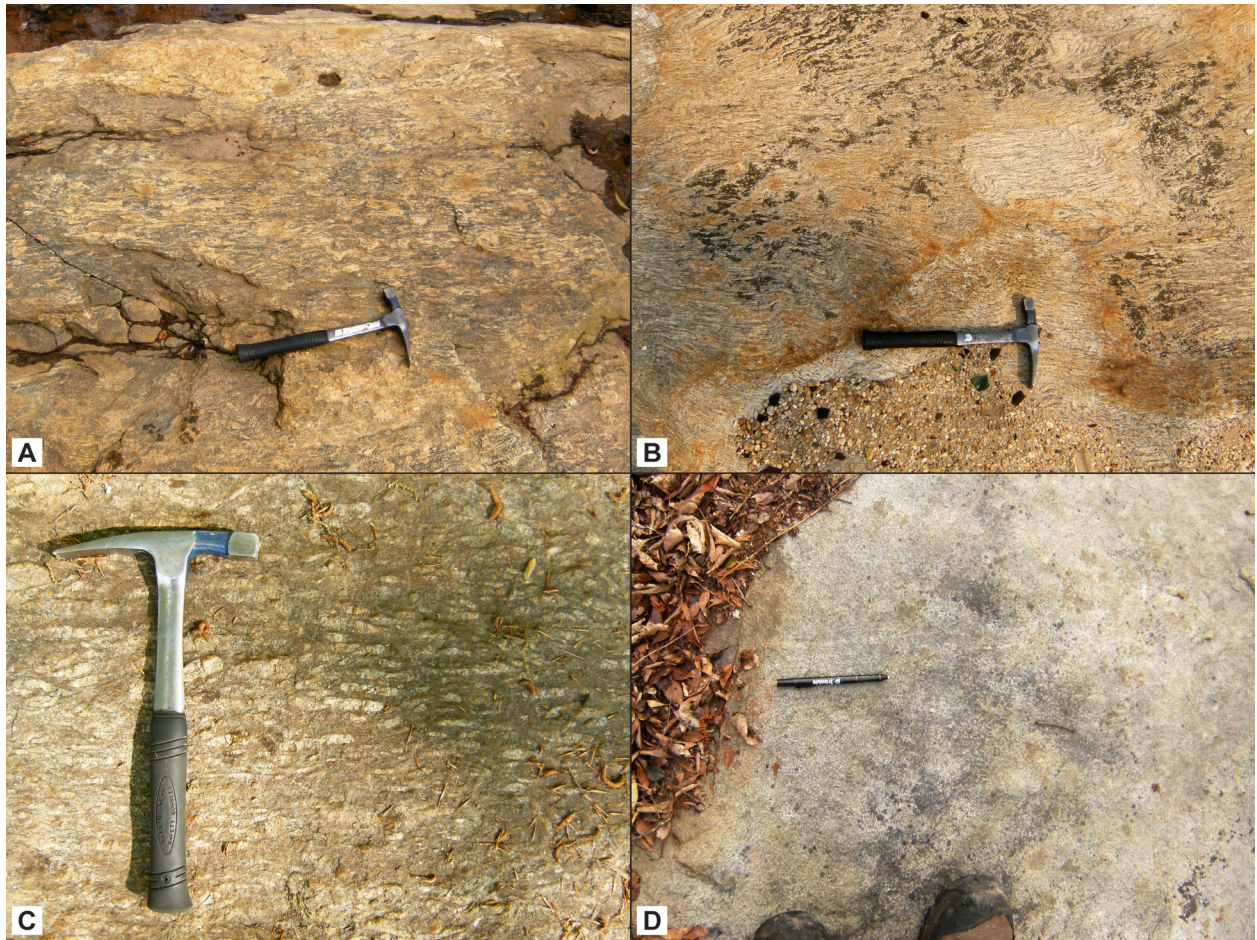


Figure 2-5: Characteristic exposures of igneous rocks selected for geochronologic analysis. (A) Pavement exposure of Snapping Shoals augen gneiss, view to the east; (B) Pavement exposure of Lithonia Gneiss, view to the northeast. F_3 folds are northwest-vergent, and deform S_2 fabric. (C) Megacrystic High Falls Granite; (D) Indian Springs granodiorite.

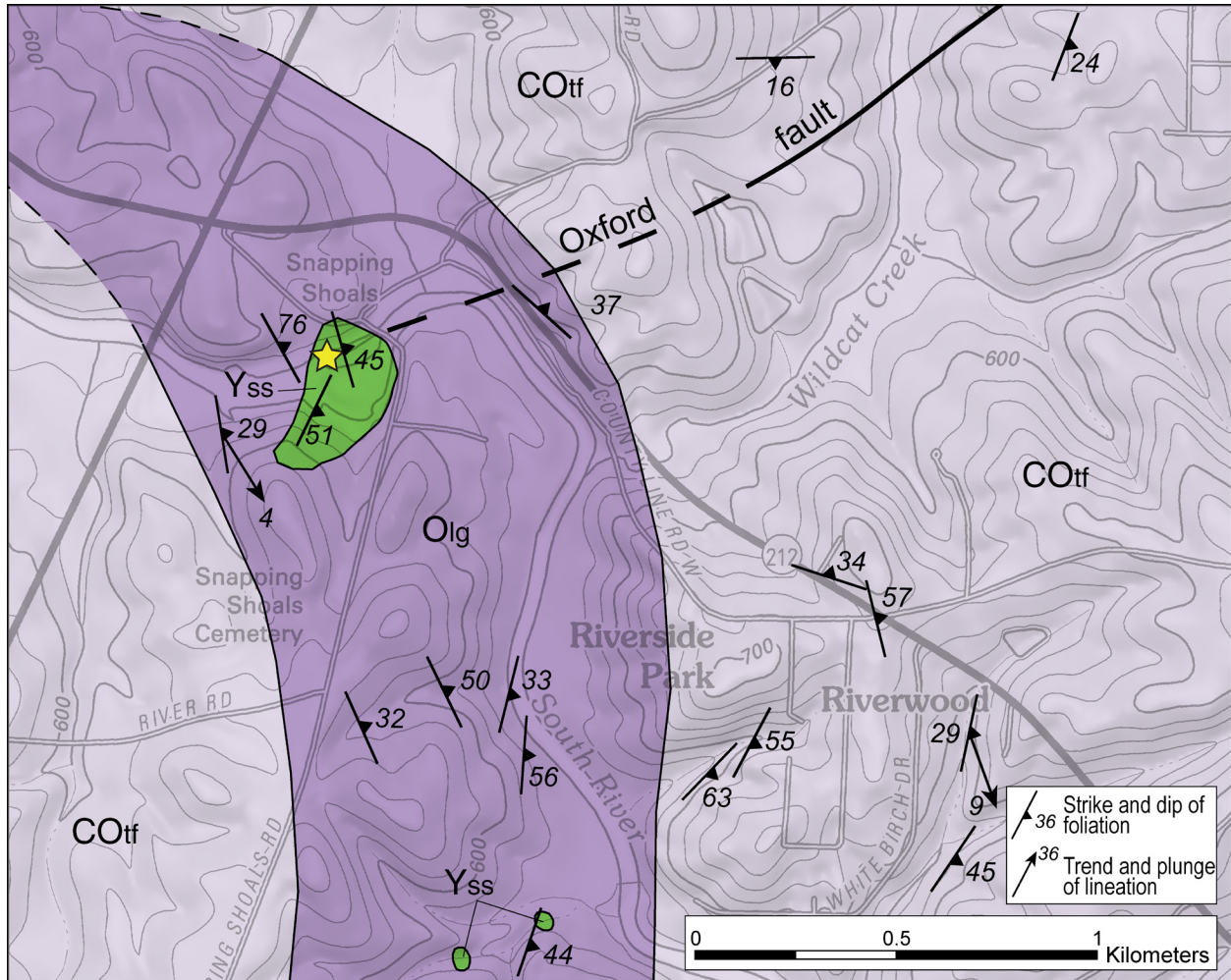


Figure 2-6: Simplified geologic map illustrating the type locality (yellow star) of the Snapping Shoals Augen Gneiss. Location of map is shown in figure 3-4. Map unit colors correspond to those in figure 3-4. COtf = lower Tallulah Falls Formation; Olg = Lithonia Gneiss; Yss = Snapping Shoals Augen Gneiss.

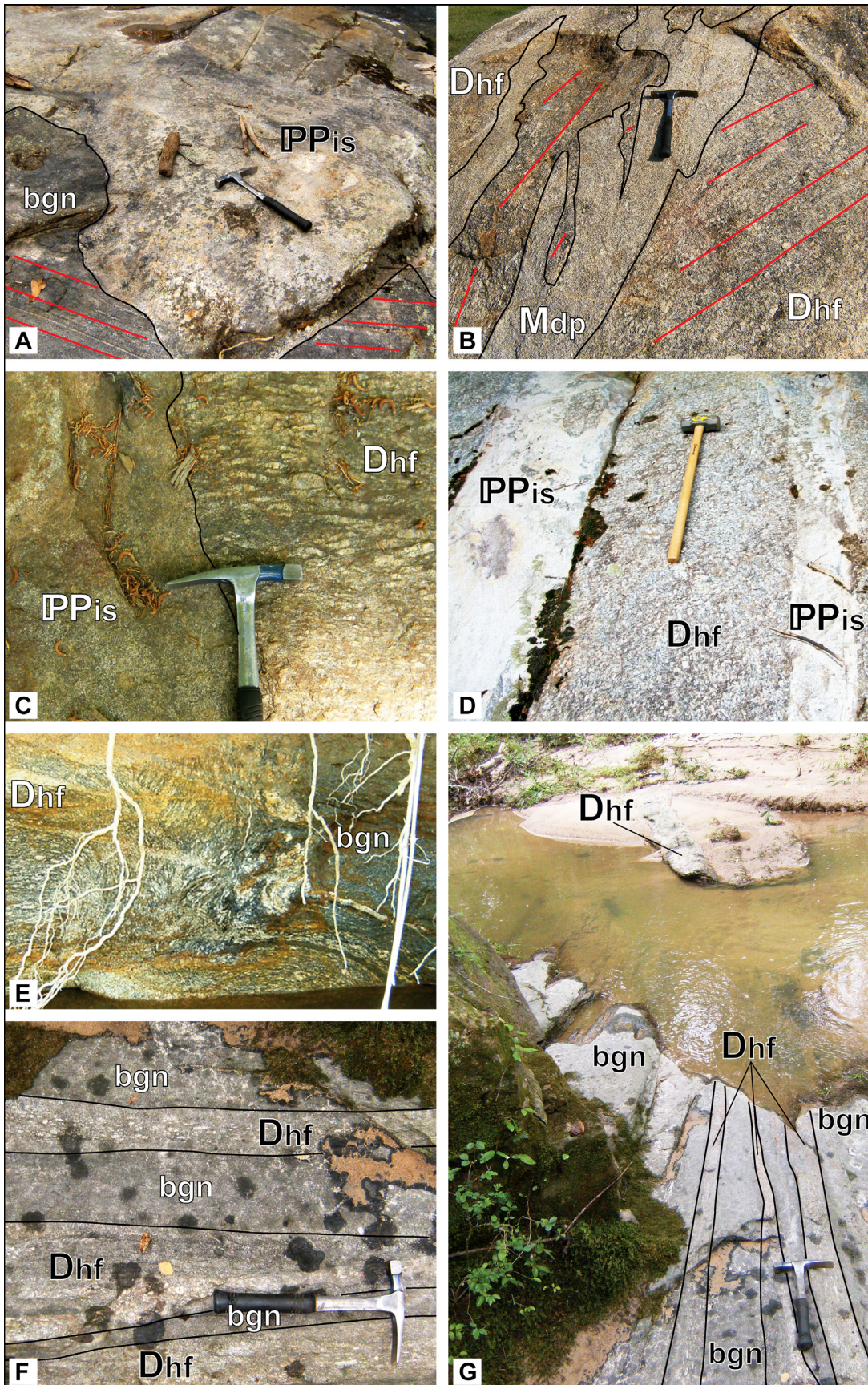
Several other less abundant granitoids have been recognized southeast of the Jackson Lake fault. The Dows Pulpit Granodiorite is a medium-coarse to coarse-grained peraluminous granodiorite that generally exhibits a weakly developed foliation oblique to the principal regional foliation, and was named by Davis (ms, 2010) for exposures around Dows Pulpit rock, Jasper County. Dominant mineralogy includes smoky quartz, plagioclase, microcline, biotite, and muscovite, with accessory sphene, apatite, zircon, and opaque minerals. This rock plots both in the granite and granodiorite fields according to IUGS classification (Streckeisen, 1976), although it more commonly plots as a granodiorite (Davis, ms, 2010). The informally named Murder Creek granite (Davis, ms, 2010) is a medium-coarse grained porphyritic granite with subhedral 1-5 cm microcline megacrysts enclosed in a matrix consisting of quartz, plagioclase, microcline, biotite, and muscovite. To date, only one small body of this granitoid has been identified.

In contrast to other granitoids in the central Georgia Inner Piedmont, the Indian Springs Granodiorite (named here, type area around Indian Springs State Park, Butts County [33°14'50" N, 83°55'14" W]; Fig. 2-8) occurs on both sides of the Jackson Lake fault, and one small body may even crosscut the fault. The Indian Springs granodiorite is a white to light gray, weakly to moderately foliated, medium- to fine-grained equigranular granodiorite that is typically exposed as large (1-5 m) rounded boulders. This rock unit occurs as dikes or isolated pods, as well as larger macroscale bodies. Internal foliation is typically parallel to the boundaries of Indian Springs Granodiorite bodies, and is interpreted as magmatic. Primary phases include plagioclase, quartz, microcline, and biotite, although muscovite can be locally abundant.

Crosscutting relationships and relative ages

Structural analysis, detailed geologic mapping, and granitoid geochronology provide valuable timing constraints related to fabric development in the Carolina Inner Piedmont. The dominant regional foliation (S_2) is concordant in both metasedimentary rocks and granitic plutons throughout the Tugaloo terrane, which indicates S_2 developed in post-Ordovician time. S_2 fabric is not disrupted by the Brindle Creek fault, and metamorphic index minerals indicate S_2 , which coincides with peak metamorphic conditions, and the mylonitic foliation within the Brindle Creek fault formed at similar metamorphic grade (for example, Giorgis, ms, 1999; Gatewood, ms, 2007; Gilliam, ms, 2010). Several deformed Devonian-Mississippian plutons (407-355 Ma) also exhibit solid-state fabric that parallels S_2 , while the plutons are truncated by the Brindle Creek fault. Several of these granitoids occur in the limbs of macroscale D_2 sheath folds, which are also truncated by the Brindle Creek fault (Mersch and Kalbas, 2002; Byars, ms, 2010). This indicates the plutons were emplaced pre- to syn- S_2 , and the final deformation along the Brindle Creek fault occurred after ~355 Ma, likely during the waning stages of S_2 fabric development. Rare, relatively small Alleghanian granitoids (~322 Ma; Gatewood, ms, 2007) truncate S_2 fabric

Figure 2-7: Mesoscale examples of spatial relationships between major lithologies in the central Georgia Inner Piedmont. (A) A small body of Indian Springs granodiorite truncates S_2 (red line) developed in biotite paragneiss, view to the southeast. (B) Dikes of Dows Pulpit Granodiorite cut S_2 fabric in High Falls Granite, view to the northeast. (C) Indian Springs Granodiorite truncates S_2 in High Falls Granite. (D) Dikes of Indian Springs Granodiorite crosscut High Falls Granite (photo by C.W. Howard). (E) Folded lithologic contact between High Falls Granite and biotite paragneiss, with S_2 parallel to contact and concordant in both lithologies, field of view ~2.5 m. View is to the northeast. (F) and (G) Apparent interlayering of High Falls Granite and biotite paragneiss, illustrating transposition of lithologic contacts parallel to S_2 . Rock hammer is in the same location in (F) and (G). bgn = biotite gneiss; Dhf = High Falls Granite; Mdp = Dows Pulpit granite-granodiorite; PPis = Indian Springs granodiorite.



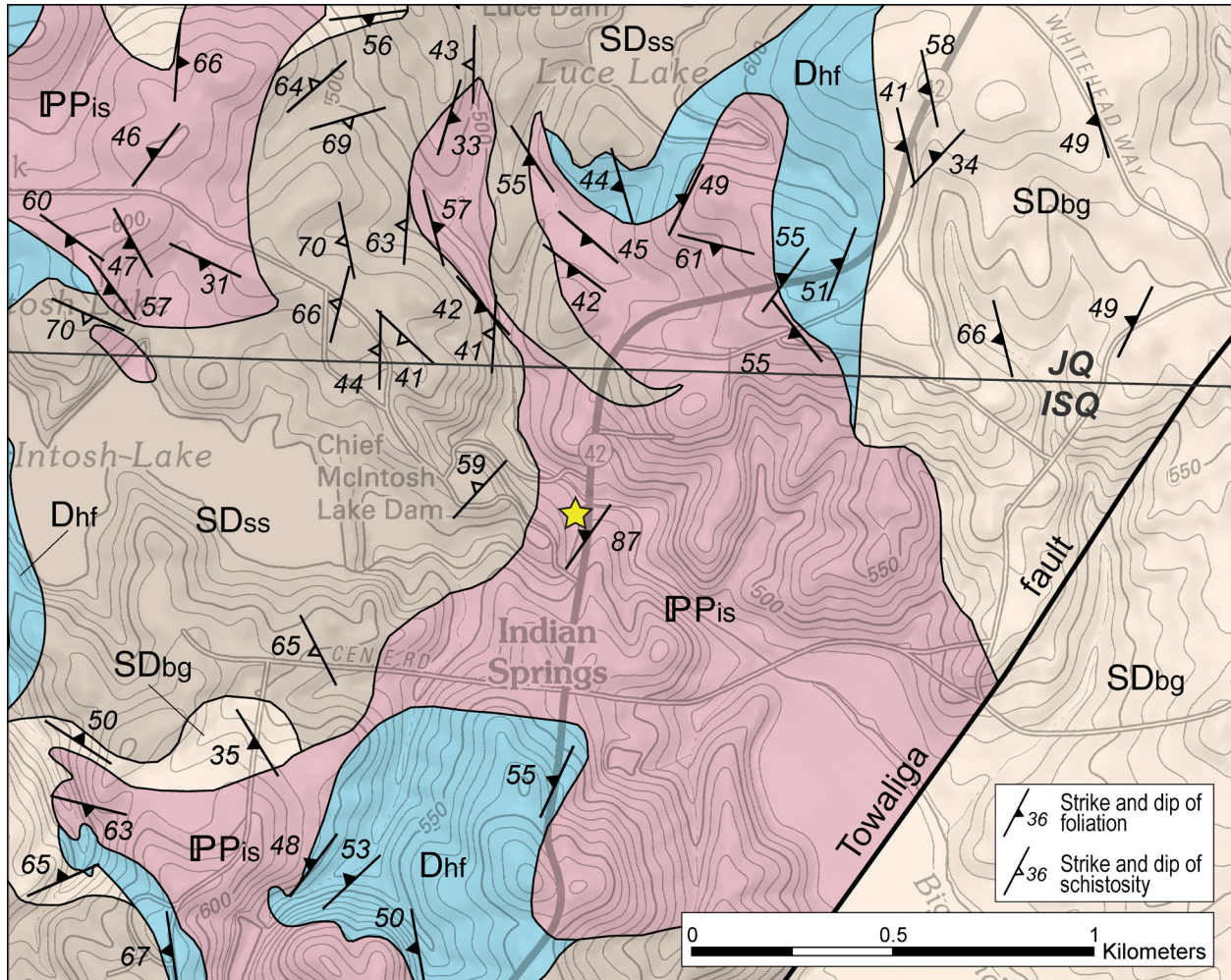


Figure 2-8: Simplified geologic map illustrating the type locality of the Indian Springs Granodiorite, indicated by the yellow star. Map unit colors correspond to figure 3-4, and map location is also shown in figure 3-4. JQ = Jackson 7.5-minute quadrangle; ISQ = Indian Springs 7.5-minute quadrangle; Dhf = High Falls Granite; **MPis** = Indian Springs Granodiorite; SDbg = biotite paragneiss; SDss = sillimanite schist.

in metasedimentary rocks and in the Walker Top Granite, which provide a minimum age limit for development of S_2 fabric. This granitoid is folded, likely during D_4 (Wilson, ms, 2006; Gatewood, ms, 2007).

Detailed geologic mapping in the central Georgia portion of the Inner Piedmont has revealed numerous crosscutting relationships that provide insight regarding the relative ages of most of the rocks in the study area, as well as the nature of the spatial relationships between the major lithologies, fault zones, and deformational events (Fig. 2-7). The Lithonia Gneiss and surrounding metasedimentary rocks share contacts concordant with regional foliation (S_2) that is also deformed, likely during the D_2 event. Lithologic contacts between the High Falls Granite and metasedimentary rocks are mostly concordant (Fig. 2-7E-G), with rare discordant foliation observed in High Falls Granite, likely a function of magmatic flow. Deformed contacts between the High Falls Granite and surrounding metasedimentary rocks indicate emplacement was pre- to syn-deformational (D_2) (Fig. 2-7E). Metasedimentary rocks, the Lithonia Gneiss, and the High Falls Granite are all truncated by the Jackson Lake fault. The Dows Pulpit, Murder Creek, and Indian Springs granitoids generally crosscut regional foliation in metasedimentary rocks and High Falls Granite (Fig. 2-7A-D), although in places these contacts are concordant. Crosscutting relationships between the Dows Pulpit and Indian Springs granitoids have not been observed in the field. All granitoids and metasedimentary rocks located in the vicinity of the Towaliga fault are obviously truncated, indicating the Towaliga fault post-dates granitic plutonism (Huebner and Hatcher, 2013).

Mesozoic diabase dikes cut all crystalline rocks through the southern Appalachian Inner Piedmont. Throughout the orogen, diabase dikes share mutually overprinting crosscutting relationships with small-displacement brittle faults, indicating roughly coeval timing (for example, Horkowitz, ms, 1984; Garihan and others, 1993; Huebner and Hatcher, 2013). Radiometric ages of diabase dikes surrounding the Atlantic margin indicate emplacement ~ 200 Ma (for example, Hames and others, 2000; Nomade and others, 2007).

Structural Geology

Abundant evidence indicates the Inner Piedmont has been multiply deformed, preserving evidence of at least six deformational events (for example, Hopson and Hatcher, 1988; Davis, ms, 1993; Merschat and others, 2005). The dominant regional foliation (S_2) formed close to peak metamorphic conditions (upper amphibolite-facies), with foliation defined by parallel alignment of high-temperature mineral assemblages, including prismatic and fibrous sillimanite, phyllosilicates, and other inequant phases. Throughout the entire Inner Piedmont, S_2 envelops amphibolite boudins that locally preserve an earlier S_1 fabric (for example, Hopson and Hatcher, 1988; Merschat and others, 2005; Davis, ms, 2010). In the northern portion of the Inner Piedmont, S_2

dips shallowly and strike becomes strongly orientated northeast-southwest toward the Brevard fault zone. Dip of S_2 steepens toward the east in the southern portion of the Inner Piedmont; the overall northeast-southwest strike remains fairly consistent, with dispersed domains of apparently chaotic or east-west striking orientations. The associated high-grade mineral stretching lineation (L_2) is defined by bladed and fibrolitic sillimanite, elongate phyllosilicates, quartz rods, and mantled feldspars, and generally plunges shallowly throughout the Inner Piedmont. Compositional and migmatitic layering parallel to S_2 are axial planar to isoclinal, meso- and macro-scale F_2 folds. In the Carolina Inner Piedmont, L_2 is coaxial with F_2 fold hinges (for example, Hopson and Hatcher, 1988; Merschat and others, 2005). Although primary sedimentary structures were obliterated by deformation that accompanied high-grade metamorphism, lithologic contacts between pelitic schists and coarser-grained metasedimentary rocks (S_0) are consistently subparallel to the dominant S_2 foliation, and are most likely the result of transposition.

A rare additional foliation (S_3) and mineral lineation (L_3) have been delineated in the Carolina Inner Piedmont (for example, Merschat and others, 2005), although they have not been observed (to date) in central Georgia. This D_3 event most noticeably deformed regional structures into tight to open folds, and generally occurred at conditions that were lower grade than peak metamorphism. Current available evidence does not delineate Neoacadian or early Alleghanian tectonism as the culprit for development of this fabric.

Throughout the entire Inner Piedmont, late-stage mesoscale open folds and coincident broad, long-wavelength macroscale synforms and antiforms are a result of a D_4 event, which also produced the Newton antiform (window). The development of the Eastern Piedmont fault system (Hatcher and others, 1977), an extensive array of Alleghanian dextral strike-slip faults that occur from the Brevard fault zone eastward to beyond the continental margin (Hatcher et al., 2007), was active at upper greenschist-facies and higher-grade conditions, and likely coincides with the D_4 event. Likewise, major crustal faults (for example, Brevard fault zone, Central Piedmont suture) were reactivated at this time (for example, Hatcher, 2001b). The emplacement of high-grade Inner Piedmont thrust nappes had ceased by the time of development of D_4 fabrics. As temperatures decreased across the Inner Piedmont, the ongoing collision with Gondwana ultimately produced the rigid composite Blue Ridge-Piedmont megathrust sheet, which was juxtaposed above the Paleozoic Laurentian platform (for example, Hatcher, 2004a).

Numerous small-scale shear zones that developed along quartz veins at relatively lower temperature conditions (450-400° C) occur throughout the central Georgia Inner Piedmont, and may be relicts of either late-stage Alleghanian or deformation associated with the early phases of the Mesozoic breakup of Pangea (Huebner and Hatcher, 2013). Numerous small-displacement brittle faults, characterized by the development of siliceous cataclasite, occur throughout the southern Appalachian orogen. These faults overprint earlier ductile fabrics, and mutually overprinting

crosscutting relationships with Mesozoic diabase dikes indicate they were active during the final stages of the breakup of Pangea (for example, Horkowitz, ms, 1984; Garihan and others 1993; Huebner and Hatcher, 2013). The current structural level exposed in the Inner Piedmont may have been at zeolite-grade conditions during this deformation episode (Huebner and Hatcher, 2011).

Metamorphism

Metamorphic isograd maps, in combination with geochronologic evidence, indicate the Inner Piedmont represents the Acadian/Neoacadian metamorphic core of the southern Appalachians, with an interior of migmatitic, upper amphibolite to granulite facies rocks (750-850° C, 500-800 MPa; Mirante and Patiño-Douce, 2000; Bier and others, 2002; Merschat, ms, 2003) bordered by relatively lower-grade rocks (kyanite grade to the southeast and kyanite, staurolite or garnet grade to the northwest) along its flanks (Fig. 2-9). Davis (ms, 2010) reported peak metamorphic conditions in central Georgia reached 4-5.3 kbars with temperatures ranging between 645 and 715° C, consistent with observed metamorphic mineral assemblages in metavolcanic and metasedimentary rocks. Assuming moderate geothermal and geobarometric gradients, metamorphic conditions in the Inner Piedmont require burial depths of 15-20 km during the Devonian Acadian/Neoacadian orogeny (Merschat and Hatcher, 2007).

The Inner Piedmont recorded Barrovian-style prograde metamorphic events during both the Devonian-Mississippian Acadian/Neoacadian and Pennsylvanian-Permian Alleghanian orogenies. If evidence of Taconic metamorphism was present prior to the Acadian/Neoacadian event, it has yet to be identified. U-Pb geochronology (monazite and zircon rims) from the Inner Piedmont across the Carolinas and northern Georgia reveals metamorphic peaks at ~360, 345, and 330-320 Ma (Dennis and Wright, 1997; Bream, ms, 2003; Merschat, ms, 2009), similar to our findings in central Georgia (peaks at ~380 and ~320 Ma, discussed in greater detail in the results section). P-T estimates and ages of plutons and metamorphism imply the Inner Piedmont underwent peak metamorphism 405-360 Ma, remained hot until ~345 Ma, cooled, and was again subjected to a thermal increase peaking 330-320 Ma (Dennis and Wright, 1997; Merschat, ms, 2009; this study). Abundant anatectic(?) granitoids coincide with regional metamorphism (407-350 Ma), with apparent pulses at ~400, ~380, and ~360 Ma (Giorgis and others, 2002; Mapes, ms, 2002; Gatewood, ms, 2007; Byars and others, 2008; this study). The dominant regional foliation (S_2), which developed during peak metamorphic conditions, crosses folded contacts between Devonian Inner Piedmont plutons, pegmatites, and granitic melts, which supports plutonism occurred pre- to syn-peak metamorphism. $^{40}\text{Ar}/^{39}\text{Ar}$ release spectra of biotite, muscovite, and hornblende from the Georgia Inner Piedmont and portions of the Carolina superterrane indicate cooling from a thermal event occurred 360-350 Ma (Secor and others, 1986; Dallmeyer, 1989).

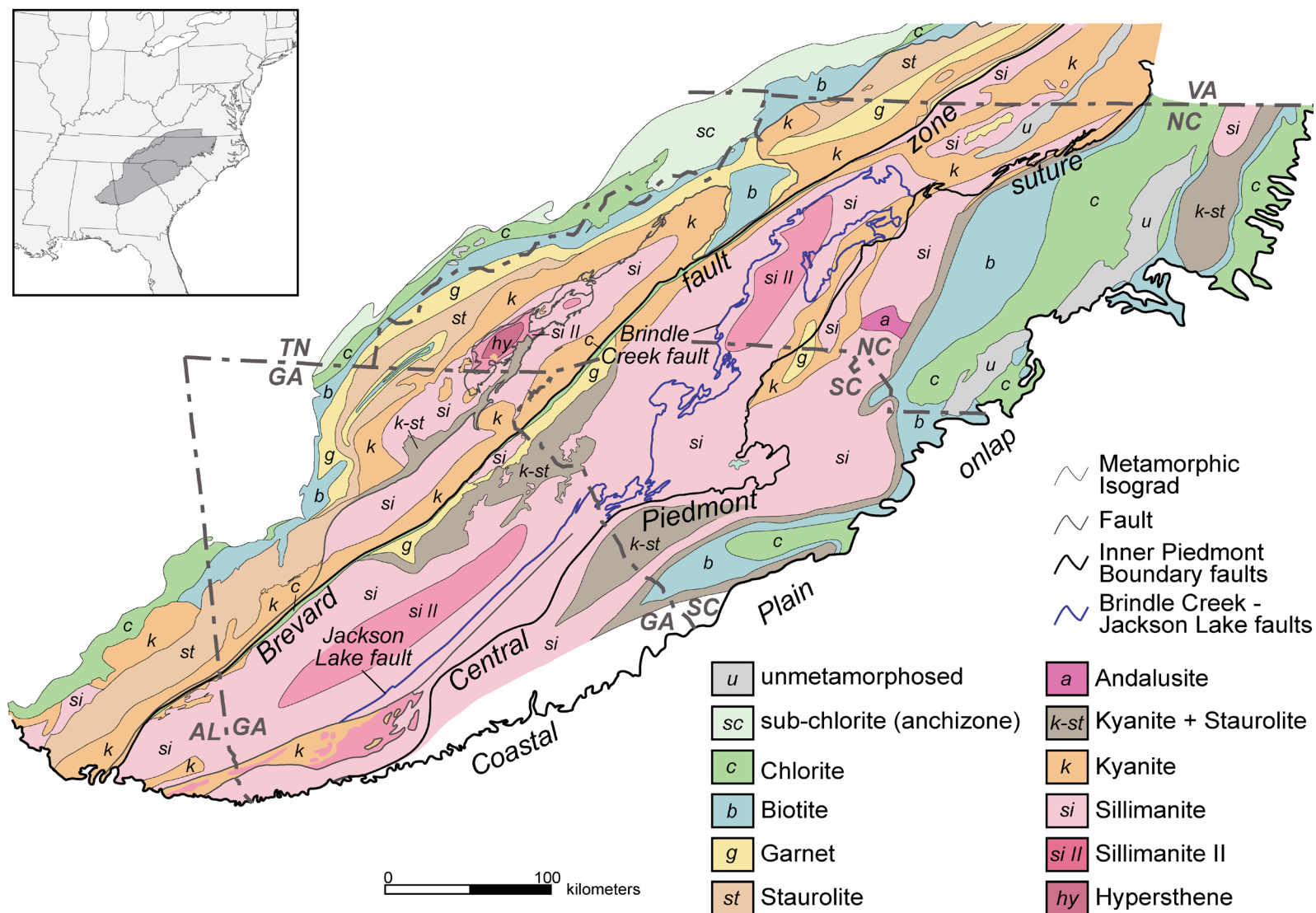


Figure 2-9: Metamorphic isograd map of the southern Appalachian orogen (modified from Mersch, ms, 2009; Hatcher, 2004b, and references therein.).

$^{40}\text{Ar}/^{39}\text{Ar}$ ages from the Gold Hill fault zone also indicate portions of the Carolina superterrane cooled from a thermal peak ~ 375 Ma (Hibbard and others, 2012), which interestingly coincides with timing of prograde upper-amphibolite facies metamorphism in the Inner Piedmont.

The nature of the boundary separating the Tugaloo and Cat Square terranes

Northern portion: The Brindle Creek fault

Giorgis (ms, 1999) first recognized the Brindle Creek fault, a boundary that involves truncation of map-scale structures (both hanging wall and footwall) and subtle changes in lithostratigraphy, in the South Mountains, NC. The Brindle Creek fault at this locality juxtaposes migmatitic metagraywacke above Poor Mountain Formation migmatitic biotite-hornblende gneiss from, and was mapped as a northwest-vergent thrust with a gentle ($10\text{--}15^\circ$) southeast dip (Giorgis, ms, 1999; Williams (ms, 2000)). The tectonic significance of the Brindle Creek fault, however, was not understood until detrital zircon analysis of Brindle Creek thrust sheet metagraywacke revealed the characteristic detrital zircon suite that warranted its separation as a distinct suspect terrane (for example, Bream and others, 2001, 2004). This fault was also traced through the Brushy Mountains to the north (Kalbas, 2003; Mersch, ms, 2003; Wilson, ms, 2006; Gatewood, ms, 2007), and was identified by the occurrence of the characteristic Hibriten mylonite, a fine- to medium-grained porphyroclastic garnetiferous biotite gneiss up to 2 km thick (Mersch and Kalbas, ms, 2002). Gatewood (ms, 2007) concluded mylonitization occurred under amphibolite facies conditions and involved dominantly dextral, top-to-the-southwest shear sense at the northeastern end of the Cat Square terrane. The Hibriten mylonite correlates with the inequigranular biotite gneiss unit of Goldsmith and others (1988), which has been used to locate the Brindle Creek fault across the Charlotte $1^\circ \times 2^\circ$ sheet (for example, Hatcher and others, 2007). In South Carolina, the fault trace has been correlated with previous mapping efforts (for example, Curl, ms, 1998; Nelson and others, 1998), and has been confirmed as the thrust fault that emplaced the Paris Mountain thrust sheet with detrital zircon analysis (Bream, ms, 2003; Mersch and others, 2010). The trace of the fault becomes increasingly tentative through southwestern South Carolina and northeastern Georgia.

The Brindle Creek fault has alternatively been interpreted as an unconformity based on the relationship of younger-over-older rocks (Dennis, 2007), similar to the Salinic basins of New England (for example, Osberg and others, 1989; Robinson and others, 1998). This interpretation, however, is not supported by: 1) truncation of structures and lithologic units on both sides of the boundary, including granitoids in the overlying rocks that are younger than the interpreted unconformity (Giorgis, ms, 1999; Williams (ms, 2000); Kalbas, 2003; Mersch, ms, 2003; Wilson, ms, 2006; Gatewood, ms, 2007; Byars, ms, 2010); 2) distinct age partitioning of granitoid ages on either side of the boundary; and 3) abundant mylonite along the boundary. A younger-over-older

relationship at a discontinuous boundary does not necessitate the occurrence of an unconformity; numerous younger-over-older thrust faults have been documented in the southern Appalachians (for example, Greenbrier fault, King, 1964; Box Ankle fault, Hooper and Hatcher, 1988).

Several key map relationships have been recognized along the Brindle Creek fault that provide insight regarding its timing. In the northeastern portion of the Cat Square terrane, the Poplar Springs map-scale sheath fold, outlined by the ~407 Ma megacrystic Walker Top Granite is truncated by the Brindle Creek fault, suggesting emplacement of the thrust sheet occurred post ~407 Ma (Gatewood, ms, 2007). This same relationship occurs in the southwestern Brushy Mountains, as the northwest limb of the Big Warrior Creek sheath fold, again outlined by ~407 Ma Walker Top Granite, is crosscut by the Brindle Creek fault (Merschhat and Kalbas, ms, 2002; Merschhat et al., 2005). At the southwest end of the Newton window, another map-scale sheath fold that includes Walker Top Granite dated at ~355 Ma is also truncated by the Brindle Creek fault (Byars, ms, 2010). These mappable truncations provide critical evidence regarding deposition in the Cat Square terrane, as well as timing constraints for the Brindle Creek fault. Merschhat and Hatcher (2007) suggested the youngest detrital zircons delimit the maximum age for Cat Square terrane rocks, although the basin itself could have been open for much longer, with the introduction of the Ordovician-Silurian suite merely a function of uplift, erosion, and deposition of the source material. The oldest anatectic granitoid, however, indicates closure and burial of the basin had to occur prior to ~407 Ma, revealing the possible short-lived nature of this basin. The youngest granitoid (~355 Ma) cut by the fault, which post-dates the age of the oldest granitoid by ~60 m.y., signifies the long, hot history of the Acadian/Neoacadian orogeny in the Inner Piedmont.

Central Georgia: The Jackson Lake fault?

The Jackson Lake fault is an ~15 m thick sillimanite-grade fault zone that dips very steeply southeast in the northeast portion of the study area in central Georgia, and changes to a moderate northwest dip toward the southwest. Granitoids and metasedimentary assemblages from both sides of the fault are truncated along this boundary. The Jackson Lake fault likely truncates against the Alleghanian Towaliga fault to the southwest, although this intersection has not been mapped in detail. The Jackson Lake fault has been traced as far northeast as Mansfield, Georgia (Fig. 2-4), and may correspond with a fault ~25 km northeast of the study area that was described by Lawton (ms, 1969) as a fault that truncates alternating bands of biotite gneiss and amphibolite (lower Tallulah Falls Formation?). Pervasive S-C fabric, along with asymmetric σ -, δ -, and θ -porphyroclasts in the fault zone dominantly exhibit dextral shear sense, while shallow-plunging mineral stretching lineations indicate chiefly strike-slip displacement (Huebner and Hatcher, 2011). Mylonite protoliths include migmatitic metagraywacke and megacrystic High Falls Gran-

ite. Mylonitic fabric is generally concordant with regional foliation and, combined with sillimanite growth within the mylonitic foliation, indicates the fault was active pre- to syn-D₂, which coincides with peak metamorphic conditions. Although granitoids from both sides of the fault are truncated, one small pod of Indian Springs Granodiorite appears to crosscut the fault, providing at least some timing constraints along this boundary. The Jackson Lake fault roughly coincides with the strong aeromagnetic lineament that Hatcher and others (2007) interpreted to represent the southwest extension of the Brindle Creek fault (Fig. 2-1B). Although we suggest the Jackson Lake fault is equivalent to the Brindle Creek fault, the motive behind introducing new nomenclature is a product of: 1) different characteristics of the fault zones; the Brindle Creek fault is a low-angle, southeast-dipping thrust fault, whereas the Jackson Lake fault is a steeply northwest-dipping strike-slip fault; 2) ambiguities in regional aeromagnetic data and a paucity of detailed geologic mapping through northeastern Georgia and southwestern South Carolina do not provide the necessary confidence to undoubtedly trace the Brindle Creek fault to central Georgia; and 3) the data presented here do not unequivocally support our hypothesis. However, we maintain this proposition, and view these data as an opportunity to gain further insight into the tectonic history of the Inner Piedmont.

METHODOLOGY

Detailed geologic mapping in the vicinity of the aeromagnetic lineament in central Georgia was conducted as part of several University of Tennessee student theses between 2008 and 2012 (Davis, ms, 2010; Howard, ms, 2012; Huebner, in prep.; Rehrer, in prep.). Fabric elements, lithology, index minerals, and spatial relationships between lithologies were carefully recorded. Samples for geochronologic and geochemical analysis were selected based on the results of detailed geologic mapping to maximize the benefits of those techniques.

Approximately 10-15 kg of specific crystalline rocks from the Inner Piedmont and adjacent Carolina superterrane were sampled for the geochronologic portion of this study, with geographic coordinates listed in table 2-1. Samples include Inner Piedmont granitoids and migmatitic meta-graywackes, one small gabbroic pluton and one sample from the corresponding contact aureole (pyroxene hornfels) of the Gladesville Gabbro from the western portion of the Carolina superterrane in central Georgia. Where possible, localities were sampled where crosscutting relationships with adjacent rocks were evident. Two additional samples were collected from the Henderson Gneiss in the northern portion of the Inner Piedmont.

Samples for whole-rock geochemistry were primarily chosen on the basis of an apparent lack of chemical weathering, and when possible, coincide with rocks selected for geochronologic analysis. Samples were initially broken into ~5 cm pieces in the field and at the University of

Tennessee, and were further reduced to < 1 cm using a 5.7 x 7.6 cm jaw crusher. Approximately 30 g of each sample (~100 g for coarse and megacrystic samples) were milled into a fine powder using an alumina ceramic mill and Shatterbox™. Individual sample powders were mixed, and 15 g of each sample were sent to Activation Laboratories in Ancaster, Ontario, for whole-rock geochemical analysis. Major elements, Sr, Ba, Y, and Zr were determined using inductively coupled plasma (ICP) emission spectroscopy employing lithium metaborate/tetraborate fusion (FUS-ICP). Trace and rare earth elements (REE) were determined by total digestion methods (TD-ICP), instrumental neutron activation analysis (INAA), and fusion methods (FUS-MS). Compositional diagrams illustrating whole-rock geochemical data were generated using Igpet® software.

Different stages of zircon separation and geochronologic sample preparation were performed at the University of Tennessee, University of North Carolina, Vanderbilt University, and Stanford University – U.S. Geological Survey Micro Analysis Center (SUMAC). Sample material was collected and processed following standard mineral separation techniques. Samples were crushed to <500 µm using a belt-driven disk pulverizer. Heavy minerals were concentrated using a water table, followed by separation of heavy phases with methylene iodide ($\rho = 3.3 \text{ g/cm}^3$). Ferromagnetic phases were removed from the sample with a hand magnet prior to density separation in methylene iodide, and with a Frantz magnetic separator subsequent to heavy liquid separation. Zircons from each sample were mounted in epoxy, polished to the approximate average grain center, and coated with ~10 nm of Au. Grains were imaged using cathodoluminescence (CL) and

Table 2-1: Geographic locations of samples collected for SHRIMP geochronologic analysis.

Lithology	Sample	Latitude	Longitude
Ordovician-Silurian Tugalo terrane Granitoids			
Henderson Gneiss	Sm-1	34°56'06.12" N	82°57'06.48" W
	HQ-1	35°21'34.38" N	82°27'07.71" W
Lithonia Gneiss	AM2	33°39'39.31" N	84°07'23.17" W
	J827	33°20'55.58" N	83°57'32.46" W
Grenville Basement Gneisses, Inner Piedmont Tugalo terrane			
Snapping Shoals Augen Gneiss	W166	33°29'02.89" N	83°57'11.60" W
Silurian-Mississippian Cat Square terrane Granitoids			
High Falls	HHF	33°08'16.1" N	84°06'02.60" W
	HFSP	33°10'42.58" N	84°01'01.18" W
	S123	33°25'25.02" N	83°48'07.30" W
	FRHF	33°27'51.27" N	83°44'17.39" W
Alleghanian Inner Piedmont Granitoids			
Indian Springs	W131	33°29'19.29" N	83°54'32.42" W
	J568	33°15'30.05" N	83°55'44.80" W
	J1210	33°21'31.24" N	83°54'51.42" W
Murder Creek	F850	33°27'47.45" N	83°43'26.09" W
Dows Pulpit	L1452	33°25'03.43" N	83°49'24.40" W
Carolina superterrane			
Metagabbroic diorite	L503	33°16'04.52" N	83°45'10.29" W
Gladesville Gabbro contact aureole	B695	33°10'32.76" N	83°47'48.44" W

reflected light to assess growth zoning, morphology, and the presence of fractures and inclusions prior to ion probe analysis. Routine operating procedures were followed for the SHRIMP-RG. The primary ion beam was run at ~15 nA, with beam diameter maintained at ~22 μm . Standards R33 (~419 Ma) and TEM (416.8 Ma), provided by SUMAC, were measured regularly. All data were reduced using the Microsoft Excel™ Add-in SQUID v. 2 (Ludwig, 2009). Zircons were analyzed during three sessions at the SUMAC facility between 2010 and 2013.

RESULTS

Results of geochronologic analyses are grouped based on their position relative to the Jackson Lake fault, which we hypothesize is the southwest equivalent of the Brindle Creek fault (Appendix II; summary of ages in table 2-2). Age calculations and plots to display data were made using Isoplot v. 3.75 (Ludwig, 2012). U-Pb data from igneous rocks were plotted using concordia diagrams (Fig. 2-10), while cumulative probability plots with histograms were used to display results of detrital zircon data (Fig. 2-11). All granitoid ages reported from this study are ^{207}Pb corrected $^{206}\text{Pb}/^{238}\text{U}$ ages unless specified otherwise. Spot analyses greater than $\pm 50\%$ discordant have been excluded from calculated weighted average ages. Interpreted metamorphic rims have been excluded from detrital zircon cumulative probability distributions.

Whole-rock geochemical results from Inner Piedmont granitoids have been subdivided into three groups based on their location relative to the Jackson Lake faults and further subdivided by age (western Piedmont, Ordovician-Silurian [Taconian]; eastern Inner Piedmont, Devonian-Mississippian [Acadian/Neoacadian]; and Pennsylvanian-Permian [Alleghanian]). It should be noted that there is a spatial separation between the Taconian and Acadian/Neoacadian granitoids, whereas Alleghanian granitoids occur throughout the western and eastern Inner Piedmont. Results are compiled with available data from the northern portion of the Inner Piedmont, which have also been separated based on their location relative to the Brindle Creek fault.

Granitoid Geochronology: Northwest of the Jackson Lake fault (Tugaloo terrane?)

Snapping Shoals augen gneiss (W166)

Sample W166 yielded large (100-300 μm long, 100-300 μm wide), subhedral, rounded zircons with acicular to equant morphologies. Concentric growth zoning is obvious in CL, with many grains showing evidence of partial resorption in apparent inherited cores. Most grains have thin ($< 5 \mu\text{m}$), bright rims in CL (low U content) that were too thin to analyze. Spot analyses of zircons yielded ages of 1109-842 Ma, with moderate discordance and the wide spread of ages signifying Pb loss. A chord drawn along an apparent Pb-loss line anchored at known Paleozoic peak metamorphism ($375 \pm 20 \text{ Ma}$) yielded an upper intercept age of $1079 \pm 26 \text{ Ma}$ (mean

squared weighted deviation [MSWD] = 1.7) (Fig. 2-10). We tentatively accept this as the age of the Snapping Shoals augen gneiss, although we recognize a more precise age is not attainable using the current data. Regardless, the bodies of Snapping Shoals augen gneiss represent fragments of granitic Grenvillian basement.

Lithonia Granitoid Gneiss

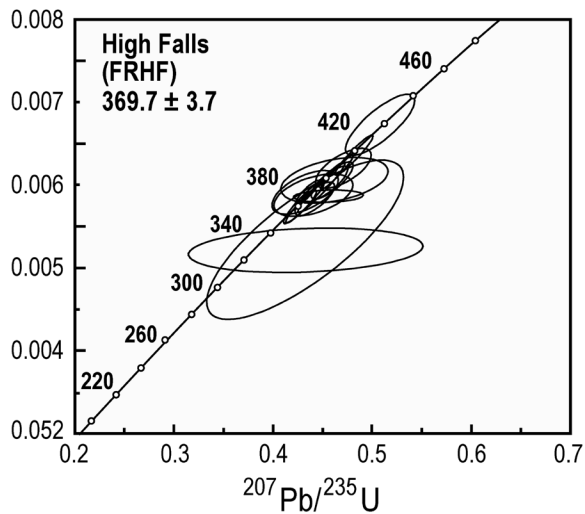
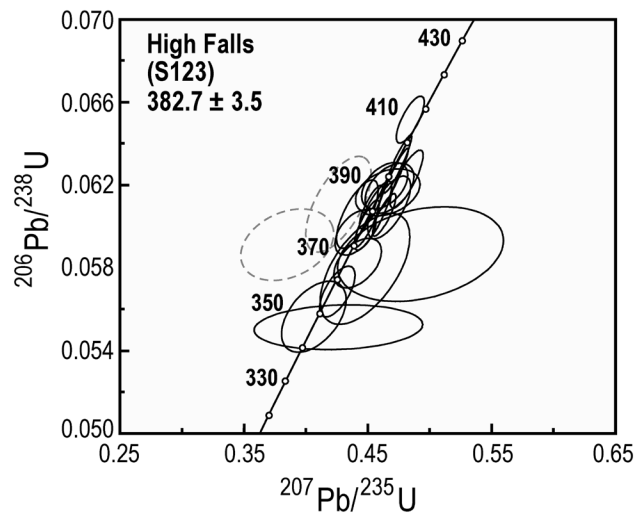
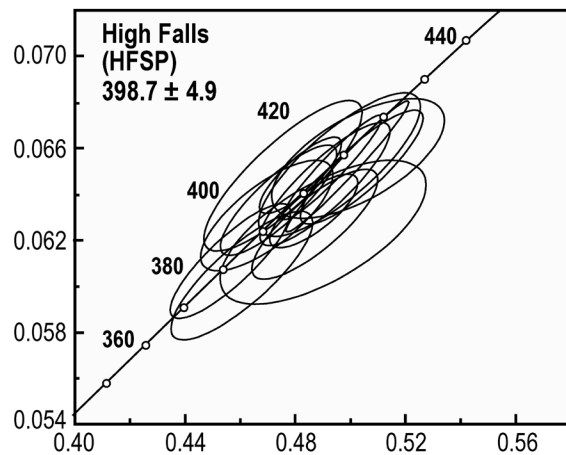
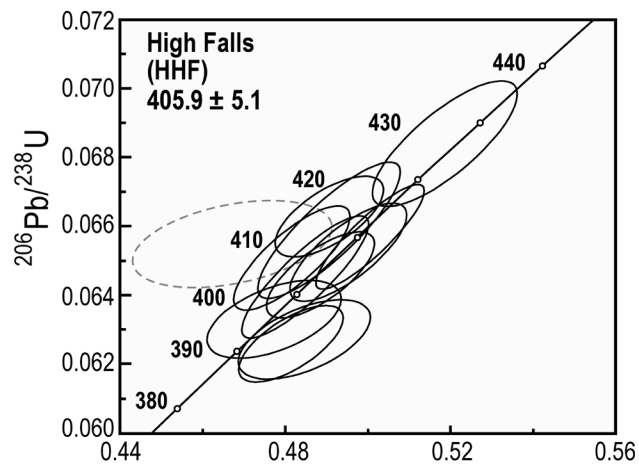
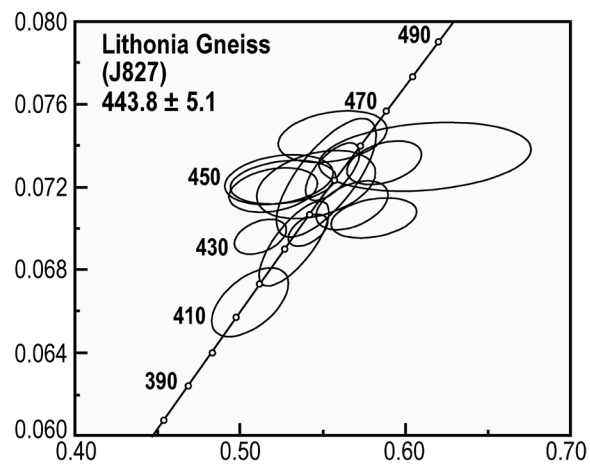
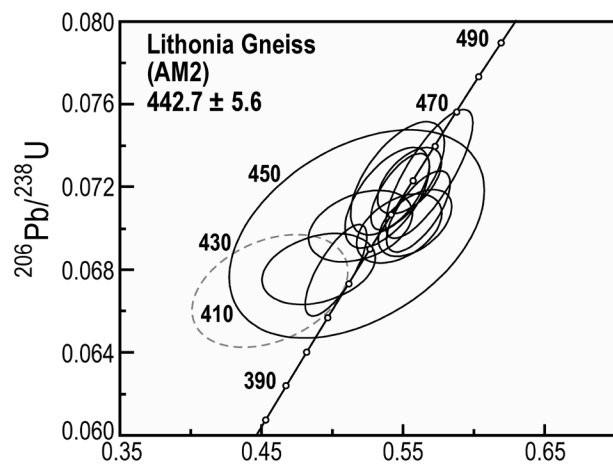
Two samples of the Lithonia Gneiss were dated in this study, as the Lithonia Gneiss is arguably the most voluminous granitoid in this portion of the Inner Piedmont. Samples were collected from an exposure at Arabia Mountain (sample AM-2), ~40 km northwest of the study area, and from a large pavement exposure in the map area (sample J827) (Fig. 2-4). Zircons from the Lithonia Gneiss are mostly acicular and euhedral with well-developed concentric zoning, with partial resorption textures common along apparent inherited cores. Zircons range from 100-300 μm long and 50-100 μm wide. Many grains appear to contain xenocrystic cores, with spot analyses from both samples yielding Middle to Late Proterozoic inheritance. A weighted average of analyses from sample AM-2, interpreted to represent crystallization, yielded an age of 442.7 ± 5.6 Ma (MSWD = 0.73). Sample J827 revealed a wider distribution of crystallization ages, with a weighted average of 443.8 ± 5.1 Ma (MSWD = 3.3). Although the MSWD for this average is high, the age is within error of sample AM-2. The largest cluster of data (eight analyses) yields a weighted average of 451.9 ± 3.6 Ma (MSWD = 0.15), although it is difficult to justify the exclusion of the younger analyses that are included in the previous weighted average. These weighted averages exclude analyses of metamorphic rims and obvious inherited cores.

Granitoid Geochronology: Southeast of the Jackson Lake fault (Cat Square terrane?)

High Falls Granite

Four samples of the High Falls Granite were analyzed in this study (HHF, HFSP, S123, FRHF), as preliminary geochronologic analyses yielded a wide spread of ages for individual samples. Samples yielded euhedral to subhedral, acicular to subequant zircons that are 100-300 μm long and 50-150 μm wide. Zircons exhibit well-developed concentric zoning, with deep embayments in most samples indicating partial resorption and occurrence of possible inherited cores. Spot analyses revealed the presence of Mesoproterozoic to Neoproterozoic inheritance in all samples but FRHF, although many core/rim paired analyses of single zircons yielded indistinguishable ages. Calculated weighted averages of samples HHF and HFSP were within error (405.9 ± 5.1 [MSWD = 1.2] and 398.7 ± 4.9 Ma [MSWD = 1.41], respectively), although samples collected farther northeast yielded weighted averages that were 20-30 m.y. younger (S123, 382.7 ± 3.5 Ma [MSWD = 1.3]; FRHF, 369.7 ± 3.7 [MSWD = 1.08]).

Figure 2-10: Zircon U-Pb concordia diagrams for plutonic rocks analyzed in this study. Gray-dashed analyses were excluded as discordant, and were not used in weighted average calculations. Reported ages are weighted averages of ^{207}Pb -corrected $^{206}\text{Pb}/^{238}\text{U}$ analyses, discussed in text. High Falls Granite samples HHF and HFSP from Howard (ms, 2012).



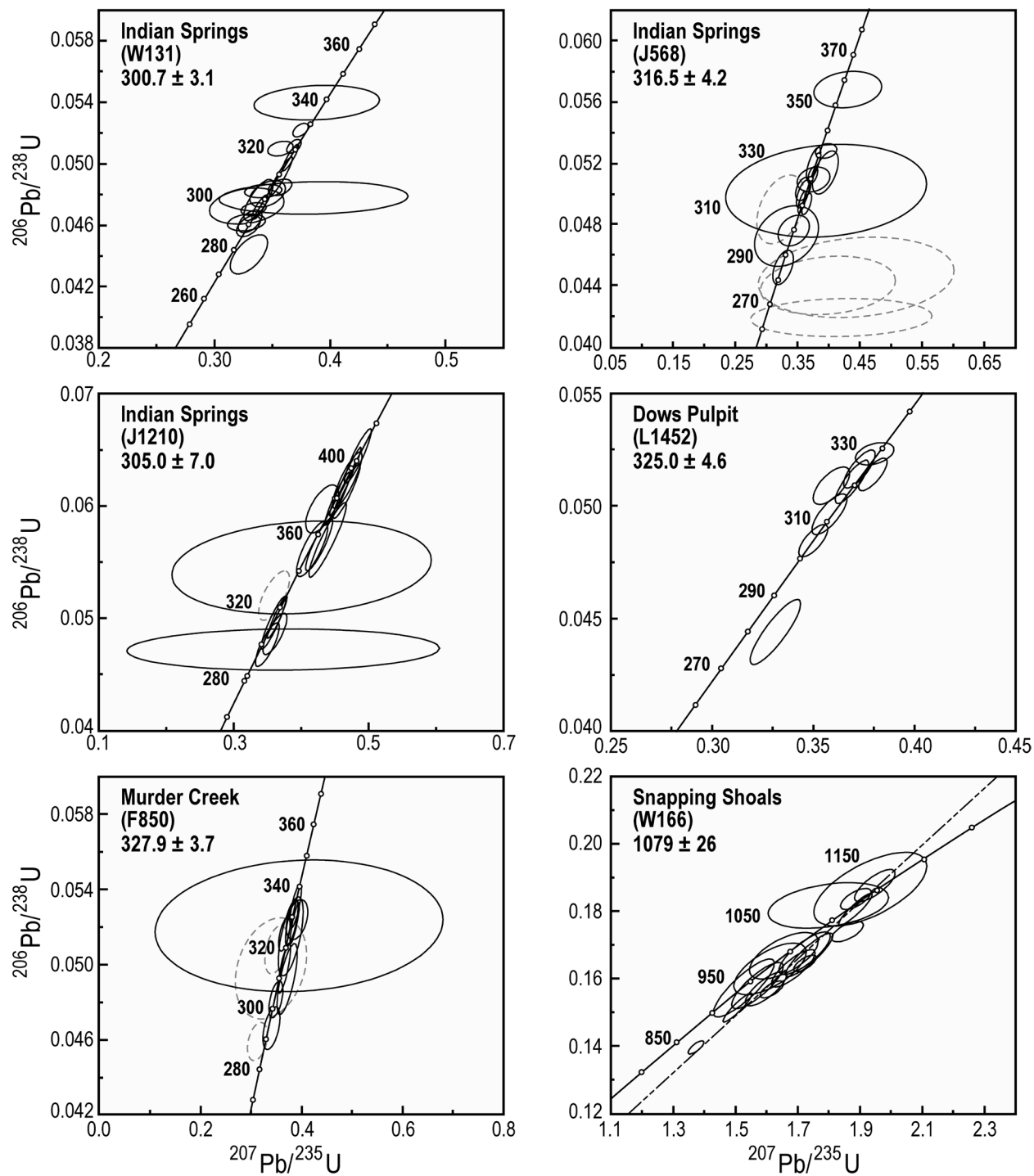


Figure 2-10 (continued)

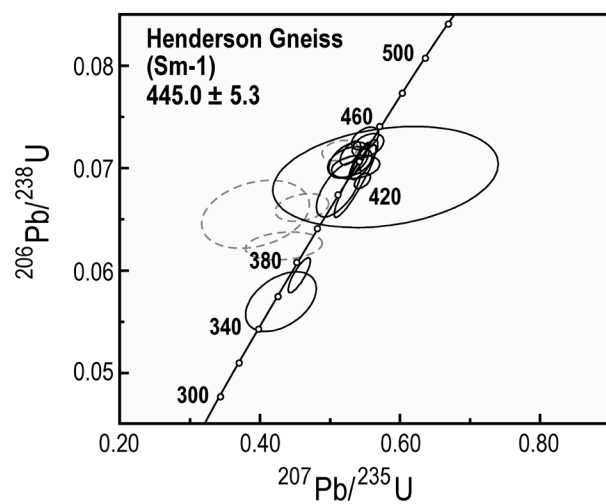
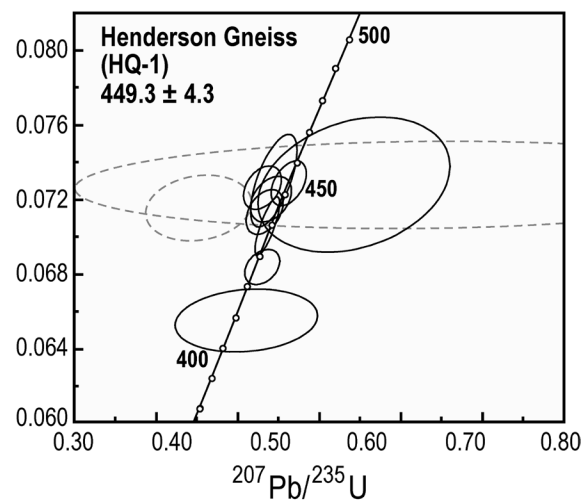
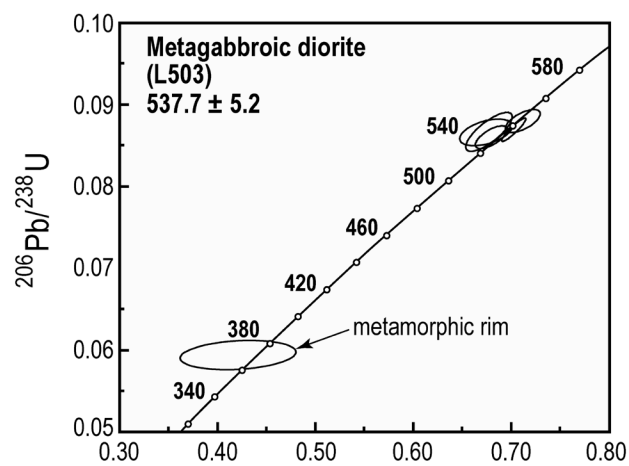


Figure 2-10 (continued)

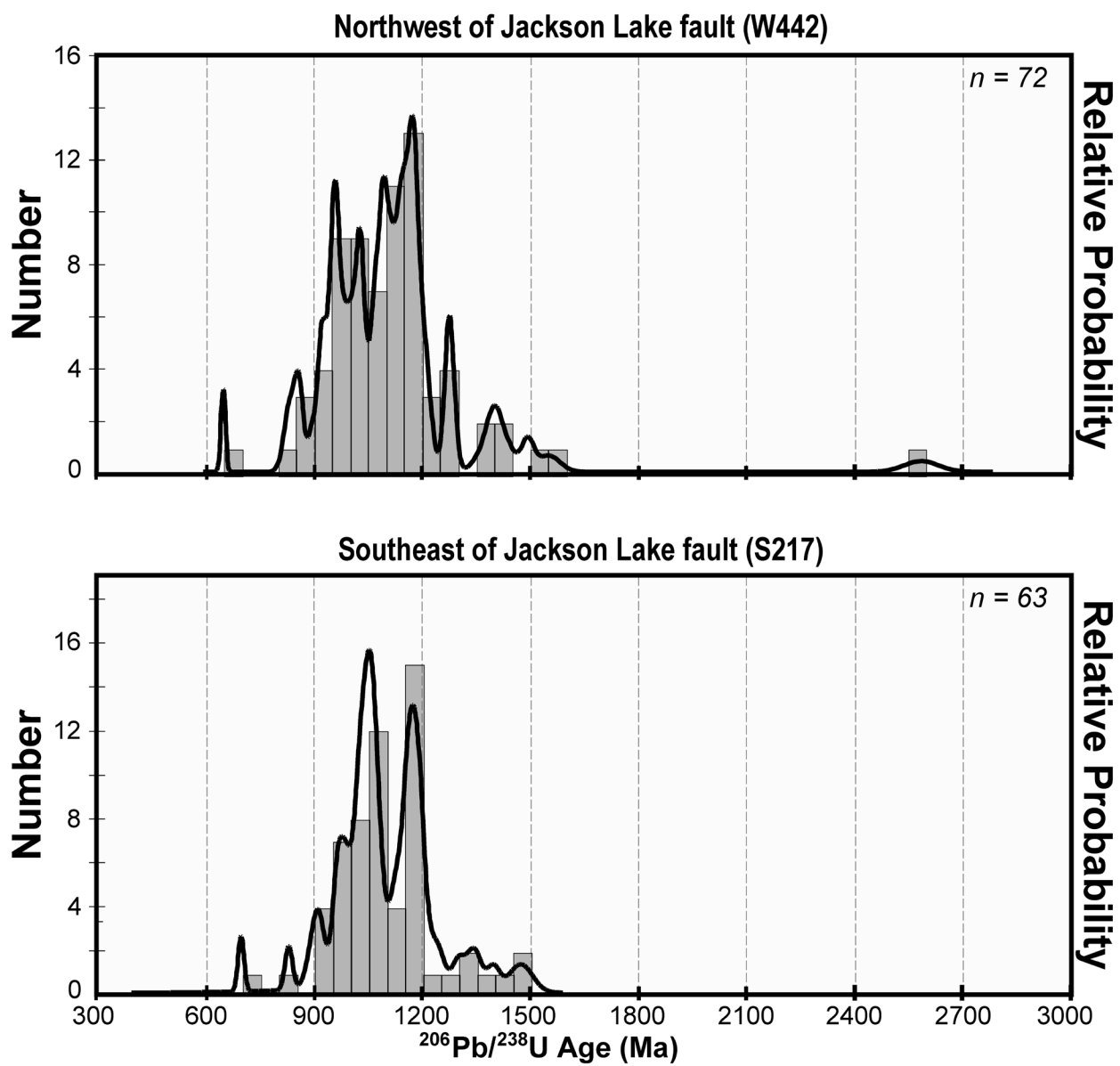


Figure 2-11: Relative probability distributions with histograms of detrital zircon data from the two samples analyzed in this study.

Dows Pulpit Granodiorite (L1452)

Zircons from sample L1452 contained mostly large (100-300 μm long, 50-150 μm wide) acicular grains. Many zircons in this sample contain rounded, U-poor cores mantled by thick (≤ 100 μm) dark, U-rich overgrowths. Cores and overgrowths exhibit well-developed concentric zoning, with embayments common in cores evidence of partial resorption. Inherited cores yield Paleoproterozoic through Devonian ages. Thick dark overgrowths and grains with no apparent inherited cores range from 329-225 Ma, with the majority of analyses occurring between 330 and 320 Ma. Several overgrowths have low Th/U ratios indicating metamorphic genesis, while whole grains in this cluster of data generally have Th/U ratios >0.1 . A weighted average of 325.0 ± 4.6 Ma (MSWD=1.7) was calculated from whole grains and overgrowths from this concentration of ages, which we interpret to represent crystallization.

Murder Creek granite (F850)

Zircons from sample F850 are mostly euhedral, acicular with some subequant to equant grains, and range 150-400 μm long by 50-200 μm wide. Most grains exhibit well-developed growth zoning. Discordant zoning in some grains indicates inheritance, although no older cores were identified. Individual spot analyses yielded ages that range 334-290 Ma, with the majority of ages 335-320 Ma. A weighted average of 327.9 ± 3.7 Ma (MSWD=0.41) is interpreted to represent crystallization of this body. No spot analyses from this sample indicate metamorphic genesis (Th/U < 0.1).

Granitoid Geochronology: The Indian Springs Granodiorite

The Indian Springs granodiorite occurs on both sides of the Jackson Lake fault, with one small body that apparently crosscuts the fault. Foliation, where developed, typically parallels sharp lithologic contacts, suggesting a magmatic origin. Bodies most commonly truncate regional foliation, although in rare instances the magmatic foliation is subparallel (Fig. 2-7). The crosscutting nature of this body, in addition to the apparent lack of strong deformation, indicates this granitoid crystallized post-D₂. Three samples were analyzed using SHRIMP, one from each side of the fault, (W131, northwest; J568, southeast), and one from the body that crosscuts the fault (J1210). All samples yielded a complex distribution of zircon ages, which include inherited cores and overgrowths with questionable petrogenetic origin. Spot analyses are plotted against Th/U ratios in figure 2-12, with cumulative probability distributions, in an effort to justify our interpretation of the crystallization ages of these bodies.

Zircons from sample W131 are mostly small (<100 μm long, <50 μm wide) acicular to equant grains, although larger grains (100-200 μm long, 50-100 μm wide) are present. Most grains exhibit distinct compositional zoning in CL, with bright U-poor cores mantled by thick, dark U-poor overgrowths. Cores tend to have well-developed concentric zoning, while overgrowths exhibit little or no zoning. Obvious xenocrystic cores yield ages that range from Proterozoic (1738-616 Ma) through Paleozoic (374- 339 Ma). Dark overgrowths range from 328-297 Ma, with a wide variation in Th/U ratios throughout the age distribution, prohibiting a clear distinction of overgrowths as magmatic or metamorphic in origin. In addition, the broad range of ages makes the assignment of a specific crystallization age problematic. The largest cluster of ages falls between 310-285 Ma (weighted average of 298.4 ± 3.6 Ma [MSWD=4.7]), although the greatest concentration of ages in this range occurs between 305 and 295 Ma. A weighted average of these eight analyses yields an age of 300.7 ± 3.1 Ma (MSWD = 2.1). Five of the eight analyses used for the weighted average were from zircon cores and/or whole grains, while three were from dark overgrowths (two of which yielded Th/U ratios < 0.1). We interpret this to represent the final crystallization age, although we recognize the complex zircon assemblage in this sample disallows the resolution of a more reliable age.

Sample J568 contains large (100-400 μm long, 50-150 μm wide) euhedral acicular to subequant zircons, many of which include rounded, relatively U-poor inherited cores mantled by thick, U-rich overgrowths. Analyses of cores reveal Neoproterozoic and Paleozoic inheritance, in addition to cores that yielded ages that overlap with ages of dark overgrowths. Ages of overgrowths and authigenic grains range from 331 to 258 Ma, with metamorphic Th/U ratios occurring throughout that spread. The largest cluster of ages yielded a weighted average of 316.5 ± 4.2 Ma (MSWD = 2.4), which includes overgrowths and whole grains, both of which cover a variety of Th/U ratios. We interpret this to represent the crystallization age, even though the majority of these analyses yield metamorphic Th/U ratios.

Zircons from sample J1210 are generally large (100-400 μm long, 50-150 μm wide) euhedral acicular to subequant zircons, many of which include rounded, relatively U-poor inherited cores. Analyses of cores reveal Paleoproterozoic through Paleozoic inheritance, with the youngest core ~300 Ma. Ages of overgrowths and grains with no apparent inherited cores range from 538 to 305 Ma, with most occurring 403-354 Ma, concentrated 389-375 Ma. A concentration of ages from one core, one whole grain, and three overgrowths (one with Th/U ratio < 0.1) occurs between 315 and 295 Ma, with a weighted average of 305.0 ± 7.0 Ma (MSWD=1.06), which we interpret to be crystallization age of the body. These data could alternatively be interpreted to represent crystallization ~382 Ma, with the Pennsylvanian-Permian ages representing a later metamorphic event.

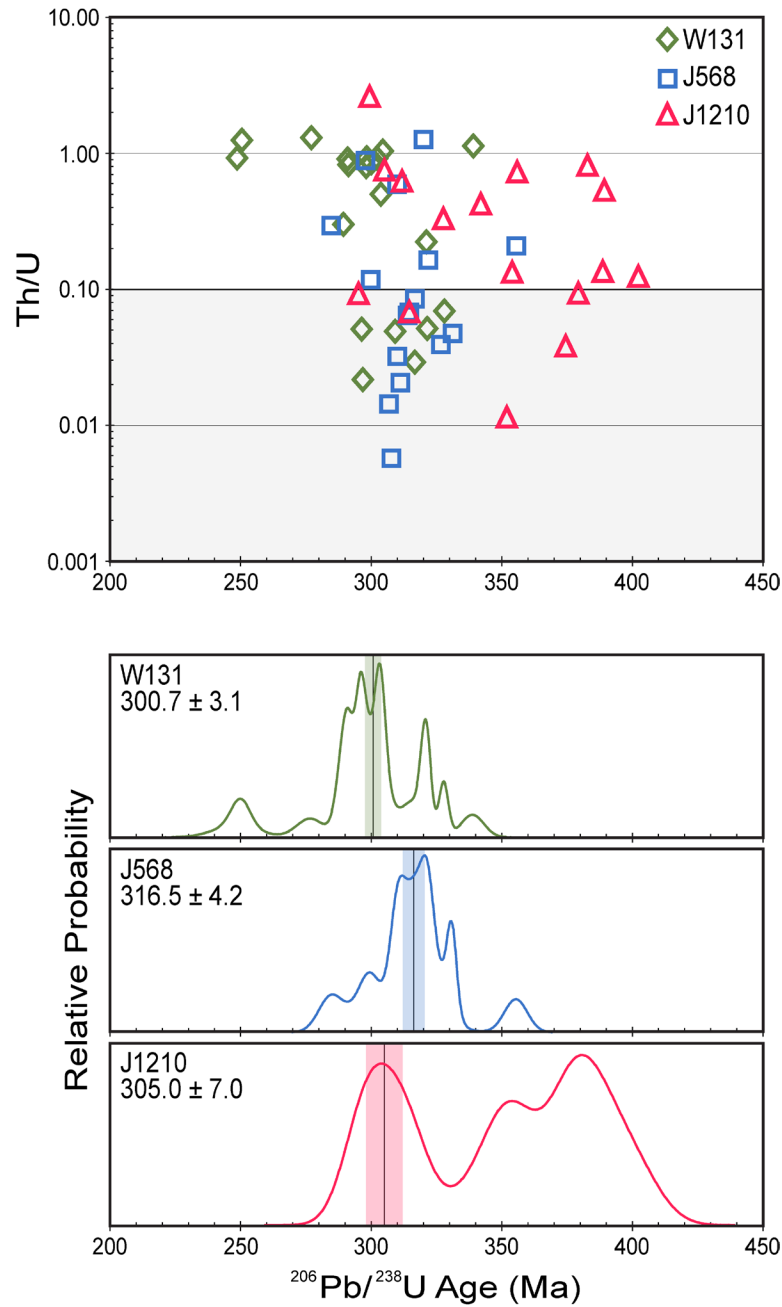


Figure 2-12: Th/U versus age plot of the three samples of Indian Springs Granodiorite, with relative probability distributions illustrating calculated weighted averages. Shaded bars in relative probability diagrams correspond to error in calculated age. In individual samples, apparent metamorphic (Th/U < 0.1) and magmatic spot analyses overlap. Determination of calculated ages is discussed in greater detail in text.

We suggest that the younger clusters of ages, many of which include apparent metamorphic overgrowths, actually represent the crystallization of this granitoid. Evidence that supports this interpretation includes: 1) field relationships, which indicate this granitoid was emplaced relatively late, at least post D_2 ; 2) inherited cores that yield age ranges from Paleoproterozoic through Paleozoic, and do not generally yield a coherent Paleozoic age; 3) overlapping ages of numerous cores, whole grains, and dark overgrowths; and 4) thick U-rich overgrowths that yield fairly consistent ages, while the bodies of granodiorite do not show any indication of a strong thermal overprint post-crystallization, nor is there any supporting evidence for strong tectonic deformation.

The suite of ages yielded by sample J1210, which crosscuts the Jackson Lake fault, is particularly interesting. This sample includes a cluster of Devonian ages and Alleghanian ages from cores, rims, and whole grains, whereas samples W131 and J568 each contain one Devonian grain. The relative abundance of Devonian cores in sample J1210 may be a product of this particular body crystallizing close to the Jackson Lake fault, where intense migmatization is prominent. It is possible that zircon that crystallized during migmatization associated with emplacement of the Jackson Lake fault may have been incorporated into this small body of Indian Springs granodiorite. Many of the inherited Devonian cores have low Th/U ratios, which may support this supposition.

Granitoid Geochronology: Southeast of the Ocmulgee fault (Carolina superterrane)

Metagabbroic diorite (L503)

Several lenticular bodies of metagabbroic diorite occur southeast of the Ocmulgee fault. These rocks are moderately foliated, medium- to coarse-grained, with dominant mineralogy consisting of hornblende, plagioclase, augite, quartz, and epidote. Structural relationships with surrounding country rock indicate the intrusion of these bodies predated deformation and metamorphism in this portion of the Carolina superterrane.

This sample yielded very large (200-400 μm wide by 250- > 400 μm long), euhedral to subhedral, equant to sub-equant zircons with clean concentric and sector zoning. Thin, U-rich rims with minor embayments are common. Analyses of six zircons yielded a weighted average of 537.7 ± 5.0 Ma (MSWD = 0.45), which coincides with magmatism in other portions of the Carolina superterrane (for example, Dennis, 1995; Dennis and Wright, 1997). One analysis of an overgrowth within a deep embayment yielded a Devonian age (~ 374 Ma), which is likely related to regional metamorphism.

Pyroxene hornfels from the Gladesville Gabbro contact aureole (B695)

Sample B695 was collected < 100 m from the main body of the Gladesville Gabbro in a well-documented contact aureole that metamorphosed layered intermediate gneissic country rock (for example, Carpenter and Hughes, 1970; Hooper, ms, 1986). The protolith of the country rock was likely a low-K felsic volcanic (Hooper, ms, 1986). This sample is a strongly foliated, migmatitic, quartzose gneiss, with foliation defined by biotite. Dominant mineralogy consists of quartz, plagioclase, biotite, hornblende, and orthopyroxene (hypersthene?). Petrographic analysis revealed relatively strain-free quartz with well-developed 120° grain boundaries, which agrees with field relations that indicate crystallization of the gabbro occurred subsequent to fabric development.

Zircons from sample B695 are subhedral, acicular to equant, and range 100-250 μm long, 50-150 μm wide. Grains commonly show well-developed concentric zoning throughout, although many zircons include very distinct inherited cores mantled by thick, U-poor rims (Fig. 2-13). Several grains exhibit very thin, bright rims that were too thin to analyze. Cores and whole grains without well-developed rims yielded ages of 578 to 474 Ma, with a weighted average of the most prominent cluster of ages 534.4 ± 4.0 Ma (MSWD = 0.21). Ages of thick overgrowths range from 445 to 349 Ma, with the largest grouping of ages at 372.7 ± 2.3 Ma (MSWD = 0.95). Th/U ratios of cores are consistently higher than younger rims, supporting metamorphic zircon growth (Fig. 2-13C). We interpret the ages of inherited cores to represent volcanism associated with the late Neoproterozoic to Cambrian event prevalent throughout the Carolina superterrane and, based on strong evidence for contact metamorphism related to the intrusion of the Gladesville Gabbro, we interpret the age of the metamorphic overgrowths to coincide with emplacement of the gabbro. An independent test of this interpretation would be to concentrate zircon from the pluton itself for geochronologic analysis, although initial attempts have been unsuccessful. We understand the inherent ambiguities with this argument, but contend that our interpretation is logical based on available data.

Granitoid Geochronology: Northern Inner Piedmont

Henderson Gneiss

Two samples of the Henderson Gneiss from northwestern South Carolina (Hatcher and Acker, 1984) and North Carolina (Vulcan Materials Hendersonville Quarry) were dated in this study (geographic coordinates of sample locations listed in table 1). Sample Sm-1 is noticeably more deformed and weathered than sample HQ-1.

Henderson Gneiss zircons are mostly acicular and euhedral with well-developed concentric zoning, and apparent inherited cores with embayments indicative of partial resorption. Sample Sm-1 yielded zircons that are slightly rounded and commonly fractured, and range from 150-

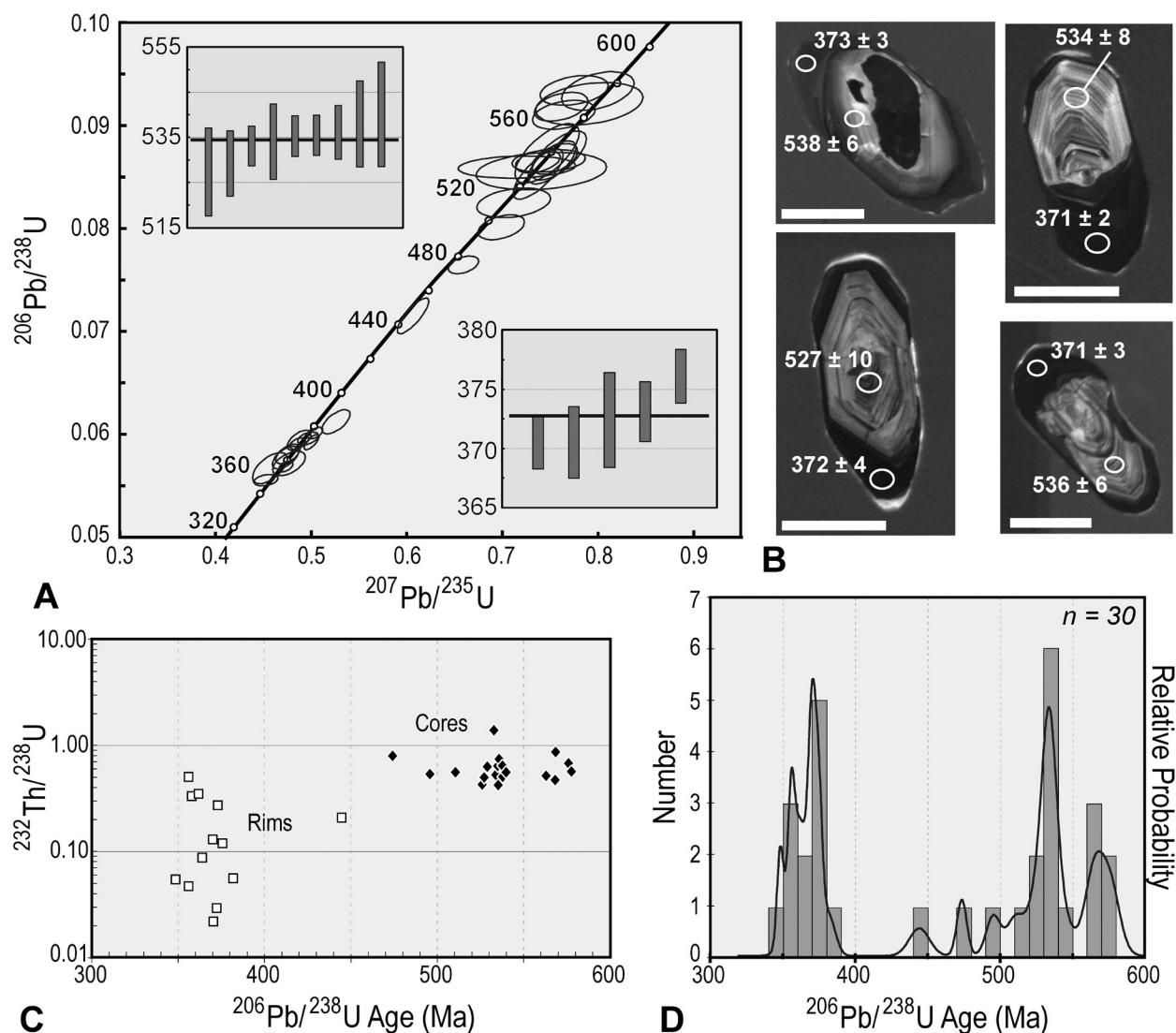


Figure 2-13: U-Pb data and images of zircons from sample B695, pyroxene hornfels surrounding the Gladesville gabbro. (A) Concordia diagram with weighted average plots of the two apparent clusters of data. (B) Images of characteristic zircons from this sample with locations of spot analyses. White bar = 100 μm (C) Th/U versus age of individual analyses, illustrating the distinct difference in Th/U ratios between cores and rims. (D) Relative probability distribution with histogram.

350 μm long and 50-150 μm wide. Many grains appear to contain xenocrystic cores, although only one spot analyses from both samples yielded a Neoproterozoic age (~ 950 Ma). A weighted average of analyses from sample HQ-1, interpreted to represent crystallization, yielded an age of 449.3 ± 4.3 Ma (MSWD = 0.82). Sample Sm-1 revealed a wider distribution of ages, including two Devonian analyses. The majority of analyses cluster 454-437 Ma, yielding a weighted average of 445.0 ± 5.3 Ma (MSWD = 1.4).

Detrital Zircon Geochronology

Detrital zircons from two samples of biotite paragneiss, one from each side of the Jackson Lake fault, were analyzed in this study. Both samples are lithologically similar: they are dark gray, medium-grained biotite-quartz-plagioclase gneisses that include accessory microcline, garnet, and muscovite. Samples are strongly foliated, with metamorphic foliation in each sample parallel to compositional banding. Both samples contain zircons with a wide variety of sizes, morphologies, and internal zoning textures. Zircons are generally rounded, mostly subequant to equant with few acicular grains, with a wide variation in size. Many zircons appear to have thin metamorphic overgrowths.

Northwest of the Jackson Lake fault (W442)

The majority of grains yielded ages of 1300 to 800 Ma, indicating dominantly Laurentian (Grenville source), with a broad double peak with individual peaks at ~ 1175 and ~ 975 Ma (Fig. 2-11). One grain yielded a relatively concordant Neoproterozoic age (~ 656 Ma), which may indicate source from the Superior province, or from possible Amazonian crust (Mersch and others, 2010). Several analyses range from 1500 to 1400 Ma, most likely sourced from the granite-rhyolite province. One Neoproterozoic grain (~ 656 Ma) is difficult to tie to a Laurentian source, and may represent limited peri-Gondwanan provenance.

Southeast of the Jackson Lake fault (S217)

The detrital zircon suite derived from sample S217 is similar to that of sample W442. Relative probability distribution of detrital zircons analyzed from sample S217 reveals an overall normal distribution with two individual peaks centered at ~ 1175 and ~ 1050 Ma (Fig. 2-11). This signature is typical of the Grenville orogen, with the two clusters of ages possibly representing the Shawingian and Ottawa orogenies that comprise the Grenville event. Several zircons yielded 1500-1300 Ma ages characteristic of the granite-rhyolite province. An age of ~ 704 Ma from zircon may represent source from the Laurentian Robertson River Igneous Suite (Aleinikoff and others, 1995).

Table 2-2: New and compiled U-Pb ages of Inner Piedmont granitoids.

Pluton	Sample	U-Pb Age (Ma)	Study
Ordovician-Silurian Tugaloo terrane Granitoids			
	HENDr9gr	447.6 ± 5.4	Moecher et al., 2011
Henderson Gneiss	Sm-1	445.0 ± 5.3	this study
	HQ-1	449.3 ± 4.3	this study
Dysartsville	VM1782	468 ± 8	Bream, 2003
Brooks Crossroads	1398DC	~461 Ma	Vinson, 1999
Caesar's Head	1617	~440 Ma	Vinson, 1999
	1688	~470 Ma	
Lithonia Gneiss	AM2	442.7 ± 5.6	this study
	J827	443.8 ± 5.1	
Toccoa		449 ± 4	Bream, 2003
Grenville Basement Gneisses, Inner Piedmont Tugaloo terrane			
Reepsville Gneiss	R29	1051 ± 18	Mersch, 2009
Snapping Shoals Augen Gneiss	W166	1079 ± 26	this study
Silurian-Mississippian Cat Square terrane Granitoids			
Anderson's Mill	AMG-1	415 ± 3	Mapes, 2002
	HHF	405.9 ± 5.1	Howard, 2012
High Falls	HFSP	398.7 ± 4.9	
	S123	382.7 ± 3.5	this study
	FRHF	369.7 ± 3.7	
	IK-WT	366 ± 3	Mapes, 2002
Walker Top	B9WT	357 ± 5	Byars, 2009
	MV-19	407 ± 2	Gatewood, 2007
Toluca	TOL-11	383 ± 2	Mapes, 2002
Pelham	PEL-1	364 ± 2	Mapes, 2002
Gray Court	GC-1	357 ± 2	Mapes, 2002
Cherryville	C-2	355 ± 2	Mapes, 2002
Alleghanian Inner Piedmont Granitoids			
Stone Mountain (GA)		337 ± 3	Mueller et al., 2011
	W131	300.7 ± 3.1	this study
Indian Springs	J568	316.5 ± 4.2	
	J1210	305.0 ± 7.0	
Murder Creek	F850	327.9 ± 3.7	this study
Reedy River	FS-1	325 ± 5	Mapes, 2002
Dows Pulpit	L1452	325 ± 5	this study
Pacolet	P-1	304 ± 2	Mapes, 2002
Elberton		302 ± 3	Mueller et al., 2011

Metamorphism

Metamorphic overgrowths on zircons in paragneisses and granitoids were also analyzed when possible. Data that were $> \pm 80\%$ discordant, in addition to low Th/U analyses that were interpreted as crystallization ages, were excluded from the compilation of metamorphic ages. Spot analyses interpreted to represent metamorphic zircon growth were selected on the basis of the truncation or embayment of interior oscillatory zoning against an overgrowth with a Th/U ratio ≤ 0.1 . We recognize these criteria alone are not always accurate to distinguish metamorphic from

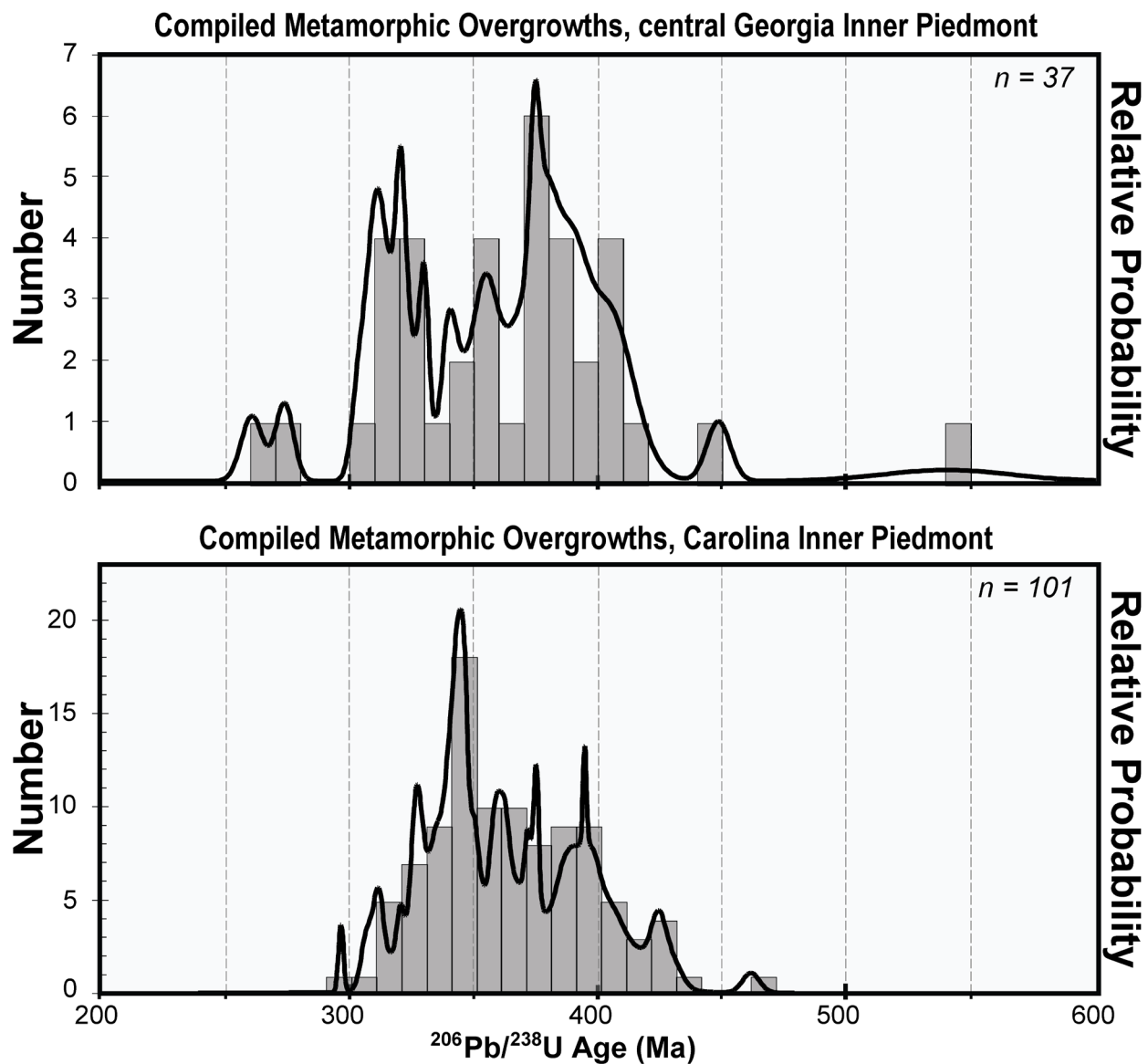


Figure 2-14: Relative probability distributions with histograms of compiled U-Pb SHRIMP analyses determined to be from metamorphic zircon growth. Northern Inner Piedmont data from Mersch (ms, 2009), and references therein.

magmatic overgrowths (for example, Harley and others, 2007). Additionally, high-U overgrowths on zircons from the Indian Springs granodiorite yielded $\text{Th/U} \leq 0.1$, although they most likely represent crystallization of that granitoid. Similar criteria were used to determine metamorphic zircon growth from U-Pb SHRIMP analyses of northern Inner Piedmont rocks (Mersch, ms, 2009), and are compared with our new data in figure 2-14.

Relative probability distributions of the compiled data from the southern portion of the Inner Piedmont yield a bimodal distribution of ages with the largest peaks occurring at ~ 380 and ~ 320 Ma (Fig. 2-14). The Devonian peak is right-skewed, and includes metamorphic zircon growth to ages as old as ~ 420 Ma, with a sharp drop at ~ 370 Ma. Ten spot analyses comprise the largest cluster of ages (390-370 Ma) within the Devonian peak, which likely coincides with upper amphibolite-facies metamorphism and the development of D_2 fabrics through the region. Several rim analyses occur from 370 to 330 Ma with an apparent minor peak ~ 355 Ma, although these ages are subordinate relative to the two larger clusters of ages. The Carboniferous peak is relatively symmetric, including ages of 330 to 300 Ma, with minor peaks at ~ 330 , ~ 322 , and ~ 315 Ma.

Whole-Rock Elemental Analyses

This discussion of Inner Piedmont granitoid whole-rock geochemistry includes new data with numerous other data compiled from other studies in the southern Appalachians (Giorgis, ms, 1999; Vinson, ms, 1999; Bier, ms, 2001; Mapes, ms, 2002; Bream, ms, 2003; Wilson, ms, 2006; Gatewood, ms, 2007; Byars, ms, 2010; Davis, ms, 2010; Howard, ms, 2012) (Appendix IV). We have taken a conservative approach to the interpretation of major and trace elements known to be mobile at high-grade metamorphic conditions (for example, K_2O , Na_2O , CaO , light ion lithophile elements [LILE]; Rollinson, 1993), as many of these granitoids either predate or are coeval with upper amphibolite facies metamorphism, and abundant petrographic evidence indicates deuteric alteration. Patterns revealed by mobile elements can however be useful as indicators of tectonic processes (for example, dehydration of subducted ocean crust and migration of fluids).

Major elements

Felsic plutonic rocks of the composite Inner Piedmont are calc-alkaline, mostly peraluminous to slightly metaluminous, and exhibit a wide range of SiO_2 concentrations. Taconian granitoids of the western Inner Piedmont are peraluminous to metaluminous, with weight percent Al_2O_3 concentrations ranging from 15.0 to 11.8% (average 13.8%) (Fig. 2-15). These mostly plot as granites to granodiorites using normative feldspar compositions (Barker, 1979), with the Dysartsville Tonalite as the lone exception (Fig. 2-15). Taconian granitoids have generally higher SiO_2 weight percent (74.0% average), and are mostly high- to medium-K affinity (Le Maitre,

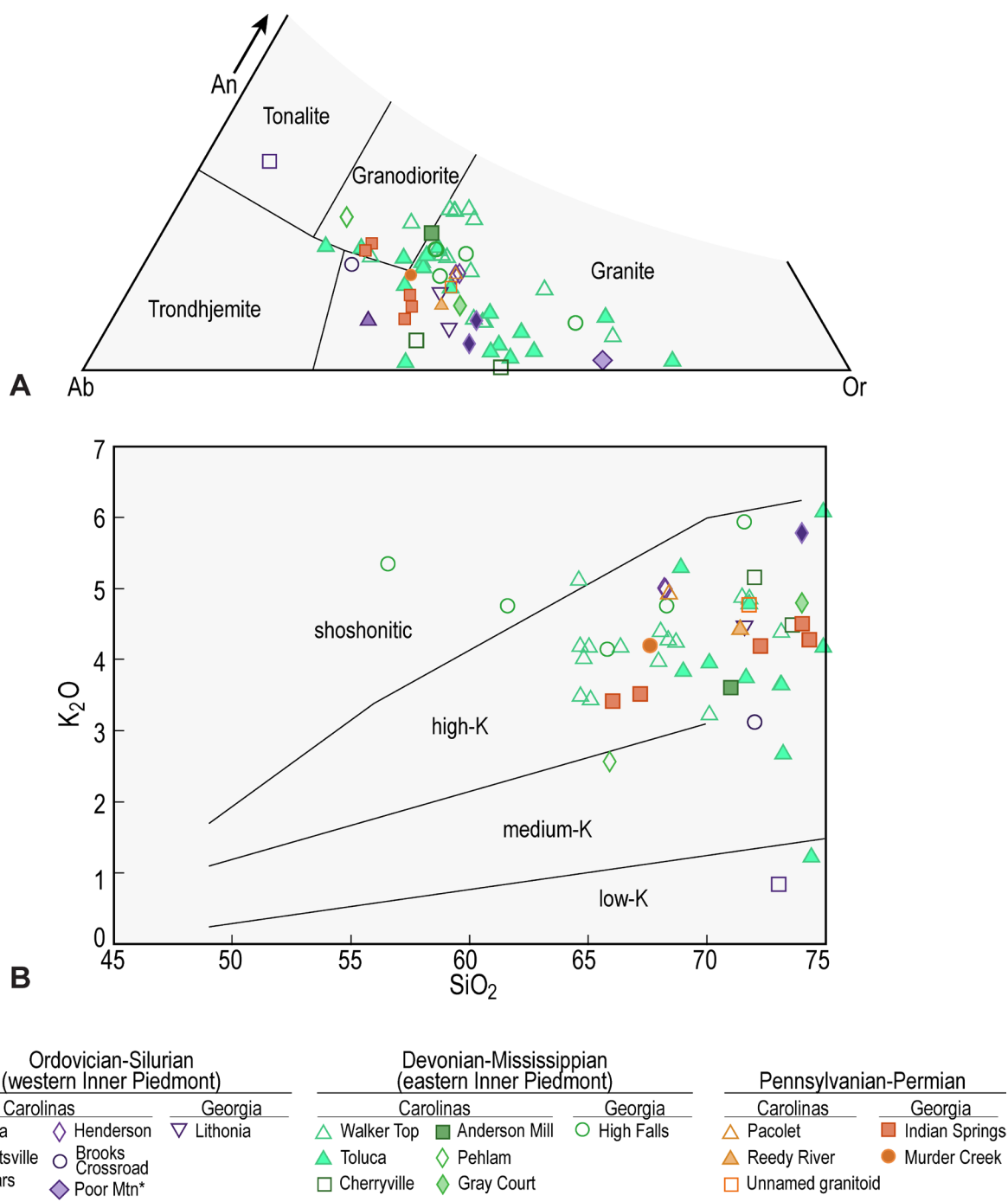


Figure 2-15: Results of major element geochemical analysis, with granitoids separated into Taconian (Ordovician-Silurian), Acadian/Neoacadian (Devonian-Mississippian), and Pennsylvanian-Permian (Alleghanian) groups. (A) Normative Ab-An-Or classification of Barker (1979). (B) SiO_2 - K_2O classification diagram of Le Maitre (1989). Data sources listed in appendix IV. *sample of Poor Mountain metatuff.

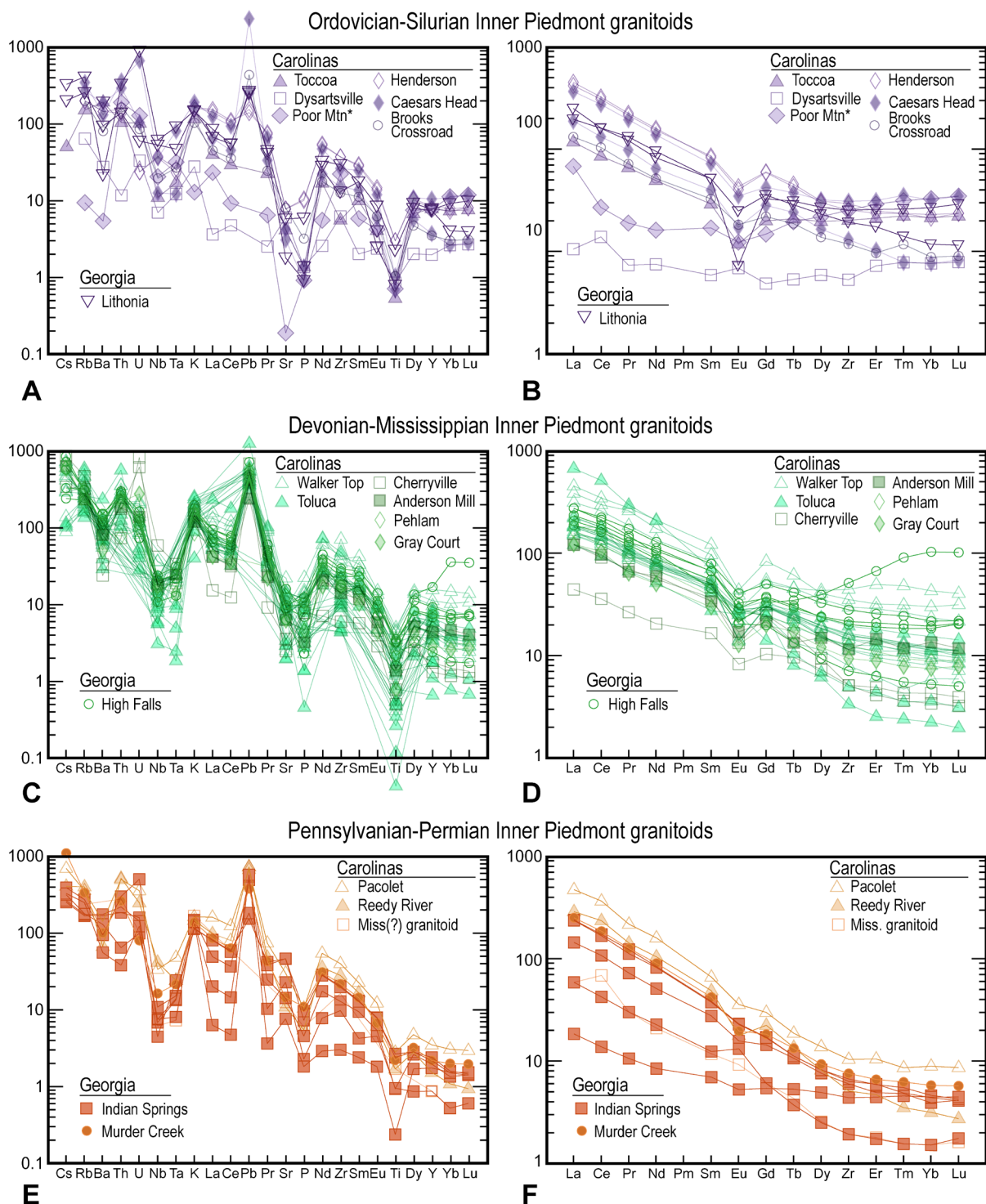


Figure 2-16: Multi-element variation diagrams, with primitive mantle normalized trace element (left column: A, C, and E) and chondrite normalized REE (right column: B, D, and F) data of the three groups of granitoids (normalization constants from Sun and McDonough, 1989). Data from the Georgia Inner Piedmont overlap compiled data from the Carolina Inner Piedmont in their respective groups, although Ordovician-Silurian and Devonian-Mississippian patterns are nearly indistinguishable. Data sources listed in appendix IV. *sample of Poor Mountain metatuff.

1989) (Fig. 2-15). The Dysartsville Tonalite is again the lone exception, with significantly lower weight percent K_2O relative to other western Inner Piedmont granitoids. Acadian/Neoacadian eastern Inner Piedmont granitoids are peraluminous granites to granodiorites, with one sample of the Toluca Granite showing trondhjemitic affinity with normative feldspar composition (Fig. 2-15). Average K_2O concentration of eastern Inner Piedmont granitoids is relatively high (average weight percent 4.55) with most samples showing high- to medium-K affinities. Several outliers exhibit low-K and shoshonitic compositions, with shoshonitic samples exclusively from the southern Inner Piedmont (High Falls Granite). Major element concentrations of Alleghanian granitoids are almost entirely intermediate between the Taconian and Acadian/Neoacadian suites. These granitoids are peraluminous to metaluminous granites to granodiorites, and are exclusively high-K affinity (Fig. 2-15). In general, there is significant overlap in major element composition through the temporally defined groups of Inner Piedmont granitoids.

Trace elements

The relative mobility of trace elements during metamorphism or hydrothermal alteration is in general orders of magnitude less than major elements; therefore, analysis of trace elements from Inner Piedmont igneous rocks permits insight into the processes and conditions under which these plutons formed. Trace element and REE analysis of Inner Piedmont granitoids yield strikingly similar patterns from all three groups (Fig. 2-16). Taconian granitoids exhibit prominent negative high field strength element (HFSE, for example, Nb, Ti) and P anomalies in primitive mantle normalized trace element spider diagrams. All samples in which Pb was analyzed show strong enrichment, with one sample of Caesar's Head Granite having a concentration of 167 ppm (average Pb concentration of Taconian granitoids is ~39 ppm). The Dysartsville Tonalite is enriched in Sr, with a slight enrichment in Eu, indicating the absence of feldspar fractionation, contrary to the rest of the Taconian granitoids, which have relative depletions in both Sr and Eu. The Dysartsville Tonalite is also strongly depleted in Th relative to the other Taconian granitoids, with concentration an order of magnitude less. Several samples, one Caesar's Head and one Lithonia Gneiss, are strongly enriched in U relative to other Taconian granitoids, with concentrations ≥ 14 ppm (average Taconian granitoids ~5 ppm). Taconian granitoids in general yield steep negative slopes in chondrite-normalized REE spider diagrams, although the Dysartsville Tonalite has a relatively flat REE curve. Chondrite-normalized La/Lu ratios (La_N/Lu_N , normalization constants from Sun and McDonough, 1989) of the Taconian granitoids average 13.3, and range from 1.3 to 22.8 (the Dysartsville Tonalite has the lowest value). Average La_N/Lu_N of Taconian granitoids between the northern and central Georgia Inner Piedmont are comparable (13.0 and 14.1, respectively). Granitoids west of the Jackson Lake fault in central Georgia geochemically overlap the majority of northern Inner Piedmont granitoids west of the Brindle Creek fault, with

the exception of the Dysartsville Tonalite, which is geochemically anomalous relative to all other Taconian granitoids.

Acadian/Neoacadian granitoids east of the Brindle Creek and Jackson Lake faults exhibit similar geochemical trends to their counterparts west of the respective faults. Acadian/Neoacadian plutons are generally depleted in HFSE relative to light ion lithophile elements (LILE), with most conspicuous negative anomalies in Nb, Ta, P, and Ti in contrast with strong enrichments in U and Pb. In general, Acadian/Neoacadian granitoids from the northern portion of the Inner Piedmont show stronger relative depletions in Ba, Sr, P, Ti, and HREE relative to granitoids from the central Georgia Inner Piedmont. Additionally, nearly ubiquitous negative Eu anomalies indicate feldspar fractionation. Virtually all Acadian/Neoacadian granitoids have steep REE curves, although one sample of the High Falls Granite exhibits strong HREE enrichment, resulting in a relatively flat curve. This sample (S123) was particularly garnetiferous, which would account for the relative Y and HREE enrichment (Howard, ms, 2012). Average La_N/Lu_N ratios vary dramatically from the northern and southern Inner Piedmont (33.7 and 18.1, respectively), although one sample of the Toluca Granite (TOL-11, Mapes, ms, 2002) has a significantly steeper REE curve, resulting in a very high La_N/Lu_N value (343.0). Exclusion of this outlier yields a more comparable average ratio of 19.0. Acadian/Neoacadian granitoids east of the Jackson Lake fault yield nearly identical trace element and REE patterns to those east of the Brindle Creek fault, although patterns from samples in the western Inner Piedmont appear to be geochemically similar.

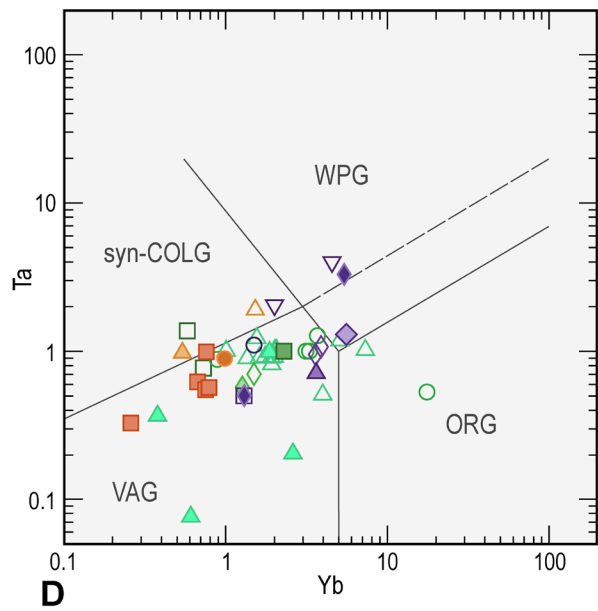
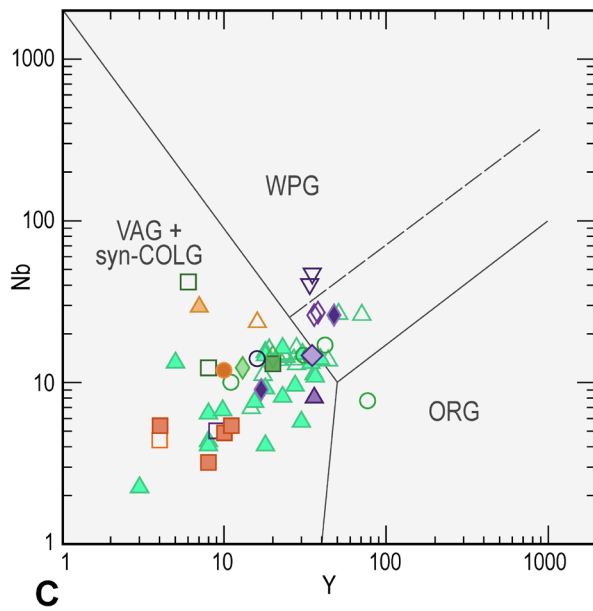
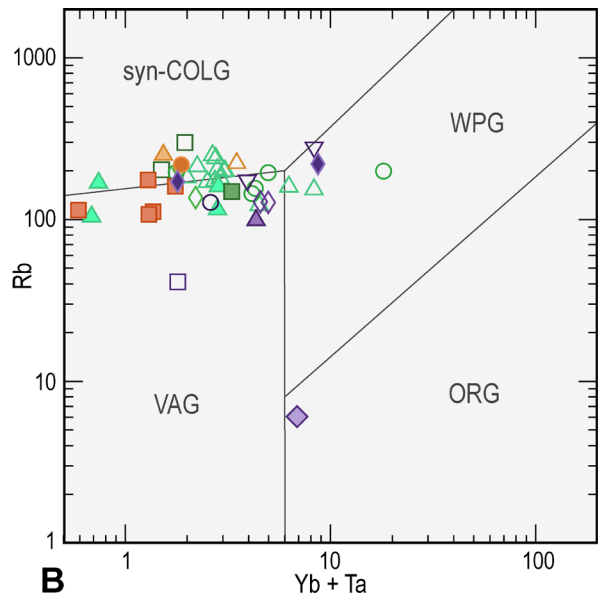
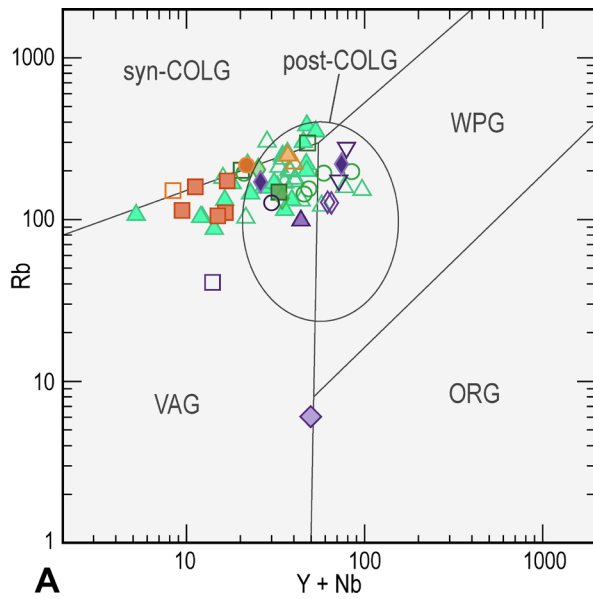
Trace and REE analysis of Alleghanian granitoids revealed several characteristics that distinguish them from the Taconian and Acadian/Neoacadian suites. Alleghanian granitoids have similar depletions in P, Ti, Nb, Ba, with strong Pb enrichment, although Alleghanian granitoids show positive Eu and Sr anomalies, indicative of plagioclase accumulation. Alleghanian granitoids overall have much lower relative HREE concentrations, resulting in steep trace element and REE element curves (average $La_N/Lu_N = 48.1$). Samples from the northern and central Georgia Inner Piedmont exhibit similar trends, although northern Inner Piedmont granitoids appear to have slightly higher REE concentrations. LREE concentrations within the group vary significantly, and can be orders of magnitude different.

Interpretation of Geochronologic and Geochemical Data and Comparisons between the Northern and Southern Portions of the Inner Piedmont

Granitoid geochemistry

While useful in determining petrogenetic origins, whole-rock geochemical data alone do not appear to be useful in distinguishing terrane affinity for pre-Alleghanian Inner Piedmont granitoids. Other workers (for example, Miller and others, 2000) have reached similar conclusions regarding the geochemical similarity between these groups of granitic rocks. However, these

Figure 2-17: Tectonic discrimination diagrams of Pearce and others (1984) (A-D) and Harris and others (1986) (E). LP-COLG = late to post collisional granite; ORG = ocean ridge granite; post-COLG = post-collisional granite; syn-COLG = syn-collisional granite; VAG = volcanic arc granite; WPG = within plate granite. *sample of Poor Mountain metatuff.



Ordovician-Silurian (western Inner Piedmont)	
Carolinas	Georgia
▲ Toccoa	◇ Henderson
□ Dysartsville	▽ Lithonia
◆ Caesars Head	○ Brooks Crossroad
	◇ Poor Mtn*

Devonian-Mississippian (eastern Inner Piedmont)	
Carolinas	Georgia
△ Walker Top	■ Anderson Mill
▲ Toluca	◇ Pehlam
□ Cherryville	◇ Gray Court

Pennsylvanian-Permian	
Carolinas	Georgia
△ Pacolet	■ Indian Springs
▲ Reedy River	● Murder Creek
□ Unnamed granitoid	

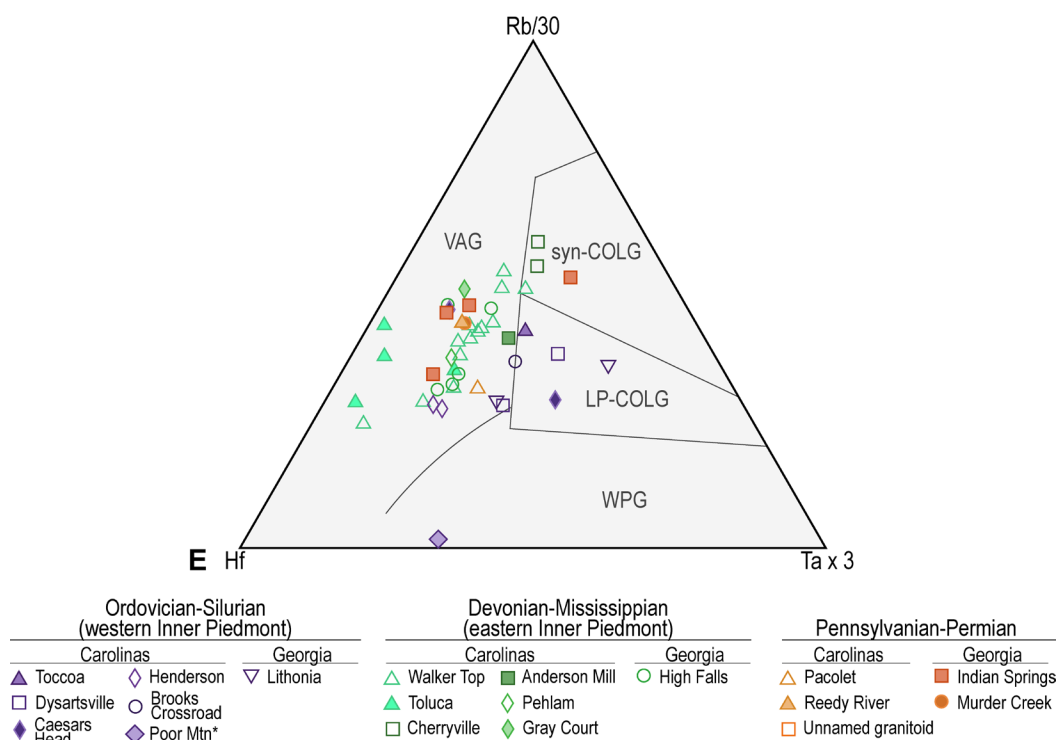


Figure 2-17 (continued)

data provide invaluable insight into the petrogenetic history of these granitoids, and in turn may yield insight into various tectonic processes at work during their genesis. Trace and REE data are plotted using several tectonic discriminant diagrams (Pearce and others, 1984; Harris and others, 1986) (Fig. 2-17), to amplify specific geochemical differences between the groups of granitoids. Alleghanian granitoids show slight geochemical differences that indicate petrogenesis distinct from the other groups, and are discussed separately.

Trace and REE spider diagrams, coupled with tectonic discriminant diagrams, illustrate significant overlap between eastern and western Inner Piedmont granitoid geochemistry, which indicates consanguinity of these rocks. Pre-Alleghanian granitoids mostly plot as volcanic arc granites or collisional granites in tectonic discriminant diagrams, with few samples that plot in other fields (Fig. 2-17). The majority of analyses from western and eastern Inner Piedmont granitoids plot within the post-collisional field of Pearce (1996) (Fig. 2-17A) and collisional fields of other diagrams, which at least indicates incorporation of a significant crustal component in these magmas (Fig. 2-17). Acadian/Neoacadian granitoid trace element chemistry reveals broad array of tectonic settings relative to western Inner Piedmont granitoids, reiterating the wider range of relative HREE concentrations evident in trace and REE spider diagrams (Fig. 2-17).

Pearce (1996) demonstrated that average continental crust plots in the volcanic arc granite field of the Rb vs. Y + Nb diagram (and likely others), and suggested moderate amounts of crustal assimilation would not affect the position of subduction-related magmas on this diagram. Harris and others (1986) also indicated that collisional granitoids generally show many geochemical similarities to volcanic arc granitoids, although those authors concluded that these can be successfully distinguished using Ta concentrations and initial $^{87}\text{Sr}/^{86}\text{Sr}$ ratios. Pre-Alleghanian granitoids throughout the Inner Piedmont generally plot as volcanic arc and collisional granitoids in tectonic discrimination diagrams, and although Sm/Nd and Rb/Sr isotopic data are sparse, available data suggest an evolved crustal component in these magmas (Fullagar and others, 1997; Mapes, ms, 2002; Bream, ms, 2003; Byars, ms, 2010).

Several workers (for example, Vinson, ms, 1999; Mapes, ms, 2002; Bream, ms, 2003) argued against Inner Piedmont granitoid genesis (both western and eastern Inner Piedmont) in a subduction zone setting, and instead suggested Inner Piedmont granitoids may be anatectic melts of “variable composition crust,” some of which was derived from a subduction-related source or local metasedimentary rocks. The absence of mafic and intermediate plutons, combined with high-K affinity, relative incompatible trace element enrichment, and ϵNd and ϵSr values characteristic of Inner Piedmont granitoids, support this hypothesis. Additionally, high $\delta^{18}\text{O}$ values from Acadian/Neoacadian northern Inner Piedmont granitoids, identical to surrounding metasedimentary rocks, indicate local derivation of these magmas (Mapes, ms, 2002). Alternatively, several geochemical characteristics support genesis in a subduction zone setting (for example, LREE enrichment, LILE enrichment relative to HFSE), and isotopic values from Inner Piedmont granitoids are similar to undoubtedly subduction-derived andesites from the Banda arc (for example, Magaritz and others, 1978; Whitford and Jezek, 1982). The common occurrence of amphibolite in Cat Square terrane metasedimentary packages could also be an expression of mafic volcanism that could support subduction-related plutonism. Although there is some ambiguity regarding the source of these magmas, current data appear to better support local derivation from quartzofeldspathic metasedimentary rocks. It should be noted that western Inner Piedmont plutons are geochemically and isotopically distinct from similar-age plutons in the eastern Blue Ridge, which exhibit characteristics that suggest arc-derived petrogenesis (for example, Mapes, ms, 2002; McDowell and others, 2002; Sinha and others, 2012).

Alleghanian granitoids occur throughout the Inner Piedmont and Carolina superterrane, crosscut the Central Piedmont suture (unnamed granitoid 326 ± 3 Ma, Dennis and Wright, 1995; Churchland pluton 320 ± 2 , Samson, 2001), and indicate the amalgamation of the outboard Laurentian terranes by the middle Carboniferous. Several contrasting hypotheses have been proposed regarding origin of this widespread, abundant suite of plutons (see Heatherington and others, 2010, and references therein), and although the petrogenetic origin of these rocks is beyond the

scope of this work, several geochemical attributes of these granitoids (at least samples from the Inner Piedmont) suggest these plutons may have a subduction-related origin. Alleghanian granitoids tend to form tighter clusters in tectonic discriminant diagrams, and exclusively plot as volcanic arc to collisional granites (Fig. 2-17). Interestingly, southern Inner Piedmont Alleghanian granitoids almost unanimously plot as volcanic-arc related, while northern Inner Piedmont samples plot as syn-collisional (Fig. 2-17). ϵNd and ϵSr values of northern Inner Piedmont Alleghanian granitoids indicate enriched mantle source (Mapes, ms, 2002).

Metamorphism

Available geochronologic data regarding metamorphism in the Inner Piedmont, combined with well-documented field relationships, strongly suggest peak upper amphibolite-facies conditions occurred during the Devonian-Carboniferous (for example, Dennis and Wright, 1997; Mersch, ms, 2009; this study) (Fig. 2-14). Interestingly, metamorphic U-Pb zircon ages between the northern and southern portions of the Inner Piedmont do not readily coincide (Fig. 2-14). Compiled data from the Carolina Inner Piedmont define a broad Gaussian distribution peaking at ~345 Ma, with individual peaks at ~400, ~375, ~345, and ~330 Ma, revealing a long history of residence at elevated temperatures (Mersch, ms, 2009). Data from the central Georgia Inner Piedmont suggest two distinct peak thermal events occurred ~380 and 320 Ma and, although data from the Carolina Inner Piedmont indicate metamorphic zircon growth at those times, the greatest concentration of ages occurs at ~345 Ma, during a relative lull in data from the Georgia Inner Piedmont (Fig. 2-14). The strong Alleghanian (330-300 Ma) overprint in samples from the central Georgia Inner Piedmont appears to be much more subordinate through the Carolinas. This lack of Alleghanian tectonism is also evident in the relative paucity of Carboniferous-Permian granitic plutonism through the northern portion of the Inner Piedmont, although Alleghanian plutons are common through the Carolina superterrane at these latitudes (for example, Hatcher and others, 2007). This raises an interesting question: Is the ~345 Ma thermal peak in the northern Inner Piedmont related to the ~380 or ~320 Ma peaks in the Georgia Inner Piedmont? Current data suggest the ~380 Ma event in the southern Inner Piedmont coincides with the ~345 Ma thermal peak in the northern Inner Piedmont. Evidence supporting this conclusion includes: 1) Carboniferous (325-300 Ma) granitoids crosscutting the dominant S_2 foliation in the Carolina and Georgia portions of the Inner Piedmont; 2) textural relationships between lithologically similar Devonian-Mississippian granitoids and S_2 , indicating these granitoids were pre- to syn-deformational; and 3) the overall expression of younger orogenesis in the Carolina Inner Piedmont, with the main pulse of Acadian/Neocadian magmatism apparently younger than similar plutonism in central Georgia. The offset of the Acadian/Neocadian thermal peak, and significant difference in duration of high temperatures, also provide insight into the nature of this orogenic event, and at least

indicate that the central Georgia Inner Piedmont cooled through the Late Devonian and early Mississippian, while the Carolina portion remained hot.

Detrital zircon geochronology

Compiled detrital zircon geochronologic data from the eastern Inner Piedmont reveal an interesting pattern of provenance from the Carolinas through central Georgia (Fig. 2-18). Three samples from the Carolina portion of the Inner Piedmont reveal a dominance of Ordovician-Silurian (480-425 Ma) detrital zircons that effectively mask the usually dominant Grenville source that blankets the entire eastern Laurentian margin. Sample GR1 from the Paris Mountain thrust sheet (South Carolina) also contains Neoarchean and Paleoproterozoic zircons, indicating a more complex evolution of the basin. Based on the wide variety of ages in Cat Square terrane detrital zircon suites, Merschat and Hatcher (2007) proposed the terrane represents a Silurian-Devonian remnant ocean basin to explain the apparent sediment recycling. Cat Square terrane samples from the Carolinas also contain a distinct suite of 600-500 Ma zircons, which likely represent source material from the exotic Carolina superterrane (Merschat and Hatcher, 2007; Merschat and others, 2010). Samples east of the Jackson Lake fault in central Georgia, however, have not yielded any Ordovician-Silurian detrital zircons, and only a few samples have contained any peri-Gondwanan zircons; these samples yielded almost entirely Grenville zircons. Detrital zircon data alone do not readily support the hypothesis that the rocks southeast of the Jackson Lake fault represent the southwest extension of the Cat Square terrane, although these observations do not refute it. The apparent lack of the Ordovician-Silurian detrital suite in these samples may be related to: 1) proximity of the southern portion of the basin to the Ordovician-Silurian source material; 2) basin dynamics (for example, drainage patterns); or 3) closure of the southern end of the basin prior to exhumation and erosion of the Ordovician-Silurian source material. Although the detrital zircon signature does not match samples from the Carolinas, the existing provenance pattern may shed vital insight into the tectonic processes associated with, and the location of the Cat Square basin prior to subduction, metamorphism, deformation, and dextral translation of the entire Inner Piedmont along the Brevard fault zone.

Granitoid ages

Granitoid ages from central Georgia provide the strongest evidence supporting the hypothesis that the Jackson Lake fault represents a significant tectonic boundary. Three distinct pulses of magmatism are evident from the geochronologic data: 1) Ordovician-Silurian (455-440 Ma); 2) Devonian Mississippian (400-350 Ma); and 3) Pennsylvanian-Permian (325-300 Ma). The Ordovician-Silurian Lithonia Gneiss occurs exclusively northwest of the Jackson Lake fault. Likewise, the High Falls Granite yielded ages 400-370 Ma, and occurs only southeast of the

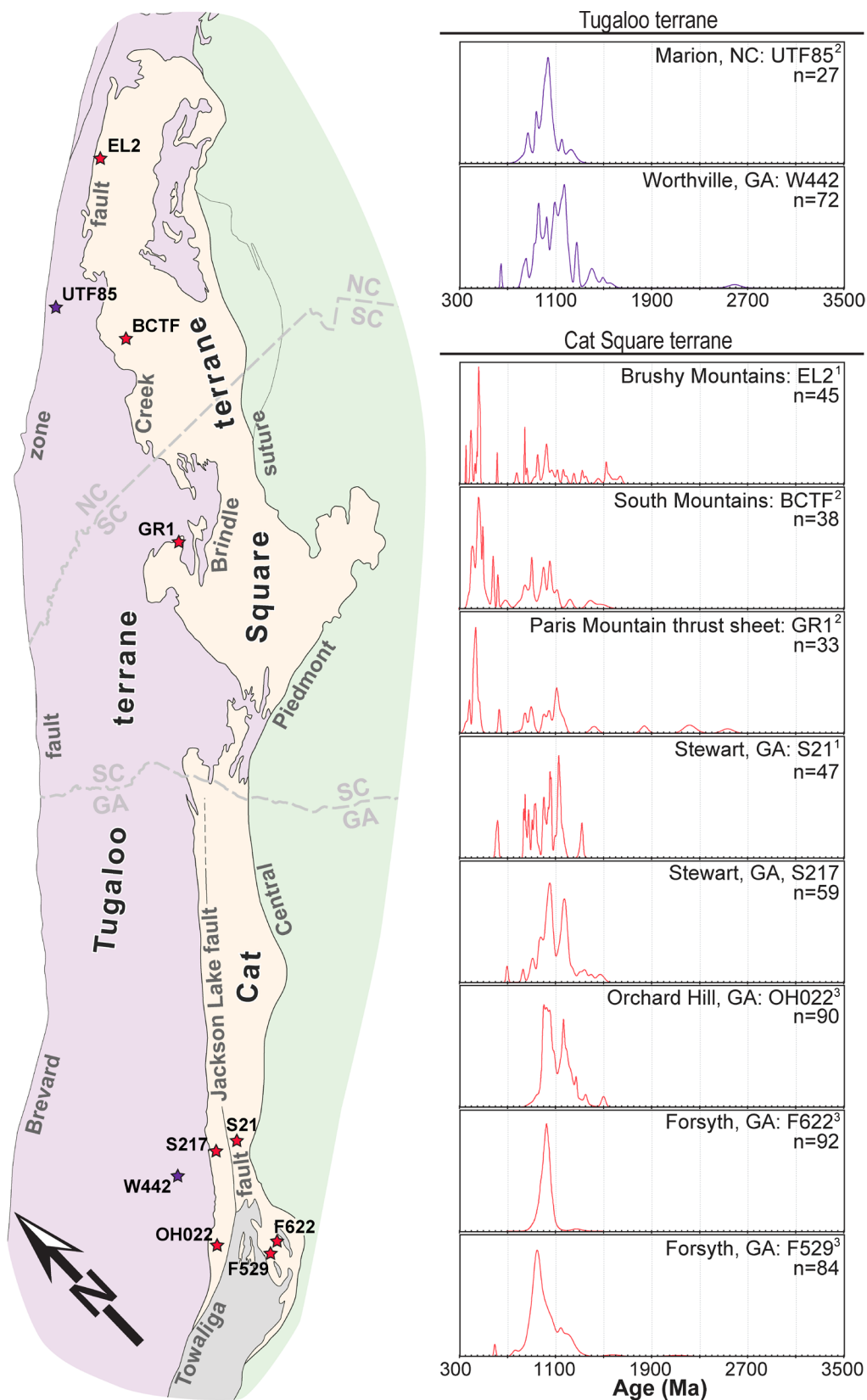


Figure 2-18: Compiled detrital zircon analyses from the Inner Piedmont. Data sources: ¹Mersch and others (2010); ²Bream (ms, 2003); ³J.R. Rehrer, unpublished data.

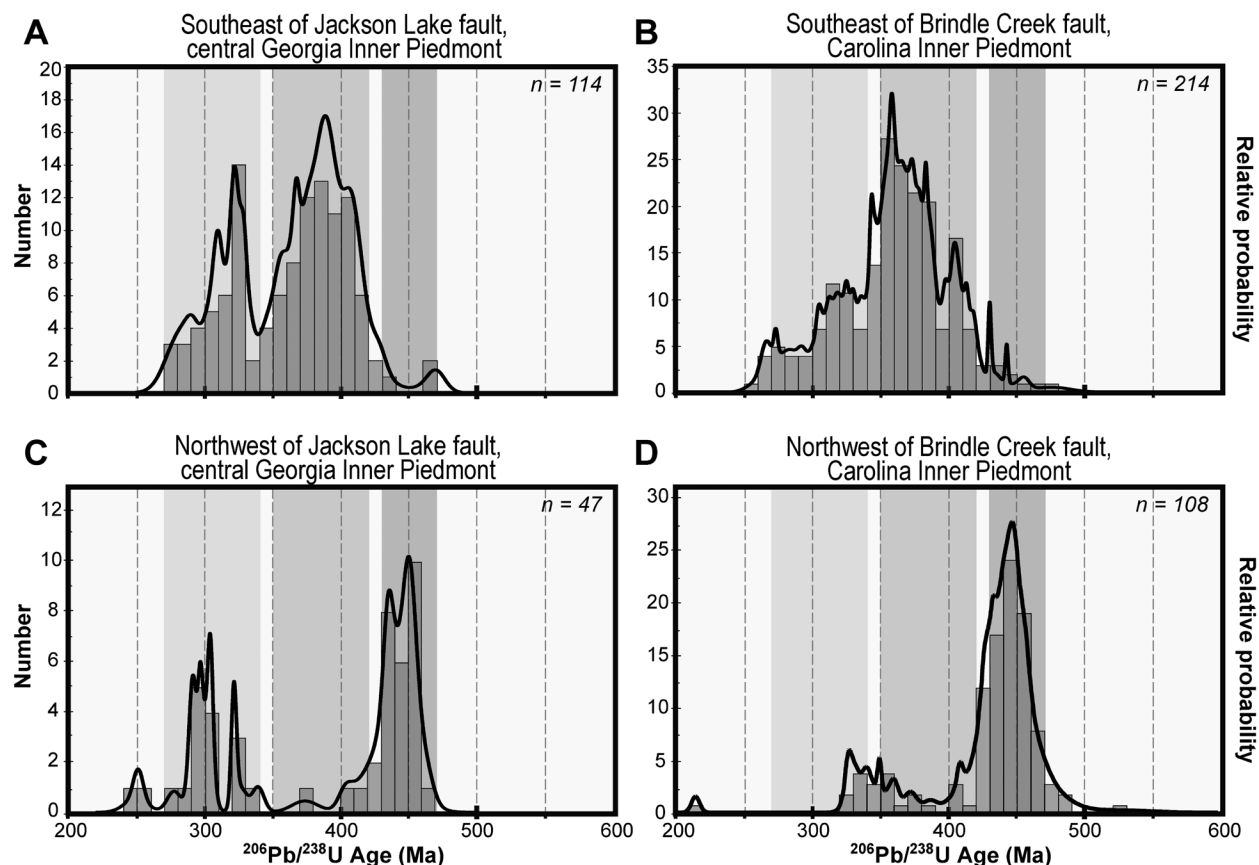


Figure 2-19: Relative probability distributions with histograms of pooled U-Pb zircon analyses from Inner Piedmont igneous rocks. Data are separated by relative position to the Jackson Lake and Brindle Creek faults (rows, A and B east of respective faults, C and D west of respective faults) and Carolina versus Georgia Inner Piedmont (columns, A and C Georgia Inner Piedmont, B and D Carolina Inner Piedmont). Shaded areas represent orogenic events: dark shading = Taconian; medium shading = Acadian/Neocadian; light shading = Alleghanian. Northern Inner Piedmont data were compiled from Vinson (ms, 1999), Mapes (ms, 2002), Bream (ms, 2003), Gatewood (ms, 2007), and Byars (ms, 2010).

fault. Pooled granitoid zircon ages from the Carolina and central Georgia portions of the Inner Piedmont separated by position relative to the Brindle Creek and Jackson Lake faults best illustrate the distinct partitioning of granitoid ages between the Inner Piedmont terranes (Fig. 2-19). The Alleghanian Indian Springs granodiorite occurs in both terranes, and also appears to crosscut the Jackson Lake fault, which indicates the Inner Piedmont terranes had been juxtaposed by the Pennsylvanian. Additionally, the truncation of the youngest body of the High Falls Granite (370 Ma) provides at least a maximum age for deformation along the Jackson Lake fault.

Based on the evidence presented above, we argue the Jackson Lake fault does represent the southwest extension of the Brindle Creek fault and terrane boundary, and that plutonic and metasedimentary rocks southeast of the Jackson Lake fault belong to the Cat Square terrane. The criteria presented for identification of the Cat Square terrane have for the most part been met, while differences between the two regions, revealed by our tests of this hypothesis, provide unique insight regarding the tectonic evolution of the Inner Piedmont. Arguably, the strongest evidence supporting this hypothesis is the clear partitioning of granitoid ages and lithologic differences across the Jackson Lake fault, which roughly corresponds with the prominent aeromagnetic lineament previously interpreted as the southwest extension of the Brindle Creek fault (Hatcher and others, 2007). The Snapping Shoals Augen Gneiss (continental Grenville basement), which only occurs northwest of the Jackson Lake fault, is consistent with similar observations from the Carolina portion of the Inner Piedmont (for example, Mersch, ms, 2009; Byars, ms, 2010). However, detrital zircon signatures, arguably the most definitive characteristic of the Cat Square terrane, are quite different between the northern and southern Inner Piedmont. The provenance pattern through the Inner Piedmont, coupled with the interpretation of detrital source location and subsequent tectonic translation along the Brevard fault, may provide a new constraint regarding the paleogeographic position of the Cat Square “basin” during deposition along the eastern Laurentian margin during the Late Silurian to Early Devonian.

DISCUSSION

One of the largest unresolved debates in the southern Appalachian orogen involves the timing and kinematics of the accretion of the exotic Carolina superterrane and its correlative effects on the eastern Laurentian margin (for example, Hibbard, 2000; Mersch and others, 2005). New and compiled data presented here can be used toward a viable, testable tectonic model that includes prograde metamorphism, magmatism, and juxtaposition of southern Appalachian terranes during the middle Paleozoic. The underlying concepts of terrane analysis, applied to ancient orogenic belts, provide an appropriate template to coherently incorporate these numerous data,

ultimately toward the resolution of one simple question: When was the Carolina superterrane accreted to the Laurentian margin?

Several observations regarding the composite Inner Piedmont, the relationship to adjacent terranes, and the mechanisms behind their genesis, are key to understanding the outboard evolution of the southern Appalachian orogen. These are (order of importance is debatable): 1) distribution of prograde metamorphism through the Inner Piedmont and Carolina superterrane; 2) timing of metamorphism, specifically the offset in thermal peak between the Carolina and central Georgia Inner Piedmont; 3) timing of plutonism, and the distinct partitioning of magmatic ages between Inner Piedmont terranes; 4) detrital zircon signatures throughout the Cat Square terrane; 5) structural juxtapositioning of terranes and the kinematics of bounding faults; 6) structural attributes of the Inner Piedmont terranes, including the regional mineral lineation pattern and the imbricate nappe-style structure throughout the Inner Piedmont; and 7) the role of the Brevard fault zone, and the proposed SW-directed lateral extrusion of the Inner Piedmont.

The provenance pattern revealed by detrital zircon analyses throughout the Inner Piedmont (Fig. 2-18) provides key insight regarding the evolution of the Cat Square terrane and collisional orogenesis during the middle Paleozoic. The characteristic detrital zircon suite observed in samples from the Carolina Inner Piedmont is dominated by Ordovician-Silurian detrital zircons, essentially masking the Grenville signature, a rare feat for sedimentary rocks along the eastern Laurentian margin (aka “The Curse of the Grenville,” S.D. Samson, 2012 personal comm.). The most likely candidate for the Ordovician-Silurian source material is a suite of arc-derived and possibly extension-related plutons in the eastern Blue Ridge of southwest Virginia (Sinha and others, 2012). These plutons crystallized at mid-crustal depths at 459-423 Ma (Sinha and others, 2012); therefore, if this material was to be available as sediment deposited in the Cat Square basin, rapid uplift of the eastern Blue Ridge during the Late Silurian is necessary. We suggest rapid exhumation of the eastern Blue Ridge at this time may be related to the approach of the Carolina superterrane, as it consumed Rheic ocean crust above an east-dipping subduction zone that resulted in Late Silurian-Devonian arc-related bimodal plutonism along the western flank of the Carolina superterrane (for example, McSween and Harvey, 1997; Esawi, 2004; Chaumba, 2010b) (Fig. 2-20). The associated peripheral bulge in the foreland of the approaching microcontinent may have been at the location of the Ordovician-Silurian plutons in the eastern Blue Ridge (Fig. 2-20), which provides a mechanism for rapid uplift, in addition to the dominance of Ordovician-Silurian ages relative to Grenville-age zircons in Carolina Cat Square terrane detrital zircon suites.

If the Ordovician-Silurian plutons in the Blue Ridge are the source material, then the pattern of detrital zircon signatures through the Cat Square terrane (Fig. 2-18) also provides information regarding its paleogeographic location during deposition. Merschat and others (2005) and Mers-

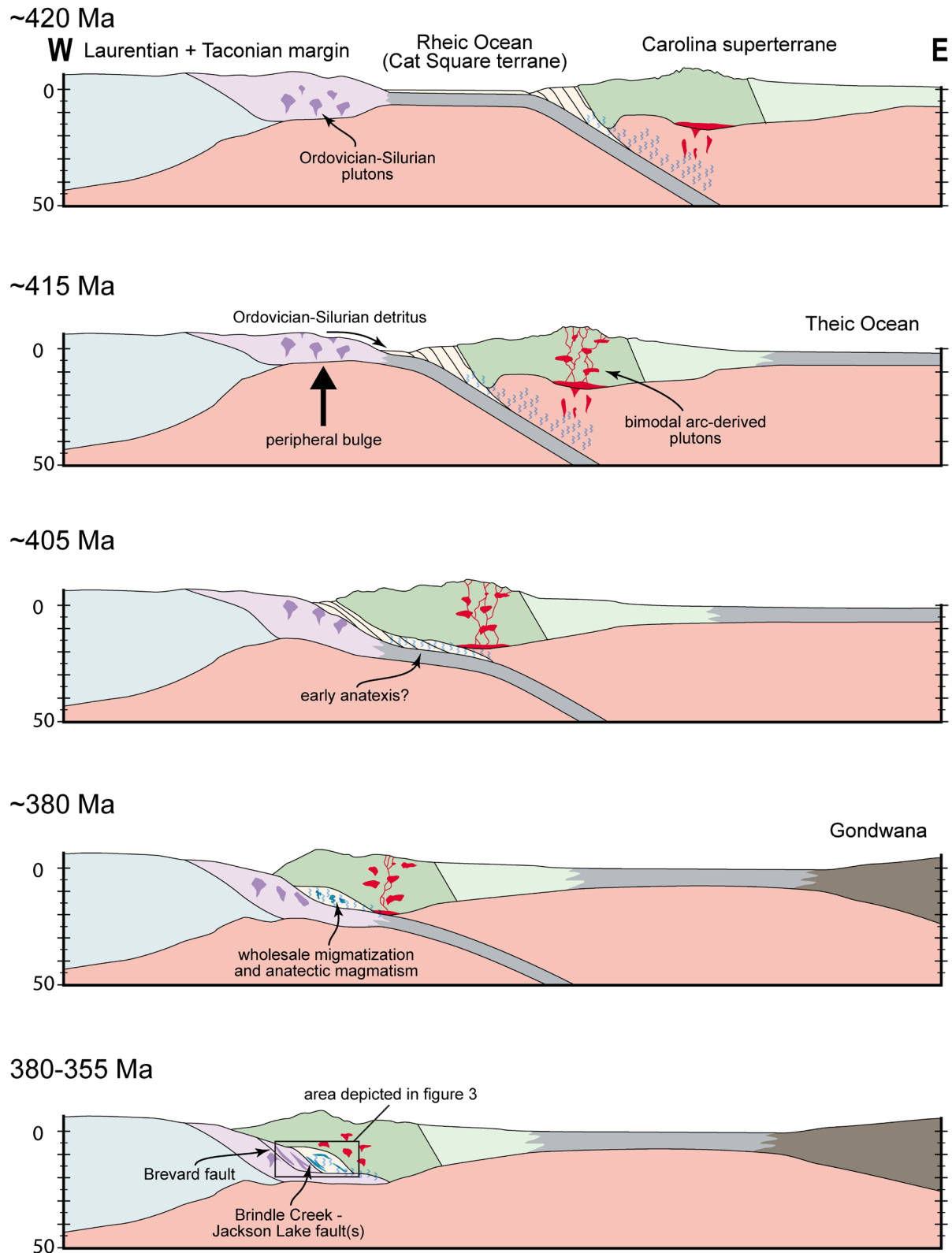


Figure 2-20: Tectonic model illustrating the evolution of the Cat Square terrane and tectonism through the Inner Piedmont during Acadian/Neoacadian accretion of the Carolina superterrane.

chat and Hatcher (2007) suggested there might be possibly 450 km of dextral southwest-directed translation of the Inner Piedmont along the Brevard fault that occurred subsequent to closure of the Cat Square basin. These authors also suggested the original site of deposition occurred at the Pennsylvania embayment, based in part by strikingly similar detrital zircon suites in metasedimentary rocks from the Silurian basins in New England (Wintsch and others, 2007; McWilliams and others, 2010); a possible southern/central Appalachian Ordovician-Silurian source had not been identified at that time. Hibbard and Waldron (2009) observed a discordance in regional structural patterns between the Carolina superterrane and the Laurentian margin, and suggested ~250 km of dextral translation had occurred based on the apparent match of their “state line flexure” with similar structural patterns in the Blue Ridge at the Virginia promontory (Fig. 2-21). Palinspastic restoration of ~250 km places the northern portion of the Cat Square terrane adjacent to the apparent Ordovician-Silurian source, while the southern portion of the Cat Square terrane is separated from the northern portion by the Virginia promontory (Fig. 2-21). This paleogeographic position, combined with tectonic exhumation of the proposed Ordovician-Silurian source material, explains the overwhelming abundance of Ordovician-Silurian detrital zircons in northern Cat Square terrane metasedimentary rocks and the relative paucity in those from the southwestern portion. Hibbard and Waldron (2009) suggested southwest translation of the outboard terranes occurred during the Devonian along a buried dextral transcurrent fault system that has yet to be identified. We suggest the Devonian Brevard fault zone is a much more reasonable (and testable) candidate. Regardless, the piercing point suggested by Hibbard and Waldron (2009) also appears to be supported by our data.

The characteristic detrital zircon signature also reveals clues regarding the depositional character of the basin, and we suggest the Cat Square terrane represents the accretionary complex that developed in the foreland of the Carolina superterrane as it approached the eastern Laurentian margin during the Late Silurian and Early Devonian (Fig. 2-20). This accretionary wedge formed in a remnant ocean basin that developed during the diachronous accretion of the Carolina superterrane (Merschhat and Hatcher, 2007). The remnant ocean basin hypothesis applied to Cat Square terrane metasedimentary rocks effectively explains the mixed Laurentian-peri-Gondwanan detrital zircon suite, although may not provide a viable mechanism to uplift and expose the proposed Ordovician-Silurian source material and make it available as clastic detritus. In the basic remnant ocean basin model, the primary sediment source, the uplifted suture zone, consists of thin-skinned, rapidly uplifted and recycled sedimentary strata (for example, Ingersoll and others, 1995), and would not adequately explain the aerial exposure of recently crystallized Ordovician-Silurian plutonic source material. We suggest that in addition to sediment derived from the uplifted suture zone, clastic input from the foreland and accreting terrane adjacent can also be significant sources of clastic detritus. In this dynamic depositional environment, sediment

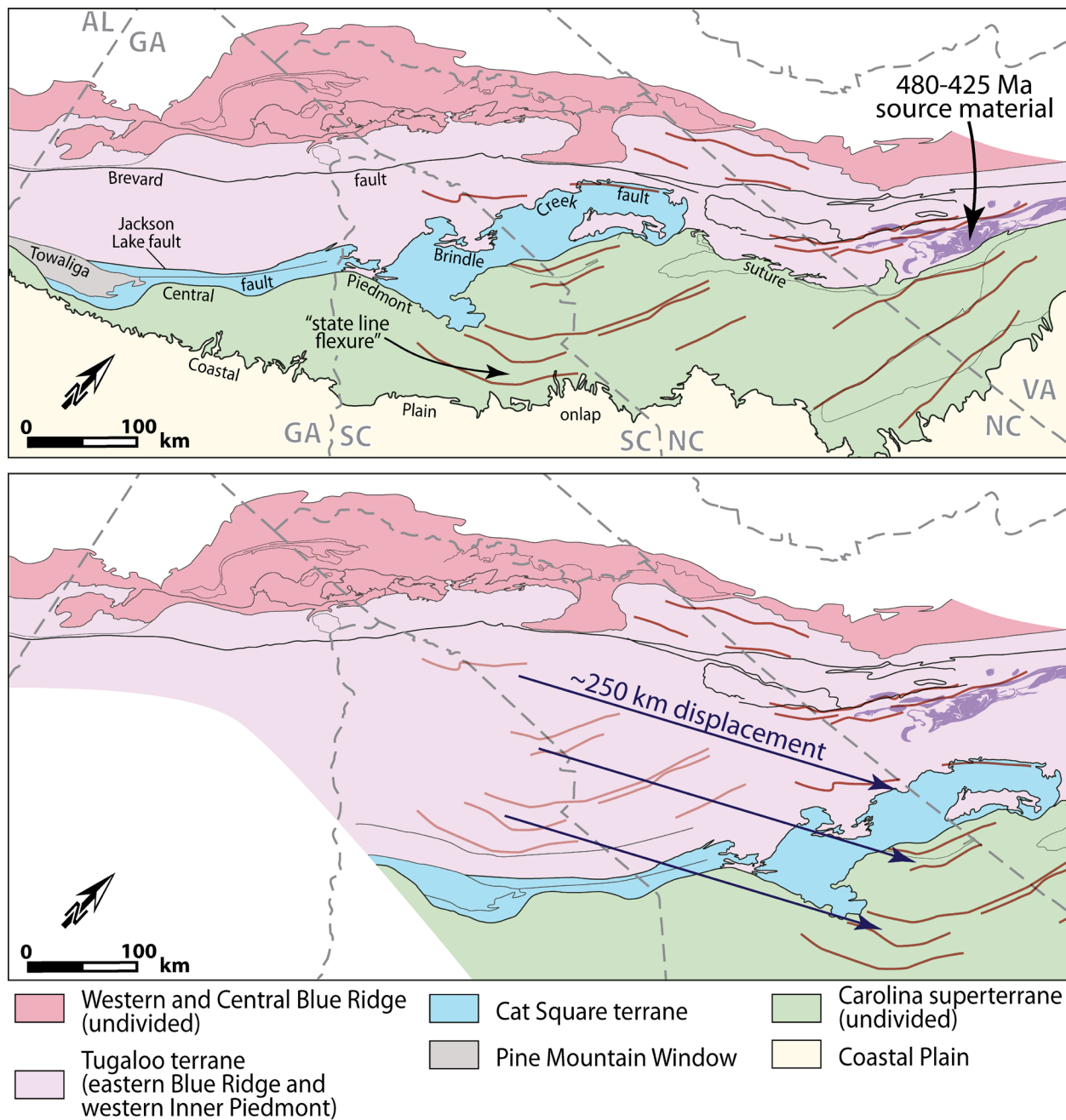


Figure 2-21: (A) Present configuration of terranes in the southern Appalachians, with regional structural trends (red lines) from Hibbard and Waldron (2009) illustrating discordance of regional fabric. (B) Palinspastic restoration of the Inner Piedmont and Carolina superterrane along the Brevard fault using the “state line flexure” as a piercing point. This figure does not account for dextral displacement along the central Piedmont suture.

is continually being reworked and deformed; this includes foreland-derived sediment that has been incorporated into the accretionary complex.

This model also elucidates the apparent younger-over-older nature of the Brindle Creek fault, an observation that prompted Dennis (2007) to suggest the Brindle Creek fault is actually a Salinic unconformity that developed on Laurentian continental crust. The interpretation of the Brindle Creek fault as an unconformity is inconsistent with the presence of Devonian-Mississippian plutons that occur *above* the boundary and are truncated by it. If these granitoids postdate the proposed unconformity, they would likely crosscut the boundary, and not be confined to the *overlying* metasedimentary package. Other evidence, including well-developed mylonitization along the boundary and truncation of regional structures (for example, Giorgis, ms, 1999; Merschchat and Kalbas, 2002), supports the interpretation that the boundary between the Inner Piedmont terranes is indeed a fault.

As the Carolina superterrane collided with the Laurentian margin, this accretionary complex was thrust over plutonic rocks and deep-water siliciclastics of the Tugaloo terrane, which were both subducted beneath the Carolina superterrane to depths required for upper amphibolite facies metamorphic conditions during the Devonian (Fig. 2-20). Interestingly, although both terranes were coevally metamorphosed to the same grade, pre- to syn-metamorphic, likely anatectic granitoids formed in the Cat Square terrane, while no similar-age plutons developed in the Tugaloo terrane. This distinct distribution of granitoid ages also provides key timing elements as constraints regarding this scenario. The distribution of granitoids in the Cat Square terrane and their truncation by the Brindle Creek fault indicate anatectic magmatism there occurred prior to final juxtaposition of the Cat Square terrane above the Tugaloo terrane, which had to occur post-crystallization of the youngest granitoid (~355 Ma). The oldest plutons (415-408 Ma) delimit the time at which the accretionary wedge, or at least a portion of it, was subducted to appropriate depths with enough time for depressed geotherms at a subduction-zone to rise to appropriate temperatures (Fig. 2-20). A relatively older mean age of plutonism and metamorphism in the southern Inner Piedmont may indicate burial predated that in the Carolina Inner Piedmont.

The pattern of timing of peak thermal event(s) recorded in metamorphic zircon growth also poses an interesting dilemma. Specifically, the northern Inner Piedmont appears to have been at relatively high-grade conditions from the Early Devonian through the middle Mississippian, peaking at ~345 Ma, while the data suggest metamorphism in central Georgia peaked through the Middle Devonian, and was relatively cool by ~345 Ma (Fig. 2-14). This phenomenon may be related to the southwest-directed orogen-parallel extrusion of the Inner Piedmont during the Acadian/Neoacadian event. Using the Himalayan orogen and southeast extrusion of the Indochina block as an analog, the extrusion of the Indochina block may result in exhumation of portions of the middle and lower crust by isostatic rebound as it escapes from areas buried by the high

topography of the Tibetan Plateau (for example, Roydin and others, 2008, their Fig. 5). Similarly, the main collision of the Carolina superterrane may have been localized over the northern Inner Piedmont, while the central Georgia portion of the Inner Piedmont may have escaped prolonged burial due to southwest lateral extrusion along the Brevard fault zone. This explanation is speculative at best, although consistent with available data.

If the Cat Square terrane represents an accretionary complex that developed in a remnant ocean basin floored by ocean crust, the subducting slab would be dewatered, not only hydrating the overlying mantle wedge resulting in Silurian-Devonian arc-related plutonism in the western Carolina superterrane, but also channeling volatiles up through the subduction zone and accretionary wedge (Fig. 2-20). As the accretionary prism was thrust over the foreland Tugaloo terrane and both were subducted beneath the Carolina superterrane, fluids driven off of the subducting slab would have fluxed through the Inner Piedmont, which may be related to the intense whole-sale migmatization and anatectic plutonism observed at the currently exposed structural level. Pearce (1996) noted that granitoids in accretionary prisms would exhibit characteristics of volcanic arc granites based on the likely assimilation of arc-like crust, and this influx of subduction-derived fluids may have also played a role in the overall geochemical signature of these plutons (for example, LILE enrichment).

Arguably, the most important elements to consider regarding the accretion of the outboard terranes is the structural position of terranes, relative metamorphic grade between adjacent terranes, and the timing of peak metamorphic events. The Inner Piedmont reached peak metamorphic conditions through the Devonian and Mississippian, conditions that require burial to depths 15-20 km. Based on the observation that the Carolina superterrane structurally overlies the Inner Piedmont, we suggest the most logical explanation for this regional metamorphic event involves accretion of the Carolina superterrane and subduction of the Inner Piedmont beneath it in the Devonian. Evidence from the Carolina superterrane suggests cooling through Ar retention (hornblende, biotite, white mica) occurred coeval with peak metamorphic conditions in the Inner Piedmont (Dallmeyer and others, 1986; Secor and others, 1986; Hibbard and others, 2012), which also supports this conclusion. Tectonic models that depict the Carolina superterrane subducting *beneath* Laurentia in an earlier accretionary event (for example, Hibbard, 2000; Miller and others, 2006) are grossly inconsistent with this most fundamental observation. While ambiguities remain regarding the overall nature of the Acadian/Neoacadian orogeny in the southern Appalachians, the delineation of terranes within the Inner Piedmont, and the observations revealed by data collected during this study, provide new constraints for proposed tectonic models, and ultimately move our understanding of middle Paleozoic collisional orogenesis along the southeastern Laurentian margin toward a coherent, testable tectonic model.

CONCLUSIONS

1. The Jackson Lake fault is likely the southwest equivalent of the Brindle Creek fault. Supporting evidence includes: 1) distinct lithologic (metasedimentary and igneous) differences on either side of the fault, similar to those in the northern Inner Piedmont; 2) partitioning of granitoid ages relative to the fault, with Ordovician-Silurian granitoids to the northwest and Devonian ages to the southeast; 3) occurrence of continental basement fragments northwest of the fault, with none (to date) southeast of the fault; 4) limited peri-Gondwanan provenance in metasedimentary rocks southeast of the fault; and 5) lithologic and geochemical similarities between rocks southeast of the Brindle Creek and Jackson Lake faults.
2. The Jackson Lake fault was active between ~371 Ma (youngest High Falls Granite) and ~305 Ma (body of Indian Springs granodiorite that crosscuts the fault). The Indian Springs granodiorite is found on both sides of the fault, indicating displacement along the fault occurred prior to the Alleghanian orogeny. This timing is similar to that of the Brindle Creek fault.
3. Cat Square terrane metasedimentary rocks were initially deposited in a remnant ocean basin setting that developed into an accretionary complex in front of the approaching Carolina superterrane. This is supported by: 1) the presence of mafic and ultramafic rocks throughout the Cat Square terrane, in addition to the Hammett Grove meta-igneous suite (possible ophiolite), which indicate the Cat Square basin was floored by ocean crust; 2) necessary rapid uplift of the eastern Blue Ridge Ordovician-Silurian source material (peripheral bulge) and dominance of Ordovician-Silurian detrital zircons relative to Grenville-age zircons; 3) younger-over-older nature of the Brindle Creek fault; 4) intense migmatization of the Inner Piedmont during peak conditions; and 5) subduction-zone geochemical signature in pre-Alleghanian plutonic rocks in the Cat Square terrane, although other evidence more strongly supports granitoid genesis as anatectic melts.
4. The pattern of detrital zircon signatures through the Cat Square terrane reveals its paleogeographic position prior to ~250 km of southwest-directed translation of the Inner Piedmont along the Brevard fault zone. The Carolina and Georgia portions of the Cat Square terrane may have straddled the Virginia promontory during deposition, which would account for the absence of the Ordovician-Silurian signature in detrital zircon suites from the southwestern portion of the Cat Square terrane.
5. The slightly older mean age of plutonism and metamorphism in the central Georgia Inner Piedmont indicates burial may have predated that in the northern end.

6. The pattern of metamorphic ages indicates the Carolina Inner Piedmont appears to have been at relatively high-grade conditions from the Early Devonian through the middle Mississippian, peaking at ~345 Ma, while central Georgia peaked through the Middle Devonian and was relatively cool by that time. This may be a product of the southwest-directed extrusion of the Inner Piedmont during the Acadian/Neoacadian event, which may have allowed the central Georgia Inner Piedmont to escape prolonged burial during orogenesis.
7. Relative grade and timing of metamorphism indicate the Inner Piedmont was structurally beneath the Carolina superterrane from the Devonian through the Mississippian.
8. Alleghanian granitoids appear to be geochemically distinct relative to their Taconian and Acadian/Neoacadian counterparts throughout the Inner Piedmont.

ACKNOWLEDGMENTS

Joe Wooden, Jorge Vasquez, and Matt Coble of the SUMAC facility were vital in the successful acquisition of ion microprobe data presented herein. Additionally, Drew Coleman, Ryan Mills, Jez Ingles, Chris Fedo, Calvin Miller, and Abe Padilla aided in zircon separations and graciously allowed use of their facilities for that purpose. Countless discussions with Chris Howard, Justin Rehrer, Brittany Davis, Mike Higgins, Ralph Crawford, John Costello, and Randy Kath helped to refine our understanding of Inner Piedmont geology and provided diverse perspectives that ultimately resulted in our interpretations of orogenesis through the southern Appalachians. REVIEWERS HERE. Detailed geologic mapping was funded by the University of Tennessee-Knoxville Science Alliance Center of Excellence, the University of Tennessee Office of Research, and USGS EDMAP Award G09AC00126. The University of Tennessee-Knoxville Science Alliance Center of Excellence provided funding for geochemical analysis and ion-microprobe geochronology.

REFERENCES CITED

- Adams, G. I., 1926, The crystalline rocks, *in* Adams, G. I., Butts, C., Stephenson, L. W., and Cooke, W., editors, *Geology of Alabama: Geological Society of Alabama Special Report 14*, p. 25-40.
- Aleinikoff, J. N., Zartman, R. E., Walter, M., Rankin, D. W., Lyttle, P. T., and Burton, W. C., 1995, U-Pb ages of metarhyolites of the Catoclin and Mount Rogers Formations, central and southern Appalachians: Evidence for two pulses of rifting: *American Journal of Science*, v. 295, p. 428-454.
- Atkins, R. L., and Lineback, J. A., 1992, Structural relations, origin and emplacement of granitic rocks in the Cedar Rock Complex, Georgia piedmont: *Georgia Geologic Survey Bulletin 115*, 40 p.
- Barker, F., 1979, Trondhjemite: Definition, environment, and hypotheses of origin, *in* Barker, F., editor, *Trondhjemites, Dacites, and Related Rocks*: Amsterdam, Elsevier, p. 1-12.
- Bentley, R. D., and Neathery, T. N., 1970, Geology of the Brevard zone and related rocks of the Inner Piedmont of Alabama: *Alabama Geological Society, Eighth Annual Field Trip Guidebook*, 119 p.
- Bier, S. E., ms, 2001, Geology of the southeastern South Mountains, North Carolina: M.S. thesis, University of Tennessee, Knoxville, 162 p.
- Bier, S. E., Bream, B. R., and Giorgis, S. D., 2002, Inner Piedmont stratigraphy, metamorphism, and deformation in the Marion-South Mountains area, North Carolina, *in* Hatcher, R. D., Jr., and Bream, B. R., editors, *Inner Piedmont geology in the South Mountains-Blue Ridge Foothills and the southwestern Brushy Mountains, central-western North Carolina: Carolina Geological Society Field Trip Guidebook*, p. 65–100.
- Bream, B. R., ms, 1999, Geology of the Glenwood and Sugar Hill quadrangles, North Carolina, and the structure of the northeast end of the Henderson Gneiss: M.S. thesis, University of Tennessee, Knoxville, 155 p.
- Bream, B. R., ms, 2003, Tectonic implications of geochronology and geochemistry of para- and orthogneisses from the southern Appalachian crystalline core: Ph.D. dissertation, University of Tennessee, Knoxville, 262 p.
- Bream, B. R., Hatcher, R. D., Jr., Miller, C. F., and Fullagar, P. D., 2001, Geochemistry and provenance of Inner Piedmont paragneisses, NC and SC: Evidence for an internal terrane boundary?: *Geological Society of America Abstracts with Programs*, v. 33, no. 2, p. 65.
- Bream, B. R., Hatcher, R. D., Jr., Miller, C. F., and Fullagar, P. D., 2004, Detrital zircon ages and Nd isotopic data from the southern Appalachian crystalline core, Georgia, South Carolina, North Carolina, and Tennessee: New provenance constraints for part of the Laurentian

- margin, *in* Tollo, R. P., Corriveau, L., McLelland, J., and Bartholomew, M. J., editors, Proterozoic tectonic evolution of the Grenville orogen in North America: Boulder, Colorado, Geological Society of America Memoir 197, p. 459-475.
- Byars, H. E., ms, 2010, Tectonic evolution of the west-central portion of the Newton window, North Carolina Inner Piedmont: Timing and implications for the emplacement of the Paleozoic Vale charnockite, Walker Top Granite, and mafic complexes: M.S. thesis, University of Tennessee, Knoxville, 248 p.
- Byars, H. E., Merschat, A. J., Hatcher, R. D., Jr., and Wooden, J. L., 2008, Timing and implications for the emplacement of the Paleozoic Vale (Cat Square) charnockite and Walker Top Granite, eastern Inner Piedmont, North Carolina: Geological Society of America Abstracts with Programs, v. 40, no. 4, p. 18.
- Carpenter, R. H., and Hughes, T. C., 1970, Geochemical and geophysical survey of the Gladesville norite, Jasper County, Georgia: Georgia Geological Survey Information Circular 37, 7 p.
- Chaumba, J. B., 2010a, The Hammett Grove meta-igneous suite, South Carolina: Bulk-rock, mineral composition, hydrogen, and oxygen isotope data from metagabbros: Geological Society of America Abstracts with Programs, v. 42, no. 1, p. 164.
- Chaumba, J. B., 2010b, Island arc origin for the Gladesville and associated bodies in the Carolina superterrane, central Georgia: Geological Society of America Abstracts with Programs, v. 42, no. 5, p. 307.
- Coney, P. J., Jones, D. L., and Monger, J. W. H., 1980, Cordilleran suspect terranes: *Nature*, v. 288, p. 329-333.
- Curl, D. C., ms, 1998, Stratigraphy and structure of Wellford and Reidville quadrangles in part of the eastern Inner Piedmont, near Spartanburg, South Carolina: M.S. thesis, University of Tennessee, Knoxville, 129 p.
- Dallmeyer, R. D., 1989, Late Paleozoic thermal evolution of crystalline terranes within portions of the U.S., Appalachian orogen, *in* Hatcher, R. D., Jr., Thomas, W. A., and Viele, G. W., editors, The Appalachian-Ouachita orogen in the United States: Boulder Colorado, Geological Society of America, The Geology of North America F-2, p. 417-444.
- Dallmeyer, R. D., Wright, J. E., Secor, D. T., Jr., and Snoke, A. W., 1986, Character of the Alleghanian orogeny in the southern Appalachians: Part II. Geochronological constraints on the tectonothermal evolution of the eastern Piedmont in South Carolina: Geological Society of America Bulletin, v. 97, p. 1329-1344.
- Davis, B. A., ms, 2010, Tectonic evolution of the southern Appalachian Inner Piedmont: Identification and interpretation of crustal features from aeromagnetic data and detailed geologic mapping in central Georgia: M.S. thesis, University of Tennessee, Knoxville, 222 p.

- Davis, T. L., ms, 1993, Lithostratigraphy, structure, and metamorphism of a crystalline thrust terrane, western Inner Piedmont, North Carolina: Ph.D. dissertation, University of Tennessee, Knoxville, 245 p.
- DeCelles, P. G., Gehrels, G. E., Quade, J., LaReau, B., and Spurlin, M., 2000, Tectonic implications of U-Pb zircon ages of the Himalayan orogenic belt in Nepal: *Science*, v. 288, p. 497-499.
- Dennis, A. J., 1991, Is the central Piedmont suture a low-angle normal fault?: *Geology*, v. 19, p. 1081-1084.
- Dennis, A. J., 1995, The Carolina terrane in northwestern South Carolina: Relative timing of events and recent tectonic models, *in* Hibbard, J. P., van Stall, C. R., and Cawood, P. A., editors, *Current Perspectives in the Appalachian-Caledonian Orogen: Geological Association of Canada Special Paper 41*, p. 173-189.
- Dennis, A. J., 2007, Cat Square basin, Catskill clastic wedge: Silurian-Devonian orogenic events in the central Appalachians and the crystalline southern Appalachians, *in* Sears, J. W., Harms, T. A., and Evenchick, C. A., editors, *Whence the Mountains? Inquiries into the evolution of orogenic systems: A volume in honor of Raymond A. Price: Boulder, Colorado, Geological Society of America Special Paper 433*, p. 313-329.
- Dennis, A. J., and Wright, J. E., 1995, Mississippian (ca. 326-323 Ma) U-Pb crystallization ages for two granitoids in Spartanburg and Union Counties, South Carolina: *South Carolina Geology*, v. 38, p. 23-28.
- Dennis, A. J., and Wright, J. E., 1997, Middle and late Paleozoic monazite U-Pb ages, Inner Piedmont, South Carolina: *Geological Society of America Abstracts with Programs*, v. 29, no. 3, p. 12.
- Esawi, E. K., 2004, Evidence from the Farmington pluton for Early Devonian subduction-related magmatism in the Carolina zone of central North Carolina: *Journal of Geodynamics*, v. 37, p. 531-548.
- Fullagar, P. D., 1997, Evidence for Grenville-age or older crust in the southern Appalachian Inner Piedmont of North and South Carolina: *Geological Society of America Abstracts with Programs*, v. 27, no. 6, p. 397.
- Fullagar, P. D., Goldberg, S. A., and Butler, J. R., 1997, Nd and Sr isotopic characterization of crystalline rocks from the southern Appalachian Piedmont and Blue Ridge, North and South Carolina, *in* Sinha, A. K., Whalen, J. B., and Hogan, J. P., editors, *The Nature of Magmatism in the Appalachian Orogen: Boulder, Colorado, Geological Society of America Memoir 191*, 165-180 p.
- Garihan, J. M., Preddy, M. S., and Ranson, W. A., 1993, Summary of mid-Mesozoic brittle faulting in the Inner Piedmont and nearby Charlotte belt of the Carolinas, *in* Hatcher, R. D., Jr.,

- and Davis, T. L., editors, *Studies of Inner Piedmont geology with a focus on the Columbus promontory*: Carolina Geological Society Field Trip Guidebook, p. 55-66.
- Gatewood, M. P., ms, 2007, Structure and tectonics of the northeastern Inner Piedmont from detailed geologic mapping, geochronologic, geochemical, and petrologic studies with macro-, meso-, and microstructural analyses of ductile fault zones: M.S. thesis, University of Tennessee, Knoxville, 279 p.
- Gilliam, W. G., ms, 2010, Structural and Metamorphic Evolution of the west-central Newton window eastern Inner Piedmont, North Carolina: M.S. thesis, University of Tennessee, Knoxville, 142 p.
- Giorgis, S. D., ms, 1999, Inner Piedmont geology of the northwestern South Mountains near Morganton, North Carolina: M.S. thesis, University of Tennessee, Knoxville, 191 p.
- Giorgis, S. D., Mapes, R. W., and Bream, B. R., 2002, The Walker Top Granite: Acadian granitoid or eastern Inner Piedmont basement?, *in* Hatcher, R. D., Jr., and Bream, B. R., editors, *Inner Piedmont geology in the South Mountains-Blue Ridge Foothills and the southwestern Brushy Mountains, central-western North Carolina*: Carolina Geological Society Field Trip Guidebook, p. 33-44.
- Goldsmith, R., Milton, D. J., and Horton, J. W., Jr., 1988, Geologic map of the Charlotte 1-degree x 2-degree quadrangle, North Carolina and South Carolina: U.S. Geological Survey Map I-1251-E, scale 1:250,000.
- Griffin, V. S., Jr., 1969, Migmatitic Inner Piedmont belt of northwestern South Carolina: South Carolina Division of Geology, *Geologic Notes*, v. 13, p. 87-104.
- Griffin, V. S., Jr., 1971, The Inner Piedmont belt of the southern crystalline Appalachians: *Geological Society of America Bulletin*, v. 82, p. 1885-1898.
- Griffin, V.S., Jr., 1978, Detailed analysis of tectonic levels in the Appalachian Piedmont: *Geologische Rundschau*, v. 67, p. 179-201.
- Griffitts, W. C., and Overstreet, W. C., 1952, Granitic rocks of the western Carolina Piedmont: *American Journal of Science*, v. 250, p. 777-789.
- Hames, W. E., Renne, P. R., and Ruppel, C., 2000, New evidence for geologically instantaneous emplacement of earliest Jurassic Central Atlantic magmatic province basalts on the North American margin: *Geology*, v. 28, p. 859-862.
- Harley, S. L., Kelly, N. M., and Möller, A., 2007, Zircon behaviour and the thermal histories of mountain chains: *Elements*, v. 3, p. 25-30.
- Harris, N. B. W., Pearce, J. A., and Tindle, A. G., 1986, Geochemical characteristics of collision-zone magmatism, *in* Coward, M. P., and Ries, A. C., editors, *Collision Tectonics*: London, Geological Society Special Publication 19, p. 67-81.

- Hatcher, R. D., Jr., 1969, Stratigraphy, petrology, and structure of the low rank belt and part of the Blue Ridge of northwesternmost South Carolina: South Carolina Division of Geology Geologic Notes, v. 13, no. 4, p. 11-32.
- Hatcher, R. D., Jr., 1971, Geology of Rabun and Habersham Counties, Georgia: A reconnaissance study: Georgia Department of Mines, Mining, and Geology Bulletin 83, 48 p.
- Hatcher, R. D., Jr., 1972, Developmental model for the southern Appalachians: Geological Society of America Bulletin, v. 83, p. 2735–2760.
- Hatcher, R. D., Jr., 1978, Tectonics of the western Piedmont and Blue Ridge: Review and speculation: American Journal of Science, v. 278, p. 276–304.
- Hatcher, R. D., Jr., 1989, Tectonic synthesis of the U.S. Appalachians, *in* Hatcher, R. D., Jr., Thomas, W. A., and Viele, G. W., editors, The Appalachian-Ouachita orogen in the United States: Boulder, Colorado, Geological Society of America, The Geology of North America, v. F-2, p. 511-535.
- Hatcher, R. D. Jr., 1993, Perspective on the tectonics of the Inner Piedmont, southern Appalachians, *in* Hatcher, R. D. Jr., and Davis, T. L., editors, Studies of Inner Piedmont geology with a focus on the Columbus Promontory: Carolina Geological Society Field Trip Guidebook, North Carolina Geological Survey, p. 17-43.
- Hatcher, R. D., Jr., 2001a, Terranes and terrane accretion in the southern Appalachians: An evolved working hypothesis: Geological Society of America Abstracts with Programs, v. 33, no. 2, p. 65.
- Hatcher, R. D., Jr., 2001b, Rheological partitioning during multiple reactivation of the Paleozoic Brevard fault zone, southern Appalachians, USA, *in* Holdsworth, R. E., Strachan, R. A., MacLoughlin, J. F., and Knipe, R. J., editors, The Nature and Significance of Fault Zone Weakening: London, Geological Society Special Publication 86, p. 255–269.
- Hatcher, R. D., Jr., 2002, An Inner Piedmont primer, *in* Hatcher, R. D., Jr., and Bream, B. R., editors, Inner Piedmont geology in the South Mountains-Blue Ridge Foothills and the southwestern Brushy Mountains, central-western North Carolina: Carolina Geological Society Field Trip Guidebook, p. 1-18.
- Hatcher, R. D., Jr., 2004a, Properties of thrusts and the upper bounds for the size of thrust sheets, *in* McClay, K. R., editor, Thrust Tectonics and Hydrocarbon Systems: American Association of Petroleum Geologists Memoir 82, p. 18–29.
- Hatcher, R. D., Jr., 2004b, Southern Appalachian Crustal Transect: Overview, *in* Merschat, A. J., and Hatcher, R. D., Jr., editors, Trans Appalachians Internides Geotraverse: 17th International Basement Tectonics Association Field Trip Guidebook, p. 1-12.
- Hatcher, R. D., Jr., and Acker, L. L., 1984, Geology of the Salem quadrangle, South Carolina: South Carolina Geological Survey, MS-26, scale 1:24,000.

- Hatcher, R. D., Jr., and Hooper, R. J. 1992, Evolution of crystalline thrust sheets in the internal parts of mountain chains, *in* McClay, K. R., editor, *Thrust Tectonics*: London, Chapman and Hall, p. 217–234.
- Hatcher, R. D., Jr., and Merschat, A. J., 2006, The Appalachian Inner Piedmont: An exhumed strike-parallel, tectonically forced orogenic channel, *in* Law, R. D., Searle, M., and Godin, L., editors, *Channel flow, ductile extrusion, and exhumation of lower-mid crust in continental collision zones*: London, Geological Society Special Publication 268, p. 517-540.
- Hatcher, R. D., Jr., Bream, B. R., and Merschat, A. J., 2007, Tectonic map of the southern and central Appalachians: A tale of three orogens and a complete Wilson Cycle *in* Hatcher, R. D., Jr., Carlson, M. P., McBride, J. H., and Martínez Catalán, J. R., editors, *4-D Framework of Continental Crust*: Boulder, Colorado, Geological Society of America Memoir 200, p. 595-632.
- Hatcher, R. D., Jr., Howell, D. E., and Talwani, P., 1977, Eastern Piedmont fault system: Speculations on its extent: *Geology*, v. 5, p. 636-640.
- Heatherington, A. L., Mueller, P. A., and Wooden, J. L., 2010, Alleghanian plutonism in the Suwanee terrane, USA: Implications for late Paleozoic tectonic models, *in* Tollo, R. P., Bartholomew, M. J., Hibbard, J. P., and Karabinos, P. M., editors, *From Rodinia to Pangea: The Lithotectonic Record of the Appalachian Region*: Boulder, Colorado, Geological Society of America Memoir 206, p. 607-620.
- Heyn, T., ms, 1984, Stratigraphic and structural relationships along the southwestern flank of the Sauratown Mountains anticlinorium: M.S. thesis, University of South Carolina, Columbia, 192 p.
- Herrmann, L. A., 1954, Geology of the Stone Mountain-Lithonia mining district, Georgia: Georgia Geological Survey Bulletin 61, 139 p.
- Hibbard, J. P., 2000, Docking Carolina: *Geology*, v. 28, p. 127-130.
- Hibbard, J., and Waldron, J. W. F., 2009, Truncation and translation of Appalachian promontories: Mid-Paleozoic strike-slip tectonics and basin initiation: *Geology*, v. 37, p. 487-490.
- Hibbard, J. P., Miller, B. V., Hames, W. E., Standard, I. D., Allen, J. S., Lavallee, S. B., and Bolland, I. B., 2012, Kinematics, U-Pb geochronology, and $^{40}\text{Ar}/^{39}\text{Ar}$ thermochronology of the Gold Hill shear zone, North Carolina: The Cherokee orogeny in Carolina, southern Appalachians: *Geological Society of America Bulletin*, v. 124, p. 643-656.
- Higgins, M. W., Atkins, R. L., Crawford, T. J., Crawford, R. F., III, Brooks, R., and Cook, R. B., 1988, The structure, stratigraphy, tectonostratigraphy and evolution of the southernmost part of the Appalachian orogen: U.S. Geological Survey Professional Paper 1475, 173 p.

- Hill, J. C., ms, 1999, Stratigraphy, structure, and tectonics of part of the southern Appalachian Inner Piedmont, near Marion, North Carolina: M.S. thesis, University of Tennessee, Knoxville, 188 p.
- Hooper, R. J., ms, 1986, Geologic studies at the east end of the Pine Mountain window and adjacent Piedmont, central Georgia: Ph.D. dissertation, University of South Carolina, Columbia, 322 p.
- Hooper, R. J., and Hatcher, R. D., Jr., 1988, Pine Mountain terrane, a complex window in the Georgia and Alabama Piedmont; evidence from the eastern termination: *Geology*, v. 16, p. 307-310.
- Hopson, J. L., and Hatcher, R. D., Jr., 1988, Structural and stratigraphic setting of the Alto allochthon, northeast Georgia: *Geological Society of America Bulletin*, v. 100, p. 339-350.
- Horkowitz, J. P., ms, 1984, Geology of the Philson Crossroads 7½ minute quadrangle, South Carolina – The nature of the boundary separating the Inner Piedmont from the Carolina/Avalon terrane in central northwestern South Carolina: M.S. thesis, University of South Carolina, Columbia, 100 p.
- Horton, J. W., Jr., and McConnell, K. I., 1991, The western Piedmont, *in* Horton, J. W., Jr., and Zullo, V. A., editors, *The Geology of the Carolinas—Carolina Geological Society 50th Anniversary Volume*: Knoxville, The University of Tennessee Press, p. 36–58.
- Howard, C. W., ms, 2012, Investigating the evolution of two southern Appalachian terrane boundaries and a plutonic complex: Tectonic implications of structural, geochemical, and geochronologic studies in the central Georgia Inner Piedmont: Knoxville, University of Tennessee, 222 p.
- Huebner, M. T., and Hatcher, R. D., Jr., editors, 2011, *The Geology of the Inner Piedmont at the Northeast End of the Pine Mountain Window*: Carrollton, Georgia Geological Society, 46th Annual Field Trip Guidebook, 136 p.
- Huebner, M. T., and Hatcher, R. D., Jr., 2013, Polyphase reactivation history of the Towaliga fault, central Georgia: Implications regarding the amalgamation and breakup of Pangea: *Journal of Geology*, v. 121, p. 75-90.
- Huebner, M. T., Wooden, J. L., and Hatcher, R. D., Jr., 2010, A terrane boundary in the central Georgia (USA) Inner Piedmont confirmed using new U-Pb SHRIMP ages of granitic rocks: *Geological Society of America Abstracts with Programs*, v. 42, no. 5, p. 196.
- Hurst, V. J., 1973, Geology of the southern Blue Ridge belt: *American Journal of Science*, v. 273, p. 643-670.
- Jubb, M. G. V., ms, 2010, Paradoxes in the deformational and metamorphic history of the eastern Blue Ridge: Evidence from the Lake Toxaway and eastern Big Ridge quadrangles, North Carolina: M.S. thesis, University of Tennessee, Knoxville, 294 p.

- Kalbas, J. L., ms, 2002, Geology of part of the southwestern Brushy Mountains, Inner Piedmont, North Carolina, and the geochemistry of western Inner Piedmont migmatite: M.S. thesis, University of Tennessee, Knoxville, 206 p.
- King, P. B., 1955, A geologic section across the southern Appalachians: An outline to the geology in the segment in Tennessee, North Carolina, and South Carolina, *in* Russell, R. J., editor, *Guides to Southeastern Geology*: New York, Geological Society of America, p. 332–373.
- King, P. B., 1964, Geology of the central Great Smoky Mountains, Tennessee: U.S. Geological Survey Professional Paper 349-C, 148 p.
- Lawton, D. E., ms, 1969, Geology of the Hard Labor Creek area in west-central Morgan County, Georgia: M.S. thesis, University of Georgia, Athens, 51 p.
- LeMaitre, R. W., 1989, *A classification of igneous rocks and glossary of terms*: Oxford, Blackwell, 193 p.
- Liu, A., ms, 1991, Structural geology and deformation history of the Brevard fault zone, Chauga belt, and Inner Piedmont, northwestern South Carolina and adjacent areas: PhD dissertation, University of Tennessee, Knoxville, 200 p.
- Ludwig, K. R., 2009, SQUID, version 2, A user's manual: Berkeley, California, Berkeley Geochronology Center Special Publication, No. 5, 110 p.
- Ludwig, K. R., 2012, Isoplot version 3.75, A geochronological toolkit for Microsoft Excel: Berkeley Geochronology Center Special Publication, No. 5, 75 p.
- Magaritz, M., Whitford, D. J., and James, D. E., 1978, Oxygen isotopes and the origin of high- $^{87}\text{Sr}/^{86}\text{Sr}$ andesites: *Earth and Planetary Science Letters*, v. 40, p. 220-230.
- Mapes, R. W., ms, 2002, Geochemistry and geochronology of mid-Paleozoic granitic plutonism in the southern Appalachian Piedmont terrane, North Carolina-South Carolina-Georgia: M.S. thesis, Vanderbilt University, Nashville, 150 p.
- McConnell, K. I., 1990, ms, Geology and geochronology of the Sauratown Mountains anticlinorium, northwestern North Carolina: Ph.D. dissertation, University of South Carolina, Columbia, 232 p.
- McSween, H. Y., Jr., and Harvey, R. P., 1997, Concord plutonic suite: Pre-Acadian gabbro-syenite intrusions in the southern Appalachians, *in* Sinha, A. K., Whalen, J. B., and Hogan, J. P., editors, *The Nature of Magmatism in the Appalachian Orogen*: Boulder, Colorado, Geological Society of America Memoir 191, p. 221-234.
- McWilliams, C. K., Walsh, G. J., and Wintsch, R. P., 2010, Silurian-Devonian age and tectonic setting of the Connecticut Valley-Gaspé trough in Vermont based on U-Pb SHRIMP analyses of detrital zircons: *American Journal of Science*, v. 310, p. 325-363.

- Merschat, A. J., ms, 2003, Inner Piedmont tectonics in the southwestern Brushy Mountains, North Carolina: Field and laboratory data revealing 3-D crustal flow and sillimanite I and II metamorphism: M.S. thesis, University of Tennessee, Knoxville, 198 p.
- Merschat, A. J., 2009, ms, Assembling the Blue Ridge and Inner Piedmont: Insights into the nature and timing of terrane accretion in the southern Appalachian orogen from geologic mapping, stratigraphy, kinematic analysis, petrology, geochemistry, and modern geochronology: Ph.D. dissertation, University of Tennessee, Knoxville, 455 p.
- Merschat, A. J., and Hatcher, R. D., Jr., 2007, The Cat Square terrane: Possible Siluro-Devonian remnant ocean basin in the Inner Piedmont, southern Appalachians, USA, *in* Hatcher, R. D., Jr., Carlson, M. P., McBride, J. H., and Martínez Catalán, J. R., editors, 4-D Framework of Continental Crust: Boulder, Colorado, Geological Society of America Memoir 197, p. 553-565.
- Merschat, A. J., and Kalbas, J. L., 2002, Geology of the southwestern Brushy Mountains, North Carolina Inner Piedmont: A summary and synthesis of recent studies, *in* Hatcher, R. D., Jr., and Bream, B. R., editors, Inner Piedmont geology in the South Mountains-Blue Ridge Foothills and the southwestern Brushy Mountains, central-western North Carolina: Carolina Geological Society Field Trip Guidebook, p. 101-126.
- Merschat, A. J., Hatcher, R. D., Jr., and Davis, T. L., 2005, The northern Inner Piedmont, southern Appalachians, USA: Kinematics of transpression and SW-directed mid-crustal flow: *Journal of Structural Geology*, 27, 1252-1281.
- Merschat, A. J., Hatcher, R. D., Jr., Byars, H. E., and Gilliam, W. G., 2008, Inner Piedmont Geotransverse from the Brushy Mountains to Lincolnton, North Carolina: Architecture of the Cat Square and Tugaloo terranes: Geological Society of America Southeastern Section, Field Trip Guidebook, 64 p.
- Merschat, A. J., Hatcher, R. D., Jr., Bream, B. R., Miller, C. F., Byars, H. E., Gatewood, M. P., and Wooden, J. L., 2010, Detrital zircon geochronology and provenance of southern Appalachian Blue Ridge and Inner Piedmont crystalline terranes, *in* Tollo, R. P., Bartholomew, M. J., Hibbard, J. P., and Karabinos, P. M., editors, From Rodinia to Pangea: The Lithotectonic Record of the Appalachian Region: Boulder, Colorado, Geological Society of America Memoir 206, p. 661-699.
- Meschter-McDowell, S., Miller, C. F., Fullagar, P. D., Bream, B. R., and Mapes, R. W., 2002, The Persimmon Creek Gneiss, eastern Blue Ridge, North Carolina-Georgia: Evidence for the missing Taconic arc?: *Southeastern Geology*, v. 41, p. 103-117.
- Miller, B. V., Fetter, A. H., and Stewart, K. G., 2006, Plutonism in three orogenic pulses, Eastern Blue Ridge province, southern Appalachians: *Geological Society of America Bulletin*, v. 118, p. 171-184.

- Miller, C. F., Hatcher, R. D., Jr., Ayers, J. C., Coath, C. D., and Harrison, T. M., 2000, Age and zircon inheritance of eastern Blue Ridge plutons, southwestern North Carolina and northeastern Georgia, with implications for magma history and evolution of the southern Appalachian orogen: *American Journal of Science*, v. 300, p. 142-172.
- Mirante, D. C., and Patiño-Douce, A. E., 2000, Melting and migmatization in the southern Appalachian Inner Piedmont of northeast Georgia; the Athens gneiss: *Geological Society of America Abstracts with Programs*, v. 33, no. 7, p. 297.
- Mittwede, S. K., 1989, The Hammett Grove meta-igneous suite; A possible ophiolite in the northwestern South Carolina Piedmont: Boulder, Colorado, Geological Society of America Special Paper 231, p. 45-62.
- Mittwede, S. K., and Fullagar, P. D., 1987, Petrology and geochronology of the Pacolet monzogranite, northwestern South Carolina: Petrogenetic implications: *Geological Society of America Abstracts with Programs*, v. 19, no. 2, p. 118.
- Mittwede, S. K., Ødegård, M., and Sharp, W. E., 1987, Major chemical characteristics of the Hammett Grove meta-igneous suite, northwestern South Carolina: *Southeastern Geology*, v. 28, p. 49-63.
- Mueller, P., Heatherington, A., Foster, D., and Wooden, J., 2011, Alleghanian granites of the southern Appalachian orogen: Keys to Pangean reconstructions, *in* Huebner, M. T., and Hatcher, R. D., Jr., editors, *The Geology of the Inner Piedmont at the Northeast End of the Pine Mountain Window: Carrollton, Georgia Geological Society, 46th Annual Field Trip Guidebook*, p. 39-47.
- Nelson, A. E., Horton, J. W., Jr., and Clarke, J. W., 1998, Geologic map of the Greenville 1-degree x 2-degree quadrangle, Georgia, South Carolina and North Carolina: U.S. Geological Survey Map I-1275, scale 1:250,000.
- Nomade, S., Knight, K. B., Beutel, E., Renne, P. R., Verati, C., Féraud, G., Marzoli, A., Youbi, N., and Bertrand, H., 2007, Chronology of the Central Atlantic Magmatic Province: Implications for the Central Atlantic rifting processes and the Triassic-Jurassic biotic crisis: *Palaeogeography, Palaeoclimatology, Palaeoecology*, v. 244, p. 326-344.
- Osberg, P. H., Tull, J. F., Robinson, P., Hon, R., and Butler, J. R., 1989, The Acadian orogen, *in* Hatcher, R. D., Jr., Thomas, W. A., and Viele, G. W., editors, *The Appalachian-Ouachita orogen in the United States: Boulder, Colorado, Geological Society of America, The Geology of North America*, v. F-2, p. 179-232.
- Pearce, J. A., 1996, Sources and settings of granitic rocks: *Episodes*, v. 19, p. 120-125.
- Pearce, J. A., Harris, N. B. W., and Tindle, A. G., 1984, Trace element discrimination diagrams for the tectonic interpretation of granitic rocks: *Journal of Petrology*, v. 25, p. 956-983.

- Privett, D. R., 1984, The Turnersburg intrusive: Petrogenesis of a metamorphosed Alpine ultramafite in the eastern Inner Piedmont Iredell County, North Carolina: *Southeastern Geology*, v. 25, p. 55-60.
- Ramos, V. A., Jordan, T. E., Allmendinger, R. W., Mpodozis, C., Kay, S. M., Cortés, J. M., and Palma, M., 1986, Paleozoic terranes of the central Argentine-Chilean Andes: *Tectonics*, v. 5, p. 855-880.
- Rankin, D. W., 1970, Stratigraphy and structure of Precambrian rocks in northwestern North Carolina, *in* Fisher, G. W., Pettijohn, F. J., Reed, J. C., Jr., and Weaver, K. N., editors, *Studies of Appalachian Geology: Central and Southern*: John Wiley and Sons, Inc., 460 p.
- Rankin, D. W., 1975, The continental margin of eastern North America in the southern Appalachians: The opening and closing of the proto-Atlantic Ocean: *American Journal of Science*, v. 275-A, p. 298-336.
- Robinson, P., Tucker, R. D., Bradley, D., Berry, H. N., IV, and Osberg, P. H., 1998, Paleozoic orogens in New England, USA: *Geologiska Föreningens Stockholm Forhandlingar*, v. 120, p. 119-148.
- Rollinson, H. R., 1993, *Using geochemical data: Evaluation, presentation, and interpretation*: John Wiley and Sons, Inc., 352 p.
- Roydin, L. H., Burchfiel, B. C., and van der Hilst, R. D., 2008, The geological evolution of the Tibetan Plateau: *Science*, v. 321, p. 1054-1058.
- Samson, S. D., 2001, Timing of Alleghanian magmatism revisited: *Geological Society of America Abstracts with Programs*, v. 33, no. 2, p. 7.
- Sears, J. W., Cook, R. B., and Brown, D. E., 1981, Tectonic evolution of the western part of the Pine Mountain window and adjacent Inner Piedmont province, *in* Sears, J. W., editors, *Contrasts in tectonic style between the Inner Piedmont terrane and the Pine Mountain window*: Alabama Geological Society, 18th Annual Field Trip Guidebook, p. 1-13.
- Secor, D. T., Jr., Snoke, A. W., and Dallmeyer, R. D., 1986, Character of the Alleghanian orogeny in the southern Appalachians: Part III. Regional Tectonics: *Geological Society of America Bulletin*, v. 97, p. 1345-1353.
- Sinha, A. K., Thomas, W. A., Hatcher, R. D., Jr., and Harrison, T. M., 2012, Geodynamic evolution of the central Appalachian orogen: Geochronology and compositional diversity of magmatism from Ordovician through Devonian: *American Journal of Science*, v. 312, p. 907-966.
- Stahr, D. W., ms, 2008, *Tectonometamorphic Evolution of the Eastern Blue Ridge: Differentiating Multiple Paleozoic Orogenic Pulses in the Glenville and Big Ridge Quadrangles, Southwestern North Carolina*: M.S. thesis, University of Tennessee, Knoxville, 277 p.

- Steltenpohl, M. G., editor, 2005, Southernmost Appalachian terranes, Alabama and Georgia: Tuscaloosa, Alabama Geological Society, Southeastern Section of the Geological Society of America Field Trip Guidebook, 162 p.
- Stose, A. J., and Stose, G. W., 1957, Geology and mineral resources of the Gossan Lead district and adjacent areas: Virginia Division of Mineral Resources Bulletin 72, 233 p.
- Streckeisen, A., 1976, Classification and nomenclature of plutonic rocks recommendations of the IUGS subcommission on the systematics of Igneous Rocks: International Journal of Earth Sciences, v. 63, no. 2, p. 773-786.
- Sun, S. S., and McDonough, W. F., 1989, Chemical and isotopic systematics of ocean basalts: implications for mantle compositions and processes, *in* Saunders, A. D., and Norry, M. J., editors, Magmatism in the Ocean Basins: Boulder, Colorado, Geological Society of America Special Publication 42, p. 313-345.
- Tull, J. F., 1978, Structural development of the Alabama Piedmont northwest of the Brevard zone: American Journal of Science, v. 278, p. 442-460.
- Vaucher, A., Babaie, H. A., & Babaie, A., 1993, Orogen-parallel tangential motion in the Late Devonian-Early Carboniferous southern Appalachians internides: Canadian Journal of Earth Sciences, v. 30, p. 1297-1305.
- Vinson, S., ms, 1999, Ion probe geochronology of granitoid gneisses of the Inner Piedmont, North Carolina and South Carolina: M.S. thesis, Vanderbilt University, Tennessee, 84 p.
- Whitford, D. J., and Jezek, P. A., 1982, Isotopic constraints on the role of subducted sialic material in Indonesian island-arc magmatism: Geological Society of America Bulletin, v. 93, p. 504-513.
- Wintsch, R. P., Aleinikoff, J. N., Walsh, G. J., Bothner, W. A., Hussey, A. M., and Fanning, C. M., 2007, SHRIMP U-Pb evidence for a Late Silurian age of metasedimentary rocks in the Merrimack and Putnam-Nashoba terranes, eastern New England: American Journal of Science, v. 307, p. 119-167.
- Williams, H., and Hatcher, R. D., Jr., 1982, Suspect terranes and accretionary history of the Appalachian orogen: Geology, v. 10, p. 530-536.
- Williams, S. T., 2000, ms, Structure, stratigraphy, and migmatization in the southwestern South Mountains, North Carolina: M.S. thesis, University of Tennessee, Knoxville, 111 p.
- Wilson, C. G., 2006, ms, Origin and tectonic evolution of the southern Appalachian Neocadian crystalline core: Evidence from the geology of the Gilreath 7.5-minute quadrangle, North Carolina: M.S. thesis, University of Tennessee, Knoxville, 200 p.

Chapter III

**The transition from B- to A-subduction during closure
of the Rheic remnant ocean: Marking the Acadian/
Neoacadian accretion of the Carolina superterrane, southern
Appalachians**

Chapter III synthesizes new geochronologic and geochemical data from Concord Plutonic Suite mafic rocks along the western flank of the Carolina superterrane with data from the Inner Piedmont, Blue Ridge, and the Appalachian foreland basin to construct a tectonic model that depicts the polyphase accretionary history of the Carolina superterrane. My coauthor is Robert D. Hatcher, Jr. A version of this manuscript will be submitted to a peer reviewed journal by late 2013. My contributions include sample and data collection, compilation of geochronologic data from the southern Appalachian orogen, synthesis and interpretation of the data, and the majority of the writing. The use of the term “we” and “our” in the text refers to the coauthor and myself.

ABSTRACT

The nature of the Paleozoic accretion of the Carolina superterrane remains a major unresolved debate regarding the tectonic history of southern Appalachian orogen. Two primary tectonic models differ in timing, kinematics, and subduction polarity: One model portrays a Late Ordovician-Silurian sinistral transpressive event with closure of an ocean basin at a west-dipping subduction zone beneath the eastern Laurentian margin, whereas the alternative depicts obduction of the Carolina superterrane onto the Laurentian margin in a Devonian-Mississippian dextral transpressive event. The Concord Plutonic Suite, an arcuate Silurian-Devonian suite of mafic plutons that intruded the western flank of the Carolina superterrane, suggest east-dipping subduction of ocean crust beneath the Carolina superterrane just prior to collision with Laurentian terranes, which supports the latter model. Geochemical and isotopic data support a subduction-related origin for the Concord Plutonic Suite, and new geochronologic data reveal the main pulse of this episode of plutonism occurred ~405 Ma. This slightly predates main phase plutonism in the adjacent Cat Square terrane, which we suggest is the product of B-subduction of ocean crust beneath the Carolina superterrane between 415 and 400 Ma, with shutoff of arc-related magmatism due to A-subduction of the eastern Laurentian margin that also resulted in prograde upper amphibolite-facies metamorphism, wholesale migmatization, and extensive anatectic plutonism in the eastern Inner Piedmont. Although these data, combined with observations from the foreland, provide compelling support for Devonian-Mississippian accretion of the Carolina superterrane, this model in itself fails to reconcile evidence that supports the alternative. We therefore propose a hybrid tectonic model that involves early (Late Ordovician) soft collision of the Carolina superterrane followed by an outboard subduction jump that resulted in the development of the Cat Square back arc basin, which then closes in the manner described above. This new model synthesizes numerous data from the foreland, crystalline interior of the Laurentian terranes, and the exotic Carolina superterrane, and provides a new perspective regarding the complex accretionary evolution of the southern Appalachian orogen.

INTRODUCTION

One of the largest unresolved debates regarding the tectonic evolution of the southern Appalachian orogen is the timing and kinematics of the Paleozoic accretion of the exotic Carolina superterrane and its collateral effects imposed on the eastern Laurentian margin. There currently are currently two dominant models that depict this tectonic event: (1) sinistral accretion of the Carolina superterrane beneath Laurentia during an Ordovician-Silurian event (e.g., Hibbard, 2000), or (2) dextral transpressive obduction of the Carolina superterrane and subduction of the eastern Laurentian margin during a Devonian-Mississippian (Acadian/Neoacadian) event (e.g., Merschat et al., 2005). Interestingly, workers who focus primarily in the exotic Carolina superterrane tend to favor the earlier model (e.g., Hibbard, 2000; Dennis, 2007), while those who work in peri-Laurentian rocks tend to favor the latter (e.g., Merschat et al., 2005; Merschat and Hatcher, 2007; Ettensohn, 2011; Huebner et al., *in review*). This debate is compounded by contrasting interpretations of the boundary between exotic and Laurentian rocks, which will be discussed herein.

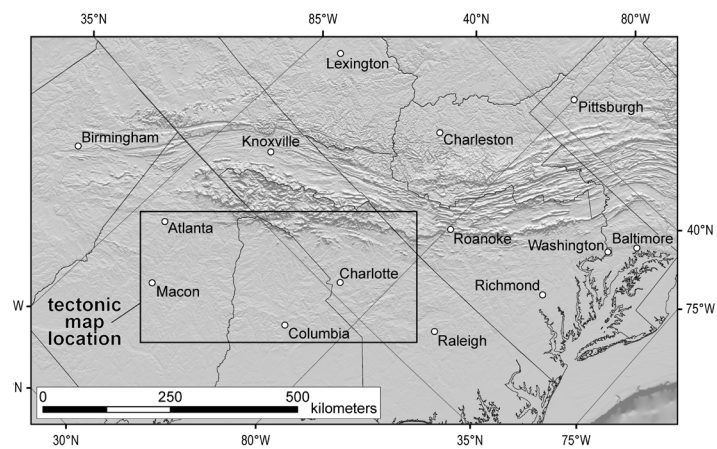
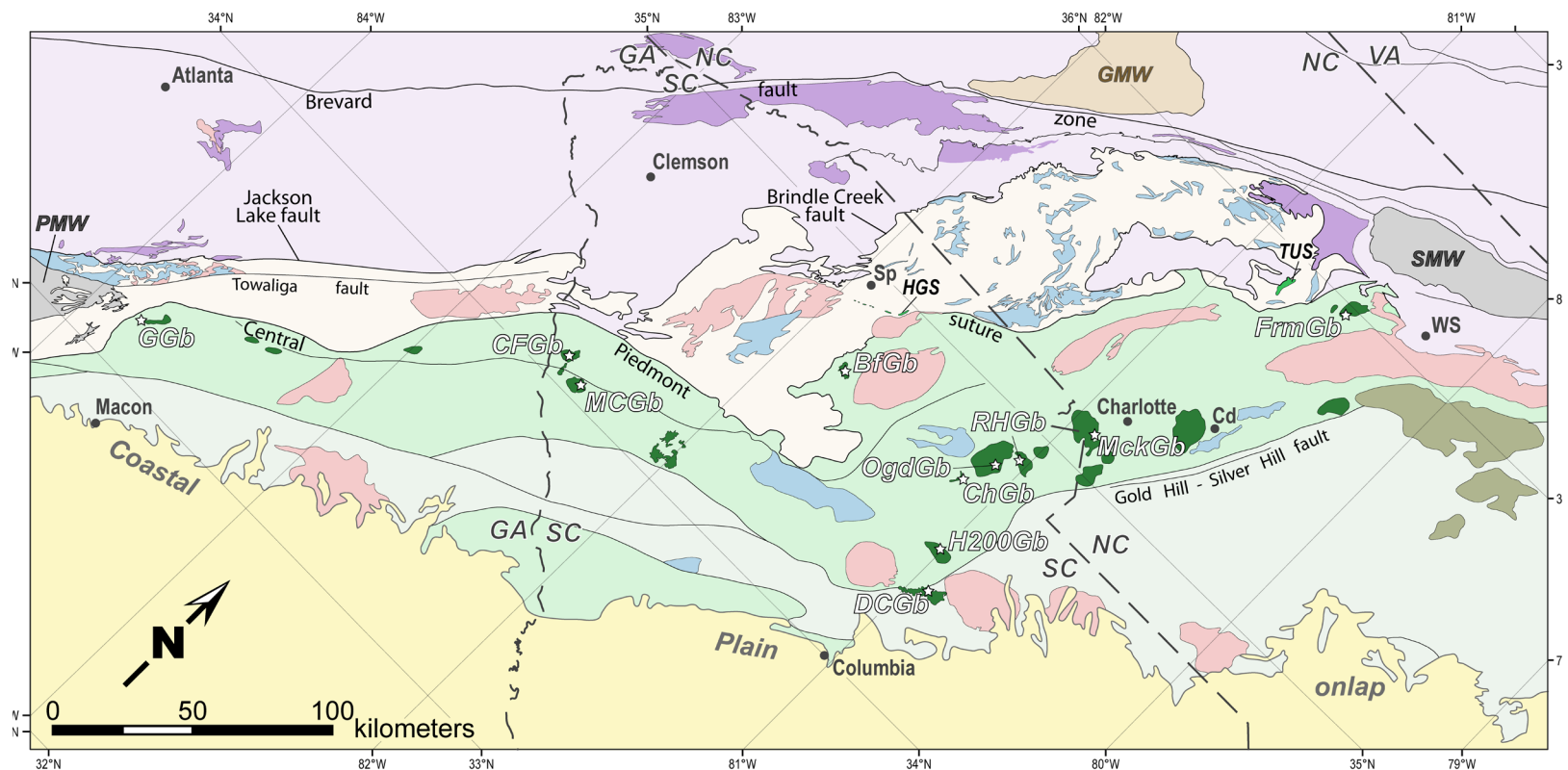
Several studies have concluded the Carolina superterrane accreted in a Late Ordovician-Silurian event, recently termed the “Cherokee orogeny” (e.g., Hibbard, 2000; Hibbard et al., 2010, 2012). The main evidence that supports accretion of the Carolina superterrane at this time includes: 1) the Tuscarora unconformity in the central Appalachian foreland (Dorsch et al., 1994; Hibbard, 2000); 2) Ordovician-Silurian arc-related magmatism in the western Inner Piedmont and eastern Blue Ridge (Tugaloo terrane) (e.g., Meschter-McDowell et al., 2002; Sinha et al., 2012); 3) paleomagnetic data that suggest the Carolina superterrane and Laurentia were at similar latitudes since the Ordovician (Vick et al., 1987; Noel et al., 1988); and 4) Late Ordovician-Silurian $^{40}\text{Ar}/^{39}\text{Ar}$ cooling ages from the Carolina terrane (Vick et al., 1987; Noel et al., 1988; Hibbard et al., 2012). In this model, west-directed (present geographic frame) subduction of Rheic ocean crust beneath the eastern Laurentian margin resulted in development of a suite of suprasubduction zone plutons in the western Inner Piedmont, with the ultimate accretion of the Carolina superterrane by sinistral transpression (e.g., Hibbard, 2000; Hibbard et al., 2010, 2012). Primary evidence for sinistral transpression is derived from a possible northeast-younging of Ordovician-Silurian plutons in the Tugaloo terrane and apparent sinistral macroscale structures within the Carolina terrane (Hibbard, 2000, 2012). This model is similar in timing and kinematics to the accretion of various peri-Gondwanan terranes in the maritime Appalachians (e.g., van Staal et al., 1998, 2008). A key attribute of this model is that the sinistral Ordovician-Silurian suture is not exposed at the surface; the fault that separates exotic from Laurentian-affinity rocks is proposed to be a late Paleozoic fault that overthrust the original suture. Therefore, proponents of this model argue that no direct evidence regarding the nature of the suture can be ascertained at

the surface, which in turn renders the timing and kinematics of this boundary as virtually untestable. Additionally, this model alone does not attempt to reconcile evidence that supports a later Devonian-Mississippian event.

In contrast, dextral transpressive Acadian/Neoacadian accretion of the Carolina superterrane and subduction of the eastern Laurentian margin has been hypothesized (Merschhat et al., 2005; Hatcher et al., 2007; Merschhat and Hatcher, 2007; Hatcher, 2010; Huebner et al., *in review*). In this model, Rheic ocean crust was consumed along an east-dipping subduction zone beneath the Carolina superterrane, followed by dextral transpressive obduction of the Carolina superterrane onto the Laurentian margin. During accretion, the Inner Piedmont was subducted to mid-crustal depths and flowed as an orogenic channel, buttressed by the dextral Devonian Brevard fault zone, as it was extruded to the southwest (Merschhat et al., 2005; Hatcher and Merschhat, 2006). The most prominent evidence that supports this model includes: 1) upper amphibolite-facies prograde metamorphism and coeval high temperature fabrics throughout most of the Inner Piedmont that occurred from latest Silurian into the Mississippian (Merschhat, 2009; Huebner et al., *in review*); 2) regional high temperature mineral lineation pattern through the northern Inner Piedmont that supports southwest-directed extrusion (Hatcher, 2001; Merschhat et al., 2005; Hatcher and Merschhat, 2006; Hatcher et al., 2007); 3) the Devonian attributes of the polyphase Brevard fault zone (Vauchez et al., 1993; Hatcher, 2001; Merschhat et al., 2005); 4) a pulse of abundant, likely anatectic felsic plutonism in the eastern Inner Piedmont (Cat Square terrane) that occurred from 415-355 Ma (Mapes, 2002; Gatewood, 2007; Byars, 2010; Huebner et al., *in review*); 5) Devonian $^{40}\text{Ar}/^{39}\text{Ar}$ cooling ages from the western and central portions of the Carolina superterrane (Dallmeyer et al., 1986; Secor et al., 1986; Dallmeyer, 1989; Hibbard et al., 2012); and 6) northeast-to-southwest younging of Devonian-Mississippian clastic wedges in the central to southern Appalachian foreland, which parallels the dextral translation of the Inner Piedmont and Carolina superterrane along the Brevard fault zone (Ettensohn, 1985, 1987; Ferrill and Thomas, 1988; Merschhat and Hatcher, 2007; Ettensohn and Lierman, 2012). We suggest the combination of these attributes, in addition to other evidence to be discussed below, provides compelling support for Acadian/Neoacadian accretion of the Carolina superterrane. However, this model in itself fails to reconcile attributes of the southern Appalachians that support earlier accretion.

Aside from the timing and kinematics of accretion, the most prominent contrast between the two models involves subduction polarity during the accretionary event. Several others have suggested that Silurian-Devonian Concord and Salisbury Plutonic Suite rocks that occur along the western flank of the Carolina superterrane (Charlotte terrane) (Fig. 3-1) were emplaced in a subduction-zone setting (e.g., McSween et al., 1984; Misra and McSween, 1984; McSween and Harvey, 1997; Esawi, 2004; Chaumba, 2010b, 2011), although other studies have indicated their petrogenesis may be related to different tectonic processes (e.g., Sinha et al., 1989; McSween

Figure 3-1: Simplified lithotectonic map of the southern Appalachian Inner Piedmont and adjacent Carolina superterrane, with sample locations of Concord Plutonic Suite gabbros analyzed in this study (*modified from* Hatcher et al., 2007). Cd-Concord; Sp-Spartanburg; WS-Winston-Salem; HGS-Hammett Grove Meta-igneous suite; TUS-Turnersburg ultramafic suite; GMW-Grandfather Mountain window; PMW-Pine Mountain window; SMW-Sauratown Mountain window; BfGb-Buffalo gabbro; CFGb-Calhoun Falls gabbro; ChGb-Chester gabbro; DCGb-Dutchman’s Creek gabbro; FrmGb-Farmington gabbro; GGb-Gladesville gabbro; H200Gb-“Highway 200” gabbro; MckGb-Mecklenburg gabbro; MCGb-Mount Carmel gabbro; OgdGb-Ogden gabbro; RHGb-Rock Hill gabbro.



Explanation	
Terranes	Igneous Rocks
Tugalo terrane	Alleghanian
Cat Square terrane	Acadian/Neoacadian
Carolina terrane	Taconian
Charlotte terrane	Concord Plutonic Suite
Coastal Plain	Neoproterozoic/Cambrian
basement massifs	
Grandfather Mountain window	

and Harvey, 1997; Dennis, 2007). We present new U-Pb SHRIMP geochronologic and whole-rock geochemical data from mafic plutonic rocks that were collected to better define the nature and timing of this pulse of plutonism. These new data, combined with compiled geochemical, geochronologic, isotopic, and structural data from the western flank of the Carolina superterrane and adjacent Inner Piedmont, strongly support Devonian-Mississippian dextral accretion of the ultimate accretion of the Carolina superterrane. However, neither model alone attempts to elucidate evidence that supports the alternative; therefore, we present a tentative hybrid model that incorporates data supporting both competing arguments, with the hope of sparking constructive discourse related to the complex Paleozoic evolution of the southern Appalachian orogen.

GEOLOGIC SETTING

The Inner Piedmont

The Inner Piedmont is a composite terrane that consists of a gently dipping stack of large, crystalline, type F thrust sheets, and has long been distinguished from surrounding rocks by contrasts in structural style and high metamorphic grade (e.g., King, 1955; Bentley and Neathery, 1970; Griffin, 1971; Hatcher and Hooper, 1992; Merschat et al., 2005). It includes two distinct lithotectonic terranes: the Tugaloo terrane, a suite of predominantly Neoproterozoic-Middle Ordovician siliciclastic and metavolcanic units that were intruded by Ordovician-Silurian plutons, and the Cat Square terrane, which is made up of Silurian-Devonian siliciclastics with latest Silurian-Mississippian peraluminous felsic magmatism (Bream, 2003; Merschat and Hatcher, 2007; Huebner et al., *in review*). The Brindle Creek-Jackson Lake fault separates the Tugaloo (western Inner Piedmont) and Cat Square terranes (eastern Inner Piedmont) (Fig. 3-1), and cross-cutting relationships with granitic rocks and macroscale structures indicate the fault was active at ~355 Ma in the Carolinas and ~370 Ma in central Georgia (Huebner et al., *in review*). The primary evidence that justifies the separation of the Inner Piedmont into two terranes includes: 1) detrital zircon signatures, and by implication, timing of deposition; 2) granitoid ages; 3) lithologic differences; and 4) occurrence of Grenville basement fragments in the Tugaloo terrane, with none identified (to date) in the Cat Square terrane. The composite Inner Piedmont is bound to the east by the Central Piedmont suture, which juxtaposes exotic peri-Gondwanan rocks of the Carolina superterrane above the Laurentian margin. Its western boundary is the Brevard fault zone, although, this boundary is not a suture by definition (Hatcher et al., 2007). While contrasts in structural style and magmatism occur across this boundary, the same lithostratigraphic successions occur on both sides of the fault zone (e.g., Hurst, 1973; Hopson and Hatcher, 1988; Hatcher, 2001; 2002). Detrital zircon data also reveal identical provenance, and confirm Laurentian affinity of western Inner Piedmont metasedimentary rocks (Bream et al., 2001; Bream, 2003;

Hatcher et al., 2007). Nonetheless, the Brevard fault zone, which bisects the Tugaloo terrane, is arguably one of the most important boundaries in the southern Appalachians (e.g., Hatcher, 2001; Merschat et al., 2005).

Tugaloo terrane lithostratigraphy is dominated by the Tallulah Falls Formation (Hatcher, 1971), which consists of Neoproterozoic-Cambrian(?) deep-water siliciclastic and mafic volcanic rocks that were likely deposited on ocean crust and fragments of Grenville basement rocks (Hatcher, 1993, 2002). The Tallulah Falls Formation is the stratigraphic equivalent of the Ashe (Rankin, 1970) and Lynchburg (Stose and Stose, 1957) Formations in North Carolina and Virginia, and the Ashland supergroup in western Georgia and Alabama (Adams, 1926; Tull, 1978). These rocks have been metamorphosed at middle- and upper-amphibolite facies conditions, and now consist of biotite paragneiss, pelitic and aluminous schist, and amphibolite; nevertheless, an intact stratigraphy is still discernable (e.g., Hatcher, 1971, 1972; Bream, 1999; Hill, 1999; Stahr, 2008). The Tallulah Falls Formation comprises a trichotomic stratigraphy that consists of a lower amphibolite-rich metagraywacke-pelitic schist unit and an upper amphibolite-poor metagraywacke-pelitic schist unit separated by a distinct, regionally continuous aluminous schist unit (e.g., Hatcher, 1978, 1993).

Throughout the western Carolinas, the Tallulah Falls Formation is conformably overlain by Cambrian-lower Ordovician(?) metasilstone, quartzite, graphitic schist, and impure marble of the Chauga River Formation (e.g., Hatcher, 1972, 2002; Bream, 1999). This unit thins dramatically northeastward in the western Inner Piedmont of the Carolinas (e.g., Bier et al., 2002), and has not been identified west of the Brevard fault. The contact with the overlying Poor Mountain Formation is sharp with limited interlayering and, when combined with the lack of evidence of faulting, has been interpreted as an unconformity (e.g., Bream, 1999; Hill, 1999; Bier et al., 2002).

The Poor Mountain Formation is characterized by a basal laminated amphibolite with interlayered felsic tuff member that grades upward into feldspathic quartzite, marble, and metatuff. It was first recognized in the western Carolinas and northeastern Georgia (Hatcher, 1969), and may correlate with the Ropes Creek Amphibolite (Bentley and Neathery, 1970; Steltenpohl, 2005) in eastern Alabama. The lower amphibolite unit is primarily a laminated amphibolite with subordinate interlayered feldspathic quartzite and amphibole gneiss (Hatcher, 1969; Bream, 1999). The relative amount of feldspathic quartzite increases upward, eventually grading into the overlying Poor Mountain Quartzite member. Ion microprobe analysis of two metatuff units from the upper quartzite member revealed Late Ordovician ages (459 ± 4 and 445 ± 4 Ma; Bream et al., 2004).

The Inner Piedmont portion of the Tugaloo terrane was intruded by mostly Ordovician-Silurian peraluminous granites and granodiorites, with Carboniferous-Permian granitoids throughout central Georgia (e.g., Vinson, 1999; Bream, 2003; Jubb, 2010; Mueller et al., 2011). Tugaloo

terrane rocks west of the Brevard fault zone include several Devonian bodies in southwestern North Carolina, with abundant Middle Ordovician through Late Devonian magmatism prevalent through the Virginia Blue Ridge (e.g., Miller et al., 2000; Sinha et al., 2012). Sinha et al. (2012) identified five discrete pulses of magmatism through the Virginia-Maryland Piedmont, mostly within Ordovician-Silurian times. Additionally, small bodies of Grenville continental basement rocks occur throughout the Tugaloo terrane (e.g., Heyn, 1984; McConnell, 1990; Fullagar, 1997; Mersch, 2009; Byars, 2010; Huebner et al., 2010).

Metasedimentary rocks of the Cat Square terrane consist of migmatized metagraywacke and aluminous schist units without a recognizable stratigraphy. Although only subtle lithologic differences are apparent in the field, the initial distinction of rocks east of the Brindle Creek-Jackson Lake fault as a separate lithotectonic terrane was primarily the result of detrital zircon data that consist of Grenville, peri-Gondwanan, and a prominent Ordovician-Silurian signature (Bream, 2003). The Ordovician-Silurian zircons are likely Laurentian, sourced from suites of arc-related and extensional plutons in the eastern Blue Ridge of Virginia (Mersch et al., 2010; Sinha et al., 2012). This signature also reveals the relative youth of the metasedimentary rocks, indicating a Silurian maximum depositional age (e.g., Bream, 2003; Mersch and Hatcher, 2007). Abundant Cat Square terrane granitoid plutons are mostly Devonian to Mississippian and appear to be dominantly anatectic (e.g., Mapes, 2002; Mersch, 2009).

Additionally, several mafic and ultramafic bodies have been identified throughout the Cat Square terrane (Privett, 1984; Mittweide et al., 1987; Goldsmith et al., 1988; Giorgis, 1999; Mersch et al., 2008; Byars, 2010). Small bodies of altered ultramafic rocks (talc-chlorite schist) occur near the western flank of the Cat Square terrane (Giorgis, 1999; Mersch et al., 2008), but the largest ultramafic and mafic bodies, the Turnersburg ultramafic and the Hammett Grove Meta-igneous Suite, occur near the central Piedmont suture to the east (Privett, 1984; Mittweide et al., 1987; Goldsmith et al., 1988). The Hammett Grove Meta-igneous Suite consists of serpentinized ultramafic rocks, metapyroxenite, metagabbro, amphibolite, and metachert, interpreted by several studies to represent a dismembered ophiolite (Mittweide et al., 1987; Mittweide, 1989; Chaumba, 2010a). Mersch and Hatcher (2007) interpreted the mafic and ultramafic rocks, lack of continental basement, and detrital zircon signatures that represent mixed Laurentian-peri-Gondwanan provenance as evidence that Cat Square terrane metasedimentary assemblages were originally deposited on oceanic crust.

Detailed structural analyses from both Inner Piedmont terranes, combined with U-Pb ion microprobe analyses of metamorphic zircons rims (Mersch, 2009; Huebner et al., *in review*), geochronologic analysis of monazite (Dennis and Wright, 1997), and $^{40}\text{Ar}/^{39}\text{Ar}$ cooling ages (Dallmeyer et al., 1986; Secor et al., 1986; Dallmeyer, 1989), indicate the composite Inner Piedmont concurrently underwent regional metamorphism through the Devonian and Mississippian.

The dominant regional foliation (S_2) is defined by parallel alignment of high-temperature mineral assemblages that indicate formation at upper amphibolite-facies conditions and, along with pervasive migmatitic layering that is ubiquitously parallel to S_2 , supports formation of the fabric during peak metamorphic conditions (e.g., Mersch, 2009; Huebner et al., *in review*). S_2 locally envelops calc-silicate and amphibolite boudins that preserve an earlier S_1 fabric (e.g., Hopson and Hatcher, 1988; Mersch et al., 2005; Davis, 2010). Lithologic contacts between metasedimentary rocks (S_0) are generally subparallel to S_2 , indicating strong transposition during deformation. S_2 dips shallowly throughout the northern Inner Piedmont, and strike becomes strongly orientated northeast-southwest close to the Brevard fault zone. In the central Georgia Inner Piedmont, S_2 consistently strikes northeast-southwest, but southeast dip dramatically steepens toward the eastern boundary with the Carolina superterrane. The associated high-grade mineral lineation (L_2) plunges shallowly throughout the Inner Piedmont, and exhibits a curved macro-scale pattern in the northern Inner Piedmont (Mersch et al., 2005; Hatcher and Mersch, 2006; Hatcher et al., 2007). Compositional and migmatitic layering, and S_2 fabric are axial planar to isoclinal, meso- and macro-scale F_2 folds. In the northern Inner Piedmont, L_2 is commonly coaxial with F_2 fold hinges, with sheath folds common at meso- and macroscales (e.g., Hopson and Hatcher, 1988; Mersch et al., 2005). Late-stage structures that are likely products of the Alleghanian orogeny consist of mesoscale to macroscale upright open folds and an extensive array of map-scale dextral strike-slip faults that occur from the Brevard fault zone eastward to beneath the Atlantic Coastal Plain (Hatcher et al., 1977).

Metamorphic isograd maps of the composite Inner Piedmont reveal a core of migmatitic, upper amphibolite to granulite facies rocks flanked by relatively lower-grade rocks along its boundaries (Mersch, 2009) (Fig. 3-2). Peak conditions in the core of the Inner Piedmont reached 750-850° C at 500-800 MPa (Mirante and Patiño-Douce, 2000; Bier et al., 2002; Mersch, 2003) through the Carolinas and northeast Georgia and 645-715° C at 400-530 MPa in central Georgia (Davis, 2010). Assuming moderate geothermal and geobarometric gradients, metamorphic conditions in the Inner Piedmont require burial depths of 15-20 km (Mersch and Hatcher, 2007). U-Pb ages of deformed plutonic rocks and metamorphic zircon rims imply the northern portion of the Inner Piedmont underwent peak metamorphism 405-360 Ma, remained hot until ~345 Ma (overall peak), cooled, and was again subjected to a thermal increase that peaked 330-320 Ma (Dennis and Wright, 1997; Mersch, 2009). Similar data from the central Georgia Inner Piedmont indicate thermal peaks occurred at ~380 and ~320 Ma, with no strong evidence for a ~345 Ma peak similar to that in the northern Inner Piedmont (Huebner et al., *in review*). Abundant anatectic(?) granitoids coincide with regional metamorphism throughout the Inner Piedmont (407-350 Ma), with apparent pulses of magmatism at ~400, ~380, and ~360 Ma (Giorgis et al., 2002; Mapes, 2002; Gatewood, 2007; Byars et al., 2008; Huebner et al., *in review*). The

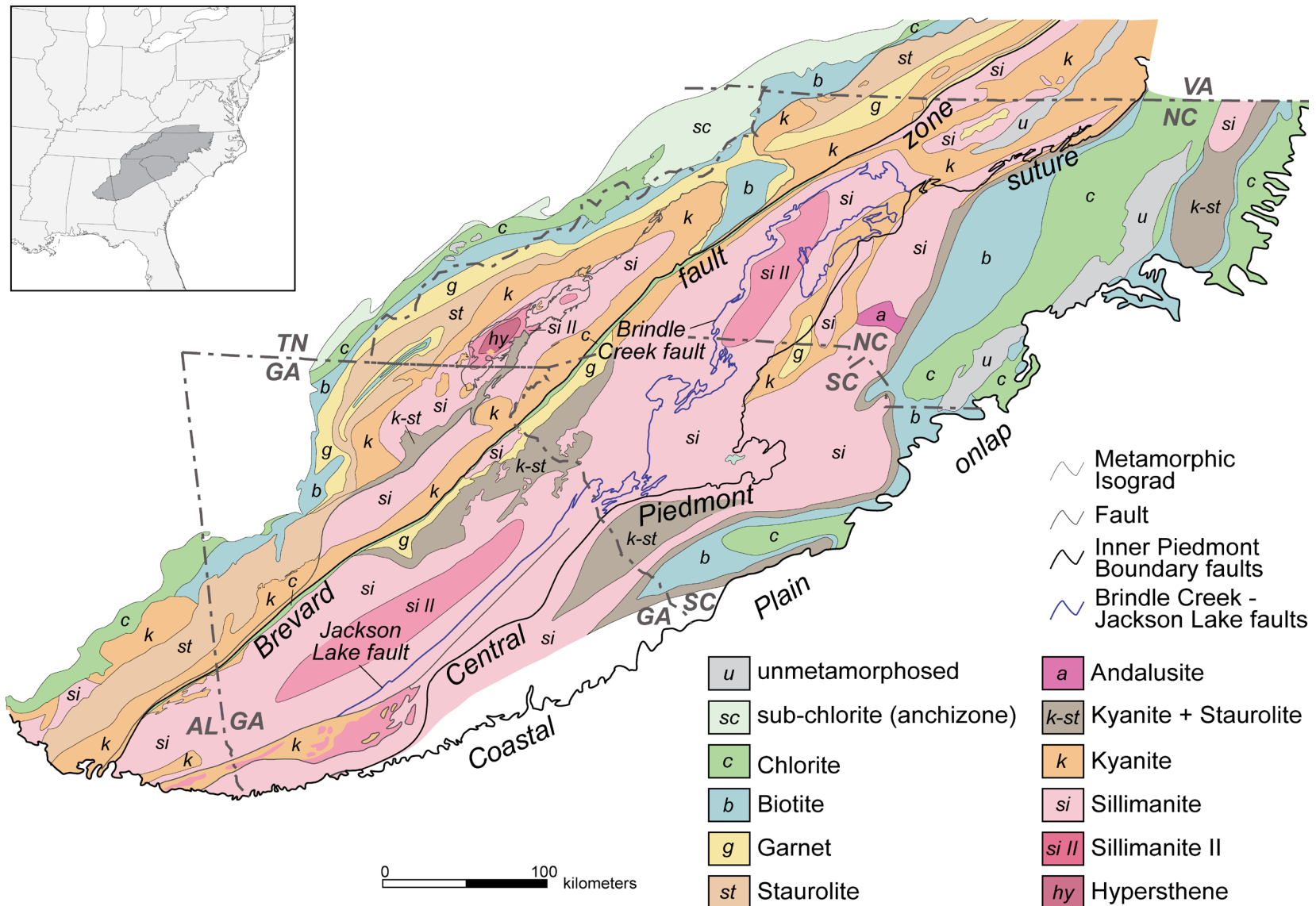


Figure 3-2: Metamorphic isograd map of the southern Appalachian orogen (*modified from Mersch, 2009; Hatcher, 2004, and references therein.*).

dominant regional foliation (S_2), which developed during peak metamorphic conditions, crosses folded contacts between Devonian Inner Piedmont plutons, pegmatites, and granitic melts, supporting the conclusion that plutonism occurred pre- to syn-peak metamorphism. Carboniferous granitoids truncate S_2 and associated structures, which confirm that development of dominant regional fabrics occurred prior to the Alleghanian orogeny (e.g., Huebner et al., *in review*).

The Carolina superterrane

The Carolina superterrane is a composite peri-Gondwanan, Neoproterozoic-early Paleozoic amalgamation of lithotectonic terranes that mostly consist of volcanic arc, volcanogenic sedimentary, and subarc plutonic components (e.g., Horton et al., 1989; Hibbard et al., 2002; Hatcher et al., 2007). The exotic nature of the Carolina superterrane was confirmed with the presence of a Middle Cambrian Atlantic province trilobite (*Acadoparadoxides*) fauna (Secor et al., 1983), and is further supported by several pulses of magmatism, deformation, metamorphism, and sedimentation that do not correspond with documented Laurentian tectonism (e.g., Harris and Glover, 1988; Hibbard and Samson, 1995; Dennis and Wright, 1997; Barker et al., 1998; Hibbard et al., 2002). Hibbard and Samson (1995) and Hibbard et al. (2002) summarized the history of tectonic events that occurred independent of Laurentia, and recognized three basic stages of tectonic activity that occurred at 700-600 Ma, 590-560 Ma, and 550-530 Ma. The youngest of these events, termed the Virgilina orogeny (Glover and Sinha, 1973; Harris and Glover, 1988), appears to have affected the entire Carolina superterrane (Barker et al., 1998). Dennis and Wright (1997) suggested that Virgilina regional metamorphism and development of the dominant foliation in the Charlotte terrane occurred prior to ~535 Ma, based on the age of a crosscutting, undeformed, unmetamorphosed biotite-hornblende diorite. Evidence for younger Paleozoic events includes Ordovician-Silurian fabric development in the Carolina terrane (e.g., Offield et al., 1995), Ordovician-Silurian, Devonian, and Carboniferous-Permian $^{40}\text{Ar}/^{39}\text{Ar}$ cooling ages (e.g., Sutter, 1983; Dallmeyer et al., 1986; Noel et al., 1988; Offield et al., 1995; Hibbard et al., 2012), and Silurian-Devonian and Carboniferous-Permian plutonism (e.g., Sinha and Zietz, 1982; McSween and Harvey, 1997; Speer and Hoff, 1997; Samson and Secor, 2000; Samson, 2001).

Although a myriad of lithotectonic terranes have been proposed to comprise the Carolina superterrane (e.g., Horton et al., 1989; Hibbard et al., 2002), the two largest and most prominent are the Charlotte and Carolina terranes (Hibbard et al., 2002). The location of the boundary that separates the Carolina and Charlotte terranes, which has been interpreted to juxtapose the lower-grade Carolina terrane above the Charlotte terrane, is not well defined; recent work has suggested that this tectonic boundary has not yet been identified (Hibbard et al., 2012). The boundary has previously been assigned to various Neoproterozoic, middle Paleozoic, and late Paleozoic fault systems (see Hibbard et al., 2002, and references therein); however, other studies have alterna-

tively argued that the boundary between the proposed terranes, mostly interpreted as the Gold Hill-Silver Hill fault zone, is simply a metamorphic gradient, as stratigraphic units appear to be continuous across that boundary (e.g., Stromquist and Sundelius, 1975; Secor et al., 1982; Halik, 1983; Dallmeyer et al., 1986; Hibbard et al., 2012).

The Carolina terrane, located east of the Charlotte terrane, is exposed along orogenic strike from central Georgia through central Virginia (e.g., Hibbard et al., 2002). Aeromagnetic data indicate much of the Carolina terrane is buried beneath the Atlantic Coastal Plain, with its eastern subsurface boundary extending to near the Atlantic shoreline (Hatcher et al., 2007). In general, the Carolina terrane is a predominantly greenschist-facies (chlorite or biotite grade) sequence of Neoproterozoic to Cambrian magmatic arc material with associated clastic and volcanogenic sedimentary rocks (e.g., Fiess, 1982; Hibbard et al., 2002). Structural geology of the Carolina terrane is characterized by tight, upright macroscale folds that are axial planar to biotite-grade slaty cleavage (e.g., Griffin, 1978; Offield, 1995; Hibbard et al., 1998). Plutonic rocks throughout the Carolina terrane are mostly Neoproterozoic to early Cambrian and Carboniferous-Permian granitoids (Samson and Secor, 2000; Samson, 2001). The event that produced the regional greenschist-facies cleavage and deformation is likely ~450 Ma, based on $^{40}\text{Ar}/^{39}\text{Ar}$ cooling ages from several studies focused within 50 km of each other in central North Carolina (e.g., Noel et al., 1988; Offield et al., 1995; Hibbard et al., 2012). Alternatively, Dallmeyer (1989), Dallmeyer et al. (1986), Secor et al. (1986) reported 350-340 and 300-280 Ma $^{40}\text{Ar}/^{39}\text{Ar}$ cooling ages from Carolina terrane samples collected in central and southwestern South Carolina.

The Charlotte terrane occupies the area between the Inner Piedmont (peri-Laurentian rocks) and the Carolina terrane to the east, from central Georgia through central North Carolina. The dominant lithologies in the Charlotte terrane include a sequence of mostly Neoproterozoic-early Paleozoic metavolcanic and metasedimentary rocks that were metamorphosed under lower amphibolite-facies conditions (e.g., King, 1955; Hibbard et al., 2002). Metaclastic rocks are intruded by Neoproterozoic and early Cambrian mafic and felsic plutons that represent two distinct magmatic pulses (Hibbard et al., 2002). The main episode of penetrative deformation and peak metamorphism in the Charlotte terrane was initially suggested to be Taconic (Butler, 1991); however, Dennis and Wright (1997) provided strong evidence supporting the regional fabric had to predate ~535 Ma. In contrast, Dallmeyer et al. (1986) reported lower amphibolite-facies rocks on the southeastern edge of the Charlotte terrane cooled through Ar-retention in hornblende (~500° C) at 350-340 Ma, which is close to the maximum temperature to which these rocks were subjected during metamorphism. Dallmeyer et al. (1986) interpreted this cooling event to be relatively rapid, supported by concordance of the Charlotte terrane cooling ages with whole-rock $^{40}\text{Ar}/^{39}\text{Ar}$ ages from Carolina terrane pelitic rocks. Additionally, Butler (1983) reported a

greenschist-facies overprint of Charlotte belt rocks that appeared to postdate Silurian-Devonian plutonic rocks.

The Concord Plutonic Suite, an arcuate group of suite of Silurian-Devonian gabbroic plutons, intruded the western flank of the Charlotte terrane (e.g., McSween and Harvey, 1997) (Fig. 3-1). These plutons occur at roughly regular intervals, which suggests at least some form of tectonic control (McSween and Harvey, 1997). Aeromagnetic maps are particularly useful in delineating the Concord plutonic suite, as the high magnetic signature of the mafic plutons starkly contrasts with surrounding country rock (Fig. 3-1). Individual plutons generally exhibit ovoid surface exposures, and geophysical modeling suggests many may be vertical cylindrical- or funnel-shaped intrusions or laccoliths (e.g., Hermes, 1968; Butler and Ragland, 1969; Chalcraft, 1970; Olsen et al., 1983; McSween and Harvey, 1997). Williams and McSween (1989) also suggested the Concord pluton resides above a much larger pluton at depth based on magnetic modeling. Gabbro bodies are relatively undeformed and unmetamorphosed, but coeval felsic plutons within the same geographic area, the Salisbury Plutonic Suite, are deformed and foliated (e.g., McSween et al., 1991; McSween and Harvey, 1997; Samson and Secor, 2000). Magmatic layering has been documented in several plutons (Matthews, 1967; Chalcraft, 1970; Fronabarger, 1984; Noble, 1993; McSween and Harvey, 1997), but most exhibit no indications of layering (McSween et al., 1991; McSween and Harvey, 1997). Contact metamorphic aureoles surround several plutons (e.g., Buffalo, Calhoun Falls, Gladesville, Presley's Mill, Mt. Carmel), with pyroxene-hornfels mineral assemblages described in several studies (Medlin, 1968; Hooper, 1986; Troyer, 1991) that appear to only have developed in the southern portion of the suite (McSween and Harvey, 1997). Altered ultramafic rocks have been documented in several plutons (e.g., Fronabarger, 1984; Hooper, 1986), whereas other plutons have associated syenites (e.g., Medlin, 1968; Olsen et al., 1983). Olsen et al. (1983) suggested syenite associated with the Concord pluton could be the product of differentiation from the same parental mafic magma as the gabbro, not from the exposed gabbro itself. Emplacement depth of gabbroic plutons from the northern portion of the suite is estimated at 12-15 km (McSween and Harvey, 1997). Available $^{87}\text{Sr}/^{86}\text{Sr}$ and $^{143}\text{Nd}/^{144}\text{Nd}$ data indicate mantle source for magmas with little evidence of crustal contamination (Fullagar, 1971; 1983; McSween et al., 1984; McSween and Harvey, 1997).

Concord suite gabbroic rocks are commonly associated amphibole-bearing metagabbros, which can occur as xenoliths within the more pristine gabbros, likely indicating they predate intrusion of the gabbros (e.g., Hermes, 1968; McSween et al., 1984; McSween and Harvey, 1997). McSween et al. (1984) interpreted the relationship between the gabbros and metagabbros to be a function of repeated pulses of magma intruded into the same pathways. However, foliated metagabbroic xenoliths may actually represent Neoproterozoic-Cambrian mafic country rock that became incorporated in the Silurian-Devonian suite. McSween and Harvey (1997) distinguished

metagabbros associated with the Concord plutonic suite as coarse-grained undeformed rocks, while strongly foliated mafic xenoliths likely represent xenolithic country rock. Based on clear evidence from a quarry in the Rock Hill Gabbro, Noble (1993) suggested Concord plutonic suite metamorphism may be fracture-controlled, and that metamorphism was localized where fluids could access the rocks.

Concord suite gabbroic rocks are commonly medium- to coarse-grained, nonfoliated gabbro and gabbro-norites that commonly exhibit cumulate textures. Olsen et al. (1983) specified that the use of the term cumulate is merely a textural description and does not necessarily indicate crystal settling. Major mineral assemblages generally consist of clinopyroxene and plagioclase with variable olivine, orthopyroxene, hornblende, and biotite, with accessory apatite, ilmenite, magnetite, pyrite, pyrrhotite, zircon, and locally baddeleyite. Whole-rock geochemistry of gabbros, coupled with the apparent fractionation to syenite, indicates parental magma composition was a likely low-silica tholeiite to alkaline basalt (McSween and Harvey, 1997). The combination of the arcuate geographic distribution of the Concord plutonic suite, initial $^{87}\text{Sr}/^{86}\text{Sr}$ and $^{143}\text{Nd}/^{144}\text{Nd}$ ratios that indicate mantle source, and whole-rock geochemical analyses, generally support subduction-zone affinity regarding the petrogenesis of these plutons (McSween and Harvey, 1997; Esawi, 2004; Chaumba, 2010a, 2010b). However, Sinha et al. (1989) argued that adiabatic melting during transtensional strike-slip accretion of the Carolina superterrane provides a better geochemical complement, based on similarities with a suite of gabbro-diorite-syenite-granite plutons from the Oslo rift, Norway. Both petrogenetic hypotheses relate the intrusion of this plutonic suite to either the onset of Acadian orogenesis or as a result of accretion of the Carolina superterrane during the Late Silurian through the Devonian.

Recent work in the Inner Piedmont indicates deformation, metamorphism, and an abundant pulse of likely anatectic plutonism occurred during the Devonian through the Mississippian, which several workers attribute to the Acadian/Neoacadian accretion of the Carolina superterrane and concurrent subduction of the eastern Laurentian margin (e.g., Mersch et al., 2005; Hatcher et al., 2007; Huebner et al., *in review*). The timing of Concord suite plutonism appears to roughly coincide with Inner Piedmont orogenesis, although available geochronologic data regarding the timing of Concord suite plutonism primarily consist of Sm-Nd internal isochron ages (Olsen et al., 1983; McSween et al., 1984), with several Rb-Sr and $^{40}\text{Ar}/^{39}\text{Ar}$ whole-rock ages (Fullagar, 1971; Sutter et al., 1983). In light of this, we collected representative samples of Concord plutonic suite gabbros from central North Carolina through central Georgia for U-Pb zircon analysis using SHRIMP in an attempt to better temporally define this pulse of magmatism. Samples were also analyzed for whole-rock geochemistry to supplement existing published geochemical data. Ultimately, our goal is to test the hypothesis that the Concord Plutonic Suite represents suprasubduction zone magmatism that developed above an east-dipping subduction of ocean crust be-

neath the Carolina superterrane, which would provide further support for the model of Acadian/Neoacadian accretion of the Carolina superterrane.

METHODS

Approximately 15-20 kg of mafic crystalline rocks from several plutons were sampled from the western flank of the Carolina superterrane for geochronologic and geochemical analysis. Samples were selected on the basis of degree of chemical weathering and were chosen where adequate geologic maps of the plutonic bodies had been previously produced (with the exception of the “Highway 200” gabbro, D. R. Privett, unpublished data). Care was taken to select samples that were characteristic of the plutons. In some instances, associated metagabbros were sampled.

Various phases of geochronologic and geochemical sample preparation were performed at The University of Tennessee, University of North Carolina, Vanderbilt University, and Stanford University–U.S. Geological Survey Micro Analysis Center (SUMAC). Samples were initially broken into ~5 cm pieces in the field and at The University of Tennessee, and were further reduced to < 1 cm using a 5.7 x 7.6 cm jaw crusher. For whole-rock geochemical analysis, ~30 g of each sample (~100 g for coarse-grained samples) were milled into a fine powder using an alumina ceramic mill and Shatterbox™. Individual sample powders were mixed, and ~15 g of each sample were sent to Activation Laboratories in Ancaster, Ontario, for analysis. Major elements, Sr, Ba, Y, and Zr were determined using inductively coupled plasma (ICP) emission spectroscopy employing lithium metaborate/tetraborate fusion (FUS-ICP). Trace and rare earth elements (REE) were determined by total digestion methods (TD-ICP), instrumental neutron activation analysis (INAA) and fusion methods (FUS-MS). Results of geochemical analyses are compiled in Appendix III. Compositional diagrams illustrating whole-rock geochemical data were generated using Igpet® software.

For zircon separation, samples were crushed to < 500 µm using a belt-driven disk pulverizer following processing through a jaw crusher. Heavy minerals were then concentrated using a water table, followed by separation of heavy phases with methylene iodide ($\rho = 3.3 \text{ g/cm}^3$). Ferromagnetic phases were removed from the sample with a hand magnet prior to density separation in methylene iodide, and with a Frantz magnetic separator following heavy liquid separation. Zircons from each sample were mounted in epoxy, polished to the approximate average grain center, and coated with ~10 nm of gold. Grains were imaged using cathodoluminescence (CL) and reflected light to assess growth zoning, morphology, and the presence of fractures and inclusions prior to ion microprobe analysis. Routine operating procedures were followed for the SHRIMP-RG. The primary $^{16}\text{O}_2^-$ ion beam was run at ~15 nA, with beam diameter kept constant at ~22 µm. Standards R33 (~419 Ma) and TEM (416.8 Ma), provided by SUMAC, were mea-

sured regularly. All data were reduced using the computer program SQUID v. 2 (Ludwig, 2009). Zircons were analyzed during two sessions at the SUMAC facility between 2011 and 2013.

RESULTS

Results of individual spot analyses from igneous rocks are presented in Appendix II, with calculated weighted averages of samples summarized in Table 3-1. Age calculations and plots to display data were made using Isoplot v. 3.75 (Ludwig, 2012) (Fig. 3-3). All igneous ages reported from this study are ^{207}Pb corrected $^{206}\text{Pb}/^{238}\text{U}$ ages unless specified otherwise. Spot analyses greater than $\pm 50\%$ discordant have been excluded from calculated weighted average ages.

Sample Descriptions and Zircon Geochronology

Calhoun Falls gabbro (CFGb)

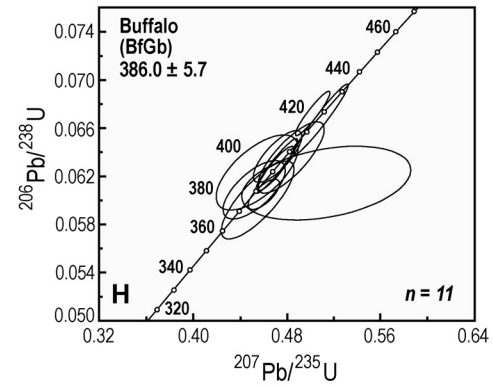
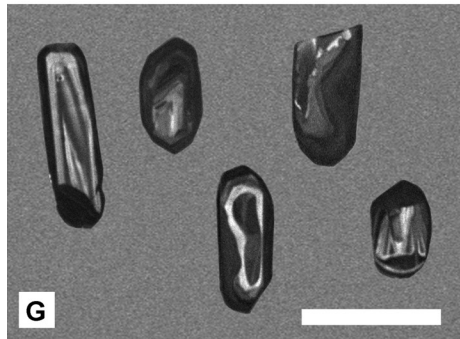
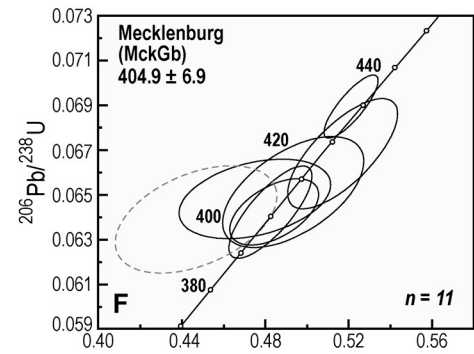
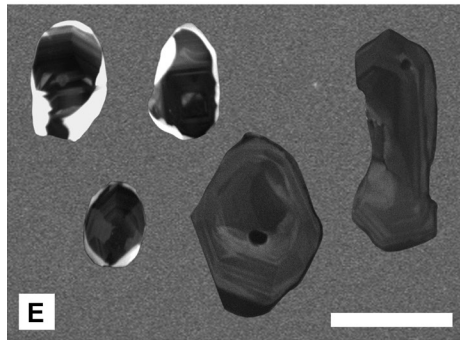
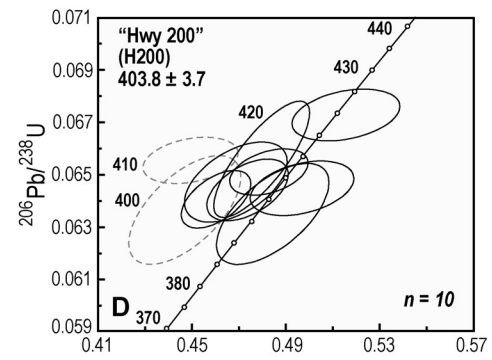
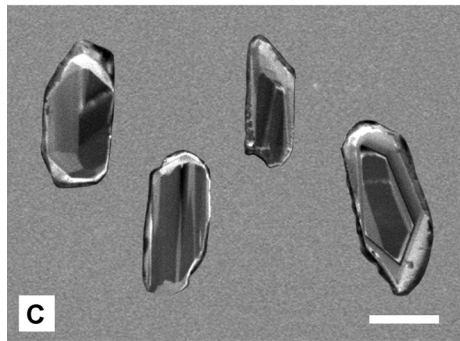
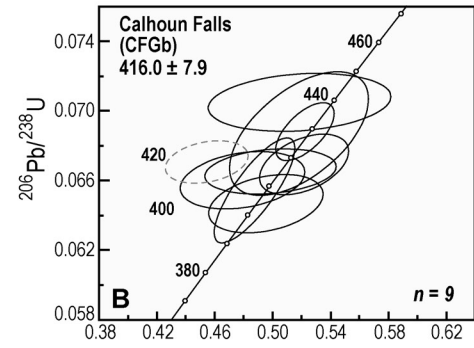
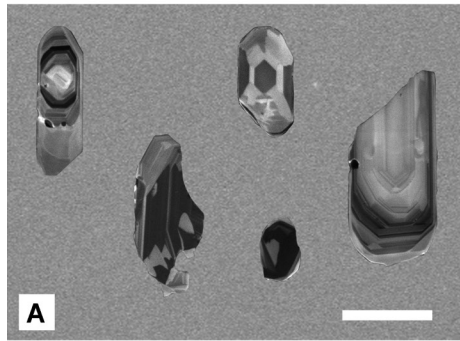
Sample CFGb was collected from the near center of the exposed pluton. This sample is medium-grained and equigranular, characterized by pink plagioclase with dark green to black pyroxene and amphibole. In thin section, subhedral plagioclase (An_{33-37}) appears to be a cumulate phase, with intercumulus material dominated by light-green to brown amphibole and augite. Interstitial poikilitic amphibole includes plagioclase, enstatite, augite, and relict olivine. Chlorite in this sample appears to have grown at the expense of augite, amphibole, and biotite. Minor phases include biotite, calcite, epidote, pyrite, magnetite, ilmenite, and zircon.

Sample CFGb contains mostly acicular to sub-equant zircons of various sizes that exhibit a variety of internal textures in CL, including concentric growth zoning, broad to faint zoning, sector zoning, and resorption textures indicative of xenocrystic cores (Fig. 3-3A). Individual spot analyses range from 440-404 Ma, with the majority of these data between 417 and 404 Ma (Fig. 3-3B). A crystallization age of 412.6 ± 6.0 Ma (mean squared weighted deviation [MSWD] = 0.62) was determined using the weighted average of the largest apparent cluster of data. Several older spot analyses (440-429 Ma) were excluded in the calculation of this age, based on the ~ 12 m.y. gap between the oldest age in the majority group (417 Ma) and the youngest age in the excluded group (429 Ma).

“Highway 200” gabbro (H200)

Sample H200 is a fine-grained, medium greenish-gray gabbro. Mineralogy consists of cumulus plagioclase (An_{51-54}) with interstitial augite, biotite, hornblende, chlorite, and opaque minerals. This sample exhibits some evidence of chemical weathering and, in places, plagioclase is almost completely broken down. Additionally, pyroxene and amphibole are commonly altered to chlorite and clay minerals.

Figure 3-3: Cathodoluminescence images of representative zircons with U-Pb concordia diagrams from plutonic rocks analyzed in this study. White bars in zircon images are 100 μm . Light dashed analyses on concordia diagrams were excluded as discordant, and were not used in weighted average calculations. Reported ages are weighted averages of ^{207}Pb -corrected $^{206}\text{Pb}/^{238}\text{U}$ analyses, discussed in text.



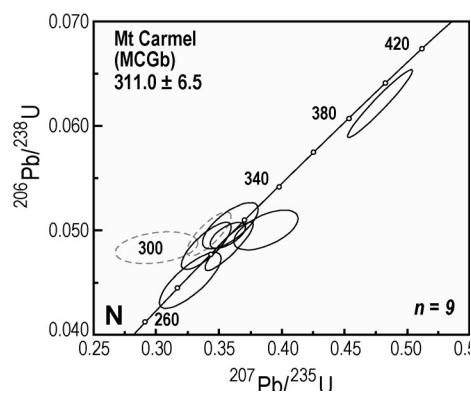
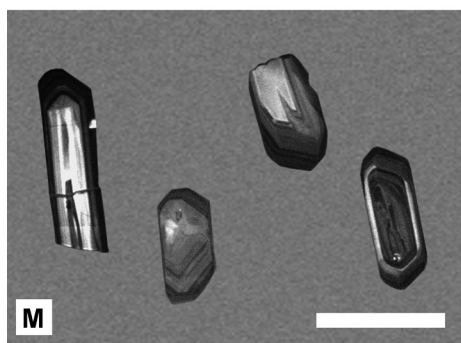
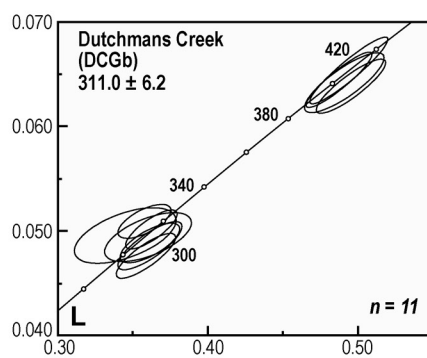
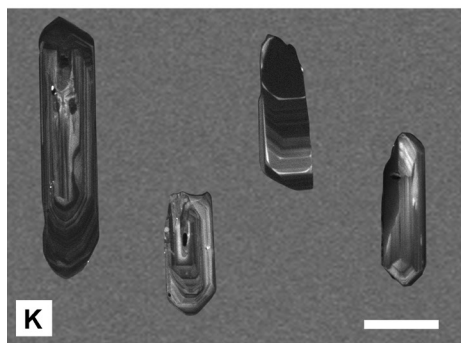
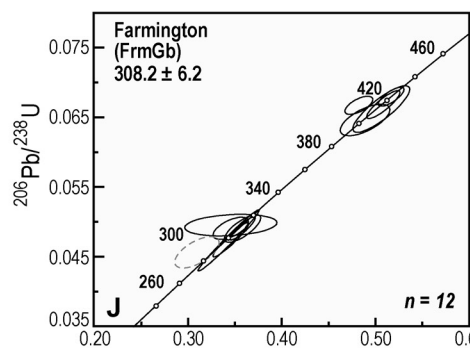
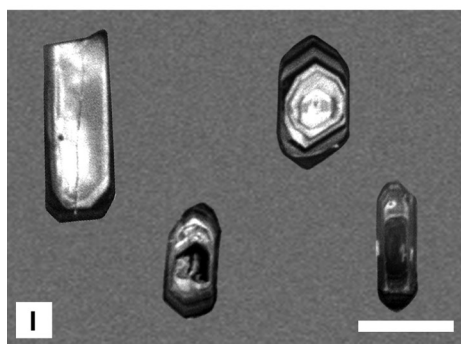


Figure 3-3 (continued)

Sample H200 yielded relatively large (>250 μm long, 100-150 μm wide), subhedral, mostly sub-equant zircons. Concentric growth zoning is mostly broad, with clear sector zoning evident in numerous grains (Fig. 3-3C). Several grains appear to contain xenocrystic cores, although none were identified with ion microprobe analysis. The majority of individual spot analyses yielded ages 410-396 Ma (Fig. 3-3D), with a weighted average of 403.8 ± 3.7 Ma (MSWD = 0.45).

Mecklenburg gabbro (MckGb)

This sample is a medium-grained, medium greenish-gray two-pyroxene hornblende gabbro that was sampled from the Vulcan Materials Pineville quarry. The dominant mineralogy consists of cumulus plagioclase (An_{54-56}) with enstatite, augite, biotite, and hornblende. Pyroxenes are generally subhedral, rounded to acicular, and are commonly included in poikilitic interstitial hornblende. Brown hornblende appears to be zoned, with inclusion-rich (mostly opaque minerals) cores mantled by relatively inclusion free rims. Opaque minerals include ilmenite, pyrite, and magnetite.

Zircons from sample MckGb can be classified into two groups based on size, texture, and morphology (Fig. 3-3E). One group contains large (~200 μm long, 100-150 μm wide), sub-equant to acicular, subhedral to euhedral zircons, with thin, well-developed concentric growth zoning and dark (1-10 μm) rims. Other zircons are relatively smaller, rounded, subequant to equant, and contain concentric and sector zoned cores mantled by bright, U-poor rims. Spot analyses of cores revealed ages 411-402 Ma (Fig. 3-3F), with a weighted average of 404.9 ± 6.9 Ma (MSWD = 0.48), likely representing crystallization of this pluton. Rim analyses are mostly discordant, although one dark overgrowth yielded a fairly concordant age ~430 Ma.

Buffalo gabbro (BfGb)

Sample BfGb is a dark gray to black, coarse-grained porphyritic gabbro that was collected from the approximate center of the exposed pluton. It is characterized by 2-6 mm augite porphyroclasts with a matrix consisting of hornblende, plagioclase (An_{44-52}), augite, and enstatite, with minor biotite, epidote, chlorite, calcite, and opaque minerals. Rare enstatite and olivine porphyroclasts generally do not exceed 2 mm. Brown hornblende appears to be interstitial, and commonly encloses anhedral plagioclase, olivine, and pyroxenes. Plagioclase occurs as subhedral inequant laths include in hornblende, and also appears as an interstitial phase. Olivine frequently exhibits resorption textures, and is commonly mantled by thin enstatite rims.

Zircons from sample BfGb are relatively small, acicular to subequant, subhedral, and appear slightly rounded (Fig. 3-3G). Most exhibit resorption textures indicating xenocrystic cores, although no obvious inheritance was identified during ion probe analysis. Two individual analyses

yielded Late Silurian ages (420 and 416 Ma), although most zircons analyzed range from 398-375 Ma (Fig. 3-3H). A weighted average of 386.0 ± 5.7 (MSWD = 0.94) was derived from the nine analyses that comprise the largest cluster of data.

Farmington metagabbro (FrmGb)

Sample FrmGb was collected from the Vulcan Materials Smith Grove quarry near Mocksville, North Carolina. It is a medium-coarse grained, equigranular, dark-gray metagabbro with common acicular hornblende megacrysts. The rock is mostly composed of plagioclase (An_{43-53}), hornblende, chlorite, and serpentine, with minor biotite, epidote, calcite, and abundant opaque minerals. Hornblende megacrysts are zoned, with inclusion-rich cores surrounded by relatively inclusion-free rims. Opaque minerals commonly form streaks along cleavage planes in hornblende. Sericitic alteration of plagioclase is common, and plagioclase also exhibits undulose extinction and deformed twins. Symplectites of serpentine, hornblende, and quartz likely represent pyroxenes that have been completely altered. This rock has undergone extensive alteration under greenschist-facies conditions.

Sample FrmGb yielded relatively small (75-150 μm long, 50-70 μm wide), euhedral to subhedral zircons with predominantly acicular morphology. Concentric growth zoning is well-developed in most grains, while few exhibit faint, broad and unzoned textures in CL (Fig. 3-3I). Spot analyses of zircons revealed a bimodal distribution of ages, clustered at ~ 418 and ~ 308 Ma (Fig. 3-3J). While no apparent differences in morphology or texture are evident between the two clusters of zircons, zircon trace element concentrations reveal these age groups are geochemically distinct. The most dramatic differences are evident in Hf concentrations (older cluster = 4,000-7,000 ppm, younger cluster = 8,500 - >11,000 ppm) and Eu* (older cluster = 0.86-1.01, younger cluster = 0.02-0.25). Th/U ratios suggest the older cluster is primarily of metamorphic origin, while values from the younger cluster indicate magmatic zircon growth. The weighted average of six analyses that comprise the younger cluster of ages is 308.2 ± 6.2 Ma (MSWD = 0.34), which we interpret to represent crystallization of this pluton.

Dutchman's Creek gabbro (DCGb)

Sample DCGb is a medium-fine grained, dark gray olivine-bearing gabbro that was collected near the center of the elongate exposure of the body. The dominant mineralogy consists of plagioclase (An_{38-41}), olivine, augite, enstatite, and biotite. Chemical zonation in plagioclase is fairly common. Subhedral, rounded olivine and pyroxenes are commonly enveloped in larger, apparently interstitial oikocrysts of enstatite, augite, and biotite. Plagioclase laths are commonly poikilitically enclosed in larger oikocrysts. Ilmenite, magnetite, and pyrrhotite appear to be interstitial and are commonly associated with biotite.

Zircons from sample DCGb are mostly large (~250 μm long, 100 μm wide), euhedral to subhedral, and acicular. Nearly all grains exhibit well-developed concentric growth zoning, with little evidence of resorption textures (Fig. 3-3K). This sample yielded a bimodal distribution of ages from spot analyses (~402 and ~311 Ma) (Fig. 3-3L), similar to sample FrmGb. Again, no textural or morphologic differences are apparent between the two age groups, while trace element concentrations show clear geochemical distinctions. Th/U ratios of younger grains are relatively higher compared to older zircons, although none indicate metamorphic genesis. The majority of zircons extracted from DCGb yielded ages in the younger cluster of data, with a weighted average of 311.0 ± 6.2 Ma (MSWD = 0.84).

Mt. Carmel metagabbro (MCGb)

One sample of Mt. Carmel metagabbro was sampled for this study, since it is the most voluminous lithology in the exposed pluton. This sample is coarse grained, dark-gray to black, with dark purplish-gray plagioclase. This rock is characterized by subhedral, rounded to acicular augite, enstatite, and hornblende with abundant serpentine, chlorite, and plagioclase (An_{55-58}). Sericitic alteration of plagioclase is abundant. Symplectites of hornblende, serpentine, and chlorite appear to replace pyroxene. Apparently interstitial hornblende poikilitically encloses rounded pyroxene and hornblende grains and plagioclase laths. Epidote, apatite, magnetite, ilmenite, and possibly some sulfides are minor constituents.

Sample MCGb yielded mostly euhedral, relatively small (75-150 μm long, 50-90 μm wide) subequant to acicular zircons. Concentric growth zoning varies from thin to broad, with several apparent xenocrystic cores (Fig. 3-3M). Most zircons analyzed revealed ages from 317-305 Ma (Fig. 3-3N), with several younger grains (285 and 223 Ma) and one inherited(?) Devonian zircon (~388 Ma). A crystallization age of 311.0 ± 6.5 Ma (MSWD = 0.34) was calculated using the weighted average of the tightest cluster of zircon ages.

Whole-Rock Geochemistry

Based on geochronologic analyses, gabbroic rocks have been separated into two groups by age for discussion of whole-rock geochemical analyses: Silurian-Devonian and Late Pennsylvanian suites. Two of the plutons discussed herein, the Rock Hill and Chester gabbros, were not dated due to unsuccessful attempts to separate zircon from collected samples. For sake of discussion, these have been included with the Silurian-Devonian group. Additionally, the Devonian Gladesville Gabbro (372 ± 2 Ma) was dated using ion-microprobe analysis of zircon overgrowths from pyroxene hornfels country rock from the associated contact aureole (Huebner et al., *in review*), and the Devonian Ogden Gabbro (411.90 ± 0.25 Ma) was dated using zircon and baddeleyite using CA-TIMS (Ibañez-Mejía, unpublished data). Additionally, many of the

Table 3-1: Compiled U-Pb ages of Concord-Salisbury suite plutons

Pluton	Sample	U-Pb Age (Ma)	Method	Reference
Granitoids				
Clouds Creek		414.9 +2.1/-1.7	TIMS	Samson and Secor, 2000
Newberry		414 ± 8	TIMS	Samson and Secor, 2000
Salisbury		415 ± 6	TIMS	Hibbard et al., 2012
Mafic Plutons				
Farmington	FrmGb	308 ± 6	SIMS	this study
Mecklenburg	MckGb	405 ± 7	SIMS	
Ogden	OgGb	412 ± 5	LA-ICPMS	Ibañez-Mejía and others, in preparation
Buffalo	BfGb	386 ± 6	SIMS	
"Highway 200"	H200	404 ± 4	SIMS	this study
Dutchman's Creek	DCGb	311 ± 6	SIMS	
Calhoun Falls	CFGb	413 ± 6	SIMS	
Mt. Carmel	MCGb	311 ± 7	SIMS	
Gladesville	GGb	372 ± 4	SIMS	Huebner et al., <i>in review</i>

mafic rocks exhibit cumulate textures (e.g., Irvine, 1982), therefore, we conservatively approach the interpretation of trace element and REE patterns, and sparingly use tectonic discrimination diagrams.

Concord plutonic suite gabbros analyzed in this study are predominantly subalkaline basalts to basaltic andesites, and exhibit both calc-alkaline and tholeiitic affinities (Fig. 3-4). Only subtle major element distinctions between Silurian-Devonian and Pennsylvanian gabbros are evident. SiO₂ abundances in Silurian-Devonian plutons occur over a relatively restricted range (49.1- 46.5 wt %) relative to their Pennsylvanian counterparts (51.1-43.0 wt %). Al₂O₃ concentrations cover a wide range from 22.1-7.9 wt % in Silurian-Devonian plutons and, on average, Pennsylvanian plutons appear to be more aluminous. Total alkalis are fairly consistent through both Silurian-Devonian and Pennsylvanian rocks, although the Buffalo gabbro has a significantly lower-than-average concentration (0.69 wt %; average = 2.63 wt %). MgO concentrations occur over a wide range in both groups, although average concentrations of the groups are fairly similar. Bivariate variation diagrams of major oxides plotted against MgO reveal mostly scatter with weak negative trends in TiO₂, P₂O₅, CaO, and K₂O (Fig. 3-5). Na₂O concentrations reveal a negative correlation with MgO occurring over a relatively narrow range (2.89-2.12 wt %), with the high MgO Buffalo gabbro as a relative outlier (~0.55 wt %).

Normalized trace element spider diagrams exhibit LILE enrichment relative to HFSE, and all samples are enriched in LILE relative to N-MORB (normalization constants of Sun and McDonough, 1989) (Fig. 3-6). All samples exhibit strong positive anomalies in Ba and Sr, with N-MORB-normalized Sr concentrations occurring over a relatively restricted range. Addition-

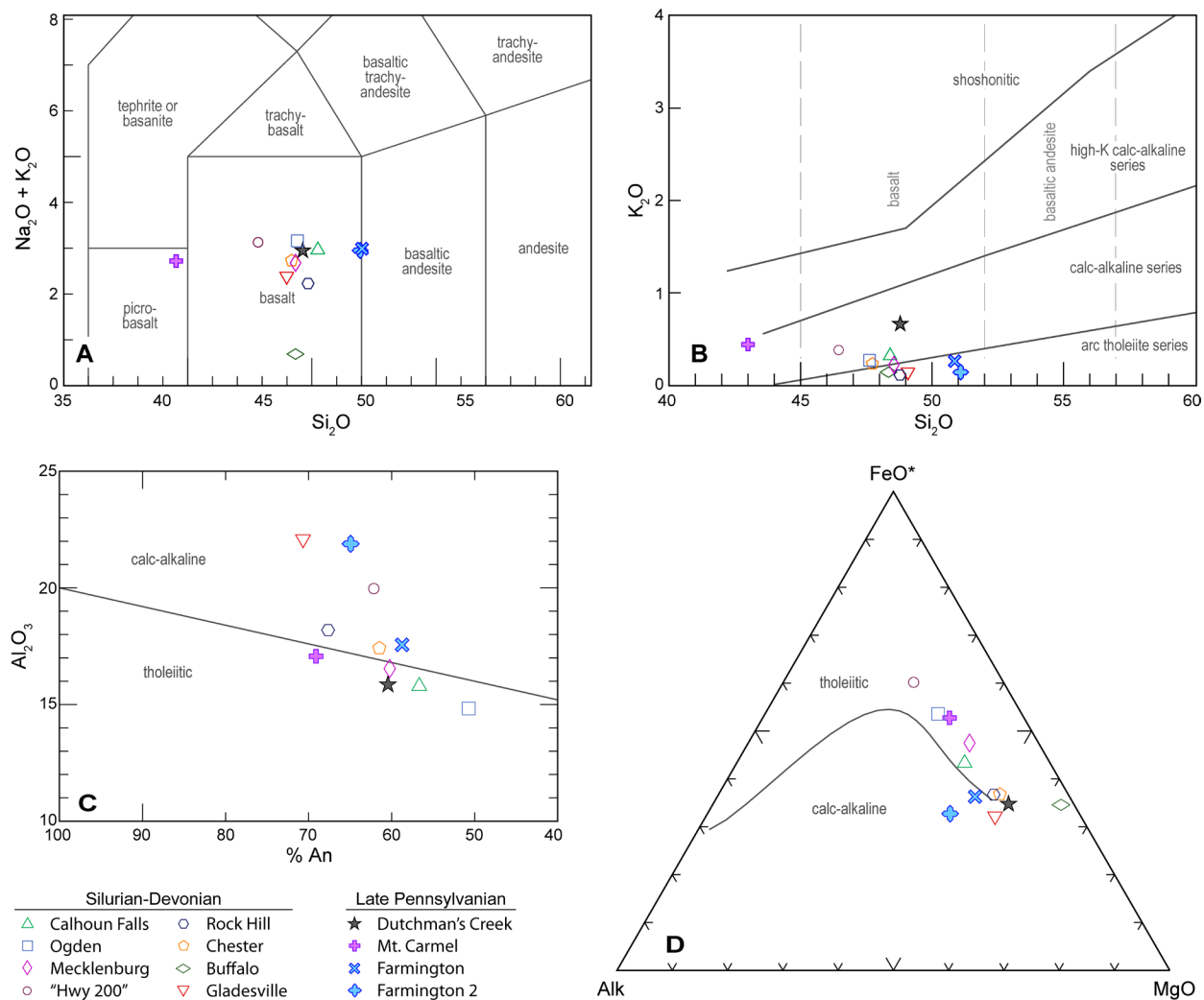


Figure 3-4: (A) Total alkali-silica and (B) K_2O -silica classification diagrams of igneous rocks (after Le Bas et al., 1986 and Le Maitre, 1989, respectively). (C) and (D) Al_2O_3 versus percent Anorthite and AFM classification of plutonic rocks in this study (after Irvine and Baragar, 1971).

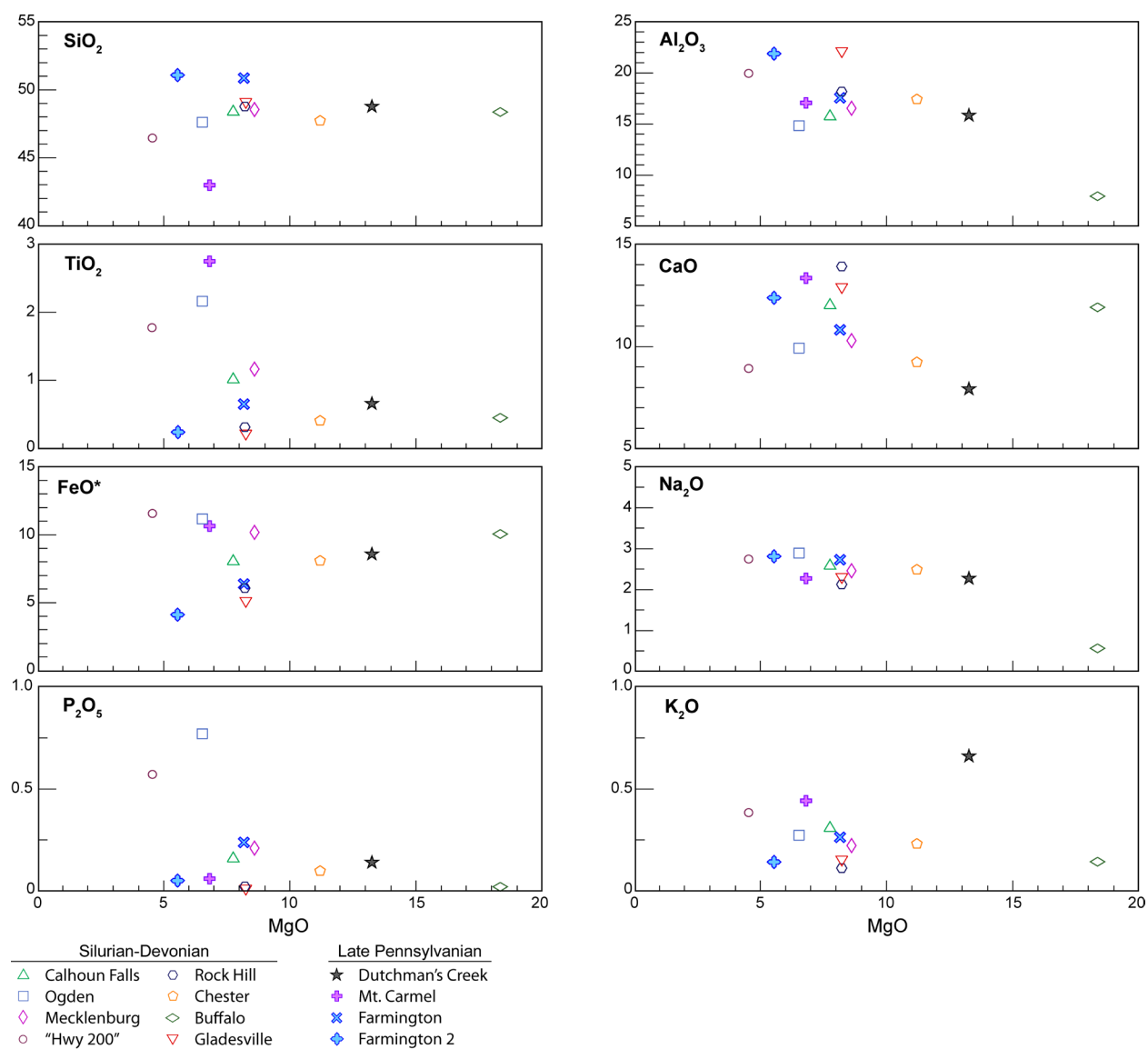
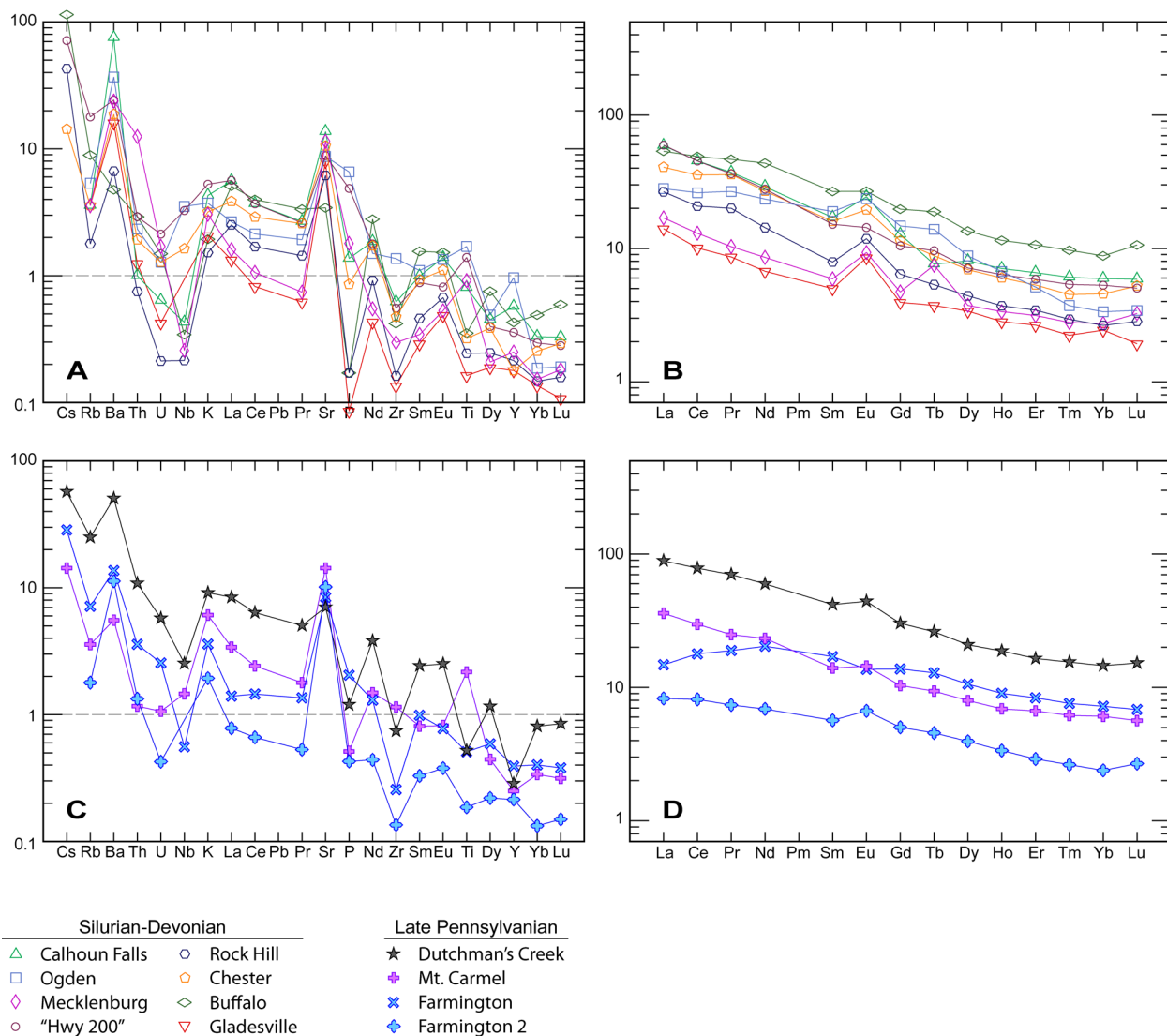


Figure 3-5: Bivariate plots of major oxides versus MgO.



ally, samples show strong negative to slightly positive Nb and Ta anomalies, with concentrations ranging from 8.2-0.5 and 0.51-0.02 ppm, respectively. Nearly all samples exhibit positive Sr and Eu anomalies, which agrees with the petrographic interpretation of plagioclase as a cumulus phase. The positive Eu anomaly appears to be more pronounced in Acadian samples, although concentrations are comparable. Overall, chondrite-normalized REE curves are relatively shallow, with La_N/Lu_N ratios of 6.3 and 7.9 for Silurian-Devonian and Pennsylvanian samples, respectively. Pb concentrations fell below detection limit (5 ppm) for all samples analyzed.

DISCUSSION

Geochemistry and tectonic setting

Several geochemical and isotopic attributes of Concord Plutonic Suite gabbros are consistent with petrogenesis in a volcanic arc setting, which has previously been suggested in several studies (e.g., McSween et al., 1984; Misra and McSween, 1984; McSween et al., 1991; McSween and Harvey, 1997; Esawi, 2004; Chaumba, 2010b, 2011). Specifically, these plutons are generally metaluminous, enriched in LILE, exhibit strong Ta and Nb depletions (MORB-normalized concentrations 0.1-3 ppm), and have $\epsilon Nd-\epsilon Sr$ isotopes that indicate mantle source (e.g., Fullagar, 1971, 1983; McSween et al., 1984; McSween and Harvey, 1997). LILE elements are thought to be mobile in the presence of a fluid phase, and enrichment in a mantle melt is interpreted to be the result of addition of these components by subduction-related fluids (e.g., Pearce, 1983; Davidson, 1996). This, in combination with HFSE depletion relative to MORB, indicates derivation from a source that has already been depleted (e.g., Davidson, 1996), which could also indicate derivation in a subduction zone environment.

The use of tectonic discrimination diagrams has been beneficial regarding the determination of genetic origin of basalts in various tectonic settings (e.g., Pearce and Cann, 1973; Pearce, 2008). Specifically, variations in Ti, Zr, Y, and Nb have been attributed to source heterogeneities (Pearce and Norry, 1979; Rollinson, 1993), and several successful tectonic discriminant diagrams have been introduced in the literature (e.g., Pearce and Cann, 1973; Pearce and Norry, 1979; Pearce, 1982; Meschede, 1986). Using the Ti-Zr-Y and Ti-Zr diagrams of Pearce and Cann (1973), rocks sampled in this study generally plot as island-arc tholeiites (Fig. 3-7). These particular diagrams have been widely criticized with regard to the discrimination of different types of MORB and problems identifying continental flood basalts (e.g., Rollinson, 1993), but our samples plot as neither. The Zr/Y-Zr diagrams of Pearce and Norry (1979) and Pearce (1983) effectively discriminate between basalts in different tectonic settings, and also can be used to distinguish island-arc basalts that were generated in an oceanic arc versus a continental arc (Fig. 3-8). Most samples plot as volcanic arc rocks and, interestingly, samples plot as both continen-

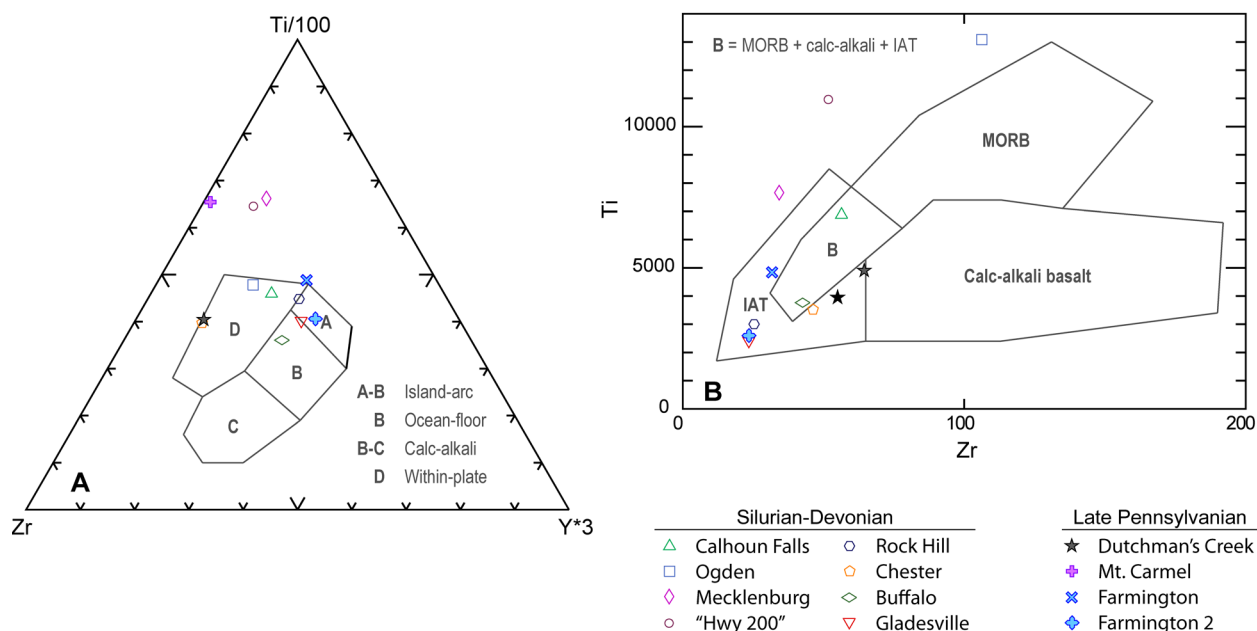


Figure 3-7: Ti-Zr-Y discrimination diagrams (after Pearce and Cann, 1973).

tal and oceanic arcs using the Pearce (1983) diagram (Fig. 3-8). This may be a consequence of the Silurian-Devonian arc being built on an existing Neoproterozoic-Paleozoic amalgamation of various arc terranes. Several other discrimination diagrams have also been successful in discriminating arc-derived mafic plutonism, particularly the Th-Hf-Ta diagram of Wood (1980) and the La-Y-Nb diagram of Cabanis and Lecolle (1989). The majority of these samples plot as volcanic arc rocks, and the Ogden gabbro consistently plots as E-MORB (Fig. 3-9). Although tectonic discriminant diagrams should never be used as absolute proof regarding the generation of magma in a specific tectonic environment (e.g., Rollinson, 1993), these diagrams generally indicate Concord Plutonic Suite gabbros were generated in a volcanic arc setting, which is consistent with other characteristics of this plutonic suite that suggest derivation in a subduction-zone setting.

Additionally, the metaluminous, calc-alkaline Salisbury Plutonic Suite, which is at least spatially and temporally related to the Concord Plutonic Suite, yields similar isotopic concentrations as Concord suite mafic plutons that also indicate mantle source (Fullagar, 1971; Butler and Fullagar, 1978; McSween et al., 1991). Butler and Fullagar (1978) suggested the Salisbury Plutonic Suite granitoids could be the result of differentiation or limited partial melt of lower crust or mantle and, based on low initial $^{87}\text{Sr}/^{86}\text{Sr}$ ratios from felsic and mafic intrusions in the Charlotte terrane. Furthermore, Fullagar (1971) concluded that this pulse of plutonism was not a product of anatexis of granites or sialic metasediments, nor does crustal contamination seem likely. We suggest that the combination of these attributes provides a strong case for subduction-related genesis

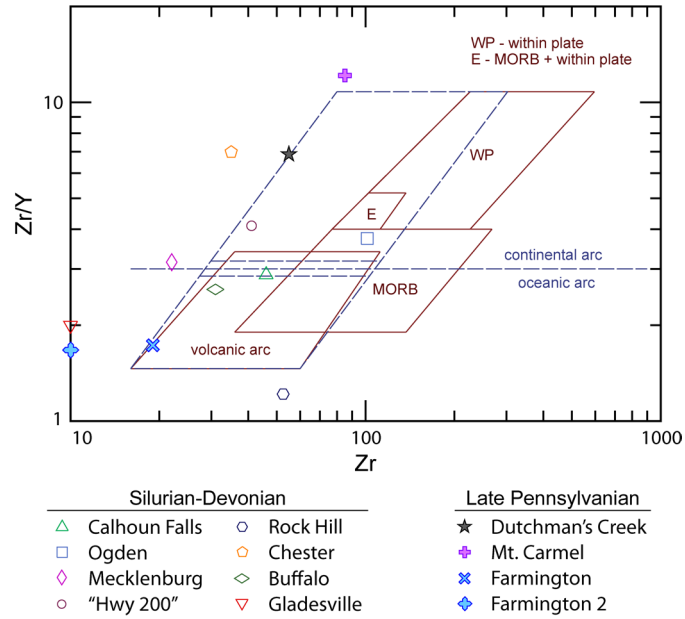


Figure 3-8: Zr-Y discrimination diagram (after Pearce and Norry, 1979 [red lines] and Pearce, 1983 [dashed blue lines]).

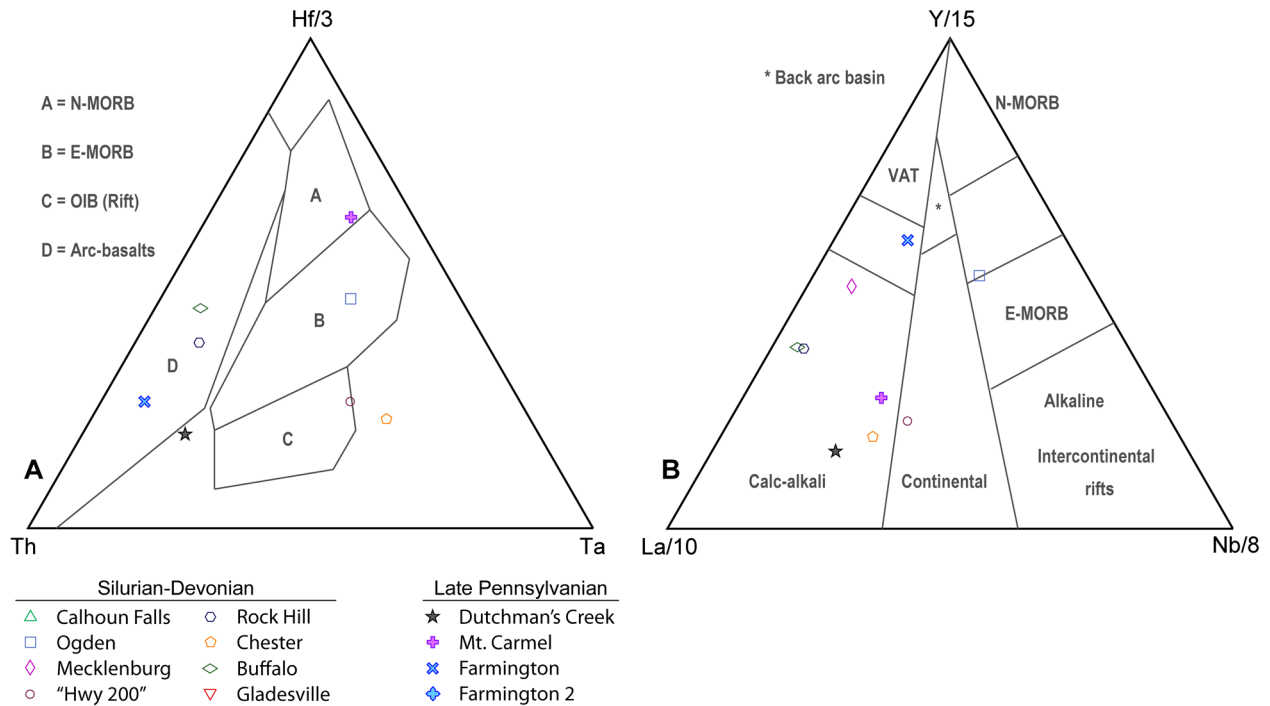


Figure 3-9: Th-Hf-Ta and La-Y-Nb discrimination diagrams (after Wood, 1980, and Cabanis and Lecolle, 1989, respectively).

of the Concord and Salisbury Plutonic Suites, although we realize other processes are also valid based on the available data.

Sinha et al. (1989) suggested Silurian-Devonian plutonism in the western flank of the Carolina superterrane is best explained by genesis in a transtensional environment, based on lithologic and geochemical similarities between Charlotte belt plutons and igneous rocks in the Oslo rift. In the Oslo rift, the trimodal gabbro-granite-syenite plutonic suite there has been attributed to decompression melting of mantle material during rifting (e.g., Neumann et al., 1992). Isotopic concentrations of syenite in the Oslo rift exhibit a wide scatter of initial $^{87}\text{Sr}/^{86}\text{Sr}$ values, over a relatively lower range of ϵNd , whereas mafic rocks form tight clusters of low ϵSr and higher ϵNd values (e.g., Neumann et al., 1992). Based on the generally high initial $^{87}\text{Sr}/^{86}\text{Sr}$ ratios that occur over a wide range, Neumann et al. (1985, 1992) suggested the petrogenesis of Oslo rift syenites required a significant component of crustal contamination. In contrast, Concord suite gabbro and syenite reveal low, overlapping initial $^{87}\text{Sr}/^{86}\text{Sr}$ values (0.7035 and 0.7038, respectively), and combined with Nd data, rule out any significant crustal contamination (Fullagar, 1971; Olsen et al., 1983). Additionally, Olsen et al. (1983) demonstrated the Concord syenite could be the product of differentiation from the same parental mafic magma of the Concord gabbro, which further distinguishes the Concord Plutonic Suite rocks from those of the Oslo rift.

Timing of emplacement

Isotopic ages of the Concord Plutonic Suite prior to this study revealed timing that was roughly Silurian-Devonian, however, calculated error in some studies approached ten percent (e.g., Fullagar, 1971; McSween et al., 1984). Results of U-Pb analyses from this study reveal similar ages, although the analytical error associated with the U-Pb technique provide a more precise assessment of the timing of this pulse of plutonism. Pooled ion-microprobe analyses of mafic plutons in this study reveal an overall peak ~ 403 Ma, which coincides with some anatectic plutonism in the Inner Piedmont, although predates the main pulse of Inner Piedmont magmatism (Fig. 3-10). We interpret this temporal relationship to represent east-dipping B-subduction of ocean crust that floored the Cat Square basin, resulting in the generation of the Concord and Salisbury plutonic suites, followed by shutoff of arc-related plutonism as eastern Laurentian margin continental crust was subducted beneath the Carolina superterrane. An extensive pulse of granitic magmatism and upper amphibolite-facies metamorphism in the Inner Piedmont followed shortly thereafter, and igneous and metamorphic ages indicate high-grade conditions in the Inner Piedmont persisted through the Devonian into the Carboniferous (Fig. 3-11). This relationship provides further support for Acadian/Neocadian accretion of the Carolina superterrane above the Laurentian margin.

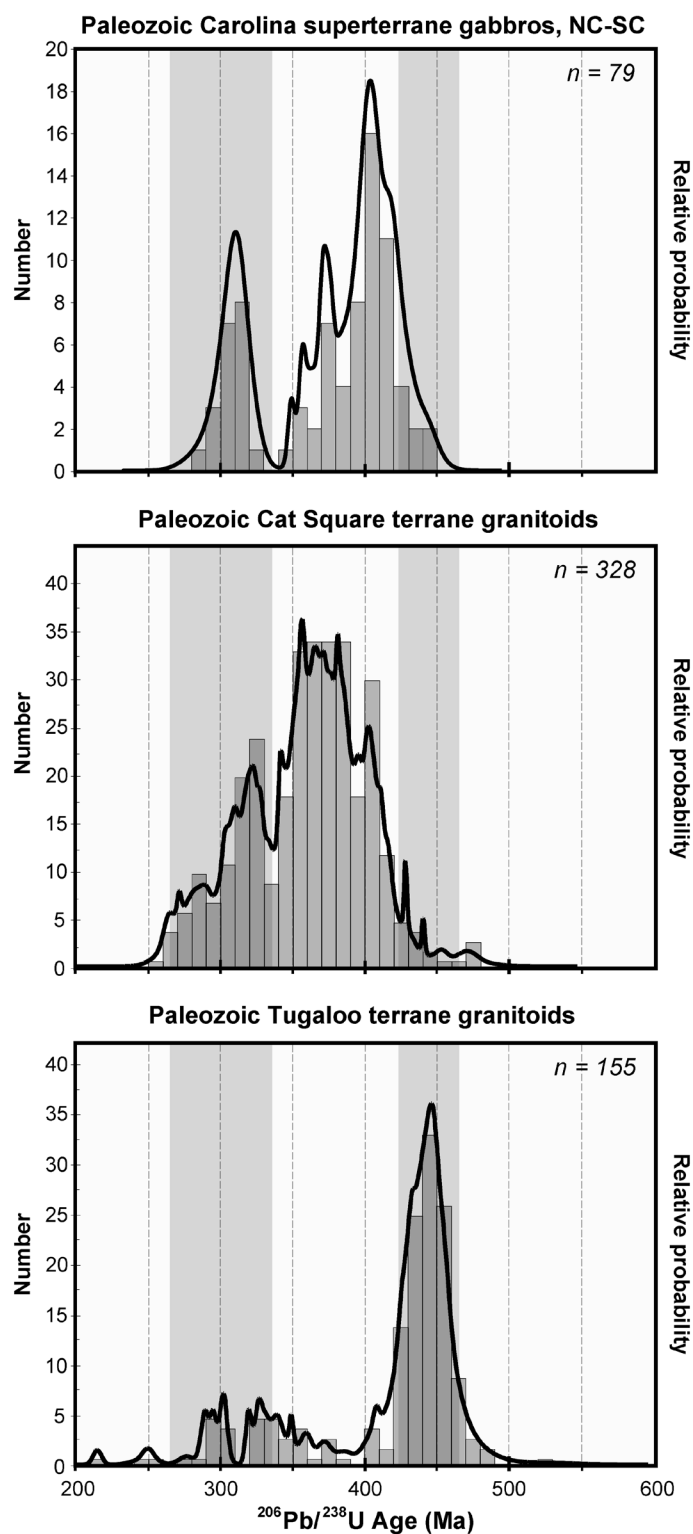


Figure 3-10: Relative probability distributions of pooled U-Pb ion microprobe ages of zircon from the Inner Piedmont (Tugaloo and Cat Square terranes; Huebner et al., *in review*, and references therein) and Concord Plutonic suite gabbros analyzed in this study. Shaded areas indicated approximate timing of the Taconian and Alleghanian events. Note the peak of Concord Plutonic suite data falls between peaks in the Tugaloo and Cat Square terranes.

Several mafic plutons from the Concord Plutonic suite are Pennsylvanian, and temporally correspond with other plutonism associated with the Alleghanian orogeny. One of the interesting characteristics of these samples is that all contain apparently inherited zircons that roughly match ages of other Concord Plutonic Suite gabbros. Considering the relatively low Zr concentrations (10-100 ppm) in these samples, it is interesting that these zircons were not resorbed in a melt that was likely near Zr-undersaturated conditions. Although isotopic data suggest little or no crustal contamination in Concord Suite gabbros, the presence of inherited zircon in these plutonic rocks may argue the contrary.

Links to the Appalachian Foreland

The relationship between plate tectonic interactions and the associated sedimentary response provides invaluable insight into the interpretation of ancient orogenic events (e.g., Dewey and Bird, 1970; Quinlan and Beaumont, 1984; Ingersoll, 1988). Consequently, analysis of the Appalachian foreland basin has provided key constraints regarding the timing, kinematics, and paleogeographic location of orogenesis throughout the Paleozoic (e.g., Ettensohn, 1985; 1987; Ferrill and Thomas, 1988; Ettensohn and Lierman, 2012). One of the most interesting observations regarding the southern and central Appalachians is the occurrence of a thick Devonian clastic wedge in the central Appalachians with no correlative metamorphic core (Fig. 3-12), and a broad Devonian metamorphic core in the southern Appalachians (Inner Piedmont) with no correlative clastic wedge (e.g., Dennis, 2007; Merschat and Hatcher, 2007). Central and southern Appalachian clastic wedges progressively young toward the southwest, and have been interpreted to represent dextral orogenesis during the Devonian through Mississippian (e.g., Ettensohn, 1985; 1986; Ferrill and Thomas, 1988). The Devonian Brevard fault zone has been interpreted to have translated the Inner Piedmont (and exotic Carolina superterrane) dextrally by up to ~450 km, which palinspastically restores the Inner Piedmont to similar latitudes as the central Appalachian clastic wedge and provides a temporal and spatial link between the two (e.g., Merschat et al., 2005; Dennis, 2007; Merschat and Hatcher, 2007). Several studies have indicated Devonian-Mississippian central and southern Appalachian clastic wedges appear to progressively young to the southwest (e.g., Ettensohn, 1985; 1986; Ferrill and Thomas, 1988; Ettensohn and Lierman, 2012), which also supports southwest-directed translation of the Inner Piedmont during Devonian-Mississippian peak metamorphism (Merschat et al., 2005). This relationship provides a strong link between foreland deposition and orogeny in the internides and, when combined with other evidence that suggests the Inner Piedmont was structurally below the Carolina superterrane during peak tectonothermal metamorphism, support dextral transpressive accretion of the Carolina superterrane above the eastern Laurentian margin through the Devonian to Mississippian.

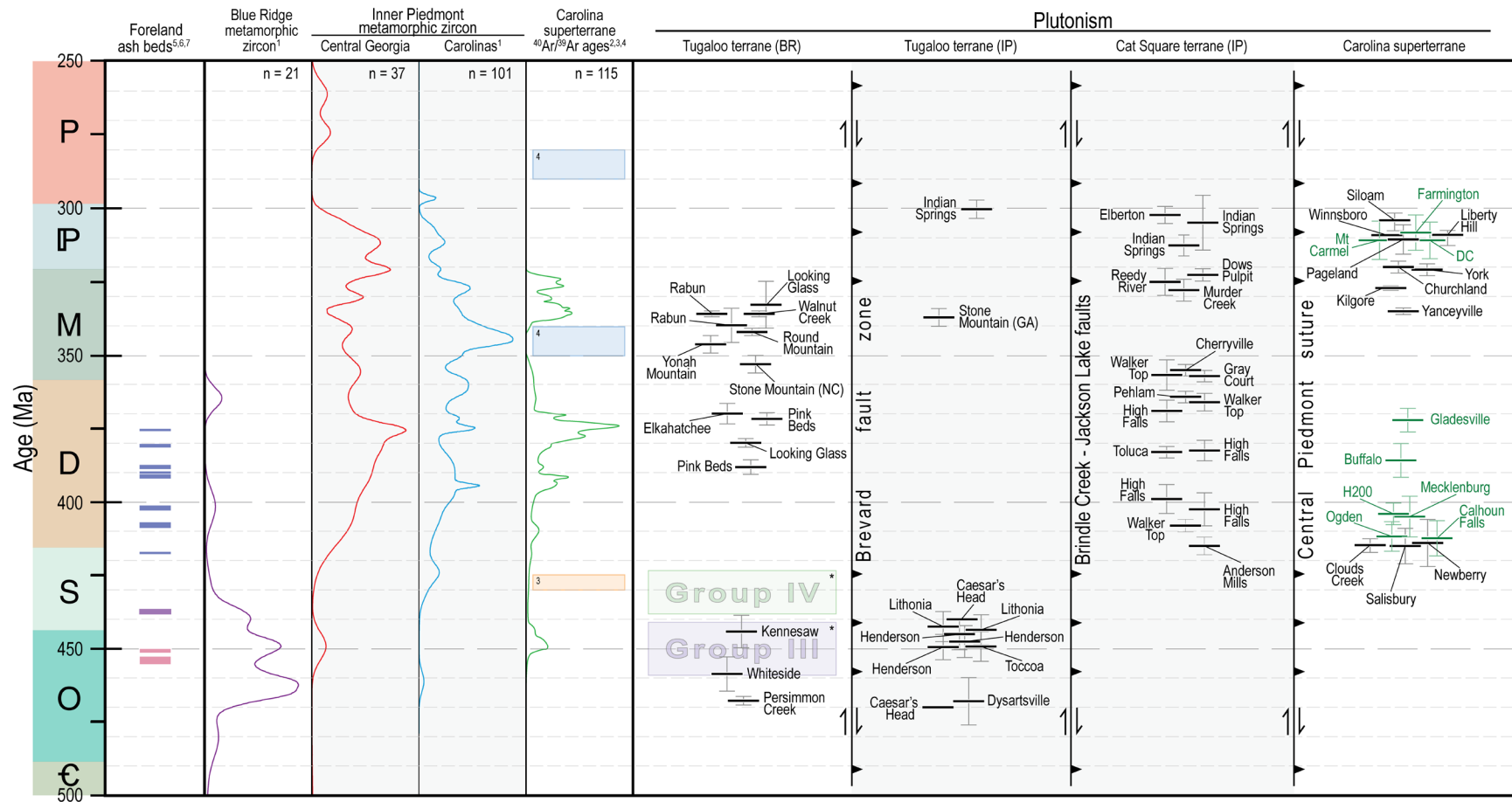


Figure 3-11: Compiled age chart of plutonic rocks, metamorphism, and cooling events in the eastern Blue Ridge, Inner Piedmont, and Carolina superterrane, with ages of ash beds in the Appalachian foreland basin. Ages of plutonic rocks and data sources are compiled in Table 4-2. * Groups III and IV of Sinha et al., 2012. Data sources: ¹Mersch, 2009; ²Hibbard et al., 2012; ³Sutter et al., 1983; ⁴Dallmeyer et al., 1986; ⁵Ver Straeten, 2010; Parrish, 2013; ⁶Bergström et al., 1998; ⁷Kolata et al., 1996.

Table 3-2: Compiled U-Pb ages of Paleozoic plutonic rocks from the eastern Blue Ridge, Inner Piedmont, and Carolina superterrane

Pluton	U-Pb Age (Ma)	Method	Reference
Ordovician-Silurian Tugaloo terrane granitoids (eastern Blue Ridge)			
Kennesaw	444 ± 11	SIMS	Bream, 2003
Persimmon Creek	468 ± 3	SIMS	Meschter McDowell et al., 2002
Whiteside	459 ± 12	SIMS	Miller et al., 2000
Devonian-Mississippian Tugaloo terrane granitoids (eastern Blue Ridge)			
Pink Beds	388 ± 5	SIMS	Miller et al., 2000
	371 ± 4	SIMS	Jubb, 2010
Looking Glass	380 ± 3	SIMS	Miller et al., 2000
	333 ± 16	SIMS	Jubb, 2010
Stone Mountain (NC)	353 ± 6	SIMS	Mapes, 2002
Yonah Mountain	346 ± 6	SIMS	Mapes, 2002
Walnut Creek	336 ± 2	SIMS	Stahr, 2008
Round Mountain	343 ± 2	SIMS	Jubb, 2010
Rabun	340 ± 12	SIMS	Stahr, 2008
	336 ± 2		
Elkahatchee	371 ± 7	SIMS	Mueller (unpub. data) cited in Barineau, 2009
Ordovician-Silurian Tugaloo terrane granitoids (Inner Piedmont)			
Henderson Gneiss	448 ± 5	SIMS	Moecher et al., 2011
	445 ± 5	SIMS	Huebner et al., in review
	449 ± 4	SIMS	Huebner et al., in review
Dysartsville	468 ± 8	SIMS	Bream, 2003
Brooks Crossroads			
Caesar's Head	~440 Ma	SIMS	Vinson, 1999
	~470 Ma		
Lithonia Gneiss	443 ± 5	SIMS	Huebner et al., in review
	444 ± 5		
Toccoa	449 ± 4	SIMS	Bream, 2003
Silurian-Mississippian Cat Square terrane granitoids			
Anderson's Mill	415 ± 3	SIMS	Mapes, 2002
	406 ± 6	SIMS	Howard, 2012
	397 ± 6	SIMS	
High Falls	383 ± 4	SIMS	Huebner et al., in review
	372 ± 6	SIMS	
	366 ± 3	SIMS	Mapes, 2002
Walker Top	357 ± 5	SIMS	Byars, 2009
	408 ± 2	SIMS	Gatewood, 2007
Toluca	383 ± 2	SIMS	Mapes, 2002
Pelham	364 ± 2	SIMS	Mapes, 2002
Gray Court	357 ± 2	SIMS	Mapes, 2002
Cherryville	355 ± 2	SIMS	Mapes, 2002
Carboniferous-Permian Inner Piedmont granitoids			
Stone Mountain (GA)	337 ± 3	SIMS	Mueller et al., 2011
	301 ± 3		
Indian Springs	316 ± 5	SIMS	Huebner et al., in review
	305 ± 7		
Murder Creek	328 ± 4	SIMS	Huebner et al., in review
Reedy River	325 ± 5	SIMS	Mapes, 2002
Dows Pulpit	325 ± 5	SIMS	Huebner et al., in review
Pacolet	304 ± 2	SIMS	Mapes, 2002
Elberton	302 ± 3	SIMS	Mueller et al., 2011
Carboniferous-Permian Carolina superterrane granitoids			
Pageland	311 ± 3	SIMS	Huebner, unpub. data
Churchland	320 ± 2	TIMS	Samson, 2001
York	321 ± 2	TIMS	Samson, 2001
Winnsboro	309 ± 1	TIMS	Samson, 2001
Liberty Hill	309 ± 3.8/-1.2	TIMS	Samson, 2001
Siloam	304 ± 3.5/-2.3	TIMS	Samson, 2001
Yanceyville	335 ± 2	TIMS	Wortman et al., 1998
Kilgore	327 ± 2	TIMS	Wortman et al., 1999

Additionally, the spatial distribution of Late Silurian-Devonian volcanic ash beds in the central and southern Appalachians, which can exceed thickness of 5 m in eastern West Virginia and west-central Virginia, strongly indicates a southern Appalachian volcanic source (Dennison and Textoris, 1970; Ver Straeten, 2010; Parrish, 2013) (Fig. 3-12). Late Silurian-Devonian ashes range from 418-376 Ma, with the thickest accumulation occurring at ~390 Ma (ver Straeten, 2010; Parrish, 2013). This at least provides additional evidence for Devonian tectonism in the southern Appalachians, however, the nature of this volcanic event is unclear. Parrish (2013) analyzed 24 samples of Tioga ash beds using SHRIMP, with weighted average ages from individual beds ranging from 397-386 Ma; the use of SHRIMP to date these ashes was crucial due to common inherited cores that prevented more precise ID-TIMS ages to be derived from zircon (Roden et al., 1990). Parrish (2013) identified numerous xenocrystic cores with mostly Mesoproterozoic (~1.5 Ga and 1.35-1.00 Ga) and several with Neoproterozoic (~800 Ma, and 600-500 Ma) ages, which strongly indicate Laurentian inheritance. This precludes any genetic connection between the Concord/Salisbury Plutonic Suite and these ash beds.

Based on whole-rock geochemical analyses and zircon trace and REE patterns of zircon from Tioga ash beds, Parrish et al. (2012) and Parrish (2013) suggested the probable magmatic source of these volcanics was felsic and peraluminous, and derived from a continental setting. Granitic rocks of the Cat Square terrane roughly coincide with ages of these ash beds (Fig. 3-11), include Laurentian xenocrystic cores, and are a suitable petrologic and geochemical match (e.g., Mapes, 2002; Parrish, 2013; Huebner et al., *in review*). However, Cat Square terrane granitoids have mostly been interpreted as anatectic melts derived from local metasedimentary material that formed during prograde upper amphibolite-facies metamorphism and wholesale migmatization of the Inner Piedmont during the Acadian/Neoacadian orogeny (Mapes, 2002; Mersch, 2009; Huebner et al., *in review*). This style of plutonism in orogenic belts rarely produces a volcanic expression. Howard (2012) suggested the Devonian High Falls pluton (central Georgia Cat Square terrane), with four dated samples that range from 406-372 Ma, may have initially developed in a volcanic arc that transitioned to a syn-collisional setting. Cat Square terrane granitoids exhibit geochemical characteristics that could be interpreted as arc-related, although isotopic data and the apparent lack of mafic or intermediate plutons support derivation from local metasedimentary rocks (Mapes, 2002). However, isotopic compositions are strikingly similar Banda arc andesites (e.g., Magaritz et al., 1978; Whitford and Jezek, 1982; Vroon et al., 1993), and abundant amphibolites through the Cat Square terrane could be an expression of mafic volcanism that accompanied arc-related plutonism. Additionally, geochemical and petrographic characteristics of Cat Square terrane granitoids indicate they are not true S-type granitoids (e.g., they do not contain tourmaline, cordierite, etc.) similar to granitoids derived from melt of sedimentary rocks in other orogens (e.g., Chappell and White, 1974; Searle et al., 1987). In light of these new

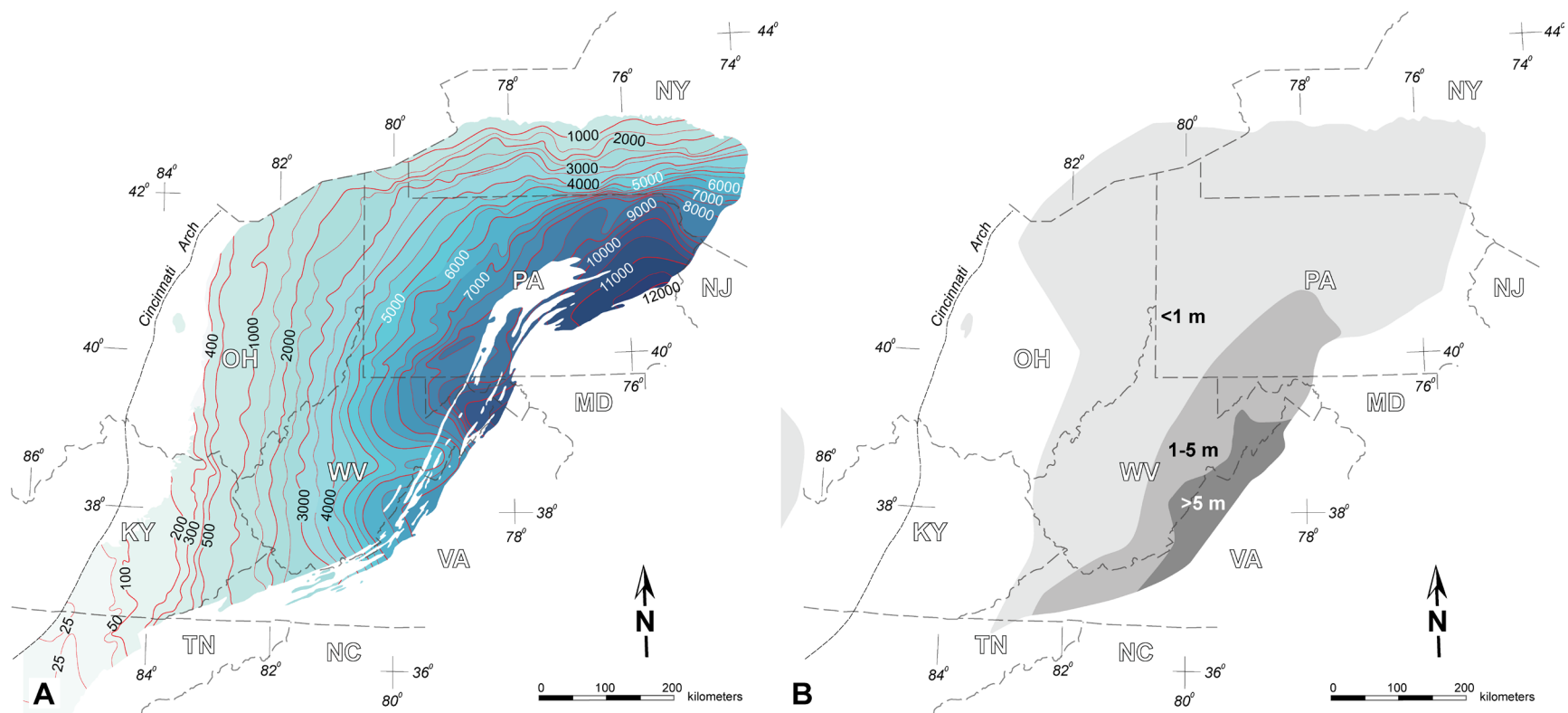


Figure 3-12: Spatial distribution of Devonian siliciclastics (A, modified from de Witt et al. (1975) and Mlici (2005) and bentonites beds (B, modified from Dennison and Textoris, 1970).

geochronologic data from the Devonian bentonites, the nature of Devonian-Mississippian Cat Square terrane plutonism may need to be reevaluated.

A Possible Alternative Model

The data that we have presented here apply to the latest Silurian through Mississippian history of the western flank of the exotic Carolina superterrane, but several key observations from the orogen that indicate tectonism prior to these times remain woefully unexplained. It is clear from the data presented here, in addition to other data from the foreland, high-grade Laurentian terranes, and exotic Carolina superterrane, that both competing accretionary models fit various aspects of the southern Appalachian orogen, while failing to reconcile other relevant observations. In light of this, we herein present a possible tectonic scenario that incorporates valuable evidence from both sides of this tectonic debate, which we hope can be the starting point for discussion toward a more coherent, all-inclusive tectonic model regarding what may be a more complex accretionary history of the exotic outboard terranes. Although the proposed scenario is logical and founded on available data, we outline the limitations and lacking evidence that would be necessary to more adequately support this proposition.

Several key elements of the central and southern Appalachians have been interpreted as evidence for the accretion of the Carolina superterrane via west-dipping subduction beneath the Laurentian margin in a Late Ordovician to Silurian event (e.g., Hibbard, 2000). These include: 1) paleomagnetic evidence that suggests the Carolina superterrane was proximal to Laurentia since Ordovician times (e.g., Vick et al., 1987; Noel et al., 1988); 2) the presence of 459-441 Ma arc-related plutonic rocks in the Tugaloo terrane in western North Carolina and Virginia (e.g., Meschter-McDowell et al., 2002; Sinha et al., 2012); 3) coeval $^{40}\text{Ar}/^{39}\text{Ar}$ cooling ages from the Carolina terrane (e.g., Vick et al., 1987; Noel et al., 1988); 4) the Sevier and Martinsburg clastic wedges, which progressively young to the northeast (e.g., Ettensohn and Lierman, 2012); 5) Ordovician-Silurian K-bentonites in the Appalachian foreland basin (e.g., Samson et al., 1989; Kolata et al., 1996); and 6) a correlative unconformity in the foreland (e.g., Dorsch et al., 1994; Hibbard, 2000). The kinematics of this accretion may be sinistral overall (e.g., Hibbard, 2000; Hibbard et al., 2012), with the strongest evidence arguably as the overlap of the Middle Ordovician Sevier clastic wedge by the Late Ordovician Martinsburg clastic wedge to the northeast (e.g., Ettensohn and Lierman, 2012). Some of the evidence originally provided as support for sinistral transpressive accretion, specifically the apparent pattern of progressive northeast younging of Tugaloo terrane Ordovician-Silurian plutons, needs to be reevaluated in light of modern geochronologic data (e.g., Sinha et al., 2012).

Even though these attributes support an Ordovician-Silurian accretionary event, this model in itself does not provide a viable explanation for 1) pervasive prograde, upper amphibolite-facies

metamorphism through the entire Inner Piedmont, which suggests it was strongly tectonized at mid-crustal levels through the Devonian into the Mississippian; 2) a distinct pulse of latest-Silurian through Mississippian, apparently anatectic magmatism concentrated in the eastern Inner Piedmont; 3) the relative youth of the Cat Square basin, with evidence that indicates it was deposited on ocean crust; 4) regional structural patterns throughout the Inner Piedmont, which suggest it flowed as an orogen-parallel mid-crustal channel, buttressed against the Brevard fault zone, during peak upper amphibolite-facies metamorphic conditions (Mersch et al., 2005; Hatcher and Mersch, 2006); 5) greenschist-facies metamorphism in the Charlotte terrane that overprints earlier (Neoproterozoic-Cambrian) fabric and post-dates intrusion of the Concord Plutonic Suite (Butler, 1983); 6) southwest progressive younging of Devonian-Mississippian clastic wedges in the central and southern Appalachian foreland (e.g., Ettensohn, 1985; Ferrill and Thomas, 1988; Ettensohn and Lierman, 2012); and 7) the spatial distribution of Devonian bentonites in the Appalachian foreland, which indicate a ~390 Ma volcanic source near central Virginia (e.g., Dennison and Textoris, 1970; van Straeten, 2010; Parrish, 2013).

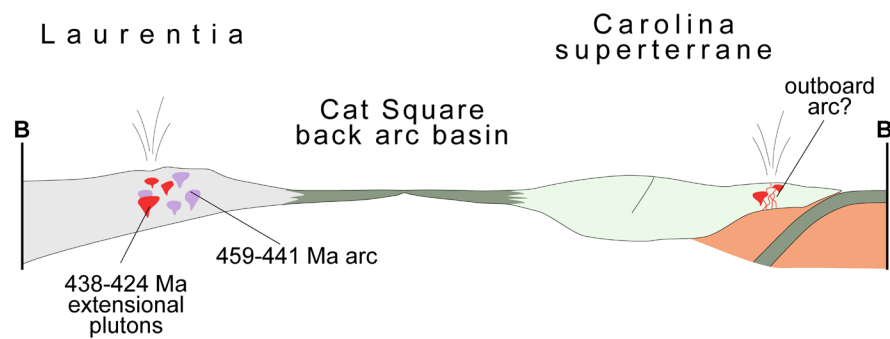
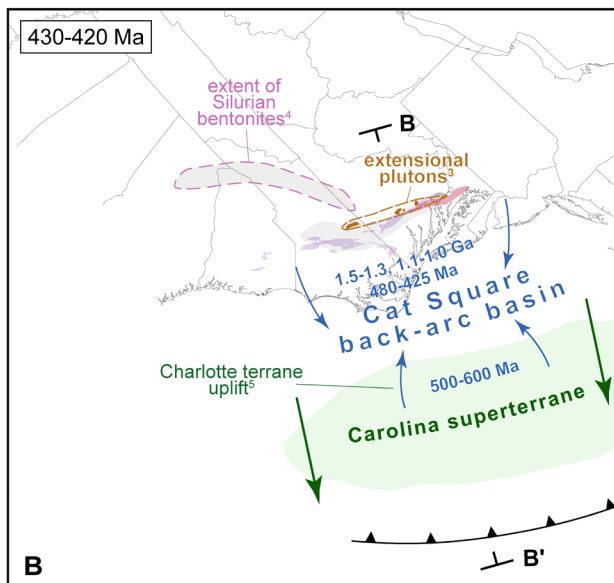
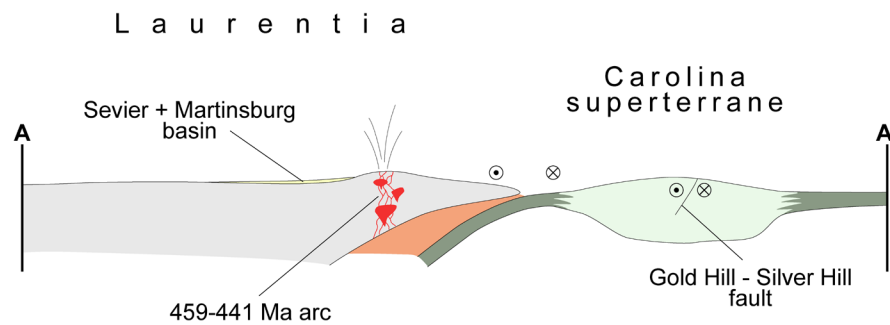
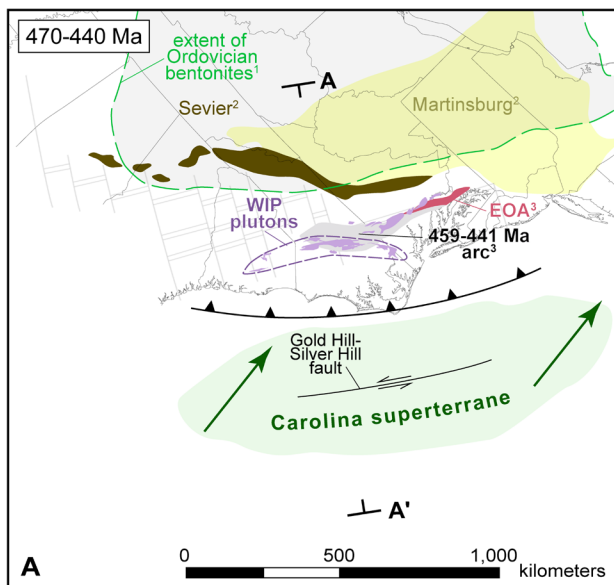
A possible solution to incorporate the aforementioned observations, in addition to data that indicate an earlier Ordovician-Silurian event, would be to rift the Carolina superterrane from Laurentia shortly after Ordovician-Silurian accretion, similar to the “terrane dispersion” model of Dennis (2007) (Fig. 3-13 A and B). This proposition is supported by 438-423 Ma extension related plutons in the eastern Blue Ridge (Sinha et al., 2012), Silurian K-bentonites in the Appalachian foreland with geochemical characteristics that indicate source magmas may have been generated in a within-plate extensional setting (Bergström et al., 1998; Manzo et al., 2002), a 430-425 Ma cooling event (uplift?) in the Charlotte terrane (Sutter, 1983), and coeval development of the inboard Cat Square basin (e.g., Bream, 2003; Mersch and Hatcher, 2007) (Fig. 3-13B). In this scenario, we suggest that, as the Carolina superterrane initially impinged on Laurentia, decreased convergence rate (possibly at a promontory?) could have resulted in the initiation of a west-dipping subduction zone outboard of the Carolina superterrane, and subsequent trench rollback resulted in the development of the Cat Square back-arc basin (Fig. 3-13). This style of accretionary complexity is similar to the initial Early Ordovician collision of the Notre Dame arc with the Humber margin and initiation of an outboard, west-directed subduction zone (e.g., Lissenberg et al., 2005; van Staal and Zagorevski, 2012). The lack of Grenvillian crustal fragments, with the presence of ultramafic and mafic rocks in the Cat Square terrane and, most importantly, the Hammett Grove Metigneous suite (possible ophiolite; Mittweide, 1989), support deposition of Cat Square terrane metasedimentary rocks on ocean crust, not as successor or intermontane basin as proposed by Dennis (2007) or Hibbard et al. (2010). Additionally, common amphibolite layers and bodies in Cat Square terrane metasedimentary assemblages reveal mixed volcanic arc and E-MORB signatures, which may indicate back-arc geochemical affinity (Wil-

son, 2006). Karig et al. (1978) suggested spreading rates in the Mariana back-arc basin varied from near zero to up to 8 cm/year; if we assume a moderate ~4 cm/year spreading rate, with the short lifespan of the Cat Square basin (say, 10-20 m.y.), the proposed back-arc basin could have been 400-800 km wide, comparable to the modern-day Sea of Japan.

The detrital zircon signature of Cat Square terrane metasedimentary rocks, coupled with an abundant pulse of mostly Devonian anatectic plutons and timing of prograde upper amphibolite-facies metamorphism, reveals the short-lived nature of the Cat Square basin. The young detrital zircons indicate deposition occurred at least during the Late Silurian and was punctuated by anatectic magmatism that indicates burial and subduction had occurred by the Devonian. Interestingly, the source of the young detrital zircons is likely from 459-441 Ma arc-related and 438-423 Ma extension-related magmatism in the Virginia Blue Ridge (e.g., Sinha et al., 2012; Huebner et al., *in review*). The characteristic detrital zircon signature of Cat Square terrane rocks exhibits a dominance of Ordovician-Silurian zircons, with minor peri-Gondwanan source and a muted Grenville signature. The nature of this signature prompted Huebner et al. (*in review*) to suggest that a peripheral bulge developed along the axis of these plutons as the Carolina superterrane approached the Laurentian margin. This would effectively cut off the strong Grenville signature common in eastern Laurentian rocks, as well as provide a mechanism for rapid uplift of this proposed source material that would allow it to be exposed, eroded, and subsequently deposited in the adjacent Cat Square basin.

The character of the Cat Square terrane detrital zircon signature changes dramatically to the southwest (Huebner et al., *in review*). In central Georgia, samples reveal dominantly Grenville source, with limited peri-Gondwanan input and no Ordovician-Silurian zircons. Huebner et al. (*in review*) suggested that this variation in provenance was likely related to proximity to the source material. Using estimates of Devonian dextral translation of the outboard terranes proposed by Hibbard and Waldron (2009), palinspastic restoration of ~250 km along the Brevard fault places the northern portion of the Cat Square terrane adjacent to the proposed source, while the southwestern portion would have been separated from this material by the Virginia promontory. Additionally, if Cat Square terrane granitoids are the plutonic equivalents of the Devonian bentonites in the Appalachian foreland, restoration of ~250 km along the Brevard fault zone would place them adjacent to the thickest deposits (Parrish, 2013) (Fig. 3-13). This adds to the validity of the piercing point proposed by Hibbard and Waldron (2009), and may provide insight regarding the paleogeographic position of the outboard Laurentian terranes in the Late Silurian to Early Devonian. However, the “state line flexure” is a nonunique piercing point and could also be matched with the New York promontory, which may be a better fit regarding the distribution of Devonian-Mississippian foreland clastic wedges (e.g., Merschhat and Hatcher, 2007; Ettensohn and Lierman, 2012).

Figure 3-13: Sequential tectonic scenario regarding the accretion of the Carolina superterrane discussed in text. The spatial distribution and geographic position of ash beds, clastic wedges, and plutons have been modified to account for Alleghanian shortening. Accompanying cross sections are schematic and vertically exaggerated. Data sources: ¹Samson et al., 1989; ²Ettensohn, 2004; ³Sinha et al., 2012; ⁴Bergström et al., 1998; ⁵Sutter et al., 1983; ⁶Dennison and Textoris, 1970.



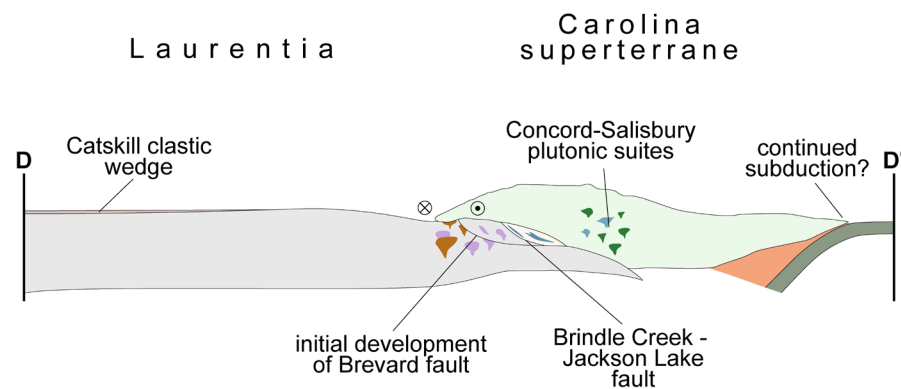
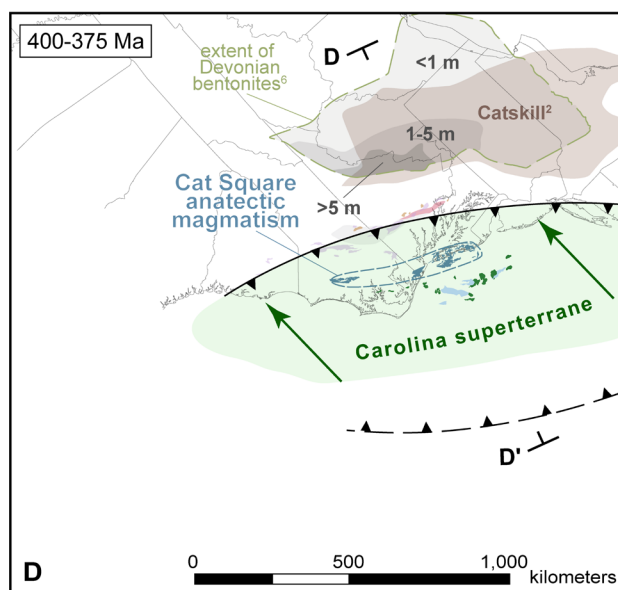
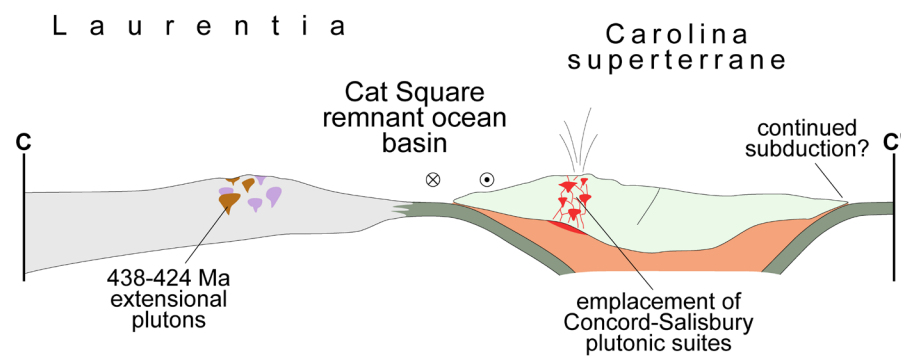
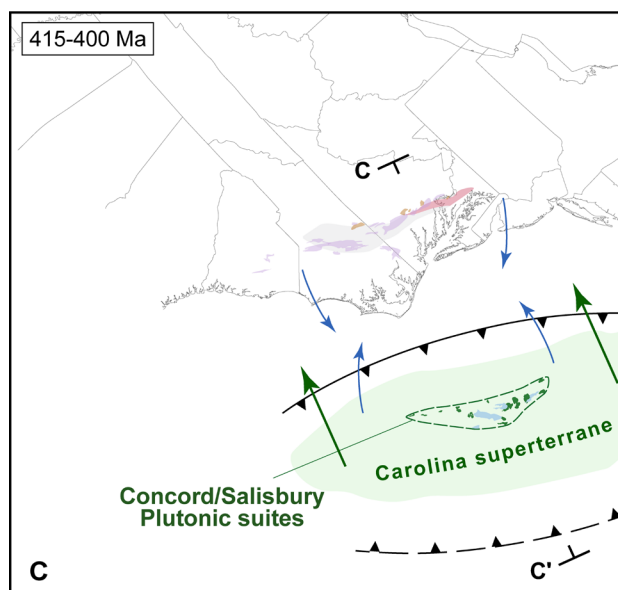


Figure 3-13 (continued)

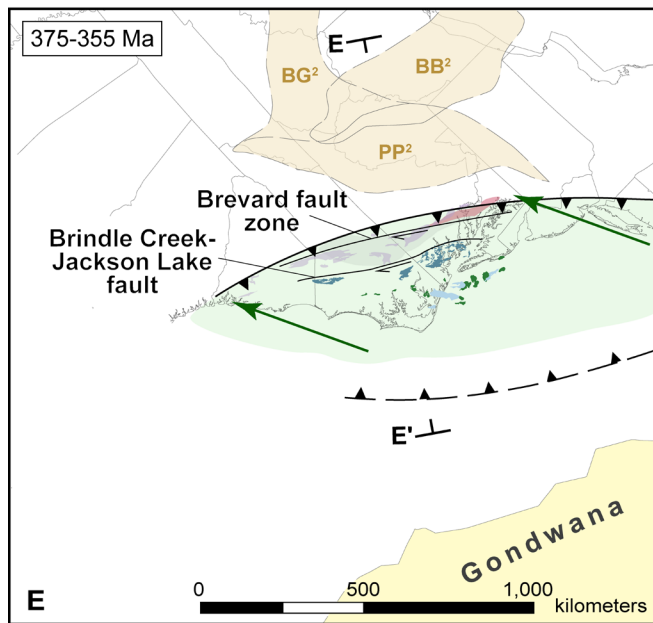
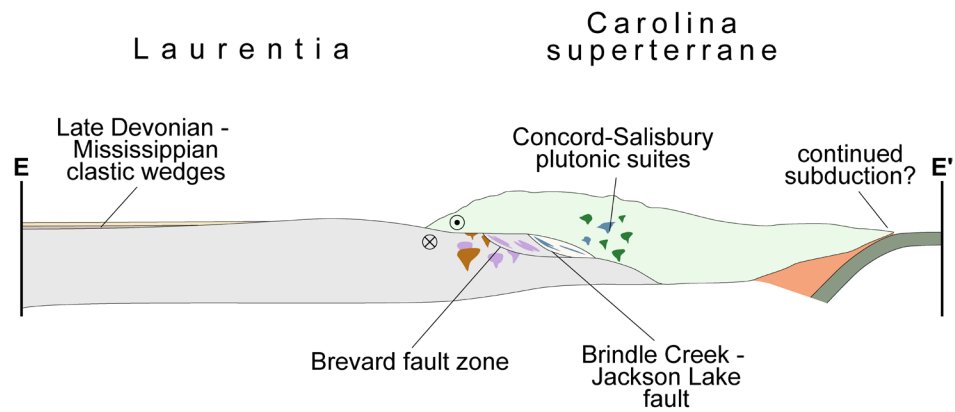


Figure 3-13 (continued)



Concord Plutonic suite arc-related rocks intruded the Charlotte terrane in the Late Silurian through Early Devonian, marking the beginnings of renewed convergence of the Carolina superterrane and subduction of the back-arc ocean crust that floored the Cat Square basin. This relatively short-lived pulse of plutonism is punctuated by the development of anatectic magmatism in the Cat Square terrane as it was subducted beneath the Carolina superterrane, which effectively shut off arc-related plutonism during the transition from B- to A-subduction that marks the tectonic burial of the Taconian + Laurentian margin, similar to the Cenozoic shutoff of magmatism in the Banda arc marking the beginning of subduction of Australian continental crust (e.g., Hamilton, 1979). Continued convergence through the Devonian resulted in burial of the Inner Piedmont beneath the Carolina superterrane to mid-crustal depths (Mirante and Patiño-Douce, 2000; Bier et al., 2002; Mersch, 2003; Davis, 2010) and orogen-parallel southwest-directed extrusion of the Inner Piedmont with dextral transpressive obduction of the Carolina superterrane (Mersch et al., 2005). This may be marked by a ~375 Ma cooling event in the Carolina superterrane that accompanied deformation along the Gold Hill-Silver Hill fault zone (Hibbard et al., 2012). Metamorphism in the northern portion of the Inner Piedmont peaked at ~345 Ma, although pooled metamorphic zircon rim data indicate the Inner Piedmont was at elevated temperatures through nearly all of the Devonian (Mersch, 2009). In contrast, data from central Georgia indicate metamorphic zircon growth peaked at ~375 Ma, and that portion of the Inner Piedmont was relatively cool until the onset of the Alleghanian orogeny (Huebner et al., *in review*). Huebner et al. (*in review*) suggested this may represent persistent high topography that kept the Carolina portion of the Inner Piedmont at mid-crustal depths, whereas the central Georgia portion may have escaped this overburden during southwest-directed lateral extrusion, similar to the escape of the Indochina block from the high topography of the Tibetan plateau (e.g., Burchfiel, 2004). Regardless, the long-lived nature of this event is contrary to recent work that indicates accretionary orogenesis is a relatively rapid process (e.g., Dewey, 2005), and we understand that this proposed model may likely represent a gross oversimplification; the orogenic evolution of the eastern Laurentian margin through the Paleozoic may rival the complexity of the present-day Indonesian region.

This leads to the nature of the exposed boundary between the Inner Piedmont and the Carolina superterrane. Hibbard et al. (1998) suggested the original suture is buried, and that the exposed boundary is an Alleghanian, post-accretionary feature that essentially decapitates the original terrane boundary. This supposition was based on the apparent young nature of their “central Piedmont shear zone” and the authors’ insistence that accretion had to occur prior to the Alleghanian orogeny (Hibbard et al., 1998). However, the ~335 Ma Yanceyville granitoid, which exhibits fabric related to the shear zone, also locally cuts gneissic layering and main-phase shear fabrics (Hibbard et al., 1998; Wortman et al., 1998). This granitoid was subsequently interpreted

as early to syn-kinematic, and by implication, the shear zone was interpreted to post-date ~335 Ma. In contrast, we suggest these fabric relationships indicate the Yanceyville granitoid intruded late syn- to post-kinematic, effectively marking the waning phases of deformation along this boundary. Additionally, several Alleghanian granitoids truncate the exposed suture (e.g., Dennis and Wright, 1995; Samson, 2001), which indicates it is a pre- or early-Alleghanian feature. With peak metamorphic conditions in the Inner Piedmont occurring less than 10 m.y. before the latest stages of deformation along this shear zone, in addition to evidence that indicates the Brindle Creek-Jackson Lake fault was still active between 355 and 325 Ma (Merschhat et al., 2005; Byars, 2010; Huebner et al., *in review*), we suggest the exposed boundary likely represents the suture between native Laurentian rocks and the exotic Carolina superterrane. Additionally, compiled metamorphic ages (Merschhat, 2009), and new plutonic ages of Carboniferous Tugaloo terrane granitoids (340-330 Ma; Stahr, 2008; Jubb, 2010; Mueller et al., 2011) obscure the boundary between the Acadian/Neoacadian and Alleghanian orogenies in the southern Appalachians (Fig. 3-11), which may indicate tectonism associated with the final accretion of the Carolina superterrane was promptly followed by the initial onset of the Alleghanian orogeny. Regardless, the tectonic model proposed here supersedes the necessity for a buried, hypothetical fault to explain the accretionary history of the Carolina superterrane, and we anticipate the new and compiled data presented herein, in addition to this tentative tectonic model that is consistent with numerous data available at the ground surface, will at least stimulate constructive discussions regarding the tectonic evolution of the southern Appalachian orogen that reconciles data used to support both competing tectonic models.

CONCLUSIONS

1. Geochemical and isotopic data are consistent with derivation of the Concord Plutonic suite in a subduction zone setting.
2. Concord Plutonic suite magmatism occurred ~403 Ma, which predates the most extensive pulse of metamorphism and possibly anatectic magmatism in the adjacent Cat Square terrane. This spatial and temporal relationship may mark the transition from B-subduction of the oceanic crust that floored the Cat Square basin to A-subduction of the eastern Laurentian margin.
3. Numerous data from the southern Appalachian foreland, crystalline internides, and exotic Carolina superterrane support both models that depict Ordovician-Silurian and Devonian-Mississippian accretion. A hybrid model that involves initial soft collision of the Carolina superterrane, followed by a period of extension and opening of the Cat Square back arc

basin, ending with final accretion during the Devonian-Mississippian, may be the optimal solution based on current available data.

4. The fault that separates the peri-Gondwanan Carolina superterrane from eastern Laurentian terranes roughly coincides with timing of late Neoacadian elements in the Inner Piedmont, and is likely the exposed suture between the exotic and native Laurentian terranes.
5. The complexity of Paleozoic accretionary orogenesis in the southern Appalachians may be much greater than depicted by current models.

ACKNOWLEDGMENTS

We thank Don Privett for his aid during gabbro sample collection in the Carolinas, in addition to Bert Bond at the Vulcan Materials Smith Grove quarry, and the people at the Vulcan Materials Pineville quarry for providing access to collect samples. Drew Coleman, Ryan Mills, Ryan Frazer, and Jez Ingles at the University of North Carolina, and Calvin Miller and Abe Padilla at Vanderbilt University permitted the use of their facilities and provided assistance for zircon separations. Joe Wooden, Jorge Vasquez, and Matt Coble are especially acknowledged for their assistance at the SUMAC facility. Insightful conversations with Justin Rehrer, Chris Howard, and Arthur Merschat helped shape the tectonic model presented herein. Funding was provided by the University of Tennessee Science Alliance Center of Excellence.

REFERENCES CITED

- Adams, G.I., 1926, The crystalline rocks, *in* Adams, G.I., Butts, C., Stephenson, L.W., and Cooke, W., eds., *Geology of Alabama: Geological Society of Alabama Special Report 14*, p. 25-40.
- Barineau, C.I., 2009, Superposed fault systems of the southernmost Appalachian Talladega belt: Implications for Paleozoic orogenesis in the southern Appalachians [Ph.D. dissertation]: Tallahassee, Florida State University, 136 p.
- Barker, C.A., Secor, D.T., Jr., Pray, J.R., and Wright, J.E., 1998, Age and deformation of the Longtown metagranite, South Carolina Piedmont: A possible constraint on the origin of the Carolina terrane: *Journal of Geology*, v. 106, p. 713-725.
- Bentley, R.D., and Neathery, T.N., 1970, *Geology of the Brevard zone and related rocks of the Inner Piedmont of Alabama: Alabama Geological Society, Eighth Annual Field Trip Guidebook*, 119 p.
- Bergström, S.M., Huff, W.D., and Kolata, D.R., 1998, Early Silurian (Llandoveryan) K-bentonites discovered in the southern Appalachian thrust belts, eastern USA: Stratigraphy, geochemistry, and tectonomagmatic and paleogeographic implications: *Geologiska Föreningens i Stockholm Förhandlingar*, v. 120, p. 149-158.
- Bier, S.E., Bream, B.R., and Giorgis, S.D., 2002, Inner Piedmont stratigraphy, metamorphism, and deformation in the Marion-South Mountains area, North Carolina, *in* Hatcher, R.D., Jr., and Bream, B.R., eds., *Inner Piedmont geology in the South Mountains-Blue Ridge Foothills and the southwestern Brushy Mountains, central-western North Carolina: Carolina Geological Society Field Trip Guidebook*, p. 65–100.
- Bream, B.R., 1999, *Geology of the Glenwood and Sugar Hill quadrangles, North Carolina, and the structure of the northeast end of the Henderson Gneiss* [M.S. thesis]: Knoxville, University of Tennessee, 155 p.
- Bream, B.R., 2003, *Tectonic implications of geochronology and geochemistry of para- and orthogneisses from the southern Appalachian crystalline core* [Ph.D. dissertation]: Knoxville, University of Tennessee, 262 p.
- Bream, B.R., Hatcher, R.D., Jr., Miller, C.F., and Fullagar, P.D., 2001, Geochemistry and provenance of Inner Piedmont paragneisses, NC and SC: Evidence for an internal terrane boundary?: *Geological Society of America Abstracts with Programs*, v. 33, no. 2, p. 65.
- Bream, B.R., Hatcher, R.D., Jr., Miller, C.F., and Fullagar, P.D., 2004, Detrital zircon ages and Nd isotopic data from the southern Appalachian crystalline core, Georgia, South Carolina, North Carolina, and Tennessee: New provenance constraints for part of the Laurentian margin, *in* Tollo, R. P., Corriveau, L., McLelland, J., and Bartholomew, M.J., eds., *Proterozoic*

- tectonic evolution of the Grenville orogen in North America: Boulder, Colorado, Geological Society of America Memoir 197, p. 459-475.
- Burchfiel, B.C., 2004, New technology: New geologic challenges: *GSA Today*, v. 14, no. 2, p. 4-9.
- Butler, J.R., 1983, Geologic history of the Charlotte belt at the old Pineville quarry, northeastern York County, South Carolina: *South Carolina Geology*, v. 27, p. 13-24.
- Butler, J.R., 1991, Metamorphism, *in* Horton, J.W., Jr., and Zullo, V.A., eds., *The geology of the Carolinas*: Knoxville, University of Tennessee Press, p. 127-141.
- Butler, J.R., and Fullagar, P.D., 1978, Petrochemical and geochronological studies of plutonic rocks in the southern Appalachians: III. Leucocratic adamellites of the Charlotte belt near Salisbury, North Carolina: *Geological Society of America Bulletin*, v. 89, p. 460-466.
- Butler, J.R., and Ragland, P.C., 1969, A petrochemical survey of plutonic intrusions in the Piedmont, southeastern Appalachians, U.S.A.: *Contributions to Mineralogy and Petrology*, v. 24, p. 164-190.
- Byars, H.E., 2010, Tectonic evolution of the west-central portion of the Newton window, North Carolina Inner Piedmont: Timing and implications for the emplacement of the Paleozoic Vale charnockite, Walker Top Granite, and mafic complexes [M.S. thesis]: Knoxville, University of Tennessee, 248 p.
- Byars, H.E., Merschat, A.J., Hatcher, R.D., Jr., and Wooden, J.L., 2008, Timing and implications for the emplacement of the Paleozoic Vale (Cat Square) charnockite and Walker Top Granite, eastern Inner Piedmont, North Carolina: *Geological Society of America Abstracts with Programs*, v. 40, no. 4, p. 18.
- Cabanis, B., and Lecolle, M., 1989, Le diagramme La/10-Y/15-Nb/8; un outil pour la discrimination des series volcaniques et la mise en evidence des processus de mélange et/ou de contamination crustale: *Comptes Rendus de l'Academie des Sciences, Serie 2, Mecanique, Physique, Chimie, Sciences de l'Univers, Sciences de la Terre*, v. 309, p. 2023-2029.
- Chalcraft, R.G., 1970, Petrography and geophysics of the Rock Hill gabbro pluton, York County, South Carolina: *Southeastern Geology*, v. 11, p. 153-171.
- Chappell, B.W., and White, A.J.R., 1974, Two contrasting granite types: *Pacific Geology*, v. 8, p. 173-174.
- Chaumba, J.B., 2010a, The Hammett Grove meta-igneous suite, South Carolina: Bulk-rock, mineral composition, hydrogen, and oxygen isotope data from metagabbros: *Geological Society of America Abstracts with Programs*, v. 42, no. 1, p. 164.
- Chaumba, J.B., 2010b, Island arc origin for the Gladesville and associated bodies in the Carolina superterrane, central Georgia: *Geological Society of America Abstracts with Programs*, v. 42, no. 5, p. 307.

- Chaumba, J.B., 2011, Bulk-rock geochemistry and mineral compositions from the Mt. Carmel complex, Carolina superterrane, southern Appalachians: Geological Society of America Abstracts with Programs, v. 34, no. 2, p. 31.
- Dallmeyer, R.D., 1989, Late Paleozoic thermal evolution of crystalline terranes within portions of the U.S., Appalachian orogen, *in* Hatcher, R.D., Jr., Thomas, W.A., and Viele, G.W., eds., The Appalachian-Ouachita orogen in the United States: Boulder, Colorado, Geological Society of America, The Geology of North America F-2, p. 417–444.
- Dallmeyer, R.D., Wright, J.E., Secor, D.T., Jr., and Snoke, A.W., 1986, Character of the Alleghanian orogeny in the southern Appalachians: Part II. Geochronological constraints on the tectonothermal evolution of the eastern Piedmont in South Carolina: Geological Society of America Bulletin, v. 97, p. 1329-1344.
- Davis, B.A., 2010, Tectonic evolution of the southern Appalachian Inner Piedmont: Identification and interpretation of crustal features from aeromagnetic data and detailed geologic mapping in central Georgia [M.S. thesis]: Knoxville, University of Tennessee, 222 p.
- Davidson, J.P., 1996, Deciphering mantle and crustal signatures in subduction zone magmatism, *in* Bebout, G.E., Scholl, D.W., Kirby, S.H., and Platt, J.P., eds., Subduction Top to Bottom: American Geophysical Union Monograph 96, p. 251-262.
- de Witt, W. Jr., Perry, W.J., Jr., and Wallace, L.G., 1975, Oil and gas data from Devonian and Silurian rocks in the Appalachian basin: U.S. Geological Survey Miscellaneous Investigations Series Map I-917B, scale 1: 2,500,000.
- Dennis, A.J., 1991, Is the central Piedmont suture a low-angle normal fault?: *Geology*, v. 19, p. 1081-1084.
- Dennis, A.J., 2007, Cat Square basin, Catskill clastic wedge: Silurian-Devonian orogenic events in the central Appalachians and the crystalline southern Appalachians, *in* Sears, J.W., Harms, T.A., and Evenchick, C.A., eds., Whence the Mountains? Inquiries into the evolution of orogenic systems: A volume in honor of Raymond A. Price: Boulder, Colorado, Geological Society of America Special Paper 433, p. 313-329.
- Dennis, A.J., and Wright, J.E., 1995, Mississippian (ca. 326-323 Ma) U-Pb crystallization ages for two granitoids in Spartanburg and Union Counties, South Carolina: *South Carolina Geology*, v. 38, p. 23-28.
- Dennis, A.J., and Wright, J.E., 1997, Middle and late Paleozoic monazite U-Pb ages, Inner Piedmont, South Carolina: Geological Society of America Abstracts with Programs, v. 29, no. 3, p. 12.
- Dennison, J.M., and Textoris, D.A., 1970, Devonian Tioga tuff in northeastern United States: *Bulletin of Volcanology*, v. 34, p. 289-294.

- Dewey, J.F., 2005, Orogeny can be very short: Proceedings of the National Academy of Sciences, v. 102, p. 15286-15293.
- Dewey, J.F., and Bird, J.M., 1970, Mountain belts and the new global tectonics: Journal of Geophysical Research, v. 75, p. 2625-2647.
- Dorsch, J., Bambach, R.K., and Driese, S.G., 1994, Basin-rebound origin for the "Tuscarora unconformity" in southwestern Virginia and its bearing on the nature of the Taconic orogeny: American Journal of Science, v. 294, p. 237-255.
- Esawi, E.K., 2004, Evidence from the Farmington pluton for Early Devonian subduction-related magmatism in the Carolina zone of central North Carolina: Journal of Geodynamics, v. 37, p. 531-548.
- Ettensohn, F.R., 1985, The Catskill Delta complex and the Acadian orogeny: A model: Boulder, Geological Society of America Special Paper 201, p. 39-49.
- Ettensohn, F.R., 1987, Rates of relative plate motion during the Acadian orogeny based on the spatial distribution of black shales: Journal of Geology, v. 95, p. 572-582.
- Ettensohn, F.R., 2011, Acadian/Neoacadian tectonic framework of Devonian-Mississippian sedimentation in the Appalachian foreland basin: Geological Society of America Abstracts with Programs, v. 43, no. 1, p. 96.
- Ettensohn, F.R., and Lierman, R.T., 2012, Large-scale tectonic controls on the origin of Paleozoic dark-shale source-rock basins: Examples from the Appalachian foreland basin, eastern United States, *in* D. Gao, ed., Tectonics and sedimentation: Implications for petroleum systems: American Association of Petroleum Geologists Memoir 100, p. 95-124.
- Ferrill, B.A., and Thomas, W.A., 1988, Acadian dextral transpression and synorogenic sedimentary successions in the Appalachians: Geology, v. 16, p. 604-608.
- Fiess, P.G., 1982, Geochemistry and tectonic setting of the volcanics of the Carolina slate belt: Economic Geology, v. 77, p. 273-293.
- Fronabarger, A.K., 1984, Petrogenesis of the Calhoun Falls, Mt. Carmel, and Greenwood complexes, South Carolina, and modeling of heat transfer in gabbro [Ph.D. dissertation]: Knoxville, University of Tennessee, 200 p.
- Fullagar, P.D., 1971, Age and origin of plutonic intrusions in the Piedmont of the southeastern Appalachians: Geological Society of America Bulletin, v. 82, p. 2845-2862.
- Fullagar, P.D., 1983, Post-metamorphic Siluro-Devonian granitic plutons in the Charlotte belt of South Carolina: Geological Society of America Abstracts with Programs, v. 15, no. 2, p. 64.
- Fullagar, P. D., 1997, Evidence for Grenville-age or older crust in the southern Appalachian Inner Piedmont of North and South Carolina: Geological Society of America Abstracts with Programs, v. 27, no. 6, p. 397.

- Gatewood, M.P., 2007, Structure and tectonics of the northeastern Inner Piedmont from detailed geologic mapping, geochronologic, geochemical, and petrologic studies with macro-, meso-, and microstructural analyses of ductile fault zones [M.S. thesis]: Knoxville, University of Tennessee, 279 p.
- Giorgis, S.D., 1999, Inner Piedmont geology of the northwestern South Mountains near Morganton, North Carolina [M.S. thesis]: Knoxville, University of Tennessee, 191 p.
- Giorgis, S.D., Mapes, R.W., and Bream, B.R., 2002, The Walker Top Granite: Acadian granitoid or eastern Inner Piedmont basement? *in* Hatcher, R.D., Jr., and Bream, B.R., eds., Inner Piedmont geology in the South Mountains-Blue Ridge Foothills and the southwestern Brushy Mountains, central-western North Carolina: Carolina Geological Society Field Trip Guidebook, p. 33-44.
- Goldsmith, R., Milton, D. J., and Horton, J. W., Jr., 1988, Geologic map of the Charlotte 1-degree x 2-degree quadrangle, North Carolina and South Carolina: U.S. Geological Survey Map I-1251-E, scale 1:250,000.
- Glover, L., and Sinha, A.K., The Virgilina deformation, a late Precambrian to Early Cambrian(?) orogenic event in the central Piedmont Virginia and North Carolina: *American Journal of Science*, v. 273, p. 234-251.
- Griffin, V.S., Jr., 1971, The Inner Piedmont belt of the southern crystalline Appalachians: *Geological Society of America Bulletin*, v. 82, p. 1885-1898.
- Griffin, V.S., Jr., 1978, Detailed analysis of tectonic levels in the Appalachian Piedmont: *Geologische Rundschau*, v. 67, p. 179-201.
- Halik, R.S., 1983, Characterization of the Charlotte/Carolina slate belt boundary in the Silverstreet and Denny quadrangles, South Carolina [M.S. thesis]: Columbia, University of South Carolina, 83 p.
- Hamilton, W., 1979, Tectonics of the Indonesian region: U.S. Geological Survey Professional Paper 1078, 345 p.
- Harris, C.W., and Glover, L., 1988, The regional extent of the ca. 600 Ma Virgilina deformation: Implications for stratigraphic correlation in the Carolina terrane: *Geological Society of America Bulletin*, v. 100, p. 200-217.
- Hatcher, R.D., Jr., 1969, Stratigraphy, petrology, and structure of the low rank belt and part of the Blue Ridge of northwesternmost South Carolina: *South Carolina Division of Geology Geologic Notes*, v. 13, no. 4, p. 11-32.
- Hatcher, R.D., Jr., 1971, Geology of Rabun and Habersham Counties, Georgia: A reconnaissance study: *Georgia Department of Mines, Mining, and Geology Bulletin* 83, 48 p.
- Hatcher, R. D., Jr., 1972, Developmental model for the southern Appalachians: *Geological Society of America Bulletin*, v. 83, p. 2735-2760.

- Hatcher, R. D., Jr., 1978, Tectonics of the western Piedmont and Blue Ridge: Review and speculation: *American Journal of Science*, v. 278, p. 276–304.
- Hatcher, R. D. Jr., 1993, Perspective on the tectonics of the Inner Piedmont, southern Appalachians, *in* Hatcher, R. D. Jr., and Davis, T. L., eds., *Studies of Inner Piedmont geology with a focus on the Columbus Promontory: Carolina Geological Society Field Trip Guidebook*, North Carolina Geological Survey, p. 17-43.
- Hatcher, R.D., Jr., 2001, Rheological partitioning during multiple reactivation of the Paleozoic Brevard fault zone, southern Appalachians, USA, *in* Holdsworth, R.E., Strachan, R.A., MacLoughin, J.F., and Knipe, R.J., eds., *The Nature and Significance of Fault Zone Weakening*: London, Geological Society Special Publication 86, p. 255–269.
- Hatcher, R. D., Jr., 2002, An Inner Piedmont primer, *in* Hatcher, R. D., Jr., and Bream, B. R., eds., *Inner Piedmont geology in the South Mountains-Blue Ridge Foothills and the southwestern Brushy Mountains, central-western North Carolina: Carolina Geological Society Field Trip Guidebook*, p. 1-18.
- Hatcher, R.D., Jr., 2004, Southern Appalachian Crustal Transect: Overview, *in* Mersch, A.J., and Hatcher, R.D., Jr., eds., *Trans Appalachians Internides Geotraverse: 17th International Basement Tectonics Association Field Trip Guidebook*, p. 1-12.
- Hatcher, R.D., Jr., 2010, The Appalachian orogen: A brief summary, *in* Tollo, R.P., Bartholomew, M.J., Hibbard, J.P., and Karabinos, P.M., eds., *From Rodinia to Pangea: The Lithotectonic Record of the Appalachian Region*: Boulder, Colorado, Geological Society of America Memoir 206, p. 1-19.
- Hatcher, R.D., Jr., and Hooper, R.J. 1992, Evolution of crystalline thrust sheets in the internal parts of mountain chains, *in* McClay, K.R., ed., *Thrust Tectonics*: London, Chapman and Hall, p. 217–234.
- Hatcher, R.D., Jr., and Mersch, A.J., 2006, The Appalachian Inner Piedmont: An exhumed strike-parallel, tectonically forced orogenic channel, *in* Law, R.D., Searle, M., and Godin, L., eds., *Channel flow, ductile extrusion, and exhumation of lower-mid crust in continental collision zones*: London, Geological Society Special Publication 268, p. 517-540.
- Hatcher, R.D., Jr., Howell, D.E., and Talwani, P., 1977, Eastern Piedmont fault system: Speculations on its extent: *Geology*, v. 5, p. 636-640.
- Hatcher, R.D., Jr., Bream, B.R., and Mersch, A.J., 2007, Tectonic map of the southern and central Appalachians: A tale of three orogens and a complete Wilson Cycle *in* Hatcher, R.D., Jr., Carlson, M.P., McBride, J.H., and Martínez Catalán, J.R., eds., *4-D Framework of Continental Crust*: Boulder, Colorado, Geological Society of America Memoir 200, p. 595-632.
- Hermes, O.D., 1968, Petrology of the Mecklenburg gabbro-metagabbro complex, North Carolina: *Contributions to Mineralogy and Petrology*, v. 18, p. 270-294.

- Heyn, T., 1984, Stratigraphic and structural relationships along the southwestern flank of the Sauratown Mountains anticlinorium [M.S. thesis]: Columbia, University of South Carolina, 192 p.
- Hibbard, J.P., 2000, Docking Carolina: *Geology*, v. 28, p. 127-130.
- Hibbard, J.P., and Samson, S.D., 1995, Orogenesis exotic to the Iapetan cycle in the southern Appalachians, *in* Hibbard, J.P., van Staal, C.R., and Cawood, P.A., eds., *Current Perspectives in the Appalachian-Caledonian Orogen: Geological Society of Canada Special Paper 41*, p. 191-205.
- Hibbard, J., and Waldron, J.W.F., 2009, Truncation and translation of Appalachian promontories: Mid-Paleozoic strike-slip tectonics and basin initiation: *Geology*, v. 37, p. 487-490.
- Hibbard, J.P., Shell, G.S., Bradley, P.J., Samson, S.D., and Wortman, G.L., 1998, The Hyco shear zone in North Carolina and southern Virginia: Implications for the Piedmont zone-Carolina zone boundary in the southern Appalachians: *American Journal of Science*, v. 298, p. 85-107.
- Hibbard, J.P., Stoddard, E.F., Secor, D.T., and Dennis, A.J., 2002, The Carolina Zone: Overview of Neoproterozoic to early Paleozoic peri-Gondwanan terranes along the eastern flank of the southern Appalachians: *Earth Science Reviews*, v. 57, p. 299-339.
- Hibbard, J.P., van Staal, C.R., and Rankin, D.W., 2010, Comparative analysis of the geological evolution of the northern and southern Appalachian orogen: Late Ordovician-Permian, *in* Tollo, R.P., Bartholomew, M.J., Hibbard, J.P., and Karabinos, P.M., eds., *From Rodinia to Pangea: The Lithotectonic Record of the Appalachian Region*: Boulder, Colorado, Geological Society of America Memoir 206, p. 51-69.
- Hibbard, J.P., Miller, B.V., Hames, W.E., Standard, I.D., Allen, J.S., Lavallee, S.B., and Boland, I.B., 2012, Kinematics, U-Pb geochronology, and $^{40}\text{Ar}/^{39}\text{Ar}$ thermochronology of the Gold Hill shear zone, North Carolina: The Cherokee orogeny in Carolina, southern Appalachians: *Geological Society of America Bulletin*, v. 124, p. 643-656.
- Hill, J. C., 1999, Stratigraphy, structure, and tectonics of part of the southern Appalachian Inner Piedmont, near Marion, North Carolina [M.S. thesis]: Knoxville, University of Tennessee, 188 p.
- Hooper, R.J., 1986, Geologic studies at the east end of the Pine Mountain window and adjacent Piedmont, central Georgia [Ph.D. dissertation]: Columbia, University of South Carolina, 322 p.
- Hopson, J.L., and Hatcher, R.D., Jr., 1988, Structural and stratigraphic setting of the Alto allochthon, northeast Georgia: *Geological Society of America Bulletin*, v. 100, p. 339-350.
- Horton, J.W., Jr., and McConnell, K.I., 1991, The western Piedmont, *in* Horton, J. W., Jr., and Zullo, V. A., editors, *The Geology of the Carolinas—Carolina Geological Society 50th Anniversary Volume*: Knoxville, The University of Tennessee Press, p. 36–58.

- Horton, J.W., Jr., Drake, A.A., and Rankin, D.W., 1989, Tectonostratigraphic terranes and their Paleozoic boundaries in the central and southern Appalachians, *in* Dallmeyer, R.D., ed., *Terranes in the Circum-Atlantic Paleozoic Orogens*: Boulder, Geological Society of America Special Paper 230, p. 213-245.
- Howard, C.W., 2012, Investigating the evolution of two southern Appalachian terrane boundaries and a plutonic complex: Tectonic implications of structural, geochemical, and geochronologic studies in the central Georgia Inner Piedmont [M.S. thesis]: Knoxville, University of Tennessee, 208 p.
- Huebner, M.T., Wooden, J.L., and Hatcher, R.D., Jr., 2010, A terrane boundary in the central Georgia (USA) Inner Piedmont confirmed using new U-Pb SHRIMP ages of granitic rocks: Geological Society of America Abstracts with Programs, v. 42, no. 5, p. 196.
- Huebner, M.T., Hatcher, R.D., Jr., and Merschat, A.J., Confirmation of the southwest continuation of the Cat Square terrane, southern Appalachian Inner Piedmont, with implications for middle Paleozoic collisional orogenesis: *American Journal of Science*, in review.
- Hurst, V.J., 1973, Geology of the southern Blue Ridge belt: *American Journal of Science*, v. 273, p. 643-670.
- Ingersoll, R.V., 1988, Tectonics of sedimentary basins: *Geological Society of America Bulletin*, v. 100, p. 1704-1719.
- Irvine, T.N., 1982, Terminology for layered intrusions: *Journal of Petrology*, v. 23, p. 127-162.
- Irvine, T.N., and Baragar, W.R.A., 1971, A guide to the chemical classification of the common volcanic rocks: *Canadian Journal of Earth Sciences*, v. 8, p. 523-548.
- Jubb, M. G. V., 2010, Paradoxes in the deformational and metamorphic history of the eastern Blue Ridge: Evidence from the Lake Toxaway and eastern Big Ridge quadrangles, North Carolina [M.S. thesis]: Knoxville, University of Tennessee, 294 p.
- Karig, D.E., Anderson, R.N., and Bibee, L.D., 1978, Characteristics of back arc spreading in the Mariana trough: *Journal of Geophysical Research*, v. 83, p. 1213-1226.
- King, P.B., 1955, A geologic section across the southern Appalachians: An outline to the geology in the segment in Tennessee, North Carolina, and South Carolina, *in* Russell, R.J., ed., *Guides to Southeastern Geology*: New York, Geological Society of America, p. 332-373.
- Kolata, D.R., Huff, W.D., and Bergström, S.M., 1996, Ordovician K-bentonites of eastern North America: Boulder, Geological Society of America Special Paper 313, 89 p.
- Le Bas, M.J., Le Maitre, R.W., Streckeisen, A., and Zanettin, B., 1986, A chemical classification of volcanic rocks based on the total alkali-silica diagram: *Journal of Petrology*, v. 27, p. 745-750.
- Le Maitre, R. W., 1989, *A classification of igneous rocks and glossary of terms*: Oxford, Blackwell, 193 p.

- Lissenberg, C.J., Zagorevski, A., McNicoll, V.J., van Staal, C.R., and Whalen, J.B., 2005, Assembly of the Annieopsquotch accretionary tract, Newfoundland Appalachians: Age and geodynamic constraints from syn-kinematic intrusions: *Journal of Geology*, v. 113, p. 553-570.
- Ludwig, K. R., 2009, SQUID v. 2, computer program.
- Ludwig, K. R., 2012, Isoplot v. 3.75, computer program.
- Magaritz, M., Whitford, D.J., and James, D.E., 1978, Oxygen isotopes and the origin of high- $^{87}\text{Sr}/^{86}\text{Sr}$ andesites: *Earth and Planetary Science Letters*, v. 40, p. 220-230.
- Manzo, D.J., Bergström, S.M., Huff, W.D., and Kolata, D.R., 2002, New data on the age and distribution of the Early Silurian (Llandoveryan) Thorn Hill K-bentonite complex in the southern Appalachians: *Geological Society of America Abstracts with Programs*, v. 34, no. 2, p. A26.
- Mapes, R.W., 2002, Geochemistry and geochronology of mid-Paleozoic granitic plutonism in the southern Appalachian Piedmont terrane, North Carolina-South Carolina-Georgia [M.S. thesis]: Nashville, Vanderbilt University, 150 p.
- Matthews, V., 1967, Geology and petrology of the pegmatite district in southwestern Jasper County, Georgia [M.S. thesis]: Athens, University of Georgia, 68 p.
- McConnell, K. I., 1990, Geology and geochronology of the Sauratown Mountains anticlinorium, northwestern North Carolina [Ph.D. dissertation]: Columbia, University of South Carolina, 232 p.
- McSween, H.Y., Jr., and Harvey, R.P., 1997, Concord plutonic suite: Pre-Acadian gabbro-syenite intrusions in the southern Appalachians *in* Sinha, A.K., Whalen, J.B., and Hogan, J.P., eds., *The Nature of Magmatism in the Appalachian Orogen*: Boulder, Colorado, Geological Society of America Memoir 191, p. 221-234.
- McSween, H.Y., Jr., Speer, J.A., and Fullagar, P.D., 1991, Plutonic Rocks, *in* Horton, J.W., Jr., and Zullo, V.A., eds., *The geology of the Carolinas*: Knoxville, University of Tennessee Press, p. 109-126.
- McSween, H.Y., Jr., Sando, T.W., Clark, S.R., Harden, J.T., and Strange, E.A., 1984, The gabbro-metagabbro association of the southern Appalachian Piedmont: *American Journal of Science*, v. 284, p. 437-461.
- Medlin, J.H., 1968, Comparative petrology of two igneous complexes in the South Carolina piedmont [Ph.D. dissertation]: State College, Pennsylvania State University, 328 p.
- Merschat, A. J., 2003, Inner Piedmont tectonics in the southwestern Brushy Mountains, North Carolina: Field and laboratory data revealing 3-D crustal flow and sillimanite I and II metamorphism [M.S. thesis]: Knoxville, University of Tennessee, 198 p.
- Merschat, A.J., 2009, Assembling the Blue Ridge and Inner Piedmont: Insights into the nature and timing of terrane accretion in the southern Appalachian orogen from geologic mapping,

- stratigraphy, kinematic analysis, petrology, geochemistry, and modern geochronology [Ph.D. dissertation]: Knoxville, University of Tennessee, 455 p.
- Merschat, A.J., and Hatcher, R.D., Jr., 2007, The Cat Square terrane: Possible Siluro-Devonian remnant ocean basin in the Inner Piedmont, southern Appalachians, USA, *in* Hatcher, R.D., Jr., Carlson, M.P., McBride, J.H., and Martínez Catalán, J.R., eds., 4-D Framework of Continental Crust: Boulder, Colorado, Geological Society of America Memoir 197, p. 553-565.
- Merschat, A.J., Hatcher, R.D., Jr., and Davis, T.L., 2005, The northern Inner Piedmont, southern Appalachians, USA: Kinematics of transpression and SW-directed mid-crustal flow: *Journal of Structural Geology*, 27, 1252-1281.
- Merschat, A.J., Hatcher, R.D., Jr., Byars, H.E., and Gilliam, W.G., 2008, Inner Piedmont Geotransverse from the Brushy Mountains to Lincolnton, North Carolina: Architecture of the Cat Square and Tugaloo terranes: Geological Society of America Southeastern Section, Field Trip Guidebook, 64 p.
- Merschat, A.J., Hatcher, R.D., Jr., Bream, B.R., Miller, C.F., Byars, H.E., Gatewood, M.P., and Wooden, J.L., 2010, Detrital zircon geochronology and provenance of southern Appalachian Blue Ridge and Inner Piedmont crystalline terranes, *in* Tollo, R.P., Bartholomew, M.J., Hibbard, J.P., and Karabinos, P.M., eds., From Rodinia to Pangea: The Lithotectonic Record of the Appalachian Region: Boulder, Colorado, Geological Society of America Memoir 206, p. 661-699.
- Meschede, M., 1986, A method of discriminating between different types of mid-ocean ridge basalts and continental tholeiites with the Nb-Zr-Y diagram: *Chemical Geology*, v. 56, p. 207-218.
- Meschter-McDowell, S., Miller, C.F., Fullagar, P.D., Bream, B.R., and Mapes, R.W., 2002, The Persimmon Creek Gneiss, eastern Blue Ridge, North Carolina-Georgia: Evidence for the missing Taconic arc?: *Southeastern Geology*, v. 41, p. 103-117.
- Milici, R.C., 2005, Assessment of undiscovered natural gas resources in Devonian black shales, Appalachian basin, eastern U.S.A.: U.S. Geological Survey Open-File Report 2005-1268.
- Miller, C.F., Hatcher, R.D., Jr., Ayers, J.C., Coath, C.D., and Harrison, T.M., 2000, Age and zircon inheritance of eastern Blue Ridge plutons, southwestern North Carolina and northeastern Georgia, with implications for magma history and evolution of the southern Appalachian orogen: *American Journal of Science*, v. 300, p. 142-172.
- Mirante, D.C., and Patiño-Douce, A.E., 2000, Melting and migmatization in the southern Appalachian Inner Piedmont of northeast Georgia; the Athens gneiss: *Geological Society of America Abstracts with Programs*, v. 33, no. 7, p. 297.
- Misra, K.C., and McSween, H.Y., Jr., 1984, Mafic rocks of the southern Appalachians: A review: *American Journal of Science*, v. 284, p. 294-318.

- Mittwede, S.K., 1989, The Hammett Grove meta-igneous suite; A possible ophiolite in the northwestern South Carolina Piedmont: Boulder, Colorado, Geological Society of America Special Paper 231, p. 45-62.
- Mittwede, S.K., Ødegård, M., and Sharp, W.E., 1987, Major chemical characteristics of the Hammett Grove meta-igneous suite, northwestern South Carolina: *Southeastern Geology*, v. 28, p. 49-63.
- Moecher, D., Hietpas, J., Samson, S., and Chakraborty, S., 2011, Insights into southern Appalachian tectonics from ages of detrital monazite and zircon in modern alluvium: *Geosphere*, v. 7, p. 494-512.
- Mueller, P., Heatherington, A., Foster, D., and Wooden, J., 2011, Alleghanian granites of the southern Appalachian orogen: Keys to Pangean reconstructions, *in* Huebner, M.T., and Hatcher, R.D., Jr., eds., *The Geology of the Inner Piedmont at the Northeast End of the Pine Mountain Window: Carrollton, Georgia Geological Society, 46th Annual Field Trip Guidebook*, p. 39-47.
- Nelson, A.E., Horton, J.W., Jr., and Clarke, J.W., 1998, Geologic map of the Greenville 1-degree x 2-degree quadrangle, Georgia, South Carolina and North Carolina: U.S. Geological Survey Map I-1275, scale 1:250,000.
- Neumann, E.R., Larsen, B.T., and Sundvoll, B., 1985, Compositional variations among gabbroic intrusions in the Oslo rift: *Lithos*, v. 18, p. 35-39.
- Neumann, E.R., Olsen, K.H., Baldrige, W.S., and Sundvoll, B., 1992, The Oslo Rift: A review: *Tectonophysics*, v. 208, p. 1-18.
- Noble, L.F., 1993, Investigation of layering in the Rock Hill gabbro pluton, South Carolina [M.S. thesis]: Knoxville, University of Tennessee, 109 p.
- Noel, J.R., Spariosu, D.J., and Dallmeyer, R.D., 1988, Paleomagnetism and $^{40}\text{Ar}/^{39}\text{Ar}$ ages from the Carolina slate belt, Albermarle, North Carolina: Implications for terrane amalgamation with North America: *Geology*, v. 16, p. 64-68.
- Offield, T.W., 1995, Structural contrasts of the Carolina slate belt and Charlotte belt in South Carolina: *South Carolina Geology*, v. 38, p. 61-70.
- Offield, T.W., Kunk, M.J., Koeppen, R.P., 1995, Style and age of deformation, Carolina slate belt, central North Carolina: *Southeastern Geology*, v. 35, p. 59-77.
- Olsen, B.A., McSween, H.Y., Jr., and Sando, T.W., 1983, Petrogenesis of the Concord gabbro-syenite complex, North Carolina: *American Mineralogist*, v. 68, p. 315-333.
- Parrish, C.B., 2013, Insights into the Appalachian Basin Middle Devonian depositional system from U-Pb zircon geochronology of volcanic ashes in the Marcellus shale and Onondaga limestone [M.S. thesis]: Morgantown, University of West Virginia, 148 p.

- Parrish, C., Toro, J., Hayward, J., Weislogel, A., and Wooden, J., 2013, U-Pb zircon geochronology from volcanic ash layers within Marcellus Formation, Appalachian basin: Understanding basin evolution during the Middle Devonian, Geological Society of America Abstracts with Programs, v. 44, p. 139.
- Pearce, J.A., 1982, Trace element characteristics of lavas from destructive plate boundaries, *in* Thorpe, R.S., ed., *Andesites*: New York, John Wiley and Sons, 525-548.
- Pearce, J.A., 1983, Role of the sub-continental lithosphere in magma genesis at active continental margins, *in* Hawkesworth, C.J., and Norry, M.J., eds., *Continental Basalts and Mantle Xenoliths*: Cheshire, Shiva Publishing Limited, p. 230-249.
- Pearce, J.A., 2008, Geochemical fingerprinting of oceanic basalts with applications to ophiolite classification and the search for Archean oceanic crust: *Lithos*, v. 100, p. 14-48.
- Pearce, J.A., and Cann, J.R., 1973, Tectonic setting of basic volcanic rocks determined using trace element analyses: *Earth and Planetary Science Letters*, v. 19, p. 290-300.
- Pearce, J.A., and Norry, M.J., 1979, Petrogenetic implications of Ti, Zr, Y, and Nb variations in volcanic rocks: *Contributions to Mineralogy and Petrology*, v. 69, p. 33-47.
- Privett, D.R., 1984, The Turnersburg intrusive: Petrogenesis of a metamorphosed Alpine ultramafite in the eastern Inner Piedmont Iredell County, North Carolina: *Southeastern Geology*, v. 25, p. 55-60.
- Quinlan, G.M., and Beaumont, C., 1984, Appalachian thrusting, lithospheric flexure, and the Paleozoic stratigraphy of the eastern interior of North America: *Canadian Journal of Earth Science*, v. 21, p. 973-996.
- Rankin, D.W., 1970, Stratigraphy and structure of Precambrian rocks in northwestern North Carolina, *in* Fisher, G.W., Pettijohn, F.J., Reed, J.C., Jr., and Weaver, K.N., eds., *Studies of Appalachian Geology: Central and Southern*: John Wiley and Sons, Inc., 460 p.
- Robinson, P., Tucker, R.D., Bradley, D., Berry, H.N., IV, and Osberg, P.H., 1998, Paleozoic orogens in New England, USA: *Geologiska Föreningens Stockholm i Förhandlingar*, v. 120, p. 119-148.
- Roden, M.K., Parrish, R.R., and Miller, D.S., 1990, The absolute age of the Eifelian Tioga ash bed, Pennsylvania: *Journal of Geology*, v. 98, p. 282-285.
- Rollinson, H. R., 1993, *Using geochemical data: Evaluation, presentation, and interpretation*: John Wiley and Sons, Inc., 352 p.
- Samson, S.D., 2001, Timing of Alleghanian magmatism revisited: Geological Society of America Abstracts with Programs, v. 33, no. 2, p. 7.
- Samson, S.D., and Secor, D., 2000, New U-Pb geochronological evidence for a Silurian magmatic event in central South Carolina: Geological Society of America Abstracts with Programs, v. 32, no. 2, p. A71.

- Samson, S.D., Patchett, P.J., Roddick, J.C., and Parrish, R.R., 1989, Origin and tectonic setting of Ordovician bentonites in North America: Isotopic and age constraints: *Geological Society of America Bulletin*, v. 101, p. 1175-1181.
- Searle, M.P., Windley, B.F., Coward, M.P., Cooper, D.J.W., Rex, A.J., Rex, D., Tingdong, L., Xuchang, X., Jan, M.Q., Thakur, V.C., and Kumar, S., 1987, The closing of Tethys and the tectonics of the Himalaya: *Geological Society of America Bulletin*, v. 98, p. 678-701.
- Secor, D.T., Jr., Peck, L.S., Pitcher, D.M., Prowell, D.C., Simpson, D.H., Smith, W.A., and Snoke, A.W., 1982, Geology of the area of induced seismic activity at Monticello Reservoir, South Carolina: *Journal of Geophysical Research*, v. 87, p. 6945-6957.
- Secor, D.T., Samson, S.L., Snoke, A.W., and Palmer, A.R., 2003, Confirmation of the Carolina slate belt as an exotic terrane: *Science*, v. 221, p. 649-651.
- Secor, D. T., Jr., Snoke, A. W., and Dallmeyer, R. D., 1986, Character of the Alleghanian orogeny in the southern Appalachians: Part III. Regional Tectonics: *Geological Society of America Bulletin*, v. 97, p. 1345-1353.
- Sinha, A.K., and Zietz, I., 1982, Geophysical and geochemical evidence for a Hercynian magmatic arc, Maryland to Georgia: *Geology*, v. 10, p. 593-596.
- Sinha, A.K., Hund, E.A., and Hogan, J.P., 1989, Paleozoic accretionary history of the North American plate margin (central and southern Appalachians): Constraints from the age, origin, and distribution of granitic rocks, *in* Hillhouse, J.W., ed., *Deep Structure and Past Kinematics of Accreted Terranes*: American Geophysical Union Monograph 50, p. 219-238.
- Sinha, A.K., Thomas, W.A., Hatcher, R.D., Jr., and Harrison, T.M., 2012, Geodynamic evolution of the central Appalachian orogen: Geochronology and compositional diversity of magmatism from Ordovician through Devonian: *American Journal of Science*, v. 312, p. 907-966.
- Speer, J.A., and Hoff, K., 1997, Elemental composition of the Alleghanian granitoid plutons of the southern Appalachians, *in* Sinha, A.K., Whalen, J.B., and Hogan, J.P., eds., *The Nature of Magmatism in the Appalachian Orogen*: Boulder, Colorado, Geological Society of America Memoir 191, p. 287-308.
- Stahr, D.W., 2008, Tectonometamorphic Evolution of the Eastern Blue Ridge: Differentiating Multiple Paleozoic Orogenic Pulses in the Glenville and Big Ridge Quadrangles, Southwestern North Carolina [M.S. thesis]: Knoxville, University of Tennessee, 277 p.
- Steltenpohl, M. G., ed., 2005, Southernmost Appalachian terranes, Alabama and Georgia: Tuscaloosa, Alabama Geological Society, Southeastern Section of the Geological Society of America Field Trip Guidebook, 162 p.
- Stromquist, A.A., and Sundelius, H.W., 1975, Interpretive geologic map of the bedrock showing radioactivity, and aeromagnetic map of the Salisbury, Southmont, Rockwell, and Gold Hill

- quadrangles, Rowan and Davidson Counties, North Carolina: U.S. Geological Survey Map I-888, scale 1:48,000.
- Stose, A.J., and Stose, G.W., 1957, Geology and mineral resources of the Gossan Lead district and adjacent areas: Virginia Division of Mineral Resources Bulletin 72, 233 p.
- Streckeisen, A., 1974, Classification and nomenclature of plutonic rocks recommendations of the IUGS subcommission on the systematics of Igneous Rocks: *International Journal of Earth Sciences*, v. 63, no. 2, p. 773-786.
- Streckeisen, A., 1976, Classification and nomenclature of plutonic rocks recommendations of the IUGS subcommission on the systematics of Igneous Rocks: *International Journal of Earth Sciences*, v. 63, no. 2, p. 773-786.
- Sun, S.S., and McDonough, W.F., 1989, Chemical and isotopic systematics of ocean basalts: implications for mantle compositions and processes, *in* Saunders, A.D., and Norry, M.J., eds., *Magmatism in the Ocean Basins*: Boulder, Colorado, Geological Society of America Special Publication 42, p. 313-345.
- Sutter, J.F., Milton, D.J., and Kunk, M.J., 1983, $^{40}\text{Ar}/^{39}\text{Ar}$ age spectrum dating of gabbro plutons and surrounding rocks in the Charlotte belt of North Carolina: *Geological Society of America Abstracts with Programs*, v. 15, no. 2, p. 110.
- Troyer, P.K., 1991, Geology of the Rock Eagle complex, central Georgia [M.S. thesis]: Tampa, University of South Florida, 59 p.
- Tull, J.F., 1978, Structural development of the Alabama Piedmont northwest of the Brevard zone: *American Journal of Science*, v. 278, p. 442-460.
- van Staal, C.R., and Zagorevski, A., 2012, Accreted terranes of the Appalachian orogen in Newfoundland: In the footsteps of Hank Williams: Geological Association of Canada – Mineralogical Association of Canada Joint Annual Meeting Field Trip Guidebook, 97 p.
- van Staal, C.R., Dewey, J.F., Mac Niocaill, C., and McKerrow, W.S., 1998, The Cambrian-Silurian tectonic evolution of the northern Appalachians and British Caledonides: History of a complex, west and southwest Pacific-type segment of Iapetus, *in* Blundell, D.J., and Scott, A.C., eds., *Lyell: The Past is the Key to the Present*: Geological Society of London Special Publication 143, p. 199-242.
- van Staal, C.R., Currie, K.L., Rowbotham, G., Goodfellow, W., and Rogers, N., 2008, Pressure-temperature paths and exhumation of Late Ordovician-Early Silurian blueschists and associated metamorphic nappes of the Salinic Brunswick subduction complex, northern Appalachians: *Geological Society of America Bulletin*, v. 120, p. 1455-1477.
- Vauchez, A., Babaie, H.A., and Babaei, A., 1993, Orogen-parallel tangential motion in the Late Devonian-Early Carboniferous southern Appalachians internides: *Canadian Journal of Earth Sciences*, v. 30, p. 1297-1305.

- Ver Straeten, C.A., 2010, Lessons from the foreland basin: Northern Appalachian basin perspectives on the Acadian orogeny, *in* Tollo, R.P., Bartholomew, M.J., Hibbard, J.P., and Karabinos, P.M., eds., *From Rodinia to Pangea: The Lithotectonic Record of the Appalachian Region*: Boulder, Colorado, Geological Society of America Memoir 206, p. 251-282.
- Vick, H.K., Channell, J.E.T., and Opdyke, N.D., 1987, Ordovician docking of the Carolina slate belt: Paleomagnetic data: *Tectonics*, v. 6, p. 573-583.
- Vinson, S., 1999, Ion probe geochronology of granitoid gneisses of the Inner Piedmont, North Carolina and South Carolina [M.S. thesis]: Nashville, Vanderbilt University, 84 p.
- Vroon, P.Z., van Bergen, M.J., White, W.M., and Varekamp, J.C., 1993, Sr-Nd-Pb isotope systematics of the Banda Arc, Indonesia: Combined subduction and assimilation of continental material: *Journal of Geophysical Research*, v. 98, p. 22349-22366.
- Whitford, D.J., and Jezek, P.A., 1982, Isotopic constraints on the role of subducted sialic material in Indonesian island-arc magmatism: *Geological Society of America Bulletin*, v. 93, p. 504-513.
- Williams, R.T., and McSween, H.Y., Jr., 1989, Geometry of the Concord, North Carolina, intrusive complex: A synthesis of potential field modeling and petrologic data: *Geology*, v. 17, p. 42-45.
- Wilson, C. G., 2006, Origin and tectonic evolution of the southern Appalachian Neoacadian crystalline core: Evidence from the geology of the Gilreath 7.5-minute quadrangle, North Carolina [M.S. thesis]: Knoxville, University of Tennessee, 200 p.
- Wood, D.A., 1980, The application of a Th-Hf-Ta diagram to problems of tectonomagmatic classification and to establishing the nature of crustal contamination of basaltic lavas of the British Tertiary volcanic province: *Earth and Planetary Science Letters*, v. 50, p. 11-30.
- Wortman, G.L., Samson, S.D., and Hibbard, J.P., 1998, Precise timing constraints on the kinematic development of the Hyco shear zone: Implications for the central Piedmont shear zone, southern Appalachian orogen: *American Journal of Science*, v. 298, p. 108-130.

Chapter IV

Polyphase reactivation history of the Towaliga fault, central Georgia: Implications regarding the amalgamation and breakup of Pangea

This chapter was published in the January 2013 volume of the *Journal of Geology*. The full citation is:

Huebner, M.T., and Hatcher, R.D., Jr., 2013, Polyphase reactivation history of the Towaliga fault, central Georgia: Implications regarding the amalgamation and breakup of Pangea: *Journal of Geology*, v. 121, p. 75-90.

My contributions to this manuscript include the majority of the writing, data collection, and structural analysis. The use of the term “we” and “our” in the text refers to the coauthor and myself.

ABSTRACT

The Towaliga fault, southern Appalachians, contains fault rocks that formed under various P-T conditions, revealing a complex reactivation history. It trends 070 along the northwest flank of the Pine Mountain window, changes to 035 at the northeast end of the window, and continues northeastward into the Inner Piedmont. Isolated, km-scale rhomboidal pods of silicified cataclasite along the Towaliga fault likely represent ancient dilational step-overs, which acted as conduits for hydrothermal fluid flow during faulting, and consequently, are sites of concentrated mineralization. Towaliga fault garnet-grade mylonite formed during large-displacement Alleghanian (~295 Ma) dextral strike-slip, while geometric and kinematic evidence suggest dilational step-overs formed in a small-displacement sinistral strike-slip system. Mutually overprinting crosscutting relationships with Mesozoic diabase dikes confirm cataclasis occurred ~200 Ma. Silicified dilational step-overs are present along both fault orientations, although the absence of step-overs at the bend in the fault suggests two separate brittle faults reactivated discrete segments of the preexisting ductile fault. Ribbon quartz mylonite (~400° C) is found locally along the Towaliga fault, but is also widespread through this part of the Piedmont. This mylonite occurs along other brittle faults in the region, and brittle fabrics exclusively overprint plastic deformation where the two fabrics occur together. Formation during the late Alleghanian or early stages of Mesozoic rifting is indicated, although precise timing is not well delimited. This phase of deformation may provide insight regarding the character of the final amalgamation or early stages of Pangea breakup in the southern Appalachians. Recognition of the rhomboidal pods as dilational step-overs resolves confusion concerning timing and kinematics of Towaliga fault brittle deformation, and has wider implications regarding the state of stress during initial stages of continental drift.

INTRODUCTION

Brittle strike-slip fault systems in the shallow crust frequently consist of numerous discrete, en echelon segments linked by step-overs, which are scale independent, mostly dilational, and commonly produce rhomboidal structures (e.g., Segall and Pollard, 1980; Bahat, 1983; Aydin and Nur, 1985; Sibson, 1987). Dilational step-overs in active fault systems are concentrated sites of earthquake swarms and aftershocks (Hill, 1977; Segall and Pollard, 1980). Based on fault plane solutions from the vicinity of dilational step-overs, Hill (1977) proposed a fault-fracture mesh of interlinked shear and extension fractures occupies these sites (Fig. 4-1). Moreover, the propagation of earthquake ruptures is commonly impeded at these locations, which Sibson (1985) attributed to a suctional force (F_s) produced by an immediately imposed pore fluid pressure gradient that results from rapid opening of extension fractures within the fault-fracture mesh in fluid-saturated crust during fault slip. F_s can easily exceed wall-rock tensile strength, yielding angular, non-attrition hydraulic implosion breccias cemented by hydrothermal precipitates (Phillips, 1972; Sibson, 1985). The induced structural permeability within the fault-fracture mesh provides conduits for hydrothermal fluid transport and, in combination with the forced fluid pressure gradient, results in concentrated mineralization (e.g., Mitcham, 1974; Sibson, 1987, 1996). Large displacement along hosting faults is not necessary to precipitate appreciable mineral deposits (Sibson, 1996).

Numerous isolated, km-scale rhomboidal to sub-rhomboidal or elongate ridges of silicified cataclasite along the length of the Towaliga fault (Fig. 4-2-4-4) may represent ancient dilational step-overs. These occur in addition to garnet-grade mylonite and chlorite-muscovite-grade ribbon quartz mylonite. As such, a range of interpretations has been proposed regarding the spatial and

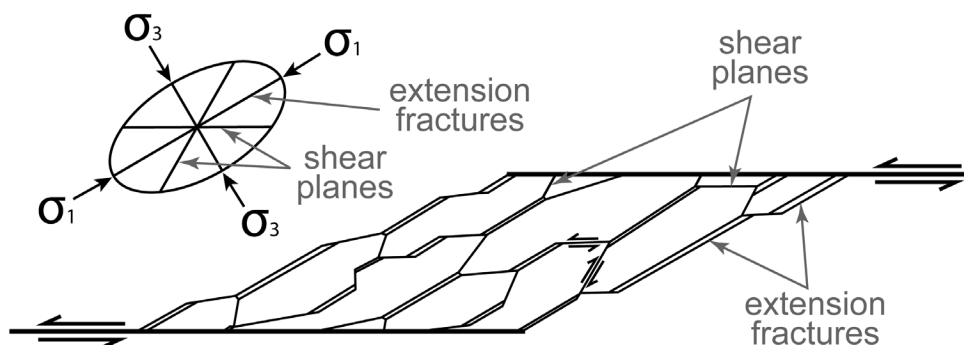


Figure 4-1: Idealized fault-fracture mesh of linked shear and extension fractures occupying a dilational step-over (from Sibson, 1985) with corresponding stress ellipse. Orientations within the fault-fracture mesh should be consistent with stresses imposed on the main fault, i.e., extension veins should form parallel to σ_1 .

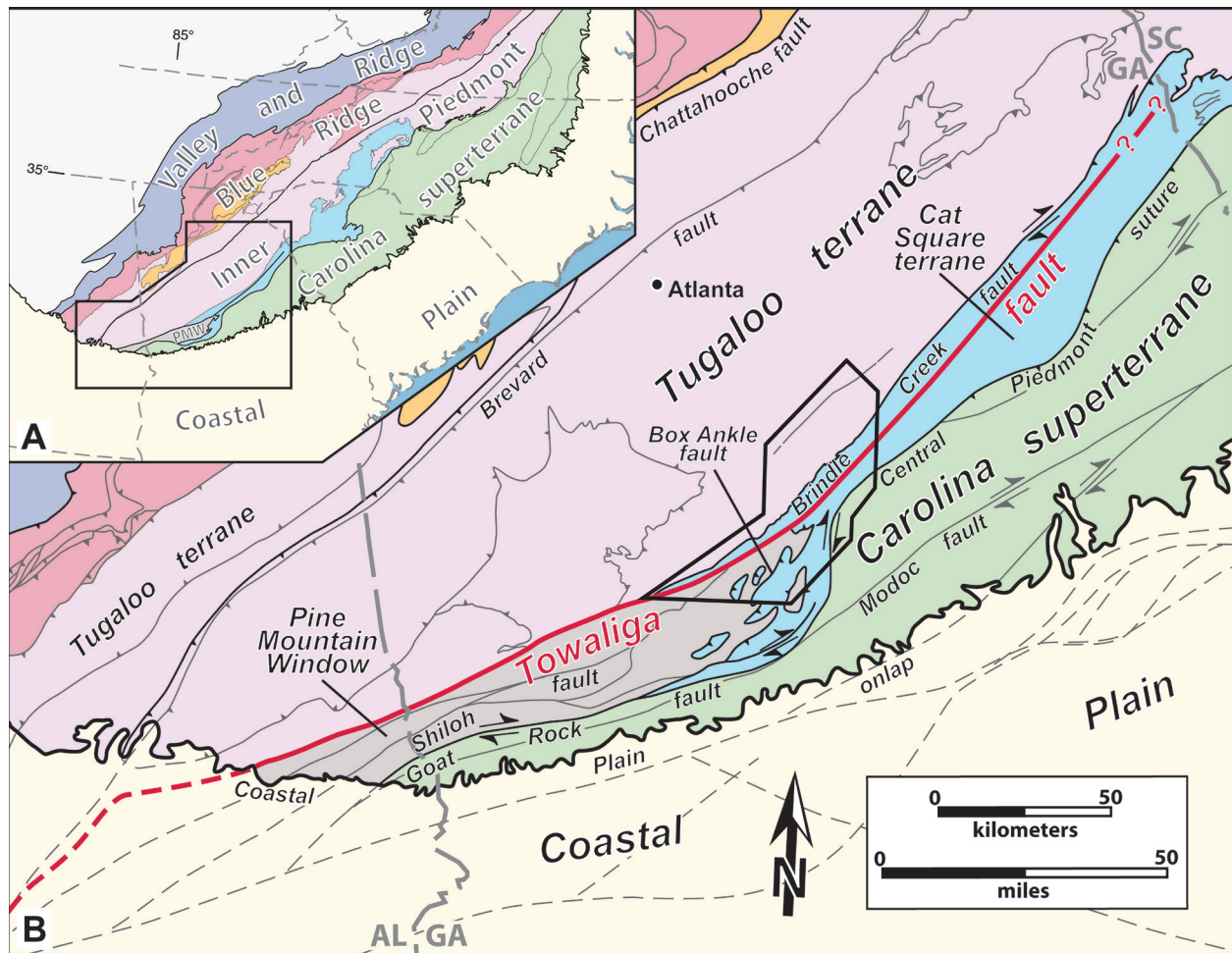


Figure 4-2: (A) Index map of the southern Appalachian orogen illustrating the location of the Inner Piedmont and major physiographic subdivisions. PMW – Pine Mountain window. (B) Simplified lithotectonic map (modified from Hatcher et al., 2007) showing the geographic extent of the Towaliga fault. Location of study area at the northeast end of the Pine Mountain window is outlined (shown in greater detail in Figure 5-3).

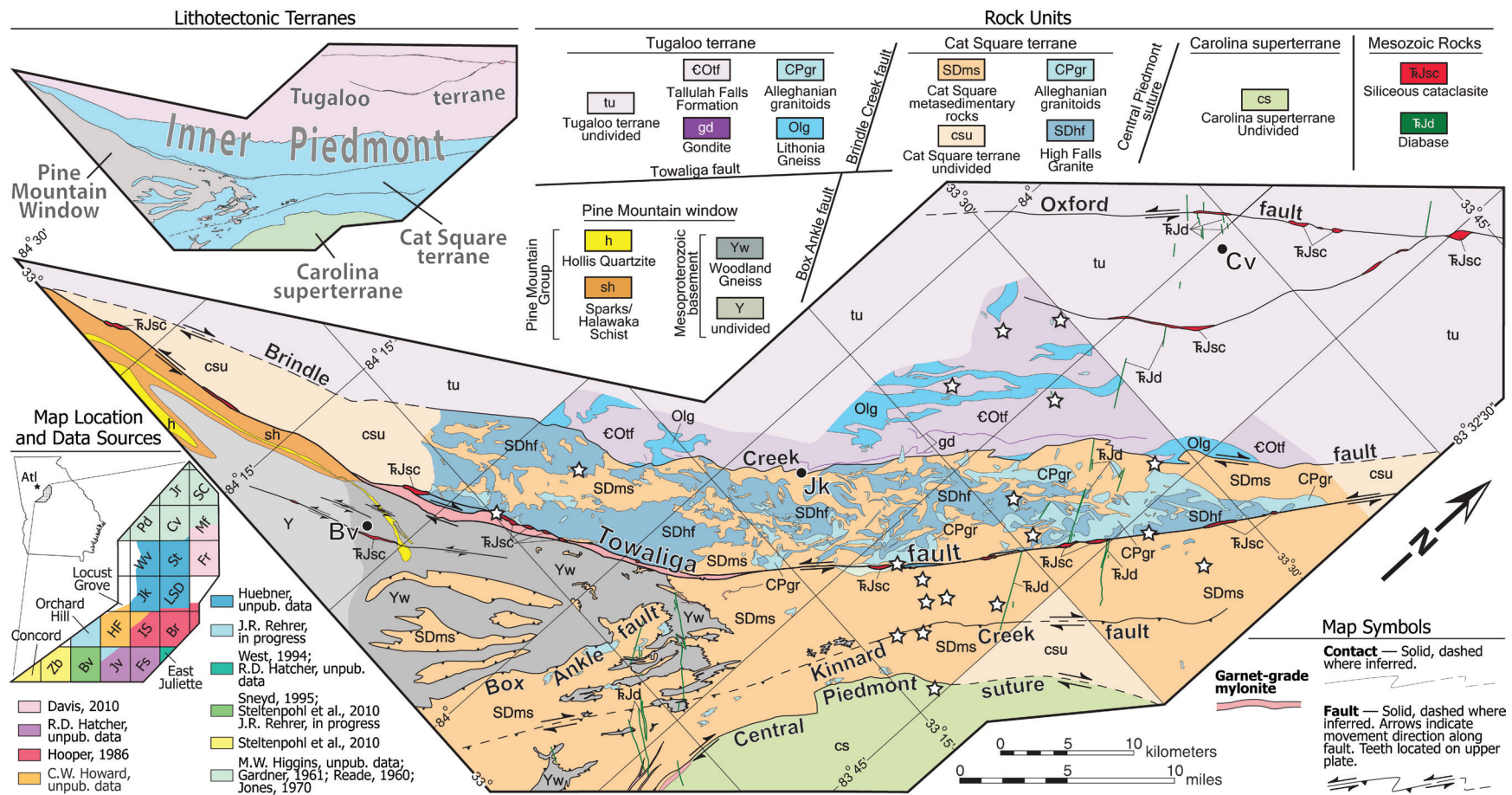


Figure 4-3: Simplified geologic map of the study area at the northeast end of the Pine Mountain window. Locations of ribbon quartz mylonite denoted by white stars. Note the conspicuous truncation of Paleozoic Inner Piedmont granitoids along the Towaliga fault. Cities: Bv – Barnesville; Cv – Covington; Jk – Jackson. 7.5-minute quadrangles: Br – Berner; Bv – Barnesville; Cv – Covington; Fr – Farrar; Fs – Forsyth; HF – High Falls; IS – Indian Springs; Jk – Jackson; Jr – Jersey; Jv – Johnstonville; LSD – Lloyd Shoals Dam; Mf – Mansfield; Pd – Porterdale; SC – Social Circle; St – Stewart; Wv – Worthville; Zb – Zebulon.

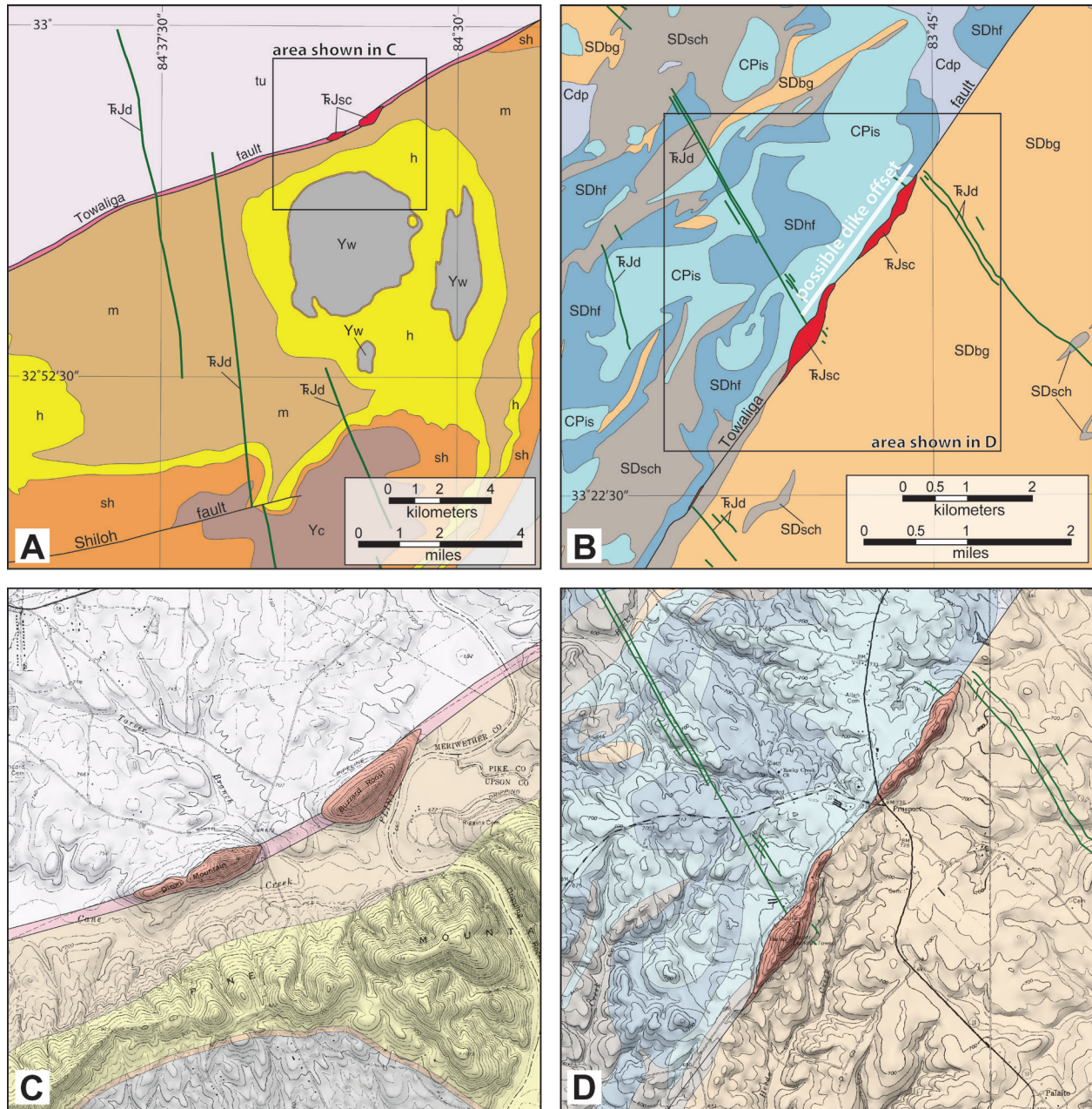


Figure 4-4: Mutually overprinting crosscutting relationships between silicified faults and CAMP diabase dikes. Diabase dikes cut the Towaliga fault (A; Woodbury 7.5-minute quadrangle) and are truncated and possibly offset by the Towaliga fault (B; Stewart 7.5-minute quadrangle). Note the offset of the diabase dikes that cut the Towaliga fault by the Shiloh fault. (C-D) Detailed geologic maps with transparent slope-shaded digital elevation models illustrating the rhomboidal nature of isolated siliceous cataclasite pods along the Towaliga fault, locations shown in (A) and (B), respectively. The Woodbury 7.5-minute quadrangle is not included in Fig. 4-3. Geologic map shown in (A) and (C) modified from Hewitt and Crickmay (1937).

temporal relationships between fault rocks, in addition to the kinematic history of the Towaliga fault. Recent detailed geologic mapping at the northeast end of the Pine Mountain window (Fig. 4-3) has provided crucial insight into the temporal and kinematic history of the Towaliga fault, and may have important implications regarding the assembly and breakup of Earth's most recent supercontinent.

GEOLOGIC SETTING

The Towaliga fault is one of the largest faults in the southern Appalachian Piedmont (Fig. 4-2). It emerges from beneath the Coastal Plain in Alabama trending ~070 as it frames the northwest side of the Pine Mountain window and suspect terrane (Steltenpohl et al., 2004), changes to ~035 at the northeast end of the window, and continues northeast along that trend through the Inner Piedmont, possibly to the Georgia–South Carolina border. The Pine Mountain window likely represents an allochthonous block of Laurentian basement plucked from the distal margin and thrust onto the platform prior to or early in the Alleghanian orogeny (Hooper and Hatcher, 1988a; McBride et al., 2005). The interior of the Pine Mountain window consists of continental basement gneisses unconformably overlain by the Pine Mountain group, a metamorphosed cover sequence of Neoproterozoic-Cambrian(?) siliciclastics and carbonates (Steltenpohl et al., 2010). Alleghanian ductile faults of different ages frame the Pine Mountain window, indicated by cross-cutting relationships and contrasting rheologic and P-T conditions during deformation (Hooper and Hatcher, 1988a).

Interpretation of COCORP seismic reflection data led to the hypothesis that the Towaliga fault is a northwest-dipping normal fault with 7-9 km of late Alleghanian or Mesozoic displacement (Nelson et al., 1985, 1987; Steltenpohl et al., 2010), but McBride et al. (2005) suggested a more conservative normal displacement of < 200 m after reprocessing the same COCORP data. Steltenpohl (1988) and Hooper and Hatcher (1988b) concluded the Towaliga fault is an Alleghanian dextral strike-slip fault with a minor normal component.

The Mesozoic breakup of Pangea in the southern Appalachians spans ~30 m.y., with evidence recording extension, basin filling, deformation and magmatism occurring from the Middle Triassic to the earliest Jurassic (e.g., Manspeizer, 1988; Olsen, 1997; Withjack et al., 1998; McHone, 2000). Northeast-southwest-trending rift basins received sediment from Middle Late Triassic times, followed by a brief period of basin inversion, reverse-sense reactivation of preexisting border faults, and deformation of basin deposits in the latest Triassic during the rift-to-drift transition (Withjack et al., 1998; Schlische et al., 2003). Undeformed diabase dikes cut these structures, and confirm northwest-southeast-directed shortening had ended by the earliest Jurassic (Withjack et al., 1998; McHone, 2000; Schlische et al., 2003).

Diabase dikes along the Atlantic margins of both Americas and Africa (the Central Atlantic Magmatic Province [CAMP]) yield tight, clustered ages 202-198 Ma (Hames et al., 2000). Although collective dike emplacement likely occurred over a few m.y. (Hames et al., 2000) or possibly less time (Nomade et al., 2007), emplacement of individual dikes was likely instantaneous (Huebner and Hatcher, 2011). Diabase dikes share mutually overprinting crosscutting relationships with numerous small-displacement faults filled with silicified cataclasite across the southern Appalachian orogen (Fig. 4-5), indicating overall coeval emplacement over the duration of CAMP magmatism (Garihan et al., 1993; Hatcher, 2006). However, it is difficult to apply a single strain ellipse to include the orientation of diabase dikes (assumed YZ plane as mode I fractures) and siliceous cataclasite faults (shear planes). Diabase dike orientations mostly trend northwest (290-345) in the southern Appalachians, rotating to a more northerly and northeast trend in the central Appalachians (Fig. 4-5). A narrow north-south-trending fanned swarm also occurs in the Carolinas, although the age of these dikes is indistinguishable from the more abundant northwest-trending set (Beutal et al., 2005). Siliceous cataclasite orientations also vary across the orogen, and generally occur in groups trending 050-070, 015-020, 305-325, and E-W (Garihan et al., 1993; Hatcher, unpublished data).

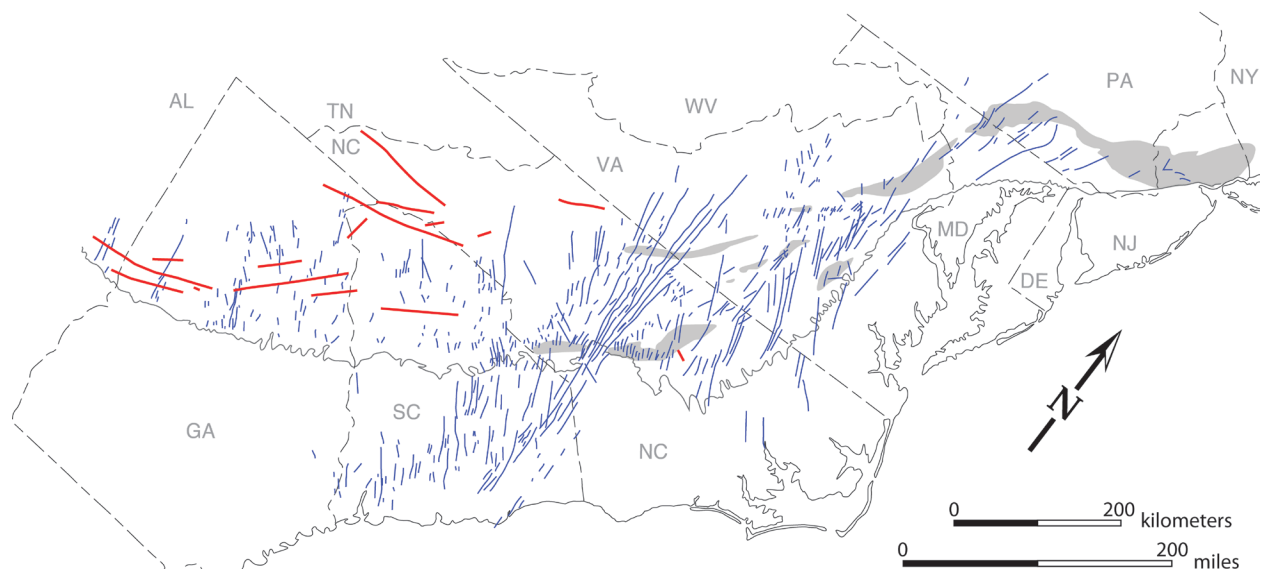


Figure 4-5: Distribution of CAMP diabase dikes (thin blue lines) and silicified cataclasites (heavy red lines) of the southern Appalachian orogen (modified from Hatcher, 1995). Dark shaded areas represent exposed Triassic rift basins.

BRITTLE AND DUCTILE FAULT ROCKS OF THE TOWALIGA FAULT ZONE

Towaliga fault garnet-grade proto- to ultramylonite protoliths include Paleozoic granitoids, Mesoproterozoic basement, and metasedimentary rocks from both the Inner Piedmont and Pine Mountain window in a zone that ranges from 10 m to 5 km wide (Steltenpohl et al., 2010). Shear-sense indicators include asymmetric σ , δ , and θ porphyroclasts, strongly developed S-C fabric, and asymmetric folds, all of which indicate dominantly dextral shear (Hooper and Hatcher, 1988b; present study). The mylonite zone dips steeply northwest with moderate- to shallow-plunging mineral stretching lineations, indicating primarily dextral strike-slip (Hooper and Hatcher, 1988b; Steltenpohl, 1988). An absolute age of ~ 295 Ma was determined for the Towaliga fault based on a whole-rock Rb-Sr isochron on the Farmville (AL) metagranite, which exhibits retrograde fabrics identical to those in the Alabama segment of the Towaliga fault zone (Goldberg and Steltenpohl, 1988). This age agrees with the truncation of the sillimanite-grade Box Ankle thrust fault (~ 303 Ma; Student and Sinha, 1992) and Alleghanian Inner Piedmont granitoids (325-299 Ma; Huebner et al., 2011) by the Towaliga fault. High-temperature Towaliga fault mylonite zones can be separated from brittle fault rocks by as much as 300 m, and are locally excised altogether by brittle faulting.

Brittle fault rocks along the Towaliga fault occur as banded cataclasite and attrition breccia (Hadizadeh et al., 1991; present study), although the most prominent features are isolated map-scale rhomboidal to sub-rhomboidal ridges of silicified breccia and cataclasite dispersed along the length of the Towaliga fault (Fig. 4-4). These rhomboidal pods are almost exclusively composed of hydrothermally precipitated quartz, and locally exhibit positive topographic relief in excess of 40 m. Northwest dip is inferred from slight asymmetry of the ridges. Rock fabrics within cataclasite pods range from massive, undeformed vein quartz to intensely brecciated quartz vein fill (Fig. 4-6). Veins mostly range from 1-2 mm to ~ 10 cm thick, and the multiple crosscutting nature of veins confirms numerous episodes of brittle deformation (Fig. 4-6). Abundant euhedral to subhedral quartz crystals grew normal to vein walls, resulting in a vuggy, “boxwork” texture evident throughout cataclasite pods. High-dilation wall-rock breccias are relatively less abundant, and reveal little evidence of attrition with low clast-matrix ratios (Fig. 4-6C). Brittle quartz fabric suggests deformation occurred $< 300^\circ\text{C}$, and Babaie et al. (1991) estimated Towaliga fault siliceous cataclasite formed at depths of 8-14 km based on fluid inclusion analysis of silicified veins. Towaliga fault siliceous cataclasite shares similar textural and compositional characteristics with Mesozoic cataclasite throughout the southern Appalachians and elsewhere in the orogen (e.g., Flint Hill fault zone, New Hampshire, Robinson, 1989; Lantern Hill fault, Connecticut, Altamura, 2001).

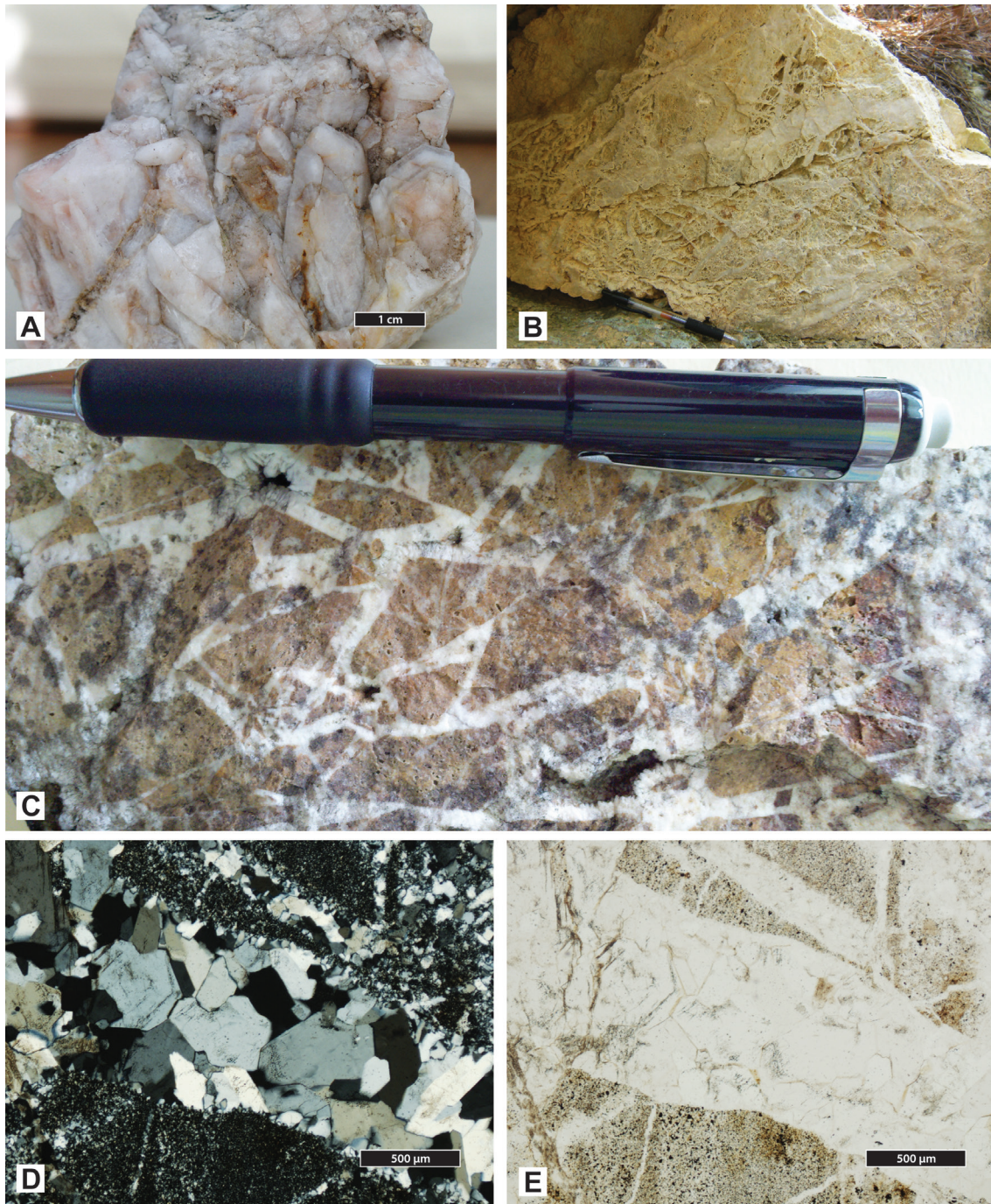


Figure 4-6: Brittle fault rocks from rhomboidal pods along the Towaliga fault. (A) Characteristic “boxwork” texture with euhedral quartz crystals growing normal to vein walls. Note the zonation in the crystal on the right side of the sample. (B) Intensely brecciated silicified cataclasite from rhomb-shaped ridge near Stewart, GA; pen for scale. Younger veins cut preexisting extension veins, indicating multiple episodes of deformation. (C) Implosion breccia from Buzzard Mountain near Concord, GA; pencil for scale (courtesy of C. Snyder). Note the lack of attrition of wall-rock clasts and common vug texture. (D) Cross-polar (XPL) and (E) plane-polarized (PPL) images of breccia shown in (C).

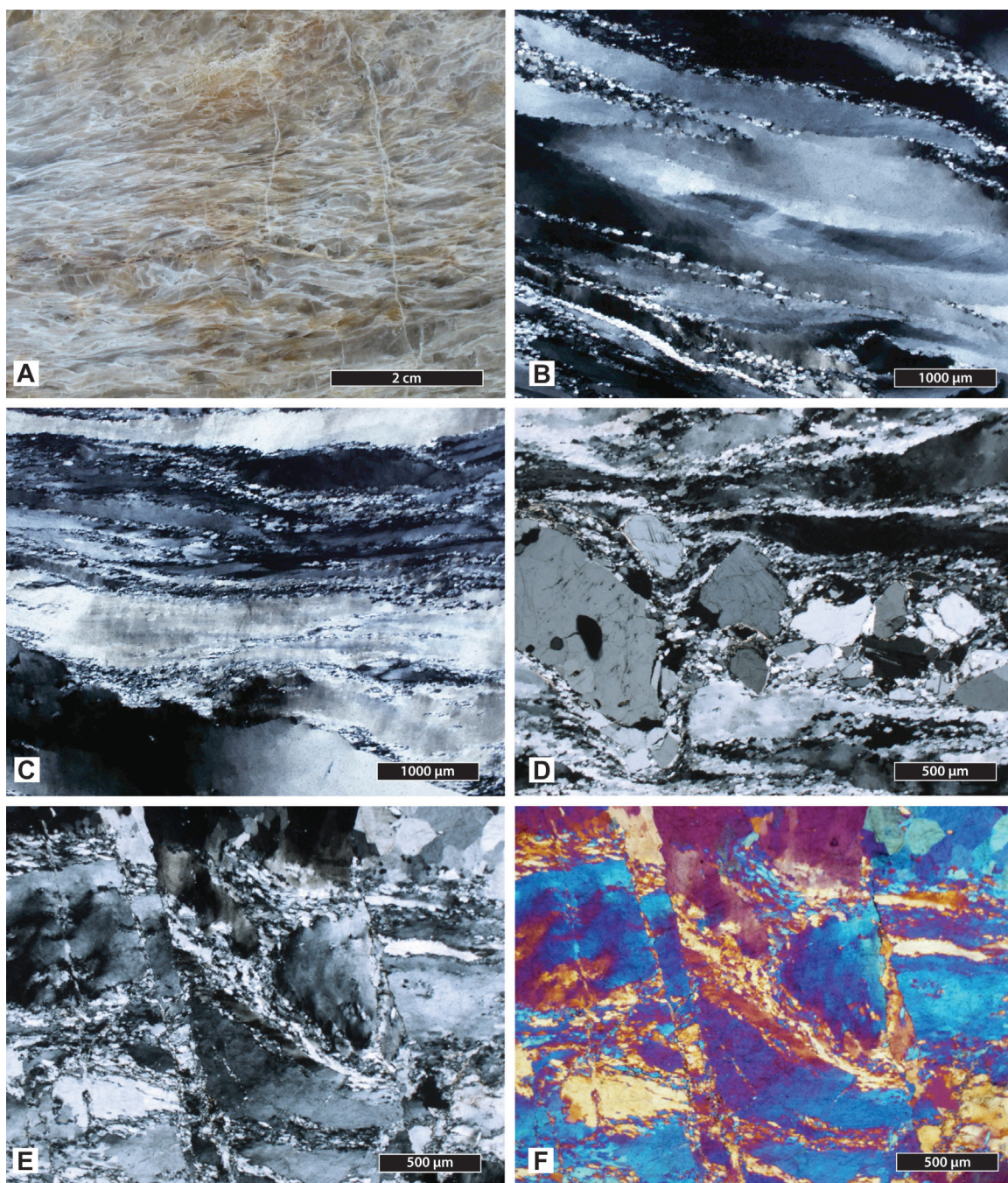


Figure 4-7: (A) Representative hand specimen of ribbon quartz mylonite. (B-D) XPL images of specimen shown in A. Recrystallization is mostly concentrated at ribbon grain boundaries, although recrystallization by subgrain rotation throughout grains is locally prevalent. Note the brittle behavior of alkali feldspar porphyroclasts in D. (E-F) Brecciated ribbon quartz mylonite from the Towaliga fault, (E) XPL and (F) XPL with accessory gypsum plate. Discrete ribbon grains are offset by brittle fractures. All thin sections were cut normal to foliation and parallel to the mineral stretching lineation.

In addition to these end-member fault fabrics, relatively low-temperature (chlorite-muscovite-grade) ribbon quartz mylonite occurs along the Towaliga fault (Fig. 4-7). This mylonite is generally composed of > 95% quartz, with minor alkali feldspar and muscovite porphyroclasts. Elongate quartz ribbons mantled by smaller recrystallized quartz grains characterize this rock, with partial to complete recrystallization of ribbons occurring locally (Fig. 4-7). Development of new grains by subgrain rotation within porphyroclasts frequently occurs, although bulging concentrated at grain boundaries remains a dominant recrystallization mechanism. We interpret these textures to represent deformation that occurred in the lower temperature portion of the zone of subgrain rotation, likely near the transition from bulging recrystallization to subgrain rotation, indicating temperature $\sim 400^{\circ}\text{C}$ (Stipp et al., 2002). Brittle behavior of feldspar porphyroclasts confirms deformation temperatures below the threshold of ductile feldspar flow ($450\text{--}500^{\circ}\text{C}$; Pryer, 1993) (Fig. 4-7). Babaie et al. (1991) acquired a muscovite K-Ar age of $\sim 269\text{ Ma}$ from a brecciated Towaliga fault quartz-ribbon ultramylonite, but dismissed the age as a result of Ar loss or mixing with later muscovite crystallization.

Ribbon quartz mylonite occurs locally along the Towaliga fault, and is also abundant throughout the region in both Laurentian lithotectonic terranes and the Carolina superterrane (Fig. 4-3). The volume of ribbon quartz mylonite, however, is miniscule relative to the volume of quartz veins showing no evidence of shear. In outcrop, most ribbon quartz mylonite occurs as < 15 cm-thick quartz veins concordant with regional foliation that does not appear to be laterally continuous. *In situ* exposures of the mylonite are rare, and we have found none in place along the Towaliga fault. Where present in outcrop, S-C fabric and asymmetric mica fish indicate dextral shear sense. Hadizadeh et al. (1991) reported micaceous quartz mylonite and quartz ultramylonite along the Towaliga fault not associated with cataclasite pods, and deduced dextral shear sense from mylonitic fabric. Previous work on other brittle faults in the region (e.g., Gardner, 1961; Schultz, 1961) reported the occurrence of sheared quartz veins on brittle faults northwest of Covington, Georgia, although none were found in outcrop. Davis (1980) described similar ribbon quartz mylonite associated with the Middleton-Lowndesville fault (Central Piedmont suture) in northeastern Georgia, and also reported exposures only as float.

The nature and significance of the relationship between ribbon quartz mylonite and brittle faults remain unclear, although there is at least some spatial affinity between the two. Where they occur together, we have found that brittle fabric exclusively overprints ductile deformation (Fig. 4-7E-F). Davis (1980) noted the same overprinting relationship, and Babaie et al. (1991) stressed the lack of recrystallization of brittle fabrics from a Towaliga fault silicified cataclasite pod. On the other hand, Hadizadeh et al. (1991) reported sheared microfractures in brecciated mylonite not associated with any cataclasite ridge along the Towaliga fault.

ISOLATED PODS OF SILICEOUS CATACLASITE AS DILATIONAL STEP-OVERS

Gillerman and Sibson (1988) presented three criteria to identify dilational step-overs in ancient fault systems: 1) the master fault should be barren of mineralization; 2) the orientation of extension veins within step-overs should reflect the shear sense of the master fault; and 3) there should be evidence of multiple episodes of deformation within step-overs. Isolated cataclasite pods along the Towaliga fault throughout central Georgia meet these criteria, in addition to other evidence that is consistent with these sites acting as dilational step-overs during faulting.

First, secondary mineralization between cataclasite pods is rare along the trace of the Towaliga fault. Hadizadeh et al. (1991) also reported a paucity of veining or secondary cementation in attrition breccias from a locality not associated with rhomboidal ridges along the Towaliga fault. Regarding the second criterion, Andersonian theory predicts the principal shortening imposed on a strike-slip fault should be horizontal, oriented $\sim 30^\circ$ from the vertical fault surface. Consequently, extension veins within a dilational step-over along this strike-slip fault should be vertical and form parallel to the principal shortening direction (Figs. 4-1, 4-8A). The orientations of silicified veins in a well-exposed rhomb-shaped ridge along the 035-trending segment of the Towaliga fault (Barnes Mountain; Fig. 4-4D) revealed significant scatter with a prominent cluster oriented ~ 005 - 185 , which corresponds to the inferred shortening direction based on fault orientation (Fig. 4-8). Copious evidence of multiple brecciation episodes throughout these pods (Fig. 4-6B) satis-

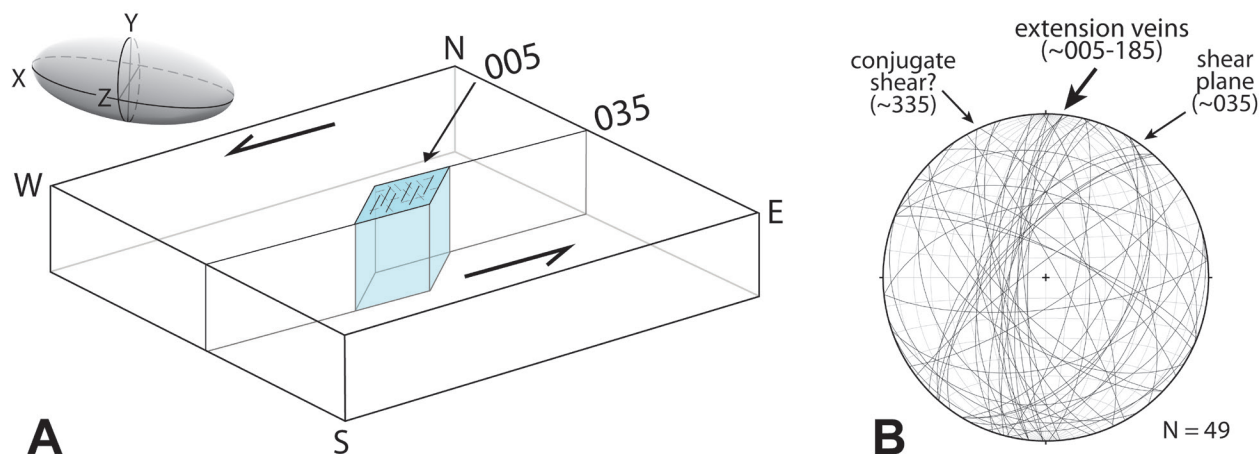


Figure 4-8: (A) Block diagram illustrating dilational step-over at Barnes Mountain (shown in figure 5-4D) along the 035-trending segment of the Towaliga fault with representative strain ellipsoid. Inferred maximum shortening direction based on Andersonian theory would be from ~ 005 . (B) Orientation of (extension?) veins measured at Barnes Mountain. Note the cluster striking ~ 005 - 185 , which corresponds to the interpreted principal shortening direction.

fies the third criterion. Zoning of vein-fill quartz (Fig. 4-6A) is at least indicative of episodic fluid influx, and could also be an indicator of incremental opening of extension veins.

The rhomboidal shape of the pods reflects step-over geometry, and ubiquitous high-dilation rock textures support the interpretation that these pods are dilational features. Additionally, rocks showing evidence of intense argillic alteration occur adjacent to some cataclasite pods (Fig. 4-9), which also indicates an influx of hydrothermal fluid occurred at these localities. Sibson's (1987) dilational step-over model provides a mechanism for concentrated mineralization at these sites along the Towaliga fault that is consistent with rock textures observed in the field. The identification of these isolated ridges as dilational step-overs provides valuable kinematic insight into this episode of faulting in an area where other indicators are difficult to ascertain.

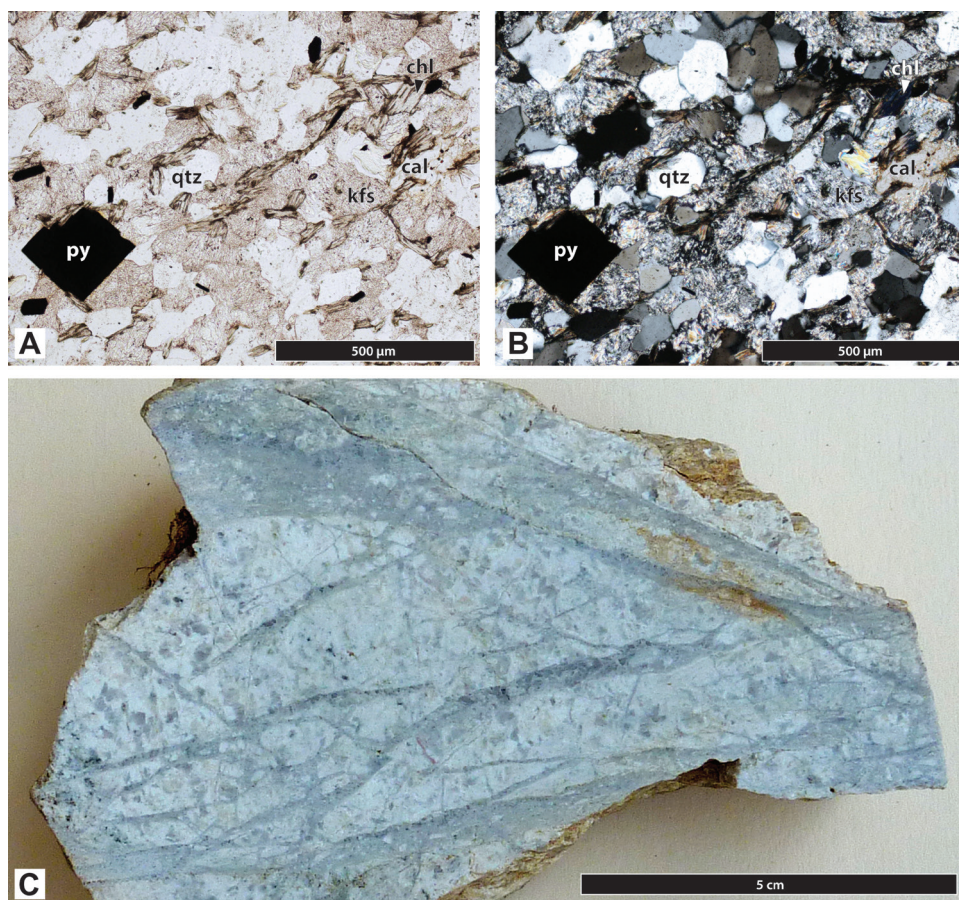


Figure 4-9: (A) PPL and (B) XPL photomicrographs of a hydrothermally altered Inner Piedmont granitoid adjacent to a dilational step-over, ~10 km east of Jackson, Georgia. Note the breakdown of feldspar, chloritization of biotite, and secondary pyrite and calcite. cal – calcite; chl – chlorite; kfs – K feldspar; py – pyrite; qtz – quartz. (C) Hand specimen of brecciated, hydrothermally altered Inner Piedmont granitoid.

DISCUSSION

The geometry of the step-overs, in addition to the dominant orientation of extension veins within cataclasite pods, suggests formation in a sinistral strike-slip system (Fig. 4-8). Cataclasite pods could alternatively be argued to be products of dextral shear involving several small left-stepping en echelon dextral strike-slip faults. However, these pods are not comprised of blocks of country rock separated by closely spaced faults, nor does this mechanism explain the concentrated mineralization, wholesale dilation, or the prominent orientation of extension veins within these structures. Additionally, our observations do not support significant normal displacement occurred during brittle faulting. These data suggest silicified cataclasites were produced during Mesozoic sinistral strike-slip reactivation of the Alleghanian Towaliga fault.

Sinistral strike-slip inverted the dominantly *dextral* strike-slip motion observed in the Alleghanian garnet-grade Towaliga mylonite (and possibly ribbon quartz mylonite), which supports a disparity in timing between formation of ductile and brittle fault rocks. Crosscutting relationships between siliceous cataclasite and ~200 Ma diabase dikes, however, provide the strongest evidence regarding timing of brittle faulting. Dikes cross the trace of the Towaliga fault (Hewett and Crickmay, 1937; present study), but are also truncated and possibly offset by the fault (Fig. 4-4). Abundant evidence of multiple deformation episodes in Towaliga fault cataclasite pods indicates recurrent brittle faulting occurred over a protracted, albeit short, amount of time, which likely overlapped CAMP diabase dike emplacement and formation of other silicified cataclasites across the orogen. Jones (1970) reported the same overprinting crosscutting relationships along the Oxford fault, located ~20 km northwest of the Towaliga fault, which contains similar isolated rhomboidal pods of silicified cataclasite (Fig. 4-3).

The exact nature of the spatial relationship between ductile and brittle fault rocks presents an interesting conundrum. Alleghanian garnet-grade mylonite can be traced through the change in strike at the northeast end of the Pine Mountain window, with silicified cataclasite pods along the 070- and 035-trending segments. Step-overs should be most abundant along a fault where curvature is greatest (Aydin and Nur, 1985), but none occur at the bend in the Towaliga fault. This suggests cataclasite pods along the Towaliga fault are products of separate brittle faults (Hooper, 1989). Brittle faults with similar orientations (035 and 070) occur in this region, but most are not associated with earlier ductile faults (e.g., Oxford fault, small faults near Barnesville, GA; Fig. 4-3). This suggests that Mesozoic brittle failure along the Towaliga fault was not purely a function of propagation along a preexisting weakness; these faults were optimally oriented in terms of the prevailing stress field during deformation. The inheritance of these fault orientations through time is certainly intriguing, considering brittle faulting is not unique to preexisting mylonite zones. The boomerang shape of the garnet-grade Towaliga fault is at least indicative of

progressive heterogeneous simple shear (polyphase Alleghanian deformation), and the bend in the fault at the northeast end of the Pine Mountain window may be a site of inherited mechanical weakness through time.

Based on the crosscutting relationships with diabase dikes along the two separate fault segments (Fig. 4-4), one could construct a temporal scenario in which the 070 segment was active prior to diabase dike emplacement (older), and the 035 segment post-dates dike intrusion (younger). However, this scenario assumes all diabase dikes spatially related to the Towaliga fault were emplaced at exactly the same time. The geochronologic precision necessary to validate this assumption is not currently available; therefore, we maintain Mesozoic reactivation along both segments was roughly coeval. Additionally, dikes that crosscut the Towaliga fault are offset by the Shiloh fault, which occurs farther southwest and shares a similar orientation with the Towaliga fault (Fig. 4-4A).

Abrupt truncation of Paleozoic Inner Piedmont granitoids along the Towaliga fault at the northeast end of the Pine Mountain window (Fig. 4-3) indicates significant displacement has occurred, which we interpret to be a product of ductile Alleghanian deformation. The size of step-overs is generally proportional to displacement on the main fault (Segall and Pollard, 1980; Sibson, 1985), suggesting Mesozoic sinistral displacement along the Towaliga fault was on the order of 1-5 km. This estimate is consistent with the possible 2.5 km offset of a diabase dike set in the study area (Fig. 4-3), although this apparent offset could also be two separate dike sets truncated by the fault. Assuming this is a dike set offset by the Towaliga fault, the temporal overlap between faulting and dike emplacement indicates this represents only minimum displacement.

Steltenpohl et al. (2010) suggested lower-temperature ribbon quartz mylonite zones link isolated pods of siliceous cataclasite along the Towaliga fault, implying coeval formation of the two fabrics. Dynamic recrystallization textures in ribbon quartz mylonite indicate deformation occurred at significantly lower temperatures than the garnet-grade Alleghanian Towaliga mylonite, but at temperatures considerably higher than those inferred from deformation fabrics in silicified cataclasite. Timing of the lower-temperature ribbon quartz mylonite, along with the nature of its relationship with the Towaliga fault, remains unclear. We have found few occurrences of ribbon quartz mylonite along > 60 km of the Towaliga fault and, to date, none have been *in situ*. Assuming an association between ribbon quartz mylonite and the Towaliga fault, scenarios that may satisfy this relationship include: 1) coeval formation of ribbon quartz mylonite and siliceous cataclasite in the ductile regime, with cataclasis resulting from transient elevated strain rates; 2) the present erosion level passing through the ductile-brittle transition during faulting, or; 3) the ribbon quartz mylonite predating cataclasis, forming 3) in the late Alleghanian or 4) during the early stages of Mesozoic rifting (Fig. 4-10). The second through fourth hypotheses are similar in that development of mylonitic fabric precedes brittle deformation, although differ in that the

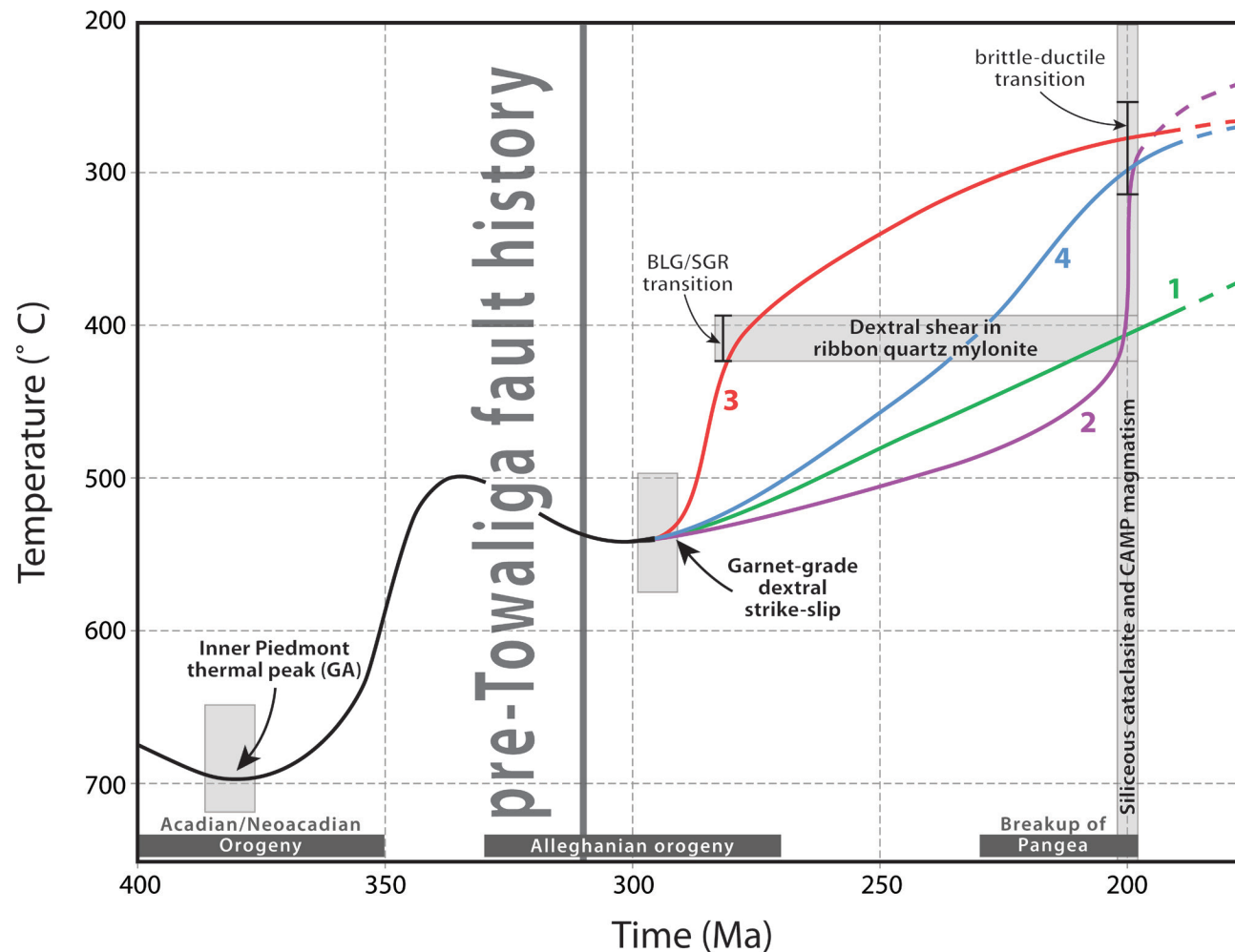


Figure 4-10: Temperature-time curves demonstrating the evolution of the Towaliga fault, illustrating the multiple working hypotheses discussed in text. (1, green line) – coeval formation of siliceous cataclasite and ribbon quartz mylonite at $\sim 400^{\circ}\text{C}$ during CAMP magmatism; (2, purple line) – formation of both fault-rock fabrics during CAMP as the exposed structural level passed through the brittle-ductile transition; (3, red line) – formation of ribbon quartz mylonite during the late Alleghanian; (4, blue line) formation of ribbon quartz mylonite during the early stages of Mesozoic rifting. Temperature ranges of the bulging recrystallization – subgrain rotation transition (BLG/SGR) and brittle-ductile transition from Stipp et al. (2002).

third and fourth scenarios imply two distinct deformation events (Fig. 4-10). Cataclasis occurring at the Triassic-Jurassic boundary is a necessary condition for all hypotheses.

Scenario 1

Evidence of plastically deformed cataclasite should be fairly common if ribbon quartz mylonite and cataclasite formed coevally at $\sim 400^{\circ}$ C. We have not observed this relationship; brittle deformation exclusively overprints mylonitic fabric in our samples, although others (Hadizadeh et al., 1991) have reported evidence of ductile overprinting of brittle fabric. The overall rarity of this relationship strongly argues against both fabrics forming concurrently in the ductile regime. Additionally, opposite shear sense of the two fault rock fabrics would preclude coeval formation altogether, assuming Towaliga fault ribbon quartz mylonite shares similar shear sense with other ribbon quartz mylonite throughout the region.

Scenario 2

An episode of rapid uplift or cooling would be required for the currently exposed structural level to pass through the ductile-brittle transition from $\sim 400^{\circ}$ to $< 300^{\circ}$ C during CAMP magmatism (say, over 2-4 m.y.). Dallmeyer (1978) concluded the Inner Piedmont was mostly exhumed by the opening of Triassic rift basins, in agreement with the occurrence of high-grade metamorphic detritus in basal conglomerates in southern Appalachian Mesozoic rift basins (e.g., Thayer, 1970). Mesozoic rift-related normal faults and basins were inverted prior to CAMP magmatism in the southern Appalachians (e.g., Withjack et al., 1998), which implies crustal thinning associated with rifting had also ceased by this time. Furthermore, opposite shear sense between ribbon quartz mylonite and siliceous cataclasite complicates formation during a single protracted deformational event, but does not refute it. Beutal et al. (2005) suggested a rapidly rotating stress field may have occurred over the time of CAMP emplacement to explain the spread of diabase dike orientations in the southern Appalachians, which is also consistent with the numerous orientations of contemporaneous silicified Mesozoic faults (Fig. 4-5). This may argue that a switch in shear sense during CAMP magmatism is possible.

Scenarios 3 and 4

Nearly ubiquitous brittle overprint of ribbon quartz mylonite and scarcity of the inverse relationship support the second through fourth hypotheses, although scenarios 3 and 4 forgo the problem of opposite shear sense between the ribbon quartz mylonite and cataclasite. Unfortunately, available data do not discriminate between late Alleghanian and early Mesozoic rift-stage formation of ribbon quartz mylonite. The K-Ar age of ~ 269 Ma acquired by Babaie et al. (1991)

supports late Alleghanian deformation, although those authors did not convey confidence in that analysis.

Alternatively, the model of Pangea breakup proposed by Swanson (1982) may be applicable to the occurrence of deformation features in the Georgia Piedmont. Swanson (1982) suggested Pangea breakup occurred via: (1) an early stage of dextral shear; (2) followed by a period of extension, normal faulting, opening of, and deposition in Triassic rift basins; and (3) ending with sinistral shear, deformation of Triassic basins, and diabase dike emplacement. Shearing events were hypothesized to take place over wide arcuate zones parallel to the continental margin as a product of counterclockwise (dextral) and later clockwise (sinistral) rotation of Africa relative to North America. Widespread sheared quartz veins throughout central Georgia could be a product of the proposed dextral shearing event that occurred prior to the main phase of rift basin fill, placing the formation of ribbon quartz mylonite sometime in the Middle Triassic. The Middle through Late Triassic was generally quiescent in this region, as Triassic basins formed more proximal to the continental margin (e.g., Manspeizer, 1988; Olsen, 1997). The rift-to-drift transition has been hypothesized to be marked by a brief period of shortening, deformation, and basin inversion that occurred immediately prior to CAMP magmatism (Withjack et al., 1998; Schlische et al., 2003). Sinistral shearing along numerous small-displacement Mesozoic faults occurred coevally with diabase dike emplacement, which corresponds to the final stage of the tectonic model proposed by Swanson (1982). This scenario indicates ~30 m.y. separates formation of ribbon quartz mylonite and silicified cataclasite, which permits sufficient time for the present erosion level to cool $> 100^{\circ}\text{C}$ indicated by the difference of deformation fabric between these two rocks. Additionally, if the emplacement of CAMP diabase dikes was related to an initial resistance to drift (e.g., Withjack et al., 1998), the spread of diabase dike and silicified fault orientations across the orogen may be the result of an unstable stress field during incipient stages of North American continental drift (Beutal et al., 2005).

The timing and rate of Inner Piedmont exhumation is likely a key variable in determining when the episode of dextral shearing recorded by ribbon quartz mylonite occurred. Other factors, such as increased geothermal gradients resulting from Alleghanian orogenesis or Mesozoic crustal extension, cannot be overlooked. In turn, more precise temporal limits regarding this intermediate deformation event that produced the widespread ribbon quartz mylonite may provide a better understanding of tectonic events that occurred between the final amalgamation and the early stages of Pangea rifting in the southern Appalachians. Additionally, these data may play an important role in deciphering the complex reactivation history of the Towaliga fault.

CONCLUSIONS

1. Isolated rhomboidal to sub-rhomboidal pods of silicified cataclasite along the Towaliga fault (and other Mesozoic faults in central Georgia) likely represent dilational step-overs in a small-displacement, sinistral strike-slip systems. Recognition of these features as dilational step-overs provides crucial insight into the kinematics of brittle deformation in an area where other kinematic indicators related to low-temperature deformation are rare. This mechanism may apply to siliceous cataclasite genesis throughout the orogen.
2. Alternating crosscutting relationships with ~200 Ma diabase dikes confirm Mesozoic reactivation of the Towaliga fault.
3. Significant displacement along the Towaliga fault likely occurred during Alleghanian deformation. Possible 2.5 km offset of diabase dikes and the size of the step-overs suggest relatively small displacement during sinistral Mesozoic reactivation.
4. The Alleghanian Towaliga fault changes trend from 070 to 035 at the northeast end of the Pine Mountain window, and both segments were reactivated as separate Mesozoic faults. The distinct bend in the garnet-grade phase of the fault also indicates polyphase deformation occurred during the Alleghanian orogeny.
5. The timing of ribbon quartz mylonite deformation remains problematic. Mylonitization likely occurred sometime between Alleghanian deformation and Triassic-Jurassic reactivation of the Towaliga fault.
6. The widespread abundance of ribbon quartz mylonite indicates an episode of dispersed dextral shear through the Piedmont, and may have important implications for tectonic models regarding the final assembly or breakup of Pangea. Events described in Swanson's (1982) model may correspond with our observations of post-Alleghanian structures.
7. Our data do not support significant normal displacement along the Towaliga fault.

ACKNOWLEDGMENTS

We thank M. Jessup, J. Langille, D. Hicks, L. Lee, and R. Leger for their input and insights during discussions regarding fluid/fault interactions. A. Merschat, J. Garihan, B. Davis, and C. Howard further refined these ideas. Funding was provided by the University of Tennessee–Knoxville Science Alliance Center of Excellence, the University of Tennessee Office of Research, and USGS EDMAP Award G09AC00126.

REFERENCES CITED

- Altamura, R.J. 2001. Geology of the Lantern Hill silicified fault zone near North Stonington, Connecticut, with integrated geochemistry and geochronology. PhD dissertation, Pennsylvania State University, State College, PA.
- Aydin, A., and Nur, A. 1985. The types and role of stepovers in strike-slip tectonics. *In* Biddle, K.T., and Christie-Blick, N. eds. *Strike-Slip Deformation, Basin Formation, and Sedimentation*. SEPM Spec. Publ. 37: 35-44.
- Babaie, H.A.; Hadizadeh, J.; Babaei, A.; and Mohammad Ghazi, A. 1991. Timing and temperature of cataclastic deformation along segments of the Towaliga fault zone, western Georgia, U.S.A. *J. Struct. Geol.* 13: 579-586.
- Bahat, D. 1983. New aspects of rhomb structures. *J. Struct. Geol.* 5: 591-601.
- Beutal, E.K.; Nomade, S.; Fronabarger, A.K.; and Renne, P.R. 2005. Pangea's complex breakup: A new rapidly changing stress field model. *Earth Planet. Sci. Lett.* 236: 471-485.
- Dallmeyer, R.D. 1978. $^{40}\text{Ar}/^{39}\text{Ar}$ incremental-release ages of hornblende and biotite across the Georgia Inner Piedmont: their bearing on late Paleozoic-early Mesozoic tectonothermal history. *Am. J. Sci.* 278: 124-149.
- Davis, B.A. 2010. Tectonic evolution of the southern Appalachian Inner Piedmont: Identification and interpretation of crustal features from aeromagnetic data and detailed geologic mapping in central Georgia. MS thesis, University of Tennessee, Knoxville, TN.
- Davis, G.J. 1980. The southwestern extension of the Middleton-Lowndesville cataclastic zone in the Greensboro, Georgia area and its regional implications. MS thesis, Athens, University of Georgia, 151 p.
- Gardner, C.H. 1961. The geology of central Newton County, Georgia. MS thesis, Emory University, Atlanta, GA.
- Garihan, J.M.; Preddy, M.S.; and Ranson, W.A. 1993. Summary of mid-Mesozoic brittle faulting in the Inner Piedmont and nearby Charlotte belt of the Carolinas. *In* Hatcher, R.D., Jr., and Davis, T.L. eds. *Studies of Inner Piedmont geology with a focus on the Columbus promontory*. Carolina Geol. Soc. Field Trip Guidebook: 55-66.
- Gillerman, V.S., and Sibson, R.H. 1988. Comment and reply on "Earthquake rupturing as a mineralizing agent in hydrothermal systems." *Geology* 16: 669-670.
- Goldberg, S.A., and Steltenpohl, M.G. 1988. Evidence for Alleghanian penetrative deformation in the Inner Piedmont of Alabama. *Geol. Soc. Am. Abstr. Program* 20: 267.
- Hadizadeh, J.; Babaie, H.A.; and Babaei, A. 1991. Development of interlaced mylonites, cataclasites and breccias: example from the Towaliga fault, south central Appalachians. *J. Struct. Geol.* 13: 63-70.

- Hames, W.E.; Renne, P.R.; and Ruppel, C. 2000. New evidence for geologically instantaneous emplacement of earliest Jurassic Central Atlantic magmatic province basalts on the North American margin. *Geology* 28: 859-862.
- Hatcher, R.D., Jr. 1995. *Structural Geology*. Upper Saddle River, NJ, Prentice-Hall, 525 p.
- Hatcher, R.D., Jr. 2006. Juxtaposed Mesozoic diabase dikes and siliceous cataclasite fault zones in the Carolinas and the mechanics of dike emplacement. *Geol. Soc. Am. Abstr. Program* 38: 8.
- Hatcher, R.D., Jr.; Bream, B.R.; and Merschat, A.J. 2007. Tectonic map of the southern and central Appalachians: A tale of three orogens and a complete Wilson cycle. *In* Hatcher, R.D. Jr.; Carlson, M.P.; McBride, J.H.; and Martínez-Catalán, J.R. eds. *4-D Framework of Continental Crust*. *Geol. Soc. Am. Mem.* 200: 595-632.
- Hewett, D.F., and Crickmay, G.W. 1937. The warm springs of Georgia, their geologic relations and origin. *U.S. Geol. Surv. Water Supply Pap.* 819, 37 p.
- Hill, D.P. 1977. A model for earthquake swarms. *J. Geophys. Res.* 82: 1347-1352.
- Hooper, R.J. 1986. Geologic studies at the east end of the Pine Mountain window and adjacent Piedmont, central Georgia. PhD dissertation, Columbia, University of South Carolina, 322 p.
- Hooper, R.J. 1989. Tectonic implications of a regionally extensive brittle fault system in the Piedmont: Evidence from central Georgia. *Geol. Soc. Am. Abstr. Program* 21: 22.
- Hooper, R.J., and Hatcher, R.D., Jr., 1988a, Pine Mountain terrane, a complex window in the Georgia and Alabama Piedmont; evidence from the eastern termination: *Geology*, v. 16, p. 307-310.
- Hooper, R.J., and Hatcher, R.D., Jr. 1988b. Mylonites from the Towaliga fault zone, central Georgia: products of heterogeneous non-coaxial deformation. *Tectonophysics* 152: 1-17.
- Huebner, M.T., and Hatcher, R.D., Jr. 2011. Evidence for sinistral Mesozoic inversion of the dextral Alleghanian Towaliga fault, central Georgia. *In* Huebner, M.T., and Hatcher, R.D., Jr. eds. *The Geology of the Inner Piedmont at the Northeast End of the Pine Mountain Window*. *Georgia Geol. Soc. Field Trip Guidebook*: 55-72.
- Huebner, M.T.; Hatcher, R.D., Jr.; and Wooden, J.L. 2011. Evidence for Paleozoic orogenies, terrane boundaries, and Mesozoic rifting from the central Georgia Inner Piedmont. *Geol. Soc. Am. Abstr. Program* 43: 21.
- Jones, D.D., Jr. 1970. Petrofabric and movement study of faults in Newton and Walton Counties, Georgia. MS thesis, Emory University, Atlanta, GA.
- Manspeizer, W. 1988. Triassic-Jurassic rifting and opening of the Atlantic: an overview. *In* Manspeizer, W. ed. *Triassic-Jurassic rifting, continental breakup and the origin of the Atlantic Ocean passive margins*, part A. New York, Elsevier: 41-79.

- McBride, J.H.; Hatcher, R.D., Jr.; Stephenson, W.J.; and Hooper, R.J. 2005. Integrating seismic reflection and geological data and interpretations across an internal basement massif: The southern Appalachian Pine Mountain window, USA. *Geol. Soc. Am. Bull.* 117: 669-686.
- McHone, J.G. 2000. Non-plume magmatism and rifting during the opening of the central Atlantic Ocean. *Tectonophysics* 316: 287-296.
- Mitcham, T.W. 1974. Origin of breccia pipes: *Econ. Geol.* 69: 412-413.
- Nelson, K.D.; Arnor, J.A.; Giguere, M.; and Schamel, S. 1987. Normal-fault boundary of an Appalachian basement massif? Results of COCORP profiling across the Pine Mountain belt in western Georgia. *Geology* 15: 832-836.
- Nelson, K.D.; Arnor, J.A.; McBride, J.H.; Willemin, J.H.; Huang, J.; Zheng, L.; Oliver, J.E.; Brown, L.D.; and Kaufman, S. 1985. New COCORP profiling in the southeastern United States. Part I: Late Paleozoic suture and Mesozoic rift basin. *Geology* 13: 714-718.
- Nomade, S.; Knight, K.B.; Beutel, E.; Renne, P.R.; Verati, C.; Féraud, G.; Marzoli, A.; Youbi, N.; and Bertrand, H. 2007. Chronology of the Central Atlantic Magmatic Province: Implications for the Central Atlantic rifting processes and the Triassic-Jurassic biotic crisis. *Palaeogeogr. Palaeoclimatol. Palaeoecol.* 244: 326-344.
- Olsen, P.E. 1997. Stratigraphic record of the early Mesozoic breakup of Pangea in the Laurasia-Gondwana rift system. *Annu. Rev. Earth Planet. Sci.* 25: 337-401.
- Phillips, W.J. 1972. Hydraulic fracturing and mineralization. *J. Geol. Soc. Lond.* 128: 337-359.
- Pryer, L.L. 1993. Microstructures in feldspars from a major crustal thrust zone: the Grenville Front, Ontario, Canada. *J. Struct. Geol.* 15: 21-36.
- Reade, E.H., Jr. 1960. The geology of a portion of Newton and Walton Counties, Georgia. MS thesis, Emory University, Atlanta, GA.
- Robinson, J.C. 1989. A brittle fracture analysis of the Flint Hill fault zone, southeastern NH. MS thesis, University of Massachusetts, Amherst, MA.
- Schliche, R.W.; Withjack, M.O.; and Olsen, P.E. 2003. Relative timing of CAMP, rifting, continental breakup, and basin inversion: tectonic significance. *In* Hames, W.E.; McHone, G.C.; Renne, P.R.; and Ruppel, C. eds. *The Central Atlantic Magmatic Province*: Washington D.C., Am. Geophys. Union Mon. 136: 33-60.
- Schultz, R.S. 1961. The geology of northwestern Newton and southeastern Walton Counties, Georgia. MS thesis, Emory University, Atlanta, GA.
- Segall, P., and Pollard, D.D. 1980. Mechanics of discontinuous faults. *J. Geophys. Res.* 85: 4337-4350.
- Sibson, R.H. 1985. Stopping of earthquake ruptures at dilational fault jogs. *Nature* 316: 248-251.
- Sibson, R.H. 1987. Earthquake rupturing as a mineralizing agent in hydrothermal systems. *Geology* 15: 701-704.

- Sibson, R.H. 1996. Structural permeability of fluid-driven fault-fracture meshes. *J. Struct. Geol.* 18: 1031-1042.
- Sneyd, D. 1995. Geology of the Barnesville Hydrologic Research Site, Lamar County, Georgia. *Geol. Surv. Info. Circ.* 98, 27 p.
- Steltenpohl, M.G. 1988. Kinematics of the Towaliga, Bartletts Ferry, and Goat Rock fault zones, Alabama: the late Paleozoic dextral shear system in the southernmost Appalachians. *Geology* 16: 852-855.
- Steltenpohl, M.G.; Heatherington, A.; Mueller, P.; and Wooden, J.L. 2004. Pre-Appalachian tectonic evolution of the Pine Mountain window in the southernmost Appalachians, Alabama and Georgia. *In* Tollo, R.P.; Corriveau, L.; McLelland, J.; and Bartholomew, M.J. eds. Proterozoic tectonic evolution of the Grenville orogen in North America: *Geol. Soc. Am. Mem.* 197: 633-646.
- Steltenpohl, M.G.; Hatcher, R.D., Jr.; Mueller, P.A.; Heatherington, A.L.; and Wooden, J.L. 2010. Geologic history of the Pine Mountain window, Alabama and Georgia: Insights from a new geologic map and U-Pb isotopic dates. *In* Tollo, R.P.; Bartholomew, M.J.; Hibbard, J.P.; and Karabinos, P.M. eds. From Rodinia to Pangea: The Lithotectonic Record of the Appalachian Region. *Geol. Soc. Am. Mem.* 206: 837-857.
- Stipp, M.; Stünitz, H.; Heilbronner, R.; and Schmid, S.M. 2002. The eastern Tonale fault zone: a 'natural laboratory' for crystal plastic deformation of quartz over a temperature range from 250 to 700° C. *J. Struct. Geol.* 24: 1861-1884.
- Student, J.J.; and Sinha, A.K. 1992. Carboniferous U-Pb ages of zircons from the Box Ankle and Ocmulgee faults, central Georgia: implications for accretionary models. *Geol. Soc. Am. Abstr. Program* 24: 69.
- Swanson, M.T. 1982. Preliminary model for an early transform history in central Atlantic rifting. *Geology* 10: 317-320.
- Thayer, P.A. 1970. Stratigraphy of the Dan River Triassic basin, North Carolina. *Southeast. Geol.* 12: 1-31.
- West, T.E., Jr. 1994. Field evidence that the Appalachian décollement is exposed in central Georgia at the east end of the Pine Mountain terrane. MS thesis, University of South Carolina, Columbia, SC.
- Withjack, M.O.; Schlische, R.W.; and Olsen, P.E. 1998. Diachronous rifting, drifting, and inversion on the passive margin of central eastern North America: an analog for other passive margins. *Am. Ass. Pet. Geol. Bull.* 82: 817-835.

Chapter V

**A new perspective on the emplacement of the Pine Mountain
terrane, southern Appalachians: Evidence from the
northeastern end of the Pine Mountain window, Georgia**

Chapter V combines the interpretation of Towaliga fault timing and kinematics discussed in Chapter IV with temporal constraints regarding fabric development in the Inner Piedmont to discuss a new model that depicts the tectonic evolution of the Pine Mountain terrane. This manuscript will be submitted to a peer reviewed journal early 2014. My coauthors are Robert D. Hatcher, Jr. and Justin R. Rehrer. My contributions to this manuscript include the majority of the writing, data collection, and structural analysis. The use of the term “we” and “our” in the text refers to the coauthor and myself.

ABSTRACT

The Pine Mountain terrane, southern Appalachians, consists of massive Grenville orthogneiss nonconformably overlain by a Neoproterozoic-Cambrian(?) metasedimentary sequence exposed in a complex fault-bounded window. It has a polyphase allochthonous emplacement history that can be delimited with evidence from its bounding faults, regional fabric relationships, and cross-cutting relationships with plutonic rocks in the region. Recent detailed geologic mapping at the northeastern end of the window, complemented by U-Pb zircon geochronology, provides new structural and temporal constraints regarding the allochthonous history of the Pine Mountain terrane. The Pine Mountain window is framed by at least four faults, and the attributes of these fault systems are crucial to unraveling the complex tectonic evolution of the window. Bounding faults of the window consist of the Towaliga fault to the northwest, the Box Ankle fault to the east, and the Bartletts Ferry-Goat Rock and Dean Creek faults to the south and southwest. Crosscutting relationships, contrasting metamorphic conditions during deformation, and varying dynamic recrystallization mechanisms in fault rocks reveal the sequential order in which these faults formed. The Box Ankle fault is a low-angle top-to-the-northwest thrust that juxtaposes Inner Piedmont rocks (Cat Square terrane) above the Pine Mountain window assemblage. The Box Ankle fault on its northwest and southeast ends by younger faults, contains the highest metamorphic grade (upper amphibolite facies) of the bounding faults, and is isoclinally folded axial planar to regional D_2 (Acadian/Neoacadian) fabric. These attributes indicate the Box Ankle fault is the oldest of the bounding faults, is likely Devonian, and should not be considered an Alleghanian fault. The Towaliga fault was active at relatively lower metamorphic grade (upper-greenschist to lower-amphibolite facies), and is an Alleghanian dextral strike-slip fault with a small-displacement sinistral Mesozoic inversion. The Towaliga fault truncates the recently identified Lloyd Shoals plutonic complex, a batholith-scale amalgamation of mostly Devonian megacrystic granite with stocks of Pennsylvanian granodiorite, which in turn provides a maximum age of ~301 Ma for the Alleghanian phase of the fault. Truncation of the Lloyd Shoals plutonic complex requires the Towaliga fault be related to Pine Mountain terrane emplacement, as the kinematics of the fault, combined with the truncation of the plutonic complex, do not permit the terrane to be emplaced

prior to displacement along the fault in a strain-compatible system. In our proposed scenario, palinspastic restoration of the bounding faults, in addition to major southern Appalachian faults (e.g., Appalachian detachment, Brevard fault), indicates the Pine Mountain terrane may have originated near the Virginia promontory. The current configuration of the Pine Mountain terrane far outboard in the orogen, combined with its near-shore Neoproterozoic-Cambrian cover strata, suggest it may represent a peri-Laurentian microcontinent that rifted from the margin sometime in the Cambrian. In contrast with the Argentine Precordillera, which rifted at approximately the same time, the Pine Mountain terrane remained proximal to Laurentia until it was accreted back in the middle Paleozoic.

INTRODUCTION

Basement massifs of the southern and central Appalachian orogen have been the focus of geologic study since their identification, and their attributes have provided numerous insights into the tectonic processes that shaped the Appalachian orogen. The internal basement massifs, or massifs that occur within the high-grade metamorphic core of the orogen (Hatcher, 1984), have been penetratively deformed during Paleozoic orogenesis, and general consensus is that all massifs are to some degree allochthonous. The Pine Mountain window (and terrane) is the southernmost exposed internal basement massif in the southern Appalachians (Steltenpohl et al., 2010) (Fig. 5-1), and its tectonic history, reviewed in light of new data from its northeastern terminus, provides new insight into the orogenic processes that shaped the Appalachians through the Paleozoic.

The tectonic evolution of the Pine Mountain terrane, central Georgia, remains one of the major unresolved tectonic problems of the southern Appalachian orogen. This is primarily a consequence of sparse detailed geologic mapping and geochronologic control, ambiguities in geophysical data, and conflicting interpretations of timing and kinematics of the faults that frame the window. Additionally, little attempt has been made to palinspastically restore the Pine Mountain terrane to its original position based on displacement estimates of major Appalachian faults (e.g., Appalachian detachment, Brevard fault, etc.). New detailed geologic mapping of the Inner Piedmont at the northeastern end of the window, complemented by U-Pb zircon geochronology and detailed microstructural analysis of fault rock fabrics, provide important limits to the complex and polyphase history of this internal Grenvillian basement massif and its associated metasedimentary cover. Synthesis of these new data, combined with recent tectonic interpretations of the history of the southern Appalachian crystalline internides, reveals a complex allochthonous history that is the product of both middle and late Paleozoic collisional orogenic events. Additionally, the metasedimentary cover sequence, which likely correlates with western Blue Ridge

Neoproterozoic-Cambrian strata (e.g., Clarke, 1952; Sears et al., 1981a; Steltenpohl et al., 2010), can be used to test our palinspastic restoration. The distribution of rifted-margin facies strata along the irregular Laurentian margin (Fig. 5-2), supports our hypothesis that the Pine Mountain terrane originated near a promontory, possibly the Virginia promontory, prior to its mid- to late Paleozoic translation. We revisit the microcontinent hypothesis regarding the tectonic history of the Pine Mountain terrane (Hooper and Hatcher, 1988a), and suggest that this hypothesis best explains the occurrence of proximal Laurentian depositional cover sequence far outboard in the orogen.

GEOLOGIC SETTING

The Pine Mountain window (Fig. 5-3) exposes a complex of felsic to mafic Grenville basement gneisses that are nonconformably overlain by an associated metasedimentary cover sequence, termed the Pine Mountain Group (e.g., Adams, 1930; Sears et al., 1981a, 1981b; Steltenpohl et al., 2004, 2010). This window is the southernmost exposed internal basement massif in the Appalachian orogen and occupies an area from central Georgia into central Alabama, where it likely continues beneath the Gulf Coastal Plain (Fig. 5-1). The Pine Mountain terrane is in fault contact with the exotic Carolina superterrane along its southwestern flank, and borders the Inner Piedmont terranes along its eastern and northern boundaries (Fig. 5-3). The Brindle Creek-Jackson Lake fault, which separates the Inner Piedmont terranes (Tugaloo and Cat Square), is truncated along the northern flank of the window (Figs. 5-1 and 5-3). Three primary faults that vary in timing, kinematics, and rheology frame the Pine Mountain window, which thus requires an allochthonous history for this massif.

Several crystalline basement units that include high-grade felsic augen gneiss, charnockite, and leucocharnockitic gneiss comprise the basement of the Pine Mountain terrane (e.g., Hewett and Crickmay, 1937; Clarke, 1952; Sears and Cook, 1984). In the northeastern portion of the window, strongly deformed augen gneiss protomylonite (Woodland Gneiss) is overlain by medium-grade, relatively less deformed quartzite and schist of the Pine Mountain Group, which indicates the contact between Grenville basement and the overlying strata is a nonconformity. The stratigraphy of the Pine Mountain Group has historically been correlated with the lower Cambrian Weisner(Chilhowee)-Shady-Rome Formations in the western Blue Ridge based on lithologic similarities and basement-cover relationships (e.g., Clarke, 1952; Schamel and Bauer, 1979; Sears et al., 1981b; Yokel and Steltenpohl, 1997; Steltenpohl et al., 2010), although no paleontologic control is available to confirm this association. Provenance of the Pine Mountain Group has been suggested to be Amazonian (Steltenpohl et al., 2004), although more recent detrital zircon geochronology indicates Laurentian affinity may be more likely (Steltenpohl et al., 2010).

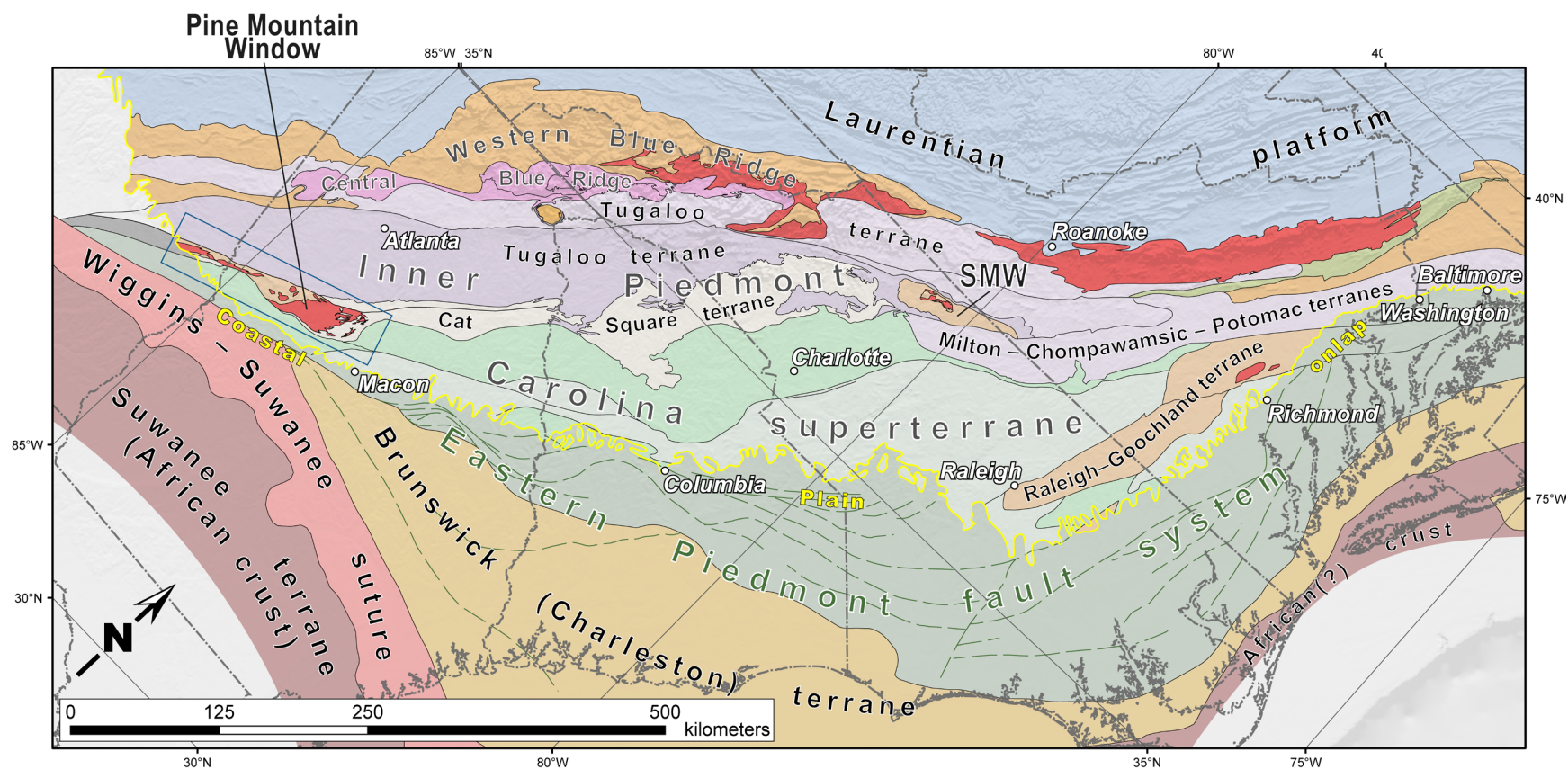


Figure 5-1: Simplified lithotectonic map of the southern Appalachian orogen illustrating the position of the Pine Mountain window (after Hatcher et al., 2007a). SMW – Sauratown Mountains window.

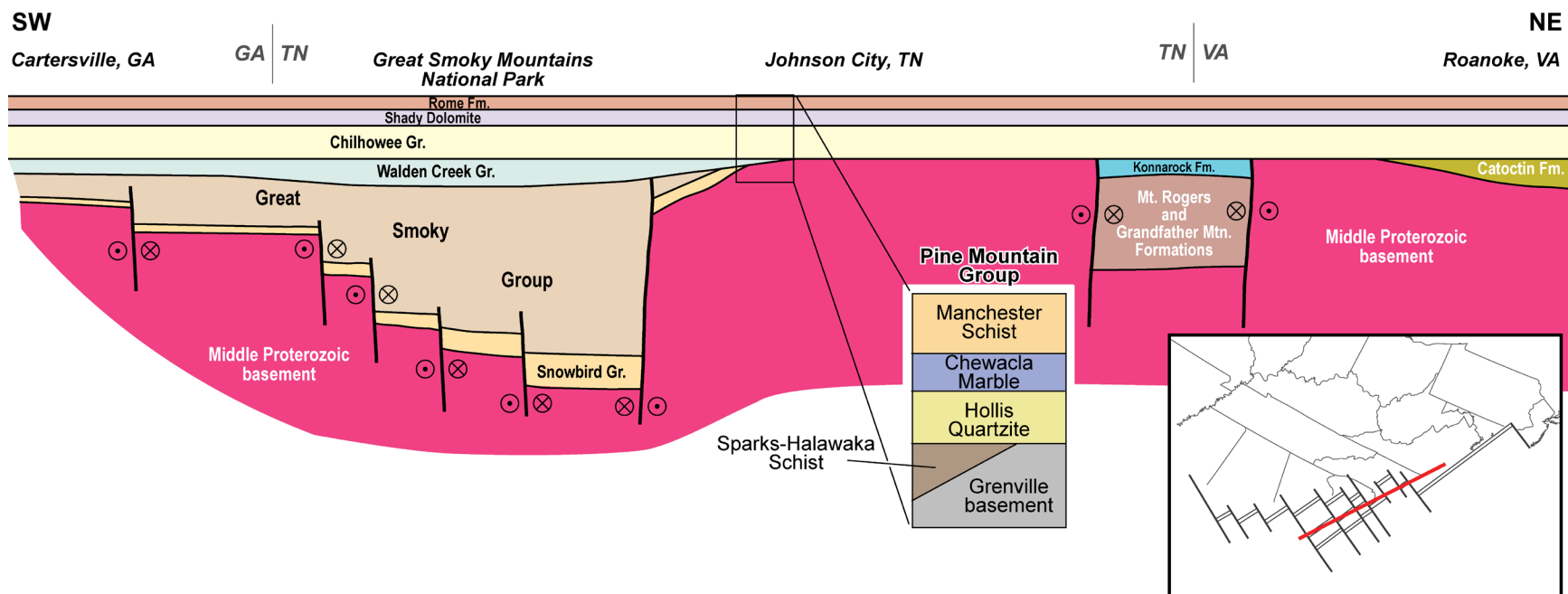


Figure 5-2: Thickness variation of Neoproterozoic-Cambrian rifted- to passive-margin strata along the eastern Laurentian margin (after Hatcher et al., 2007a), with possible stratigraphic correlation to Pine Mountain Group. Inset shows approximate location of schematic cross-section (red line) prior to northwest translation along the Appalachian detachment.

The Pine Mountain Group consists of ~2 km of schist, quartzite, and carbonate units (e.g., Galpin, 1915; Clarke, 1952; Sears and Cook, 1984; Steltenpohl et al., 2010). The stratigraphically lowest member of the Pine Mountain Group appears to be the Sparks-Halawaka Schist, which is primarily feldspathic muscovite-biotite schist that locally contains lenses of graphitic muscovite schist, coarse arkosic schist, layered metasandstone, aluminous schist, and quartzite (Schamel and Bauer, 1979; Sears et al., 1981b; Raymond et al., 1988; Steltenpohl et al., 2010). Schamel and Bauer (1979) suggested the Sparks-Halawaka Schist was deposited in narrow fault-bounded basins based on compositional immaturity and highly variable stratigraphic thickness (zero to 900 m; Sears et al., 1981b). It has been correlated with Ocoee Supergroup rifted-margin facies strata based on lithologic and depositional characteristics (Steltenpohl et al., 2004).

The contact between the Sparks-Halawaka Schist and the overlying Hollis Quartzite has been described as locally gradational, but elsewhere the Hollis Quartzite was deposited directly on crystalline basement (Schamel and Bauer, 1979). The Hollis Quartzite consists predominantly of meta-quartz arenite with intermittent schistose layers, is locally feldspathic and micaceous, and can be thick to thin bedded (e.g., Adams, 1926; Hewett and Crickmay, 1937; Clarke, 1952; Sears et al., 1981b). Thickness of the Hollis Quartzite averages ~100 m, although it can be up to 325 m thick (Clarke, 1952; Sears and Cook, 1984). Some of this variation in thickness could be tectonic. As a result of its quartzose lithology, the Hollis Quartzite generally holds up relatively high topography in the Pine Mountain window.

Hollis Quartzite is overlain by the Manchester Schist, which is the stratigraphically highest member of the Pine Mountain Group. The Manchester Schist consists mostly of aluminous and feldspathic schist with interlayered metasandstone, and appears to average ~600 m thickness (Sears et al., 1981b). Clarke (1952) and Raymond et al. (1988) suggested a three-part stratigraphy for the Manchester Schist that consists of a lower graphitic and aluminous schist member, a middle quartzite unit, and an upper two-mica schist and feldspathic schist unit.

At the southwestern end of the window, 10-300 m of Chewacla Marble, a medium- to coarse-grained dolomitic marble that is locally siliceous, lies stratigraphically between the Hollis Quartzite and Manchester Schist (Clarke, 1952; Raymond et al., 1988; Yokel and Steltenpohl, 1997). This rock unit is geographically confined to the southwestern portion of the window. The stratigraphic position of the Chewacla Marble is debated; most workers assign a stratigraphic position between the Hollis Quartzite and Manchester Schist (e.g., Clarke, 1952; Schamel and Bauer, 1979; Raymond et al., 1988; Steltenpohl et al., 2010), whereas Sears et al. (1981b) suggested it is the highest stratigraphic unit in the Pine Mountain Group, and interpreted it as the uppermost member of the Manchester Schist.

The current configuration of lithologic units exposed in the Pine Mountain window is controlled by deformation of basement and cover rocks that occurred under kyanite-staurolite to

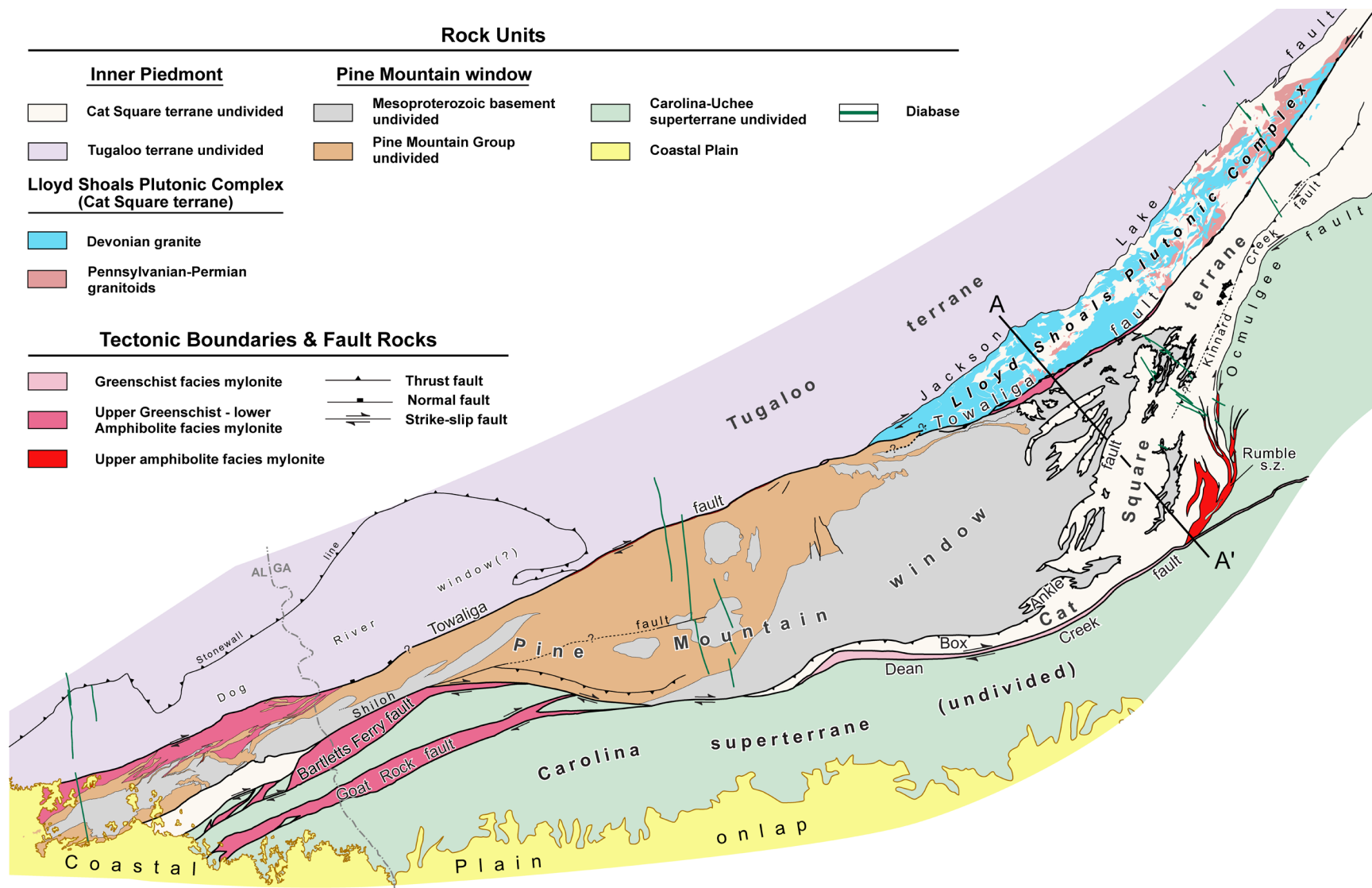


Figure 5-3: Simplified geologic map of the Pine Mountain window and the Inner Piedmont at its northeastern terminus (after Steltenpohl et al., 2010).

sillimanite-grade conditions, which we herein suggest occurred during the Acadian/Neoacadian orogeny. Structurally, the window consists of at least three northwest-vergent, basement-cored recumbent crystalline thrust nappes (Fig. 5-4), which may be stacked with inverted metamorphic isograds; i.e., the lowest metamorphic grade is at the lowest structural position (Sears and Cook, 1984). These nappes are coaxially refolded, producing macro-scale overturned antiforms and synforms (Sears and Cook, 1984). Emplacement of these nappes and deformation within the window likely precedes or at least coincides with the initial juxtaposition of the Inner Piedmont above the Pine Mountain terrane along the Box Ankle thrust fault.

The Box Ankle fault frames the eastern portion of the Pine Mountain window, and bounds several klippen within the window along with smaller windows east of its main trace (Fig. 5-3). It is a deformed thrust fault that was active under upper amphibolite-facies conditions, similar to peak metamorphic conditions and parallel development of the dominant fabric elements in the Inner Piedmont. The northern trace of the Box Ankle fault is truncated by the Towaliga fault, and to the south by the Dean Creek and Goat Rock-Bartletts Ferry faults, which indicate it is the oldest of the faults that frame the window (Fig. 5-3).

The Towaliga fault frames the northwest flank of the window from beneath the Coastal Plain in central Alabama to central Georgia, and at the northeastern end of the window, changes strike from ~070 to ~035 and continues northeast through the Inner Piedmont (Fig. 5-3). Various kinematic interpretations of the Towaliga fault have been proposed based on seismic reflection data (e.g., Nelson et al., 1985, 1987) and fault-rock fabrics that range from lower amphibolite to zeolite(?) facies (e.g., Steltenpohl, 1988; Hooper and Hatcher, 1988b; Huebner and Hatcher, 2013). Several studies have concluded that the Towaliga fault was active as a dextral strike-slip fault at garnet-grade conditions during the Alleghanian orogeny (Steltenpohl, 1988; Hooper and Hatcher, 1988a, 1988b; Huebner and Hatcher, 2013). The Towaliga fault was reactivated during the Mesozoic by small-displacement, sinistral strike-slip faults (Huebner and Hatcher, 2013). The change in strike of the Alleghanian phase of the fault also suggests polyphase deformation during the Alleghanian orogeny, discussed in detail below.

To the south and west, the window is framed by the dextral Bartletts Ferry-Goat Rock fault zone(s), which in turn are cut by the late Alleghanian(?) Dean Creek and Mesozoic Shiloh faults (Fig. 5-3). The Bartletts Ferry-Goat Rock faults are similar to the Alleghanian phase of the Towaliga fault in metamorphic grade and kinematics (Steltenpohl, 1988), whereas the dextral Dean Creek fault exhibits ductile fabrics that indicate lower greenschist-facies conditions during deformation (Steltenpohl et al., 2010). A paucity of detailed geologic mapping at the southeastern terminus of the window in Georgia prohibits the delineation of more reliable crosscutting relationships and, although limited reconnaissance mapping here indicates the Dean Creek fault truncates the Bartletts Ferry-Goat Rock faults, its western extent is not well defined (Fig. 5-3). The

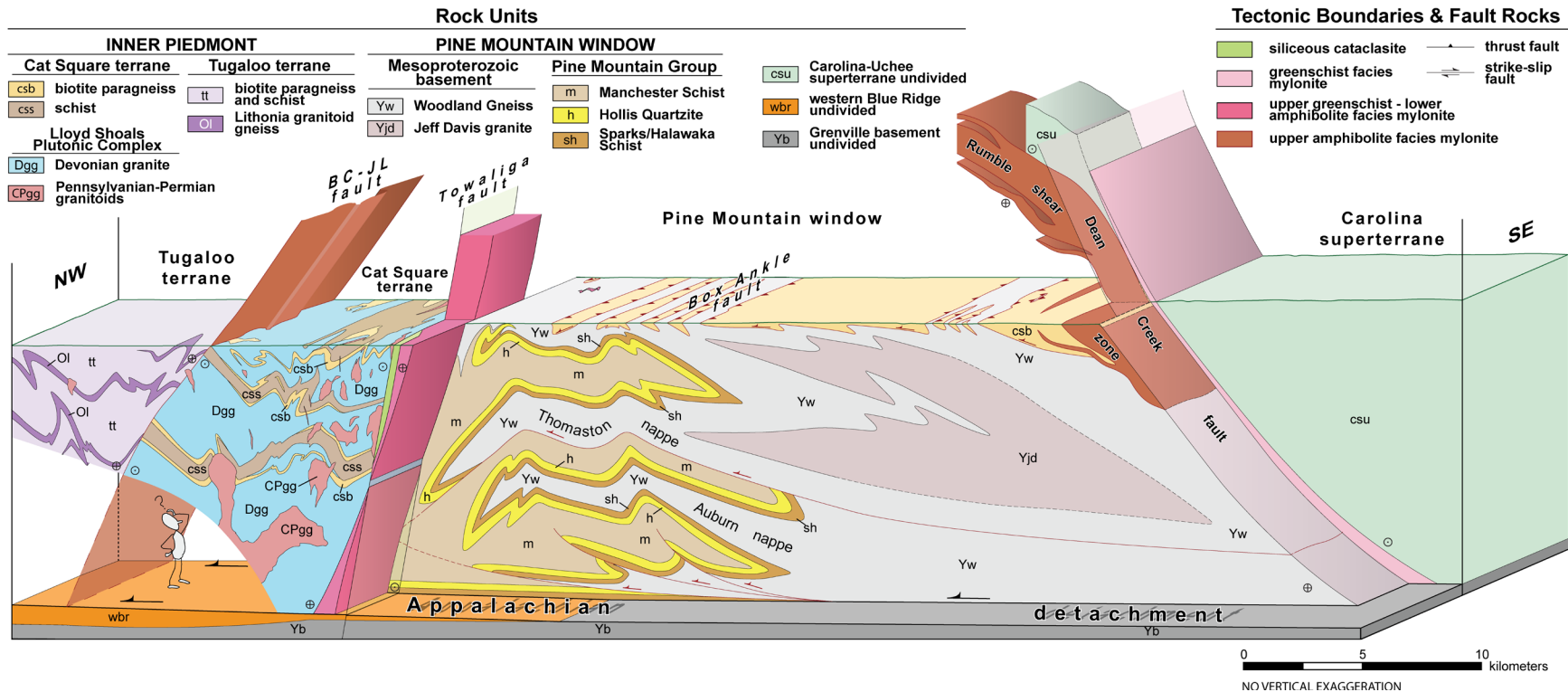


Figure 5-4: Cross section and block diagram through the Carolina superterrane, Pine Mountain terrane, and Inner Piedmont at the northeastern end of the Pine Mountain window. Location of cross section shown in Figure 6-3. Imbricate nappe structure of the Pine Mountain terrane adapted from Sears and Cook (1984). BC-JL – Brindle Creek-Jackson Lake fault.

Shiloh fault may truncate the Dean Creek fault, and has been interpreted as a southeast-dipping Mesozoic normal fault that extends from just south of Warm Springs, Georgia, through central Alabama (e.g., Sears et al., 1981a; Steltenpohl et al., 2010). The fault was originally mapped by Hewett and Crickmay (1937), however, was depicted as a < 5 km-long fault that sinistrally offset a large diabase dike (~200 Ma) by < 1 km southeast of Warm Springs, Georgia. No surface evidence has been identified that confirms significant normal slip during the Mesozoic, nor has its trace been confirmed through western Georgia. Its interpretation as a regional-scale normal fault is herein considered suspect.

Based on the configuration, kinematics, and various timing of faults that frame the window, Hooper and Hatcher (1988a) concluded that the window cannot be a simple window through the master Appalachian detachment (e.g., Sears and Cook, 1984; Nelson et al., 1987; West et al., 1995), and that the Pine Mountain terrane as a whole must be allochthonous (e.g., McBride et al., 2005). We agree with this conclusion and, based on new data revealed by detailed geologic mapping and geochronology at the northeastern end of the window, provide a new perspective on the nature and timing of Pine Mountain terrane emplacement. Our findings are considered in light of recent tectonic models that describe middle and late Paleozoic collisional orogenesis, and, based on palinspastic restoration of relevant faults throughout the southern Appalachian orogen, we propose a viable geographic origin of the Pine Mountain terrane along the eastern Laurentian margin.

NEW OBSERVATIONS FROM DETAILED MAPPING AT THE NORTHEAST END OF THE PINE MOUNTAIN WINDOW

Fault kinematics

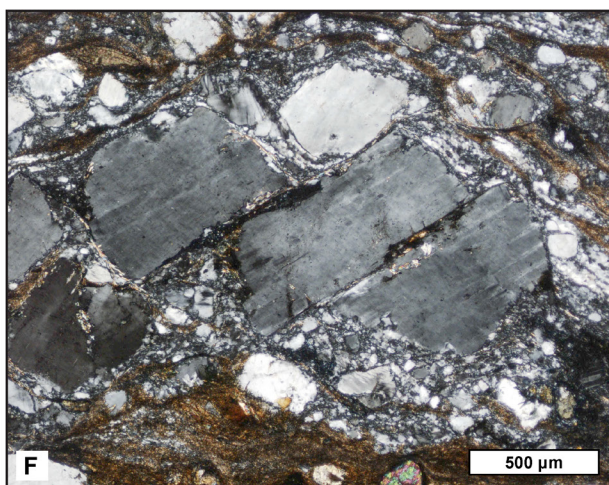
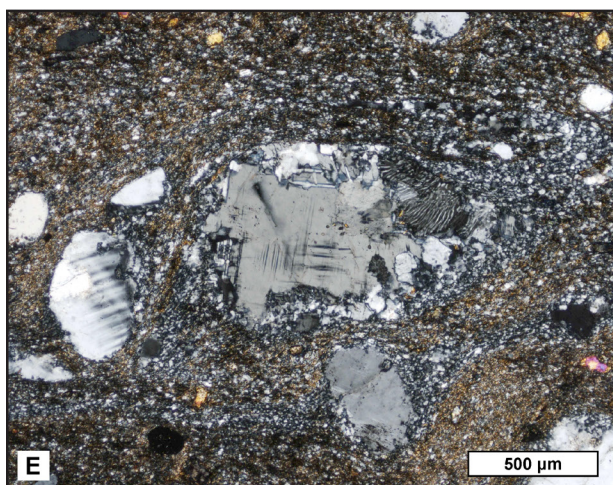
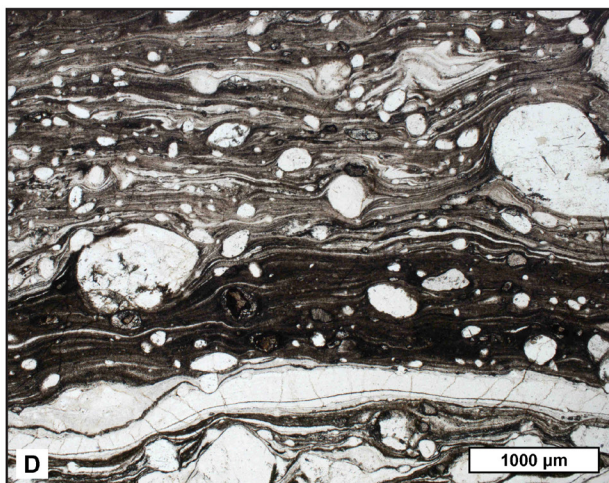
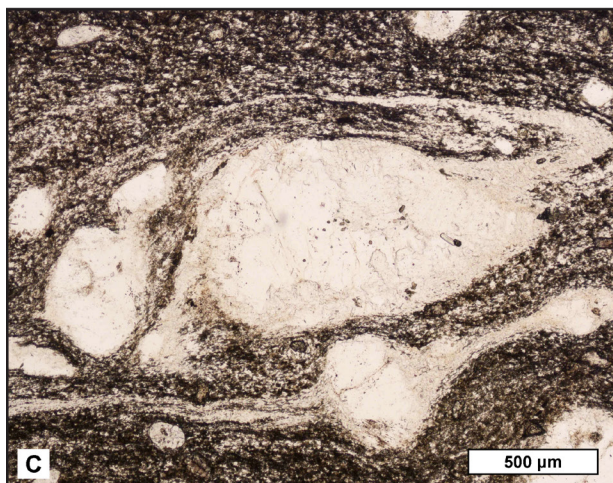
Box Ankle fault mylonite has previously been considered the 2-4 km thick, coarse-grained augen protomylonite to mylonite that characterizes the Woodland Gneiss in the eastern and central portions of Pine Mountain window (e.g., West et al., 1995). However, this pervasive mylonitic fabric also occurs directly beneath the nonconformable contact with the overlying Pine Mountain Group, which is significantly less deformed (Clarke, 1952; J.R. Rehrer, unpublished data). We therefore suggest that much of the mylonite that has been considered to represent the Box Ankle fault may be likely a product of Grenvillian deformation, or at least deformation that occurred prior to the Neoproterozoic-Cambrian deposition of the Pine Mountain Group. Additionally, the type locality of the Woodland Gneiss, > 20 km from the closest trace of the Box Ankle fault, is described by Hewett and Crickmay (1937) as “coarse-grained biotite augen gneiss,” is deformed much like Woodland Gneiss that is adjacent to the Box Ankle fault and considered to be a product of deformation associated with the Paleozoic emplacement of the fault.

Instead, the Box Ankle fault is much thinner (< 100 m), with relatively finer-grained mylonite that incorporates Inner Piedmont and Pine Mountain terrane rocks in the shear zone (e.g., Hooper et al., 1997) (Fig. 5-5). Mylonite here contains upper amphibolite-facies mineral assemblages, well-developed S-C fabric, and abundant σ - and δ -feldspar porphyroclasts with myrmekite rims and recrystallized K-feldspar tails (Hooper and Hatcher, 1988a; Rehrer et al., 2012). Petrographic evidence indicates Box Ankle fault mylonite is relatively free of unrecovered strain (Hooper and Hatcher, 1988a), which at least indicates an episode of thermal equilibration post-deformation. Shear-sense indicators, combined with shallow southeast- and northwest-dipping foliation and pervasive northwest mineral lineation, indicate the Box Ankle fault is a folded, northwest-vergent thrust that juxtaposes Cat Square terrane rocks above Pine Mountain terrane rocks in the footwall.

The Towaliga fault has a complex reactivation history, which includes an Alleghanian upper greenschist to lower amphibolite-facies dextral strike-slip phase overprinted by small-displacement sinistral strike-slip faults active at ~200 Ma under zeolite(?) facies conditions (Huebner and Hatcher, 2013). The Alleghanian phase consists of garnet-grade proto- to ultramylonite in shear zones that range from 10 m to 5 km wide (e.g., Steltenpohl et al., 2010; this study). Mylonite protoliths include Mesoproterozoic basement, Paleozoic granitoids, and metasedimentary rocks from both the Inner Piedmont and Pine Mountain terranes (Steltenpohl et al., 2010; Huebner and Hatcher, 2013). Shear sense indicators include asymmetric σ , δ , and θ porphyroclasts, synthetic domino-type fragmented feldspar porphyroclasts, strongly developed S-C fabric, and asymmetric folds (Hooper and Hatcher, 1988b; Steltenpohl, 1988; this study) (Fig. 5-5). Feldspar porphyroclasts characteristically exhibit quartz-mica pressure shadows with no recrystallized feldspar in tails (Rehrer et al., 2012). The mylonite zone dips steeply northwest with moderate- to shallow-plunging northeast-southwest mineral stretching lineations and, when combined with shear-sense indicators, indicates the Alleghanian Towaliga fault is a dextral strike-slip fault (e.g., Hooper and Hatcher, 1988a, 1988b; Steltenpohl, 1988; Huebner and Hatcher, 2013). The Towaliga fault has been interpreted as a northwest-dipping normal fault based on COCORP seismic reflection data (Nelson et al., 1985; 1987), although fault-rock fabrics indicate only a minor dip-slip component (Steltenpohl, 1988).

The most striking aspect of the Towaliga fault is arguably the occurrence of isolated, km-scale rhomboidal ridges of silicified breccia and cataclasite that occur along its length. Huebner and Hatcher (2013) interpreted these to represent ancient dilational step-overs that formed in a small-displacement sinistral strike-slip regime based on their geometry and overwhelming dilational rock fabrics (Fig. 5-5). Additionally, this brittle episode of faulting shares mutually overprinting crosscutting relationships with ~200 Ma Central Atlantic Magmatic Province (CAMP)

Figure 5-5: Hand specimen, outcrop, and photomicrographs of Box Ankle (left column) and Towaliga fault (right column) mylonites. All images shown (except B) are normal to foliation, parallel to mineral lineation. (A) Sawed surface of Box Ankle mylonite. (B) Outcrop of Woodland Gneiss with a band of ultramylonite (center) and mylonite (above) associated with the Towaliga fault. (C) Plane-polarized light and (E) cross-polarized light photomicrographs of Box Ankle fault mylonite. Note internal deformation of feldspar porphyroclast (center). (D) Plane-polarized light image of Towaliga fault mylonite with abundant δ - and θ - feldspar porphyroclasts. (F) Cross-polarized light image of domino-style fractured feldspar porphyroclast in Towaliga fault mylonite, indicating dextral shear sense.



diabase dikes, which delimits the timing of faulting, and sinistral offset of these dikes supports the interpretation of shear sense (Huebner and Hatcher, 2013).

Timing of deformation, metamorphism, and fabric development

The central Georgia Inner Piedmont has been multiply deformed, and records at least six deformational events. The dominant regional foliation (S_2) formed close to peak metamorphic conditions (upper amphibolite-facies), with foliation in metasedimentary rocks defined by high-temperature mineral assemblages that include prismatic and fibrous sillimanite, phyllosilicates, and other inequant phases. Timing of S_2 development at the northeast end of the Pine Mountain window is bracketed by well-documented crosscutting relationships with isotopically dated granitoids (Fig. 5-6). S_2 is concordant with pre- to synmetamorphic granitoids that range from 406-369 Ma, and is obviously truncated by post-metamorphic granitoids ranging from 328-301 Ma (Huebner et al., *in review*) (Fig. 5-6). Ion microprobe analyses of metamorphic zircon rims also indicate peak metamorphic conditions took place in the Middle to Late Devonian (400-380 Ma; Huebner et al., *in review*), all of which provide a strong case for fabric development during the Acadian/Neoacadian orogeny.

Continuity of S_2 fabric and related structures across the Box Ankle fault into the eastern portion of the Pine Mountain window, in addition to structural data that indicate the fault is folded axial planar to S_2 , is evidence that the Pine Mountain terrane and Inner Piedmont were deformed coevally post-emplacement of the Box Ankle fault (Hooper and Hatcher, 1988a, 1989). This dictates that displacement along the fault had to occur prior to the development of S_2 and peak metamorphism, which are products of the Acadian/Neoacadian orogeny. Therefore, thrusting of the Inner Piedmont above the Pine Mountain terrane occurred no later than the Devonian, requiring the ~303 Ma age for the Box Ankle fault (Student and Sinha, 1992) be abandoned.

The Box Ankle fault is truncated to the north by the Towaliga fault at the northeast terminus of the window. The Towaliga fault truncates S_2 fabric and related structures, in addition to the Lloyd Shoals plutonic complex, a batholith-scale amalgamation of mostly Devonian granite with smaller stocks of Pennsylvanian-Permian post-deformational granitoids (Huebner et al., GSA MAP) (Fig. 5-3). The youngest granitoid in the Lloyd Shoals plutonic complex (~301 Ma) provides a maximum age for the Towaliga fault, which is consistent with previous estimates of fault activity (~295 Ma; Goldberg and Steltenpohl, 1988). The Bartletts Ferry-Goat Rock fault system, which is rheologically and kinematically similar to the Towaliga fault, was active at similar metamorphic grade, and truncates the Box Ankle fault to the south (Steltenpohl, 1988) (Fig. 5-3). The Dean Creek fault likely truncates the Box Ankle and Bartletts Ferry-Goat Rock faults based on its assumed younger age inferred from its lower metamorphic grade, although the crosscutting relationships here are less certain due to a lack of detailed geologic mapping (Fig. 5-3).

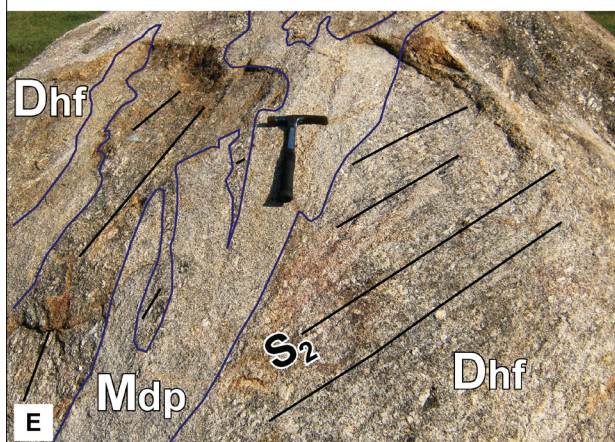
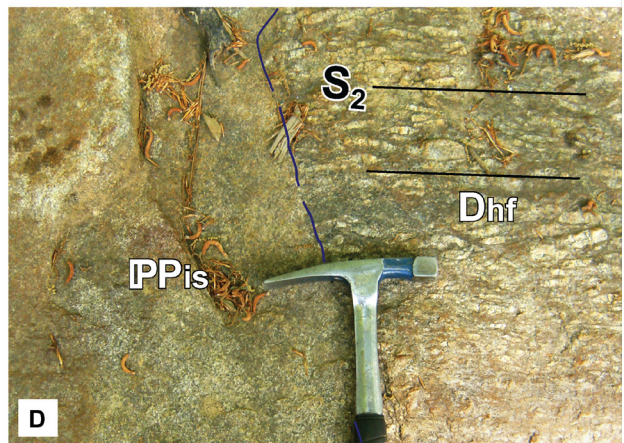
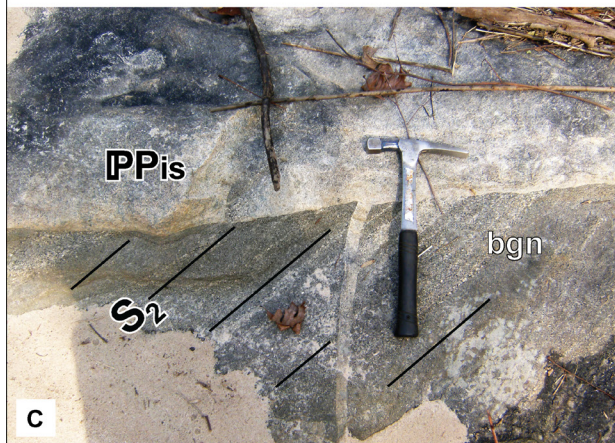
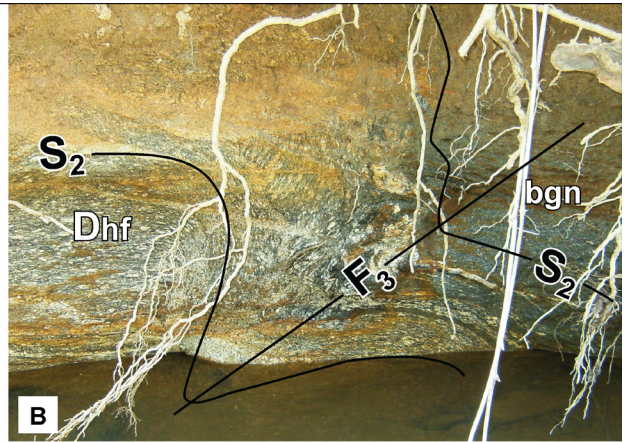
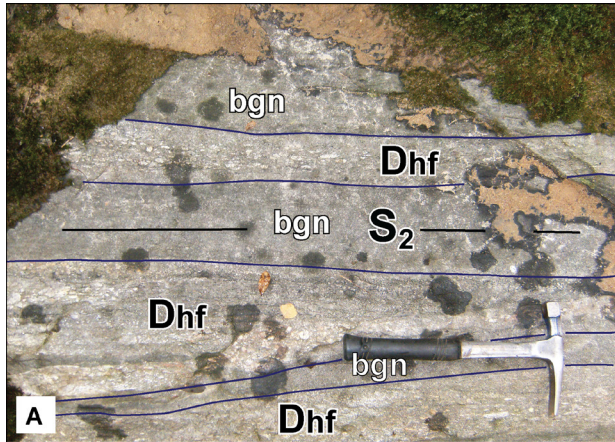
The Lloyd Shoals plutonic complex: Can the Pine Mountain terrane be emplaced prior to the Alleghanian phase of the Towaliga fault?

The truncation of the Lloyd Shoals plutonic complex not only provides a maximum age for the Towaliga fault, it also suggests that a significant amount of displacement has occurred along the fault. The question arises as to whether the displacement that truncates the Lloyd Shoals plutonic complex occurred during the Alleghanian or Mesozoic movement phases of the Towaliga fault, because the maximum age determined from crosscutting relationships does not discriminate between the two. Huebner and Hatcher (2013) suggested that the Mesozoic component of the Towaliga fault system involved < 5 km of sinistral displacement, based on the size and geometry of dilational step-overs along the fault and apparent sinistral offset of a diabase dike set along the northeastern ~035 segment. Another conclusion of that study is that no evidence for significant normal offset is evident at the surface for either phase of faulting, as has been suggested by several previous studies (e.g., Schamel and Bauer, 1979; Nelson et al., 1985; 1987; Steltenpohl et al., 2004). Therefore, the Alleghanian phase of the Towaliga fault, which was predominantly strike-slip at upper greenschist to lower amphibolite-facies conditions, involved a significant amount of dextral displacement. This has important implications regarding the allochthonous history of the Pine Mountain terrane relative to surrounding terranes. An obvious structural discrepancy results if the Pine Mountain terrane was emplaced prior to Alleghanian strike-slip movement on the Towaliga fault; the displaced portion of the Lloyd Shoals plutonic complex would have to override the Pine Mountain terrane, for which there is no evidence. Based on this relationship, we suggest that the polyphase Alleghanian Towaliga fault moved the Pine Mountain terrane relative to the Inner Piedmont and Carolina superterrane to its current configuration, which occurred post ~301 Ma.

A REVISED TECTONIC HISTORY OF THE PINE MOUNTAIN TERRANE

Recent detailed mapping, coupled with ion microprobe U-Pb geochronologic analyses in the Inner Piedmont at the northeastern end of the Pine Mountain window, have yielded crucial insight regarding the nature of the emplacement of the Pine Mountain terrane. In addition to these new data, the overall tectonic history of southern Appalachian orogen, specifically major large-displacement faults, has to be accounted for when attempting any tectonic reconstructions that depict the emplacement and geographic origin of this allochthonous terrane. Key elements that should be considered include: 1) timing and kinematics of faults that bound the Pine Mountain window; 2) fabric development in the Pine Mountain terrane and surrounding terranes; 3) spatial relationships between surrounding rocks and bounding faults; 4) palinspastic restoration of other

Figure 5-6: Inner Piedmont fabric and granitoid relationships used as temporal brackets in this study. (A) Apparent interlayering of Devonian (406-372 Ma) High Falls granite with Cat Square terrane biotite paragneiss. S_2 is concordant in both lithologies and is parallel to contacts. (B) Folded contact between High Falls Granite and biotite gneiss, view to the northeast. (C) and (D) Discordant contacts between Pennsylvanian-Permian Indian Springs Granodiorite (316-299 Ma) and biotite gneiss (C) and High Falls Granite (D). (E) Dikes of Dows Pulpit Granodiorite (~325 Ma) cut S_2 in High Falls Granite, view to the northeast. Ages from Huebner et al. (*in review*).



major tectonic boundaries, primarily the Appalachian master detachment and Brevard fault zone; and 5) possible original position of the Pine Mountain terrane based on stratigraphic similarities at promontories and embayments along the eastern Laurentian margin. Synthesis of these data provides a unique perspective regarding the original position of the Pine Mountain terrane along the eastern Laurentian margin. The following discussion is an attempt to briefly summarize the major tectonic events that shaped the southern Appalachian orogen, with a focus on the allochthonous history of the Pine Mountain terrane.

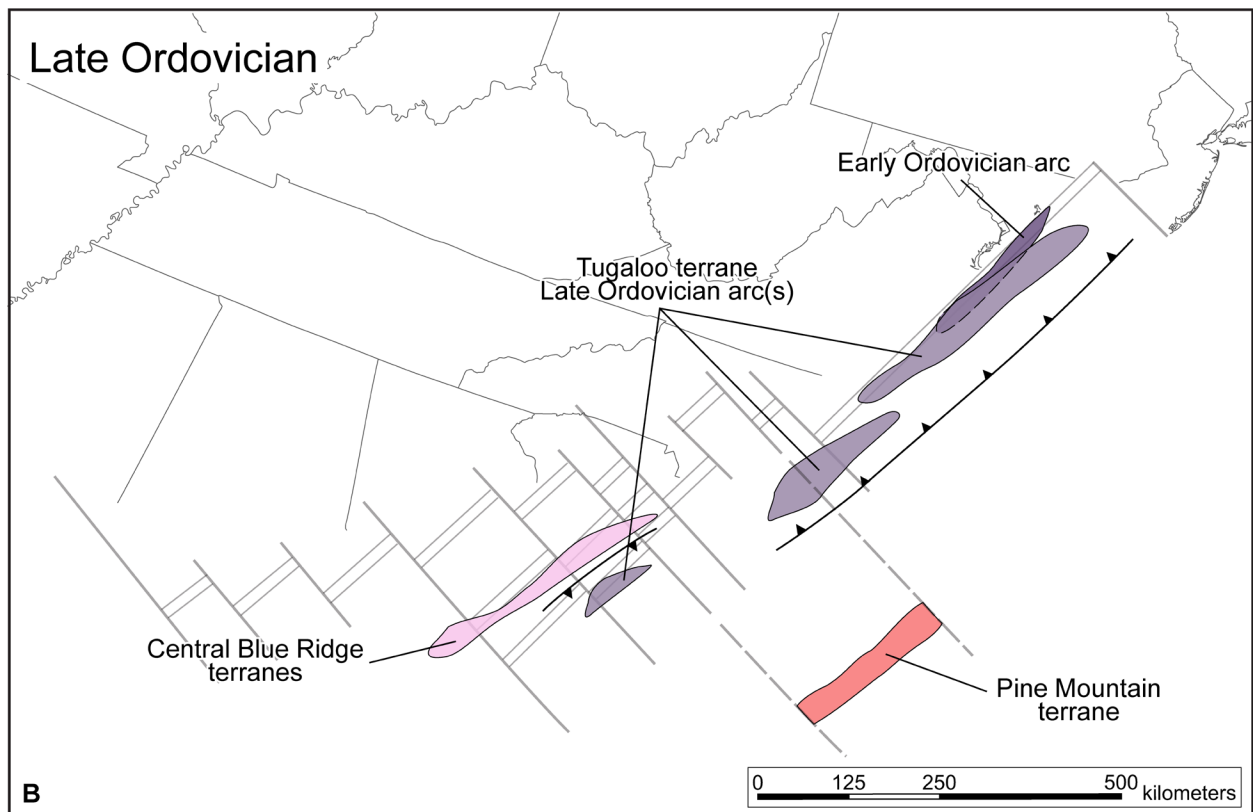
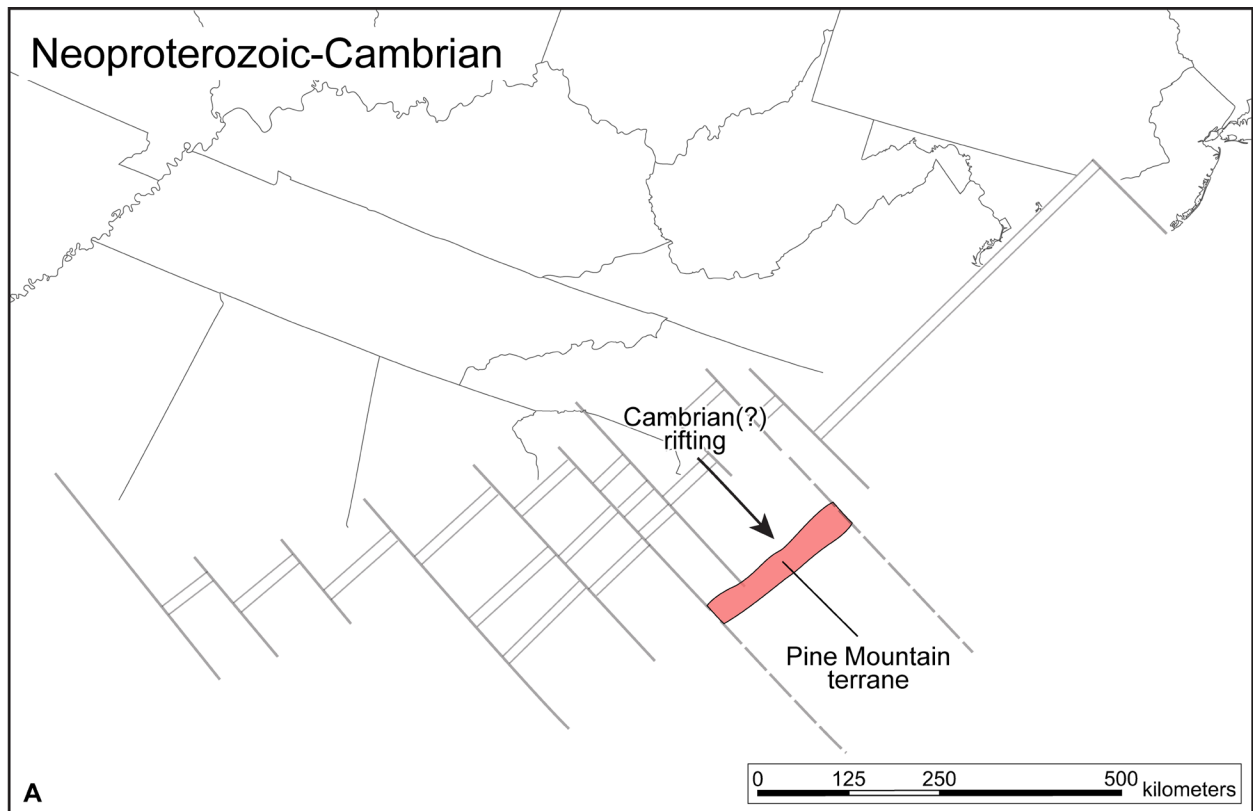
The Neoproterozoic breakup of Rodinia produced an irregular continental margin that consisted of promontories and embayments controlled by northwest-striking transform faults (e.g., Thomas, 1991). Relatively thick (10-15 km) sections of rift- and post-rift-to-drift facies (Ocoee Supergroup) rocks were deposited at embayments, while these rocks thin dramatically at promontories and locally pinch out completely (e.g., Hatcher et al., 2007a) (Fig. 5-2). The transition from rifted- to passive-margin strata is marked by the deposition of the lower Cambrian Chilhowee Group sandstone and overlying Shady Dolomite, which stratigraphically overlie the Ocoee Supergroup. The eastern Laurentian margin evolved into a collisional margin in the Middle Ordovician (480-460 Ma), which involved accretion of several(?) island arcs that now comprise the central Blue Ridge terranes (e.g., Moecher et al., 2004; Miller et al., 2006; Merschat, 2009). Additionally, an early Ordovician (489-470 Ma) arc was accreted in the eastern Blue Ridge in central to northern Virginia (Sinha et al., 2012). The central Blue Ridge terranes (Cowrock, Cartoogechaye, Dahlenega gold belt) were probably accreted near present-day central South Carolina through southeastern Georgia (Fig. 5-7), based on shortening estimates from restored Valley and Ridge cross sections through East Tennessee (e.g., Thomas, 1991; Hatcher, 2002; Hatcher et al., 2007b). During the Late Ordovician, west-dipping subduction of ocean crust may have initiated, resulting in the development of a 459-441 Ma continental island arc along the eastern Laurentian margin (e.g., Sinha et al., 2012). While several workers attribute the termination of this pulse of plutonism to mark the accretion of the Carolina superterrane (e.g. Hibbard, 2000), evidence of ultimate Devonian-Mississippian accretion during the Acadian/Neoacadian orogeny is overwhelming (e.g., Merschat et al., 2005; Hatcher, 2010; Hatcher et al., 2007a; Huebner et al., *in review*). During this orogeny, the eastern Laurentian margin was partially subducted beneath the Carolina superterrane during its dextral transpressive accretion, and the composite Inner Piedmont was extruded to the southwest, buttressed against the Brevard fault, in an orogen-parallel, mid-crustal orogenic channel (Merschat et al., 2005; Hatcher and Merschat, 2006).

Fabric relations between the Box Ankle fault and S_2 indicate juxtaposition of the Inner Piedmont above the Pine Mountain terrane occurred either prior to or during the early stages of Acadian/Neoacadian S_2 development (e.g., Hooper and Hatcher, 1988a; Huebner et al., *in*

review). Based on this critical fabric relationship, the Box Ankle fault cannot be considered an Alleghanian fault as suggested by several authors (e.g., Student and Sinha, 1992; West et al., 1995; McBride et al., 2005; Hatcher et al., 2007a; Steltenpohl et al., 2010). Additionally, imbricate stacking of ductile thrust nappes in the Pine Mountain terrane and folding of the Box Ankle fault likely occurred during this event. An implication of this temporal constraint is that when the composite Inner Piedmont was laterally extruded to the southwest during dextral transpressive accretion of the Carolina superterrane, it had already been juxtaposed above the Pine Mountain terrane, and the Pine Mountain terrane was incorporated in the southwest-directed mid-crustal orogenic channel. The proposition that the Box Ankle fault was emplaced prior to orogen-parallel extrusion is supported by the lack of southwest-directed fault rock fabrics. Pervasive mylonitic foliation and mineral lineation data from Box Ankle fault rocks indicate top to the northwest translation (present configuration). Dextral translation of the Inner Piedmont and outboard terranes along the Brevard fault zone in the middle Paleozoic involved significant displacement (e.g., Vauchez et al., 1993; Hatcher, 2001; Merschhat et al., 2005), which is likely on the order of ~250 km (Huebner et al., *in review*).

The Box Ankle fault is truncated at both ends by Alleghanian faults of the Eastern Piedmont Fault System (Hatcher et al., 1977), which includes the Towaliga and Bartletts Ferry-Goat Rock fault systems (Fig. 5-3). The extent of the Towaliga fault, which trends ~035 along its northeastern segment and ~070 along its southwestern segment, provides key insight regarding the next phase of the journey of the Pine Mountain terrane. We suggest that translation of the Pine Mountain terrane along the Towaliga fault initially occurred along the northeastern ~035 segment, followed by rotation of the block and translation along the southwestern ~070 segment. This polyphase episode of movement of the Pine Mountain terrane is supported by the abrupt truncation of the Lloyd Shoals plutonic complex by the Towaliga fault at the northeast end of the window. The Pine Mountain terrane cannot be in place prior to dextral Alleghanian strike-slip displacement along the Towaliga fault because the portion of the Lloyd Shoals plutonic complex that has been excised would have had to be juxtaposed above the Pine Mountain terrane. For the Pine Mountain terrane to be in place prior to Alleghanian movement along the Towaliga fault, there would have to be either 1) a southwest-directed thrust fault that juxtaposed the Inner Piedmont above the Pine Mountain window; or 2) southwest-directed reactivation of the Box Ankle fault at lower metamorphic grade. There is currently no evidence that supports either alternative; therefore, we suggest that the Towaliga fault translated the Pine Mountain terrane to its current position relative to the Inner Piedmont and Carolina superterrane. Crosscutting relationships with the youngest plutonic rocks in the Lloyd Shoals plutonic complex indicate this episode of translation occurred post ~301 Ma.

Figure 5-7: Tectonic history of the allochthonous Pine Mountain terrane. (A) Initial early to middle Cambrian rifting of the Pine Mountain terrane from the Laurentian margin, likely in the vicinity of the Virginia Promontory. (B) Development and accretion of central and eastern Blue Ridge arc terranes occurred inboard of the rifted Pine Mountain microcontinent. (C) Acadian/Neoacadian (Devonian-Mississippian) transpressive obduction of the Carolina superterrane subducts the Inner Piedmont to mid-crustal depths, where it flows to the southwest as an orogenic channel. The Cat Square terrane is thrust over the Tugaloo and Pine Mountain terranes at this time. Displacement on the Brevard fault, which buttressed the orogenic channel, may be ~250 km. (D) Polyphase translation of the Pine Mountain terrane along the ~035 and ~070 segments of the Towaliga fault. (E) Northwest-directed thrusting of the Blue Ridge-Inner Piedmont mega-thrust sheet along the Appalachian detachment translates the southern Appalachian orogen to its current configuration (F).



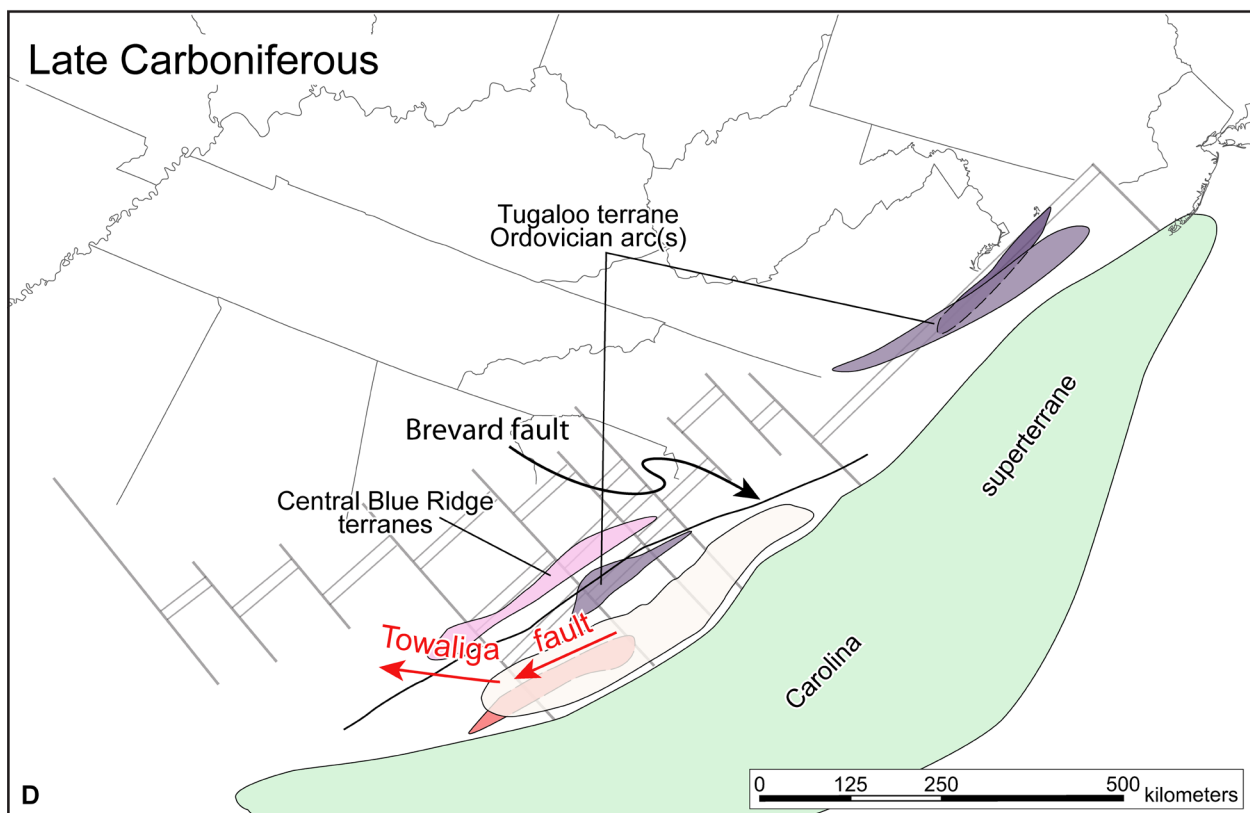
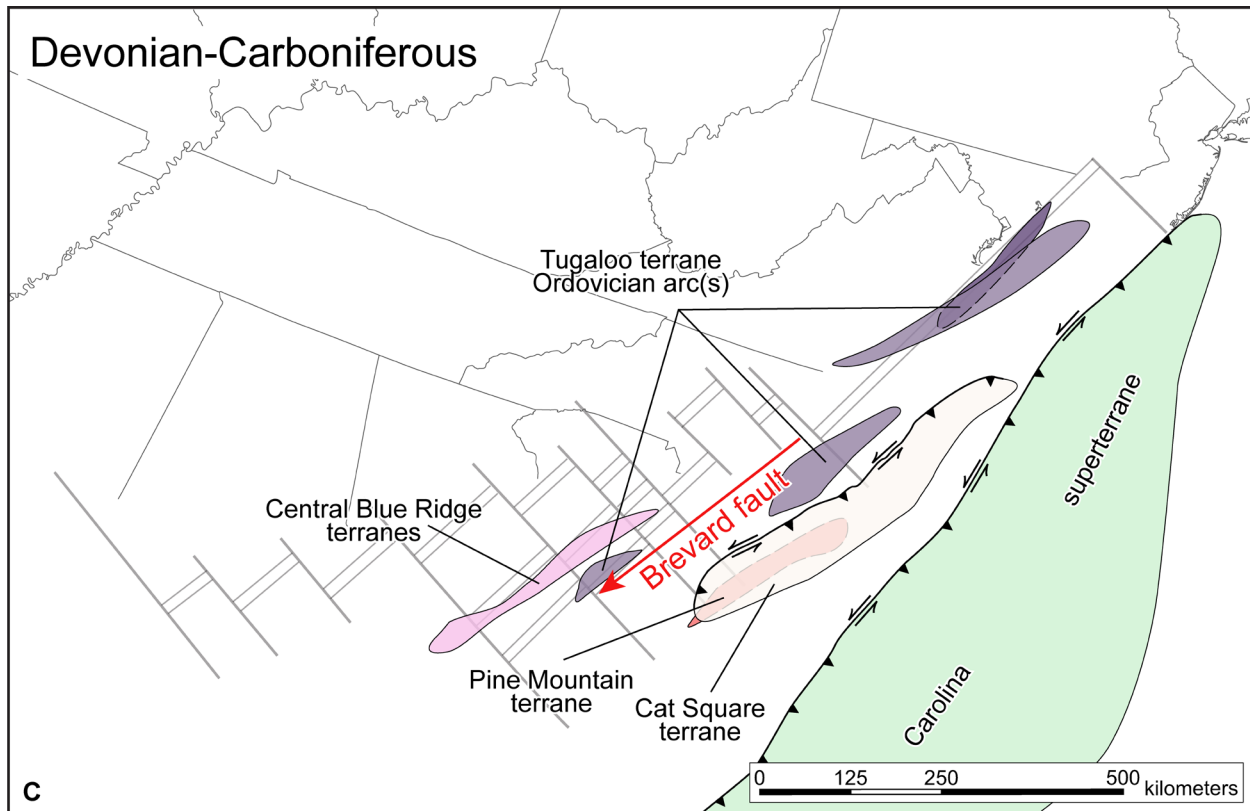


Figure 5-7 (continued)

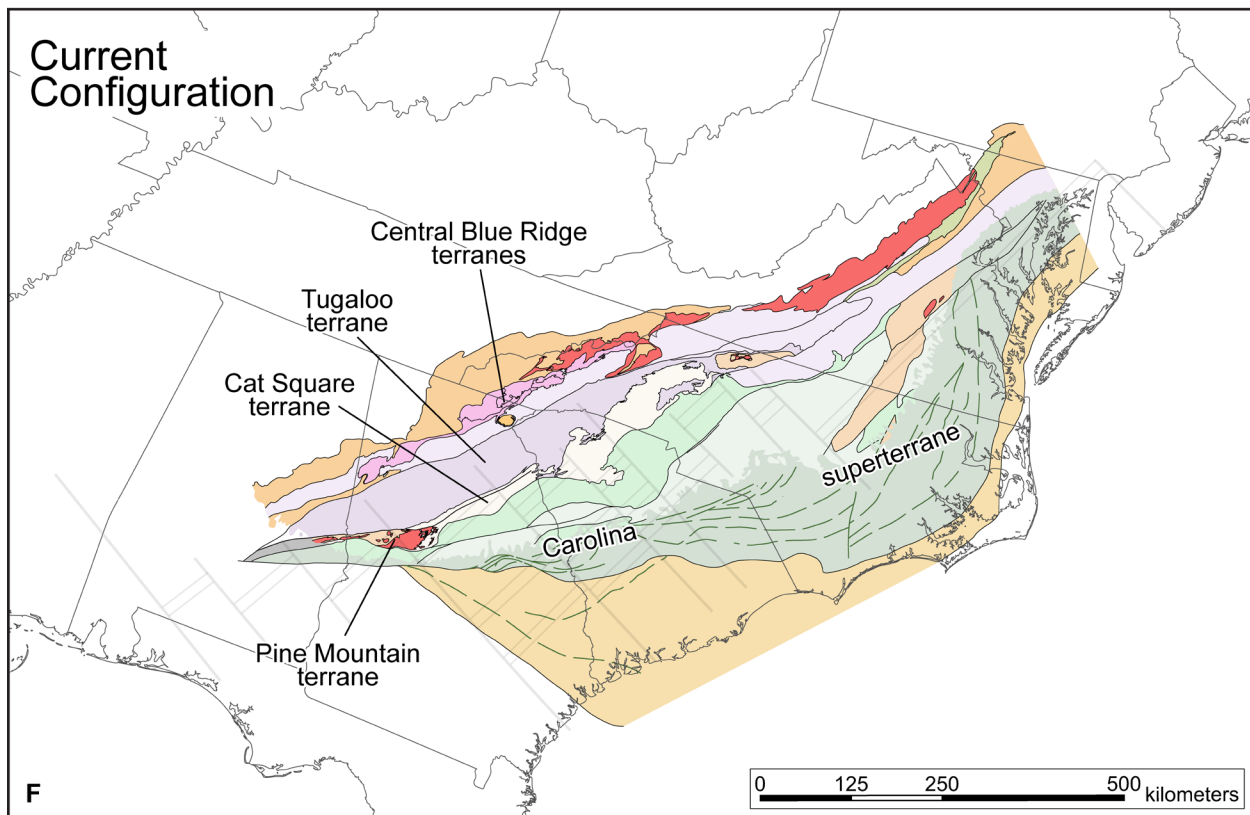
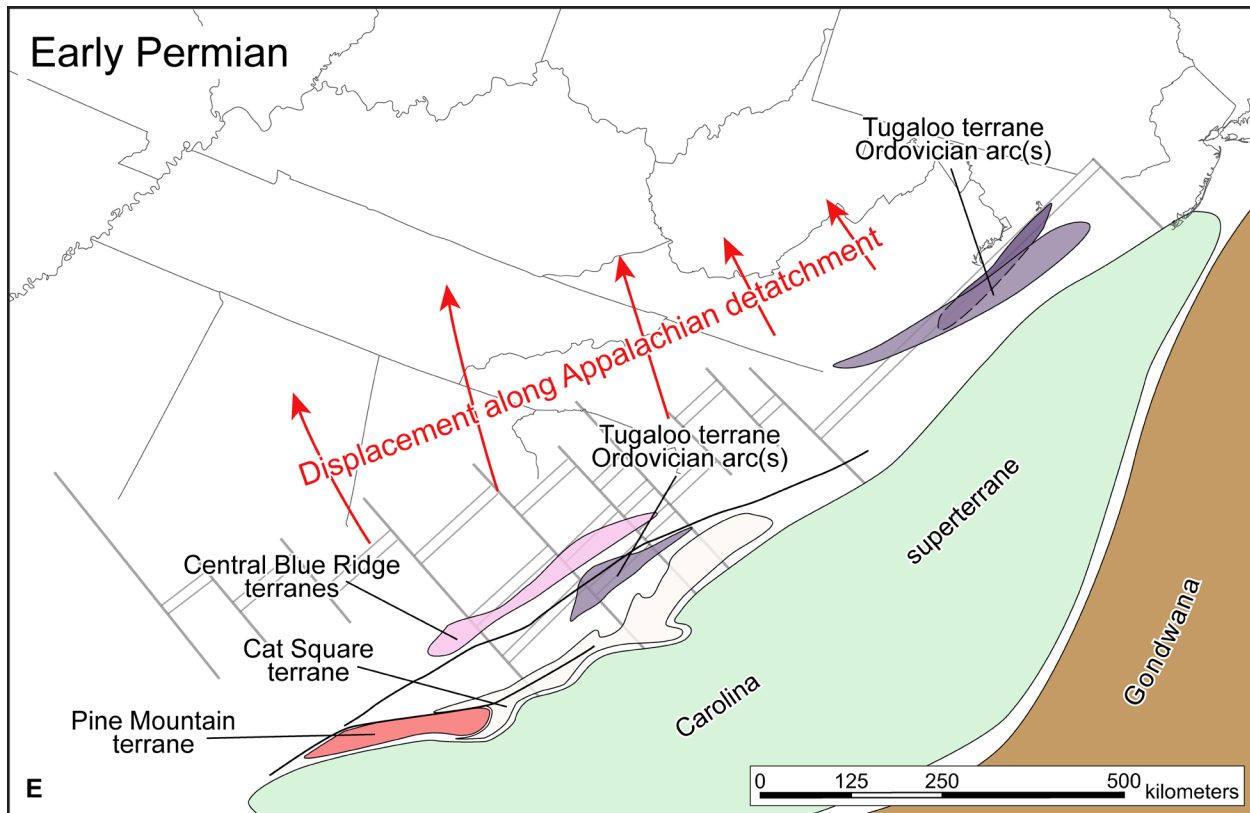


Figure 5-7 (continued)

Additionally, several authors have suggested the Towaliga fault may record a significant normal component (7-9 km), primarily based on COCORP seismic reflection data (e.g., Nelson et al., 1985, 1987). Reprocessing of those data indicate less than 200 m of normal offset of subsurface basement reflectors along the Towaliga fault (McBride et al., 2005). However, based on the current configuration of terranes and seismic data, the Pine Mountain terrane, which is juxtaposed against ~7 km of Inner Piedmont to the northwest (Fig. 5-4), had to be uplifted relative to the Inner Piedmont post emplacement of the Box Ankle fault. The interpretation of the Towaliga fault as a normal fault satisfies this observation, although fault-rock fabrics from both Alleghanian and Mesozoic phases of the Towaliga fault reveal no evidence for significant normal slip (Huebner and Hatcher, 2013). The large-displacement, primarily strike-slip Alleghanian phase, however, included an oblique northeast-down (southwest-up) dip-slip component, based shallow northeast-southwest-plunging mineral lineation data from fault rocks (Steltenpohl, 1988; Huebner and Hatcher, 2013). Considering the extent of the Towaliga fault, up to 250 km of displacement on the ~035 and ~070 segments combined is possible, which would require a $< 5^\circ$ oblique dip-slip component to uplift the Pine Mountain terrane relative to the adjacent Inner Piedmont by the observed offset.

One key aspect of the southern Appalachian orogen is that the entire orogen has been juxtaposed above the Laurentian platform on the Appalachian master detachment (e.g., Hatcher, 2010), with northwest displacement up to 400 km during the final rotational head-on collision with Gondwana (e.g., Hatcher, 2002). It must be kept in mind that all previous accretionary orogenies occurred significantly outboard relative to the current geographic configuration of terranes. Based on palinspastic restoration of the master Appalachian detachment, the Towaliga fault, and the Brevard fault zone, we suggest that an estimate of the original position of the Pine Mountain basement block along the eastern Laurentian margin can be ascertained (Fig. 5-7). Additionally, the distribution of rifted-margin facies along orogenic strike relative to structural promontories and embayments (Fig. 5-2) may provide a further test of our restoration estimate. Assuming the correlation of the Pine Mountain Group with Neoproterozoic-Cambrian passive-margin strata of the western Blue Ridge is valid, our estimate of the original position of the Pine Mountain terrane along the Laurentian margin would coincide with stratigraphic thicknesses at the Virginia promontory, which at that location along the margin consists of a thin veneer of Ocoee Supergroup rocks beneath the Chilhowee-Shady-Rome sequence (Fig. 5-2). The lithology and stratigraphic position of the Pine Mountain Group are consistent with this interpretation, and thickness of the strata, compared with thicknesses of correlative strata along the Neoproterozoic-Cambrian Laurentian margin, are compatible with our restoration of the original position of the Pine Mountain terrane.

DISCUSSION

Based on restoration of Blue Ridge and Inner Piedmont lithotectonic terranes along the master Appalachian detachment, Paleozoic orogenic events occurred significantly outboard relative to their current geographic configuration. The proximal shallow-water passive-margin facies Pine Mountain Group far into the internal portions of the orogen poses a significant problem considering our proposed temporal constraints with the current distribution of Blue Ridge and Inner Piedmont terranes (Fig. 5-7). Thrusting of the Inner Piedmont above the Pine Mountain terrane during Permian emplacement of the Blue Ridge-Inner Piedmont megathrust sheet is the most obvious solution; however, fabric relations between the Box Ankle fault and Inner Piedmont indicate the Inner Piedmont was thrust over the Pine Mountain terrane during the Acadian/Neoacadian orogeny sometime in the Devonian. Alternatively, thrusting of the Inner Piedmont, eastern, and central Blue Ridge terranes above the Laurentian platform during accretion of the Carolina superterrane would also solve this problem, but there is no evidence for significant foreland-directed thrusting of the central Blue Ridge terranes at that time. Therefore, the solution that best fits available data is early to middle Cambrian rifting of the Pine Mountain terrane from the Laurentian margin (e.g., Hooper and Hatcher, 1988a), similar to the departure of the Argentine Precordillera from southern Laurentia (e.g., Thomas, 1991; Thomas and Astini, 2003) and the Dashwoods microcontinent in the Newfoundland Appalachians (Waldron and van Staal, 2001). We suggest this rifting event had to occur post-deposition of the Pine Mountain Group (assuming the Manchester Schist is the highest stratigraphic unit), but prior to the development of Taconian island-arc terranes that comprise the central and eastern Blue Ridge (i.e., by ~480 Ma). This suggested rifting event would place the Pine Mountain terrane at a suitable position in the orogen based on the restoration of major faults and their timing, and also reconciles the paradox of proximal Laurentian strata of the Pine Mountain Group far out in the orogen with timing constraints that warrant overthrusting by the Inner Piedmont in the Devonian.

Another implication of this tectonic scenario is the relationship between the Box Ankle fault and northern portion of the Brindle Creek-Jackson Lake fault, which are similar in timing, metamorphic grade, and tectonic position in the orogen prior to translation along the Towaliga fault. It is interesting to consider the hypothesis that the Box Ankle fault may be a dismembered portion of the Brindle Creek thrust fault that was translated to the southwest during Alleghanian deformation along the Towaliga fault. We suggest that, when the Cat Square terrane was thrust over the Tugaloo terrane along the Brindle Creek-Jackson Lake fault in the Devonian (e.g., Merschat and Hatcher, 2007), what is now termed the Box Ankle fault could have been a portion of the Brindle Creek-Jackson Lake fault that was thrust over the Pine Mountain terrane instead of the Tugaloo terrane (Fig. 5-8). In this scenario, the development of the Towaliga and Bartletts Ferry-

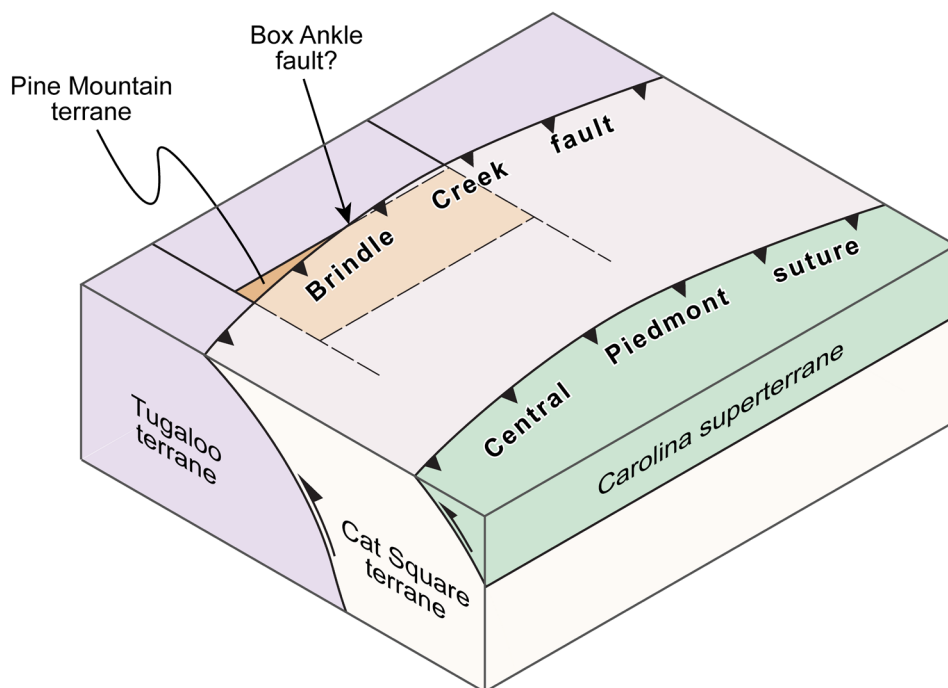


Figure 5-8: Schematic block diagram illustrating the hypothesis that the Box Ankle fault is a dismembered portion of the Brindle Creek-Jackson Lake fault.

Goat Rock fault systems may have localized at the margins of the Pine Mountain microcontinent, utilizing preexisting weaknesses, translated the block to the southwest during deformation along the Eastern Piedmont Fault System, and essentially separated this portion of the thrust that juxtaposes the Cat Square terrane above peri-Laurentian rocks. This would have juxtaposed this portion of the Inner Piedmont to what is now central Georgia, where the Jackson Lake fault (*sensu stricto*) is primarily strike-slip.

Translation along the Towaliga fault marks the final movement of the block relative to the Inner Piedmont and Carolina superterrane. The bend in the Towaliga fault at the northeast end of the window is indicative of polyphase deformation during the Alleghanian orogeny, which appears to be a common pattern throughout the Eastern Piedmont fault system (Fig. 5-1). In terms of the rotational transpressive terminal collision with Gondwana that formed Pangea, the north-south- and ~035-oriented faults of the Eastern Piedmont Fault System may coincide with the initial collision and development of step-over basins in New England, whereas the ~070-oriented segments of these faults may coincide with the Lackawanna phase of the Alleghanian orogeny during the initial rotation of Gondwana and head-on collision in the southern Appalachian orogen. We suggest this may be a corollary to the zipper tectonics model that depicts the final amalgamation of Pangea (Hatcher, 2002), which most likely represents an episode of extrusion

tectonics that slightly predates(?) head-on collision that emplaced the Blue Ridge-Inner Piedmont thrust sheet along the master Appalachian detachment.

Although the tectonic model proposed here regarding the allochthonous history of the Pine Mountain terrane is consistent with attributes of the southern Appalachian orogen discussed above, more supporting evidence is necessary for the hypothesis that depicts the Pine Mountain terrane as a peri-Laurentian microcontinent that rifted off of Laurentia, likely in the Cambrian. However, we argue its necessity based on our temporal constraints of the bounding faults, palinspastic restoration of those faults and major southern Appalachian fault systems, and the proximal nature of the Pine Mountain Group far outboard in the orogen. Future tests of this hypothesis may reveal yet unexplored ideas about the tectonic evolution of the southern Appalachians, and provide new clues regarding the complex amalgamation of Pangea through the Paleozoic.

CONCLUSIONS

1. The Pine Mountain window is framed by faults that vary in timing and kinematics, which structurally demands the Pine Mountain terrane be allochthonous.
2. Fabric relationships indicate the Box Ankle fault was active prior to development of S_2 fabric and peak metamorphism in the Inner Piedmont, which occurred during the Acadian/Neoacadian orogeny.
3. Timing and kinematics of the bounding faults and major southern Appalachian fault systems indicate a multi-stage allochthonous history for the Pine Mountain terrane, and palinspastic restoration of these fault systems restore it to the vicinity of the Virginia promontory.
4. The distribution of rifted- and passive-margin facies strata along the Laurentian margin supports restoration of the Pine Mountain terrane to the Virginia promontory.
5. The current configuration of the Pine Mountain terrane far outboard in the orogen, coupled with the temporal constraints of the bounding faults and proximal Neoproterozoic-Cambrian strata of Pine Mountain Group, suggest the Pine Mountain terrane may have rifted off of Laurentia post-deposition of its cover strata (middle Cambrian?) and reaccreted during the Acadian/Neoacadian orogeny.

REFERENCES CITED

- Adams, G.I., 1926, The crystalline rocks, *in* Adams, G.I., Butts, C., Stephenson, L.W., and Cooke, W., eds., *Geology of Alabama: Geological Society of Alabama Special Report 14*, p. 25-40.
- Adams, G.I., 1930, The significance of the quartzites of the Pine Mountain in the crystallines of west central Georgia: *Journal of Geology*, v. 38, p. 271-279.
- Clarke, J.W., 1952, *Geology and mineral resources of the Thomaston quadrangle, Georgia: Georgia Geological Survey Bulletin 59*, 99 p.
- Galpin, S.L., 1915, A preliminary report on the feldspar and mica deposits of Georgia: *Georgia Geological Survey Bulletin 30*, 190 p.
- Goldberg, S.A., and Steltenpohl, M.G., 1988, Evidence for Alleghanian penetrative deformation in the Inner Piedmont of Alabama: *Geological Society of America Abstracts with Programs*, v. 20, p. 267.
- Hatcher, R.D., Jr., 1984, Southern and central Appalachian basement massifs, *in* Bartholomew, M.J., Force, E.R., Sinha, A.K., and Herz, N., *The Grenville Event in the Appalachians and Related Topics: Boulder, Colorado, Geological Society of America Special Paper 194*, p. 149-153.
- Hatcher, R.D., Jr., 2001, Rheological partitioning during multiple reactivation of the Paleozoic Brevard fault zone, southern Appalachians, USA, *in* Holdsworth, R.E., Strachan, R.A., MacLoughlin, J.F., and Knipe, R.J., eds., *The Nature and Significance of Fault Zone Weakening: London, Geological Society Special Publication 86*, p. 255–269.
- Hatcher, R.D., Jr., 2002, Alleghanian (Appalachian) orogeny, a product of zipper tectonics: Rotational transpressive continent-continent collision and closing of ancient oceans along irregular margins, *in* Martínez Catalán, J.R., Hatcher, R.D., Jr., Arenas, R., and Díaz García, F., eds., *Variscan-Appalachian dynamics: The building of the late Paleozoic basement: Boulder, Colorado, Geological Society of America Special Paper 364*, p. 199-208.
- Hatcher, R.D., Jr., 2010, The Appalachian orogen: A brief summary, *in* Tollo, R.P., Bartholomew, M.J., Hibbard, J.P., and Karabinos, P.M., eds., *From Rodinia to Pangea: The Lithotectonic Record of the Appalachian Region: Boulder, Colorado, Geological Society of America Memoir 206*, p. 1-19.
- Hatcher, R.D., Jr., and Merschat, A.J., 2006, The Appalachian Inner Piedmont: An exhumed strike-parallel, tectonically forced orogenic channel, *in* Law, R.D., Searle, M., and Godin, L., eds., *Channel flow, ductile extrusion, and exhumation of lower-mid crust in continental collision zones: London, Geological Society Special Publication 268*, p. 517-540.

- Hatcher, R.D., Jr., Howell, D.E., and Talwani, P., 1977, Eastern Piedmont fault system: Speculations on its extent: *Geology*, v. 5, p. 636-640.
- Hatcher, R.D., Jr., Bream, B.R., and Merschat, A.J., 2007a, Tectonic map of the southern and central Appalachians: A tale of three orogens and a complete Wilson Cycle *in* Hatcher, R.D., Jr., Carlson, M.P., McBride, J.H., and Martínez Catalán, J.R., eds., 4-D Framework of Continental Crust: Boulder, Colorado, Geological Society of America Memoir 200, p. 595-632.
- Hatcher, R.D., Jr., Lemiszki, P.J., and Whisner, J.B., 2007b, Character of rigid boundaries and internal deformation of the southern Appalachian foreland fold-thrust belt, *in* Sears, J.W., Harms, T.A., and Evenchick, C.A., eds., Whence the Mountains? Inquiries into the Evolution of Orogenic Systems: A Volume in Honor of Raymond A. Price: Boulder, Colorado, Geological Society of America Special Paper 433, p. 243-276.
- Hewett, D.F., and Crickmay, G.W., 1937, The warm springs of Georgia, their geologic relations and origin: U.S. Geologic Survey Water Supply Paper 819, 37 p.
- Hibbard, J.P., 2000, Docking Carolina: *Geology*, v. 28, p. 127-130.
- Hooper, R.J., and Hatcher, R.D., Jr., 1988a, Pine Mountain terrane, a complex window in the Georgia and Alabama Piedmont; evidence from the eastern termination: *Geology*, v. 16, p. 307-310.
- Hooper, R.J., and Hatcher, R.D., Jr. 1988b. Mylonites from the Towaliga fault zone, central Georgia: products of heterogeneous non-coaxial deformation: *Tectonophysics*, v. 152, p. 1-17.
- Hooper, R.J., and Hatcher, R.D., Jr., 1989, The geology of the east end of the Pine Mountain window and adjacent Piedmont, central Georgia, *in* Fritz, W.J., ed., Premeeting field guide, Southeastern Section of the Geological Society of America: Atlanta, Georgia Geological Society, 37 p.
- Hooper, R.J., Hatcher, R.D., Jr., Troyer, P.K., Dawson, R.J., and Redmond, C.G., 1997, The character of the Avalon terrane and its boundary with the Piedmont terrane in central Georgia, *in* Glover, L., III, and Gates, A.E., eds., Central and Southern Appalachian Sutures: Results of the EDGE Project and Related Studies: Boulder, Colorado, Geological Society of America Special Paper 314, p. 1-14.
- Huebner, M. T., and Hatcher, R. D., Jr., 2013, Polyphase reactivation history of the Towaliga fault, central Georgia: Implications regarding the amalgamation and breakup of Pangea: *Journal of Geology*, v. 121, p. 75-90.
- Huebner, M.T., Hatcher, R.D., Jr., and Merschat, A.J., Confirmation of the southwest continuation of the Cat Square terrane, southern Appalachian Inner Piedmont, with implications for middle Paleozoic collisional orogenesis: *American Journal of Science*, in review.

- Huebner M.T., Rehner, J.R., Hatcher, R.D., Jr., and Wunderlich, A.L., Detailed geologic map of the Inner Piedmont at the northeast end of the Pine Mountain window, Georgia: 1:50,000 scale, Geological Society of America Map Series, in review.
- McBride, J.H., Hatcher, R.D., Jr., Stephenson, W.J., and Hooper, R.J., 2005, Integrating seismic reflection and geological data and interpretations across an internal basement massif: The southern Appalachian Pine Mountain window, USA: Geological Society of America Bulletin, v. 117, p. 669-686.
- Merschat, A.J., 2009, Assembling the Blue Ridge and Inner Piedmont: Insights into the nature and timing of terrane accretion in the southern Appalachian orogen from geologic mapping, stratigraphy, kinematic analysis, petrology, geochemistry, and modern geochronology [Ph.D. dissertation]: Knoxville, University of Tennessee, 455 p.
- Merschat, A.J., and Hatcher, R.D., Jr., 2007, The Cat Square terrane: Possible Siluro-Devonian remnant ocean basin in the Inner Piedmont, southern Appalachians, USA, *in* Hatcher, R.D., Jr., Carlson, M.P., McBride, J.H., and Martínez Catalán, J.R., eds., 4-D Framework of Continental Crust: Boulder, Colorado, Geological Society of America Memoir 197, p. 553-565.
- Merschat, A.J., Hatcher, R.D., Jr., and Davis, T.L., 2005, The northern Inner Piedmont, southern Appalachians, USA: Kinematics of transpression and SW-directed mid-crustal flow: Journal of Structural Geology, v. 27, p. 1252-1281.
- Miller, B.V., Fetter, A.H., and Stewart, K.G., 2006, Plutonism in three orogenic pulses, Eastern Blue Ridge Province, southern Appalachians: Geological Society of America Bulletin, v. 118, p. 171-184.
- Moecher, D.P., Samson, S.D., and Miller, C.F., 2004, Precise time and conditions of peak Taconian granulite facies metamorphism in the southern Appalachian orogen, U.S.A., with implications for zircon behavior during crustal melting events: Journal of Geology, v. 112, p. 289-304.
- Nelson, K.D., Arnou, J.A., Giguere, M., and Schamel, S., 1987, Normal-fault boundary of an Appalachian basement massif? Results of COCORP profiling across the Pine Mountain belt in western Georgia: Geology, v. 15, p. 832-836.
- Nelson, K.D., Arnou, J.A., McBride, J.H., Willemin, J.H., Huang, J., Zheng, L., Oliver, J.E., Brown, L.D., and Kaufman, S., 1985, New COCORP profiling in the southeastern United States. Part I: Late Paleozoic suture and Mesozoic rift basin: Geology, v. 13, p. 714-718.
- Raymond, D.E., Osborne, W.E., Copeland, C.W., and Neathery, T.L., 1988, Alabama Stratigraphy: Alabama Geological Survey Circular 140, 97 p.
- Rehner, J.R., Huebner, M.T., and Hatcher, R.D., Jr., 2012, Rheological and timing contrasts of major faults framing the northeastern end of the Pine Mountain window, central Georgia: Geological Society of America Abstracts with Programs, v. 44, no. 7, p. 595.

- Schamel, S., and Bauer, D.T., 1979, Remobilized Grenville basement in the Pine Mountain window, *in* Wones, D.R., ed., *Proceedings of the Caledonides in the U.S.A.: Department of Geosciences, Virginia Polytechnic Institute and State University, Memoir 2*, p. 313-316.
- Sears, J.W., and Cook, R.B., 1984, An overview of the Grenville basement complex of the Pine Mountain window, Alabama and Georgia, *in* Bartholomew, M.J., Force, E.R., Sinha, A.K., and Herz, N., eds., *The Grenville Event in the Appalachians and Related Topics: Boulder, Colorado, Geological Society of America Special Paper 194*, p. 281-287.
- Sears, J. W., Cook, R. B., and Brown, D. E., 1981a, Tectonic evolution of the western part of the Pine Mountain window and adjacent Inner Piedmont province, *in* Sears, J. W., ed., *Contrasts in tectonic style between the Inner Piedmont terrane and the Pine Mountain window: Alabama Geological Society, 18th Annual Field Trip Guidebook*, p. 1-13.
- Sears, J.W., Cook, R.B., Gilbert, O.E., Jr., Carrington, T.J., and Schamel, S., 1981b, Stratigraphy and structure of the Pine Mountain window in Georgia and Alabama, *in* Wigley, P.B., ed., *Latest Thinking on the Stratigraphy of Selected Areas in Georgia: Georgia Geological Survey Information Circular 54A*, p. 41-54.
- Sinha, A.K., Thomas, W.A., Hatcher, R.D., Jr., and Harrison, T.M., 2012, Geodynamic evolution of the central Appalachian orogen: Geochronology and compositional diversity of magmatism from Ordovician through Devonian: *American Journal of Science*, v. 312, p. 907-966.
- Steltenpohl, M.G., 1988, Kinematics of the Towaliga, Bartletts Ferry, and Goat Rock fault zones, Alabama: the late Paleozoic dextral shear system in the southernmost Appalachians: *Geology*, v. 16, p. 852-855.
- Steltenpohl, M.G., Heatherington, A., Mueller, P., and Wooden, J.L., 2004, Pre-Appalachian tectonic evolution of the Pine Mountain window in the southernmost Appalachians, Alabama and Georgia, *in* Tollo, R.P., Corriveau, L., McLelland, J., and Bartholomew, M.J., eds., *Proterozoic tectonic evolution of the Grenville orogen in North America: Boulder, Colorado, Geological Society of America Memoir 197*, p. 633-646.
- Steltenpohl, M.G., Hatcher, R.D., Jr., Mueller, P.A., Heatherington, A.L., and Wooden, J.L., 2010, Geologic history of the Pine Mountain window, Alabama and Georgia: Insights from a new geologic map and U-Pb isotopic dates, *in* Tollo, R.P., Bartholomew, M.J., Hibbard, J.P., and Karabinos, P.M., eds., *From Rodinia to Pangea: The Lithotectonic Record of the Appalachian Region: Boulder, Colorado, Geological Society of America Memoir 206*, p. 837-857.
- Student, J.J., and Sinha, A.K., 1992, Carboniferous U-Pb ages of zircons from the Box Ankle and Ocmulgee faults, central Georgia: implications for accretionary models: *Geological Society of America Abstracts with Programs*, v. 24, p. 69.
- Thomas, W.A., 1991, The Appalachian-Ouachita rifted margin of southeastern North America: *Geological Society of America Bulletin*, v. 103, p. 415-431.

- Thomas, W.A., and Astini, R.A., 2003, Ordovician accretion of the Argentine Precordillera terrane to Gondwana: a review: *Journal of South American Earth Sciences*, v. 16, p. 67-79.
- Vaucher, A., Babaie, H. A., and Babaie, A., 1993, Orogen-parallel tangential motion in the Late Devonian-Early Carboniferous southern Appalachians internides: *Canadian Journal of Earth Sciences*, v. 30, p. 1297-1305.
- Waldron, J.W.F., and van Staal, C.R., 2001, Taconian orogeny and the accretion of the Dashwoods block: A peri-Laurentian microcontinent in the Iapetus Ocean: *Geology*, v. 29, p. 811-814.
- West, T.E., Jr., Secor, D.T., Jr., Pray, J.R., Boland, I.B., and Maher, H.D., Jr., 1995, New evidence for an exposure of the Appalachian décollements at the east end of the Pine Mountain terrane, Georgia: *Geology*, v. 23, p. 621-624.
- Yokel, L.S., and Steltenpohl, M.G., 1997, Laurentian cover lithologies of the Pine Mountain massif, Alabama, and potential correlations with the Valley and Ridge and Western Blue Ridge units, *in* Bearce, D., ed., *Comparison of the Pine Mountain Block Basement-Cover Sequence with the Lower Cambrian Clastic-Carbonate Sequence in the Talladega Slate Belt: Tuscaloosa, Alabama Geological Society, Field Trip Guidebook*, p. 1-26.

APPENDICES

Appendix I

Structural Measurements and Outcrop Descriptions from the Covington, Jackson, Lloyd Shoals Dam, Stewart, and Worthville 7.5-minute Quadrangles

Note: Stations correspond to locations shown in Plate II.

ABBREVIATIONS

7.5-minute Quadrangles:

CV - Covington
JK - Jackson
LS - Lloyd Shoals Dam
ST - Stewart
WV - Worthville

Textures:

ALT - hydrothermally altered
MIG - migmatitic
MYL - mylonitic

Lithologies:

AM - amphibolite
CALC-SI - calc-silicate
CHL SCH - chlorite schist
DD - diabase
DPG - Dows Pulpit Granodiorite
GG - granitic gneiss
GTD - granitoid
HFG - High Falls Granite
ISG - Indian Springs Granodiorite
MGW - metagraywacke
PEG - pegmatite
QZ - quartzite
RQ - ribbon quartz mylonite
SCH - schist
SCH MGW - schistose metagraywacke
SI CAT - siliceous cataclasite
SSCH - sillimanite schist

			FOLIATION		LINEATION			FOLD AXIS		AXIAL SURFACE		ILA	VERG	JOINT	
QUAD	STATION	LITHOLOGY	STRIKE	DIP	TREND	PLUNGE	TYPE	TREND	PLUNGE	STRIKE	DIP			STRIKE	DIP
CV	1	MYL MGW, AM	45	88											
CV	1	MYL MGW, AM	42	81											
CV	1	MYL MGW, AM			130	81	BN								
CV	3	MIG MGW	211	64											
CV	4	MYL MGW			211	22	STR								
CV	5	MYL MGW, AM	10	75											
CV	6	GG	32	61											

			FOLIATION		LINEATION			FOLD AXIS		AXIAL SURFACE		ILA	VERG	JOINT	
QUAD	STATION	LITHOLOGY	STRIKE	DIP	TREND	PLUNGE	TYPE	TREND	PLUNGE	STRIKE	DIP			STRIKE	DIP
JK	13	MIG MGW	196	56											
JK	14	MGW	191	16											
JK	15	MGW	139	51											
JK	19	HFG	64	59											
JK	23	HFG	196	51											
JK	24	HFG	149	24											
JK	24	HFG			237	22									
JK	25	HFG	221	73											
JK	26	HFG	177	66											
JK	27	HFG								56	79	150	NW		
JK	27	HFG						221	31			150	NW		
JK	28	GG	81	22											
JK	28	GG	81	22											
JK	29	ISG	161	65											
JK	32	HFG, ISG	191	47											
JK	33	MGW, GTD	221	61											
JK	34	SSCH, RQ	204	41											
JK	35	MGW	209	64											
JK	36	MIG MGW	194	41											
JK	37	GTD	207	64											
JK	38	GTD	141	39											
JK	39	GTD												34	90
JK	39	GTD												103	90
JK	41	MGW, PEG	244	73											
JK	42	QZ	36	59											
JK	45	MGW, QZ	234	56											
JK	47	MGW, ISG	21	56											
JK	48	MIG MGW	61	37											
JK	49	MIG MGW	354	49											
JK	50	MIG MGW	241	66											
JK	51	MIG MGW	354	46											
JK	51	MIG MGW												259	79
JK	52	MIG MGW	299	42											
JK	53	MIG MGW	316	59											
JK	54	MGW, QZ	201	61											
JK	55	MGW, QZ	184	51											
JK	56	SCH MGW	192	35											
JK	57	MGW	56	39											
JK	57	MGW												157	90
JK	57	MGW			194	17									
JK	58	MIG MGW	181	48											
JK	59	MGW	161	51											
JK	60	MGW	184	65											
JK	61	GTD	147	56											
JK	62	MIG MGW	229	56											
JK	63	MIG MGW	202	51											
JK	64	MIG MGW, GTD	166	31											
JK	65	MIG MGW	185	51											
JK	65	MIG MGW								345	71	30	SSW		
JK	65	MIG MGW						4	26			30	SSW		
JK	66	MIG MGW	184	59											
JK	67	MIG MGW	164	49											
JK	68	MIG MGW	201	51											
JK	69	MIG MGW	223	34											
JK	70	MIG MGW	167	41											
JK	71	MIG MGW	166	66											
JK	72	MIG MGW	141	40											
JK	74	GG	199	60											

			FOLIATION		LINEATION			FOLD AXIS		AXIAL SURFACE		ILA	VERG	JOINT	
QUAD	STATION	LITHOLOGY	STRIKE	DIP	TREND	PLUNGE	TYPE	TREND	PLUNGE	STRIKE	DIP			STRIKE	DIP
JK	75	MIG MGW	204	56											
JK	76	HFG	186	67											
JK	77	MIG MGW	189	38											
JK	78	HFG, GTD	204	64											
JK	79	HFG, GTD	209	59											
JK	82	MGW, ISG	238	77											
JK	82	MGW, ISG								238	77	10	NW		
JK	82	MGW, ISG						239	41			10	NW		
JK	82	MGW, ISG												76	90
JK	82	MGW, ISG												31	90
JK	83	MGW	184	64											
JK	83	MGW												311	90
JK	84	MGW, ISG	216	63											
JK	85	MGW	182	61											
JK	86	MGW	204	59											
JK	87	MGW	223	59											
JK	88	MGW	189	46											
JK	89	MGW	191	51											
JK	90	MGW	81	51											
JK	92	GG	111	41											
JK	93	SCH	209	69											
JK	94	HFG	236	65											
JK	96	SCH	34	49											
JK	98	ISG	26	74											
JK	99	ISG	162	54											
JK	101	ISG	125	34											
JK	104	DPG	69	74											
JK	105	MGW	111	28											
JK	106	HFG	252	53											
JK	107	ISG, PEG	99	76											
JK	108	MGW	233	24											
JK	109	MGW	236	57											
JK	112	HFG	62	53											
JK	113	ISG	104	39											
JK	114	ISG	65	65											
JK	116	MGW	185	36											
JK	117	MGW, PEG	176	44											
JK	118	MGW, ISG	171	46											
JK	119	MGW	98	29											
JK	120	MIG SCH	311	61											
JK	123	ISG	182	64											
JK	124	MGW	166	53											
JK	124	MGW			226	39									
JK	125	MGW	146	51											
JK	126	ISG	196	45											
JK	129	MGW	32	45											
JK	130	HFG	94	35											
JK	133	SCH MGW	171	56											
JK	134	SCH MGW	168	47											
JK	135	MGW	197	36											
JK	136	ISG	34	46											
JK	137	MYL MGW	14	30											
JK	139	ISG	336	61											
JK	140	HFG	65	64											
JK	141	HFG	52	45											
JK	144	HFG	65	52											
JK	147	HFG	224	64											
JK	148	HFG	218	48											

			FOLIATION		LINEATION			FOLD AXIS		AXIAL SURFACE		ILA	VERG	JOINT	
QUAD	STATION	LITHOLOGY	STRIKE	DIP	TREND	PLUNGE	TYPE	TREND	PLUNGE	STRIKE	DIP			STRIKE	DIP
JK	149	HFG	248	72											
JK	150	HFG	206	67											
JK	151	MIG SSCH								269	79	35	S		
JK	151	MIG SSCH						270	43			35	S		
JK	152	ISG	135	49											
JK	154	HFG	17	54											
JK	155	HFG	262	59											
JK	156	HFG	125	42											
JK	157	ISG	216	68											
JK	158	HFG	49	46											
JK	159	HFG	36	31											
JK	160	HFG, ISG	201	51											
JK	160	HFG, ISG	87	62											
JK	162	DPG	358	51											
JK	163	MIG MGW	206	66											
JK	164	HFG	186	43											
JK	165	HFG	208	49											
JK	166	HFG	207	44											
JK	167	HFG	61	45											
JK	170	HFG	41	46											
JK	172	HFG	218	51											
JK	174	MGW, AM	68	54											
JK	175	MGW	91	60											
JK	178	MGW	34	74											
JK	179	DPG	6	75											
JK	180	MGW	104	44											
JK	183	MGW, ISG	27	60											
JK	184	MGW	213	51											
JK	185	HFG	174	41											
JK	186	ISG	170	56											
JK	189	MGW	195	43											
JK	193	DPG	241	66											
JK	194	DPG	49	62											
JK	195	ISG	200	61											
JK	196	DPG	144	56											
JK	197	DPG	31	77											
JK	198	DPG	118	44											
JK	200	HFG, SCH	49	82											
JK	200	HFG, SCH								50	70	60	NW		
JK	200	HFG, SCH						52	40			60	NW		
JK	202	MGW	174	64											
JK	203	MIG MGW	154	39											
JK	205	DPG	21	72											
JK	206	HFG	49	59											
JK	207	HFG	44	71											
JK	208	HFG	119	44											
JK	210	HFG	41	70											
JK	211	HFG	244	71											
JK	212	MIG MGW, GTD, MY	211	61											
JK	213	SCH MGW	226	50											
JK	214	MIG SCH MGW	206	53											
JK	215	MIG MGW	217	44											
JK	216	SCH MGW	216	54											
JK	217	SCH MGW	135	46											
JK	219	HFG	45	66											
JK	220	HFG	121	64											
JK	221	HFG	172	43											
JK	223	HFG, SCH	154	48											

			FOLIATION		LINEATION			FOLD AXIS		AXIAL SURFACE		ILA	VERG	JOINT	
QUAD	STATION	LITHOLOGY	STRIKE	DIP	TREND	PLUNGE	TYPE	TREND	PLUNGE	STRIKE	DIP			STRIKE	DIP
JK	225	HFG	113	70											
JK	226	ISG	126	44											
JK	227	ISG	132	48											
JK	229	HFG	62	58											
JK	230	MGW	73	55											
JK	232	MGW, ISG	179	64											
JK	233	HFG	73	76											
JK	234	HFG, PEG	66	66											
JK	235	ISG	122	74											
JK	236	HFG	46	58											
JK	238	MGW	41	43											
JK	240	HFG	225	66											
JK	242	MGW	133	39											
JK	243	HFG	110	44											
JK	244	SSCH			54	14									
JK	245	HFG	29	66											
JK	246	HFG	37	69											
JK	248	GG	219	51											
JK	249	GG	88	42											
JK	250	GG	41	56											
JK	251	GG	234	72											
JK	252	GG	292	56											
JK	253	GG	216	42											
JK	254	GG	116	48											
JK	255	GG	226	26											
JK	256	GG	229	36											
JK	257	SCH MGW, AM	231	70											
JK	258	SCH MGW, AM	232	68											
JK	259	MGW, AM	199	80											
JK	260	MGW, AM	241	63											
JK	261	SCH MGW	190	71											
JK	262	SCH MGW, AM	152	79											
JK	263	SCH, AM								92	66	25	N		
JK	263	SCH, AM						275	76			25	N		
JK	265	MIG SCH MGW	124	52											
JK	266	MGW, AM	191	56											
JK	267	SCH MGW	181	62											
JK	268	MGW	186	31											
JK	270	SSCH			211	32									
JK	271	HFG, SCH	211	65											
JK	273	HFG	81	41											
JK	280	GTD	84	66											
JK	281	HFG	265	74											
JK	283	ISG	209	64											
JK	284	ISG, HFG	201	43											
JK	285	HFG	232	62											
JK	286	ISG	74	60											
JK	286	ISG												315	82
JK	287	HFG	95	64											
JK	288	SI CAT, ALT GG												289	84
JK	288	SI CAT, ALT GG												124	72
JK	288	SI CAT, ALT GG												220	72
JK	288	SI CAT, ALT GG												59	82
JK	288	SI CAT, ALT GG												176	41
JK	288	SI CAT, ALT GG												257	56
JK	288	SI CAT, ALT GG												201	41
JK	288	SI CAT, ALT GG												324	46
JK	288	SI CAT, ALT GG												255	38

			FOLIATION		LINEATION			FOLD AXIS		AXIAL SURFACE		ILA	VERG	JOINT	
QUAD	STATION	LITHOLOGY	STRIKE	DIP	TREND	PLUNGE	TYPE	TREND	PLUNGE	STRIKE	DIP			STRIKE	DIP
JK	288	SI CAT, ALT GG												231	51
JK	288	SI CAT, ALT GG			21	19	STR								
JK	288	SI CAT, ALT GG	79	72											
JK	291	HFG, ISG	84	53											
JK	291	HFG, ISG								164	86	25	NNE		
JK	291	HFG, ISG						158	66			25	NNE		
JK	293	HFG, ISG	66	71											
JK	294	ISG	234	48											
JK	295	HFG	31	80											
JK	296	ISG	31	81											
JK	297	ISG	41	72											
JK	298	HFG, ISG	85	73											
JK	299	HFG, ISG	63	79											
JK	300	ISG	134	61											
JK	301	ISG	138	81											
JK	302	ISG	116	51											
JK	303	HFG	49	44											
JK	304	HFG	27	71											
JK	305	ISG, SCH	88	65											
JK	308	SCH												331	71
JK	310	SCH	81	43											
JK	312	HFG, SCH	141	61											
JK	315	MGW	46	74											
JK	328	HFG	71	59											
JK	329	ISG	41	48											
JK	330	ISG	75	59											
JK	331	HFG	216	44											
JK	332	ISG	26	66											
JK	333	ISG, HFG	44	79											
JK	334	HFG, ISG	231	53											
JK	335	HFG, ISG	65	76											
JK	337	SSCH												318	81
JK	339	HFG	72	39											
JK	344	ISG	263	48											
JK	346	ISG	124	34											
JK	347	ISG	259	48											
JK	348	HFG	59	86											
JK	349	ISG	85	72											
JK	350	ISG	79	44											
JK	351	HFG	93	58											
JK	352	HFG	55	74											
JK	353	ISG	178	46											
JK	354	HFG	172	51											
JK	355	MGW	192	55											
JK	356	MGW	217	51											
JK	357	MGW, ISG	231	52											
JK	357	MGW, ISG	196	79											
JK	358	ISG	158	72											
JK	359	ISG	72	66											
JK	360	ISG	69	74											
JK	361	MGW, ISG	223	76											
JK	361	MGW, ISG												306	68
JK	362	MGW	66	63											
JK	363	MGW, HFG	244	72											
JK	364	HFG	259	78											
JK	365	HFG	229	66											
JK	366	HFG	252	77											
JK	367	ISG	156	62											

			FOLIATION		LINEATION			FOLD AXIS		AXIAL SURFACE		ILA	VERG	JOINT	
QUAD	STATION	LITHOLOGY	STRIKE	DIP	TREND	PLUNGE	TYPE	TREND	PLUNGE	STRIKE	DIP			STRIKE	DIP
JK	368	MGW	96	81											
JK	379	HFG	248	68											
JK	380	ISG, MGW	32	54											
JK	380	ISG, MGW	86	84											
JK	381	HFG	146	62											
JK	387	HFG	228	60											
JK	388	ISG, MGW	99	82											
JK	389	ISG	214	68											
JK	390	HFG	221	59											
JK	391	HFG	228	56											
JK	393	ISG	292	56											
JK	394	HFG, ISG	264	65											
JK	395	HFG	242	85											
JK	396	ISG, HFG	276	55											
JK	397	ISG	69	60											
JK	398	HFG	64	41											
JK	399	HFG	56	31											
JK	400	HFG	338	38											
JK	401	HFG	86	52											
JK	402	HFG	61	68											
JK	403	SCH, HFG			243	34									
JK	404	HFG	64	42											
JK	405	SCH								86	54	60	N		
JK	405	SCH						244	37			60	N		
JK	406	HFG	64	69											
JK	407	HFG	122	41											
JK	408	HFG	61	47											
JK	409	HFG	59	38											
JK	419	ISG	290	42											
JK	422	HFG	231	63											
JK	425	HFG	62	62											
JK	426	HFG	110	61											
JK	429	MIG SCH MGW	141	37											
JK	429	SCH MGW			244	26									
JK	430	SCH	184	49											
JK	431	SCH MGW	139	36											
JK	434	HFG	109	68											
JK	436	HFG	72	74											
JK	437	ISG	26	46											
JK	440	ISG	244	44											
JK	442	SCH MGW	66	80											
JK	443	HFG, PEG	77	65											
JK	444	HFG	174	44											
JK	445	HFG	121	51											
JK	446	HFG	90	72											
JK	447	HFG	77	58											
JK	448	HFG	86	52											
JK	449	HFG	96	51											
JK	451	HFG	69	64											
JK	452	ISG	104	59											
JK	453	MGW, HFG, CALC-S	56	77											
JK	454	HFG	253	69											
JK	456	HFG	13	76											
JK	457	MGW, SCH	31	55											
JK	462	HFG	135	43											
JK	463	HFG	74	75											
JK	466	ISG	124	44											
JK	468	HFG, ISG	103	31											

			FOLIATION		LINEATION			FOLD AXIS		AXIAL SURFACE		ILA	VERG	JOINT	
QUAD	STATION	LITHOLOGY	STRIKE	DIP	TREND	PLUNGE	TYPE	TREND	PLUNGE	STRIKE	DIP			STRIKE	DIP
JK	470	HFG, ISG	169	79											
JK	471	ISG	109	77											
JK	472	HFG	87	46											
JK	473	HFG	119	63											
JK	475	HFG	112	63											
JK	476	HFG	74	38											
JK	477	HFG	106	82											
JK	478	HFG	95	51											
JK	479	HFG	114	77											
JK	480	HFG	79	42											
JK	481	ISG	151	67											
JK	483	HFG	86	69											
JK	484	HFG	102	74											
JK	485	HFG, ISG	194	64											
JK	486	ISG	131	44											
JK	487	HFG	144	68											
JK	488	HFG	103	52											
JK	489	HFG	219	65											
JK	490	HFG	252	81											
JK	491	HFG	72	53											
JK	492	HFG	80	56											
JK	497	HFG, PEG	97	63											
JK	501	HFG	222	69											
JK	502	GTD, HFG, SCH MGW	212	59											
JK	503	HFG, ISG	194	66											
JK	505	ISG	69	50											
JK	506	ISG	239	76											
JK	507	ISG	46	37											
JK	508	ISG	65	53											
JK	514	SCH MGW, PEG, HFG	104	34											
JK	514	SCH MGW, PEG, HFG			224	21									
JK	516	HFG	41	59											
JK	517	HFG, ISG	51	82											
JK	520	ISG	83	68											
JK	521	HFG	66	49											
JK	522	HFG	59	57											
JK	523	HFG	51	51											
JK	524	HFG	87	67											
JK	526	HFG, PEG	81	64											
JK	528	HFG	105	53											
JK	529	HFG	132	41											
JK	530	HFG	71	51											
JK	532	HFG	153	31											
JK	533	HFG	52	77											
JK	537	HFG	58	59											
JK	540	HFG	102	68											
JK	541	SCH			233	35									
JK	542	ISG	91	51											
JK	543	HFG	74	37											
JK	545	SCH MGW, ISG	188	76											
JK	548	SCH MGW	179	52											
JK	550	HFG, ISG	222	67											
JK	553	GTD, Gd	46	47											
JK	554	MGW, AM	148	37											
JK	555	GG, AM	54	46											
JK	556	MGW, AM	41	48											
JK	557	MGW	26	71											
JK	558	SCH MGW	33	57											

			FOLIATION		LINEATION			FOLD AXIS		AXIAL SURFACE		ILA	VERG	JOINT	
QUAD	STATION	LITHOLOGY	STRIKE	DIP	TREND	PLUNGE	TYPE	TREND	PLUNGE	STRIKE	DIP			STRIKE	DIP
JK	559	HFG, ISG	63	53											
JK	561	HFG	217	46											
JK	563	ISG	4	66											
JK	564	SCH MGW	146	52											
JK	565	MIG MGW								46	73	80	SE		
JK	565	MIG MGW						228	34			80	SE		
JK	566	MGW, ISG	235	66											
JK	566	MGW, ISG	255	49											
JK	567	ISG	104	37											
JK	568	ISG	101	43											
JK	568	ISG												216	68
JK	568	ISG												113	90
JK	569	SCH MGW	261	79											
JK	570	MIG MGW	240	64											
JK	570	MIG MGW								203	71	40	NW		
JK	570	MIG MGW						14	39			40	NW		
JK	571	MIG MGW	261	64											
JK	571	MIG MGW												96	75
JK	572	SCH MGW	81	74											
JK	576	ISG	70	56											
JK	578	MGW, ISG	137	48											
JK	579	HFG	77	46											
JK	580	HFG	246	47											
JK	581	MGW	111	56											
JK	581	MGW			264	30									
JK	582	HFG	236	62											
JK	583	HFG	124	40											
JK	584	HFG	61	66											
JK	586	HFG	111	43											
JK	587	HFG	81	79											
JK	588	HFG	45	76											
JK	589	MGW, HFG	119	67											
JK	590	HFG	67	69											
JK	591	HFG, MGW	149	55											
JK	592	SCH MGW	71	60											
JK	601	HFG	168	70											
JK	603	SSCH								321	71	45	SW		
JK	603	SSCH						131	39			45	SW		
JK	604	ISG	345	57											
JK	607	ISG	138	41											
JK	613	ISG	17	33											
JK	615	ISG	136	35											
JK	615	ISG												124	82
JK	616	HFG, ISG	191	63											
JK	620	MGW	148	67											
JK	621	MGW	134	44											
JK	622	MIG MGW	165	57											
JK	623	MIG MGW	195	72											
JK	623	MIG MGW								168	69				
JK	623	MIG MGW						162	53						
JK	628	ISG	255	74											
JK	629	SCH MGW	191	34											
JK	630	ISG	128	37											
JK	631	HFG	42	61											
JK	632	ISG	176	46											
JK	633	HFG	92	66											
JK	634	HFG	58	62											
JK	636	HFG	51	64											

			FOLIATION		LINEATION			FOLD AXIS		AXIAL SURFACE		ILA	VERG	JOINT	
QUAD	STATION	LITHOLOGY	STRIKE	DIP	TREND	PLUNGE	TYPE	TREND	PLUNGE	STRIKE	DIP			STRIKE	DIP
JK	640	ISG	193	56											
JK	641	MGW	140	38											
JK	642	ISG	191	58											
JK	643	MGW	226	41											
JK	644	MGW	197	61											
JK	645	MGW	211	64											
JK	646	HFG, MGW	221	70											
JK	647	HFG, MGW	221	60											
JK	647	HFG, MGW								131	48				
JK	647	HFG, MGW						268	36						
JK	648	ISG	71	41											
JK	649	SCH MGW	214	59											
JK	650	SCH MGW	192	74											
JK	651	HFG	215	79											
JK	652	HFG	227	67											
JK	653	HFG	236	68											
JK	653	HFG												318	90
JK	661	HFG, ISG	254	63											
JK	662	HFG	65	67											
JK	664	SCH MGW	151	60											
JK	665	SCH	143	79											
JK	667	MIG MGW, ISG	83	56											
JK	672	ISG	258	61											
JK	676	HFG, SCH	73	54											
JK	678	HFG, MGW	63	78											
JK	679	MGW	57	54											
JK	689	SSCH			105	44									
JK	691	ISG	66	59											
JK	695	SCH	39	73											
JK	697	SCH								341	84	95	NE		
JK	697	SCH						148	53			95	NE		
JK	705	ISG	63	64											
JK	706	HFG	36	68											
JK	707	ISG, HFG	65	49											
JK	711	HFG	90	75											
JK	712	ISG	343	67											
JK	716	HFG	66	66											
JK	717	ISG, HFG	116	63											
JK	724	HFG	144	45											
JK	725	MGW	88	65											
JK	727	HFG	105	65											
JK	728	HFG	59	50											
JK	736	HFG, ISG	65	64											
JK	737	ISG, HFG	33	62											
JK	743	HFG	246	47											
JK	745	HFG, ISG	273	56											
JK	746	MGW, ISG, HFG	61	58											
JK	747	HFG, ISG	104	37											
JK	748	HFG	64	59											
JK	753	HFG, ISG	222	62											
JK	754	ISG, MGW	214	43											
JK	754	ISG, MGW	145	68											
JK	755	HFG	245	78											
JK	759	MIG MGW	185	78											
JK	761	HFG	247	75											
JK	769	HFG, ISG	67	67											
JK	770	ISG	76	58											
JK	771	ISG	107	56											

			FOLIATION		LINEATION			FOLD AXIS		AXIAL SURFACE		ILA	VERG	JOINT	
QUAD	STATION	LITHOLOGY	STRIKE	DIP	TREND	PLUNGE	TYPE	TREND	PLUNGE	STRIKE	DIP			STRIKE	DIP
JK	772	HFG	69	65											
JK	774	HFG	163	66											
JK	778	MGW, AM	211	44											
JK	779	MGW, AM	158	58											
JK	780	MGW, AM	131	26											
JK	781	SSCH	134	54											
JK	782	SCH MGW	121	56											
JK	784	SCH MGW	129	56											
JK	787	MGW	142	38											
JK	788	HFG	204	56											
JK	789	ISG, HFG	163	73											
JK	790	ISG	211	43											
JK	791	HFG	241	44											
JK	792	DPG	221	40											
JK	792	DPG, SI CAT												286	73
JK	792	DPG, SI CAT												175	47
JK	792	DPG, SI CAT												308	90
JK	794	SSCH												135	72
JK	799	GG	229	68											
JK	799	GG								166	80	80	WSW		
JK	799	GG						334	37			80	WSW		
JK	800	GG	307	77											
JK	801	GG								102	77				
JK	801	GG						111	56						
JK	802	GG								128	75		SW		
JK	802	GG						306	64				SW		
JK	803	GG								92	76		SSW		
JK	803	GG						276	44				SSW		
JK	804	GG	70	69											
JK	805	GG	261	75											
JK	805	GG								106	79	ISO			
JK	805	GG						104	53			ISO			
JK	806	GG	88	73											
JK	807	GG	62	57											
JK	808	MGW	23	56											
JK	809	MGW	204	49											
JK	809	MGW												108	83
JK	810	MGW								122	65	75	NE		
JK	810	MGW						313	21			75	NE		
JK	811	GG	88	46											
JK	812	MIG MGW	57	72											
JK	812	MIG MGW								247	74				
JK	812	MIG MGW						64	46						
JK	814	GG	134	61											
JK	821	GG	167	52											
JK	823	GG, AM	46	63											
JK	824	GG	103	56											
JK	825	GTD	122	49											
JK	826	GG, AM	212	46											
JK	827	GG	61	56											
JK	828	GG	75	66											
JK	828	GG								95	79	ISO	SW		
JK	828	GG						104	46			ISO	SW		
JK	829	GG	289	77											
JK	829	GG								75	80				
JK	829	GG						84	52						
JK	830	GG	251	73											
JK	831	GG	81	76											

			FOLIATION		LINEATION			FOLD AXIS		AXIAL SURFACE		ILA	VERG	JOINT	
QUAD	STATION	LITHOLOGY	STRIKE	DIP	TREND	PLUNGE	TYPE	TREND	PLUNGE	STRIKE	DIP			STRIKE	DIP
JK	832	GG								66	81				
JK	832	GG						242	56						
JK	833	GG								97	82				
JK	833	GG						271	46						
JK	834	GG								98	77				
JK	834	GG						277	48						
JK	835	GG								96	76				
JK	835	GG						92	57						
JK	836	GG								101	70				
JK	836	GG						110	49						
JK	837	GG								107	75		WSW		
JK	837	GG								256	74		NW		
JK	837	GG						122	71				WSW		
JK	837	GG						236	62				NW		
JK	839	MGW	194	64											
JK	840	MGW	206	67											
JK	841	MGW	49	25											
JK	842	MGW	146	56											
JK	843	MGW	202	64											
JK	844	MGW	146	36											
JK	845	MGW	36	76											
JK	846	MGW	39	66											
JK	847	MGW	233	62											
JK	850	MGW	21	75											
JK	853	ISG	359	39											
JK	854	HFG, ISG	54	46											
JK	856	SCH MGW	197	57											
JK	857	SCH MGW	206	55											
JK	860	HFG	44	77											
JK	862	SCH MGW	62	73											
JK	863	HFG	35	70											
JK	864	HFG	197	66											
JK	865	HFG, ISG	37	72											
JK	866	HFG, SCH MGW	221	55											
JK	866	HFG, SCH MGW												298	80
JK	866	HFG, SCH MGW			205	25									
JK	867	HFG, SCH MGW	211	70											
JK	870	SCH MGW	38	65											
JK	874	Gd	226	68											
JK	875	SCH MGW	154	38											
JK	876	HFG	233	52											
JK	877	SCH								213	36	80	NW		
JK	877	SCH						309	39			80	NW		
JK	879	ISG	141	55											
JK	885	MGW	31	50											
JK	886	ISG, SCH	154	63											
JK	887	HFG	216	59											
JK	888	ISG, HFG	122	42											
JK	889	ISG, HFG	154	46											
JK	890	MGW, ISG	200	57											
JK	890	MGW, ISG	356	71											
JK	891	HFG	227	74											
JK	892	HFG	165	39											
JK	899	HFG	187	69											
JK	902	HFG	156	54											
JK	903	MGW, PEG	176	57											
JK	903	MGW, PEG			160	11									
JK	905	MGW, PEG	126	49											

			FOLIATION		LINEATION			FOLD AXIS		AXIAL SURFACE		ILA	VERG	JOINT	
QUAD	STATION	LITHOLOGY	STRIKE	DIP	TREND	PLUNGE	TYPE	TREND	PLUNGE	STRIKE	DIP			STRIKE	DIP
JK	906	ISG	140	44											
JK	909	ISG	93	59											
JK	910	ISG	51	71											
JK	911	ISG	334	63											
JK	912	ISG	324	62											
JK	913	HFG, SCH	141	49											
JK	914	ISG	183	51											
JK	915	ISG, HFG, MGW	156	70											
JK	918	MGW	132	36											
JK	919	MGW	152	34											
JK	920	MGW	201	46											
JK	921	GG	164	38											
JK	922	GG	56	16											
JK	922	GG												253	68
JK	923	GG	65	23											
JK	924	GG	6	27											
JK	924	GG								24	59				
JK	924	GG			42	44									
JK	925	MGW, GG												93	60
JK	926	MGW, GG	24	34											
JK	926	MGW, GG								199	69	25	NW		
JK	926	MGW, GG						201	26			25	NW		
JK	926	MGW, GG			204	11									
JK	927	MGW, GG	259	27											
JK	927	MGW, GG			360	24									
JK	928	MGW, GG	9	61											
JK	928	MGW, GG								356	56				
JK	928	MGW, GG						69	40						
JK	928	MGW, GG			11	8									
JK	929	MGW, GG	77	24											
JK	930	MGW	144	36											
JK	931	GG, MGW	212	36											
JK	931	GG, MGW	31	54											
JK	932	MIG MGW	31	24											
JK	933	GG								209	64	30	NNW		
JK	933	GG						206	44			30	NNW		
JK	934	ISG, SCH	219	54											
JK	935	ISG	124	67											
JK	938	HFG	9	49											
JK	939	HFG	21	74											
JK	941	HFG	24	28											
JK	942	HFG	126	38											
JK	945	HFG	76	41											
JK	948	GG	14	22											
JK	950	SCH, GG	48	31											
JK	951	GTD	126	58											
JK	955	ISG	227	69											
JK	962	ISG	306	51											
JK	963	SCH			206	38									
JK	970	HFG	125	37											
JK	971	ISG	356	39											
JK	972	ISG	140	45											
JK	973	MGW	111	46											
JK	974	SCH, HFG	166	66											
JK	975	MIG SCH, HFG	224	46											
JK	975	MIG SCH, HFG								6	77				
JK	975	MIG SCH, HFG						9	50						
JK	976	HFG	211	58											

			FOLIATION		LINEATION			FOLD AXIS		AXIAL SURFACE		ILA	VERG	JOINT	
QUAD	STATION	LITHOLOGY	STRIKE	DIP	TREND	PLUNGE	TYPE	TREND	PLUNGE	STRIKE	DIP			STRIKE	DIP
JK	977	MGW	211	70											
JK	978	MGW	212	72											
JK	979	MGW	204	71											
JK	980	MGW	211	73											
JK	981	HFG	202	62											
JK	982	HFG	351	76											
JK	983	HFG	134	56											
JK	984	HFG	184	64											
JK	985	HFG	144	53											
JK	987	MGW	184	56											
JK	987	MGW												311	90
JK	988	HFG	211	46											
JK	989	ISG	210	52											
JK	990	SCH MGW	194	58											
JK	991	HFG	172	76											
JK	997	ISG	126	60											
JK	998	MGW	111	56											
JK	1000	HFG, ISG	222	54											
JK	1003	ISG	144	57											
JK	1004	ISG	151	47											
JK	1005	ISG	115	31											
JK	1013	ISG, HFG	147	55											
JK	1019	ISG, PEG	164	44											
JK	1022	ISG	206	49											
JK	1024	ISG	104	61											
JK	1026	ISG	131	45											
JK	1028	ISG	127	42											
JK	1034	MIG SCH								80	62				
JK	1034	MIG SCH						242	26						
JK	1038	GG	206	49											
JK	1039	GG, MGW	163	54											
JK	1040	HFG	185	78											
JK	1041	HFG	228	42											
JK	1042	ISG	186	68											
JK	1043	HFG	216	55											
JK	1044	ISG, MGW	168	58											
JK	1045	HFG, PEG, MGW	209	51											
JK	1047	HFG, ISG	76	58											
JK	1048	MGW	230	80											
JK	1049	MGW, ISG	101	41											
JK	1051	SCH								133	85	150			
JK	1051	SCH						152	53			150			
JK	1052	SCH								211	83	30			
JK	1052	SCH						209	40			30			
JK	1054	HFG	35	63											
JK	1055	SCH	76	58											
JK	1062	MIG SCH	71	39											
JK	1062	MIG SCH								289	80	90	SSE		
JK	1062	MIG SCH						274	78			90	SSE		
JK	1064	MGW	222	71											
JK	1066	HFG	52	49											
JK	1066	HFG								119	65	70	W		
JK	1066	HFG						129	47			70	W		
JK	1067	ISG	208	68											
JK	1068	HFG	54	67											
JK	1069	HFG	95	56											
JK	1070	HFG	41	48											
JK	1071	HFG	39	60											

			FOLIATION		LINEATION			FOLD AXIS		AXIAL SURFACE		ILA	VERG	JOINT	
QUAD	STATION	LITHOLOGY	STRIKE	DIP	TREND	PLUNGE	TYPE	TREND	PLUNGE	STRIKE	DIP			STRIKE	DIP
JK	1072	HFG	170	80											
JK	1073	HFG	305	48											
JK	1074	HFG	138	57											
JK	1075	HFG	94	83											
JK	1076	HFG	264	64											
JK	1077	SCH MGW	233	72											
JK	1078	SCH MGW								177	59	75	W		
JK	1078	SCH MGW						221	50			75	W		
JK	1079	HFG, ISG	107	51											
JK	1080	HFG, ISG	304	50											
JK	1081	HFG, ISG	88	75											
JK	1082	HFG	58	64											
JK	1083	HFG	103	68											
JK	1084	HFG	61	54											
JK	1085	HFG	124	67											
JK	1086	MGW, ISG	63	64											
JK	1087	HFG	66	65											
JK	1088	HFG, ISG	245	76											
JK	1089	ISG	66	58											
JK	1090	ISG	39	55											
JK	1093	SCH MGW	191	56											
JK	1096	SCH MGW, ISG	191	74											
JK	1097	GTD	56	37											
JK	1100	SCH MGW	96	51											
JK	1102	HFG	238	41											
JK	1103	HFG	81	48											
JK	1104	HFG	40	50											
JK	1105	HFG, ISG	46	76											
JK	1106	HFG	247	72											
JK	1108	SCH	84	66											
JK	1109	SCH MGW	215	47											
JK	1109	SSCH MGW								227	77	20			
JK	1109	SSCH MGW						45	34			20			
JK	1110	SCH	42	51											
JK	1112	ISG	142	45											
JK	1114	HFG	92	38											
JK	1120	MIG SCH MGW	86	59											
JK	1122	MIG SCH MGW	59	51											
JK	1123	ISG	223	66											
JK	1123	ISG												119	79
JK	1127	HFG	301	67											
JK	1128	GG	56	52											
JK	1129	GG	42	60											
JK	1130	GG	211	40											
JK	1131	GG	207	21											
JK	1133	HFG	54	59											
JK	1135	HFG	46	60											
JK	1136	HFG, MGW	101	59											
JK	1137	HFG	234	78											
JK	1138	HFG	191	80											
JK	1139	HFG	233	78											
JK	1140	HFG	119	56											
JK	1141	HFG	141	64											
JK	1142	HFG, ISG	222	69											
JK	1143	MGW	222	65											
JK	1145	ISG	129	41											
JK	1146	MGW, HFG	90	54											
JK	1147	HFG	289	51											

			FOLIATION		LINEATION			FOLD AXIS		AXIAL SURFACE		ILA	VERG	JOINT	
QUAD	STATION	LITHOLOGY	STRIKE	DIP	TREND	PLUNGE	TYPE	TREND	PLUNGE	STRIKE	DIP			STRIKE	DIP
JK	1148	ISG	188	54											
JK	1149	ISG	103	54											
JK	1150	HFG	95	68											
JK	1151	HFG	171	49											
JK	1153	GG	17	44											
JK	1154	GG, AM	225	37											
JK	1156	MGW, GG	259	76											
JK	1156	MGW, GG	73	35											
JK	1158	GG	351	46											
JK	1159	GG	113	38											
JK	1160	GG	193	31											
JK	1161	GG, MGW								180	56	80	W		
JK	1161	GG, MGW						264	66			80	W		
JK	1162	GG, MGW								51	81	ISO			
JK	1162	GG, MGW						226	16			ISO			
JK	1163	SCH MGW	193	68											
JK	1164	GG	54	66											
JK	1165	MGW	219	21											
JK	1165	MGW			250	18									
JK	1166	MGW	201	29											
JK	1167	MGW	147	77											
JK	1168	AM	223	70											
JK	1169	GG	200	65											
JK	1170	GG	234	76											
JK	1171	GG	51	69											
JK	1172	GG	234	73											
JK	1173	GG								125	84	95	E		
JK	1173	GG						306	56			95	E		
JK	1174	GG	221	83											
JK	1175	GG	224	66											
JK	1176	GG	191	53											
JK	1177	AM	211	83											
JK	1178	SCH MGW	171	54											
JK	1179	HFG	66	55											
JK	1180	HFG	197	69											
JK	1181	HFG	175	48											
JK	1182	HFG								171	74	60	E		
JK	1182	HFG						175	71			60	E		
JK	1184	HFG	205	56											
JK	1185	MGW	217	49											
JK	1186	HFG, ISG	31	46											
JK	1188	ISG	6	61											
JK	1189	HFG	143	72											
JK	1190	HFG	163	52											
JK	1191	HDR	225	64											
JK	1193	HDR, ISG	243	75											
JK	1194	HFG	115	37											
JK	1197	ISG	241	45											
JK	1200	HFG	204	54											
JK	1201	SCH MGW	61	41											
JK	1202	SCH MGW	126	51											
JK	1203	MGW, AM	151	34											
JK	1204	SCH MGW	129	37											
JK	1205	MGW			258	22									
JK	1210	ISG	46	47											

			FOLIATION		LINEATION			FOLD AXIS		AXIAL SURFACE		ILA	VERG	JOINT	
QUAD	STATION	LITHOLOGY	STRIKE	DIP	TREND	PLUNGE	TYPE	TREND	PLUNGE	STRIKE	DIP			STRIKE	DIP
LS	2	MGW	340	25											
LS	4	MGW	37	15											
LS	5	MGW	20	35											
LS	6	MGW			225	40	STR								
LS	7	MGW	15	22											
LS	8	MGW	0	18											
LS	9	MGW	45	15											
LS	10	MGW	345	15											
LS	21	MGW	52	18											
LS	22	MGW	42	21											
LS	23	RQ	106	4											
LS	23	QZ			220	3	STR								
LS	24	QZ	66	19											
LS	24	QZ												283	90
LS	25	MGW	341	24											
LS	26	MGW	15	21											
LS	27	MGW	69	26											
LS	28	MGW	66	28											
LS	31	MGW	23	29											
LS	32	MGW	66	11											
LS	37	MGW	40	31											
LS	41	MYL MGW	246	7											
LS	42	AM	65	39											
LS	42	AM												302	71
LS	43	MGW	116	14											
LS	44	MGW	131	16											
LS	45	MGW	116	11											
LS	46	MGW	139	16											
LS	47	MGW	144	9											
LS	47	MGW			203	5	STR								
LS	48	MGW	143	9											
LS	48	MGW												198	68
LS	48	MGW												133	90
LS	49	MGW	134	6											
LS	49	MGW												76	84
LS	49	MGW												126	86
LS	50	MGW	162	19											
LS	50	MGW												310	79
LS	51	MGW	116	33											
LS	52	MGW	144	12											
LS	52	MGW												188	90
LS	52	MGW			174	9	STR								
LS	53	MGW	109	6											
LS	53	MGW												105	90
LS	54	MGW	126	11											
LS	55	MYL MGW	105	13											
LS	56	MYL MGW	209	7											
LS	57	MYL MGW	114	14											
LS	58	MYL MGW	101	10											
LS	59	QZ	165	27											
LS	60	MGW	101	12											
LS	61	MGW	21	11											
LS	61	MGW												250	67
LS	62	MGW	31	11											
LS	63	MGW												71	87
LS	63	MGW			250	16	STR								
LS	63	MYL MGW	127	24											

			FOLIATION		LINEATION			FOLD AXIS		AXIAL SURFACE		ILA	VERG	JOINT	
QUAD	STATION	LITHOLOGY	STRIKE	DIP	TREND	PLUNGE	TYPE	TREND	PLUNGE	STRIKE	DIP			STRIKE	DIP
LS	64	MYL MGW	106	7											
LS	65	MGW												145	90
LS	65	MYL MGW	85	12											
LS	66	MYL MGW	160	9											
LS	67	MGW												158	90
LS	67	MYL MGW	181	6											
LS	68	MGW												121	90
LS	68	MGW												135	90
LS	68	MGW			201	4	STR								
LS	68	MYL MGW	116	9											
LS	69	MYL MGW	92	16											
LS	70	MYL MGW	113	11											
LS	71	MGW	343	31											
LS	72	MGW	75	16											
LS	73	MGW	81	12											
LS	75	MGW	113	7											
LS	76	MGW												301	77
LS	76	MYL MGW	137	21											
LS	77	MYL MGW	159	13											
LS	79	MYL MGW	338	26											
LS	81	MYL MGW	156	14											
LS	83	MYL MGW	85	19											
LS	86	MYL MGW	175	12											
LS	88	MGW	155	21											
LS	90	MGW	123	11											
LS	91	MGW	76	19											
LS	92	MYL MGW	10	16											
LS	93	MYL MGW	35	39											
LS	94	MGW												162	83
LS	94	MYL MGW	116	19											
LS	95	MYL MGW	98	25											
LS	96	MYL MGW	73	19											
LS	101	MGW	29	44											
LS	102	MGW	14	31											
LS	104	MGW	33	14											
LS	105	MYL MGW	63	24											
LS	106	MYL MGW	26	31											
LS	107	MIG MGW	41	11											
LS	108	MIG MGW	42	14											
LS	109	MIG MGW												291	67
LS	110	MIG MGW	51	12											
LS	111	MGW	313	31											
LS	112	MIG MGW	185	21											
LS	112	MIG MGW												96	86
LS	114	MGW	83	16											
LS	115	MGW	68	13											
LS	115	MGW												176	84
LS	116	MGW	51	24											
LS	117	MGW	63	26											
LS	119	MGW	127	16											
LS	121	MGW	24	46											
LS	122	MIG MGW	52	24											
LS	122	MIG MGW												128	90
LS	123	MIG MGW	341	18											
LS	123	MIG MGW												151	90
LS	124	MIG MGW	6	21											
LS	124	MIG MGW												151	61

			FOLIATION		LINEATION			FOLD AXIS		AXIAL SURFACE		ILA	VERG	JOINT	
QUAD	STATION	LITHOLOGY	STRIKE	DIP	TREND	PLUNGE	TYPE	TREND	PLUNGE	STRIKE	DIP			STRIKE	DIP
LS	125	MIG MGW	11	19											
LS	125	MIG MGW												127	66
LS	126	MIG MGW	21	6											
LS	127	MIG MGW	21	21											
LS	127	MIG MGW												317	79
LS	128	MIG MGW	347	6											
LS	130	MIG MGW	6	11											
LS	130	MIG MGW												134	90
LS	131	MIG MGW	3	16											
LS	132	MIG MGW	38	16											
LS	133	MIG MGW	21	14											
LS	134	MIG MGW	24	19											
LS	134	MIG MGW												109	86
LS	135	MIG MGW	33	26											
LS	136	MIG MGW	336	10											
LS	137	MIG MGW	55	26											
LS	142	MIG MGW	22	9											
LS	143	MIG MGW	356	16											
LS	144	MIG MGW	282	16											
LS	145	MIG MGW	133	12											
LS	146	MIG MGW	278	6											
LS	147	MIG MGW	336	11											
LS	147	MIG MGW												146	90
LS	148	MIG MGW	9	27											
LS	149	MIG MGW	14	22											
LS	150	MIG MGW	358	25											
LS	150	MIG MGW												126	90
LS	152	MGW	41	31											
LS	153	MGW												139	90
LS	156	MGW												286	84
LS	156	MIG MGW	16	38											
LS	157	MIG MGW	349	22											
LS	157	MIG MGW												311	84
LS	157	MIG MGW												325	75
LS	158	MIG MGW	13	16											
LS	159	MIG MGW	351	27											
LS	159	MIG MGW												287	82
LS	161	MIG MGW	313	16											
LS	162	MIG MGW	328	21											
LS	162	MIG MGW												77	75
LS	163	MIG MGW	341	16											
LS	163	MIG MGW												134	71
LS	164	MIG MGW	321	14											
LS	165	MIG MGW	358	19											
LS	166	MIG MGW	349	8											
LS	167	MIG MGW	334	19											
LS	167	MIG MGW												173	84
LS	167	MIG MGW												106	79
LS	168	MIG MGW	317	21											
LS	169	MIG MGW	296	7											
LS	170	MIG MGW	61	35											
LS	170	MIG MGW												141	84
LS	171	MIG MGW	37	32											
LS	171	MIG MGW												126	82
LS	172	MIG MGW	351	24											
LS	173	MIG MGW	355	12											
LS	173	MIG MGW												119	79

			FOLIATION		LINEATION			FOLD AXIS		AXIAL SURFACE		ILA	VERG	JOINT	
QUAD	STATION	LITHOLOGY	STRIKE	DIP	TREND	PLUNGE	TYPE	TREND	PLUNGE	STRIKE	DIP			STRIKE	DIP
LS	174	MIG MGW	344	9											
LS	175	MIG MGW	6	13											
LS	175	MIG MGW												313	81
LS	176	MIG MGW	4	24											
LS	177	MIG MGW	14	43											
LS	177	MIG MGW												112	90
LS	178	MIG MGW	16	37											
LS	180	MIG MGW	33	25											
LS	181	MIG MGW	51	40											
LS	182	MIG MGW	34	21											
LS	183	AM	29	18											
LS	186	MIG MGW												111	82
LS	187	MGW	34	21											
LS	188	MIG MGW	21	21											
LS	189	MIG MGW	37	24											
LS	190	MIG MGW								295	81	150			
LS	190	MIG MGW						144	29			150			
LS	191	MIG MGW								26	29	30	SW		
LS	191	MIG MGW						121	30			30	SW		
LS	192	MIG MGW	24	16											
LS	193	MIG MGW	41	30											
LS	194	MIG MGW	51	12											
LS	195	MIG MGW	37	26											
LS	196	MGW	346	13											
LS	197	MIG MGW	33	24											
LS	198	MIG MGW	46	19											
LS	200	MIG MGW	73	29											
LS	201	MIG MGW	116	29											
LS	202	MIG MGW	335	19											
LS	203	MIG MGW	94	15											
LS	204	MIG MGW	46	25											
LS	205	MIG MGW	37	41											
LS	205	MIG MGW												294	80
LS	205	MIG MGW												315	86
LS	206	MIG MGW	66	24											
LS	207	MIG MGW	48	21											
LS	208	MIG MGW	39	19											
LS	208	MIG MGW												136	79
LS	209	MIG MGW	41	39											
LS	210	MIG MGW	28	40											
LS	211	MIG MGW	41	26											
LS	212	MIG MGW	52	25											
LS	213	MIG MGW	49	43											
LS	214	MIG MGW	59	31											
LS	215	MIG MGW	29	33											
LS	216	MIG MGW	34	31											
LS	217	MIG MGW	22	26											
LS	218	MIG MGW	41	21											
LS	219	MIG MGW	46	34											
LS	220	MIG MGW	55	26											
LS	221	MIG MGW	58	31											
LS	222	MIG MGW	26	33											
LS	223	MIG MGW	11	50											
LS	224	MIG MGW	41	34											
LS	225	MIG MGW	46	31											
LS	226	MIG MGW	29	57											
LS	227	MIG MGW	35	37											

			FOLIATION		LINEATION			FOLD AXIS		AXIAL SURFACE		ILA	VERG	JOINT	
QUAD	STATION	LITHOLOGY	STRIKE	DIP	TREND	PLUNGE	TYPE	TREND	PLUNGE	STRIKE	DIP			STRIKE	DIP
LS	228	MIG MGW	44	32											
LS	229	SI CAT												24	57
LS	230	MIG MGW	36	19											
LS	231	MIG MGW	187	12											
LS	232	MIG MGW	186	22											
LS	235	MIG MGW	208	21											
LS	236	QZ												344	87
LS	237	MIG MGW	51	31											
LS	238	MIG MGW	35	15											
LS	239	MIG MGW	16	14											
LS	240	MGW	51	59											
LS	242	MIG MGW	24	37											
LS	243	MIG MGW	126	13											
LS	244	MIG MGW	67	19											
LS	245	MIG MGW	291	21											
LS	246	MIG MGW	111	16											
LS	247	MIG MGW	74	34											
LS	248	MIG MGW	31	53											
LS	250	MIG MGW	39	34											
LS	251	MIG MGW	55	67											
LS	252	MIG MGW	62	51											
LS	253	MIG MGW	64	79											
LS	254	MIG MGW	44	41											
LS	255	MIG MGW	52	34											
LS	256	MIG MGW	39	54											
LS	257	MIG MGW	56	56											
LS	258	MIG MGW	40	56											
LS	259	MIG MGW	41	77											
LS	260	MIG MGW	46	59											
LS	261	MIG MGW	61	80											
LS	262	MIG MGW	38	36											
LS	263	MIG MGW	53	46											
LS	264	MIG MGW	59	41											
LS	266	MIG MGW	32	51											
LS	268	RQ	36	48											
LS	269	MGW	36	29											
LS	270	MGW	52	64											
LS	271	MGW	56	44											
LS	274	MIG MGW	26	12											
LS	277	MIG MGW	46	17											
LS	278	MIG MGW	39	19											
LS	280	MIG MGW	358	29											
LS	281	MIG MGW								255	52	150	S		
LS	281	MIG MGW						71	16			150	S		
LS	282	MIG MGW	339	16											
LS	283	MIG MGW	344	29											
LS	284	MIG MGW	14	26											
LS	285	MIG MGW	186	50											
LS	285	MIG MGW												314	86
LS	285	MIG MGW												251	90
LS	286	MIG MGW	14	63											
LS	287	MIG MGW	18	31											
LS	287	MIG MGW												304	86
LS	288	SI CAT												214	39
LS	288	SI CAT												154	79
LS	289	SI CAT												182	74
LS	304	SCH												104	78

			FOLIATION		LINEATION			FOLD AXIS		AXIAL SURFACE		ILA	VERG	JOINT	
QUAD	STATION	LITHOLOGY	STRIKE	DIP	TREND	PLUNGE	TYPE	TREND	PLUNGE	STRIKE	DIP			STRIKE	DIP
LS	304	SCH			21	34	STR								
LS	306	QZ	213	46											
LS	310	SI CAT												220	44
LS	313	MIG MGW	64	25											
LS	314	MIG MGW	66	39											
LS	315	MIG MGW	71	26											
LS	316	MGW	46	63											
LS	317	MIG MGW	43	34											
LS	318	MIG MGW	46	58											
LS	319	MGW								226	55	40			
LS	319	MGW						226	22			40			
LS	320	MIG MGW	41	42											
LS	321	MIG MGW								22	29	18			
LS	321	MIG MGW						101	37			18			
LS	322	MIG MGW	46	67											
LS	323	MIG MGW	42	64											
LS	324	AM	42	16											
LS	324	AM												79	46
LS	329	MIG MGW	36	36											
LS	330	MGW	59	29											
LS	332	MIG MGW	39	34											
LS	334	MIG MGW	41	63											
LS	335	MIG MGW	38	44											
LS	336	MIG MGW								51	53	60			
LS	336	MIG MGW						218	34			60			
LS	336	MIG MGW	27	64											
LS	338	MIG MGW	48	81											
LS	339	MIG MGW	38	69											
LS	340	MIG MGW	46	42											
LS	341	MIG MGW	51	46											
LS	342	MIG MGW	37	55											
LS	343	MIG MGW	53	48											
LS	344	MIG MGW	55	49											
LS	345	MIG MGW	36	53											
LS	349	ISG	143	21											
LS	353	MGW								211	35	70			
LS	353	MGW						346	24			70			
LS	361	ISG	189	46											
LS	364	GG	194	36											
LS	370	SCH												81	62
LS	373	HFG	249	47											
LS	375	DPW	148	64											
LS	376	DPW												94	71
LS	377	HFG	169	74											
LS	378	MGW	209	84											
LS	379	DPW	184	36											
LS	380	HFG	151	63											
LS	382	HFG	126	31											
LS	382	HFG												307	29
LS	383	HFG	154	31											
LS	384	ISG												104	84
LS	385	HFG	164	44											
LS	386	ISG	155	45											
LS	387	MIG MGW								19	56	110	W		
LS	387	MIG MGW						24	22			110	W		
LS	388	GG								204	75	160	W		
LS	388	GG						24	19			160	W		

			FOLIATION		LINEATION			FOLD AXIS		AXIAL SURFACE		ILA	VERG	JOINT	
QUAD	STATION	LITHOLOGY	STRIKE	DIP	TREND	PLUNGE	TYPE	TREND	PLUNGE	STRIKE	DIP			STRIKE	DIP
LS	388	GG												112	67
LS	389	HFG	196	38											
LS	390	HFG	0	0											
LS	391	HFG	94	27											
LS	392	DPW	277	34											
LS	393	HFG	71	24											
LS	394	DPW	116	37											
LS	395	DPW, SCH	101	34											
LS	397	SCH	121	34											
LS	398	SCH								105	75	75	N		
LS	398	SCH						101	26			75	N		
LS	399	DPW	251	36											
LS	400	HFG	279	44											
LS	401	HFG	74	24											
LS	402	HFG	232	65											
LS	402	HFG												108	82
LS	404	ISG								301	75	110	WSW		
LS	404	ISG						281	34			110	WSW		
LS	404	ISG												351	29
LS	405	HFG	119	64											
LS	405	HFG												224	85
LS	406	SCH												177	76
LS	418	MGW	101	11											
LS	418	MGW												334	90
LS	419	MGW								119	71	170	NE		
LS	419	MGW						314	21			170	NE		
LS	419	MGW												270	84
LS	419	MGW												301	86
LS	426	HFG, SSCH	219	66											
LS	429	ISG	77	72											
LS	448	MGW, RQ	118	15											
LS	449	MGW	33	54											
LS	449	MGW												169	67
LS	450	MGW	28	47											
LS	450	MGW												149	90
LS	450	MGW			31	19	STR								
LS	451	MIG MGW	28	51											
LS	451	MIG MGW												162	85
LS	452	MGW	22	46											
LS	453	MGW	29	45											
LS	454	MGW	59	56											
LS	455	MGW	37	71											
LS	456	MGW	61	52											
LS	456	MGW												119	90
LS	457	MGW	46	61											
LS	457	MGW			214	14	STR								
LS	458	MGW	49	61											
LS	459	MGW	51	61											
LS	460	MGW	30	64											
LS	461	MGW	34	65											
LS	463	MGW	38	45											
LS	465	MGW	42	57											
LS	466	MGW	23	66											
LS	467	MGW	37	59											
LS	467	MGW			216	19	STR								
LS	468	MGW	33	44											
LS	469	MGW	32	47											

			FOLIATION		LINEATION			FOLD AXIS		AXIAL SURFACE		ILA	VERG	JOINT	
QUAD	STATION	LITHOLOGY	STRIKE	DIP	TREND	PLUNGE	TYPE	TREND	PLUNGE	STRIKE	DIP			STRIKE	DIP
LS	469	MGW												325	79
LS	470	MGW	19	76											
LS	471	MGW	38	37											
LS	471	MGW												159	90
LS	471	MGW			201	16	STR								
LS	472	MGW	31	44											
LS	472	MGW			163	26	STR								
LS	473	MGW	49	37											
LS	473	MGW												277	77
LS	474	MGW	24	41											
LS	474	MGW												150	86
LS	474	MGW			221	4	STR								
LS	475	MGW	34	51											
LS	476	MIG MGW	36	54											
LS	477	MIG MGW	27	45											
LS	477	MIG MGW			77	45	BN								
LS	478	MGW	25	46											
LS	479	MGW	21	59											
LS	480	MGW	24	64											
LS	482	MGW	41	53											
LS	482	MGW												151	87
LS	483	MGW	47	46											
LS	484	MGW	51	63											
LS	485	MGW	45	56											
LS	486	MGW	49	52											
LS	487	MGW	39	54											
LS	488	SCH MGW	44	61											
LS	489	MGW	35	60											
LS	490	SCH MGW, AM	41	59											
LS	490	SCH MGW, AM			150	44	BN								
LS	491	MIG MGW	66	61											
LS	492	MGW	36	70											
LS	492	MGW												125	90
LS	493	MGW	34	46											
LS	494	MGW	41	47											
LS	495	MGW	56	45											
LS	496	MGW	46	45											
LS	497	MGW	46	71											
LS	499	CHL SCH	74	56											
LS	499	CHL SCH												6	86
LS	500	CHL SCH	59	65											
LS	501	MGW	209	68											
LS	506	MGD	215	50											
LS	507	MGW	31	52											
LS	508	MGW	32	46											
LS	509	MGW	24	44											
LS	510	MGW	23	44											
LS	511	MGW	21	51											
LS	512	MIG MGW	24	57											
LS	513	MGW	18	46											
LS	514	MGW	348	56											
LS	515	MGW	12	43											
LS	516	MGW	16	41											
LS	517	MGW	3	49											
LS	518	MGW	31	54											
LS	518	MGW			115	54	BN								
LS	519	MGW	6	61											

			FOLIATION		LINEATION			FOLD AXIS		AXIAL SURFACE		ILA	VERG	JOINT	
QUAD	STATION	LITHOLOGY	STRIKE	DIP	TREND	PLUNGE	TYPE	TREND	PLUNGE	STRIKE	DIP			STRIKE	DIP
LS	521	MGW	11	48											
LS	522	MGW	41	44											
LS	523	MGW	26	55											
LS	524	MGW	12	59											
LS	525	MGW	33	54											
LS	525	MGW			104	49	BN								
LS	526	MGW	41	53											
LS	527	MGW	24	46											
LS	528	MGW	37	49											
LS	529	MGW	37	76											
LS	530	MGW	46	46											
LS	531	MGW	31	42											
LS	532	MGW	34	39											
LS	534	MGW	31	49											
LS	535	MGW	36	46											
LS	536	MGW	34	47											
LS	537	MGW	46	42											
LS	537	MGW			174	30	STR								
LS	538	MGW	216	80											
LS	539	MGW	61	61											
LS	540	MGW	41	64											
LS	541	MIG MGW								56	42	10	SE		
LS	541	MIG MGW						58	76			10	SE		
LS	541	MIG MGW	56	42											
LS	542	MIG MGW	45	47											
LS	543	MIG MGW, AM	66	71											
LS	544	MIG MGW, AM	65	68											
LS	545	MGW	39	59											
LS	546	MIG MGW	41	53											
LS	547	MIG MGW	47	64											
LS	548	MIG MGW	61	66											
LS	549	MIG MGW	41	39											
LS	550	MIG MGW	47	65											
LS	551	MIG MGW								21	71	15	SE		
LS	551	MIG MGW						211	61			15	SE		
LS	551	MIG MGW	46	35											
LS	551	MIG MGW			82	22	STR								
LS	552	MIG MGW	47	50											
LS	553	MGW	36	44											
LS	554	MGW	46	64											
LS	555	MGW	39	65											
LS	556	MGW	61	52											
LS	557	MGW	63	54											
LS	559	MGW	47	49											
LS	560	MGW	42	69											
LS	560	MGW			206	19	STR								
LS	561	MGW	42	76											
LS	562	MIG MGW	24	74											
LS	563	MIG MGW	36	44											
LS	563	MIG MGW			54	17	STR								
LS	564	MIG MGW	39	71											
LS	566	MIG MGW	46	64											
LS	567	MIG MGW	42	64											
LS	568	MIG MGW	37	49											
LS	569	MIG MGW	36	46											
LS	570	MIG MGW	46	59											
LS	571	MIG MGW	41	44											

			FOLIATION		LINEATION			FOLD AXIS		AXIAL SURFACE		ILA	VERG	JOINT	
QUAD	STATION	LITHOLOGY	STRIKE	DIP	TREND	PLUNGE	TYPE	TREND	PLUNGE	STRIKE	DIP			STRIKE	DIP
LS	572	MIG MGW	46	64											
LS	573	MIG MGW, AM	43	56											
LS	574	MIG MGW	39	49											
LS	575	MIG MGW	46	46											
LS	576	MIG MGW	36	47											
LS	577	MIG MGW	49	80											
LS	578	MIG MGW	36	44											
LS	578	MIG MGW			49	15	STR								
LS	579	MIG MGW	41	51											
LS	579	MIG MGW												279	90
LS	580	MIG MGW	29	59											
LS	581	MIG MGW	38	76											
LS	582	MGW	46	27											
LS	586	MGW	49	52											
LS	588	MGW	51	57											
LS	590	DD												337	71
LS	591	MGW, DD	32	63											
LS	593	MGW	46	53											
LS	594	MIG MGW	21	58											
LS	596	MIG MGW	22	74											
LS	597	MGW, DD	43	62											
LS	598	DD												336	51
LS	599	MGW	24	68											
LS	600	MIG MGW	36	62											
LS	604	MIG MGW	48	61											
LS	606	MGW	28	56											
LS	607	MGW	35	44											
LS	608	MGW	196	44											
LS	609	SCH MGW	24	36											
LS	611	SCH MGW	39	51											
LS	612	MGW, AM	34	42											
LS	613	MGW, AM	26	31											
LS	614	MGW, AM	46	69											
LS	614	MGW, AM	61	32											
LS	615	MIG MGW	46	50											
LS	616	MIG MGW	41	60											
LS	617	MIG MGW, QZ	32	49											
LS	618	MIG MGW	36	63											
LS	619	MIG MGW	31	46											
LS	619	MIG MGW			56	21	STR								
LS	620	MIG MGW	33	64											
LS	621	SCH MGW	316	26											
LS	621	SCH MGW			4	11	STR								
LS	622	MGW	164	65											
LS	623	MIG MGW	36	44											
LS	624	MIG MGW	29	37											
LS	625	MIG MGW	36	59											
LS	626	MIG MGW	30	56											
LS	627	MIG MGW	31	51											
LS	628	MIG MGW	44	26											
LS	629	MIG MGW	26	44											
LS	630	MIG MGW	33	52											
LS	631	MIG MGW	29	46											
LS	632	MIG MGW	42	41											
LS	633	MIG MGW	51	44											
LS	634	MIG MGW, CALC-S	19	38											
LS	635	MIG MGW, CALC-S	36	46											

			FOLIATION		LINEATION			FOLD AXIS		AXIAL SURFACE		ILA	VERG	JOINT	
QUAD	STATION	LITHOLOGY	STRIKE	DIP	TREND	PLUNGE	TYPE	TREND	PLUNGE	STRIKE	DIP			STRIKE	DIP
LS	636	MIG MGW	40	44											
LS	637	MGW	39	44											
LS	638	MIG MGW, CALC-SI	31	39											
LS	638	MIG MGW, CALC-SI			131	35	BN								
LS	639	MGW	24	41											
LS	640	MGW	36	54											
LS	641	MGW	31	65											
LS	642	MIG MGW	38	31											
LS	643	MIG MGW	41	45											
LS	644	MIG MGW	21	34											
LS	645	MGW	46	34											
LS	646	MGW	32	37											
LS	647	MGW	31	40											
LS	647	MGW												103	90
LS	648	MIG MGW	33	55											
LS	649	MIG MGW	36	59											
LS	650	MIG MGW	42	40											
LS	651	MGW	46	51											
LS	651	MGW			73	29	STR								
LS	652	MGW	39	37											
LS	653	MGW	40	46											
LS	654	MGW	51	49											
LS	655	MGW	26	65											
LS	656	MGW	19	44											
LS	657	MGW	34	47											
LS	658	MGW	46	49											
LS	659	MGW	21	66											
LS	660	MGW	66	29											
LS	661	MIG MGW	14	37											
LS	661	MIG MGW												331	90
LS	662	MIG MGW	24	59											
LS	663	MIG MGW	14	42											
LS	664	MIG MGW	21	46											
LS	665	MIG MGW	34	49											
LS	666	MIG MGW	26	45											
LS	667	MIG MGW	46	48											
LS	668	MIG MGW	26	43											
LS	669	MIG MGW	16	51											
LS	670	MIG MGW	14	26											
LS	670	MIG MGW												314	90
LS	671	MIG MGW	11	44											
LS	672	MGW	21	39											
LS	672	MGW			170	14	STR								
LS	673	MGW	251	24											
LS	674	QZ	216	49											
LS	675	MIG MGW	211	40											
LS	676	MIG MGW	221	49											
LS	677	MGW	4	36											
LS	678	MIG MGW	6	40											
LS	679	MIG MGW								351	47	30	SW		
LS	679	MIG MGW						21	34			30	SW		
LS	679	MIG MGW	356	45											
LS	680	MIG MGW	359	34											
LS	680	MIG MGW												96	76
LS	681	MGW, QZ	222	37											
LS	682	MGW, QZ	106	44											
LS	683	QZ	316	70											

			FOLIATION		LINEATION			FOLD AXIS		AXIAL SURFACE		ILA	VERG	JOINT	
QUAD	STATION	LITHOLOGY	STRIKE	DIP	TREND	PLUNGE	TYPE	TREND	PLUNGE	STRIKE	DIP			STRIKE	DIP
LS	684	MIG MGW, DD	36	22											
LS	685	MGW	36	39											
LS	685	MGW			54	8	STR								
LS	686	MGW	29	35											
LS	687	MGW	41	31											
LS	688	MGW	24	31											
LS	689	MGW	34	31											
LS	690	MGW	69	61											
LS	691	MGW	35	56											
LS	692	MGW	29	47											
LS	693	MGW	41	47											
LS	694	MGW	66	56											
LS	695	MIG MGW	56	41											
LS	695	MIG MGW			216	21	STR								
LS	696	MGW	46	39											
LS	697	MGW	49	32											
LS	699	MIG MGW	56	42											
LS	700	MGW	17	66											
LS	701	MGW, AM	9	46											
LS	701	MGW, AM			14	11	BN								
LS	702	MGW	9	45											
LS	703	MGW	11	37											
LS	704	MIG MGW	4	30											
LS	705	MIG MGW	351	42											
LS	706	MIG MGW	14	34											
LS	707	MIG MGW	21	42											
LS	708	MIG MGW	13	52											
LS	709	MIG MGW	5	39											
LS	710	MIG MGW	354	44											
LS	711	MIG MGW	340	47											
LS	712	ALT GG	216	34											
LS	713	ALT GG	219	47											
LS	714	CALC-SI												31	80
LS	714	CALC-SI												92	78
LS	715	ALT GG	201	37											
LS	716	ALT GG	154	36											
LS	717	CALC-SI	191	41											
LS	718	ALT GG	154	54											
LS	719	ALT GG	186	56											
LS	720	ALT GG	221	46											
LS	721	ALT GG	231	39											
LS	722	ALT GG	196	56											
LS	723	ALT GG	214	46											
LS	724	ALT GG	206	58											
LS	725	ALT GG	196	54											
LS	726	ALT GG	216	45											
LS	727	ALT GG	201	49											
LS	728	ALT GG	193	61											
LS	729	ALT GG	178	19											
LS	730	MIG MGW	135	33											
LS	731	MIG MGW	51	66											
LS	732	MIG MGW	36	41											
LS	733	MIG MGW	21	57											
LS	734	MIG MGW	51	37											
LS	735	MIG MGW	39	41											
LS	736	MIG MGW	21	47											
LS	737	MGW	16	46											

			FOLIATION		LINEATION			FOLD AXIS		AXIAL SURFACE		ILA	VERG	JOINT	
QUAD	STATION	LITHOLOGY	STRIKE	DIP	TREND	PLUNGE	TYPE	TREND	PLUNGE	STRIKE	DIP			STRIKE	DIP
LS	738	MGW	6	37											
LS	739	SCH MGW	7	39											
LS	740	SCH MGW	11	44											
LS	741	MIG SCH MGW	28	74											
LS	742	MIG MGW	16	65											
LS	743	MIG MGW	16	69											
LS	744	MIG MGW	16	64											
LS	745	MIG MGW	21	51											
LS	746	MIG MGW	9	39											
LS	747	MIG MGW	17	51											
LS	748	MIG MGW	11	19											
LS	749	MIG MGW	9	69											
LS	750	MIG MGW	11	34											
LS	751	MIG MGW	16	36											
LS	752	MIG MGW	17	51											
LS	753	MIG MGW	29	47											
LS	754	MIG MGW	21	31											
LS	754	MIG MGW			196	10	STR								
LS	755	MIG MGW	33	31											
LS	756	MIG MGW	17	37											
LS	757	MIG MGW	11	36											
LS	758	MIG MGW	36	57											
LS	759	SCH MGW	34	49											
LS	760	SCH MGW	24	46											
LS	761	MIG MGW	44	59											
LS	762	SCH MGW	22	36											
LS	763	MIG MGW	27	53											
LS	764	SCH MGW	18	64											
LS	765	MIG MGW	14	51											
LS	766	MIG MGW	26	43											
LS	767	MIG MGW	22	51											
LS	768	MIG SCH MGW	24	46											
LS	769	SCH MGW	39	60											
LS	770	MIG MGW	31	42											
LS	771	MIG MGW	24	40											
LS	772	MIG MGW	13	45											
LS	773	MIG SCH MGW	11	44											
LS	774	SCH	9	74											
LS	775	MGW	341	51											
LS	776	SCH	167	52											
LS	777	SCH	198	61											
LS	778	ISG, SSCH	211	41											
LS	779	ISG, SSCH	231	34											
LS	780	ISG, SSCH	201	39											
LS	781	HFG	189	42											
LS	782	MIG SCH, HFG	211	32											
LS	783	HFG	212	44											
LS	784	HFG	210	46											
LS	785	HFG	201	51											
LS	786	SSCH, ISG	203	59											
LS	787	MIG SCH								190	68	20	W		
LS	787	MIG SCH						11	16			20	W		
LS	788	MIG SCH	216	62											
LS	789	CHL SCH	201	56											
LS	790	CHL SCH	197	51											
LS	790	CHL SCH	246	31											
LS	791	CHL SCH	206	39											

			FOLIATION		LINEATION			FOLD AXIS		AXIAL SURFACE		ILA	VERG	JOINT	
QUAD	STATION	LITHOLOGY	STRIKE	DIP	TREND	PLUNGE	TYPE	TREND	PLUNGE	STRIKE	DIP			STRIKE	DIP
LS	791	CHL SCH			13	24	STR								
LS	792	MGW	9	37											
LS	794	MGW	221	56											
LS	795	MGW	209	48											
LS	797	MIG SCH	211	41											
LS	799	MIG MGW, ISG	204	56											
LS	799	MIG MGW, ISG			356	19	STR								
LS	801	MGW	221	64											
LS	803	MGW, PEG	211	53											
LS	804	MGW	202	65											
LS	805	MIG MGW	216	59											
LS	806	MGW	200	66											
LS	806	MGW												117	90
LS	807	MGW	219	54											
LS	808	MGW	196	48											
LS	809	MGW	226	55											
LS	810	DPW	199	41											
LS	812	MIG MGW	173	51											
LS	813	MIG MGW	168	36											
LS	814	MIG MGW	198	52											
LS	815	MIG MGW	191	48											
LS	818	MGW	135	61											
LS	821	SCH	202	51											
LS	823	MGW	161	37											
LS	824	MIG MGW	251	65											
LS	825	MIG MGW	216	53											
LS	826	MIG MGW	189	68											
LS	827	MIG MGW, PEG	196	66											
LS	827	MIG MGW, PEG												306	81
LS	828	MIG MGW, PEG	199	63											
LS	829	MGW, ISG	86	65											
LS	830	ISG, MGW	85	43											
LS	831	MGW	192	56											
LS	832	SCH	224	43											
LS	833	SCH, GTD	212	57											
LS	834	MGW	93	72											
LS	835	ISG	188	51											
LS	836	MIG SCH MGW	186	56											
LS	837	MIG SCH MGW	139	41											
LS	838	MIG SCH MGW	221	55											
LS	839	MGW, PEG	216	69											
LS	840	SCH, GTD	100	54											
LS	841	MGW	207	62											
LS	842	MIG SCH MGW	194	52											
LS	843	MIG SCH MGW	199	67											
LS	844	MIG SCH MGW	221	64											
LS	845	ISG	194	41											
LS	846	MGW	57	34											
LS	849	DPW	154	63											
LS	854	HFG	180	72											
LS	861	GG, SCH	209	64											
LS	862	MIG MGW, HFG	44	63											
LS	864	HFG	195	69											
LS	870	HFG	209	85											
LS	872	MGW	219	31											
LS	873	MIG MGW	61	35											
LS	874	MIG MGW	34	59											

			FOLIATION		LINEATION			FOLD AXIS		AXIAL SURFACE		ILA	VERG	JOINT	
QUAD	STATION	LITHOLOGY	STRIKE	DIP	TREND	PLUNGE	TYPE	TREND	PLUNGE	STRIKE	DIP			STRIKE	DIP
LS	875	MIG MGW	44	49											
LS	876	MIG MGW	41	55											
LS	877	MIG MGW	44	56											
LS	878	MIG MGW	36	63											
LS	879	MIG MGW	31	56											
LS	881	CALC-SI	173	64											
LS	884	SCH	163	41											
LS	889	MGW	196	41											
LS	890	MGW	202	55											
LS	891	MGW	204	57											
LS	892	MGW	194	46											
LS	893	MGW	221	53											
LS	896	MGW	206	47											
LS	897	MGW	200	61											
LS	899	MGW	196	45											
LS	900	MGW, PEG	227	43											
LS	902	MGW	214	51											
LS	907	HFG, ISG	211	68											
LS	912	MGW, SCH	41	31											
LS	913	MIG SCH MGW	114	17											
LS	914	MIG SCH MGW	84	31											
LS	915	MGW	119	26											
LS	915	MGW												68	90
LS	915	MGW			223	22	STR								
LS	916	MGW	71	51											
LS	917	SCH MGW	44	17											
LS	918	MGW	36	28											
LS	919	MGW	35	34											
LS	920	MGW	58	22											
LS	921	MGW	114	31											
LS	922	MGW	165	30											
LS	923	MGW	35	16											
LS	923	MGW			179	11	STR								
LS	924	MGW	184	21											
LS	925	MGW	14	20											
LS	926	MGW	29	27											
LS	927	MGW	109	19											
LS	928	MIG MGW	37	30											
LS	929	MIG MGW	31	44											
LS	931	MGW	216	31											
LS	931	MGW			23	14	STR								
LS	933	MGW	51	37											
LS	934	MGW	32	35											
LS	935	MGW	21	31											
LS	937	MGW	217	36											
LS	938	HFG	156	57											
LS	939	HFG	146	57											
LS	940	HFG	186	44											
LS	943	MGW	76	46											
LS	944	GTD	65	70											
LS	945	DPW	236	55											
LS	946	MIG MGW	193	62											
LS	947	MGW	221	46											
LS	948	SCH MGW	41	49											
LS	949	MIG MGW	34	56											
LS	950	MIG MGW	221	45											
LS	951	MIG MGW	204	66											

			FOLIATION		LINEATION			FOLD AXIS		AXIAL SURFACE		ILA	VERG	JOINT	
QUAD	STATION	LITHOLOGY	STRIKE	DIP	TREND	PLUNGE	TYPE	TREND	PLUNGE	STRIKE	DIP			STRIKE	DIP
LS	952	MIG MGW	47	36											
LS	953	MIG MGW	29	46											
LS	954	MIG MGW	41	52											
LS	955	MIG MGW	34	44											
LS	956	MIG MGW	34	49											
LS	956	MIG MGW												146	90
LS	957	MIG MGW	29	35											
LS	957	MIG MGW			184	9	STR								
LS	958	MIG MGW	27	34											
LS	959	MIG MGW	11	41											
LS	960	MIG MGW	36	51											
LS	961	MIG MGW	11	39											
LS	962	MIG MGW	31	34											
LS	963	MGW	14	31											
LS	964	MGW	21	57											
LS	965	MIG MGW	11	46											
LS	966	MIG MGW	26	37											
LS	967	MIG MGW	36	36											
LS	968	MIG MGW	26	47											
LS	969	MIG MGW	29	34											
LS	970	MIG MGW	24	41											
LS	971	MIG MGW	11	38											
LS	972	MIG MGW	31	44											
LS	976	MIG MGW	44	35											
LS	977	SCH MGW	19	29											
LS	978	SCH MGW	44	35											
LS	979	SCH MGW	69	24											
LS	981	MGW	255	24											
LS	981	MGW			36	13	STR								
LS	982	MGW	201	30											
LS	983	MGW	234	41											
LS	984	MGW	16	37											
LS	985	MGW	283	33											
LS	986	MGW	12	37											
LS	987	MGW	11	44											
LS	987	MGW			26	7	STR								
LS	989	SCH MGW	356	35											
LS	990	MGW	11	31											
LS	991	MIG MGW	18	29											
LS	991	MIG MGW												107	90
LS	992	MIG MGW	21	27											
LS	993	MIG MGW	36	24											
LS	994	MGW	354	22											
LS	995	MGW	11	39											
LS	996	MGW	344	51											
LS	998	MGW	221	33											
LS	1000	MGW	169	41											
LS	1000	MGW			319	11	STR								
LS	1001	MGW	9	31											
LS	1002	MGW						196	34						
LS	1003	ISG, SCH	185	69											
LS	1006	SCH	235	49											
LS	1007	ISG	31	64											
LS	1010	HFG	89	26											
LS	1012	HFG	250	64											
LS	1013	HFG	265	58											
LS	1015	HFG	51	54											

			FOLIATION		LINEATION			FOLD AXIS		AXIAL SURFACE		ILA	VERG	JOINT	
QUAD	STATION	LITHOLOGY	STRIKE	DIP	TREND	PLUNGE	TYPE	TREND	PLUNGE	STRIKE	DIP			STRIKE	DIP
LS	1016	HFG	133	29											
LS	1017	HFG	261	59											
LS	1018	ISG	276	58											
LS	1019	HFG	39	44											
LS	1020	HFG	337	37											
LS	1021	HFG	183	64											
LS	1022	HFG	224	68											
LS	1023	HFG	23	58											
LS	1024	HFG	163	64											
LS	1025	HFG	51	55											
LS	1026	HFG	314	69											
LS	1027	HFG	296	44											
LS	1028	HFG	70	69											
LS	1029	HFG	34	76											
LS	1030	HFG	357	56											
LS	1031	HFG	295	61											
LS	1032	HFG	221	55											
LS	1033	HFG	29	46											
LS	1034	HFG	71	41											
LS	1035	HFG	346	61											
LS	1036	HFG	27	61											
LS	1037	HFG	135	46											
LS	1038	HFG	37	60											
LS	1041	HFG	308	41											
LS	1042	HFG	250	62											
LS	1043	ISG	97	51											
LS	1044	HFG	137	31											
LS	1045	ISG	34	65											
LS	1046	HFG	294	61											
LS	1047	DPW	217	66											
LS	1049	ISG	136	38											
LS	1050	ISG	121	33											
LS	1051	ISG	172	71											
LS	1052	ISG	194	56											
LS	1053	ISG	198	61											
LS	1054	ISG	201	69											
LS	1055	ISG, HFG	209	61											
LS	1056	ISG	34	49											
LS	1057	HFG, SCH	179	71											
LS	1058	ISG	204	64											
LS	1059	ISG	189	40											
LS	1061	HFG	220	41											
LS	1062	HFG	202	47											
LS	1063	HFG	186	38											
LS	1064	ISG	203	77											
LS	1065	ISG	174	62											
LS	1066	ISG	204	55											
LS	1067	ISG	176	66											
LS	1068	ISG	197	53											
LS	1071	ISG	181	64											
LS	1072	ISG	184	77											
LS	1073	MGW	209	67											
LS	1074	ISG	184	47											
LS	1075	MGW	221	45											
LS	1076	ISG	192	70											
LS	1077	MGW	186	50											
LS	1078	MGW	202	55											

			FOLIATION		LINEATION			FOLD AXIS		AXIAL SURFACE		ILA	VERG	JOINT	
QUAD	STATION	LITHOLOGY	STRIKE	DIP	TREND	PLUNGE	TYPE	TREND	PLUNGE	STRIKE	DIP			STRIKE	DIP
LS	1079	MGW	174	48											
LS	1080	MGW	166	41											
LS	1081	HFG	226	72											
LS	1082	MGW	202	51											
LS	1083	MGW	229	63											
LS	1084	ISG	168	53											
LS	1085	ISG	33	66											
LS	1086	MGW	161	51											
LS	1087	HFG	207	67											
LS	1088	HFG	189	54											
LS	1090	HFG	186	69											
LS	1091	ISG	194	66											
LS	1092	HFG	204	57											
LS	1093	HFG	193	56											
LS	1094	HFG	211	65											
LS	1095	HFG	189	49											
LS	1096	ISG	195	52											
LS	1097	HFG	233	65											
LS	1098	HFG	226	68											
LS	1099	ISG	221	56											
LS	1100	HFG, ISG	209	49											
LS	1100	HFG, ISG	186	62											
LS	1101	HFG	214	51											
LS	1102	ISG	27	54											
LS	1103	ISG	214	66											
LS	1104	HFG	213	64											
LS	1106	HFG	214	53											
LS	1110	MGW	197	43											
LS	1112	MGW	166	57											
LS	1113	SCH MGW	211	65											
LS	1114	HFG	196	60											
LS	1115	HFG	203	52											
LS	1116	HFG	242	64											
LS	1117	HFG	224	46											
LS	1119	ISG	354	52											
LS	1120	ISG	336	64											
LS	1121	HFG	59	49											
LS	1122	HFG	141	57											
LS	1123	HFG	224	50											
LS	1125	HFG	114	47											
LS	1126	HFG	186	64											
LS	1128	HFG	146	61											
LS	1129	HFG	96	71											
LS	1130	HFG	244	75											
LS	1131	ISG, HFG	166	43											
LS	1132	HFG	226	68											
LS	1134	SCH MGW	231	62											
LS	1153	ISG	171	57											
LS	1154	ISG	226	61											
LS	1155	ISG	177	59											
LS	1156	ISG	31	49											
LS	1157	ISG	26	72											
LS	1158	HFG	22	75											
LS	1159	HFG	248	47											
LS	1163	MIG SSCH						227	24			95	SE		
LS	1163	MIG SSCH								230	76	95	SE		
LS	1163	MIG SSCH						241	17			10	NW		

			FOLIATION		LINEATION			FOLD AXIS		AXIAL SURFACE		ILA	VERG	JOINT	
QUAD	STATION	LITHOLOGY	STRIKE	DIP	TREND	PLUNGE	TYPE	TREND	PLUNGE	STRIKE	DIP			STRIKE	DIP
LS	1163	MIG SSCH								239	88	10	NW		
LS	1163	MIG SSCH						231	4			15	SSE		
LS	1163	MIG SSCH								251	38	15	SSE		
LS	1163	MIG SSCH						225	15			70	SE		
LS	1163	MIG SSCH								241	64	70	SE		
LS	1163	MIG SSCH						239	21			15	SSE		
LS	1163	MIG SSCH								57	70	15	SSE		
LS	1163	MIG SSCH						232	26			75	SE		
LS	1163	MIG SSCH								227	69	75	SE		
LS	1163	MIG SSCH						57	25			80	NNW		
LS	1163	MIG SSCH								250	41	80	NNW		
LS	1163	MIG SSCH						243	17			45	SE		
LS	1163	MIG SSCH								251	73	45	SE		
LS	1163	MIG SSCH						225	13			ISO	NW		
LS	1163	MIG SSCH								41	80	ISO	NW		
LS	1163	MIG SSCH			231	17	STR								
LS	1163	MIG SSCH						211	21			10	SE		
LS	1163	MIG SSCH								227	69	10	SE		
LS	1163	MIG SSCH						35	16			90	NW		
LS	1163	MIG SSCH								358	66	90	NW		
LS	1163	MIG SSCH						219	16			20	NW		
LS	1163	MIG SSCH								215	79	20	NW		
LS	1163	MIG SSCH						223	12			80	SE		
LS	1163	MIG SSCH								211	76	80	SE		
LS	1163	MIG SSCH						231	20			75	SE		
LS	1163	MIG SSCH								222	67	75	SE		
LS	1163	MIG SSCH						207	3			90	SE		
LS	1163	MIG SSCH								226	66	90	SE		
LS	1163	MIG SSCH						214	4			90	SE		
LS	1163	MIG SSCH								231	55	90	SE		
LS	1163	MIG SSCH						345	37			10	N		
LS	1163	MIG SSCH								244	35	10	N		
LS	1163	MIG SSCH						31	29			30	NW		
LS	1163	MIG SSCH								226	81	30	NW		
LS	1163	MIG SSCH						233	23			35	NW		
LS	1163	MIG SSCH								221	77	35	NW		
LS	1163	MIG SSCH						3	38			15	SE		
LS	1163	MIG SSCH								238	75	15	SE		
LS	1163	MIG SSCH						46	16			50	SE		
LS	1163	MIG SSCH								231	75	50	SE		
LS	1163	MIG SSCH						218	28			80	SE		
LS	1163	MIG SSCH								220	69	80	SE		
LS	1163	MIG SSCH						221	18			70	SE		
LS	1163	MIG SSCH								226	75	70	SE		
LS	1165	ISG	101	66											
LS	1166	MIG SCH								54	82	45	SE		
LS	1166	MIG SSCH						41	52			45	SE		
LS	1167	HFG	46	62											
LS	1168	ISG	239	57											
LS	1169	HFG	37	77											
LS	1170	HFG	47	55											
LS	1173	HFG	203	54											
LS	1174	HFG	64	78											
LS	1175	HFG	152	58											
LS	1177	HFG	344	33											
LS	1178	HFG	47	34											
LS	1180	HFG	67	42											

			FOLIATION		LINEATION			FOLD AXIS		AXIAL SURFACE		ILA	VERG	JOINT	
QUAD	STATION	LITHOLOGY	STRIKE	DIP	TREND	PLUNGE	TYPE	TREND	PLUNGE	STRIKE	DIP			STRIKE	DIP
LS	1182	HFG	53	50											
LS	1183	ISG	333	74											
LS	1185	HFG	129	49											
LS	1186	HFG	110	41											
LS	1187	HFG	233	48											
LS	1188	HFG	166	79											
LS	1189	MIG SCH, ALT GG	205	37											
LS	1190	ISG	189	60											
LS	1191	ISG	190	52											
LS	1192	HFG	207	44											
LS	1193	HFG	222	77											
LS	1194	ISG	6	79											
LS	1195	SCH MGW, AM	14	76											
LS	1196	MIG MGW, AM	355	79											
LS	1197	SCH MGW	21	66											
LS	2001	HFG	33	69											
LS	2006	MYL MGW	46	50											
LS	2007	MGW			72	18	STR								
LS	2008	MGW	52	75											
LS	2008	MGW			226	15	STR								
LS	2009	MGW												105	90
LS	2010	MYL MGW	47	57											
LS	2010	MYL MGW	221	19											
LS	2011	MIG MGW	46	49											
LS	2012	MIG MGW	43	53											
LS	2013	MGW	36	45											
LS	2013	MGW												156	90
LS	2014	MIG MGW	41	34											
LS	2015	MGW	33	37											
LS	2016	MGW	25	42											
LS	2017	MGW												131	80
LS	2018	MGW			211	12	STR								
LS	2018	MYL MGW	55	34											
LS	2021	SI CAT												256	52
LS	2022	SI CAT												221	44
LS	2025	SI CAT												359	68
LS	2025	SI CAT												347	73
LS	2025	SI CAT												282	81
LS	2033	SI CAT												189	63
LS	2035	ISG	31	63											
LS	2045	ISG	141	40											
LS	2051	MGW	164	38											
LS	2054	MGW, GG	207	43											
LS	2055	HFG	193	42											
LS	2056	HFG	204	53											
LS	2063	HFG	174	65											
LS	2066	HFG, SCH MGW	208	49											
LS	2071	MGW	21	41											
LS	2072	QZ			201	17	STR								
LS	2072	QZ, MGW	28	73											
LS	2074	MGW	44	51											
LS	2076	HFG	216	60											
LS	2077	HFG	204	70											
LS	2085	HFG	149	53											
LS	2086	HFG	146	42											
LS	2087	HFG, ISG	171	47											
LS	2088	HFG	201	64											

			FOLIATION		LINEATION			FOLD AXIS		AXIAL SURFACE		ILA	VERG	JOINT	
QUAD	STATION	LITHOLOGY	STRIKE	DIP	TREND	PLUNGE	TYPE	TREND	PLUNGE	STRIKE	DIP			STRIKE	DIP
LS	2089	ISG, HFG	131	49											
LS	2090	HFG	189	66											
LS	2091	ISG	154	52											
LS	2092	HFG	284	65											
LS	2093	ISG	330	69											
LS	2094	HFG, ISG	61	75											
LS	2095	HFG	46	65											
LS	2096	HFG	54	68											
LS	2097	HFG	54	54											
LS	2098	HFG	41	58											
LS	2099	HFG, ISG	191	56											
LS	2100	ISG	180	56											
LS	2101	ISG	191	78											
LS	2102	HFG	131	38											
LS	2103	ISG	156	66											
LS	2105	HFG	221	53											
LS	2106	HFG	229	61											
LS	2107	HFG	204	46											
LS	2108	ISG	358	68											
LS	2109	HFG, ISG	259	62											
LS	2109	HFG, ISG	335	54											
LS	2113	HFG, ISG	51	75											
LS	2114	HFG	55	68											
LS	2115	HFG	229	77											
LS	2116	HFG	242	58											

			FOLIATION		LINEATION			FOLD AXIS		AXIAL SURFACE		ILA	VERG	JOINT	
QUAD	STATION	MAJOR_1	STRIKE	DIP	TREND	PLUNGE	TYPE	TREND	PLUNGE	STRIKE	DIP			STRIKE	DIP
ST	2	MGW	28	18											
ST	3	MGW	68	11											
ST	5	MYL MGW	200	21											
ST	6	MYL MGW	70	14											
ST	7	MYL MGW	10	11											
ST	9	MYL MGW	180	21											
ST	10	MYL MGW												320	68
ST	11	MYL MGW	140	31											
ST	12	MGW	80	11											
ST	12	MGW	195	7											
ST	13	MGW	201	13											
ST	14	MGW	202	31											
ST	15	MGW	131	36											
ST	17	MYL MGW	71	21											
ST	18	MYL MGW	125	16											
ST	19	MYL MGW	162	11											
ST	20	MYL MGW	138	19											
ST	21	MYL MGW	104	24											
ST	22	MYL MGW	154	17											
ST	23	MYL MGW	126	21											
ST	24	MYL MGW	105	19											
ST	25	MYL MGW	154	9											
ST	26	MYL MGW	169	8											
ST	27	MYL MGW	156	12											
ST	28	MYL MGW	124	9											
ST	29	MYL MGW	39	21											
ST	30	MYL MGW	89	11											
ST	31	MYL MGW	132	11											
ST	43	HFG	158	83											
ST	58	DPG	112	30											
ST	58	DPG												50	32
ST	59	DPG	112	13											
ST	59	DPG												84	37
ST	61	DPG	123	21											
ST	65	DPG	86	5											
ST	67	DPG	125	16											
ST	69	DPG	105	14											
ST	74	DPG	98	18											
ST	75	DPG	98	18											
ST	86	ISG	115	6											
ST	88	DPG	335	6											
ST	89	DPG	338	24											
ST	104	DPG	221	68											
ST	105	DPG												160	90
ST	106	DPG	270	15											
ST	107	MGW	215	31											
ST	108	MGW	225	13											
ST	109	SI CAT	30	71											
ST	113	SI CAT, DD	330	18											
ST	115	SI CAT	314	29											
ST	117	HFG	220	60											
ST	119	HFG	130	25											
ST	120	MGW						5	11			150	ESE		
ST	121	HFG	31	15											
ST	122	HFG	59	10											
ST	124	HFG	58	66											
ST	125	HFG	23	65											
ST	137	SI CAT												318	76

			FOLIATION		LINEATION			FOLD AXIS		AXIAL SURFACE		ILA	VERG	JOINT	
QUAD	STATION	MAJOR_1	STRIKE	DIP	TREND	PLUNGE	TYPE	TREND	PLUNGE	STRIKE	DIP			STRIKE	DIP
ST	138	MGW	62	16											
ST	139	HFG	256	22											
ST	140	SI CAT												216	34
ST	141	SI CAT												346	75
ST	142	SI CAT												255	61
ST	143	SI CAT												339	71
ST	143	SI CAT												150	88
ST	144	SI CAT												275	69
ST	145	SI CAT												109	61
ST	146	SI CAT												176	85
ST	147	SI CAT												196	58
ST	148	ISG	316	31											
ST	149	ISG	76	14											
ST	151	ISG												353	0
ST	153	ISG	256	64											
ST	153	ISG												145	76
ST	154	AM												229	69
ST	155	HFG	66	75											
ST	159	ISG												235	84
ST	161	ISG	198	14											
ST	162	ISG												31	79
ST	169	HFG, ISG												104	64
ST	169	HFG, ISG	258	29											
ST	170	HFG	248	17											
ST	191	HFG	160	12											
ST	205	HFG	95	6											
ST	216	MYL MGW	99	31											
ST	224	MYL MGW	176	45											
ST	225	MYL MGW	130	17											
ST	228	MYL MGW	185	61											
ST	235	MYL MGW	193	49											
ST	241	MGW	211	20											
ST	248	MGW	89	21											
ST	249	MGW	114	29											
ST	250	MGW	77	11											
ST	256	CALC-SI, MGW						173	19						
ST	256	CALC-SI, MGW								47	24				
ST	257	SI CAT												354	64
ST	257	SI CAT												291	87
ST	258	SI CAT												7	26
ST	258	SI CAT												112	33
ST	258	SI CAT												134	62
ST	258	SI CAT												292	76
ST	258	SI CAT												84	74
ST	258	SI CAT												57	77
ST	258	SI CAT												180	62
ST	258	SI CAT												292	49
ST	258	SI CAT												196	59
ST	258	SI CAT												321	49
ST	258	SI CAT												134	70
ST	258	SI CAT												186	76
ST	258	SI CAT												162	67
ST	258	SI CAT												14	75
ST	258	SI CAT												193	72
ST	258	SI CAT												155	71
ST	258	SI CAT												233	83
ST	258	SI CAT												186	72
ST	258	SI CAT												222	67

			FOLIATION		LINEATION			FOLD AXIS		AXIAL SURFACE		ILA	VERG	JOINT	
QUAD	STATION	MAJOR_1	STRIKE	DIP	TREND	PLUNGE	TYPE	TREND	PLUNGE	STRIKE	DIP			STRIKE	DIP
ST	258	SI CAT												359	68
ST	258	SI CAT												296	76
ST	258	SI CAT												221	69
ST	258	SI CAT												216	61
ST	258	SI CAT												186	69
ST	258	SI CAT												264	53
ST	258	SI CAT												31	58
ST	258	SI CAT												336	69
ST	258	SI CAT												226	66
ST	258	SI CAT												175	79
ST	258	SI CAT												199	72
ST	258	SI CAT												195	77
ST	258	SI CAT												221	58
ST	258	SI CAT												188	56
ST	258	SI CAT												71	45
ST	258	SI CAT												122	56
ST	258	SI CAT												164	57
ST	258	SI CAT												146	29
ST	258	SI CAT												181	81
ST	258	SI CAT												13	38
ST	258	SI CAT												31	44
ST	258	SI CAT												75	24
ST	258	SI CAT												21	46
ST	258	SI CAT												307	72
ST	258	SI CAT												181	76
ST	258	SI CAT												28	31
ST	258	SI CAT												176	67
ST	258	SI CAT												294	26
ST	258	SI CAT												31	46
ST	258	SI CAT												331	84
ST	258	SI CAT												113	13
ST	258	SI CAT												71	7
ST	258	SI CAT												205	80
ST	266	SI CAT												119	55
ST	266	SI CAT												104	86
ST	267	SI CAT												191	74
ST	268	SI CAT												297	61
ST	269	SI CAT												196	73
ST	270	MIG MGW	194	73											
ST	271	MIG MGW												138	84
ST	272	MIG MGW						19	23				SE		
ST	272	MIG MGW								33	47				
ST	272	MIG MGW	29	27											
ST	272	MIG MGW	233	84											
ST	273	MIG MGW	211	69											
ST	274	MIG MGW						54	61						
ST	274	MIG MGW								56	77				
ST	274	MIG MGW	58	76											
ST	275	MIG MGW													
ST	275	MIG MGW	201	29											
ST	276	DPG						189	44				W		
ST	276	DPG	157	76											
ST	291	MIG MGW	178	31											
ST	291	MIG MGW												107	74
ST	292	MIG MGW	26	44				201	90			32			
ST	292	MIG MGW								28	41				
ST	292	MIG MGW												111	79
ST	293	MIG MGW						27	54			40	NW		

			FOLIATION		LINEATION			FOLD AXIS		AXIAL SURFACE		ILA	VERG	JOINT	
QUAD	STATION	MAJOR_1	STRIKE	DIP	TREND	PLUNGE	TYPE	TREND	PLUNGE	STRIKE	DIP			STRIKE	DIP
ST	293	MIG MGW								36	46				
ST	295	MIG MGW	203	66											
ST	296	MIG MGW												122	74
ST	297	MIG MGW			352	71	BN								
ST	298	MIG MGW						224	68			15	NW		
ST	298	MIG MGW								220	83				
ST	299	MIG MGW												111	66
ST	299	MIG MGW												79	38
ST	300	MIG MGW						219	74			40	NW		
ST	300	MIG MGW								211	71				
ST	301	MIG MGW	216	64											
ST	302	MIG MGW	46	76											
ST	303	MIG MGW								36	55				
ST	303	MIG MGW	221	84											
ST	304	MIG MGW	36	79											
ST	305	MIG MGW	198	71											
ST	308	MGW	36	58											
ST	309	MIG MGW	67	11											
ST	320	MGW	84	44											
ST	321	SCH	201	46											
ST	331	ISG	206	24											
ST	340	MIG MGW	116	32											
ST	347	HFG	256	56											
ST	348	HFG	202	61											
ST	352	HFG	45	35											
ST	352	HFG												326	77
ST	356	HFG	204	31											
ST	358	HFG	176	51											
ST	359	HFG	244	35											
ST	365	MGW						244	59			20	NW		
ST	365	MGW								64	73				
ST	366	MGW	224	68											
ST	367	MGW						262	31			115	SSW		
ST	367	MGW								76	58				
ST	369	MGW	193	76											
ST	370	MGW	187	54											
ST	372	MGW	174	56											
ST	376	MGW, AM	99	34											
ST	378	MGW, SCH	216	36											
ST	378	MGW, SSCH												124	76
ST	381	HFG, ISG	171	41											
ST	384	MGW	184	56											
ST	398	MIG MGW	186	56											
ST	400	MGW						214	31						
ST	400	MGW								46	69				
ST	404	MGW, AM	21	84											
ST	406	MGW	71	63											
ST	407	MYL GG	221	44											
ST	408	MYL GG	209	46											
ST	409	MYL GG	198	34											
ST	410	GG	228	56											
ST	411	SCH	224	59											
ST	415	GG	214	27											
ST	418	MIG MGW	191	58											
ST	424	MIG MGW	219	54											
ST	425	MIG MGW								241	46				
ST	425	MIG MGW	149	51											
ST	426	MIG MGW												124	79

			FOLIATION		LINEATION			FOLD AXIS		AXIAL SURFACE		ILA	VERG	JOINT	
QUAD	STATION	MAJOR_1	STRIKE	DIP	TREND	PLUNGE	TYPE	TREND	PLUNGE	STRIKE	DIP			STRIKE	DIP
ST	427	MIG MGW	221	71											
ST	428	MIG MGW	229	61											
ST	430	MIG MGW	189	56											
ST	431	HFG	201	66											
ST	442	GG	191	55											
ST	446	AM	71	32											
ST	463	ISG	237	72											
ST	466	MIG MGW	214	79											
ST	467	GG	201	44											
ST	468	GG	207	31											
ST	470	MYL GG	204	52											
ST	472	GG	209	59											
ST	473	GG	212	79											
ST	479	MIG MGW	158	58											
ST	480	MIG MGW	61	64											
ST	485	MGW	29	78											
ST	486	MIG MGW	21	54											
ST	489	MIG MGW	37	71											
ST	490	MIG MGW	214	64											
ST	491	MIG MGW	241	64											
ST	493	MIG MGW								201	65				
ST	493	MIG MGW	211	56											
ST	493	MIG MGW	44	59											
ST	494	MIG MGW	39	69											
ST	495	MIG MGW	42	81											
ST	495	MIG MGW												319	83
ST	496	MIG MGW	219	74											
ST	496	MIG MGW												125	86
ST	497	MIG MGW	51	47											
ST	498	MIG MGW	37	51											
ST	499	MIG MGW	219	79											
ST	504	MGW	41	72											
ST	512	MIG MGW, AM	43	61											
ST	512	MIG MGW, AM												81	90
ST	513	MIG MGW	41	58											
ST	514	MIG MGW	47	55											
ST	515	MIG MGW	221	78											
ST	516	MIG MGW	43	80											
ST	517	MIG MGW	221	74											
ST	519	MGW	355	80											
ST	520	MGW	111	26											
ST	520	MGW												144	79
ST	522	DPG	236	35											
ST	523	HFG	104	33											
ST	524	HFG	201	54											
ST	525	DPG	224	59											
ST	526	HFG	195	34											
ST	526	HFG												301	90
ST	527	HFG	226	49											
ST	528	DPG	218	69											
ST	529	HFG	265	64											
ST	530	MIG MGW	156	23											
ST	531	DPG	194	23											
ST	532	HFG	166	29											
ST	533	DPG	249	37											
ST	534	MYL GG	205	66											
ST	536	CALC-SI	194	87											
ST	536	CALC-SI, AM												305	90

			FOLIATION		LINEATION			FOLD AXIS		AXIAL SURFACE		ILA	VERG	JOINT	
QUAD	STATION	MAJOR_1	STRIKE	DIP	TREND	PLUNGE	TYPE	TREND	PLUNGE	STRIKE	DIP			STRIKE	DIP
ST	537	MGW	41	55											
ST	540	MGW	194	65											
ST	542	HFG	229	61											
ST	543	MIG MGW												291	82
ST	544	ISG												291	90
ST	552	ISG												287	74
ST	558	HFG	46	36											
ST	560	ISG, HFG	19	54											
ST	562	HFG	174	39											
ST	565	ISG												16	86
ST	574	HFG	242	64											
ST	575	HFG	242	69											
ST	576	HFG	267	81											
ST	583	HFG	221	53											
ST	585	MGW												124	84
ST	592	ISG												126	87
ST	606	MGW	168	36											
ST	606	MGW												314	76
ST	607	MGW	189	34											
ST	608	MGW	186	27											
ST	609	MGW	191	30											
ST	610	MGW	178	37											
ST	614	MGW	24	88											
ST	619	ISG	194	68											
ST	619	ISG												329	90
ST	638	HFG	39	47											
ST	650	MGW	126	24											
ST	651	MIG MGW	189	44											
ST	652	MIG MGW	182	47											
ST	655	MIG MGW	187	75											
ST	672	MIG MGW, DD	219	81											
ST	673	MIG MGW	221	74											
ST	674	MIG MGW	228	81											
ST	676	MIG MGW	215	79											
ST	677	MIG MGW	204	56											
ST	679	MIG MGW			313	79	BN								
ST	679	MIG MGW	221	79											
ST	694	MIG MGW	198	34											
ST	699	MGW	246	11											
ST	700	MIG MGW	194	61											
ST	703	MIG MGW	181	33											
ST	703	MIG MGW												137	87
ST	704	HFG	239	46											
ST	707	HFG	81	74											
ST	751	HFG	166	74											
ST	752	HFG	114	61											
ST	760	HFG	249	9											
ST	793	HFG	248	70											
ST	802	HFG	204	51											
ST	803	HFG, ISG	181	47											
ST	804	HFG	171	34											
ST	805	HFG	94	46											
ST	813	HFG	101	24											
ST	814	HFG	71	54											
ST	835	HFG	59	32											
ST	845	DPG, HFG	153	34											
ST	850	HFG	241	67											
ST	886	HFG, ISG	21	73											

			FOLIATION		LINEATION			FOLD AXIS		AXIAL SURFACE		ILA	VERG	JOINT	
QUAD	STATION	MAJOR_1	STRIKE	DIP	TREND	PLUNGE	TYPE	TREND	PLUNGE	STRIKE	DIP			STRIKE	DIP
ST	909	SSCH												306	51
ST	914	HFG	94	17											
ST	916	MGW												313	84
ST	917	HFG	229	76											
ST	918	MGW			254	24	STR								
ST	918	MGW	186	39											
ST	919	MGW			231	13	STR								
ST	919	MGW	193	16											
ST	920	HFG	227	66											
ST	921	MGW	234	39											
ST	931	SSCH												197	84
ST	932	MGW						144	12						
ST	932	MGW								111	24				
ST	936	ISG	11	21											
ST	940	HFG	249	54											
ST	955	MGW	282	19											
ST	956	MGW	167	76											
ST	957	MGW	119	51											
ST	959	HFG	114	39											
ST	960	DPG	66	25											
ST	970	HFG	229	55											
ST	973	MGW	199	42											
ST	975	HFG	221	61											
ST	976	ISG	226	66											
ST	978	HFG	224	58											
ST	987	HFG, ISG	72	70											
ST	988	HFG	358	11											
ST	989	HFG, SCH	155	50											
ST	999	SCH												81	83
ST	1012	DPG, SCH	15	76											
ST	1017	HFG	57	75											
ST	1025	HFG	64	55											
ST	1030	MIG MGW	219	78											
ST	1031	MIG MGW	226	74											
ST	1032	MIG MGW								26	74				
ST	1032	MIG MGW	205	82											
ST	1033	MIG MGW	216	56											
ST	1034	MIG MGW	171	37											
ST	1035	MIG MGW	211	40											
ST	1035	MIG MGW												309	90
ST	1038	MIG MGW												119	81
ST	1039	MIG MGW	222	74											
ST	1039	MIG MGW												107	87
ST	1040	MIG MGW	213	61											
ST	1041	MIG MGW	205	47											
ST	1042	MIG MGW	216	61											
ST	1043	MIG MGW	41	54											
ST	1044	MIG MGW	39	59											
ST	1045	MIG MGW	86	39											
ST	1054	SSCH												125	79
ST	1057	HFG	234	41											
ST	1077	MGW	84	51											
ST	1081	HFG	244	74											
ST	1082	HFG	196	79											
ST	1088	DPG	274	44											
ST	1122	MGW	216	62											
ST	1124	MGW	229	60											
ST	1125	MIG MGW	221	73											

			FOLIATION		LINEATION			FOLD AXIS		AXIAL SURFACE		ILA	VERG	JOINT	
QUAD	STATION	MAJOR_1	STRIKE	DIP	TREND	PLUNGE	TYPE	TREND	PLUNGE	STRIKE	DIP			STRIKE	DIP
ST	1132	DPG	92	29											
ST	1134	DPG	76	18											
ST	1139	GG	214	71											
ST	1144	MGW	209	72											
ST	1150	GG	26	35											
ST	1151	MYL GG	46	71											
ST	1152	MGW	189	42											
ST	1153	GG	236	29											
ST	1155	ISG	52	54											
ST	1155	ISG												348	44
ST	1155	ISG												306	76
ST	1157	DPG, SCH	82	79											
ST	1158	DPG, SCH	72	62											
ST	1173	GG	126	43											
ST	1180	MGW	214	52											
ST	1183	MGW	211	61											
ST	1188	MGW, AM	242	62											
ST	1193	MGW	41	78											
ST	1194	MGW	29	62											
ST	1196	MGW	219	65											
ST	1207	GG	49	56											
ST	1211	MGW, AM			144	56	BN								
ST	1211	MGW, AM	66	72											
ST	1212	MGW	207	55											
ST	1213	MGW	29	77											
ST	1216	MGW	212	74											
ST	1217	MGW						216	34			40	W		
ST	1217	MGW								34	69				
ST	1219	DPG	184	61											
ST	1220	DPG, HFG	171	81											
ST	1220	DPG, HFG	204	59											
ST	1222	HFG	214	79											
ST	1233	DPG, HFG	196	78											
ST	1234	DPG	129	76											
ST	1235	DPG	110	36											
ST	1235	DPG												206	69
ST	1239	MGW	176	62											
ST	1240	GG	172	36											
ST	1241	MGW	212	26											
ST	1242	MYL GG	186	34											
ST	1243	GG	172	29											
ST	1243	GG												294	52
ST	1244	HFG	235	64											
ST	1245	MGW	342	68											
ST	1246	MGW	335	65											
ST	1248	MGW	191	26											
ST	1249	MGW, SSCH	180	76											
ST	1250	MGW, SSCH	174	74											
ST	1251	MIG MGW, AM								329	69				
ST	1251	MIG MGW, AM	160	44											
ST	1252	MGW	204	73											
ST	1253	MGW	186	69											
ST	1254	MGW	140	79											
ST	1256	MGW	350	79											
ST	1259	MIG MGW								194	76				
ST	1259	MIG MGW	6	54											
ST	1260	MGW	230	72											
ST	1262	MYL MGW	200	74											

			FOLIATION		LINEATION			FOLD AXIS		AXIAL SURFACE		ILA	VERG	JOINT	
QUAD	STATION	MAJOR_1	STRIKE	DIP	TREND	PLUNGE	TYPE	TREND	PLUNGE	STRIKE	DIP			STRIKE	DIP
ST	1263	MIG MGW	39	61											
ST	1264	MIG MGW								356	61				
ST	1264	MIG MGW	55	44											
ST	1265	MGW	35	84											
ST	1266	MYL MGW	215	79											
ST	1267	MGW	186	75											
ST	1268	MGW	47	79											
ST	1269	MYL MGW	15	82											
ST	1270	MGW	204	76											
ST	1271	MGW	209	71											
ST	1272	MGW	46	66											
ST	1273	MIG MGW	135	36											
ST	1275	MIG MGW	216	61											
ST	1276	SSCH	219	74											
ST	1278	SSCH	39	84											
ST	1279	SSCH	37	85											
ST	1280	MIG MGW			139	84	BN								
ST	1280	MIG MGW	41	84											
ST	1281	MIG MGW	42	76											
ST	1282	MIG MGW								204	79				
ST	1282	MIG MGW	196	53											
ST	1282	MIG MGW	44	84											
ST	1283	MIG MGW	221	76											
ST	1284	SSCH			69	24	STR								
ST	1285	MGW	184	61											
ST	1286	MGW	64	64											
ST	1288	MGW	106	55											
ST	1289	MIG MGW, CALC-S	158	60											
ST	1289	MIG MGW, CALC-SI												311	81
ST	1290	MGW	76	54											
ST	1291	MIG MGW			136	54	BN								
ST	1291	MIG MGW	67	54											
ST	1292	MIG MGW	49	60											
ST	1293	MGW	42	57											
ST	1294	MGW	39	72											
ST	1295	MGW	46	59											
ST	1297	MGW	64	49											
ST	1298	MGW, AM			164	22	STR								
ST	1298	MGW, AM	49	49											
ST	1299	MGW	42	69											
ST	1300	MIG MGW			304	56	BN								
ST	1300	MIG MGW						12	51			30	SE		
ST	1300	MIG MGW								12	86				
ST	1300	MIG MGW	210	56											
ST	1301	MGW	52	60											
ST	1302	MGW	131	52											
ST	1303	MGW	76	31											
ST	1304	MGW	164	50											
ST	1304	MGW	86	34											
ST	1305	MGW	42	72											
ST	1306	MGW	49	66											
ST	1308	MGW	47	71											
ST	1310	MIG MGW	42	61											
ST	1311	MIG MGW	207	79											
ST	1312	MIG MGW	46	60											
ST	1313	Granite	32	64											
ST	1315	MGW			184	16	STR								
ST	1315	MGW						156	25			60	SSW		

			FOLIATION		LINEATION			FOLD AXIS		AXIAL SURFACE		ILA	VERG	JOINT	
QUAD	STATION	MAJOR_1	STRIKE	DIP	TREND	PLUNGE	TYPE	TREND	PLUNGE	STRIKE	DIP			STRIKE	DIP
ST	1315	MGW								124	20				
ST	1315	MGW	24	74											
ST	1317	MGW	51	49											
ST	1318	MGW	48	72											
ST	1319	Granite	27	27											
ST	1319	Granite												226	80
ST	1320	MGW						232	44			60	NW		
ST	1320	MGW								51	61				
ST	1320	MIG MGW	42	71											
ST	1321	MGW	61	46											
ST	1322	Granite	136	21											
ST	1323	MGW	81	29											
ST	1325	MGW	42	69											
ST	1326	MIG MGW	53	52											
ST	1327	MIG MGW	207	46											
ST	1328	MIG MGW	37	74											
ST	1329	MIG MGW	31	65											
ST	1330	MIG MGW	24	66											
ST	1332	MGW	56	69											
ST	1333	MIG MGW	29	59											
ST	1334	MIG MGW	36	67											
ST	1335	MIG MGW	37	71											
ST	1336	MIG MGW	28	72											
ST	1337	HFG	234	66											
ST	1339	MGW	7	79											
ST	1340	HFG	66	72											
ST	1341	DPG	61	59											
ST	1343	MGW	54	84											
ST	1346	MIG MGW			171	26	BN								
ST	1346	MIG MGW								89	85				
ST	1346	MIG MGW	265	46											
ST	1347	MGW	86	71											
ST	1349	GG, SCH	54	57											
ST	1350	MIG SCH	197	51											
ST	1351	MGW	129	69											
ST	1353	GG, SCH	204	46											
ST	1354	HFG	215	61											
ST	1355	MGW	249	79											
ST	1355	MGW			77	24	STR								
ST	1356	MGW	26	42											
ST	1357	MGW	27	61											
ST	1359	MIG MGW	31	64											
ST	1360	MIG MGW	201	77											
ST	1361	MIG MGW	199	65											
ST	1362	MIG MGW			312	77	BN								
ST	1362	MIG MGW	211	77											
ST	1363	MIG MGW	206	77											
ST	1365	MIG MGW	236	86											
ST	1366	MIG MGW			218	27	STR								
ST	1366	MIG MGW	218	82											
ST	1367	MIG MGW								26	65				
ST	1367	MIG MGW	46	31											
ST	1367	MIG MGW	45	52											
ST	1368	MIG MGW	216	81											
ST	1369	MIG MGW	237	26											
ST	1369	MIG MGW	42	59											
ST	1369	MIG MGW	59	87											
ST	1370	MIG MGW	217	63											

			FOLIATION		LINEATION			FOLD AXIS		AXIAL SURFACE		ILA	VERG	JOINT	
QUAD	STATION	MAJOR_1	STRIKE	DIP	TREND	PLUNGE	TYPE	TREND	PLUNGE	STRIKE	DIP			STRIKE	DIP
ST	1371	MIG MGW	44	84											
ST	1372	MIG MGW	34	78											
ST	1373	MIG MGW	36	72											
ST	1374	MIG MGW	209	66											
ST	1375	MIG MGW	221	62											
ST	1376	MGW	207	61											
ST	1378	MIG MGW								219	46				
ST	1378	MIG MGW	349	21											
ST	1378	MIG MGW	199	64											
ST	1380	MIG MGW	46	62											
ST	1381	MIG MGW	48	64											
ST	1382	MIG MGW								81	74				
ST	1382	MIG MGW	255	39											
ST	1383	MIG MGW	46	56											
ST	1385	HFG	201	61											
ST	1386	HFG	111	36											
ST	1387	HFG	132	76											
ST	1388	SCH			219	21	STR								
ST	1389	MGW	221	64											
ST	1390	HFG	87	51											
ST	1391	DPG	204	63											
ST	1392	HFG	21	48											
ST	1393	HFG	43	26											
ST	1394	ISG	163	51											
ST	1395	ISG	188	57											
ST	1396	HFG	252	65											
ST	1397	HFG	17	53											
ST	1398	HFG	264	69											
ST	1399	HFG	216	70											
ST	1400	HFG	65	46											
ST	1401	HFG	47	56											
ST	1402	ISG	183	64											
ST	1403	ISG	349	36											
ST	1404	HFG	77	51											
ST	1405	ISG	84	66											
ST	1406	HFG	92	70											
ST	1407	DPG	196	56											
ST	1408	DPG	105	58											
ST	1409	HFG	344	64											
ST	1410	HFG	44	49											
ST	1411	HFG	47	62											
ST	1412	HFG	130	24											
ST	1413	ISG	346	38											
ST	1414	ISG	334	74											
ST	1415	HFG	226	39											
ST	1416	ISG	131	61											
ST	1417	HFG	94	45											
ST	1418	HFG	76	37											
ST	1419	ISG	31	47											
ST	1420	ISG	96	24											
ST	1421	ISG	56	64											
ST	1422	HFG	237	62											
ST	1423	HFG	224	41											
ST	1424	HFG	166	44											
ST	1425	HFG	191	41											
ST	1426	SCH MGW	245	44											
ST	1427	HFG	156	49											
ST	1428	MGW	204	43											

			FOLIATION		LINEATION			FOLD AXIS		AXIAL SURFACE		ILA	VERG	JOINT	
QUAD	STATION	MAJOR_1	STRIKE	DIP	TREND	PLUNGE	TYPE	TREND	PLUNGE	STRIKE	DIP			STRIKE	DIP
ST	1429	MGW	216	56											
ST	1430	MGW	201	46											
ST	1431	MGW	271	61											
ST	1432	HFG	224	71											
ST	1433	HFG	314	52											
ST	1434	HFG	228	48											
ST	1436	HFG	331	65											
ST	1437	HFG	216	67											
ST	1443	HFG	300	41											
ST	1445	HFG	214	71											
ST	1446	HFG	54	55											
ST	1447	MIG MGW	74	66											
ST	1448	DPG	207	32											
ST	1449	DPG	74	44											
ST	1452	DPG	164	41											
ST	1453	DPG	209	59											
ST	1454	HFG	220	73											
ST	1455	DPG	196	66											
ST	1456	DPG	70	49											
ST	1457	DPG	36	36											
ST	1458	DPG	46	66											
ST	1459	DPG	76	44											
ST	1460	DPG	37	61											
ST	1461	DPG	32	58											
ST	1462	MIG MGW	201	61											
ST	1464	HFG	64	71											
ST	1465	ISG	33	62											
ST	1466	HFG	34	67											
ST	1467	HFG	224	48											
ST	1468	ISG	4	46											
ST	1471	DPG	64	47											
ST	1472	HFG	82	66											
ST	1473	ISG	93	64											
ST	1474	MGW	53	46											
ST	1475	MGW	11	41											
ST	1477	MGW	29	80											
ST	1478	MIG MGW	221	67											
ST	1479	MIG MGW	34	85											
ST	1480	MIG MGW, AM	55	77											
ST	1481	MIG MGW	191	63											
ST	1483	MIG MGW	54	74											
ST	1485	HFG	14	60											
ST	1486	HFG	52	59											
ST	1489	DPG	136	54											
ST	1490	DPG	201	31											
ST	1491	DPG	221	59											
ST	1492	DPG, ISG	71	39											
ST	1493	DPG	211	74											
ST	1495	DPG	4	61											
ST	1498	ISG	33	62											
ST	1499	HFG	84	51											
ST	1500	HFG	17	69											
ST	1501	MIG MGW	296	31											
ST	1503	DPG	71	36											
ST	1504	DPG, SCH	204	63											
ST	1507	MIG MGW	49	36											
ST	1508	MIG MGW	35	66											
ST	1509	MIG MGW	41	56											

			FOLIATION		LINEATION			FOLD AXIS		AXIAL SURFACE		ILA	VERG	JOINT	
QUAD	STATION	MAJOR_1	STRIKE	DIP	TREND	PLUNGE	TYPE	TREND	PLUNGE	STRIKE	DIP			STRIKE	DIP
ST	1510	MGW, SSCH	191	26											
ST	1511	MGW	29	61											
ST	1512	ISG	131	41											
ST	1513	ISG	196	34											
ST	1514	ISG	171	57											
ST	1515	MGW, AM	49	49											
ST	1516	SCH MGW, AM	214	79											
ST	1517	SCH MGW	224	81											
ST	1518	MGW	164	48											
ST	1519	SCH MGW	211	84											
ST	1521	DPG	92	54											
ST	1522	ISG	109	67											
ST	1523	ISG	84	58											
ST	1524	MGW	209	71											
ST	1525	MGW, AM	130	43											
ST	1526	SCH MGW	34	71											
ST	1527	SCH MGW, AM	33	64											
ST	1529	MGW	55	58											
ST	1530	MGW	218	66											
ST	1531	SCH MGW	184	72											
ST	1532	SCH MGW	36	75											
ST	1533	MGW	215	67											
ST	1534	SCH MGW	176	50											
ST	1539	GG	83	55											
ST	1544	MGW	229	71											
ST	1546	MIG MGW	44	74											
ST	1547	MIG MGW	224	76											
ST	1552	MIG MGW			246	16	STR								
ST	1553	MGW	36	84											
ST	1554	GG	19	74											
ST	1250-1	SCH	121	24											
ST	1250-1	SCH												306	90
ST	1256-1	DPG	41	64											
ST	1257-1	DPG												181	69

			FOLIATION		LINEATION			FOLD AXIS		AXIAL SURFACE		ILA	VERG	JOINT	
QUAD	STATION	LITHOLOGY	STRIKE	DIP	TREND	PLUNGE	TYPE	TREND	PLUNGE	STRIKE	DIP			STRIKE	DIP
WV	5	MGW	138	41											
WV	7	MGW, AM	109	31											
WV	10	MGW	167	36											
WV	11	SCH	174	29											
WV	11	SCH												312	90
WV	13	MYL MGW	203	64											
WV	18	MIG MGW	86	48											
WV	19	MGW	99	31											
WV	25	MGW	109	31											
WV	26	GG												271	90
WV	29	SCH	231	36											
WV	29	SCH												171	84
WV	42	ISG	68	27											
WV	44	GG	241	61											
WV	45	GG	224	35											
WV	46	CALC-SI, SSCH	206	64											
WV	47	MIG SCH MGW						255	17			30	NE		
WV	47	MIG SCH MGW								284	21	30	NE		
WV	47	MIG SCH MGW						18	10			80	ENE		
WV	47	MIG SCH MGW								343	16	80	ENE		
WV	47	MIG SCH MGW						176	23			30	ENE		
WV	47	MIG SCH MGW								352	31	30	ENE		
WV	47	MIG SCH MGW						27	29			75	SE		
WV	47	MIG SCH MGW								19	51	75	SE		
WV	47	MIG SCH MGW						231	36			15	NW		
WV	47	MIG SCH MGW								229	53	15	NW		
WV	47	MIG SCH MGW						34	25			15	SE		
WV	47	MIG SCH MGW								211	66	15	SE		
WV	47	MIG SCH MGW						11	11				SSE		
WV	47	MIG SCH MGW								321	36		SSE		
WV	47	MIG SCH MGW						21	12			75	SE		
WV	47	MIG SCH MGW								194	73	75	SE		
WV	47	MIG SCH MGW						184	16			50	SSE		
WV	47	MIG SCH MGW								274	10	50	SSE		
WV	47	MIG SCH MGW						21	29			10	W		
WV	47	MIG SCH MGW								12	62	10	W		
WV	47	MIG SCH MGW						26	26			30	SE		
WV	47	MIG SCH MGW								25	69	30	SE		
WV	47	MIG SCH MGW						36	34			80	SE		
WV	47	MIG SCH MGW								257	46	80	SE		
WV	47	MIG SCH MGW						19	26			35	W		
WV	47	MIG SCH MGW								14	55	35	W		
WV	47	MIG SCH MGW						189	7			25	SW		
WV	47	MIG SCH MGW								195	33	25	SW		
WV	48	MIG SCH MGW						181	9			30	W		
WV	48	MIG SCH MGW								34	35	30	W		
WV	48	MIG SCH MGW						346	21			30	NW		
WV	48	MIG SCH MGW								189	49	30	NW		
WV	48	MIG SCH MGW						209	23			40	SE		
WV	48	MIG SCH MGW								203	79	40	SE		
WV	48	MIG SCH MGW						2	14			15	W		
WV	48	MIG SCH MGW								348	60	15	W		
WV	48	MIG SCH MGW						191	15			90	W		
WV	48	MIG SCH MGW								169	76	90	W		
WV	48	MIG SCH MGW						217	29			35	ESE		
WV	48	MIG SCH MGW								209	77	35	ESE		
WV	48	MIG SCH MGW						180	6			15	SE		
WV	48	MIG SCH MGW								338	26	15	SE		
WV	48	MIG SCH MGW						186	11			90	SE		

			FOLIATION		LINEATION			FOLD AXIS		AXIAL SURFACE		ILA	VERG	JOINT	
QUAD	STATION	LITHOLOGY	STRIKE	DIP	TREND	PLUNGE	TYPE	TREND	PLUNGE	STRIKE	DIP			STRIKE	DIP
WV	48	MIG SCH MGW								14	85	90	SE		
WV	48	MIG SCH MGW						197	8			110	ESE		
WV	48	MIG SCH MGW								271	9	110	ESE		
WV	48	MIG SCH MGW						163	13			35	SW		
WV	48	MIG SCH MGW								102	27	35	SW		
WV	48	MIG SCH MGW						231	16			95	SE		
WV	48	MIG SCH MGW								224	45	95	SE		
WV	48	MIG SCH MGW						34	37			30	W		
WV	48	MIG SCH MGW								220	64	30	W		
WV	48	MIG SCH MGW						206	13			40	NW		
WV	48	MIG SCH MGW								11	62	40	NW		
WV	48	MIG SCH MGW						156	13			10	W		
WV	48	MIG SCH MGW								181	64	10	W		
WV	48	MIG SCH MGW						339	15			20	SE		
WV	48	MIG SCH MGW								217	46	20	SE		
WV	50	MGW	68	52											
WV	51	MGW	67	59											
WV	53	MGW	39	59											
WV	54	MGW	216	29											
WV	55	MGW	27	73											
WV	56	MIG MGW	27	76											
WV	57	MIG MGW	34	61											
WV	59	SCH	36	67											
WV	61	SCH	21	48											
WV	64	QZ	34	44											
WV	65	MGW	24	56											
WV	66	MIG MGW	27	59											
WV	67	MIG MGW	31	60											
WV	68	MIG MGW	30	62											
WV	69	MIG MGW, AM	26	76											
WV	70	MIG MGW	27	70											
WV	71	MIG MGW	121	59											
WV	72	MIG MGW	34	44											
WV	73	MIG MGW	29	38											
WV	74	MIG MGW	37	49											
WV	75	QZ	39	63											
WV	75	QZ			209	31	STR								
WV	77	MGW	16	51											
WV	78	MGW	36	42											
WV	79	MGW	61	41											
WV	80	MGW	51	56											
WV	81	MGW	23	44											
WV	82	MGW	345	45											
WV	83	MGW	26	47											
WV	84	MGW	36	42											
WV	85	MGW	29	42											
WV	86	MGW	126	35											
WV	87	MGW	46	49											
WV	88	MGW	27	32											
WV	90	MGW, ISG	21	56											
WV	91	MGW, ISG	26	38											
WV	92	MIG MGW	136	43											
WV	93	MIG MGW	36	75											
WV	94	MIG MGW	43	66											
WV	95	MIG MGW	179	76											
WV	96	MIG MGW	226	71											
WV	97	MIG MGW	64	72											
WV	98	MIG MGW	44	61											
WV	99	MIG MGW	42	66											

			FOLIATION		LINEATION			FOLD AXIS		AXIAL SURFACE		ILA	VERG	JOINT	
QUAD	STATION	LITHOLOGY	STRIKE	DIP	TREND	PLUNGE	TYPE	TREND	PLUNGE	STRIKE	DIP			STRIKE	DIP
WV	100	MIG MGW	65	65											
WV	101	MIG MGW	64	56											
WV	102	MIG MGW	69	67											
WV	103	MIG MGW	129	38											
WV	104	MIG MGW	41	59											
WV	105	MIG MGW	44	70											
WV	106	MIG MGW	44	72											
WV	107	MIG MGW	46	57											
WV	108	MIG MGW	66	31											
WV	109	MIG MGW	36	62											
WV	110	MIG MGW	16	80											
WV	110	MIG MGW												284	69
WV	111	MIG MGW								91	26	50	NW		
WV	111	MIG MGW						165	34			50	NW		
WV	112	MIG MGW	46	41											
WV	112	MIG MGW	76	52											
WV	113	MIG MGW								84	29	35	NNW		
WV	113	MIG MGW						163	24			35	NNW		
WV	114	MGW	12	56											
WV	115	MGW								193	39	65	SE		
WV	115	MGW						309	24			65	SE		
WV	116	MIG MGW	339	61											
WV	117	MIG MGW	326	31											
WV	118	MIG MGW, RQ	331	61											
WV	119	MIG MGW	339	36											
WV	120	MIG MGW	302	42											
WV	121	MIG MGW	334	29											
WV	122	MGW	327	27											
WV	123	MGW	329	22											
WV	124	MGW	333	49											
WV	125	MGW	320	27											
WV	126	MGW	19	34											
WV	127	MGW	15	34											
WV	128	MGW	26	34											
WV	129	MGW	4	55											
WV	130	MGW	14	26											
WV	132	MGW	57	74											
WV	133	MIG MGW	17	34											
WV	134	MIG MGW	36	73											
WV	135	MGW	16	61											
WV	136	MIG MGW, AM								31	65				
WV	136	MIG MGW, AM						36	71						
WV	136	MIG MGW, AM						209	68						
WV	136	MIG MGW, AM	34	66											
WV	137	MGW	21	41											
WV	137	MGW												91	84
WV	138	MGW, AM	16	24											
WV	138	MGW, AM												98	83
WV	139	MGW, AM	21	74											
WV	140	MGW	36	67											
WV	141	MGW	29	76											
WV	142	MGW	42	66											
WV	143	MGW	25	80											
WV	144	MGW	25	74											
WV	145	MGW	32	71											
WV	146	MGW	51	82											
WV	147	MIG MGW	126	47											
WV	148	MGW	34	76											
WV	149	MIG MGW	36	76											

			FOLIATION		LINEATION			FOLD AXIS		AXIAL SURFACE		ILA	VERG	JOINT	
QUAD	STATION	LITHOLOGY	STRIKE	DIP	TREND	PLUNGE	TYPE	TREND	PLUNGE	STRIKE	DIP			STRIKE	DIP
WV	150	MIG MGW	39	77											
WV	151	MIG MGW	46	71											
WV	152	MIG MGW								41	86	90	NW		
WV	152	MIG MGW						222	6			90	NW		
WV	153	MIG MGW								37	79	60	NW		
WV	153	MIG MGW						35	27			60	NW		
WV	154	MIG MGW	41	75											
WV	155	MGW	41	59											
WV	156	MGW	41	66											
WV	157	MIG MGW	35	72											
WV	158	MGW	44	66											
WV	159	MGW	46	44											
WV	160	MGW	40	64											
WV	161	MIG MGW	44	68											
WV	162	MIG MGW	49	52											
WV	163	MIG MGW	64	47											
WV	164	MIG MGW	331	76											
WV	165	MGW								330	82	20	W		
WV	165	MGW						326	71			20	W		
WV	165	MGW	326	86											
WV	166	GG	344	45											
WV	167	GG	354	71											
WV	168	GG								300	38	10	NE		
WV	168	GG						346	5			10	NE		
WV	168	GG	346	50											
WV	169	MGW, AM	193	71											
WV	170	MIG MGW, AM	27	64											
WV	171	MIG MGW, AM	9	82											
WV	172	MIG MGW	46	80											
WV	177	MIG MGW	198	66											
WV	179	MIG MGW, AM	46	81											
WV	180	MIG MGW, AM	6	69											
WV	181	MGW	193	59											
WV	182	MGW	324	36											
WV	183	MGW	288	34											
WV	184	MGW	28	55											
WV	185	MGW	44	63											
WV	187	MGW	346	57											
WV	188	MGW	334	50											
WV	189	MGW	322	41											
WV	190	MGW	346	46											
WV	191	MIG MGW	14	33											
WV	192	MIG MGW	4	56											
WV	193	MIG MGW	41	14											
WV	194	MGW	11	40											
WV	195	MIG MGW	19	44											
WV	196	MGW, GG	309	79											
WV	197	MGW	335	46											
WV	198	MGW	308	39											
WV	199	MGW	213	19											
WV	200	MGW	107	56											
WV	201	MIG MGW	335	49											
WV	202	MIG MGW	344	26											
WV	202	MIG MGW												113	90
WV	203	MIG MGW	319	61											
WV	204	MIG MGW	352	41											
WV	205	MIG MGW	335	42											
WV	206	MIG MGW	22	33											
WV	207	MIG MGW	11	51											

			FOLIATION		LINEATION			FOLD AXIS		AXIAL SURFACE		ILA	VERG	JOINT	
QUAD	STATION	LITHOLOGY	STRIKE	DIP	TREND	PLUNGE	TYPE	TREND	PLUNGE	STRIKE	DIP			STRIKE	DIP
WV	208	MIG MGW	9	42											
WV	209	MIG MGW	3	41											
WV	210	MIG MGW	14	49											
WV	211	MIG MGW	332	36											
WV	212	GG	348	61											
WV	212	GG	127	56											
WV	213	GG	17	54											
WV	214	MGW	336	32											
WV	215	MIG MGW	216	22											
WV	216	MIG MGW	316	24											
WV	216	MIG MGW			39	24	BN								
WV	217	MGW	96	41											
WV	217	MGW												192	90
WV	217	MGW			154	28	STR								
WV	218	MIG MGW	356	28											
WV	222	MIG MGW	116	53											
WV	223	MIG MGW	279	17											
WV	227	MGW	69	41											
WV	228	MGW	109	31											
WV	229	MGW	85	33											
WV	230	MGW	29	81											
WV	230	MGW			162	32	STR								
WV	232	MGW	31	76											
WV	233	MGW	34	77											
WV	234	MGW	44	59											
WV	235	MGW	46	69											
WV	236	MGW	9	74											
WV	237	MGW	59	41											
WV	238	MGW	83	63											
WV	239	MGW	26	66											
WV	240	MGW	51	42											
WV	241	MGW	16	29											
WV	242	MGW	354	65											
WV	243	MGW	6	66											
WV	244	MGW	8	52											
WV	245	MGW	12	29											
WV	245	MGW												69	84
WV	245	MGW			160	9	STR								
WV	246	MGW	8	64											
WV	247	MGW	4	49											
WV	248	MGW	24	41											
WV	249	MGW	34	45											
WV	250	MGW	7	57											
WV	251	MGW	41	37											
WV	252	MGW	11	54											
WV	253	MGW	7	48											
WV	254	MGW	143	26											
WV	254	MGW			162	11	STR								
WV	256	CALC-SI	246	79											
WV	256	CALC-SI												4	90
WV	257	MGW	17	46											
WV	258	MGW	26	46											
WV	259	MGW	2	54											
WV	260	MIG MGW	24	33											
WV	261	MIG MGW	71	56											
WV	262	MIG MGW	71	37											
WV	263	MIG MGW	359	48											
WV	263	MIG MGW												56	90
WV	264	MIG MGW								174	44	150	E		

			FOLIATION		LINEATION			FOLD AXIS		AXIAL SURFACE		ILA	VERG	JOINT	
QUAD	STATION	LITHOLOGY	STRIKE	DIP	TREND	PLUNGE	TYPE	TREND	PLUNGE	STRIKE	DIP			STRIKE	DIP
WV	264	MIG MGW						171	6			150	E		
WV	265	MIG MGW	326	41											
WV	266	MIG MGW	11	68											
WV	266	MIG MGW			349	17	STR								
WV	267	MGW	56	49											
WV	268	MIG MGW	21	50											
WV	269	MIG MGW	37	64											
WV	271	MGW	37	40											
WV	272	MGW	26	41											
WV	273	MIG MGW	326	27											
WV	274	MGW, AM	141	41											
WV	275	MGW, AM	226	51											
WV	276	MGW, AM	206	61											
WV	277	MGW, AM	191	59											
WV	278	MGW, AM	184	64											
WV	279	MGW, AM	346	81											
WV	280	MGW, AM	34	79											
WV	281	MGW, AM	21	74											
WV	282	MIG MGW	41	50											
WV	283	MGW	229	59											
WV	283	MGW												39	80
WV	283	MGW			212	41	STR								
WV	285	MGW	49	61											
WV	286	MGW	54	56											
WV	287	MGW	54	64											
WV	288	MGW	31	55											
WV	289	MGW	41	74											
WV	293	MGW	28	72											
WV	293	MGW			204	26	STR								
WV	295	MGW	204	57											
WV	296	MGW, PEG	36	80											
WV	297	MGW	204	59											
WV	298	MGW, AM, PEG	191	47											
WV	298	MGW, AM, PEG			354	14	STR								
WV	299	MGW	194	65											
WV	301	GG	239	74											
WV	302	GG, PEG	36	44											
WV	303	GG, ISG								106	71	45	S		
WV	303	GG, ISG						277	40			45	S		
WV	303	GG, ISG	79	64											
WV	304	GG, ISG	217	74											
WV	305	GG, ISG, PEG	214	56											
WV	306	GG, ISG, PEG	226	64											
WV	307	GG	234	68											
WV	308	GG, PEG	221	66											
WV	309	GG	228	65											
WV	310	GG	206	79											
WV	311	GG	209	60											
WV	312	GG	216	73											
WV	313	GG, ISG	34	79											
WV	315	AM	226	77											
WV	316	MGW	191	76											
WV	317	GG, AM	37	74											
WV	318	GG, AM	47	86											
WV	319	GG	243	69											
WV	320	MGW	51	49											
WV	321	MGW	31	76											
WV	322	MGW	29	65											
WV	323	MGW, AM, ISG	26	67											

			FOLIATION		LINEATION			FOLD AXIS		AXIAL SURFACE		ILA	VERG	JOINT	
QUAD	STATION	LITHOLOGY	STRIKE	DIP	TREND	PLUNGE	TYPE	TREND	PLUNGE	STRIKE	DIP			STRIKE	DIP
WV	324	MGW, PEG	69	77											
WV	325	MGW	56	74											
WV	326	MIG MGW, AM	206	69											
WV	327	MGW	41	72											
WV	329	MIG MGW	56	39											
WV	330	MGW	31	66											
WV	333	SCH MGW	306	34											
WV	334	SCH MGW	16	21											
WV	335	SCH MGW	9	16											
WV	336	SCH MGW	26	37											
WV	337	SCH MGW	31	36											
WV	338	SCH MGW	21	24											
WV	339	MGW	234	29											
WV	340	SCH MGW	9	16											
WV	341	SCH MGW	89	16											
WV	342	SCH MGW	358	29											
WV	342	SCH MGW	106	26											
WV	343	SCH MGW	339	21											
WV	344	MGW	309	56											
WV	345	MGW	33	44											
WV	346	MIG MGW								208	74	20	SE		
WV	346	MIG MGW						201	24			20	SE		
WV	346	MIG MGW	34	36											
WV	347	MGW	129	49											
WV	348	MIG MGW	41	46											
WV	349	MIG MGW	39	64											
WV	350	MIG MGW	31	44											
WV	351	MIG MGW	45	67											
WV	352	MIG MGW	56	41											
WV	353	MIG MGW	48	61											
WV	354	MIG MGW	51	44											
WV	355	GG	54	37											
WV	356	MGW	81	39											
WV	357	SCH MGW	109	39											
WV	358	GG	21	29											
WV	359	GG	337	21											
WV	360	GG	345	57											
WV	361	MIG MGW	176	68											
WV	362	AG	26	51											
WV	362	AG			2	19	STR								
WV	363	AG	21	66											
WV	364	AG	26	33											
WV	366	MIG MGW, SCH	201	43											
WV	367	MIG MGW	198	76											
WV	368	MIG MGW	41	60											
WV	369	MGW	164	61											
WV	370	MGW	164	41											
WV	371	MGW	183	64											
WV	372	ISG	196	60											
WV	373	SCH MGW	189	50											
WV	374	SCH MGW	191	72											
WV	375	ISG	189	54											
WV	376	MGW	205	81											
WV	377	MGW	44	60											
WV	378	GG	194	57											
WV	379	SCH MGW, AM	353	79											
WV	380	SCH MGW, AM	186	81											
WV	381	SCH MGW, AM	191	60											
WV	382	MIG MGW, AM	219	61											

			FOLIATION		LINEATION			FOLD AXIS		AXIAL SURFACE		ILA	VERG	JOINT	
QUAD	STATION	LITHOLOGY	STRIKE	DIP	TREND	PLUNGE	TYPE	TREND	PLUNGE	STRIKE	DIP			STRIKE	DIP
WV	384	MGW	209	63											
WV	385	SCH MGW, AM	32	74											
WV	386	MIG SCH MGW, AM	358	81											
WV	387	MIG SCH MGW, AM	196	85											
WV	388	MGW, AM	13	84											
WV	389	SCH MGW, AM								204	74	10	ESE		
WV	389	SCH MGW, AM						29	14			10	ESE		
WV	389	SCH MGW, AM	202	74											
WV	390	MIG SCH MGW, AM	198	76											
WV	391	SSCH, AM	353	79											
WV	391	SSCH, AM	177	77											
WV	392	MIG SCH MGW, AM	119	61											
WV	393	MIG SCH MGW, AM	197	72											
WV	394	MIG SCH MGW, AM	125	44											
WV	395	MIG SCH MGW, AM	200	67											
WV	396	MIG SCH MGW, AM	184	48											
WV	397	MGW, AM	191	33											
WV	398	MIG SCH MGW, AM	106	66											
WV	399	MGW	194	47											
WV	400	SSCH	56	58											
WV	401	SCH MGW	86	65											
WV	402	SCH MGW	252	73											
WV	403	SCH MGW, AM	101	44											
WV	404	SCH MGW, GD	155	45											
WV	405	SCH MGW, GD	6	39											
WV	406	SCH MGW	44	36											
WV	407	MGW, GD, AM	136	37											
WV	408	MGW	53	54											
WV	409	MIG MGW	25	50											
WV	410	SSCH	51	54											
WV	411	MGW	24	90											
WV	412	SCH MGW	32	56											
WV	413	MGW	197	55											
WV	414	SCH MGW	216	72											
WV	415	MIG MGW	221	77											
WV	416	SCH MGW	210	82											
WV	417	SCH MGW, AM	92	38											
WV	419	AM	26	73											
WV	421	MGW	85	60											
WV	422	GG	61	42											
WV	423	GG	194	41											
WV	424	GG			211	18	STR								
WV	425	GG	224	34											
WV	426	GG	224	55											
WV	427	GG	55	59											
WV	428	GG						102	49						
WV	429	GG								88	73	70	WSW		
WV	430	GG	60	63								70	WSW		
WV	431	GG	41	54											
WV	432	GG	66	69											
WV	433	GG	234	42											
WV	435	GG	39	74											
WV	436	GG	215	56											
WV	438	MGW	162	53											
WV	439	MGW	183	77											
WV	440	GG	312	37											
WV	441	MGW	298	19											
WV	446	SCH MGW	16	69											
WV	447	GG	182	45											

			FOLIATION		LINEATION			FOLD AXIS		AXIAL SURFACE		ILA	VERG	JOINT	
QUAD	STATION	LITHOLOGY	STRIKE	DIP	TREND	PLUNGE	TYPE	TREND	PLUNGE	STRIKE	DIP			STRIKE	DIP
WV	451	MGW	351	55											
WV	451	MGW			148	4	STR								
WV	452	GG	44	60											
WV	453	SCH MGW	21	31											
WV	454	GG	21	46											
WV	455	MGW	191	41											
WV	456	MGW	164	43											
WV	457	SSCH						218	19						
WV	457	SSCH	183	34											
WV	457	SSCH												291	66
WV	458	SSCH	222	67											
WV	458	SSCH												314	80
WV	459	GG	141	24											
WV	460	SSCH, GG, AM	178	69											
WV	461	SCH MGW	56	43											
WV	462	GG	31	71											
WV	463	GG	222	70											
WV	464	GG	200	57											
WV	465	GG	52	58											
WV	466	GG	44	57											
WV	467	GG	42	64											
WV	468	SCH MGW	29	69											
WV	469	SCH MGW	47	66											
WV	470	GG	51	63											
WV	471	GG	39	51											
WV	472	SCH MGW	54	69											
WV	473	GG	27	55											
WV	474	GG	211	37											
WV	475	GG	216	74											
WV	476	GG								103	81	ISO			
WV	476	GG						127	66			ISO			
WV	476	GG	198	54											
WV	478	GG	228	76											
WV	479	GG	213	52											
WV	480	GG	209	73											
WV	481	GG	183	77											
WV	482	SCH MGW	42	76											
WV	483	GG	209	78											
WV	484	MGW	36	86											
WV	485	MGW, AM								234	75	70	SE		
WV	485	MGW, AM						231	67			70	SE		
WV	486	SCH MGW	39	74											
WV	487	MGW	126	53											
WV	488	GG	34	76											

Appendix II

SHRIMP U-Th-Pb data from analysis of igneous and metasedimentary rocks from the Inner Piedmont and Carolina superterrane

sample	measured ²⁰⁴ Pb/ ²⁰⁶ Pb	measured ²⁰⁷ Pb/ ²⁰⁶ Pb	% com ²⁰⁶ Pb	U (ppm)	Th (ppm)	Th/U	Age in Ma				% disc	²⁰⁷ Pb/ ²³⁵ U	% err	²⁰⁶ Pb/ ²³⁸ U	% err	err correl
							²⁰⁶ Pb/ ²³⁸ U	err	²⁰⁷ Pb/ ²⁰⁶ Pb	err						
<i>Snapping Shoals augen gneiss</i>																
W166-1	-0.000008	0.0756	0.06	308.52	128.80	0.43	1069.2	17.6	1086.7	14.9	2	1.88	1.9	0.1805	1.7	0.917
W166-2	0.000047	0.0782	0.55	92.96	46.06	0.51	1029.5	11.4	1133.7	27.5	10	1.86	1.8	0.1740	1.1	0.638
W166-3	-0.000012	0.0758	0.48	188.29	60.57	0.33	977.5	9.2	1092.4	19.8	11	1.72	1.4	0.1646	1.0	0.701
W166-3.2	0.000000	0.0751	-0.15	253.38	85.88	0.35	1104.3	41.4	1071.0	97.4	-3	1.93	6.2	0.1866	3.9	0.623
W166-4	0.000020	0.0720	-0.41	108.51	57.20	0.54	1080.8	26.2	978.2	135.6	-11	1.80	7.1	0.1817	2.5	0.346
W166-4.2	0.000007	0.0739	0.43	322.68	143.97	0.46	936.7	19.4	1034.4	34.1	10	1.60	2.7	0.1570	2.1	0.786
W166-6	0.000045	0.0754	0.62	131.95	62.80	0.49	934.3	9.4	1061.1	22.3	12	1.62	1.5	0.1568	1.0	0.685
W166-6.2	-0.000008	0.0748	0.40	275.01	110.37	0.41	970.1	21.0	1066.5	32.0	9	1.69	2.7	0.1631	2.2	0.815
W166-7	0.000000	0.0745	0.26	339.64	77.03	0.23	996.3	24.0	1055.1	38.8	6	1.72	3.2	0.1676	2.5	0.791
W166-8	0.000000	0.0745	-0.16	82.38	48.10	0.60	1088.6	11.8	1053.4	25.9	-3	1.89	1.7	0.1837	1.1	0.657
W166-9	-0.000022	0.0749	-0.20	175.04	117.79	0.70	1110.2	18.0	1074.6	28.6	-3	1.95	2.2	0.1876	1.7	0.762
W166-10	0.000000	0.0721	0.34	251.77	86.42	0.35	906.0	16.2	988.7	15.9	9	1.51	2.0	0.1514	1.9	0.922
W166-11	0.000037	0.0718	0.58	327.51	72.21	0.23	838.4	7.4	965.5	15.9	14	1.37	1.2	0.1396	0.9	0.761
W166-11.2R	0.000153	0.0739	0.28	339.14	142.72	0.43	972.7	29.3	976.9	73.2	0	1.61	4.8	0.1629	3.1	0.654
W166-12	0.000019	0.0757	0.41	430.50	144.92	0.35	992.6	24.3	1078.0	26.9	8	1.74	2.9	0.1671	2.5	0.884
W166-13.2	0.000010	0.0722	0.20	471.16	127.31	0.28	943.8	26.1	988.1	39.8	5	1.57	3.5	0.1580	2.9	0.825
W166-13R	0.000026	0.0723	0.00	321.62	129.50	0.42	995.0	26.4	983.6	70.3	-1	1.65	4.4	0.1668	2.7	0.621
W166-14	0.000027	0.0708	0.04	409.24	219.52	0.55	941.5	32.8	939.4	45.4	0	1.53	4.2	0.1572	3.6	0.852
<i>Lithonia granitoid gneiss</i>																
AM2-1	0.001661	0.0781	2.78	114.72	50.69	0.46	435.4	20.1	362.5	235.6	-21	0.52	11.5	0.0697	4.8	0.415
AM2-2	0.000260	0.0561	0.09	124.74	113.77	0.94	425.9	6.9	297.0	116.5	-44	0.49	5.4	0.0680	1.7	0.310
AM2-3	0.000091	0.0550	-0.04	301.86	165.86	0.57	424.8	8.9	355.3	42.4	-20	0.50	2.9	0.0680	2.1	0.752
AM2-4	-0.000061	0.0568	0.14	135.39	85.76	0.65	436.6	6.5	515.8	58.6	16	0.56	3.1	0.0703	1.5	0.494
AM2-5	0.000174	0.0563	0.08	80.05	81.84	1.06	437.8	7.0	361.7	98.3	-21	0.52	4.7	0.0701	1.6	0.350
AM2-6	—	0.0547	-0.14	79.80	73.68	0.95	445.7	9.8	398.3	64.6	-12	0.54	3.7	0.0715	2.2	0.614
AM2-7	0.000100	0.0589	0.39	286.94	347.12	1.25	440.1	7.9	507.7	42.0	14	0.56	2.6	0.0708	1.8	0.691
AM2-8	0.000078	0.0578	0.28	92.57	86.78	0.97	435.6	6.8	479.4	72.1	9	0.55	3.6	0.0700	1.6	0.435
AM2-9	0.000189	0.0564	0.43	420.18	37.43	0.09	326.2	4.5	354.4	61.0	8	0.38	3.0	0.0519	1.4	0.465
AM2-9.2R	0.006110	0.1403	11.04	1504.38	112.42	0.08	275.0	3.6	220.8	152.9	-25	0.30	6.8	0.0435	1.4	0.205

sample	measured ²⁰⁴ Pb/ ²⁰⁶ Pb	measured ²⁰⁷ Pb/ ²⁰⁶ Pb	% com ²⁰⁶ Pb	U (ppm)	Th (ppm)	Th/U	Age in Ma					% disc	²⁰⁷ Pb/ ²³⁵ U	% err	²⁰⁶ Pb/ ²³⁸ U	% err	err correl
							²⁰⁶ Pb/ ²³⁸ U	err	²⁰⁷ Pb/ ²⁰⁶ Pb	err							
<i>Lithonia granitoid gneiss</i>																	
AM2-10	-0.000072	0.0537	-0.29	104.01	72.86	0.72	451.4	11.0	399.0	70.0	-13	0.55	4.0	0.0724	2.5	0.623	
AM2-11	—	0.0790	0.79	25.35	6.77	0.28	995.2	20.7	1170.4	54.2	15	1.83	3.5	0.1683	2.1	0.615	
AM2-11.2R	0.000095	0.0573	0.31	2291.88	531.61	0.24	404.0	5.2	449.6	15.1	10	0.50	1.5	0.0648	1.3	0.889	
AM2-12	—	0.0568	0.09	121.98	176.31	1.49	451.5	12.5	481.7	48.5	6	0.57	3.6	0.0726	2.8	0.790	
AM2-13	0.000044	0.0563	0.04	162.78	75.87	0.48	450.2	6.5	437.0	50.0	-3	0.55	2.7	0.0723	1.5	0.547	
AM2-14	0.000448	0.0560	0.09	62.67	36.62	0.60	420.7	10.9	164.3	176.7	-159	0.46	8.0	0.0669	2.7	0.331	
AM2-14.2R	0.000134	0.0545	0.14	1392.47	97.38	0.07	344.0	4.5	306.3	27.6	-13	0.40	1.8	0.0548	1.3	0.740	
AM2-15	0.000031	0.0558	-0.01	225.55	120.75	0.55	447.1	7.4	426.4	40.3	-5	0.55	2.5	0.0718	1.7	0.685	
J827-1	0.000189	0.0577	0.21	202.46	102.94	0.53	449.5	6.7	407.2	91.1	-11	0.55	4.3	0.0721	1.5	0.346	
J827-2	—	0.0554	-0.08	236.29	275.15	1.20	452.9	5.6	428.5	32.7	-6	0.56	1.9	0.0727	1.3	0.650	
J827-2.2R	0.000054	0.0542	-0.18	289.41	114.41	0.41	434.9	3.4	343.5	42.0	-27	0.51	2.0	0.0696	0.8	0.394	
J827-3	0.000029	0.0562	0.08	264.77	145.88	0.57	431.6	8.2	441.9	38.8	2	0.53	2.6	0.0693	1.9	0.745	
J827-3.2R	0.000562	0.0613	1.28	2694.57	1087.81	0.42	242.3	1.3	331.4	40.4	27	0.28	1.9	0.0384	0.6	0.296	
J827-4	0.000015	0.0563	0.09	398.48	355.12	0.92	435.4	3.1	456.3	27.8	5	0.54	1.4	0.0699	0.7	0.499	
J827-5	0.000190	0.0556	-0.05	117.17	107.95	0.95	451.3	4.2	319.9	88.1	-42	0.53	4.0	0.0722	1.0	0.240	
J827-6	-0.000006	0.0800	0.28	448.76	9.08	0.02	1135.5	18.0	1197.6	12.2	5	2.13	1.8	0.1932	1.6	0.936	
J827-6.2R	0.000099	0.0537	0.04	1256.45	11.18	0.01	340.8	2.9	293.7	26.9	-16	0.39	1.5	0.0542	0.9	0.596	
J827-7	—	0.0552	0.02	95.03	54.07	0.59	414.6	6.7	420.7	56.7	1	0.51	3.0	0.0664	1.6	0.543	
J827-8	—	0.0579	0.26	108.83	57.17	0.54	441.7	4.8	525.0	50.0	16	0.57	2.5	0.0711	1.1	0.432	
J827-9	-0.000112	0.0581	0.31	131.94	59.42	0.47	437.0	3.9	593.5	60.7	27	0.58	2.9	0.0705	0.9	0.307	
J827-10	—	0.0582	0.26	121.36	91.76	0.78	454.1	4.3	536.4	51.5	16	0.59	2.5	0.0732	0.9	0.374	
J827-11	0.000051	0.0560	0.00	175.87	111.27	0.65	451.2	11.5	422.4	55.5	-7	0.55	3.6	0.0724	2.6	0.723	
J827-12	-0.000344	0.0554	-0.08	42.88	34.12	0.82	454.6	6.4	617.2	145.9	27	0.61	6.9	0.0735	1.5	0.215	
J827-13	0.000151	0.0547	-0.15	155.40	92.03	0.61	449.1	4.3	305.9	74.2	-48	0.52	3.4	0.0719	1.0	0.289	
J827-14	0.000096	0.0539	-0.27	85.63	61.41	0.74	452.2	4.9	304.9	90.7	-49	0.52	4.1	0.0724	1.1	0.265	
J827-15	0.000090	0.0555	-0.10	78.994	116.073	1.52	463.9	5.0	377.2	84.2	-23	0.56	3.9	0.0744	1.1	0.283	

sample	measured ²⁰⁴ Pb/ ²⁰⁶ Pb	measured ²⁰⁷ Pb/ ²⁰⁶ Pb	% com ²⁰⁶ Pb	U (ppm)	Th (ppm)	Th/U	Age in Ma				²⁰⁷ Pb/ ²³⁵ U	% err	²⁰⁶ Pb/ ²³⁸ U	% err	err correl	
							²⁰⁶ Pb/ ²³⁸ U	err	²⁰⁷ Pb/ ²⁰⁶ Pb	err						
High Falls granite																
HHF-1	0.000609	0.0885	3.32	424.073	41.0861	0.10	647.4	23.7	1192.3	146.9	47	1.19	8.3	0.1081	3.7	0.446
HHF-2	-0.000074	0.0550	0.05	420.939	137.049	0.34	391.4	4.7	453.1	40.2	14	0.48	2.2	0.0627	1.2	0.557
HHF-3	—	0.0551	0.02	584.254	110.071	0.19	407.4	5.8	413.4	27.3	1	0.50	1.9	0.0652	1.4	0.763
HHF-4	0.000022	0.0540	-0.11	916.635	183.708	0.21	407.0	6.1	356.1	26.6	-15	0.48	1.9	0.0651	1.5	0.793
HHF-5	0.000110	0.0563	0.21	482.178	115.614	0.25	395.6	4.6	398.4	42.9	1	0.48	2.2	0.0633	1.2	0.524
HHF-6	0.000014	0.0555	0.06	1336.23	459.854	0.36	410.0	6.1	421.9	18.4	3	0.50	1.7	0.0657	1.5	0.879
HHF-7	0.011435	0.2236	20.91	1106.21	203.778	0.19	397.5	22.2	491.0	1702.0	19	0.50	77.4	0.0638	6.3	0.081
HHF-8	-0.000017	0.0534	-0.20	666.517	72.5415	0.11	414.4	4.7	357.0	30.0	-16	0.49	1.8	0.0663	1.2	0.660
HHF-9	0.000028	0.0553	0.06	839.595	219.658	0.27	403.4	5.1	405.3	27.3	0	0.49	1.8	0.0646	1.3	0.723
HHF-10	0.000028	0.0544	-0.07	731.137	25.1161	0.04	411.8	8.0	370.3	27.5	-11	0.49	2.3	0.0659	2.0	0.852
HHF-11	—	0.0558	0.16	520.32	146.52	0.29	390.7	4.5	442.5	28.6	12	0.48	1.7	0.0626	1.2	0.673
HHF-12	0.000058	0.0558	0.06	735.007	208.185	0.29	426.7	7.4	411.1	30.9	-4	0.52	2.2	0.0684	1.8	0.786
HHF-13	0.001649	0.0790	3.15	387.263	71.8039	0.19	355.3	5.6	407.5	176.8	13	0.43	8.1	0.0567	1.6	0.203
HHF-14	-0.000012	0.0543	-0.06	954.065	137.621	0.15	403.2	7.2	390.4	23.5	-3	0.48	2.1	0.0645	1.8	0.866
HHF-15	0.000171	0.0542	-0.09	254.18	70.934	0.29	410.5	5.1	272.2	72.5	-52	0.47	3.4	0.0655	1.3	0.372
HFSP-1	-0.000020	0.0536	-0.13	507.955	114.103	0.23	398.7	9.7	367.0	35.8	-9	0.47	2.9	0.0637	2.5	0.842
HFSP-2.1	0.000091	0.0735	0.29	44.1573	15.5092	0.36	957.7	42.4	990.6	67.2	3	1.60	5.6	0.1604	4.6	0.811
HFSP-2.2R	0.000264	0.0591	0.53	1393.66	26.0718	0.02	402.4	10.8	421.0	35.9	5	0.49	3.2	0.0644	2.7	0.861
HFSP-3	0.000065	0.0549	0.04	336.647	102.194	0.31	394.6	9.7	370.2	50.8	-7	0.47	3.4	0.0631	2.5	0.744
HFSP-4	0.000102	0.0557	0.17	723.66	241.744	0.35	382.3	10.1	377.6	37.3	-1	0.46	3.2	0.0611	2.7	0.851
HFSP-5	-0.000042	0.0619	0.67	454.341	88.7208	0.20	469.9	6.0	691.7	33.2	33	0.66	2.0	0.0762	1.3	0.642
HFSP-6.1	0.000020	0.0806	-0.25	154.801	54.5112	0.36	1261.4	36.0	1202.7	28.4	-5	2.39	3.3	0.2155	3.0	0.899
HFSP-6.2R	—	0.0552	0.13	250.11	29.5741	0.12	378.0	11.3	421.2	46.4	10	0.46	3.7	0.0605	3.0	0.826
HFSP-7.1	—	0.0551	0.02	201.782	28.2372	0.14	407.6	12.6	415.7	51.8	2	0.50	3.9	0.0653	3.1	0.805
HFSP-7.2R	0.000005	0.0550	0.01	1834.91	115.295	0.06	406.9	9.1	407.7	16.9	0	0.49	2.4	0.0652	2.3	0.950
HFSP-8	—	0.0793	0.25	191.084	45.1382	0.24	1126.0	84.6	1179.1	138.7	5	2.09	10.5	0.1913	7.8	0.742
HFSP-9	-0.000035	0.0556	0.09	529.088	209.927	0.41	406.4	10.0	455.4	33.0	11	0.50	2.9	0.0652	2.5	0.860
HFSP-10.1	0.000093	0.0769	0.97	165.243	41.9984	0.26	891.2	30.8	1082.4	91.0	18	1.56	5.8	0.1495	3.6	0.617
HFSP-10.2R	0.000021	0.0542	-0.08	952.171	10.3594	0.01	405.3	6.7	366.4	25.8	-11	0.48	2.0	0.0648	1.7	0.827
HFSP-11	-0.000047	0.0557	0.14	422.228	128.548	0.31	391.1	9.7	465.0	40.0	16	0.49	3.1	0.0627	2.5	0.812

sample	measured ²⁰⁴ Pb/ ²⁰⁶ Pb	measured ²⁰⁷ Pb/ ²⁰⁶ Pb	% com ²⁰⁶ Pb	U (ppm)	Th (ppm)	Th/U	Age in Ma				% disc	²⁰⁷ Pb/ ²³⁵ U	% err	²⁰⁶ Pb/ ²³⁸ U	% err	err correl
							²⁰⁶ Pb/ ²³⁸ U	err	²⁰⁷ Pb/ ²⁰⁶ Pb	err						
High Falls granite																
HFSP-12	0.000028	0.0562	0.20	772.032	312.091	0.42	395.0	6.5	442.9	31.0	11	0.49	2.2	0.0633	1.7	0.766
HFSP-13	0.000060	0.0541	-0.09	305.638	135.24	0.46	405.6	13.3	337.3	49.8	-21	0.48	4.0	0.0648	3.3	0.835
HFSP-14	0.000108	0.0572	0.28	184.713	48.9246	0.27	409.0	10.5	436.5	70.8	6	0.50	4.1	0.0656	2.6	0.636
HFSP-15.1	0.000479	0.0640	1.18	632.75	544.133	0.89	388.7	12.6	491.0	83.9	21	0.49	5.0	0.0624	3.3	0.656
HFSP-15.2R	—	0.0555	0.07	2415.42	153.245	0.07	406.9	11.5	431.1	13.9	6	0.50	2.9	0.0652	2.9	0.977
S123-1	-0.000012	0.0559	0.18	711.326	48.1307	0.07	388.8	5.7	453.8	23.4	15	0.48	1.8	0.0623	1.5	0.815
S123-2	0.000020	0.0542	-0.08	621.821	106.663	0.18	407.4	4.6	366.9	22.9	-11	0.48	1.5	0.0652	1.1	0.748
S123-20	0.000401	0.0589	0.67	290.077	143.045	0.51	349.2	7.0	328.1	84.2	-7	0.41	4.2	0.0556	2.0	0.481
S123-3	0.000691	0.0662	1.53	319.782	147.972	0.48	362.2	10.9	454.6	96.8	21	0.45	5.3	0.0580	3.1	0.574
S123-5	0.000013	0.0558	0.19	558.606	345.619	0.64	380.6	6.1	437.1	40.3	13	0.47	2.4	0.0609	1.6	0.671
S123-6	0.000013	0.0617	0.07	449.156	251.805	0.58	641.5	13.4	655.0	22.5	2	0.89	2.4	0.1047	2.1	0.898
S123-6.2R	0.000024	0.0552	0.09	4302.89	63.6793	0.02	389.2	6.1	404.7	11.7	4	0.47	1.7	0.0623	1.6	0.950
S123-7	0.000066	0.0544	0.04	346.074	126.69	0.38	374.1	4.4	348.0	49.1	-8	0.44	2.5	0.0597	1.2	0.486
S123-8	0.000193	0.0534	-0.11	292.116	86.7877	0.31	384.0	9.4	221.7	73.6	-75	0.43	4.0	0.0611	2.5	0.617
S123-9	0.000161	0.0566	0.27	416.42	173.526	0.43	387.7	4.6	381.7	53.2	-2	0.46	2.7	0.0620	1.2	0.452
S123-10	0.000169	0.0573	0.36	808.027	472.151	0.60	386.6	4.9	405.0	54.9	5	0.47	2.8	0.0618	1.3	0.466
S123-11.2	0.001877	0.0749	2.58	790.025	506.288	0.66	373.4	7.0	59.4	146.6	-539	0.38	6.4	0.0591	1.9	0.297
S123-11R	—	0.0546	0.00	2570.58	24.173	0.01	393.9	5.7	394.6	12.3	0	0.47	1.6	0.0630	1.5	0.936
S123-12.2	0.000375	0.0603	0.74	323.119	186.537	0.60	385.5	4.6	405.4	77.7	5	0.47	3.7	0.0617	1.2	0.330
S123-12R	-0.000006	0.0554	0.15	1509.58	117.958	0.08	378.4	4.2	431.5	16.2	13	0.46	1.3	0.0606	1.1	0.838
S123-13	0.001172	0.0732	2.46	606.414	121.012	0.21	344.8	4.2	456.1	231.7	25	0.43	10.5	0.0551	1.3	0.123
S123-13.2R	0.000006	0.0540	-0.04	1627.51	107.9	0.07	381.6	4.2	365.1	17.0	-5	0.45	1.4	0.0609	1.1	0.829
S123-14	0.000066	0.0538	-0.05	422.091	156.793	0.38	379.8	6.7	322.5	40.2	-18	0.44	2.5	0.0606	1.8	0.711
S123-15	0.003789	0.1158	7.69	538.174	275.991	0.53	364.4	9.1	635.5	184.7	43	0.49	9.0	0.0587	2.6	0.287
S123-15.2R	0.000012	0.0544	0.03	1503.43	105.914	0.07	376.5	4.6	377.7	17.4	0	0.45	1.5	0.0601	1.3	0.850
S123-16	0.000242	0.0578	0.52	1049.36	455.51	0.45	356.2	5.0	382.2	38.1	7	0.43	2.2	0.0569	1.4	0.643
S123-17	0.000160	0.0574	0.44	335.72	134.701	0.41	364.3	4.8	413.2	56.9	12	0.44	2.9	0.0582	1.4	0.470
S123-18	—	0.0545	0.03	649.173	199.693	0.32	378.7	6.8	389.4	26.4	3	0.45	2.2	0.0605	1.8	0.839
S123-19	0.001762	0.0789	3.27	2605.16	274.331	0.11	314.0	9.3	334.0	151.9	6	0.37	7.3	0.0499	3.0	0.410

sample	measured ²⁰⁴ Pb/ ²⁰⁶ Pb	measured ²⁰⁷ Pb/ ²⁰⁶ Pb	% com ²⁰⁶ Pb	U (ppm)	Th (ppm)	Th/U	Age in Ma					²⁰⁷ Pb/ ²³⁵ U	% err	²⁰⁶ Pb/ ²³⁸ U	% err	err correl
							²⁰⁶ Pb/ ²³⁸ U	err	²⁰⁷ Pb/ ²⁰⁶ Pb	err	% disc					
High Falls granite																
FRHF-1	0.000404	0.0612	0.87	1026.55	585.814	0.59	378.5	11.1	424.7	158.6	11	0.46	7.7	0.0606	3.0	0.387
FRHF-2	—	0.0550	0.10	564.049	70.5972	0.13	376.9	7.9	410.5	34.9	8	0.46	2.7	0.0603	2.1	0.809
FRHF-3	-0.000004	0.0547	0.04	2506.29	190.094	0.08	384.7	8.4	400.9	15.6	4	0.46	2.3	0.0615	2.2	0.954
FRHF-4	0.000420	0.0592	0.65	282.032	82.47	0.30	370.5	10.7	331.3	94.2	-12	0.43	5.1	0.0591	3.0	0.579
FRHF-5	0.000086	0.0563	0.30	523.978	490.026	0.97	364.8	8.2	411.4	42.5	12	0.44	3.0	0.0583	2.3	0.767
FRHF-6.1	0.000131	0.0563	0.29	87.7666	44.7197	0.53	367.9	10.3	386.6	117.5	5	0.44	6.0	0.0588	2.9	0.480
FRHF-6.2R	0.000006	0.0543	0.07	1985.54	36.8788	0.02	359.3	8.0	377.4	19.0	5	0.43	2.4	0.0573	2.3	0.936
FRHF-7.1	0.000428	0.0626	1.08	251.4	97.4134	0.40	366.3	2.8	466.5	111.0	22	0.46	5.1	0.0586	0.8	0.161
FRHF-8.1	—	0.0551	0.11	332.17	195.165	0.61	378.4	9.1	414.6	40.6	9	0.46	3.0	0.0605	2.4	0.802
FRHF-8.2	-0.000006	0.0548	0.02	1639.35	74.4598	0.05	397.3	9.7	408.7	18.5	3	0.48	2.6	0.0636	2.5	0.949
FRHF-9	0.000044	0.0551	0.13	1299.62	227.645	0.18	373.9	12.4	391.0	22.6	4	0.45	3.5	0.0597	3.4	0.958
FRHF-10	0.000185	0.0578	0.42	679.513	222.668	0.34	387.4	9.8	416.0	66.4	7	0.47	3.9	0.0620	2.6	0.654
FRHF-11	0.000089	0.0600	0.86	1525.51	545.156	0.37	333.0	38.9	557.1	205.7	41	0.43	15.2	0.0534	11.9	0.783
FRHF-12	0.000105	0.0555	0.21	1572.54	167.72	0.11	363.0	10.5	370.0	25.4	2	0.43	3.2	0.0579	2.9	0.934
FRHF-13.1	0.001627	0.0839	3.85	435.529	357.482	0.85	324.6	11.1	612.0	382.4	48	0.43	18.0	0.0521	3.4	0.188
FRHF-13.2R	0.000006	0.0534	-0.07	1932.1	37.5279	0.02	370.3	5.9	343.2	18.5	-8	0.43	1.8	0.0591	1.6	0.894
FRHF-14	0.000050	0.0555	0.04	454.834	152.512	0.35	419.7	14.9	403.0	61.6	-4	0.51	4.5	0.0672	3.6	0.795
Murder Creek granite																
F850-1	0.000083	0.0527	-0.03	634.716	624.761	1.02	324.9	3.7	260.0	37.6	-25	0.37	2.0	0.0516	1.1	0.573
F850-2	0.000131	0.0552	0.32	6964.75	753.581	0.11	313.1	5.4	340.8	31.2	8	0.37	2.2	0.0498	1.8	0.787
F850-3	0.000832	0.0605	1.25	441.725	162.825	0.38	218.7	2.8	111.7	133.9	-97	0.23	5.8	0.0344	1.3	0.229
F850-4	0.000357	0.0600	0.92	710.013	323.181	0.47	308.9	7.7	401.4	55.1	23	0.37	3.5	0.0492	2.5	0.717
F850-5	0.002709	0.0894	4.56	761.064	976.015	1.32	314.5	11.1	172.1	308.8	-84	0.34	13.7	0.0498	3.5	0.259
F850-6	0.000134	0.0546	0.27	416.605	382.284	0.95	302.9	4.0	312.8	50.3	3	0.35	2.6	0.0481	1.3	0.516
F850-7	0.000627	0.0588	0.83	578.154	128.166	0.23	290.2	4.1	172.4	89.6	-69	0.31	4.1	0.0459	1.4	0.351
F850-8	0.000006	0.0538	0.10	1610.05	379.665	0.24	327.7	4.4	358.0	17.0	9	0.39	1.6	0.0522	1.4	0.878
F850-9	0.000071	0.0544	0.18	282.358	359.782	1.32	323.5	8.6	342.4	75.6	6	0.38	4.3	0.0515	2.7	0.627
F850-10	0.000183	0.0529	0.01	432.541	103.641	0.25	320.3	5.2	202.7	92.8	-59	0.35	4.3	0.0508	1.6	0.379
F850-11	0.000353	0.0582	0.75	1353.9	1397.45	1.07	293.3	4.6	328.7	64.8	11	0.34	3.3	0.0466	1.6	0.491
F850-12	0.019219	0.3357	35.14	606.111	163.045	0.28	326.3	13.4	413.5	1058.2	21	0.40	47.5	0.0521	4.4	0.094

sample	measured ²⁰⁴ Pb/ ²⁰⁶ Pb	measured ²⁰⁷ Pb/ ²⁰⁶ Pb	% com ²⁰⁶ Pb	U (ppm)	Th (ppm)	Th/U	Age in Ma				% disc	²⁰⁷ Pb/ ²³⁵ U	% err	²⁰⁶ Pb/ ²³⁸ U	% err	err correl
							²⁰⁶ Pb/ ²³⁸ U	err	²⁰⁷ Pb/ ²⁰⁶ Pb	err						
<i>Murder Creek granite</i>																
F850-13.2	0.000065	0.0538	0.10	737.822	125.279	0.18	328.1	5.1	323.0	34.6	-2	0.38	2.2	0.0522	1.6	0.718
F850-13R	0.000094	0.0544	0.16	1716.4	231.939	0.14	333.6	4.8	329.3	28.5	-1	0.39	1.9	0.0531	1.4	0.755
F850-14	-0.000076	0.0530	0.00	162.523	91.708	0.58	328.7	4.4	376.6	74.7	13	0.39	3.6	0.0524	1.3	0.374
<i>Dows Pulpit granodiorite</i>																
L1452-1	0.000216	0.0573	0.67	2917.55	103.591	0.04	279.3	5.9	374.5	27.9	26	0.33	2.5	0.0444	2.1	0.865
L1452-1.2	0.000096	0.0719	-0.40	106.304	46.0587	0.45	1074.7	10.7	941.8	38.2	-15	1.75	2.1	0.1804	1.0	0.483
L1452-1.3R	0.000037	0.0529	0.06	1700.93	101.89	0.06	305.0	2.9	301.1	21.2	-1	0.35	1.3	0.0484	1.0	0.722
L1452-2	—	0.0856	1.45	185.975	72.0111	0.40	1024.7	19.6	1328.1	18.7	24	2.06	2.2	0.1748	2.0	0.898
L1452-2.2R	0.000013	0.0526	-0.03	1962.09	13.5468	0.01	321.2	3.9	302.7	18.1	-6	0.37	1.5	0.0511	1.2	0.842
L1452-3	0.000011	0.1289	1.84	476.469	73.5912	0.16	1844.6	12.9	2080.4	7.0	11	5.99	0.8	0.3374	0.7	0.871
L1452-4	0.000012	0.0722	0.43	321.519	135.949	0.44	885.7	15.9	985.1	18.8	10	1.47	2.1	0.1479	1.9	0.895
L1452-5	0.000027	0.0545	0.07	1551.4	1626.24	1.08	367.6	2.1	373.2	18.8	2	0.44	1.0	0.0587	0.6	0.565
L1452-6.2	0.000065	0.0521	-0.09	1126	515.541	0.47	320.6	3.4	246.5	28.8	-31	0.36	1.7	0.0509	1.1	0.654
L1452-6R	0.001071	0.0692	2.31	2593.15	1091.4	0.43	225.4	3.2	349.7	61.3	36	0.26	3.1	0.0357	1.4	0.469
L1452-7	0.000025	0.0927	-0.06	422.281	206.017	0.50	1491.7	10.3	1473.6	10.4	-1	3.31	0.9	0.2601	0.7	0.793
L1452-7.2R	0.000027	0.0527	-0.02	1628.62	62.0311	0.04	324.7	3.4	299.8	19.6	-8	0.37	1.4	0.0516	1.1	0.781
L1452-8	0.000452	0.0583	0.94	303.416	29.7359	0.10	229.2	6.9	268.5	126.5	15	0.26	6.3	0.0362	3.1	0.485
L1452-9	0.009058	0.1736	15.72	522.263	206.675	0.41	125.8	3.0	-448.1	846.3	129	0.10	32.2	0.0195	2.6	0.082
L1452-10	0.000040	0.0828	1.58	280.12	44.4219	0.16	916.7	17.6	1251.1	18.9	28	1.76	2.2	0.1552	2.0	0.899
L1452-10.2R	0.000011	0.0525	-0.02	1093.54	67.1286	0.06	312.3	3.7	298.2	23.7	-5	0.36	1.6	0.0496	1.2	0.757
L1452-11	0.000016	0.0779	0.44	254.762	63.8087	0.26	1045.9	8.8	1137.6	37.1	8	1.89	2.1	0.1769	0.9	0.416
L1452-12	0.000016	0.0942	-0.28	135.854	75.9898	0.58	1559.5	14.0	1506.9	33.0	-4	3.54	2.0	0.2728	0.9	0.461
L1452-13	0.000039	0.0533	0.03	610.467	137.661	0.23	328.8	2.0	316.0	34.5	-4	0.38	1.6	0.0523	0.6	0.381
L1452-14	0.000007	0.0536	0.09	1512.02	485.99	0.33	322.8	2.9	350.8	17.8	8	0.38	1.2	0.0514	0.9	0.762

sample	measured ²⁰⁴ Pb/ ²⁰⁶ Pb	measured ²⁰⁷ Pb/ ²⁰⁶ Pb	% com ²⁰⁶ Pb	U (ppm)	Th (ppm)	Th/U	Age in Ma					²⁰⁷ Pb/ ²³⁵ U	% err	²⁰⁶ Pb/ ²³⁸ U	% err	err correl
							²⁰⁶ Pb/ ²³⁸ U	err	²⁰⁷ Pb/ ²⁰⁶ Pb	err	% disc					
Indian Springs granodiorite																
J568-1	-0.000032	0.0607	0.20	223.252	3.71599	0.02	568.1	5.0	642.8	37.3	12	0.78	1.9	0.0924	0.9	0.456
J568-1.2R	0.001475	0.0740	2.74	2105.08	600.132	0.29	284.8	4.6	301.8	65.1	6	0.33	3.3	0.0452	1.7	0.501
J568-2	—	0.0500	-0.31	177.433	0.98077	0.01	307.7	3.0	195.3	58.4	-58	0.34	2.7	0.0487	1.0	0.358
J568-3	—	0.0494	-0.38	81.7093	1.13454	0.01	306.9	3.5	167.4	87.3	-85	0.33	3.9	0.0486	1.1	0.292
J568-3.2R	0.000572	0.0627	1.20	1931.05	88.0688	0.05	331.3	1.8	384.3	61.7	14	0.40	2.8	0.0528	0.6	0.209
J568-4	0.000135	0.0586	0.07	586.686	25.114	0.04	530.9	5.1	477.9	30.9	-11	0.67	1.7	0.0857	1.0	0.573
J568-5	0.000768	0.0623	1.24	295.171	252.802	0.88	297.9	8.2	240.8	223.7	-24	0.33	10.1	0.0472	2.8	0.275
J568-6	0.001942	0.0929	4.41	508.649	285.79	0.58	493.2	3.1	768.2	85.8	37	0.72	4.1	0.0803	0.7	0.169
J568-6.2R	0.014888	0.2866	28.91	445.056	85.6311	0.20	355.2	6.8	1054.1	616.3	67	0.60	30.7	0.0582	2.4	0.077
J568-7	0.000209	0.0560	0.39	2446.22	386.507	0.16	322.0	2.3	324.7	28.0	1	0.37	1.4	0.0512	0.7	0.511
J568-7.2R	0.000049	0.0612	0.14	112.535	46.3216	0.43	604.2	19.6	618.7	48.9	2	0.82	4.0	0.0983	3.3	0.826
J568-8	—	0.0559	0.09	135.041	92.5726	0.71	418.5	6.5	446.9	48.9	6	0.52	2.7	0.0671	1.6	0.580
J568-9.2R	0.000542	0.0603	0.99	2206.98	250.502	0.12	299.8	4.0	298.7	104.2	0	0.34	4.8	0.0476	1.4	0.289
J568-10	0.009432	0.2070	19.35	137.627	73.6042	0.55	273.9	9.8	991.2	467.6	73	0.44	23.3	0.0445	3.9	0.167
J568-10.2R	0.000250	0.0557	0.37	1642.14	107.591	0.07	314.7	3.7	284.0	35.4	-11	0.36	2.0	0.0500	1.2	0.608
J568-11	0.000116	0.0582	0.35	72.3489	16.7335	0.24	428.2	5.0	472.5	96.2	10	0.54	4.5	0.0688	1.2	0.265
J568-12	0.000794	0.0660	1.03	180.47	121.445	0.70	513.8	4.3	385.3	121.3	-34	0.62	5.5	0.0826	0.9	0.167
J568-13	0.000349	0.0530	0.05	102.044	58.3775	0.59	309.9	9.2	91.9	170.3	-241	0.32	7.8	0.0490	3.0	0.389
J568-14	0.000112	0.0551	0.28	101.808	124.029	1.26	320.0	3.3	345.6	101.6	8	0.38	4.6	0.0509	1.1	0.229
J568-15	0.000076	0.0595	0.19	1530.23	1192.94	0.81	526.1	3.0	544.0	16.6	3	0.69	1.0	0.0851	0.6	0.602
J568-16.1	0.000458	0.0679	1.42	1371.22	1896.64	1.43	467.6	8.7	647.1	125.8	28	0.64	6.2	0.0757	1.9	0.307
J568-17.1	0.000203	0.0554	0.34	5306.87	105.417	0.02	311.2	2.9	301.2	19.8	-3	0.36	1.3	0.0494	0.9	0.734
J568-18.1	0.000167	0.0610	0.31	575.271	280.785	0.50	545.2	5.5	548.7	34.1	1	0.71	1.9	0.0883	1.0	0.552
J568-19.1	0.004648	0.1327	10.09	213.673	102.696	0.50	272.9	6.9	796.5	370.2	67	0.40	17.9	0.0440	2.9	0.162
J568-19.2	0.000458	0.0585	0.72	1956.54	160.514	0.08	316.8	3.0	275.7	46.7	-15	0.36	2.3	0.0503	1.0	0.433
J568-20.1	0.000227	0.0557	0.34	3009.3	114.104	0.04	326.8	4.5	301.5	32.1	-8	0.38	2.0	0.0520	1.4	0.704
J568-21.1	0.001811	0.0814	3.44	2106.42	224.453	0.11	355.8	4.4	407.8	182.8	13	0.43	8.3	0.0568	1.4	0.166
J568-22.1	0.000081	0.0548	0.28	2485	77.2327	0.03	310.0	2.8	354.0	25.2	13	0.36	1.5	0.0493	0.9	0.641
J568-23.1	0.003105	0.1024	6.18	3999.6	248.456	0.06	314.0	12.6	496.9	588.0	37	0.40	27.0	0.0502	4.0	0.147
J1210-1.1	0.000135	0.0553	0.37	741.576	1894.56	2.64	299.6	7.9	342.9	43.8	13	0.35	3.3	0.0476	2.7	0.811

sample	measured ²⁰⁴ Pb/ ²⁰⁶ Pb	measured ²⁰⁷ Pb/ ²⁰⁶ Pb	% com ²⁰⁶ Pb	U (ppm)	Th (ppm)	Th/U	Age in Ma						²⁰⁷ Pb/ ²³⁵ U	% err	²⁰⁶ Pb/ ²³⁸ U	% err	err correl
							²⁰⁶ Pb/ ²³⁸ U	err	²⁰⁷ Pb/ ²⁰⁶ Pb	err	% disc						
Indian Springs granodiorite																	
J1210-1.2R	0.000157	0.0549	0.28	1366.69	834.141	0.63	312.0	9.6	309.8	30.5	-1	0.36	3.4	0.0496	3.1	0.919	
J1210-2.1	—	0.1209	0.29	91.8697	47.4212	0.53	1931.5	49.9	1969.3	18.1	2	5.84	2.8	0.3504	2.6	0.932	
J1210-2.2R	—	0.0538	0.03	285.298	3.19063	0.01	352.1	10.0	362.7	50.2	3	0.42	3.7	0.0562	2.9	0.793	
J1210-3	-0.000020	0.0543	-0.02	495.705	257.677	0.54	389.4	10.1	394.8	34.2	1	0.47	3.1	0.0623	2.7	0.867	
J1210-4.1R	0.002472	0.0895	4.50	962.459	394.693	0.42	342.1	17.5	344.1	707.4	1	0.40	31.7	0.0545	5.0	0.158	
J1210-4.2R	0.000041	0.0535	0.09	2044.71	135.833	0.07	314.9	7.6	321.7	20.7	2	0.36	2.6	0.0501	2.5	0.938	
J1210-5.1	0.000159	0.0584	0.02	89.7904	74.4521	0.86	537.4	5.4	453.1	92.8	-19	0.67	4.3	0.0867	1.0	0.241	
J1210-5.2R	0.003407	0.1071	6.82	2159.79	195.156	0.09	295.4	7.6	507.9	897.6	42	0.37	40.9	0.0472	2.6	0.063	
J1210-6	0.000008	0.0545	0.03	1291.33	117.901	0.09	379.5	9.5	385.3	21.4	2	0.45	2.7	0.0606	2.6	0.937	
J1210-7.1	-0.000054	0.0552	0.19	465.765	330.494	0.73	356.1	13.4	450.9	35.3	21	0.44	4.2	0.0570	3.8	0.924	
J1210-8	0.000057	0.0511	-0.23	199.551	64.1904	0.33	327.9	9.0	206.8	72.4	-60	0.36	4.2	0.0520	2.8	0.665	
J1210-9	0.000092	0.0557	0.16	3111.97	411.879	0.14	388.8	12.3	385.4	16.3	-1	0.47	3.3	0.0622	3.2	0.976	
J1210-10	0.000019	0.0548	0.01	1439.61	174.821	0.13	402.6	9.8	393.2	24.2	-2	0.48	2.7	0.0644	2.5	0.917	
J1210-11	0.000705	0.0627	1.07	872.236	32.6713	0.04	374.7	8.7	303.0	65.9	-24	0.43	3.7	0.0597	2.4	0.632	
J1210-12	0.000025	0.0593	0.13	1058.76	597.556	0.58	537.9	7.9	564.9	18.3	5	0.71	1.7	0.0871	1.5	0.872	
J1210-13	-0.000032	0.0543	0.09	655.83	85.678	0.13	354.1	9.5	402.6	32.3	12	0.43	3.1	0.0566	2.7	0.884	
J1210-14	-0.000019	0.0551	0.10	995.835	788.034	0.82	383.0	9.8	426.1	23.8	10	0.47	2.8	0.0613	2.6	0.925	
J1210-15	0.000108	0.0555	0.38	620.024	452.868	0.75	305.3	7.5	368.8	46.2	17	0.36	3.2	0.0486	2.5	0.771	
W131-1	-0.000031	0.0809	0.47	101.8	38.6542	0.39	1119.4	11.0	1228.8	28.3	9	2.14	1.8	0.1906	1.0	0.574	
W131-1.2R	0.000538	0.0594	0.87	1269.72	609.772	0.50	303.9	1.7	262.3	70.0	-16	0.34	3.1	0.0482	0.6	0.191	
W131-2	0.000064	0.0529	0.09	616.592	487.758	0.82	291.5	3.0	280.7	39.8	-4	0.33	2.0	0.0462	1.0	0.515	
W131-3	-0.000028	0.0530	0.07	409.141	406.395	1.03	304.7	2.2	345.5	39.2	12	0.36	1.9	0.0485	0.7	0.387	
W131-4	0.000779	0.0630	1.47	1556.57	1378.05	0.91	248.9	8.5	263.9	482.0	6	0.28	21.3	0.0394	3.5	0.165	
W131-5	-0.000016	0.0753	0.25	208.38	30.2991	0.15	1020.1	19.4	1082.6	21.0	6	1.79	2.2	0.1719	2.0	0.883	
W131-5.2R	0.000161	0.0532	0.04	1129.19	242.247	0.22	321.3	1.9	232.2	44.4	-39	0.36	2.0	0.0510	0.6	0.305	
W131-6	0.000031	0.0528	-0.01	1256.78	61.8045	0.05	321.6	1.8	299.2	21.2	-8	0.37	1.1	0.0511	0.6	0.527	
W131-7	0.000214	0.0546	0.31	346.55	302.184	0.90	291.2	2.2	262.6	73.4	-11	0.33	3.3	0.0462	0.8	0.238	
W131-8	0.000380	0.0571	0.60	1494.38	73.075	0.05	296.6	1.7	262.1	47.5	-13	0.33	2.1	0.0470	0.6	0.271	
W131-9	0.000441	0.0627	1.06	883.946	428.649	0.50	373.9	9.7	460.8	56.6	19	0.46	3.7	0.0599	2.7	0.721	
W131-9.2R	0.000048	0.0535	0.11	2946.75	138.094	0.05	309.3	5.1	317.3	15.5	3	0.36	1.8	0.0492	1.7	0.926	

sample	measured ²⁰⁴ Pb/ ²⁰⁶ Pb	measured ²⁰⁷ Pb/ ²⁰⁶ Pb	% com ²⁰⁶ Pb	U (ppm)	Th (ppm)	Th/U	Age in Ma				% disc	²⁰⁷ Pb/ ²³⁵ U	% err	²⁰⁶ Pb/ ²³⁸ U	% err	err correl
							²⁰⁶ Pb/ ²³⁸ U	err	²⁰⁷ Pb/ ²⁰⁶ Pb	err						
Indian Springs granodiorite																
W131-10	0.000043	0.0521	-0.03	511.155	417.556	0.84	300.2	5.5	262.9	37.2	-14	0.34	2.5	0.0476	1.9	0.753
W131-11	0.001077	0.0674	1.41	136.401	59.1862	0.45	450.2	4.1	265.4	185.4	-71	0.51	8.1	0.0719	1.0	0.127
W131-12	0.000014	0.1190	1.45	110.202	61.8276	0.58	1738.3	18.1	1937.8	14.1	10	5.14	1.3	0.3140	1.1	0.803
W131-12.2R	0.000085	0.0533	0.04	1990.64	132.167	0.07	328.3	1.8	287.6	23.1	-14	0.37	1.2	0.0522	0.6	0.483
W131-13	0.000032	0.0639	0.36	162.707	92.7171	0.59	637.5	5.3	723.6	42.3	12	0.91	2.2	0.1043	0.8	0.390
W131-14	0.000226	0.0537	0.17	182.207	139.062	0.79	298.3	4.9	211.4	145.4	-42	0.33	6.5	0.0472	1.6	0.252
W131-15	0.000497	0.0595	0.78	53.6299	58.2909	1.12	339.3	4.4	294.5	208.0	-15	0.39	9.2	0.0540	1.4	0.150
W131-15.2R	0.000004	0.0527	0.00	3076.32	85.7562	0.03	317.0	3.5	313.6	12.7	-1	0.37	1.3	0.0504	1.1	0.896
W131-16.1	0.000037	0.0607	0.04	177.857	91.2009	0.53	616.1	7.3	608.9	44.8	-1	0.83	2.4	0.1003	1.2	0.507
W131-17.1	0.000160	0.0544	0.28	1029.8	296.341	0.30	289.5	2.8	286.0	40.8	-1	0.33	2.0	0.0459	1.0	0.485
W131-18.1	0.000153	0.0565	0.58	390.665	486.285	1.29	277.3	5.2	382.1	58.1	28	0.33	3.2	0.0441	1.9	0.595
W131-19.1	0.002348	0.0877	4.55	535.039	638.333	1.23	250.7	3.6	340.7	201.1	27	0.29	9.0	0.0398	1.6	0.172
W131-20.1	0.000005	0.0523	0.00	2645.23	54.7364	0.02	297.1	3.3	293.4	16.8	-1	0.34	1.3	0.0472	1.1	0.834
W131-21.1	0.004833	0.1289	9.53	351.116	311.509	0.92	298.5	3.7	551.4	302.7	47	0.39	13.9	0.0478	1.5	0.105
W131-22.1	-0.000084	0.0511	-0.17	290.771	255.346	0.91	302.5	3.5	296.5	61.0	-2	0.35	2.9	0.0480	1.2	0.404
W131-23.1	0.000120	0.0699	0.66	88.155	163.36	1.91	755.2	28.1	873.0	60.1	14	1.17	4.8	0.1249	3.8	0.797
Gladesville gabbro contact aureole																
B695-1C	0.000066	0.0594	0.17	263.456	124.931	0.49	527.4	9.7	543.9	35.8	3	0.69	2.5	0.0853	1.9	0.755
B695-1.2R	0.000000	0.0534	-0.09	1204.49	34.1027	0.03	372.4	4.0	343.2	33.4	-9	0.44	1.8	0.0594	1.1	0.593
B695-2C	0.000139	0.0588	-0.01	127.255	62.4774	0.51	563.3	5.6	483.7	63.0	-17	0.71	3.0	0.0911	1.0	0.336
B695-2.2R	-0.000045	0.0557	0.17	735.966	39.7848	0.06	382.1	4.7	465.6	35.0	18	0.48	2.0	0.0612	1.3	0.623
B695-3C	0.000081	0.0590	0.08	138.616	73.5775	0.55	540.1	11.5	521.4	50.7	-4	0.70	3.2	0.0873	2.2	0.687
B695-3.2R	0.000019	0.0543	0.07	945.33	42.9623	0.05	356.5	2.1	369.6	22.1	4	0.42	1.1	0.0569	0.6	0.522
B695-4C	0.000502	0.0592	0.12	86.3735	41.6424	0.50	538.1	5.6	279.3	138.7	-95	0.62	6.2	0.0864	1.1	0.179
B695-4.2R	0.000000	0.0543	0.03	367.845	97.3604	0.27	373.1	2.5	384.0	32.4	3	0.45	1.6	0.0596	0.7	0.427
B695-5	0.000046	0.0594	0.27	134.012	68.4605	0.53	496.1	4.9	554.5	49.0	11	0.65	2.5	0.0801	1.0	0.407
B695-6.2R	0.000031	0.0539	-0.01	1059.53	131.833	0.13	370.5	2.2	347.2	24.1	-7	0.44	1.2	0.0591	0.6	0.492
B695-6C	0.000030	0.0593	0.14	196.808	98.8405	0.52	534.1	8.3	560.5	37.3	5	0.70	2.3	0.0865	1.6	0.682
B695-7	0.000208	0.0593	-0.01	152.304	82.2054	0.56	578.0	5.7	460.6	68.1	-26	0.72	3.2	0.0935	1.0	0.315
B695-8R	0.000014	0.0566	0.10	508.426	101.983	0.21	445.0	7.0	468.0	24.6	5	0.56	1.9	0.0715	1.6	0.821

sample	measured ²⁰⁴ Pb/ ²⁰⁶ Pb	measured ²⁰⁷ Pb/ ²⁰⁶ Pb	% com ²⁰⁶ Pb	U (ppm)	Th (ppm)	Th/U	Age in Ma						²⁰⁷ Pb/ ²³⁵ U	% err	²⁰⁶ Pb/ ²³⁸ U	% err	err correl
							²⁰⁶ Pb/ ²³⁸ U	err	²⁰⁷ Pb/ ²⁰⁶ Pb	err	% disc						
Gladesville gabbro contact aureole																	
B695-9	0.000780	0.0674	1.14	200.399	264.877	1.37	533.2	4.4	453.7	133.8	-18	0.66	6.1	0.0860	0.8	0.136	
B695-10.1R	-0.000010	0.0546	0.06	863.639	99.5835	0.12	376.1	2.3	401.3	21.4	6	0.45	1.1	0.0601	0.6	0.536	
B695-10.2C	0.000025	0.0581	0.19	275.359	208.436	0.78	474.4	3.4	519.1	34.3	9	0.61	1.7	0.0765	0.7	0.424	
B695-11.1C	0.000273	0.0624	0.54	49.6005	29.7091	0.62	529.3	7.2	546.4	139.0	3	0.69	6.5	0.0856	1.4	0.216	
B695-11.2R	0.000119	0.0538	0.01	287.913	139.45	0.50	356.3	6.2	285.1	53.8	-25	0.41	2.9	0.0567	1.8	0.601	
B695-12C	0.000082	0.0573	-0.21	134.167	60.2233	0.46	568.5	5.6	456.2	53.1	-25	0.71	2.6	0.0919	1.0	0.386	
B695-13C	0.000131	0.0600	0.31	93.2736	49.5885	0.55	510.8	5.8	533.7	79.8	4	0.66	3.8	0.0825	1.2	0.303	
B695-14.1C	0.000037	0.0595	0.16	160.908	98.166	0.63	538.0	9.5	566.0	42.5	5	0.71	2.7	0.0871	1.8	0.679	
B695-14.2R	0.000109	0.0541	0.08	507.789	26.561	0.05	348.9	2.2	308.6	44.4	-13	0.40	2.1	0.0555	0.6	0.311	
B695-15.1C	0.000000	0.0582	-0.14	47.4586	30.5727	0.67	576.4	7.5	535.4	67.0	-8	0.75	3.3	0.0934	1.3	0.397	
B695-15.2R	0.000045	0.0538	-0.01	455.042	38.4951	0.09	364.3	3.9	333.2	37.5	-9	0.43	2.0	0.0581	1.1	0.550	
B695-16C	0.000261	0.0568	-0.14	84.0674	34.183	0.42	526.3	5.4	326.5	99.8	-63	0.62	4.5	0.0846	1.1	0.236	
B695-17C	0.000040	0.0581	-0.01	159.942	64.401	0.42	535.5	4.4	511.2	45.3	-5	0.69	2.2	0.0866	0.8	0.379	
B695-18.1C	0.000083	0.0601	0.23	214.123	151.304	0.73	536.1	6.0	560.7	41.6	4	0.70	2.2	0.0868	1.1	0.511	
B695-18.2R	-0.000013	0.0549	0.12	1362.63	28.7399	0.02	370.6	3.0	416.5	16.9	11	0.45	1.1	0.0592	0.8	0.737	
B695-19C	0.000208	0.0613	0.27	52.603	43.352	0.85	568.8	8.1	538.8	104.4	-6	0.74	5.0	0.0922	1.5	0.296	
B695-20C	0.000096	0.0598	0.21	153.449	93.4884	0.63	535.3	4.5	545.4	76.7	2	0.70	3.6	0.0866	0.8	0.231	
B695-21R	0.000028	0.0536	-0.03	300.722	101.741	0.35	362.2	4.5	334.1	39.1	-9	0.42	2.1	0.0577	1.3	0.588	
B695-22R	0.000097	0.0555	0.23	271.42	87.4463	0.33	358.2	4.8	375.3	50.9	5	0.43	2.6	0.0572	1.4	0.516	
Metagabbroic diorite																	
L503-1.1	0.000042	0.0571	-0.14	173.107	84.0859	0.50	536.3	6.5	470.3	51.4	-14	0.67	2.6	0.0866	1.2	0.468	
L503-2.1	0.000171	0.0564	-0.24	163.057	135.312	0.86	540.7	6.7	365.3	113.7	-49	0.65	5.2	0.0870	1.2	0.238	
L503-3.1	-0.000029	0.0583	-0.02	492.064	601.144	1.26	543.3	5.5	554.3	27.8	2	0.71	1.6	0.0880	1.0	0.634	
L503-4.1	-0.000024	0.0569	-0.14	610.736	749.54	1.27	532.4	5.5	502.0	25.5	-6	0.68	1.6	0.0860	1.1	0.675	
L503-4.2	0.000000	0.0586	0.05	3444.16	1689.22	0.51	536.9	5.5	552.3	9.5	3	0.70	1.1	0.0869	1.1	0.925	
L503-5.1	0.000000	0.0567	-0.19	319.532	266.025	0.86	536.7	9.4	478.2	32.6	-13	0.68	2.3	0.0867	1.8	0.773	
L503-5.2	0.000252	0.0549	0.10	42.3912	5.05782	0.12	374.4	7.1	249.9	208.8	-51	0.42	9.3	0.0596	1.9	0.210	
L503-6.1	0.000264	0.0559	-0.29	147.892	66.6086	0.47	538.5	12.9	284.4	94.8	-92	0.62	4.8	0.0865	2.5	0.510	

sample	measured ²⁰⁴ Pb/ ²⁰⁶ Pb	measured ²⁰⁷ Pb/ ²⁰⁶ Pb	% com ²⁰⁶ Pb	U (ppm)	Th (ppm)	Th/U	Age in Ma					% disc	²⁰⁷ Pb/ ²³⁵ U	% err	²⁰⁶ Pb/ ²³⁸ U	% err	err correl
							²⁰⁶ Pb/ ²³⁸ U	err	²⁰⁷ Pb/ ²⁰⁶ Pb	err							
<i>Henderson Gneiss</i>																	
SM-1.1	0.000169	0.0572	0.23	114.014	66.2892	0.60	423.8	10.8	400.1	70.3	-6	0.51	4.1	0.0679	2.6	0.639	
SM-2.1	0.001171	0.0610	0.74	50.3048	50.5342	1.04	414.0	13.3	-130.3	309.2	427	0.39	12.9	0.0654	3.3	0.256	
SM-3.1	0.001260	0.0833	4.39	466.696	572.863	1.27	119.0	5.4	777.5	120.4	85	0.17	7.4	0.0190	4.6	0.628	
SM-4.1	0.000000	0.0555	-0.01	94.5253	60.5091	0.66	436.8	4.8	432.4	91.3	-1	0.54	4.2	0.0701	1.1	0.257	
SM-5.1	0.001614	0.0842	3.56	403.449	535.665	1.37	428.0	19.7	631.3	381.9	33	0.58	18.4	0.0691	4.7	0.258	
SM-6.1	0.000045	0.0544	-0.19	322.357	200.731	0.64	446.0	4.7	357.8	32.8	-25	0.53	1.8	0.0715	1.1	0.594	
SM-7.1	0.000285	0.0562	0.03	177.824	108.511	0.63	448.4	4.0	285.0	72.6	-59	0.51	3.3	0.0717	0.9	0.275	
SM-8.1	0.000081	0.0555	-0.03	68.29	51.7322	0.78	440.4	6.1	381.9	83.2	-16	0.53	4.0	0.0706	1.4	0.357	
SM-9.1	0.000352	0.0617	0.78	997.53	432.722	0.45	427.7	14.2	474.1	32.4	10	0.54	3.7	0.0687	3.4	0.918	
SM-10.1	0.000248	0.0541	-0.12	63.3619	43.2784	0.71	415.0	5.3	215.4	124.6	-95	0.46	5.5	0.0661	1.3	0.239	
SM-11.1	0.000142	0.0561	0.04	103.42	130.369	1.30	441.7	7.1	369.5	72.0	-20	0.53	3.6	0.0708	1.6	0.456	
SM-12.1	0.001081	0.0706	2.10	91.6587	83.8148	0.94	356.4	11.8	402.3	156.1	12	0.43	7.7	0.0569	3.4	0.437	
SM-13.1	0.000016	0.0565	0.09	300.401	159.056	0.55	440.8	7.9	461.6	31.0	5	0.55	2.3	0.0708	1.8	0.794	
SM-14.1	0.000000	0.0548	-0.16	122.289	68.437	0.58	454.2	4.5	401.4	46.8	-13	0.55	2.3	0.0729	1.0	0.432	
SM-15.1	-0.000031	0.0572	0.22	461.448	274.718	0.62	427.4	3.0	515.5	25.8	17	0.55	1.4	0.0687	0.7	0.518	
SM-16.1	0.001378	0.0707	2.00	158.103	176.285	1.15	391.9	5.3	213.6	192.2	-85	0.43	8.4	0.0624	1.4	0.168	
SM-17.1	0.000070	0.0566	0.32	1932.29	569.224	0.30	371.9	6.9	434.8	28.6	15	0.46	2.3	0.0595	1.9	0.827	
SM-18.1	0.005217	0.1280	9.95	369.943	471.923	1.32	138.6	6.2	262.3	737.8	48	0.15	32.5	0.0218	5.0	0.152	
SM-19.1	0.000016	0.0557	0.00	1111.54	292.253	0.27	441.1	6.7	430.3	15.1	-3	0.54	1.7	0.0708	1.6	0.916	
SM-20.1	0.000077	0.0568	0.10	133.767	87.3466	0.67	449.5	4.7	438.4	54.8	-3	0.55	2.7	0.0722	1.1	0.396	
HQ1-1.1	0.000027	0.0712	0.05	183.318	46.9226	0.26	950.3	8.4	950.8	24.1	0	1.55	1.5	0.1588	0.9	0.611	
HQ1-2.1	0.000010	0.0553	-0.05	493.524	233.742	0.49	439.8	6.4	416.7	24.8	-6	0.54	1.9	0.0706	1.5	0.801	
HQ1-3.1	-0.000055	0.0537	-0.28	95.2653	46.3823	0.50	449.1	5.0	388.9	64.1	-16	0.54	3.1	0.0720	1.1	0.365	
HQ1-4.1	0.001521	0.0787	2.94	59.1694	37.7875	0.66	408.1	6.3	473.3	246.5	14	0.51	11.3	0.0655	1.7	0.151	
HQ1-5.1	0.007385	0.1765	14.89	64.397	108.978	1.75	444.7	13.9	949.1	775.8	54	0.71	38.0	0.0728	2.1	0.056	
HQ1-5.2	0.000037	0.0565	0.06	147.172	76.8897	0.54	453.4	4.9	451.4	50.6	0	0.56	2.5	0.0729	1.1	0.432	
HQ1-6.1	0.000048	0.0548	-0.16	107.79	87.0087	0.83	455.4	10.1	372.7	58.8	-23	0.54	3.4	0.0730	2.3	0.653	
HQ1-7.1	0.000687	0.0560	0.00	58.1559	45.0439	0.80	450.8	6.9	-11.8	225.7	4002	0.45	9.5	0.0715	1.6	0.172	
HQ1-8.1	0.000000	0.0542	-0.20	92.9858	52.248	0.58	445.0	4.9	377.8	57.9	-18	0.53	2.8	0.0713	1.1	0.398	
HQ1-9.1	0.000049	0.0537	-0.29	107.323	53.0698	0.51	453.7	4.7	326.1	60.9	-40	0.53	2.9	0.0726	1.1	0.367	
HQ1-10.1	0.001717	0.0888	4.06	218.735	121.408	0.57	448.6	14.1	741.2	245.6	40	0.64	12.1	0.0728	3.3	0.273	
HQ1-11.1	0.000130	0.0581	0.34	165.512	142.907	0.89	425.9	3.8	460.7	55.7	8	0.53	2.7	0.0684	0.9	0.341	

Appendix III

SHRIMP U-Th-Pb data from analysis of Concord Plutonic Suite mafic plutons

sample	measured ²⁰⁴ Pb/ ²⁰⁶ Pb	measured ²⁰⁷ Pb/ ²⁰⁶ Pb	% com ²⁰⁶ Pb	U (ppm)	Th (ppm)	Th/U	Age in Ma					²⁰⁷ Pb/ ²³⁵ U	% err	²⁰⁶ Pb/ ²³⁸ U	% err	err correl
							²⁰⁶ Pb/ ²³⁸ U	err	²⁰⁷ Pb/ ²⁰⁶ Pb	err	% disc					
<i>Farmington metagabbro</i>																
FRMGB-1.1	0.000000	0.0515	0.42	210.28	124.50	0.61	107.0	2.7	262.6	106.1	60	0.12	5.3	0.0168	2.5	0.475
FRMGB-1.1	0.000022	0.0555	0.02	517.47	17.30	0.03	423.7	5.5	418.7	25.3	-1	0.52	1.7	0.0679	1.3	0.761
FRMGB-2	0.000387	0.0550	0.36	708.09	410.43	0.60	288.7	9.0	159.7	90.5	-82	0.31	5.0	0.0456	3.2	0.632
FRMGB-2.1	-0.000090	0.0499	-0.34	145.61	84.77	0.60	309.2	6.5	248.3	66.1	-25	0.35	3.6	0.0490	2.1	0.597
FRMGB-3	0.000022	0.0555	0.05	889.41	207.11	0.24	416.8	8.1	419.9	25.5	1	0.51	2.3	0.0668	2.0	0.866
FRMGB-3.1	0.000267	0.0541	0.42	1429.33	745.29	0.54	231.4	6.2	203.9	41.5	-14	0.25	3.2	0.0365	2.7	0.834
FRMGB-4	0.000034	0.0560	0.12	245.21	183.46	0.77	412.7	13.5	431.7	46.6	4	0.51	3.9	0.0662	3.3	0.847
FRMGB-4.1	0.001293	0.0697	2.12	959.39	1155.96	1.24	312.2	6.3	227.0	210.9	-38	0.35	9.4	0.0495	2.1	0.220
FRMGB-5	0.000000	0.0549	0.01	179.47	9.96	0.06	403.5	9.2	407.6	60.6	1	0.49	3.6	0.0646	2.3	0.649
FRMGB-5.1	0.000030	0.0535	0.12	1060.19	1317.44	1.28	308.5	6.7	329.9	24.4	7	0.36	2.5	0.0490	2.2	0.900
FRMGB-6	0.000095	0.0543	0.25	1409.08	591.52	0.43	298.4	10.0	326.0	27.6	9	0.35	3.6	0.0474	3.4	0.942
FRMGB-6.1	-0.000039	0.0525	-0.01	209.99	187.81	0.92	308.4	8.1	330.3	52.6	7	0.36	3.5	0.0490	2.7	0.756
FRMGB-7	0.000027	0.0531	0.10	1500.14	772.39	0.53	297.8	18.0	315.6	24.5	6	0.34	6.2	0.0473	6.1	0.985
FRMGB-7.1	0.000083	0.0537	-0.18	401.18	30.32	0.08	417.5	5.2	304.7	35.5	-38	0.48	2.0	0.0667	1.3	0.634
<i>Mecklenburg gabbro</i>																
MCKGB-1.1	0.000000	0.0545	-0.03	379.36	233.98	0.64	401.4	8.4	390.4	38.4	-3	0.48	2.7	0.0642	2.1	0.778
MCKGB-1.2R	0.000040	0.0554	-0.01	2007.48	626.16	0.32	430.1	5.7	404.2	20.9	-7	0.52	1.6	0.0689	1.4	0.822
MCKGB-2	-0.000086	0.0537	-0.15	240.80	103.72	0.44	406.6	10.1	409.5	84.2	1	0.49	4.5	0.0651	2.5	0.555
MCKGB-3.1	-0.000115	0.0515	-0.42	96.94	77.83	0.83	405.6	7.2	334.8	106.9	-22	0.48	5.1	0.0648	1.8	0.358
MCKGB-3.2R	-0.000336	0.0670	1.45	29.41	30.28	1.06	423.1	9.4	979.4	302.3	58	0.69	15.0	0.0692	2.0	0.134
MCKGB-4.1	0.000000	0.0547	-0.01	199.38	163.63	0.85	401.3	6.0	398.5	55.3	-1	0.48	2.9	0.0642	1.5	0.525
MCKGB-4.2R	0.006797	0.0942	4.75	17.56	23.45	1.38	442.4	16.2	#NUM!	#NUM!	#NUM!	0.12	317.8	0.0654	7.2	0.023
MCKGB-5.1	0.000291	0.0550	0.03	141.18	270.48	1.98	401.2	9.6	227.3	119.7	-78	0.45	5.7	0.0639	2.5	0.429
MCKGB-5.2R	0.000000	0.0989	5.34	25.00	13.92	0.58	437.9	14.3	1603.3	183.6	74	1.01	10.3	0.0743	3.1	0.298
MCKGB-6.1	0.000000	0.0561	0.12	198.05	430.20	2.24	416.5	10.0	456.2	51.5	9	0.52	3.4	0.0668	2.4	0.723
MCKGB-6.2R	0.004552	0.0720	2.05	2.99	2.98	1.03	429.3	70.4	#NUM!	#NUM!	#NUM!	0.01	6902.9	0.0645	18.9	0.003

sample	measured ²⁰⁴ Pb/ ²⁰⁶ Pb	measured ²⁰⁷ Pb/ ²⁰⁶ Pb	% com ²⁰⁶ Pb	U (ppm)	Th (ppm)	Th/U	Age in Ma				% disc	²⁰⁷ Pb/ ²³⁵ U	% err	²⁰⁶ Pb/ ²³⁸ U	% err	err correl
							²⁰⁶ Pb/ ²³⁸ U	err	²⁰⁷ Pb/ ²⁰⁶ Pb	err						
<i>Dutchman's Creek Gabbro</i>																
DCGB-1	0.000000	0.0562	0.19	404.92	133.12	0.34	398.2	10.5	461.1	33.3	14	0.50	3.1	0.0638	2.7	0.872
DCGB-11	0.000013	0.0550	0.01	655.35	108.91	0.17	408.2	12.9	402.2	28.0	-2	0.49	3.5	0.0654	3.2	0.932
DCGB-2	0.000000	0.0548	0.00	571.61	437.04	0.79	402.6	10.7	403.5	27.1	0	0.49	3.0	0.0645	2.7	0.913
DCGB-3	-0.000128	0.0486	-0.50	88.99	94.62	1.10	312.4	10.9	218.2	125.0	-44	0.35	6.5	0.0495	3.6	0.549
DCGB-4	-0.000094	0.0526	0.02	350.49	520.88	1.54	305.1	9.4	369.7	52.1	18	0.36	3.9	0.0486	3.1	0.804
DCGB-5	-0.000161	0.0505	-0.26	121.69	95.14	0.81	310.6	9.6	323.8	96.6	4	0.36	5.3	0.0494	3.1	0.593
DCGB-6	0.000029	0.0559	0.14	314.07	111.37	0.37	400.6	11.6	429.4	44.3	7	0.49	3.6	0.0642	2.9	0.829
DCGB-7	-0.000034	0.0542	0.23	384.95	634.61	1.70	298.8	8.8	398.5	46.2	25	0.36	3.6	0.0476	3.0	0.822
DCGB-8	0.000000	0.0525	-0.03	296.73	530.13	1.85	315.3	7.7	304.4	43.3	-4	0.36	3.1	0.0501	2.5	0.792
DCGB-9	0.000000	0.0510	-0.23	236.63	231.66	1.01	320.7	6.7	239.8	56.7	-34	0.36	3.2	0.0509	2.1	0.650
DCGB-10	-0.000078	0.0526	0.01	271.83	361.47	1.37	306.8	7.8	357.4	57.4	14	0.36	3.6	0.0488	2.6	0.711
<i>"Highway 200" gabbro</i>																
H200-1.1	0.000060	0.0530	-0.22	305.55	669.12	2.26	401.4	4.5	290.4	41.0	-39	0.46	2.1	0.0640	1.1	0.535
H200-2.1	-0.000124	0.0538	-0.17	136.35	139.73	1.06	419.5	4.0	435.7	61.8	4	0.52	2.9	0.0673	1.0	0.331
H200-3.1	0.000000	0.0554	0.09	80.61	94.00	1.20	396.4	7.8	425.6	57.3	7	0.48	3.3	0.0635	2.0	0.616
H200-4.1	0.000078	0.0545	-0.04	207.48	378.18	1.88	403.0	4.8	343.2	47.2	-18	0.47	2.4	0.0644	1.2	0.502
H200-5.1	0.000174	0.0535	-0.15	185.03	219.93	1.23	399.4	8.4	238.7	63.7	-69	0.45	3.5	0.0636	2.2	0.615
H200-6.1	0.000053	0.0567	0.24	103.80	100.14	1.00	402.2	4.3	448.3	60.7	10	0.50	2.9	0.0645	1.1	0.365
H200-7.1	0.000131	0.0545	-0.05	158.80	219.01	1.43	405.3	6.2	308.6	60.5	-32	0.47	3.1	0.0647	1.6	0.508
H200-8.1	-0.000034	0.0533	-0.19	172.53	186.97	1.12	407.0	3.6	362.2	47.2	-13	0.48	2.3	0.0651	0.9	0.395
H200-9.1	0.000041	0.0537	-0.16	269.79	301.12	1.15	410.4	9.0	331.0	38.3	-24	0.48	2.8	0.0656	2.2	0.799
H200-10.1	0.000155	0.0520	-0.37	172.43	225.09	1.35	411.8	3.6	182.6	65.5	-128	0.45	2.9	0.0655	0.9	0.299

sample	measured $^{204}\text{Pb}/^{206}\text{Pb}$	measured $^{207}\text{Pb}/^{206}\text{Pb}$	% com ^{206}Pb	U (ppm)	Th (ppm)	Th/U	Age in Ma					$^{207}\text{Pb}/^{235}\text{U}$	% err	$^{206}\text{Pb}/^{238}\text{U}$	% err	err correl
							$^{206}\text{Pb}/^{238}\text{U}$	err	$^{207}\text{Pb}/^{206}\text{Pb}$	err	% disc					
<i>Buffalo Gabbro</i>																
BFGB-1	0.000000	0.0544	-0.02	1249.17	157.20	0.13	393.0	9.2	384.8	20.1	-2	0.47	2.5	0.0628	2.4	0.936
BFGB-2	0.000632	0.0631	1.10	877.59	214.15	0.25	381.1	9.8	364.5	64.1	-5	0.45	3.9	0.0609	2.6	0.679
BFGB-3	0.000583	0.0635	1.16	1087.39	428.82	0.41	375.4	13.1	411.1	61.6	9	0.46	4.5	0.0600	3.6	0.791
BFGB-4.1	-0.000016	0.0550	0.10	873.25	522.46	0.62	378.1	5.1	419.1	30.3	10	0.46	1.9	0.0605	1.4	0.709
BFGB-5	0.000054	0.0553	0.09	2001.19	145.84	0.08	391.8	7.4	389.8	21.0	-1	0.47	2.1	0.0627	1.9	0.899
BFGB-6	0.000322	0.0653	1.37	784.29	204.61	0.27	381.3	12.4	625.9	187.0	40	0.51	9.3	0.0614	3.3	0.355
BFGB-7	0.000127	0.0572	0.26	2689.97	224.94	0.09	416.2	11.9	425.6	17.1	2	0.51	3.0	0.0667	2.9	0.967
BFGB-8	-0.000026	0.0534	-0.16	337.59	206.57	0.63	398.1	8.7	362.0	41.5	-10	0.47	2.9	0.0636	2.2	0.772
BFGB-9.1	0.000035	0.0534	-0.13	235.11	175.01	0.77	390.4	12.7	324.5	87.6	-21	0.45	5.1	0.0623	3.3	0.651
BFGB-9.2R	0.000043	0.0548	-0.05	2569.91	134.83	0.05	419.9	7.4	377.5	15.3	-11	0.50	1.9	0.0672	1.8	0.935
BFGB-10	0.000389	0.0608	0.77	819.94	208.68	0.26	397.0	12.0	418.2	52.8	5	0.48	3.9	0.0636	3.1	0.793
<i>Calhoun Falls Gabbro</i>																
CFGB-1	0.000000	0.0491	-0.76	92.86	113.61	1.26	421.7	5.0	151.3	93.0	-183	0.45	4.1	0.0671	1.2	0.287
CFGB-2.1	-0.000157	0.0520	-0.38	84.73	114.93	1.40	415.6	5.2	383.5	131.8	-9	0.50	6.0	0.0665	1.3	0.215
CFGB-2.2R	0.000000	0.0526	-0.30	49.56	51.06	1.06	413.4	6.9	311.1	129.7	-34	0.48	5.9	0.0660	1.7	0.278
CFGB-3.1	0.000075	0.0576	0.30	259.31	317.48	1.26	417.0	7.0	471.3	77.4	12	0.52	3.9	0.0669	1.7	0.441
CFGB-3.2R	-0.000228	0.0500	-0.71	58.78	46.99	0.83	440.5	6.6	341.8	178.5	-29	0.52	8.0	0.0705	1.6	0.194
CFGB-4	0.000000	0.0550	-0.05	343.64	586.01	1.76	429.3	6.7	411.9	44.5	-4	0.52	2.6	0.0688	1.6	0.625
CFGB-5	0.000000	0.0555	0.09	53.67	78.11	1.50	403.7	6.9	432.4	111.1	7	0.50	5.3	0.0647	1.7	0.325
CFGB-6	0.000065	0.0549	0.00	429.82	364.77	0.88	409.1	12.2	370.1	50.2	-11	0.49	3.8	0.0654	3.0	0.806
CFGB-7	-0.000207	0.0517	-0.47	126.25	188.33	1.54	428.8	14.3	398.1	113.8	-8	0.52	6.1	0.0687	3.4	0.558

sample	measured ²⁰⁴ Pb/ ²⁰⁶ Pb	measured ²⁰⁷ Pb/ ²⁰⁶ Pb	% com ²⁰⁶ Pb	U (ppm)	Th (ppm)	Th/U	Age in Ma						²⁰⁷ Pb/ ²³⁵ U	% err	²⁰⁶ Pb/ ²³⁸ U	% err	err correl
							²⁰⁶ Pb/ ²³⁸ U	err	²⁰⁷ Pb/ ²⁰⁶ Pb	err	% disc						
<i>Mt. Carmel metagabbro</i>																	
MCGB-1	0.000302	0.0495	-0.37	134.81	94.36	0.72	307.0	6.2	-51.9	168.1	702	0.30	7.2	0.0483	2.1	0.285	
MCGB-2	0.000008	0.0560	0.19	972.40	169.27	0.18	387.8	13.1	445.9	20.7	13	0.48	3.6	0.0621	3.4	0.965	
MCGB-3.1	-0.000225	0.0493	-0.16	197.32	156.17	0.82	223.3	1.9	311.6	126.0	29	0.26	5.6	0.0353	0.9	0.157	
MCGB-4	0.000051	0.0507	-0.24	394.80	160.68	0.42	313.3	8.5	192.4	47.9	-64	0.34	3.4	0.0496	2.8	0.801	
MCGB-5	-0.000037	0.0531	0.08	571.91	210.42	0.38	304.6	9.5	354.3	35.5	14	0.36	3.5	0.0484	3.2	0.896	
MCGB-6	0.000087	0.0529	0.02	255.49	85.39	0.35	317.5	9.1	270.1	65.4	-18	0.36	4.1	0.0504	2.9	0.713	
MCGB-7	-0.000132	0.0543	0.20	173.37	76.01	0.45	313.2	7.7	459.8	79.0	32	0.39	4.4	0.0500	2.5	0.576	
MCGB-8	0.000063	0.0518	-0.09	372.71	246.56	0.68	305.9	9.3	232.9	53.9	-32	0.34	3.9	0.0485	3.1	0.796	
MCGB-9	0.000363	0.0578	0.73	405.39	423.58	1.08	284.7	11.0	307.0	69.4	7	0.33	5.0	0.0452	3.9	0.788	
MCGB-10	-0.000090	0.0510	-0.20	501.30	666.91	1.37	311.5	5.1	299.3	45.7	-4	0.36	2.6	0.0495	1.7	0.639	

Appendix IV

Compiled whole-rock geochemical data of granitoids from the Inner Piedmont

Granitoid	High Falls					Walker Top		
Sample	HFSP ¹	HF862 ¹	IS370 ¹	FRHF ²	S123	B9WT ³	RP281 ³	MV-566 ⁴
Age	399			372	383	357		
Major Elements								
SiO ₂	56.56	61.60	65.80	68.30	71.57	64.67	64.81	73.13
Al ₂ O ₃	21.17	18.89	15.83	15.38	13.88	15.01	15.35	14.64
Fe ₂ O ₃ (T)	5.31	5.38	5.38	2.86	3.41	7.21	5.90	2.22
MnO	0.082	0.093	0.116	0.062	0.273	0.124	0.088	0.042
MgO	1.26	1.14	1.14	0.90	0.69	1.84	1.41	0.50
CaO	3.48	2.99	2.40	2.28	0.89	3.22	3.11	1.16
Na ₂ O	4.27	3.82	2.74	3.68	2.08	2.56	2.50	2.76
K ₂ O	5.35	4.76	4.15	4.76	5.94	3.47	4.00	4.37
TiO ₂	0.763	0.718	0.689	0.471	0.346	0.990	0.950	0.321
P ₂ O ₅	0.27	0.15	0.23	0.19	0.05	0.33	0.30	0.24
LOI	0.57	0.60	1.18	0.22	0.14	0.23	0.72	1.28
Total	99.08	100.10	99.66	99.10	99.26	99.67	99.13	100.70
Trace Elements								
Sc	14.6	13.2	11.5	6.82	15.3	17.1	13.2	
V	67	63	63	44	31	78	75	22
Cr	30.0	14.9	21.7	13.3	< 0.5	33.1	31.0	8.6
Co	9.6	9.1	11.7	4.7	5.2	14.1	11.0	3.5
Ni	9.0	14.0	17.0	5.0	5.0	15.0	16.0	2.0
Cu	< 1	2.0	17.0	4.0	< 1	13.0	20.0	1.0
Zn	84.0	91.0	91.0	61.0	41.0	110.0	77.0	65.0
Ga	29.0	23.0	21.0	20.0	13.0	26.0	20.0	18.0
Rb	194	155	144	194	198	150	120	209
Sr	208	190	187	337	133	184	217	155
Y	42.0	34.0	31.0	11.0	77.0	71.0	44.0	18.0
Zr	329	303	260	186	201	388	484	136
Nb	17.0	14.6	14.7	10.0	7.7	25.7	13.4	15.1
Cs	5.7	4.5	1.9	6.7	2.6	1.1	0.7	2.3
Ba	1036	851	905	1066	765	679	869	389
La	65.1	55.7	49.0	65.4	44.7	74.8	91.7	37.1
Ce	137	116	105	130	99	159	183	84
Pr	16.6	13.4	12.2	14.1	11.5	17.8	24.8	9.5
Nd	60.5	52.3	49.4	47.0	41.2	63.1	81.7	36.0
Sm	12.10	10.20	10.30	6.89	8.48	12.70	14.80	8.16
Eu	2.36	1.89	1.68	1.19	1.23	1.61	2.26	0.80
Gd	10.30	7.48	7.73	4.06	6.77	10.40	11.20	6.23
Tb	1.55	1.10	1.15	0.50	1.30	1.70	1.71	0.87
Dy	8.32	6.12	6.01	2.38	9.98	11.00	9.06	4.06
Ho	1.59	1.22	1.14	0.40	2.91	2.52	1.69	0.64
Er	4.24	3.46	3.15	1.05	11.10	8.21	4.76	1.59
Tm	0.62	0.51	0.47	0.14	2.32	1.23	0.68	0.22
Yb	3.70	3.30	3.14	0.89	17.60	7.31	3.99	1.36
Lu	0.56	0.53	0.52	0.13	2.59	1.03	0.55	0.18
Hf	8.60	8.40	7.10	4.60	5.60	9.60	11.10	4.10
Ta	1.27	1.00	1.00	0.88	0.53	1.00	0.50	0.88
Pb	35	35	30	32	51	27	27	27
Th	25.3	24.1	20.1	22.5	25.2	29.9	30.4	17.7
U	2.74	2.29	2.53	1.53	3.44	1.72	1.06	4.35

Granitoid		Walker Top						
Sample	MV-566B ⁴	MV-564 ⁴	MV-19 ⁴	MV-19B ⁴	MV-249 ⁴	GL-1 ⁴	GL-1B ⁴	GL-2 ⁴
Age	408							
Major Elements								
SiO ₂	71.79	71.48	67.96	68.37	68.05	66.36	65.03	64.66
Al ₂ O ₃	15.01	15.09	15.18	15.35	15.38	15.74	15.77	15.85
Fe ₂ O ₃ (T)	2.29	2.30	3.48	3.45	3.38	4.54	4.56	4.67
MnO	0.049	0.052	0.062	0.064	0.063	0.085	0.086	0.090
MgO	0.50	0.51	1.33	1.34	1.30	1.99	2.03	2.09
CaO	1.17	1.17	2.55	2.57	2.55	3.47	3.57	3.59
Na ₂ O	2.91	2.89	3.10	3.28	3.26	2.69	2.96	2.98
K ₂ O	4.84	4.86	3.96	4.26	4.38	4.16	4.16	4.17
TiO ₂	0.319	0.318	0.576	0.561	0.538	0.756	0.753	0.774
P ₂ O ₅	0.24	0.24	0.22	0.21	0.22	0.26	0.26	0.26
LOI	1.06	0.87	0.82	0.76	0.80	0.82	0.70	0.74
Total	100.20	99.75	99.22	100.20	99.93	100.90	99.87	99.85
Trace Elements								
Sc								
V	19	19	64	62	61	94	96	97
Cr	6.2	3.9	50.1	42.3	32.2	73.6	58.3	61.3
Co	3.0	2.7	8.8	7.0	6.5	12.9	9.9	11.0
Ni	2.0	2.0	12.0	11.0	9.0	19.0	16.0	17.0
Cu	2.0	1.0	2.0	4.0	4.0	10.0	10.0	9.0
Zn	58.0	56.0	61.0	51.0	49.0	71.0	63.0	64.0
Ga	21.0	22.0	16.0	19.0	18.0	20.0	20.0	20.0
Rb	234	244	167	176	170	200	195	195
Sr	163	162	195	202	204	297	304	305
Y	19.0	19.0	22.0	27.0	28.0	23.0	24.0	24.0
Zr	148	156	157	203	235	247	235	253
Nb	15.7	15.6	13.5	13.6	12.7	14.7	14.1	14.3
Cs	2.4	4.8	3.8	3.6	3.3	5.4	5.7	5.8
Ba	416	429	572	603	628	719	676	664
La	36.8	35.7	44.2	43.3	44.9	38.6	54.3	35.7
Ce	81	77	93	89	91	82	109	73
Pr	9.2	8.8	10.3	9.9	10.1	9.5	12.2	8.3
Nd	34.7	33.2	38.6	35.6	36.4	34.6	43.4	31.5
Sm	7.82	7.51	7.71	7.36	7.54	6.99	8.24	6.75
Eu	0.82	0.82	1.28	1.27	1.26	1.64	1.68	1.61
Gd	6.31	6.11	6.24	6.26	6.36	6.07	7.01	6.18
Tb	0.84	0.84	0.90	0.92	0.94	0.86	0.96	0.90
Dy	3.97	3.89	4.74	5.03	5.03	4.65	4.91	4.71
Ho	0.65	0.69	0.82	0.93	0.91	0.82	0.90	0.87
Er	1.70	1.84	2.11	2.49	2.34	2.27	2.38	2.42
Tm	0.25	0.28	0.28	0.34	0.33	0.32	0.33	0.34
Yb	1.56	1.76	1.62	2.00	1.93	1.92	2.02	2.06
Lu	0.21	0.24	0.22	0.28	0.25	0.27	0.28	0.29
Hf	4.00	4.20	4.40	5.10	6.00	6.00	5.90	6.40
Ta	1.20	0.90	0.89	0.90	0.80	0.89	1.00	1.00
Pb	24	25	39	32	32	28	26	20
Th	18.3	17.4	23.6	21.9	22.8	9.3	15.6	8.1
U	4.61	4.26	2.13	2.41	3.21	1.82	2.21	1.82

Granitoid	Walker Top					Toluca		
Sample	BK150 ⁵	D734 ⁵	MS13 ⁵	IK-WT ⁶	WT-1 ⁷	GQ1303 ⁸	GQ1170 ⁸	TOL-1 ⁶
Age				366				
Major Elements								
SiO ₂	71.40	68.70	70.10	64.60	61.50	73.21	71.78	73.10
Al ₂ O ₃	16.50	17.70	16.40	16.13	18.00	13.76	15.17	15.04
Fe ₂ O ₃ (T)	0.90	3.48	2.78	4.05	6.37	2.55	1.34	2.10
MnO	0.020	0.120	0.060	0.045	0.080	0.040	0.021	0.038
MgO	0.36	0.67	0.93	1.15	2.03	0.87	0.42	0.26
CaO	0.75	1.19	2.36	2.49	3.48	2.23	1.78	2.22
Na ₂ O	2.02	1.74	3.93	3.27	3.27	3.52	3.45	3.56
K ₂ O	7.18	4.23	3.21	5.10	3.42	2.66	4.77	3.63
TiO ₂	0.090	0.260	0.540	0.690	1.080	0.286	0.172	0.120
P ₂ O ₅	0.08	0.05	0.09	0.31	0.49	0.07	0.08	0.03
LOI				0.92	0.60	0.65	0.63	0.26
Total				98.71	103.90	99.84	99.60	100.40
Trace Elements								
Sc				7.1	11.4			3.47
V	nd	nd	60	49	88			8
Cr	nd	nd	nd	12.4				0.5
Co				8.1	14.0			1.8
Ni	nd	nd	nd					
Cu				6.4	4.7			
Zn				88.1	112.0			31.2
Ga								
Rb	299	129	101	178	156	86	105	102
Sr	53	150	468	194	186	157	233	199
Y	17.4	28.0	14.7	16.0	51.0	8.0	3.0	8.0
Zr	101	797	302	285	436	103	66	126
Nb	10.9	16.0	6.8		26.0	6.3	2.2	4.2
Cs				2.3				0.8
Ba				811	709			661
La				42.9	108.0			28.8
Ce				110	213			58
Pr				8.6	26.4			6.4
Nd				41.0	99.0			24.1
Sm				7.29	18.70			4.21
Eu				1.63	2.53			1.47
Gd				5.01	17.20			2.89
Tb				0.50	2.30			0.39
Dy				2.87	10.30			1.74
Ho				0.45	2.00			0.28
Er				1.03	5.30			0.73
Tm				0.12	0.80			0.09
Yb				1.01	5.10			0.61
Lu				0.15	0.80			0.08
Hf				6.90	8.00			4.19
Ta				0.99	1.16	0.40	0.10	0.08
Pb				29	17			29
Th				21.4	25.9	12.7	8.7	10.6
U				2.20		1.14	0.59	0.95

Granitoid	Toluca							
Sample	TOL-10 ⁶	TOL-11 ⁶	BK 238 ⁹	BK 372 ⁹	BK 431 ⁹	BK 529 ⁹	BK 955 ⁹	BK 1052 ⁹
Age	383							
Major Elements								
SiO ₂	70.10	68.90	74.40	69.00	76.70	76.30	74.90	77.10
Al ₂ O ₃	15.10	14.93	14.30	16.50	16.40	15.40	17.50	16.40
Fe ₂ O ₃ (T)	2.43	2.78	2.08	3.37	1.02	1.00	0.74	0.88
MnO	0.024	0.024	0.010	0.020	0.006	0.005	0.033	0.006
MgO	0.74	0.74	0.96	1.82	0.46	0.46	0.23	0.49
CaO	1.35	1.35	1.21	2.27	0.58	0.91	0.53	0.43
Na ₂ O	3.04	3.04	2.10	3.32	3.22	3.05	3.50	2.81
K ₂ O	5.25	5.28	1.21	3.82	5.84	6.28	6.06	5.40
TiO ₂	0.370	0.630	0.320	0.490	0.102	0.106	nd	0.026
P ₂ O ₅	0.19	0.19	0.01	0.18	0.06	0.10	0.12	0.17
LOI	0.77	0.77						
Total	99.29	98.58	96.60	100.79	104.39	103.62	103.61	103.72
Trace Elements								
Sc	6.13	3.13						
V	37	44	16	30	10	10	15	6
Cr	9.7	2.9	nd	15.0	nd	nd	64.0	nd
Co	4.5	5.8	5.0	6.0	3.0	2.9	26.0	2.8
Ni			8.0	19	6.0	3.4	3.0	3.0
Cu	2.4	8.1	nd	11.0	3.0	1.6	3.0	nd
Zn	46.8	90.2	48.0	70	41.0	36.2	36.0	42.3
Ga								
Rb	157	165	155	217	166	197	215	297
Sr	244	280	151	62	215	62	306	42
Y	18.0	5.0	18.0	36	23.0	36.6	18.0	30.5
Zr	254	536	176	115	124	115	49	53
Nb	14.4	13.0	9.0	11	8.0	10.7	4.0	14.7
Cs	4.3	0.9						
Ba	832	1642	682	614	561	797	482	204
La	52.6	160.0						
Ce	111	316						
Pr	10.2	28.2						
Nd	38.1	97.4						
Sm	6.29	10.81						
Eu	1.53	1.68						
Gd	5.16	5.14						
Tb	0.72	0.30						
Dy	3.87	1.57						
Ho	0.72	0.19						
Er	2.07	0.42						
Tm	0.29	0.06						
Yb	1.87	0.38						
Lu	0.29	0.05						
Hf	6.96	12.84						
Ta	0.97	0.36						
Pb	33	26	31	26	45	39	89	37
Th	23.3	47.8						
U	2.47	0.85						

Granitoid	Toluca							
Sample	BK 1079 ⁹	BK 1357 ⁹	BK 1365 ⁹	CA 40 ⁹	CA 63 ⁹	CA-AR1 ⁹	TOL-1 ⁹	CH117 ³
Age								
Major Elements								
SiO ₂	72.30	77.80	74.90	75.70	70.60	76.70	73.14	71.65
Al ₂ O ₃	15.40	16.10	16.90	15.90	17.30	16.40	15.04	14.85
Fe ₂ O ₃ (T)	2.38	1.23	0.70	0.88	2.91	2.13	2.10	3.01
MnO	0.019	nd	nd	nd	0.027	0.016	0.040	0.100
MgO	1.26	0.49	0.64	0.43	0.86	0.79	0.26	0.47
CaO	1.32	0.28	1.86	0.57	0.50	2.08	2.22	2.19
Na ₂ O	2.06	4.03	3.97	2.57	1.49	3.37	3.56	3.16
K ₂ O	7.18	4.43	4.16	5.62	7.63	3.92	3.63	3.73
TiO ₂	0.270	0.057	0.076	0.009	0.392	0.117	0.120	0.189
P ₂ O ₅	0.20	0.10	0.07	0.19	0.26	0.09	0.03	0.06
LOI								0.31
Total	102.39	104.52	103.28	101.87	101.97	105.62	100.14	99.72
Trace Elements								
Sc								9.5
V	17	6	9	5	21	14	10	13
Cr	nd	nd	nd	nd	12.5	nd	na	8.0
Co	4.7	3.0	2.7	2.9	5.3	4.4	1.8	3.0
Ni	7.8	3.0	4.8	1.3	11.8	4.7	2.0	< 1
Cu	1.9	nd	nd	nd	6.4	nd	nd	37.0
Zn	39.0	42.0	43.1	42.8	56.2	44.4	31.0	40.0
Ga								15.0
Rb	255	130	130	376	346	142	102	113
Sr	191	129	232	41	72	194	199	204
Y	27.5	23.0	9.8	34.5	39.4	15.4	8.0	30.0
Zr	147	50	111	54	288	134	126	190
Nb	9.4	16.0	6.6	12.9	13.7	7.4	4.0	5.6
Cs								0.9
Ba	961	274	499	770	462	823	661	477
La								42.8
Ce								89
Pr								10.9
Nd								37.3
Sm								7.77
Eu								1.46
Gd								6.57
Tb								1.03
Dy								5.98
Ho								1.10
Er								3.00
Tm								0.42
Yb								2.61
Lu								0.36
Hf								5.70
Ta								0.20
Pb	32	42	35	40	39	28	29	39
Th								18.5
U								2.93

Granitoid	Cherryville		Anderson Mill	Pelham	Gray Court
Sample	C-2 ⁶	C-10 ⁶	AMG ⁶	PEL-1 ⁶	GC-1 ⁶
Age	355		415	364	357
Major Elements					
SiO ₂	73.60	72.00	71.00	65.90	74.00
Al ₂ O ₃	15.35	14.93	14.30	17.03	13.78
Fe ₂ O ₃ (T)	0.74	0.96	2.99	4.60	1.44
MnO	0.170	0.021	0.070	0.053	0.026
MgO	0.01	0.22	0.67	1.23	0.30
CaO	0.80	0.19	2.61	3.38	1.38
Na ₂ O	3.89	2.84	2.99	4.00	3.28
K ₂ O	4.49	5.16	3.61	2.57	4.80
TiO ₂	0.110	0.170	0.300	0.750	0.170
P ₂ O ₅	0.17	0.17	0.07	0.23	0.10
LOI	0.95	2.34	1.35	0.68	0.39
Total	100.20	98.95	99.96	100.40	99.67
Trace Elements					
Sc	3.88	2.36	5.2	9.8	2.83
V		6	35	53	11
Cr	1.6	3.2	3.0	10.4	2.1
Co	1.3	2.6	4.0	8.0	1.9
Ni					
Cu	1.9	1.4	1.1	2.8	3.9
Zn	22.9	54.6	60.4	64.6	39.4
Ga					
Rb	202	298	148	136	204
Sr	75	52	133	270	132
Y	8.0	6.0	20.0	20.0	13.0
Zr	67	197	158	213	194
Nb	12.3	41.8	13.0	14.4	12.3
Cs	2.7	6.8	5.0	4.6	4.8
Ba	167	233	564	588	355
La	10.5	28.7	28.9	40.3	29.2
Ce	22	56	59	73	64
Pr	2.5	6.6	6.3	8.6	6.1
Nd	9.6	26.2	28.0	32.4	23.5
Sm	2.54	5.61	5.20	5.87	4.56
Eu	0.48	0.77	0.99	1.66	0.74
Gd	2.13	5.11	4.40	4.93	4.10
Tb	0.36	0.62	0.50	0.75	0.64
Dy	1.86	2.39	3.80	3.78	3.07
Ho	0.29	0.29	0.65	0.71	0.53
Er	0.81	0.68	2.40	1.82	1.47
Tm	0.11	0.09	0.30	0.24	0.20
Yb	0.73	0.58	2.30	1.50	1.27
Lu	0.10	0.08	0.30	0.23	0.20
Hf	2.13	3.86	4.00	5.47	4.83
Ta	0.77	1.37	1.00	0.70	0.57
Pb	30	49	17		40
Th	6.2	14.9	15.6	6.6	18.6
U	17.21	12.87	2.90	1.96	5.77

Granitoid	Lithonia		Toccoa	Dysartsville	Poor Mtn	Brooks Crossroad
Sample	AM2	J827	TOC 1 ¹⁰	VM1782 ¹⁰	POMTN ¹⁰	1398DC ⁷
Age						
Major Elements						
SiO ₂	76.09	71.61	77.18	73.00	84.50	72.00
Al ₂ O ₃	11.79	13.61	12.99	14.40	14.30	14.50
Fe ₂ O ₃ (T)	1.31	3.15	0.81	3.12	0.05	2.22
MnO	0.054	0.075	0.040	0.050	nd	0.050
MgO	0.17	0.66	0.17	0.62	nd	0.67
CaO	0.78	1.65	0.94	3.66	0.01	2.34
Na ₂ O	3.29	3.40	4.10	3.84	0.12	4.33
K ₂ O	4.52	4.43	3.54	0.84	0.39	3.13
TiO ₂	0.173	0.495	0.116	0.186	0.155	0.226
P ₂ O ₅	0.02	0.13	0.03	0.03	0.02	0.07
LOI	0.42	0.29	0.32	0.40	0.72	0.15
Total	98.61	99.50	100.23	100.20	100.27	99.80
Trace Elements						
Sc	6.14	9.72				3.2
V	8	29	nd	43	nd	22
Cr	11.3	12.7				
Co	1.4	4.0				4.0
Ni	2.0	4.0				4.0
Cu	2.0	3.0				2.4
Zn	32.0	76.0				28.3
Ga	19.0	21.0				19.0
Rb	262	164	97	41	6	127
Sr	38	123	88	128	4	170
Y	35.0	34.0	36.0	9.0	35.0	16.0
Zr	147	331	63	70	250	142
Nb	44.0	38.0	7.9	5.0	14.7	14.0
Cs	2.6	1.6	0.4	nd	nd	
Ba	153	662	1350	193	38	565
La	46.3	58.9	27.8	2.5	16.1	31.1
Ce	98	98	52	9	17	64
Pr	11.5	12.5	6.3	0.7	1.8	6.8
Nd	38.4	44.4	23.0	3.5	7.5	24.1
Sm	7.87	7.88	4.45	0.90	2.60	5.00
Eu	0.42	1.44	0.69	0.40	0.71	1.06
Gd	6.71	7.30	4.10	1.00	3.04	4.50
Tb	1.16	1.07	0.78	0.20	0.73	0.70
Dy	6.88	5.89	4.99	1.50	5.56	3.50
Ho	1.43	1.09	1.14	0.30	1.43	0.67
Er	4.26	2.89	3.50	1.20	4.80	1.60
Tm	0.66	0.36	0.57	0.20	0.80	0.30
Yb	4.55	2.00	3.64	1.30	5.58	1.50
Lu	0.74	0.29	0.56	0.20	0.88	0.23
Hf	4.90	8.20	2.30	2.00	7.70	4.00
Ta	3.75	1.92	0.70	0.50	1.30	1.10
Pb	19	18				31
Th	28.2	11.9	8.9	1.0	16.3	14.0
U	18.80	1.26	2.16	0.70	2.72	1.80

Granitoid	Henderson		Caesars Head		Pacolet	Reedy River	Miss(?) granitoid
Sample	HG-1⁷	HG-1_dup⁷	16177	16637	P-1⁶	FS-1⁶	GL30⁸
Age							
Major Elements							
SiO ₂	68.20	68.30	74.00	75.10	68.40	71.40	70.63
Al ₂ O ₃	15.00	15.00	13.40	12.60	15.08	14.95	14.95
Fe ₂ O ₃ (T)	3.71	3.72	1.31	1.13	2.96	1.98	1.92
MnO	0.070	0.070	0.030	0.030	0.068	0.036	0.021
MgO	0.88	0.88	0.22	0.27	1.09	0.61	0.58
CaO	2.37	2.38	0.63	1.01	2.32	1.36	1.22
Na ₂ O	3.49	3.50	3.74	3.19	3.46	3.36	3.46
K ₂ O	5.00	4.98	5.78	5.13	4.93	4.42	5.06
TiO ₂	0.654	0.653	0.227	0.150	0.610	0.370	0.372
P ₂ O ₅	0.22	0.23	0.02	0.03	0.23	0.12	0.13
LOI	0.20	0.20	0.20	0.25	0.92	1.49	1.19
Total	100.00	100.20	99.70	99.10	100.10	100.10	
Trace Elements							99.52
Sc	6.7	6.7	3.6	3.1	5.25	4.65	
V	46	46	7	10	48	30	
Cr					10.7	6.4	
Co	5.0	7.0	1.0	3.0	6.1	3.3	
Ni	5.0	4.0	2.0	2.0			
Cu	4.5	5.4	3.1	3.8	5.6	2.8	
Zn	60.8	61.2	23.7	24.7	94.0	68.9	
Ga	22.0	23.0	17.0	13.0			
Rb	128	127	221	172	227	255	151
Sr	164	165	65	90	638	231	269
Y	36.0	38.0	48.0	17.0	16.0	7.0	4.0
Zr	418	418	296	170	450	316	184
Nb	26.0	27.0	26.0	9.0	24.1	29.9	4.4
Cs					5.5	3.2	
Ba	1020	1020	921	1290	997	470	
La	106.0	98.5	86.4	44.7	111.0	67.8	
Ce	197	188	167	81	222	143	
Pr	21.2	20.3	18.4	9.3	20.5	13.5	
Nd	74.2	71.3	64.3	30.2	74.2	48.5	
Sm	12.60	13.10	11.00	6.10	10.10	7.44	
Eu	2.33	2.49	2.02	1.00	2.07	1.03	
Gd	12.10	12.30	8.70	5.80	6.14	4.60	
Tb	1.60	1.70	1.40	0.90	0.70	0.51	
Dy	7.60	7.90	8.10	4.20	3.52	2.08	
Ho	1.44	1.66	1.75	0.74	0.59	0.29	
Er	3.90	4.10	5.20	1.70	1.74	0.78	
Tm	0.60	0.60	0.90	0.20	0.22	0.09	
Yb	3.60	3.90	5.40	1.30	1.52	0.54	
Lu	0.60	0.60	0.88	0.21	0.22	0.07	
Hf	8.00	8.00	8.00	5.00	10.45	7.58	
Ta	0.95	1.07	3.30	0.50	1.97	0.99	0.30
Pb	10	11	18	167	48	52	
Th	13.3	11.8	31.0	25.0	42.7	44.2	23.7
U	0.50	0.50	14.00	2.20	7.50	5.23	2.19

Granitoid	Indian Springs					Murder Creek
Sample	L429	F-1337 ²	F432 ²	HF1465 ¹	IS470 ¹	MC ²
Age						
Major Elements						
SiO ₂	74.00	66.05	67.20	72.28	74.36	67.60
Al ₂ O ₃	14.58	17.18	16.45	15.25	14.72	15.31
Fe ₂ O ₃ (T)	1.27	3.17	3.22	1.38	0.57	3.07
MnO	0.032	0.045	0.046	0.028	0.019	0.070
MgO	0.27	1.31	1.18	0.38	0.09	0.94
CaO	1.54	2.93	2.96	1.59	1.08	2.35
Na ₂ O	4.09	4.22	4.49	3.86	3.99	3.87
K ₂ O	4.50	3.41	3.51	4.19	4.27	4.19
TiO ₂	0.204	0.525	0.580	0.208	0.052	0.482
P ₂ O ₅	0.10	0.16	0.21	0.05	0.04	0.24
LOI	0.15	0.68	0.67	0.57	0.51	0.54
Total						
Trace Elements	100.7	99.68	100.5	99.78	99.7	98.67
Sc	2.96	3.63	5.6	3.7	2	7.29
V	14	63	66	23	< 5	49
Cr	5.0	6.2	6.6	5.3	< 0.5	14.0
Co	1.9	4.7	7.7	2.9	2.6	5.5
Ni	2.0	5.0	6.0	5.0	2.0	5.0
Cu	3.0	21.0	24.0	5.0	2.0	2.0
Zn	34.0	57.0	57.0	39.0	14.0	67.0
Ga	19.0	20.0	21.0	19.0	19.0	22.0
Rb	174	107	111	114	159	214
Sr	303	981	986	485	162	309
Y	9.0	10.0	11.0	4.0	8.0	10.0
Zr	145	230	222	110	34	244
Nb	7.8	4.9	5.4	5.4	3.2	11.7
Cs	3.1	2.0	2.1	2.5	2.6	8.7
Ba	664	1185	1226	911	391	706
La	34.0	56.3	55.6	13.9	4.4	59.2
Ce	66	105	102	26	8	113
Pr	6.9	11.6	10.6	2.9	1.0	11.9
Nd	23.8	39.0	38.2	10.6	4.0	42.0
Sm	4.23	5.86	5.74	1.90	1.07	6.44
Eu	0.91	1.34	1.32	0.77	0.31	1.14
Gd	2.96	3.53	3.48	1.25	1.12	3.76
Tb	0.40	0.42	0.42	0.14	0.20	0.50
Dy	1.94	2.10	2.09	0.64	1.26	2.38
Ho	0.34	0.36	0.38	0.11	0.25	0.43
Er	0.82	0.99	0.98	0.29	0.74	1.10
Tm	0.12	0.13	0.14	0.04	0.12	0.16
Yb	0.67	0.75	0.79	0.26	0.76	0.99
Lu	0.11	0.11	0.11	0.05	0.11	0.15
Hf	4.50	5.20	5.40	3.40	1.70	6.40
Ta	0.62	0.55	0.57	0.33	0.99	0.88
Pb	35	11	13	39	41	27
Th	25.6	15.8	18.7	5.5	3.3	22.3
U	10.60	3.36	3.01	2.09	2.59	1.69

Data sources: ¹Howard (ms, 2012); ²Davis (ms, 2010); ³Byars (ms, 2010); ⁴Gatewood (ms, 2007); ⁵Giorgis (ms, 1999); ⁶Mapes (ms, 2002); ⁷Vinson (ms, 1999); ⁸Wilson (ms, 2006); ⁹Bier (ms, 2001); ¹⁰Bream (ms, 2003).

Appendix V

Whole-rock geochemical data of mafic plutons from the Concord Plutonic Suite

Sample	BFGb	CFGb	CHGb	DCGb	FrmGb	GGB	H200	MCGb	MKGb	OgdGb	RHGb	FrmSy
Major Elements												
SiO ₂	48.35	48.41	47.73	48.79	50.86	49.09	46.45	43.00	48.55	47.62	48.78	51.09
Al ₂ O ₃	7.93	15.80	17.42	15.86	17.56	22.08	19.97	17.07	16.54	14.83	18.19	21.89
FeO(T)	10.06	8.09	8.09	8.61	6.35	5.11	11.58	10.64	10.19	11.17	6.06	4.13
MnO	0.171	0.132	0.133	0.141	0.128	0.087	0.175	0.117	0.171	0.217	0.109	0.081
MgO	18.35	7.75	11.20	13.26	8.16	8.26	4.54	6.82	8.59	6.53	8.22	5.54
CaO	11.94	12.06	9.24	7.91	10.84	12.90	8.92	13.37	10.29	9.91	13.94	12.39
Na ₂ O	0.55	2.60	2.49	2.27	2.73	2.29	2.75	2.28	2.46	2.89	2.12	2.81
K ₂ O	0.14	0.31	0.23	0.66	0.26	0.15	0.38	0.44	0.22	0.27	0.11	0.14
TiO ₂	0.447	1.021	0.405	0.659	0.645	0.207	1.767	2.751	1.161	2.156	0.310	0.236
P ₂ O ₅	0.02	0.16	0.10	0.14	0.24	0.01	0.57	0.06	0.21	0.77	0.02	0.05
LOI	0.95	1.64	0.67	0.96	1.52	0.19	1.36	1.61	0.22	1.97	1.33	0.33
Total	100.00	98.87	98.61	100.20	100.00	100.90	99.76	99.33	99.74	99.58	99.86	99.15
Trace Elements												
Sc	52.1	48.8	14.4	14.4	27.6	18.9	24.9	39.9	30.4	38	40.4	20.5
V	176	218	73	92	125	51	339	436	243	280	116	67
Cr	550.0	274.0	140.0	103.0	93.9	177.0	93.3	208.0	271.0	173.0	725.0	79.6
Co	79.0	37.8	59.1	61.4	37.2	41.5	33.1	43.9	42.9	38.1	34.1	25.7
Ni	353.0	64.0	227.0	250.0	104.0	188.0	41.0	142.0	134.0	52.0	99.0	75.0
Cu	39.0	113.0	75.0	27.0	42.0	30.0	46.0	33.0	131.0	63.0	113.0	35.0
Zn	104.0	62.0	58.0	62.0	152.0	33.0	100.0	53.0	73.0	88.0	27.0	27.0
Ga	10.0	17.0	14.0	15.0	17.0	16.0	24.0	21.0	18.0	19.0	15.0	18.0
Rb	5	2	2	14	4	2	10	2	2	3	1	1
Sr	309	1231	948	632	758	721	794	1287	1033	784	555	914
Y	12.0	16.0	5.0	8.0	11.0	5.0	10.0	7.0	7.0	27.0	6.0	6.0
Zr	31	46	35	55	19	10	41	85	22	101	12	10
Nb	0.8	1.0	3.8	5.9	1.3	< 0.2	7.6	3.4	0.6	8.2	0.5	< 0.2
Cs	0.8	< 0.1	0.1	0.4	0.2	< 0.1	0.5	0.1	< 0.1	< 0.1	0.3	< 0.1
Ba	30	473	118	319	86	101	153	35	150	232	42	71
La	12.7	14.0	9.6	21.1	3.5	3.3	14.1	8.5	4.0	6.7	6.3	2.0
Ce	30	28	22	48	11	6	28	18	8	16	13	5
Pr	4.4	3.5	3.4	6.7	1.8	0.8	3.5	2.4	1.0	2.5	1.9	0.7
Nd	20.4	13.6	12.6	27.9	9.5	3.2	13.0	10.9	4.0	11.0	6.7	3.2
Sm	4.09	2.61	2.44	6.39	2.60	0.77	2.32	2.14	0.91	2.89	1.21	0.87
Eu	1.56	1.42	1.13	2.56	0.79	0.50	0.83	0.84	0.54	1.37	0.69	0.39
Gd	4.05	2.62	2.34	6.20	2.82	0.81	2.15	2.12	0.97	3.03	1.32	1.03
Tb	0.71	0.29	0.33	0.98	0.48	0.14	0.36	0.35	0.28	0.52	0.20	0.17
Dy	3.43	2.05	1.76	5.29	2.68	0.86	1.81	2.02	0.95	2.23	1.12	1.00
Ho	0.65	0.40	0.34	1.06	0.51	0.16	0.36	0.39	0.19	0.38	0.21	0.19
Er	1.76	1.09	0.88	2.72	1.38	0.44	0.97	1.10	0.52	0.85	0.57	0.48
Tm	0.25	0.16	0.12	0.39	0.19	0.06	0.14	0.16	0.07	0.10	0.08	0.07
Yb	1.50	1.01	0.78	2.47	1.23	0.42	0.90	1.03	0.47	0.57	0.45	0.41
Lu	0.27	0.15	0.13	0.39	0.17	0.05	0.13	0.14	0.08	0.09	0.07	0.07
Hf	1.00	1.30	0.60	1.20	0.50	0.20	0.90	2.40	0.50	2.00	0.20	0.20
Ta	0.06	< 0.01	0.47	0.38	0.05	< 0.01	0.51	0.32	< 0.01	0.48	0.02	< 0.01
Pb	< 5	< 5	< 5	< 5	< 5	< 5	< 5	< 5	< 5	< 5	< 5	< 5
Th	0.4	0.1	0.2	1.3	0.4	0.2	0.4	0.1	1.5	0.3	0.1	0.2
U	0.07	0.03	0.06	0.27	0.12	0.02	0.10	0.05	0.08	0.06	0.01	0.02

Vita

Matthew Tiesher Huebner was born on September 15, 1980, in Harrisburg, Pennsylvania, in the heart of the central Pennsylvania Valley and Ridge province. His parents, Deanna and John, along with his older brother Chris, spent much of the mid- to late 80's in various walk-in clinics and emergency rooms, as Matt quite often found his way into trouble that often involved stitches and/or concussions. Matt miraculously survived to graduate from Central Dauphin High School in 1999, and decided to forego further education to get a head start on the job market. After pursuing several not-so-fulfilling career paths, Matt was persuaded by his then girlfriend, Alexandra (Ali), to attend courses at Harrisburg Area Community College. Following several semesters of full-time work with part-time coursework in the evenings, Matt and Ali resigned from their careers in the health insurance industry to pursue full-time collegiate coursework at beautiful Bloomsburg University. It was there that Matt embraced his passion for earth science, and soon after developed an affinity for field-based study. Matt graduated with a B.S. in geology *summa cum laude* from Bloomsburg in May of 2007 (second in the College of Arts and Sciences), and he and his wife, Ali, moved to Knoxville that summer to pursue their graduate degrees. Matt will earn his Ph.D. in December, 2013, and he and his family will eagerly begin the next phase of their journey. Like his undergraduate mentor, Joe Hill, Matt also hates to refer to himself in the third person.